PETROLOGIC AND EXPERIMENTAL STUDIES ON THE PETROGENESIS OF PAPUA NEW GUINEA OPHIOLITES

by

Alan Lynton Jaques, B.Sc. (Hons.)

Submitted in fulfillment of the requirements

for the degree of Doctor of Philosophy.

University of Tasmania

HOBART

1980

This thesis contains no material which has been accepted for the award of any other degree or diploma in any university, and to the best of my knowledge and belief, contains no copy or paraphrase of material previously published or written by another person, except where due reference is made in the text of this thesis.

A.L. Jaques
January, 1980.

page

CONCLUSIONS 212

REFERENCES 217

APPENDIX 1. ANALYTICAL TECHNIQUES

APPENDIX 2. SAMPLE LOCALITY DATA

APPENDIX 3. THE CONTINENT/ISLAND-ARC COLLISION IN NORTHERN PAPUA NEW GUINEA

APPENDIX 4. DETERMINATION OF LIQUID COMPOSITION IN HIGH PRESSURE MELTING OF PERIDOTITE

ABSTRACT

The late Mesozoic Marum and Papuan ophiolites of Papua New Guinea dip from the continental margin towards accreted Paleogene island-arcs and appear to represent frontal-arc basement emplaced as a result of mid-Tertiary continent/arc collision. Both ophiolites comprise thick sequences of layered ultramafic and mafic cumulates overlying tectonite peridotite and have associated basaltic pillow lavas. The petrology and geochemistry of the cumulate sequences are not consistent with an origin from common mid-ocean ridge basalts (MORB). Discrimination between mid-ocean ridge or marginal basin origins for the Papua New Guinea ophiolites is more dependent on accurate dating of the rocks rather than geochemical characteristics.

The tectonite peridotites (mainly harzburgite) are characterized by extremely refractory mineralogy and chemistry, and are believed to be the residue from large degrees of partial melting of depleted mantle peridotite at low pressure. Relic protogranular textures and mineral assemblages in the Marum harzburgites indicate a high temperature (1200-1300^{o}C), low pressure (< 5 kb) origin followed by deformation and progressive subsolidus re-equilibration and cooling to much lower temperatures which are recorded by the different blocking temperatures of various cation exchange equilibria.

A number of cyclic units are superimposed on the gross layering (peridotite to gabbro) of the cumulate sequences which together with the igneous layering and cumulus textures indicate formation by magmatic crystallization in a large magma chamber(s) from a magma(s) of gradually evolving composition. The main cumulus phases - olivine, chrome spinel, clinopyroxene, orthopyroxene and plagioclase - show cryptic variation from highly magnesian and calcic early cumulates to more fractionated compositions. Various geothermometers and geobarometers, together with thermodynamic calculations involving silica buffers, indicate that the Marum cumulates crystallized at high temperature (1200-1300^{o}C) and low pressure (1-2 kb) under low f_{O_2}, and subsequently re-equilibrated under subsolidus conditions and cooled. The

presence of cumulus magnesian (Mg_{90}) orthopyroxene in the PNG ophiolites conflicts with the low pressure crystallization behaviour of MORB studied previously and with that found in an experimental study of a low-Ti olivine tholeiite basalt from a marginal basin. The cumulate sequences of these ophiolites are inferred to have accumulated from magnesian olivine-poor or quartz tholeiite parent magmas rich in Ni and Cr but poor in alkalies and other large-ion-lithophile (LIL) elements and high valence cations. Fractionated examples of these magmas are found among the lavas directly overlying the gabbro layer in the Papuan ophiolite and, although resembling MORB in terms of their very low contents of LIL elements, mostly have lower abundances of Ti, Zr, and Y than MORB of comparable Mg/(Mg + ΣFe) ratio.

Models of formation of oceanic crust based on ophiolites such as the PNG examples suggest segregation of magma from residual peridotite at shallow depth. An experimental study of the anhydrous melting behaviour of two possible upper mantle peridotite compositions at 0-15 kb pressure has been carried out to determine the composition of partial melts from peridotite at low to moderate pressure and the nature of the residual phases. Partial melts at low pressure are saturated to oversaturated in silica, magnesian olivine-poor tholeiite and quartz tholeiite, and co-exist with refractory harzburgite and dunite, consistent with the evidence from the ophiolites. Partial melts in the spinel lherzolite field are richer in normative olivine, ranging from alkali olivine basalt at low degrees of partial melting (for pyrolite) through olivine tholeiite and tholeiitic picrite to komatiitic compositions at high degrees of partial melting. It is concluded that high-alumina olivine tholeiites are not derived by segregation from harzburgite at shallow depths (< 25 km). This is consistent with crystallization studies on 'primitive' MORB and the marginal basin basalt studied here which suggest that such magmas are derived by fractionation of olivine from tholeiitic picrite parents which segregated at about 60-70 km depth.

ACKNOWLEDGEMENTS

I wish to express my sincere thanks to my supervisor Professor D.H. Green for his constant encouragement, guidance and advice during the course of this study. I also wish to thank him and his wife Helen for their friendship, hospitality and many kindnesses extended to my family and I during our time in Hobart.

This thesis was commenced at the Research School of Earth Science (RSES), Australian National University, and I wish to acknowledge the support, both in analytical facilities and in funding of a field trip to Papua New Guinea, provided by the School. I also gratefully acknowledge receipt of an Australian Public Service Board Scholarship and the continued interest and support of my employer, the Bureau of Mineral Resources. The bulk of the mapping and sampling was carried out while I was employed by the Geological Survey of Papua New Guinea and I wish to thank the Survey and, particularly Dr. H.L. Davies, for their support and encouragement.

Because of the wide ranging nature of this thesis many people have given instruction or assistance in the various analytical techniques. I particularly wish to thank Dr. B.W. Chappell of the Department of Geology, ANU for his generous collaboration and assistance with the XRF analyses, Messrs. W.O. Hibberson and K.L. Harris for their assistance with the experimental work and fellow student Mr. B.J. Griffin for his generous contribution in automating the energy-dispersive probe at Hobart. I am grateful to Dr. S.R. Taylor (RSES) for access to his laboratory and wish to thank him and Ms. P. Muir and Mr. M. Shelley for instruction and assistance in operation of the MS7. I also wish to thank Mr. N.G. Ware, Dr. A. McKee and Mr. B. Griffin for assistance and instruction with the microprobe work, Messrs. P. Beazely, R. Freeman, E. Kiss, P. Robinson and J. Wasik for assistance with XRF, AAS and wet chemical analyses, and Dr. R.W. Page for the isotopic analyses. Drs. J. Walshe, M. Owen, A. Glikson

and Mr. R.J. Ryburn kindly gave assistance with computing and data processing.

I have benefited from discussions with a number of people on various aspects of this work - Dr. R. Arculus, Mr. C.M. Brown, Dr. H.L. Davies, Dr. D.J. Ellis, Mr. J. Foden, Dr. F.A. Frey, Mr. B.J. Griffin, Mr. K.L. Harris, Mr. G. Jenner, Dr. R.W. Johnson, Dr. T. Mori, Mr. C.J. Pigram, Dr. G.P. Robinson, Dr. S.R. Taylor, and Dr. R. Varne.

I would finally like to thank my wife Barbara for her patience and understanding during the course of this study and her care and endurance in typing the thesis.

INTRODUCTION

Ophiolites (as defined by the Geological Society of America's Penrose Conference on ophiolites, Anonymous, 1972) are generally held to be segments of oceanic lithosphere obducted onto a continental margin. As such they should afford opportunity for detailed study of the nature of the deeper oceanic crust and mantle not revealed by sampling of the ocean basins. Geological and geophysical studies of ophiolites over the past decade have emphasized the similarities between ophiolites and oceanic crust, and current models of the oceanic crust rely heavily on the ophiolite analogue for information on the nature and relationship of lower crustal lithologies. While there is general agreement that ophiolites form in an oceanic environment doubts have been raised as to whether they are in fact representative of oceanic crust formed at mid-ocean ridges. It has been argued that many ophiolites formed in small back-arc basins or marginal seas; others have suggested that ophiolites may form in young island-arcs.

This thesis represents a contribution to the understanding of the petrology and petrogenesis of ophiolites in general but with particular regard to the ophiolites of Papua New Guinea. Study of the ophiolites of Papua New Guinea is attractive in view of their relative youth and well preserved state. The Papua New Guinea ophiolites are also of economic interest since the peridotites have associated lateritic nickel mineralization and are a source of chromite-rich (and possibly platinoids) mineral sands. An understanding of the mode of emplacement of the ophiolites and the subsequent tectonic history of the former plate boundary is important in understanding the tectonic evolution of Papua New Guinea, and is relevant to exploration for hydrocarbons in the sedimentary basins lying to the north and east of the ophiolites.

The thesis comprises four distinct but interrelated investigations which are presented as separate parts.

PART 1 consists of a study of the geology, petrology and geochemistry of the Marum ophiolite complex in northern Papua New Guinea. Mapping and sampling were carried out largely while I was employed by the Geological Survey of Papua New Guinea.

PART 2 consists of a petrologic and geochemical study of a representative suite of samples from the Papuan Ultramafic Belt in southeast Papua. The samples were collected in collaboration with Dr. H.L. Davies. No mapping was undertaken.

PART 3 is an experimental study of the anhydrous melting of two peridotites at 0 to 15 kb pressure with the aim of examining the nature of the melt compositions and of the residual phases formed on melting of peridotite at comparatively low pressure.

PART 4 is a study of the experimental petrology of a marginal basin basalt with the aim of comparing the low-pressure liquidus and near-liquidus phases with the mineralogy of accumulate sequences in ophiolites.

A substantial proportion of PARTS 1 and 2 is devoted to a consideration of the petrology and geochemistry of the *cumulate sequences* in the ophiolites. Study of the cumulate rocks is considered to be of importance in understanding the petrogenesis of ophiolites, particularly since the Deep Sea Drilling Project (DSDP) program and the French-American-Mid-Ocean-Undersea-Study (FAMOUS) project have resulted in a large amount of information on the petrology and geochemistry of the basaltic layer of the oceanic crust but have, with some exceptions, yielded very little information on the lower crust and mantle.

Significantly, both the DSDP and FAMOUS project studies have emphasized the importance of low pressure crystal fractionation in the evolution of ocean floor basalts, and it is now widely accepted that ultramafic and mafic rocks formed by fractional crystallization of mafic magmas comprise a significant component of present day oceanic crust. To date however few detailed studies of the petrology of the cumulates exposed in ophiolites have been made and there has been little opportunity to compare the nature of these accumulates with the petrologic or chemical characteristics of ocean floor basalts.

Implicit in popular models of formation of oceanic crust based on the ophiolite analogue is the assumption that mid-ocean ridge basalts (MORB) form by melting of peridotite at comparatively shallow depth. This model of oceanic crust formation is explored in PART 3 where the nature of the melt compositions and of the residual phases formed by anhydrous melting of peridotite at comparatively low pressure are examined in detail. From the results of this study and complementary melting studies of mid-ocean ridge-type olivine tholeiites a model for the petrogenesis of MORB and other tholeiitic basalts is developed.

A number of authors have pointed out the petrologic and chemical similarities between basalts erupted in marginal basins and those formed at mid-ocean ridges. Currently marginal basins attract considerable interest as possible sites for formation of ophiolites. At present direct comparison of ophiolite sequences with crustal sections of marginal basins is precluded by a lack of fundamental knowledge concerning the petrology of the lower crust beneath marginal basins and island-arcs. Sampling of marginal basins both in the Western Pacific and, particularly, in the South Atlantic region, has revealed that although marginal basin basalts lie broadly within the compositional spectrum exhibited by MORB many have features transitional with the island-arc tholeiite suite. PART 4 consists

of a study of the experimental petrology of a selected marginal basin basalt. The liquidus and near-liquidus phases at low pressure of this basalt are compared with the accumulate sequences in ophiolites to evaluate the proposal that ophiolites such as those of Papua New Guinea might have formed in a marginal basin.

Two published papers are also presented in support of the thesis as Appendices 3 and 4. The first paper describes the continent/island-arc collision in northern Papua New Guinea and bears directly on the emplacement of the Marum ophiolite. The second discusses technical problems involved in conducting partial melting experiments and is relevant to PART 3. My contribution to both papers was the greater part of the data and the bulk of the writing of each paper.

PART 1

THE MARUM OPHIOLITE COMPLEX

Contents *page*

SUMMARY			6
CHAPTER	1.	GEOLOGY	8
	2.	TECTONITE PERIDOTITES	14
	3.	PETROLOGY OF THE CUMULATE PERIDOTITES AND GABBROS	37
	4.	GEOCHEMISTRY OF CUMULATE PERIDOTITES AND GABBROS	76
	5.	ASSOCIATED BASALTS AND SEDIMENTS	87
	6.	ORIGIN OF THE MARUM OPHIOLITE COMPLEX	106

SUMMARY

The Marum ophiolite complex in northern Papua New Guinea consists of two main thrust sheets; a larger peridotite-gabbro massif and a smaller allochthon of spilitic pillow basalt (Tumu River basalt) which lies to the south of, and partly beneath, the peridotites and gabbros. The ophiolite dips from the continental margin northwards towards an accreted Tertiary island-arc which comprises the northern coastal ranges, and was emplaced as a result of collision between the continent and the Paleogene arc in the mid-Tertiary.

The base of the peridotite-gabbro massif consists of weakly foliated harzburgite, with interfingering lenses of dunite, characterized by extremely refractory mineralogy (olivine Mg_{92}, enstatite Mg_{93}, and chrome-rich spinel) and chemistry (< 0.3% CaO, Al_2O_3, < 0.1 ppm Rb, Sr, > 2400 ppm Ni). Cation exchange equilibria between olivine, pyroxene and spinel, coupled with the protogranular textures, suggests an origin at high temperatures (1200-1300^{o}C) and low pressure. Superimposed on the high temperature origin is a subsolidus history involving varying degrees of deformation and re-equilibration recorded by exchange equilibria which show a range of equilibration temperatures from about 900^{o}C down to very low temperatures ($\sim$ 600^{o}C) which probably represent cooling.

The tectonite peridotites are overlain by a thick (3-4 km) sequence of layered ultramafic and mafic cumulates, ranging from dunite at the base upwards through wehrlite, lherzolite, and pyroxenite to norite-gabbro. Superimposed on the gross layering are a number of cyclic units of variable thickness. Igneous layering and structures, and cumulus textures indicate an origin by magmatic crystallization in a large magma chamber(s) from a magma(s) of gradually evolving composition. The major cumulus phases are olivine, clinopyroxene, orthopyroxene and plagioclase and show cryptic variation from highly magnesian and calcic early cumulates

to lower temperature end-members, e.g. olivine Mg_{92-78}. Various geothermometers and geobarometers, together with thermodynamic calculations involving silica buffers, suggest that the cumulates crystallized at high temperatures (1200-1300°C) and low pressure (1-2 kb) under low f_{O_2} from a magnesian olivine-poor or quartz tholeiite parent magma ($Mg_{78 \pm 2}$). Most of the layered rocks show textural and mineralogical evidence of subsolidus re-equilibration during consolidation of the crystal pile; some rocks are foliated and folded with structures indicating deformation in the plane of the layering. The subsolidus history is recorded by various cation exchange reactions which indicate progressive cooling to temperatures below 600°C at low pressure. Superimposed on the solidus and subsolidus history is a weak, sporadically developed greenschist facies metamorphic event.

The upper portion of the peridotite-gabbro massif has been removed by erosion and/or dismembering during solid-state emplacement of the ophiolite. However volume-composition considerations for the ultramafic and mafic cumulates requires the existence of a suite of co-magmatic differentiated (probably iron-rich) basaltic rocks. The geochemistry of the cumulates implies that the parent magma(s) were highly depleted in LREE and other LIL elements similar to the most depleted MORB (e.g. DSDP Leg 3 basalts) but had significantly lower abundances of REE, Ti, Zr and Y. The spatially associated Tumu River basalts are strongly differentiated and range to TiO_2-rich ferrotholeiite compositions. These basalts are enriched in LREE, Ti, Zr, Y and Nb compared to common MORB, and are genetically unrelated to the cumulate sequence.

The harzburgites are considered to represent the refractory residue of large degrees of partial melting of depleted mantle peridotite under anhydrous conditions at shallow depth ($\sim$ 5 kb) which generated the olivine-poor tholeiite magmas parental to the cumulate sequence. Shallow segregation of melt resulted in a complex relationship between residual phases and overlying cumulates.

CHAPTER 1

GEOLOGY

1-1. Distribution of ophiolites in Papua New Guinea

Ophiolites form a conspicuous belt at the northern and north-eastern margin of the central cordillera of mainland Papua New Guinea extending westwards into Irian Jaya (Fig. 1-1). By far the largest and best preserved is the Papuan Ultramafic Belt (Davies, 1971, 1977) which extends some 400 km in a 40 km wide belt along the northern slopes of the Owen Stanley Ranges in the southeast Papuan peninsula. The next largest body, the Marum ophiolite complex, forms a 90 km long north-westerly-trending belt at the northern foothills of the Bismarck Range in northern Papua New Guinea between longitude 144°45' E and 145°20' E Fig. 1-1). West of the Marum complex in the Schrader Range (144° E). smaller faulted bodies of peridotite (commonly serpentinized), pyroxenite and gabbro (dismembered ophiolites) occur as klippen on, and thrust slices within, low-grade metamorphic rocks. Farther west (142-143° E) in the south Sepik region fault-bounded serpentinized ultramafic and mafic rocks (April Ultramafics) are associated with glaucophane schist and lower grade metamorphic rocks (Dow & others, 1972). A small body of peridotite (including cumulate wehrlite) crops out at Mt Turu in the north Sepik region.

1-2. Regional geology

The Marum ophiolite lies at the deformed outer (northern and northeastern) margin of the central orogenic belt, one of three major geotectonic provinces of Papua New Guinea. This province is comprised mainly of a thick sequence of Mesozoic and early Tertiary geosynclinal sediments and volcanics which have been strongly folded, faulted (including extensive foreland-type thrusting) and metamorphosed along the outer margin. The orogenic belt lies between sialic crust of the stable platform (Paleozoic metamorphic and granitic rocks overlain by Mesozoic

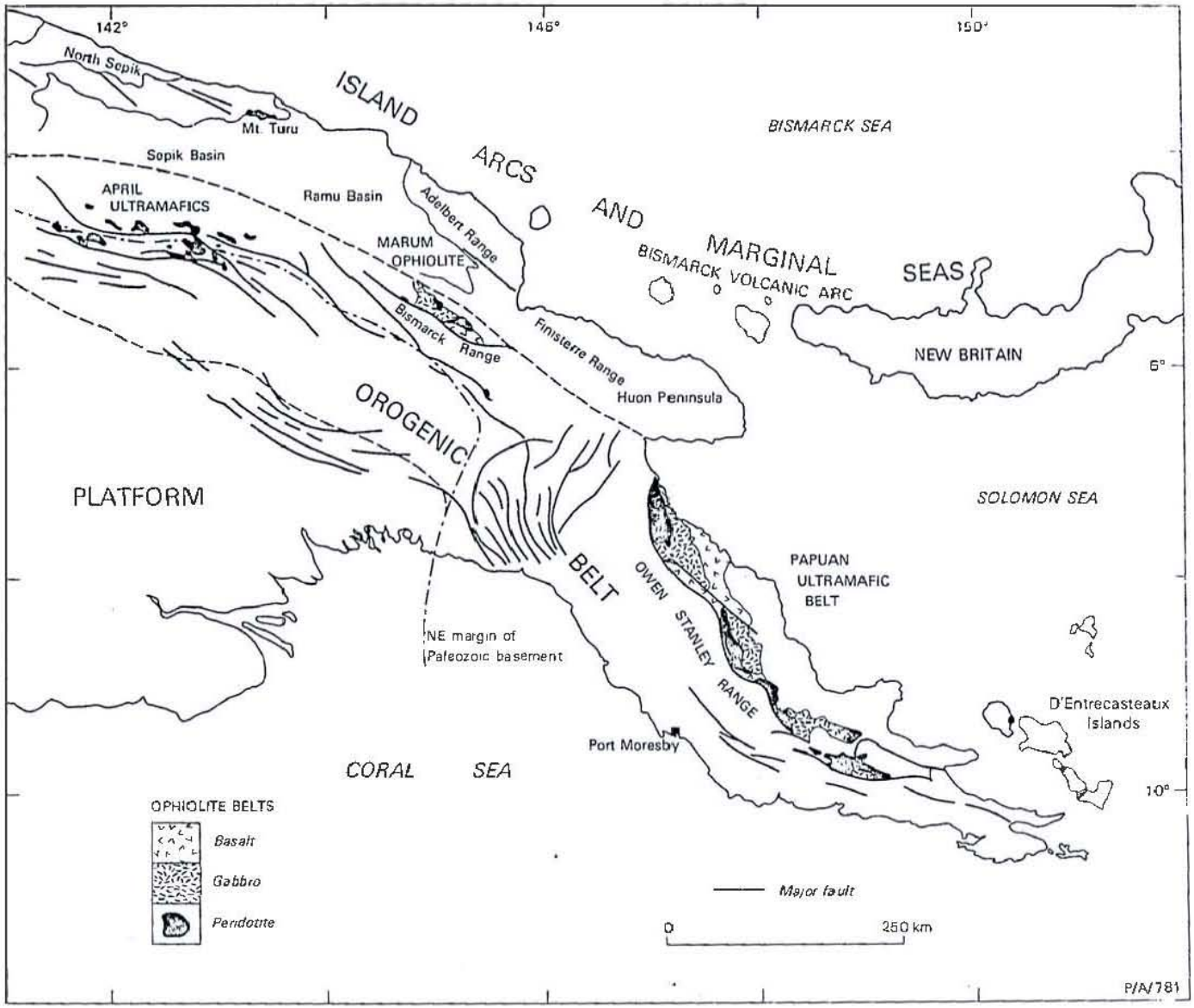

Fig. 1-1. Tectonic map of Papua New Guinea showing the distribution of ophiolites.

and Cainozoic shelf sediments) to the south, and Cainozic volcanic and sedimentary rocks of the island-arc province to the north. A synthesis of the regional geology of northern Papua New Guinea is provided by Jaques & Robinson (1977) (Appendix 3). The Marum ophiolite has been thrust over the low-grade metasediments of the orogenic belt, and is separated from the Tertiary volcanic and sedimentary rocks of the Adelbert-Finisterre Ranges-Huon Peninsula region to the north by the Ramu-Markham fault zone which occupies the alluviated Ramu-Markham valley and extends some 300 km in a northwesterly direction.

Emplacement of the Marum ophiolite occurred in the late Oligocene-early Miocene as a result of collision between the Australian continent to the south with the Tertiary island-arc which lay to the northeast. Jaques & Robinson (1977) (Appendix 3) presented a detailed model of the collision proposing a northward-dipping subduction zone associated with the Tertiary Adelbert-Finisterre-Huon arc into which a thick welt of sediments at the continental margin were subducted, forming a 'choked subduction zone'. The ophiolite is thought to be oceanic crust and mantle of the upper plate bearing the island-arc, thrust from the arc-trench gap region over the choked subduction zone, and probably represents frontal-arc basement to the Tertiary arc. Subsequent to emplacement the ophiolite has been affected by faulting related to both post-collision compression and late Neogene regional uplift.

1-3. Geology of the Marum ophiolite

The simplified geological map of the Marum ophiolite shown in Figure 1-2 is based on the 1:100 000 scale preliminary map (Jaques, 1978 unpubl.), copies of which are available from the Geological Survey of Papua New Guinea (GSPNG), Port Moresby, and the Bureau of Mineral Resources (BMR), Canberra. The area occupied by the Marum ophiolite is virtually uninhabited and access is by foot from the Ramu River valley or from Bundi patrol post in the southwest ($145^{o}14'E$, $5^{o}44'S$).

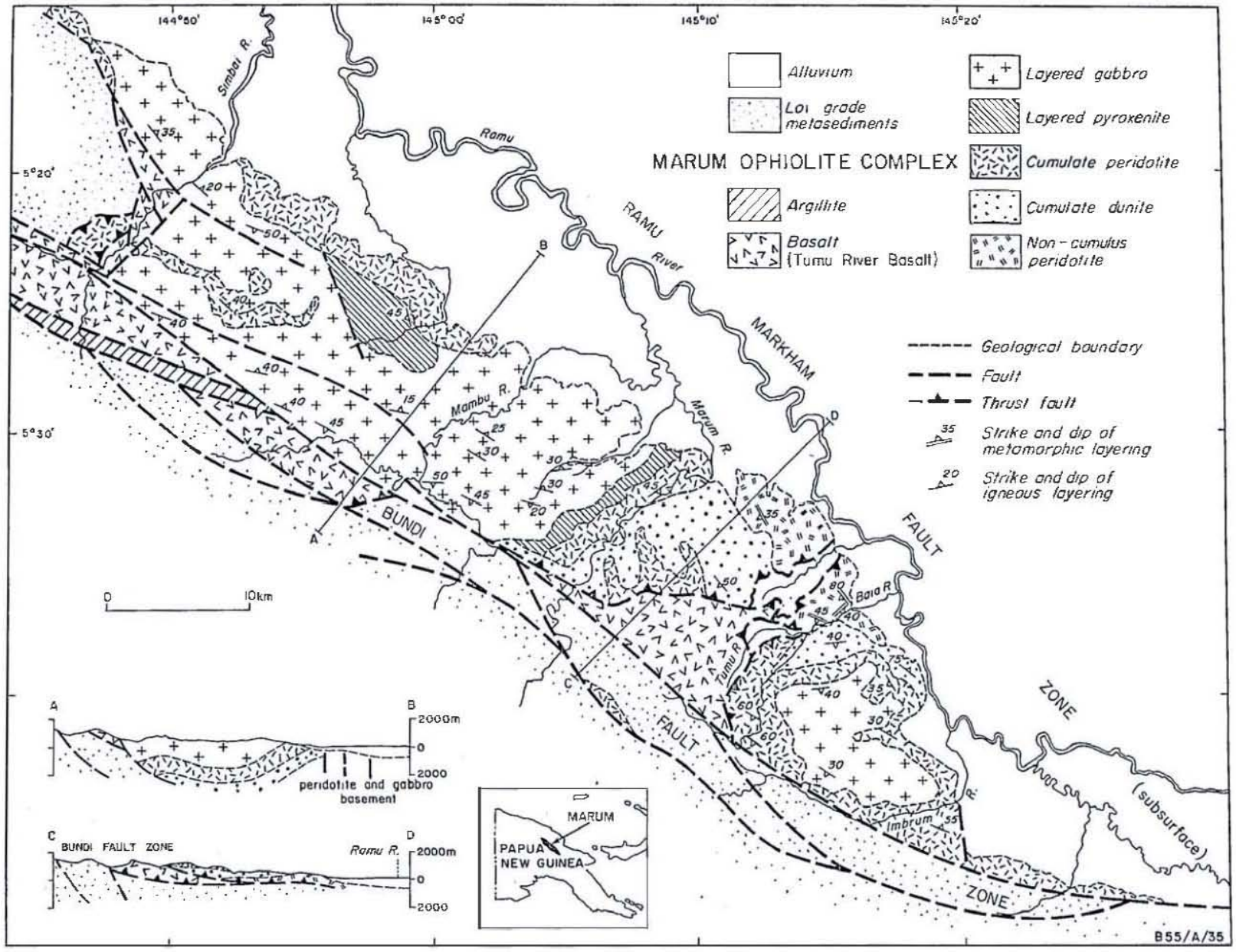

Fig. 1-2. Simplified geological map of the Marum ophiolite complex.

Outcrop is largely confined to rivers and streams, and the hillslopes are clad in tropical rain forest, except for the lower slopes immediately adjacent to the Ramu River valley which are covered by kunai grass. Mapping and sampling were carried out by the author and C.J. Pigram (GSPNG) by helicopter-assisted traverses of 1 to 5 days duration of the drainage system in July-September, 1974 with further sampling by the author in mid-1975 and 1976.

The Marum ophiolite complex consists of two major thrust sheets, a main peridotite-gabbro massif which covers some 1000 km^2, and a smaller, much-faulted allochthon of spilitic pillow basalt (Tumu River basalt) and pelagic sediments. The thrust sheets are faulted against low-grade metasedimentary rocks, mostly dark calcareous shale, siltstone and mudstone (Asai Shale) of late Cretaceous to Eocene age. To the south-east and east both the ophiolite and the Asai Shale are faulted against indurated graphitic shale, slate and phyllite of the Goroka Formation. The peridotite-gabbro massif forms a large northerly-to-northeasterly-dipping thrust sheet bounded to the north by the Ramu-Markham fault zone which forms the southern boundary of the Ramu basin, a major Neogene sedimentary basin containing some 4000 m of clastic sediments and overlain by Quaternary alluvium. To the south the peridotite-gabbro massif is bounded by the Bundi fault zone, a zone of intense shearing and anastomosing faults with vertical strata and serpentinite bodies. Windows exposed in rivers transecting the ophiolite (e.g. Tumu River) reveal an imbricate zone of low-grade metasediments and metabasalt beneath the sole of the thrust (Fig. 1-2). The thrust surface dips gently ($<10^{o}$) northeast, and the base of the massif is marked by a narrow band (1 m thick) of metasomatized peridotite and serpentinite. The sheet-like nature of the massif has been confirmed by regional gravity surveys (St John, 1970; Milsom, 1975) which also showed that the highest gravity values lie offset

to the north of the ophiolite, suggesting subsurface extension of the ophiolite beneath the alluvium and Neogene clastic sediments of the Ramu Basin. Further evidence for an oceanic floor beneath the Ramu valley is the occurrence of Jurassic gabbro-peridotite basement unconformably overlain by Neogene sediments at a depth of 2000 m in Keram No. 1 wildcat well drilled on the southern margin of the Ramu Basin northwest of the Marum ophiolite at $4^{o}26'$ S, $144^{o}09'$ E (Jaques & Robinson, 1977).

Faulting is common throughout the ophiolite, particularly within the Tumu River basalts. Some faults are considered to be high-angle curvilinear thrusts, whereas others are clearly strike-slip. A north-northwest/east-northeast trending set of fractures may represent conjugate shears related to northeast - southwest compression. Normal faults on the northern slopes of the ophiolite adjacent to the Ramu valley are probably mainly related to late Neogene regional uplift but some may be associated with faulting in the Ramu-Markham fault zone. The age of formation of the Marum ophiolite is uncertain but thought to be late Mesozoic or, possibly, earliest Tertiary. K-Ar dating of plagioclase separates from cumulate gabbros has shown that, because of the extremely low K contents of the separates, apparent 'age' depends directly on the K level (i.e. the oldest 'ages' are given by rocks with the lowest K content). For this reason the youngest age of 173 m.y. must be regarded as a maximum age (A.W. Webb, writ. report, 1975). A much younger date of 59 ± 2.5 m.y. was obtained from hornblende in a granophyric diorite (A.W. Webb, writ. report,1976), suggesting that formation of the ophiolite may, in fact, be as young as Paleocene. The age of formation of the Tumu River basalts are also not well defined; they are thought to be mainly of early Tertiary age since radiolarian argillites overlying the basalts are of probable Eocene age, although faunas are too poorly

preserved for positive determination (D. Belford, pers. comm., 1976).

The ophiolite is considered to have been emplaced in the late Oligocene or early Miocene, coinciding with the timing of the continent-arc collision (Jaques & Robinson, 1977). The age of emplacement clearly post-dates the (?) early Eocene since it is thrust over low-grade metasedimentary rocks of late Cretaceous to early Eocene age. An upper limit of middle Miocene is suggested by the unconformable relationship between the gabbro-peridotite basement (interpreted as a subsurface extension of the ophiolite) and Neogene strata in Keram well. Farther west in the south Sepik region stratigraphic evidence indicates that ophiolitic bodies occupying a similar tectonic and stratigraphic setting were emplaced in post-Eocene and pre-middle Miocene times (Dow & others, 1972).

1-4. Subdivision of the ophiolite

The ultramafic rocks of the peridotite-gabbro massif are of two types:

1) *ultramafic tectonite* consisting of weakly foliated harzburgite and subordinate dunite cut by narrow enstatite-rich pyroxenite dykes and veins;
2) *cumulate peridotite* - dunite, wehrlite, lherzolite, plagioclase lherzolite and olivine pyroxenite which shows cumulate layering and textures.

Poor outcrop precludes clear definition of the boundary between cumulate and non-cumulate peridotite. Above the inferred contact layered dunite and chromitite show cumulate textures, and features such as mineral-graded* layering and cross-stratification. Below the contact harzburgite and dunite (present as concordant bands up to 15 cms thick, and lenses and tabular bodies up to several tens of metres thick) are generally

---

* Defined in Chapter 3

more strongly deformed and foliated. Du

sequence is generally more deformed and recrystallized than the overlying cumulate pyroxene-bearing peridotites and some appears transitional to the tectonite peridotites. However, unlike the cumulate peridotites which exhibit cryptic variation, the harzburgites are of uniform composition and highly refractory mineralogy (Chapter 2). The harzburgites therefore appear to form basement to the thick sequence (3-4 km) of relatively undeformed ultramafic and mafic cumulates. The thickness of the harzburgite-dunite body is unknown but exceeds 400 m. A nickeliferous laterite profile developed on the ultramafics in the area between the Marum and Baia Rivers is described by Holmes & Hall (1975).

Mafic cumulates, conformably overlie the ultramafic cumulates from which they are distinguished by the presence of cumulus plagioclase. The sequence is layered on a gross scale from troctolite and plagioclase pyroxenite at the base through norite-gabbro to ferrogabbro and anorthositic gabbro at the top. Rare microgabbro and quartz dolerite dykes intrude the uppermost gabbros, and dykes and veins of gabbro pegmatite or mafic pegmatoid intrude the entire cumulate sequence. The attitude of cumulus layering varies from northeastward dips roughly parallel to the base of the massif and the gross lithologic layering to steep southward dips; much of the layering is arched over a central area (Fig. 1-2).

Volcanic rocks (Tumu River basalts) lie faulted against the peridotite-gabbro massif in the south. The Tumu River basalts consist mainly of spilitic pillow basalt, basalt lava and lava breccia with some hyaloclastite and intercalated radiolarian argillite. Narrow dolerite and basaltic dykes intrude the basalt sequence at a high angle in a number of localities, and the sequence is overlain by argillite and radiolarian argillite. The argillite sequence becomes tuffaceous higher in the sequence with interbedded volcanolithic greywacke, and basalt, trachybasalt and trachyandesite occur near the top.

CHAPTER 2

TECTONITE PERIDOTITES

2-1. Structures and textures

Structures

The ultramafic tectonite unit consists predominantly of relatively homogeneous harzburgite with subordinate dunite and minor enstatolite, and crops out on the northern side of the ophiolite adjacent to the Ramu River between the Marum and Baia Rivers (Fig. 1-2). Outcrops in the area southwest of the Marum River are generally of massive harzburgite with irregular, interfingering lenses and tabular masses of dunite up to several metres thick which appear broadly concordant. In the vicinity of the Baia River the harzburgite has a weak but pervasive foliation defined by concordant olivine-rich and pyroxene-rich layers from 1 to 15 cms thick (Fig. 1-3A). Contacts between dunitic and pyroxenitic layers are commonly sharp due to abrupt change in the ratio of pyroxene to olivine. Chrome spinel is sparsely disseminated in the harzburgite, and is commonly flattened in the plane of the foliation. Small isoclinal and near-isoclinal folds with disrupted limbs and isolated hinges (Fig. 1-3B) occur in places. Mesoscopic warps in the foliation and minor pyroxene-rich boudins are additional evidence of deformation but, overall, the degree of tectonization is low.

Enstatite-rich pyroxenite dykes intrude the harzburgite-dunite mass as dykes and veins from 2 cms to 3 m wide (Fig. 1-3C), and have sharp contacts with the harzburgite. The dykes cut accross the foliation in the harzburgite, indicating formation after deformation of the harzburgite.

Poor outcrop precludes precise definition of the contact between the harzburgite-dunite and the overlying cumulus peridotites and gabbros. In at least one area the contact is clearly tectonic and accompanied by extensive shearing and serpentinization. Elsewhere the contact appears

Fig. 1-3. Structures and textures in Marum harzburgites.

A. Orthopyroxene-rich bands (p) in banded harzburgite, lower Baia River.

B. Small-scale isoclinal folding and disruption of orthopyroxene-rich bands in peridotite.

C. Narrow veins and dykes of orthopyroxenite cutting harzburgite, lower Baia River.

D. Photomicrograph showing curvilinear interlocking grain boundaries between olivine (OL) and enstatite (OPX) in harzburgite. Sample 425. Crossed polarizers, x 12.

E. Photomicrograph showing kink-banding and undulatory extinction in xenoblastic olivine in harzburgite. Sample 087. Crossed polarizers, x 12.

F. Photomicrograph showing both subhedral to euhedral (some embayed) and interstitial chrome spinel (SP) in harzburgite. Sample 426. Plane polarized light, x 12.

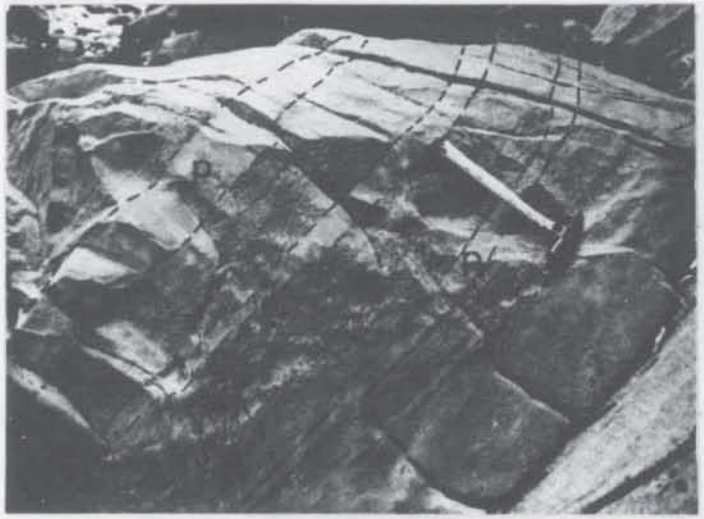

A

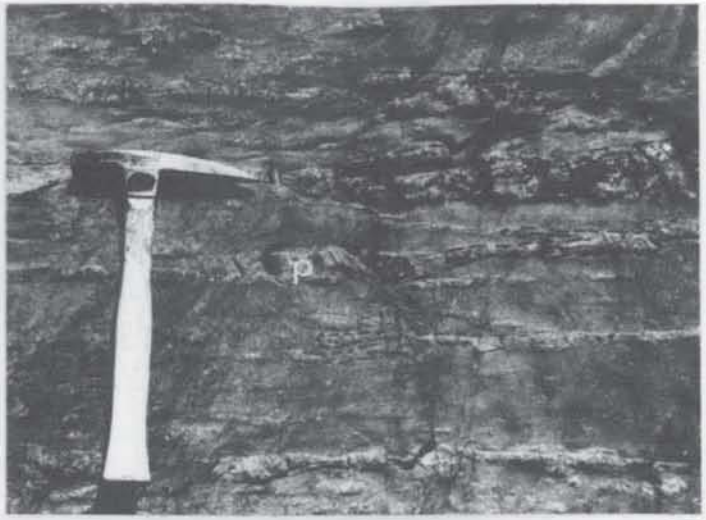

B

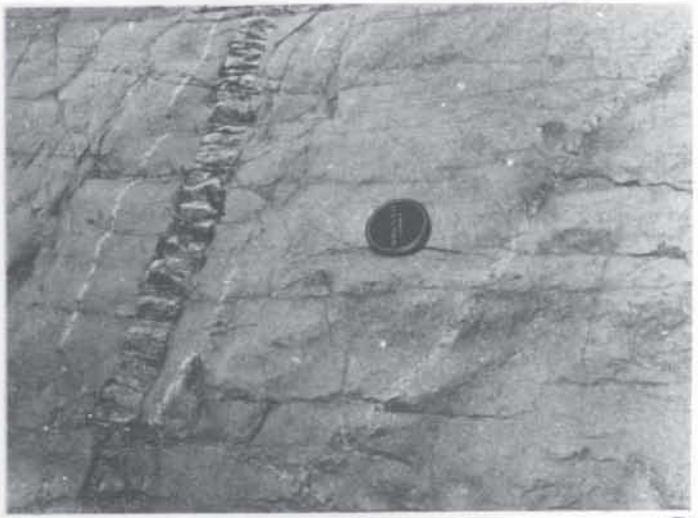

C

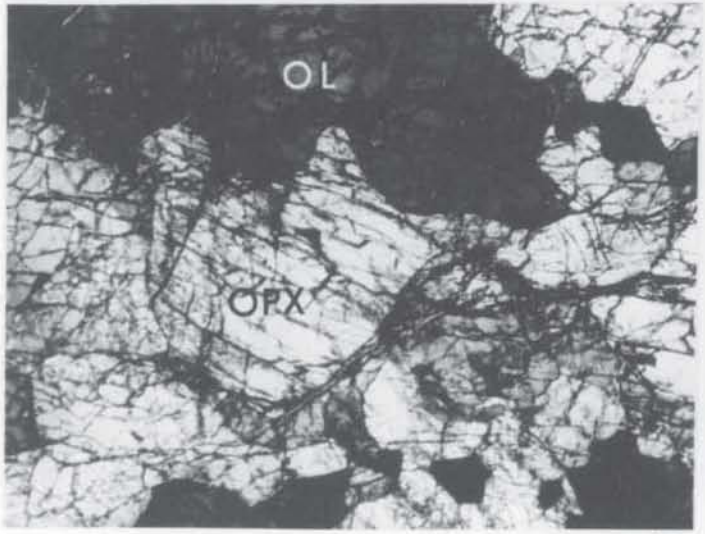

D

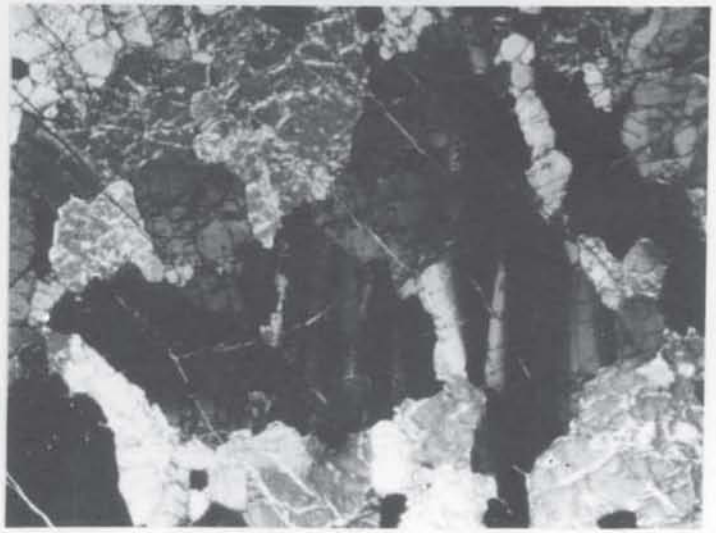

E

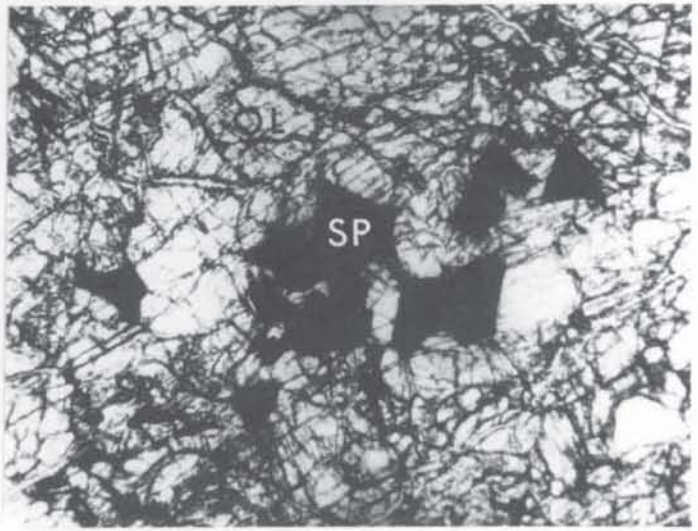

F

transitional and marked mainly by an increase in the number of dunite lenses towards the cumulus dunite and chromitite.

Textures

The harzburgite has a xenoblastic granular texture comprised of interlocking olivine and orthopyroxene grains ranging from 2.5 to 7 mm across (average 3-4 mm), and accessory red-brown chrome spinel. The orthopyroxene content is generally in the range 15-25% (vol.) but ranges up to about 60% (vol.) in pyroxene-rich layers. Some harzburgites contain small amounts of chrome diopside, either as exsolved (100) lamellae in enstatite, or as small, recrystallized, polygonal grains at the margins of orthopyroxene.

The least deformed harzburgites have a protogranular texture (terminology of Mercier & Nicolas, 1975) characterized by curvilinear, lobate and cuspate grain boundaries between olivine and orthopyroxene (Fig. 1-3D). Olivine grain boundaries are commonly embayed and have thin mantles of interstitial orthopyroxene; in some cases small, rounded olivine grains are enclosed in orthopyroxene. Both olivine and orthopyroxene have suffered mild plastic deformation, and exhibit a moderate degree of undulatory extinction, kink-banding, and deformation bands and lamellae (Fig. 1-3E). Chrome spinel is of two forms: 1) sub-to euhedral grains up to 500μ diameter which contain inclusions of olivine or orthopyroxene, and commonly show curvilinear grain boundaries with olivine and orthopyroxene, 2) smaller, $\leq$ 50μ interstitial grains with amoeboid and irregular cuspate grain boundaries (Fig. 1-3F).

More deformed harzburgites have a weak porphyroclastic texture characterized by the presence of elongated, more strongly deformed enstatite grains with abundant kink-banding and deformation bands, surrounded by smaller, strain-free, polygonal and sub-polygonal grains (neoblasts) of olivine and orthopyroxene. Recrystallized grains have

straight grain boundaries and commonly intersect at triple junctions. Both olivine and pyroxene have preferred orientations and define a weak foliation. Enstatite porphyroclasts commonly have fine polysynthetic (100) lamellae with inclined extinction suggestive of intergrown clino-enstatite (cf. Boland, 1974). Clinopyroxene exsolved from orthopyroxene forms neoblasts at kink-band boundaries in the orthopyroxene. Spinel grains define a lineation and commonly show "pull-apart" texture.

Dunite also has a xenoblastic granular texture, with interlocking olivine grains 2-5 mm across and some 2-4% (vol.) disseminated subhedral to euhedral chrome spinel. The degree of deformation is similar to that of the harzburgite, and textures range from protogranular, with ubiquitous curvilinear grain boundaries and limited kink-banding, to more plastically deformed dunite with a variable degree of recrystallization. Spinel is generally of smaller grainsize and more abundant in dunite than harzburgite, and generally of sub-to euhedral habit. Spinel also occurs as subrounded inclusions within olivine grains, a feature which, according to Mercier & Nicolas (1975), is characteristic of secondary (i.e. second generation) fabrics. In this case the dunites must have undergone extensive high temperature recrystallization. Alternatively, the dunite spinels may have crystallized from a melt since the spinel textures are similar to those in the overlying cumulate dunites.

The pyroxenite dykes and veins intruding the harzburgite contain coarse (3-4 mm) interlocking pyroxene with undulatory extinction and kink-banding, and interstitial olivine and clinopyroxene subgrains. Contacts with the harzburgite are commonly marked by a narrow zone in which olivine of the host peridotite is strongly embayed.

Interpretation

Harzburgite-dunite masses with metamorphic (tectonite) fabric comprise the harzburgite subtype of alpine-type peridotites (see Jackson

& Thayer, 1972; Nicolas & Jackson, 1972 for definition), and have been described from the basal portion of a number of ophiolites where they are overlain by ultramafic cumulates (e.g. Davies, 1971; England & Davies, 1973; Jackson & others, 1975; Menzies & Allen, 1974; Coleman, 1977; Malpas, 1978). Detailed studies of harzburgite masses have commonly revealed the existence of several phases of high-temperature, plastic deformation (e.g. Loney & Himmelberg, 1976), and the tectonite peridotite in ophiolites has been commonly interpreted as a deformed, metamorphic basement to overlying magmatic cumulates (e.g. Davies, 1971; England & Davies, 1973; Jackson & others, 1975; Coleman, 1977).

The origin of compositional layering of the Marum harzburgites is problematic. Similar layering in alpine-type peridotites is commonly ascribed to metamorphic processes (e.g. differentiation during deformation that produced the foliation, Loney & Himmelberg, 1976: or mineral segregation, Sinton, 1977). However, some compositional layering appears primary (e.g. Thayer, 1969; Loney & others, 1971; Coleman, 1977). In view of the lack of any obvious cumulus textures or structures (such as chromitite layers with mineral grading)the Marum compositional layering might be of metamorphic origin, although the exact nature of the process of formation is unknown. Alternatively, the layering might have been formed by settling of residual crystals during segregation of a basaltic melt (see later).

Protogranular textures in peridotite, characterized by abundant curvilinear grain boundaries and interlocking grains, are commonly interpreted as resulting from partial melting (Mercier & Nicolas, 1975; Menzies & Allen, 1974; Dick, 1977). This interpretation is supported by the fact that similar textures in metamorphic rocks are generally accepted to indicate resorption of mineral grains or dissolution-reprecipitation processes (Spry, 1969). Studies on the melting behaviour of felsic gneiss has shown that melting begins at places

where three or more grains are in contact, and with further melting the liquid forms films at each grain boundary (Mehnert & others, 1973). Melting of peridotite probably proceeds in a similar fashion and, for all except very small (< 5%?) degrees of partial melting, the residual phases are completely disaggregated and separated by melt (Arndt, 1977a). At higher degrees of partial melting residual phases are subhedral to euhedral (PART 3; Appendix 4; Arndt, 1977a). Protogranular textures characterized by xenoblastic interlocking grains with curvilinear grain boundaries are, therefore, not likely to represent textures formed *during* partial melting, but could have formed by recrystallization involving dissolution-precipitation creep at near-solidus temperatures *after* extraction of a melt fraction.

Evidence for an origin by recrystallization following a partial melting event for the Marum harzburgites includes 1) the abundance of curvilinear and lobate grain boundaries of olivine and orthopyroxene, 2) the mainly euhedral but partly cuspate boundaries of chrome spinel, 3) the comparatively low degree of plastic deformation, and 4) the high equilibration temperatures of the kink-controlled exsolution of clinopyroxene from enstatite (900°C, see later). Although these features appear best explained by partial melting an origin by cumulus-type processes with subsequent textural modification and re-equilibration at near-solidus temperatures cannot be entirely ruled out. Subsequent plastic deformation of the protogranular harzburgites resulted in modified protogranular texture, and textures transitional between protogranular and porphyroclastic.

2-2. Mineral Chemistry

Microprobe analyses were obtained by energy-dispersive (TPD) electron microprobe following the method of Reed & Ware (1973, 1975) (Appendix 1). NiO concentrations in olivine were measured by JEOL JX 50A

wavelength-dispersive crystal spectrometer using an accelerating voltage of 25 kV and a specimen current of 60 nannoamps with on-line data reduction for ZAF corrections (Griffin, 1979).

Olivine

Olivine within the harzburgite has a very restricted range of compositions, 100Mg/(Mg+Fe) = 91.6 - 93.8; the mean of 140 analyses from 12 harzburgites is 92.3 $\pm$ 0.4 (1 σ). Representative analyses are presented in Table 1-1. Individual grains are homogenous and mostly show less than 0.5 mol.% variation: where variation exists the rims are more Mg-rich. Small polygonal neoblasts were found to be mostly of the same compositions as larger grains, except where in contact with chrome spinel. Similarly, olivine inclusions in chrome spinel were markedly more magnesian ($Mg_{93-93.8}$) than the large xenoblastic grains, $Mg_{92.2-92.4}$. Cr, Mn and Ca were not detected in any of the analyses. The very low Ca contents are typical of olivine equilibrated at comparatively low temperature. NiO contents are high, 0.3-0.4%, consistent with the magnesian nature of the olivine.

Olivine in the dunite lenses lies in the range $Mg_{90.0-92.4}$, averaging Mg_{91}, and is more iron-rich than olivine in the harzburgite. NiO contents are appreciably lower in the dunite olivine, 0.2-0.3%, than in the harzburgite (Table 1-1). Small olivine grains in the enstatite-rich pyroxenite dykes are generally of similar composition to olivine in the dunite lenses.

The highly uniform magnesian olivine compositions of the Marum tectonite harzburgites and dunites are typical of those found in harzburgite-subtype alpine peridotites (e.g. Challis, 1965; Loney & others, 1971; Medaris, 1972; Himmelberg & Loney, 1973; Dick, 1977), and from harzburgitic basement in other ophiolite sequences (e.g. England & Davies, 1973; Irvine & Findlay, 1972; Menzies & Allen, 1974; Jackson & others, 1975; Sinton, 1977; Malpas, 1978). Such compositions are more

TABLE 1-1. REPRESENTATIVE ANALYSES OF OLIVINE FROM TECTONITE PERIDOTITES

	Harzburgite															
Sample	087	490		488		492		425			423		473		418	
		core	rim	core	rim	core	rim	core	incl.*	rim	core	incl.*	core	rim	core	rim
SiO_2	41.49	41.15	40.92	41.18	41.15	41.05	41.24	41.16	41.70	41.12	41.22	41.63	40.98	41.31	40.97	41.06
FeO	6.18	7.49	7.18	7.48	7.08	7.66	7.46	7.51	6.20	7.52	7.71	6.41	7.68	7.24	7.77	7.29
NiO	0.34	-	-	0.37	-	0.40	-	-	-	-	0.41	-	0.43	-	-	-
MnO	<0.09	<0.09	<0.09	<0.09	<0.09	<0.09	<0.09	<0.09	<0.09	<0.09	<0.09	<0.09	<0.09	<0.09	<0.09	<0.09
MgO	52.33	51.27	51.20	51.34	51.59	50.99	51.06	51.43	52.56	51.43	51.06	52.24	50.95	51.62	52.21	51.95
Total	100.34	99.91	99.30	100.37	99.82	100.10	99.76	100.10	100.46	100.06	100.40	100.28	100.03	100.17	99.95	100.30
Cations per 4 oxygens																
Si	0.997	0.998	0.997	0.996	0.997	0.996	1.001	0.996	0.999	0.996	0.997	1.000	0.995	0.998	0.995	0.992
Fe	0.124	0.152	0.146	0.151	0.143	0.155	0.152	0.152	0.124	0.152	0.156	0.129	0.156	0.146	0.158	0.147
Ni	0.007	-	-	0.007	-	0.008	-	-	-	-	0.008	-	0.008	-	-	-
Mn	-	-	-	-	-	-	-	-	-	-	-	-	-	-	-	-
Mg	1.875	1.853	1.859	1.850	1.863	1.844	1.847	1.856	1.877	1.856	1.841	1.871	1.845	1.858	1.853	1.869
Total	3.003	3.003	3.003	3.004	3.003	3.004	3.000	3.004	3.000	3.004	3.003	3.000	3.005	3.002	3.006	3.008
$\frac{100\ Mg}{Mg+Fe}$	93.8	92.4	92.7	92.4	92.9	92.2	92.4	92.2	93.8	92.4	92.2	93.6	92.2	92.7	92.2	92.4

	Harzburgite cont.				Dunite				Pyroxenite
Sample	489		474	046	410	414	414	411	491
	core	rim							
SiO_2	41.16	41.47	41.07	40.84	40.70	40.94	40.93	40.60	41.03
FeO	7.78	7.54	7.88	8.23	8.07	8.74	7.53	8.92	8.16
NiO	0.37	-	-	-	0.19	0.21	(0.40)**	0.27	0.46
MnO	<0.09	<0.09	<0.09	<0.09	<0.09	<0.09	<0.09	<0.09	0.09
MgO	50.96	51.51	50.80	50.69	50.71	50.31	51.25	50.00	50.97
Total	100.27	100.52	99.75	99.76	99.67	100.20	100.10	99.79	100.62
Cations per 4 oxygens									
Si	0.997	0.999	0.999	0.995	0.993	0.996	0.992	0.994	0.993
Fe	0.158	0.152	0.160	0.168	0.165	0.178	0.153	0.183	0.165
Ni	0.007	-	-	-	0.004	0.004	(0.003)	0.005	0.009
Mn	-	-	-	-	-	-	-	-	-
Mg	1.840	1.850	1.842	1.841	1.845	1.825	1.852	1.824	1.839
Total	3.003	3.001	3.001	3.005	3.007	3.004	3.005	3.006	3.007
$\frac{100\ Mg}{Mg+Fe}$	92.1	92.4	92.0	91.7	91.8	91.1	92.4	90.9	91.8

* Indicates inclusion in chrome spinel

** Contains 0.40 % Cr_2O_3

magnesian than olivine crystallized in most stratiform intrusions (Wager & Brown, 1968), but in the Marum ophiolite the compositions of olivines in the harzburgites overlaps that of olivine in the overlying cumulates (see Chapter 3).

Orthopyroxene

Representative orthopyroxene analyses are presented in Table 1-2. Orthopyroxene compositions from the harzburgites have 100Mg/(Mg+Fe) ratios in the range 92.3-94.5; the mean of more than 100 analyses is 92.8±0.4 (1σ). A feature of the Marum orthopyroxenes is their uniformly low CaO and R_2O_3 contents; Al_2O_3 contents are mostly less than 0.6% but range up to 0.9% in the cores of some of the least deformed harzburgites. CaO contents lie within the range 0.1-0.9% and vary sympathetically with Al_2O_3 contents. Cr_2O_3 contents are less than 0.4%. Compositional variation exists between the cores and rims of the larger xenoblastic grains, and between the xenoblastic grains and secondary polygonal neoblasts. Rims and neoblasts are poorer in Al and Ca than the xenoblast cores. CaO and Al_2O_3 contents show a correlation with Mg-value (Fig. 1-4), and with the degree of plastic deformation and recrystallization. Orthopyroxene from protogranular-textured harzburgites with little deformation have the highest Al_2O_3 contents (0.6-0.9%) whereas those from more deformed harzburgites have much lower Al_2O_3. Neoblasts and orthopyroxene grains with kink-controlled exsolution of clinopyroxene have very low Al and Ca contents compared to the primary orthopyroxene hosts (Fig. 1-4). The decrease in Al_2O_3 content between orthopyroxene in protogranular-textured harzburgite and orthopyroxene in more plastically deformed porphyroclastic harzburgite is consistent with recrystallization under lower temperature (see 2-3). Orthopyroxene from enstatite-rich dykes is slightly less magnesian than that in the harzburgite but has comparable CaO and R_2O_3

TABLE 1-2. REPRESENTATIVE ORTHOPYROXENE ANALYSES FROM TECTONITE PERIDOTITES

	Harzburgite																				Pyroxenite	
Sample	087		490		488		492		425		423		473		418		489		474		046		491	257
	core	rim	core	rim	core	rim	core	rim	core	rim	core	rim	core	rim	core	rim	core	rim	core	rim	core	rim		
SiO_2	58.50	58.63	57.92	58.06	57.83	58.83	57.71	57.86	57.72	57.69	57.77	57.73	57.96	56.60	57.93	58.19	57.66	57.88	58.11	57.78	57.83	57.50	58.15	58.20
Al_2O_3	0.15	<0.09	0.46	<0.09	0.58	0.11	0.37	0.29	0.65	0.39	0.84	0.57	0.91	0.66	0.54	0.45	0.64	0.21	0.72	0.55	0.65	0.44	0.60	0.12
Cr_2O_3	0.18	0.17	0.30	<0.07	0.38	<0.07	0.25	<0.07	0.32	0.18	0.38	0.28	0.24	0.22	0.34	0.20	0.35	<0.07	0.31	0.19	0.32	0.31	0.30	0.12
FeO	3.91	3.94	4.78	5.06	4.90	4.99	4.92	5.17	4.98	4.91	5.10	5.22	5.21	5.32	4.89	4.94	4.94	5.07	5.15	5.31	5.24	5.34	5.50	6.12
MnO	<0.09	<0.09	<0.09	<0.09	<0.09	<0.09	<0.09	<0.09	<0.09	<0.09	<0.09	<0.09	<0.09	<0.09	<0.09	<0.09	<0.09	<0.09	<0.09	<0.09	<0.09	<0.09	<0.09	<0.09
MgO	36.86	36.75	36.01	36.00	35.99	36.65	35.52	35.96	35.70	36.03	35.62	35.57	35.63	35.16	35.72	35.81	35.46	36.30	35.59	35.79	35.48	35.26	35.83	35.53
CaO	0.43	0.53	0.50	0.26	0.59	0.18	0.76	0.22	0.66	0.36	0.69	0.60	0.58	0.54	0.55	0.60	0.68	0.30	0.68	0.51	0.56	0.67	0 27	0.25
Total	100.03	100.02	99.97	99.38	99.94	100.76	99.53	99.50	100.02	99.56	100.40	99.97	100.53	98.50	99.97	100.19	99.93	99.76	100.56	100.13	100.08	99.52	100.65	100.33
Si	1.993	1.998	1.984	1.999	1.983	1.996	1.987	1.991	1.978	1.984	1.974	1.981	1.977	1.974	1.985	1.989	1.979	1.987	1.981	1.980	1.982	1.984	1.982	1.995
Al^{IV}	0.006	-	0.016	-	0.017	0.004	0.013	0.009	0.022	0.016	0.026	0,019	0.023	0.026	0.015	0.011	0.021	0.008	0.019	0.020	0.018	0.016	0.018	0.005
Al^{VI}	-	-	0,003	-	0.006	-	0.002	0.003	0.004	-	0.008	0.004	0.014	0.001	0.007	0.007	0.005	-	0.010	0.002	0.009	0.002	0.006	-
Cr	0.005	0.005	0.008	-	0.010	-	0.007	-	0.009	0.005	0.010	0.008	0.007	0.006	0.009	0.005	0.009	-	0.008	0.007	0.009	0.008	0.008	0.003
Fe	0.111	0.112	0.137	0.146	0.140	0.142	0.142	0.149	0.143	0.141	0.146	0.150	0.149	0.155	0.140	0.141	0.142	0.145	0.147	0.152	0.150	0.154	0.157	0.175
Mn	-	-	-	-	-	-	-	-	-	-	-	-	-	-	-	-	-	-	-	-	-	-	-	-
Mg	1.872	1.866	1.838	1.847	1.822	1.853	1.823	1.844	1.824	1.847	1.814	1.820	1.811	1.828	1.824	1.824	1.814	1.857	1.809	1.828	1.813	1.813	1.820	1.814
Ca	0.016	0.019	0.018	0.010	0.022	0.007	0.028	0.008	0.024	0.013	0.025	0.022	0.021	0.020	0.020	0.022	0.032	0.011	0.025	0.019	0.021	0.025	0.010	0.009
Total	4.003	4.000	4.003	4.002	4.000	4.002	4.002	4.004	4.004	4.005	4.003	4.004	4.002	4.010	4.000	3.999	4.003	4.008	3.999	4.006	4.002	4.003	4.001	4.001
$\frac{100}{Mg+Fe}$	94.4	94.3	93.1	92.7	92.8	92.9	92.8	92.5	92.7	92.9	92.6	92.4	92.4	92.2	92.9	92.8	92.7	92.7	92.5	92.3	92.3	92.2	92.1	91.2
Ca	0.8	1.0	0.9	0.5	1.1	0.3	1.4	0.4	1.2	0.6	1.2	1.1	1.1	1.0	1.0	1.1	1.6	0.5	1.3	1.0	1.0	1.3	0.5	0.5
Mg	93.6	93.4	92.2	92.2	91.8	92.6	91.5	92.2	91.6	92.3	91.4	91.4	91.4	91.3	91.9	91.8	91.2	92.3	91.3	91.4	91.4	91.0	91.6	90.8
Fe	5.6	5.6	6.9	7.3	7.1	7.1	7.1	7.4	7.2	7.1	7.4	7.5	7.5	7.7	7.1	7.1	7.1	7.2	7.4	7.6	7.6	7.7	7.9	8.8

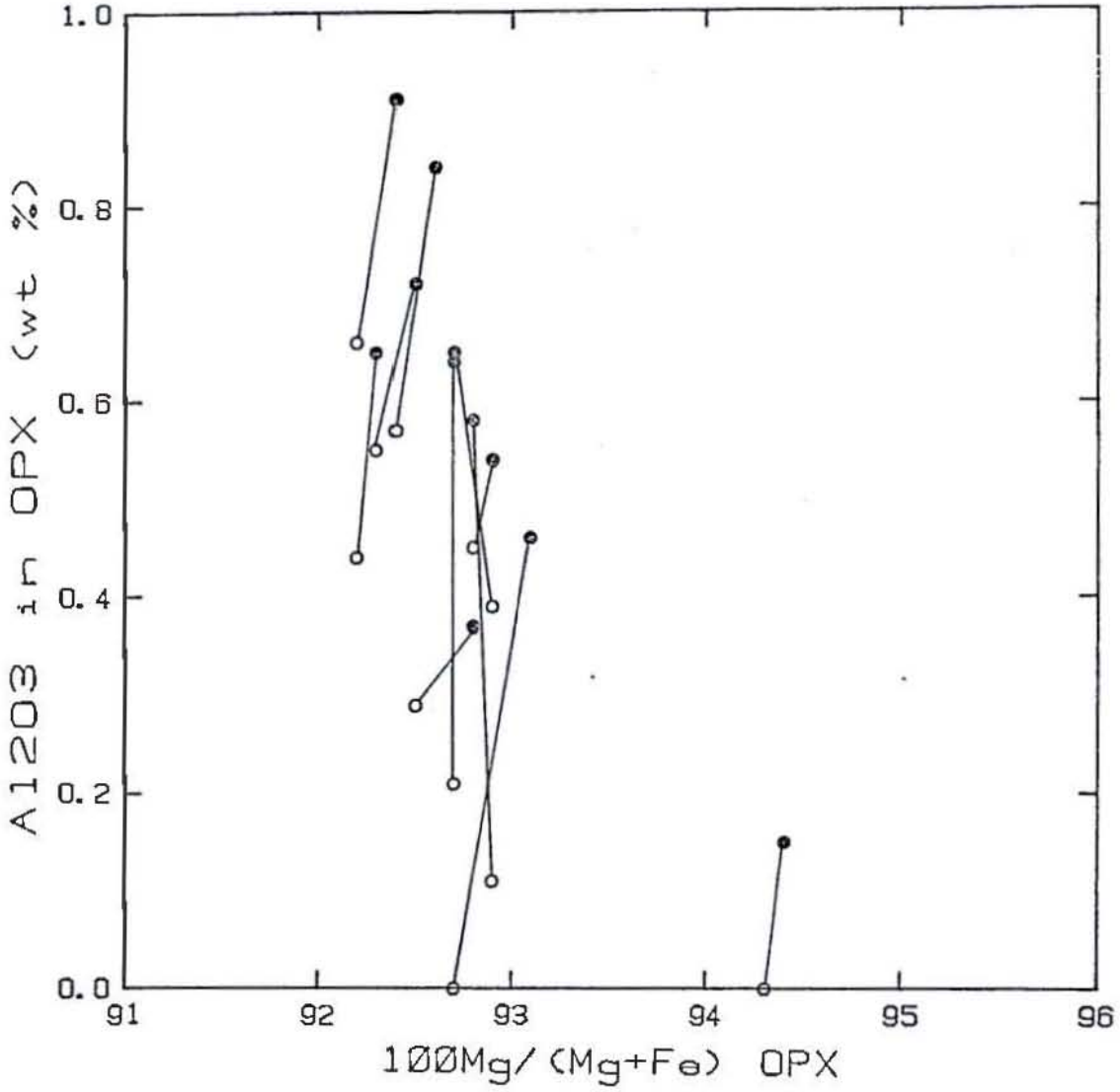

Fig. 1-4. Variation of Al_2O_3 content with 100Mg/(Mg + Fe) in orthopyroxene from Marum harzburgites. The lines connect mineral cores (solid circles) to rims (open circles). Note that the Al_2O_3 content is lower in the rims.

content.

Compared to orthopyroxenes from alpine peridotites orthopyroxenes from the Marum harzburgites are characterized by higher 100Mg/(Mg+Fe) ratios and decidedly lower Al_2O_3 and CaO contents (Fig. 1-5). Orthopyroxenes from harzburgite-subtype alpine peridotites typically have Al_2O_3 contents in the range 1.3-3% (e.g. Himmelberg & Loney, 1973; Dick, 1977). Orthopyroxenes in the Marum harzburgites are also more magnesian and have lower R_2O_3 content than orthopyroxenes from harzburgite in the majority of other documented ophiolites (Fig. 1-5; Sinton, 1977; Dick, 1977) although the Marum pyroxenes are not as refractory as enstatites from tectonite harzburgite in the Papuan Ultramafic Belt (See PART 2).

Clinopyroxene

Rare clinopyroxene occurs as exsolved lamellae parallel to (100) direction and at kink-band boundaries in enstatite, and as small (50-100μ) polygonal grains, both at kink-band and grain boundaries, in the more plastically deformed harzburgites. The exsolved lamellae and recrystallized neoblasts are of similar composition, i.e. magnesian chrome diopside (Table 1-3) with the compositional range $Mg_{50-51}Ca_{48-46}Fe_{2-3}$. The clinopyroxenes are highly magnesian, Mg_{94-96}, and have very low Al_2O_3 contents, comparable with that of co-existing orthopyroxene. Co-existing pyroxenes are shown by tie lines in Figure 1-6. TiO_2, MnO and Na_2O contents are very low and were not detected in any of the analyses.

Consistent with the orthopyroxenes, Marum clinopyroxenes are more magnesian and have lower R_2O_3 content than clinopyroxenes from alpine-type peridotites (e.g. Medaris, 1972; Himmelberg & Loney, 1973) and from tectonite peridotite in most other ophiolites, but are comparable with exsolved clinopyroxenes in the tectonite harzburgites from the Papuan Ultramafic Belt (England & Davies, 1973).

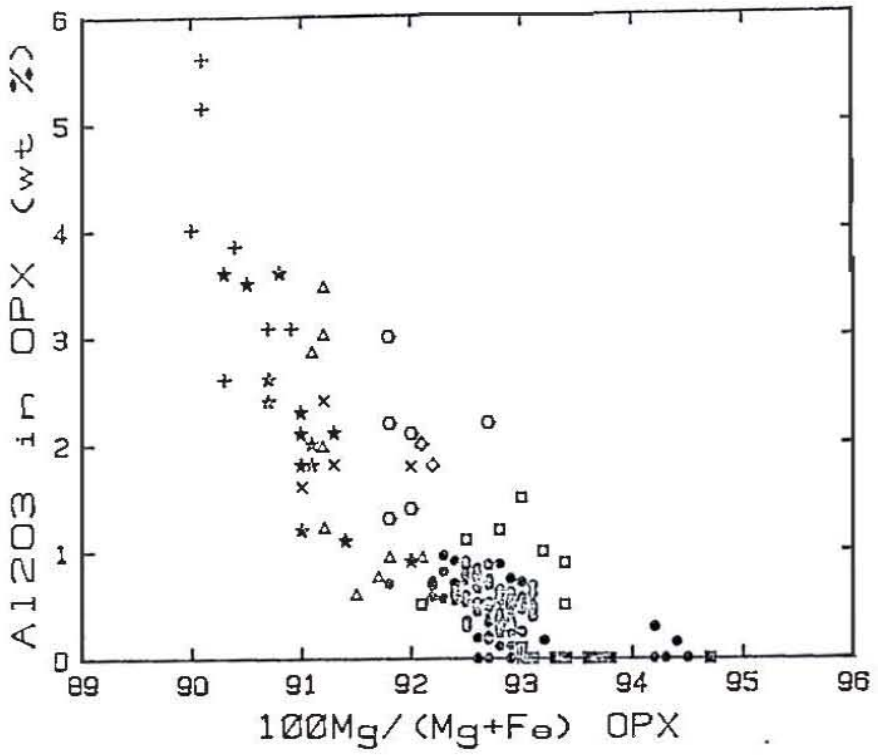

Fig. 1-5. Variation of Al_2O_3 with 100Mg/(Mg+Fe) for orthopyroxenes from alpine peridotites and ophiolites. Closed squares = Papuan Ultramafic Belt (PART 2), Open squares = England & Davies, (1973), solid circles = Marum, crosses = Troodos (from Dick, 1977), + = Oregon, U.S.A. (Medaris, 1972), stars = Josephine peridotite, U.S.A. (Dick, 1977), triangle = Red Mountain, N.Z. (Sinton, 1977), octagons = Burro Mountain, U.S.A. (Loney & others, 1971), diamonds = Vulcan Peak, U.S.A. (Himmelberg & Loney, 1973). Note that the PNG examples are the most magnesian and Al-poor of the population.

TABLE 1-3. REPRESENTATIVE CLINOPYROXENE ANALYSES FROM TECTONITE PERIDOTITES

	Harzburgite			Pyroxenite		Dunite
	488	492	425	491	257	414*
SiO_2	55.17	54.33	54.62	55.00	54.70	53.62
Al_2O_3	0.37	0.37	0.88	0.61	0.31	1.13
Cr_2O_3	0.50	0.72	0.61	0.83	0.82	1.25
FeO	1.43	1.56	1.56	1.55	1.97	1.71
MnO	<0.09	<0.09	<0.09	<0.09	<0.09	<0.09
MgO	18.65	18.09	18.58	17.89	18.18	17.03
CaO	24.36	23.93	23.92	24.90	23.71	25.07
Na_2O	<0.17	<0.17	<0.17	<0.17	<0.17	<0.17
Total	100.48	99.00	100.17	100.78	99.69	99.82
	Cations per 6 oxygens					
Si	1.986	1.987	1.972	1.980	1.988	1.957
Al^{IV}	0.014	0.013	0.028	0.020	0.012	0.043
Al^{VI}	0.002	0.003	0.010	0.006	0.001	0.006
Cr	0.014	0.021	0.017	0.024	0.024	0.036
Fe	0.043	0.048	0.047	0.047	0.060	0.052
Mn	-	-	-	-	-	-
Mg	1.001	0.986	1.000	0.960	0.985	0.926
Ca	0.939	0.938	0.925	0.961	0.923	0.980
Na	-	-	-	-	-	-
Total	3.999	3.996	4.000	3.995	3.993	4.001
$\frac{100\ Mg}{Mg+Fe}$	95.9	95.4	95.5	95.3	94.3	94.7
Ca	47.4	47.6	46.9	48.8	46.9	50.0
Mg	50.5	50.0	50.7	48.8	50.0	47.3
Fe	2.2	2.4	2.4	2.4	3.0	2.7

* indicates inclusion in chrome spinel. All TiO_2 <0.07%.

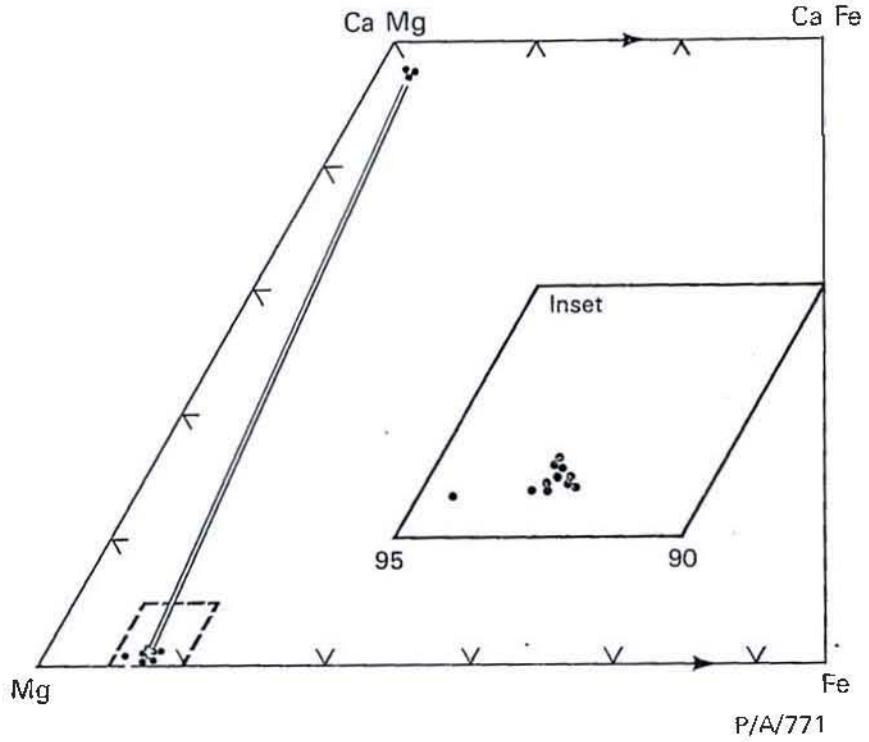

Fig. 1-6. Portion of pyroxene quadrilateral showing co-existing pyroxenes in Marum harzburgites.

Chrome-rich diopside (Table 1-3) also occurs as inclusions (up to 50μ) in chrome spinel in dunite 414. The inclusions have variable Al_2O_3 contents (0.44-1.18%) and contain between 1.05 and 1.45% Cr_2O_3. The distribution coefficient K_D, where $K_D = (\frac{Al}{Cr})^{cpx} / (\frac{Al}{Cr})^{sp}$, varies between 1.2 and 3. The most likely explanation of these chromian pyroxenes is by reaction of trapped basaltic melt with the chrome spinel host according the reaction;

Chrome spinel + liquid = chromian pyroxene.

Clinopyroxene in the pyroxenite dykes is extremely Cr-rich, containing up to 2% Cr_2O_3, and co-exists with tiny, chrome-rich spinel.

Chrome spinel

Chrome spinel comprises about 0.5-2 volume % of the harzburgite and up to 4% of the dunite. Representative analyses are presented in Table 1-4. Iron was determined as FeO and distributed among FeO and Fe_2O_3 by assuming ideal $R^{2+}R_2^{3+}O_4$ stoichiometry so that $RO:R_2O_3 = 1:1$.

Chrome spinel in the harzburgite is highly chrome-rich with Cr/(Cr+Al) ratios of 0.65-0.86, and of uniform composition (Table 1-4). Variation among the harzburgite spinels is dominated by Cr-Al substitution Figs. 1-7,8); $Mg/(Mg+Fe^{2+})$ ratios are relatively constant (Fig. 1-7a). Calculated Fe^{3+} contents are low, 0.04 or less, and vary little with $Mg/(Mg+Fe^{2+})$ (Fig. 1-7b). Spinel compositions show a direct correlation with orthopyroxene compositions; spinel Cr/(Cr+Al) ratios vary directly with both the Mg and the alumina content of the co-existing pyroxene (Fig. 1-9). The most chrome-rich spinels, Cr/(Cr+Al) = 0.86, are associated with the most magnesian olivine ($Mg_{93.8}$) and most Mg-rich, Al-poor pyroxene (Fig. 1-9), and the more Al-rich spinel with more aluminous, less magnesian orthopyroxenes of the least-deformed protogranular harzburgites. The rims of most spinel grains are consistently more Al-rich than the cores, and commonly less magnesian but have higher Fe^{3+}.

TABLE 1-4. REPRESENTATIVE CHROME SPINEL ANALYSES FROM TECTONITE PERIDOTITES

	Harzburgites																								Dunite			Pyroxenite
Sample	087		490			488		492		425			423		473		418		489			474		046			410	411	414	257
	core	inter*	core	rim	inter*	core	rim	core	rim	core	rim	inter*	core	inter*	core	rim	core	rim	core	rim	inter*	core	rim	core	rim					
TiO_2	<0.07	<0.07	<0.07	<0.07	<0.07	<0.07	<0.07	<0.07	<0.07	<0.07	<0.07	<0.07	<0.07	<0.07	0.12	<0.07	<0,07	<0.07	<0.07	0.12	0.18	<0.07	<0.07	<0.07	<0.07		0.14	0.14	0.22	0.19
Al_2O_3	6.88	6.70	11.82	12.82	12.98	14.22	15.67	10.76	10.83	14.36	16.03	17.54	14.16	14.98	15.19	15.95	14.21	14.98	13.72	14.35	14.99	15.57	16.19	14.70	14.92		8.63	7.88	14.07	6.22
Cr_2O_3	62.84	62.36	58.39	57.06	57.37	55.51	54.47	59.38	59.00	55.33	53.26	49.90	54.88	53.37	53.47	52.37	55.17	54.18	56.18	54.86	53.86	52.68	51.71	53.83	52.68		53.85	52.81	49.56	57.86
Fe_2O_3**	3.19	3.03	1.55	1.91	1.39	1.48	0.89	2.00	1.60	2.48	2.58	3.18	2.99	3.34	3.68	3.57	2.71	2.37	1.64	1.75	1.36	3.06	3.39	3.28	3.48		8.90	9.63	6.86	6.76
FeO	16.72	17.07	16.69	17.85	16.36	16.68	17.78	17.28	18.00	16.65	16.50	17.70	16.64	17.23	16.60	16.96	16.87	17.37	17.34	17.24	20.05	17.46	17.68	18.56	18.73		20.08	21.64	18.92	22.57
MnO	0.26	<0,09	0.27	<0.09	<0.09	0.36	<0.09	<0.09	<0.09	<0.09	<0.09	<0.09	<0.09	0.25	0.34	0.32	<0.09	<0.09	<0.09	<0.09	<0.09	0.37	<0.09	<0.09	<0.09		<0.09	<0.09	0.93	<0.07
MgO	10.53	10.22	11.06	10.60	11.43	11.08	10.89	10.73	10.28	11.63	11.80	10.98	11.42	10.98	11.49	11.29	11.47	11.09	11.03	10.96	9.36	10.89	10.95	10.45	10.18		8.56	7.40	9.50	6.81
CaO	0.19	0.18	0.07	0.09	0.11	0.10	0.07	0.12	0.07	0.07	0.07	0.11	0.20	0.19	0.20	0.15	<0.07	0.07	<0.07	0.10	<0.07	<0.07	0.11	0.08	0.07		0.20	0.07	0.11	0.13
Total	100.61	99.56	99.78	100.33	99.64	99.43	99.70	100.27	99.71	100.45	100.26	99.41	100.29	100.34	101.09	100.61	100.43	100.06	99.91	99.36	99.80	100.03	99.99	100.90	100.06		100.36	99.61	99.77	100.53
Cations per 4 oxygens																														
Ti	-	-	-	-	-	-	-	-	-	-	-	-	-	-	0.003	-	-	-	-	0.003	0.004	-	-	-	-		0.004	0.004	0.005	0.003
Al	0.270	0.265	0.455	0.490	0.496	0.543	0.594	0.415	0.421	0.541	0,600	0.662	0.535	0.566	0.568	0.598	0.537	0.567	0.523	0.548	0.576	0.589	0.610	0.556	0.567		0.341	0.318	0,543	0.252
Cr	1.651	1,658	1.507	1.463	1.470	1.421	1.385	1.536	1.539	1.399	1.338	1.262	1.392	1.353	1.341	1.317	1.398	1.376	1.437	1.406	1.387	1.337	1.309	1,365	1.348		1.430	1,430	1.283	1.569
Fe^{3+}	0.080	0.077	0.038	0.047	0.034	0.036	0.021	0.049	0,040	0.060	0,062	0.076	0.073	0.081	0.088	0.085	0,085	0.057	0.040	0.043	0.033	0.074	0.081	0.079	0.085		0.225	0.248	0.169	0.174
Fe^{2+}	0.464	0.480	0.455	0.484	0.443	0.452	0.478	0.473	0.494	0.445	0.438	0.473	0.447	0.462	0.440	0,451	0.452	0.467	0.469	0.468	0.546	0.469	0.473	0.498	0.509		0.564	0.620	0,518	0.647
Mn	0.007	-	0.007	-	-	0.010	-	-	-	-	-	-	-	0.007	0.009	0.009	-	-	-	-	-	0.010	-	-	-		-	-	0.014	-
Mg	0.522	0.512	0.538	0.513	0.553	0.535	0.522	0.523	0.506	0.555	0.559	0.523	0.546	0.525	0.544	0.535	0.548	0,531	0.531	0.529	0.454	0,521	0.523	0.499	0,491		0.429	0.378	0.464	0.348
Ca	0.007	0.007	-	0.003	0.004	0.003	-	0.004	-	-	0.003	0.004	0.007	0.006	0.007	0.005	-	0.002	-	0.003	-	-	0.004	0.003	0.003		0.007	0.003	0.004	0.005
$\frac{100\ Mg}{Mg+Fe}$	52.9	51.6	54.3	51.4	55.5	54.2	52.2	52.5	50.6	55.5	56.0	52.5	55.0	53.2	55.2	54.3	54.8	53.2	53.1	53.1	45.4	52.7	52.5	50.1	49.2		43.1	37.9	47.3	35.0
$\frac{Cr}{Cr+Al+Fe^{3+}}$	0.825	0.829	0.753	0.732	0.735	0.711	0.692	0.768	0.770	0.700	0.669	0.631	0.696	0.677	0.671	0.658	0.699	0.688	0.718	0.704	0.695	0,669	0.654	0.682	0.674		0.717	0,716	0.643	0,786
$\frac{Al}{Cr+Al+Fe^{3+}}$	0,135	0.133	0.228	0.245	0.248	0.271	0.297	0.207	0.211	0.271	0.300	0.331	0.268	0.283	0.284	0.299	0.268	0.283	0.262	0.275	0.289	0.295	0.305	0.278	0.284		0.171	0.159	0.272	0,126
$\frac{Fe^{3+}}{Cr+Al+Fe^{3+}}$	0.040	0.038	0.019	0.023	0.017	0.018	0.011	0.025	0,020	0.029	0.031	0.038	0.036	0.040	0.044	0.043	0.033	0.029	0.020	0.021	0.017	0.037	0.040	0.040	0.042		0.112	0,124	0.085	0.087
$\frac{Cr}{Cr+Al}$	0.860	0.862	0.768	0.749	0.748	0.724	0.700	0.787	0.785	0.721	0.690	0.656	0.722	0,705	0.702	0.688	0.723	0.708	0.733	0.719	0.707	0.694	0.682	0.711	0.704		0.807	0.818	0.703	0.862

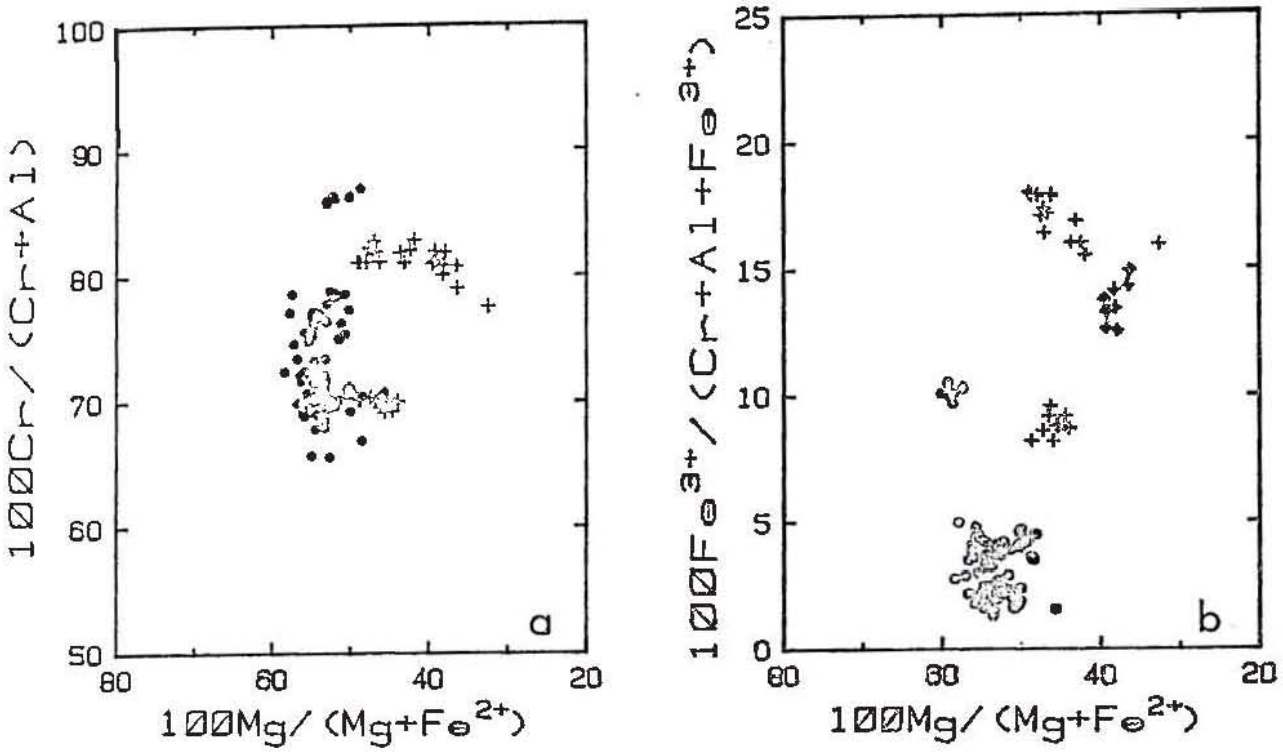

Fig. 1-7. Variation in composition of spinels from Marum tectonite peridotites in terms of $100Mg/(Mg+Fe^{2+})$ versus $100Cr/(Cr+Al)$, and $100Fe^{3+}/(Fe+Cr+Al)$. Circles = harzburgite, crosses = dunite. Note the higher Fe^{3+} and lower $100Mg/(Mg+Fe^{2+})$ of the dunite spinels.

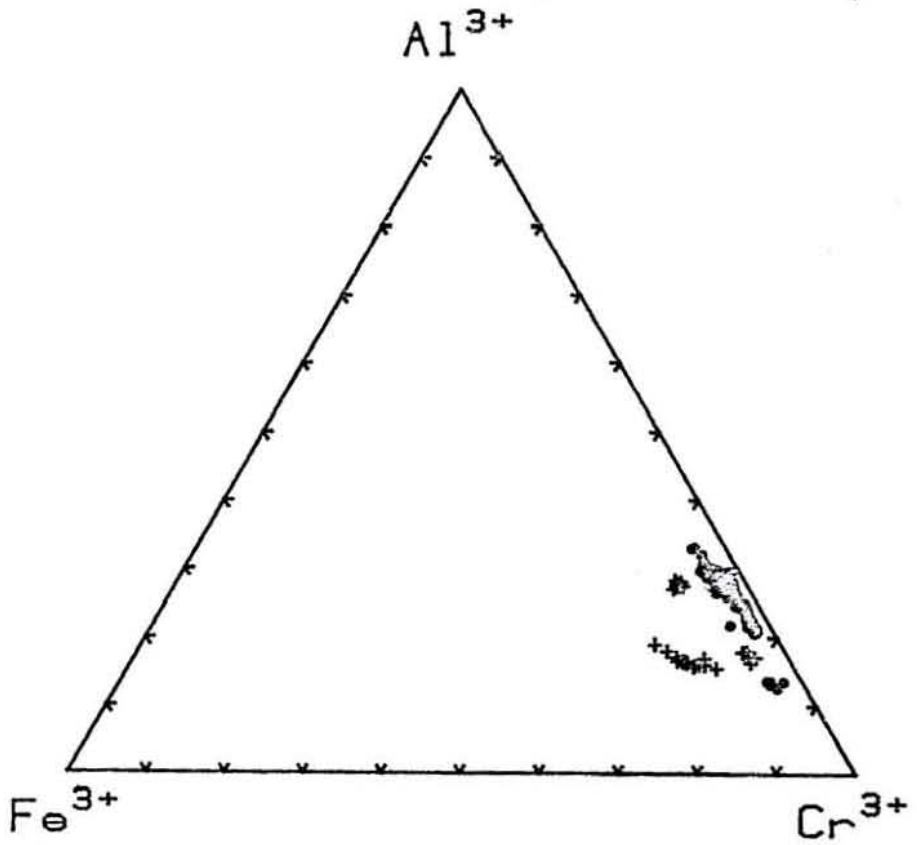

Fig. 1-8. Ternary plot of trivalent cations showing compositional variation exhibited by Marum tectonite spinels. Note Cr-Al trend of harzburgite spinels and higher Fe^{3+} of dunite spinels.

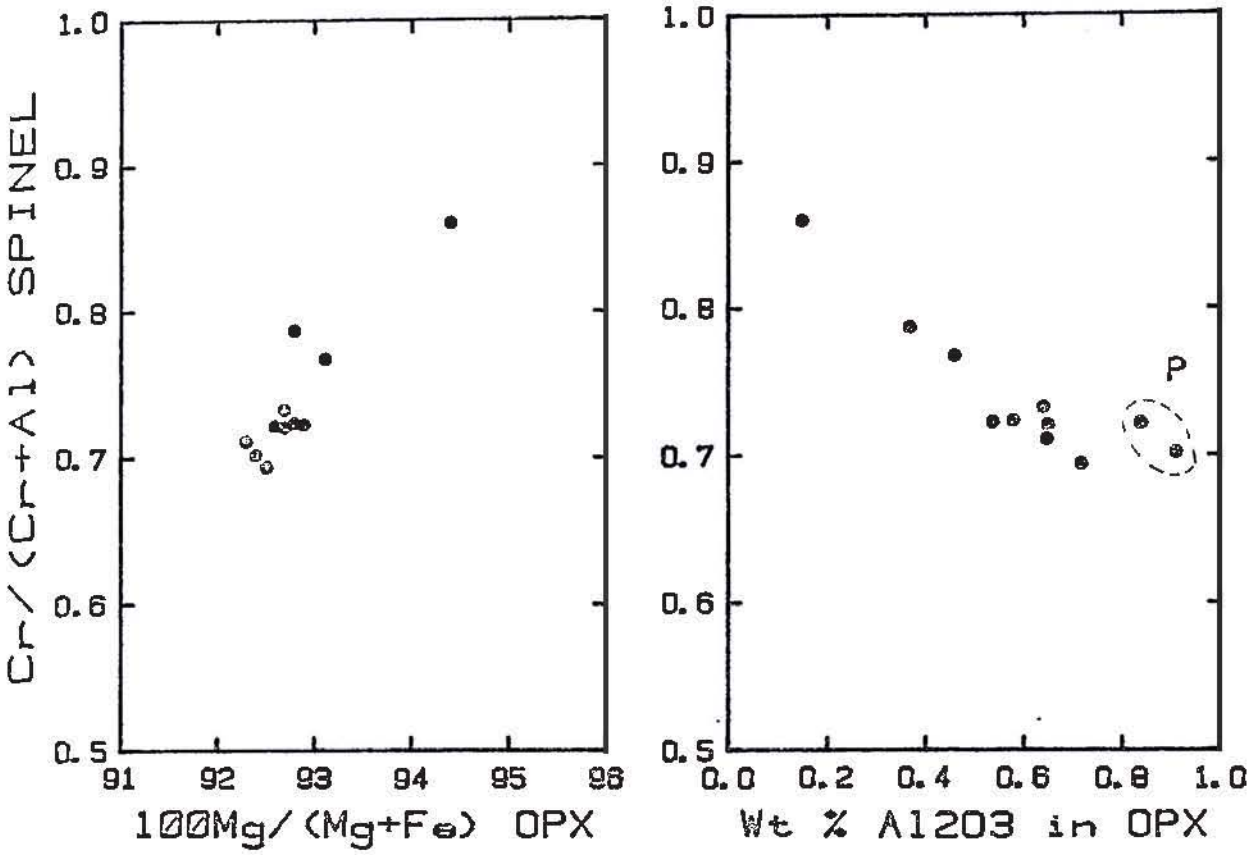

Fig. 1-9. Diagram showing co-variance of spinel and orthopyroxene compositions from Marum harzburgites. Field (P) is for least deformed protogranular harzburgites.

The irregularly shaped spinels are commonly (but not exclusively) more Al-rich than the larger sub-to euhedra.

Chrome spinel from the dunites are compositionally distinct from those of the harzburgite by virtue of their appreciably higher Fe^{3+} content (0.09-0.12) and more variable $Mg/(Mg+Fe^{2+})$ ratios (Figs. 1-7, 8). On a trivalent ion ($Cr-Al-Fe^{3+}$) plot the dunite spinels show a trend towards Fe^{3+} enrichment compared to the harzburgite spinels which show only Cr-Al variation. Spinels in the dunite also have higher Cr/(Cr+Al) ratios than many of the harzburgite spinels. This might suggest a magmatic origin for the dunites since Cr-enrichment would be favoured by the large octahedral site preference energy of Cr^{3+} compared to Al^{3+} and Fe^{3+} (Burns, 1970). Spinel in the pyroxenite dykes is highly chrome-rich (Table 1-4) and has a high Fe^{3+} content. The low $100Mg/(Mg+Fe^{2+})$ ratios suggests extensive subsolidus re-equilibration.

The Marum harzburgite spinels are more Cr-rich than spinels from most alpine peridotites (cf. Irvine & Findlay, 1972; Himmelberg & Loney, 1973), and from harzburgites in many ophiolites (e.g. Sinton, 1977; Malpas & Strong, 1975; Menzies, 1975). The more Cr-rich spinels of the tectonites compositionally overlap the more Cr-rich spinels of the overlying cumulate peridotites but, compared to the cumulate spinels show only limited Cr-Al substitution and are more Mg-rich.

Secondary alteration

The harzburgites and dunites have been affected by variable degrees of serpentinization. Near fault zones peridotites are extensively serpentinized but elsewhere the degree of serpentinization is low ($\leq$ 10%) and consists of fine irregular veinlets with disseminated secondary magnetite and traces of secondary sulphides, mainly pentlandite and pyrrhotite. In more strongly serpentinized peridotites secondary magnetite forms ragged rims on chrome spinel. In strongly altered harzburgites and

pyroxenite dykes orthopyroxene is altered in part to bastite, and clinopyroxene is replaced by tremolite.

2-3. Mineral equilibria and conditions of equilibration

Olivine-spinel

Irvine (1965) showed that the Fe^{2+}-Mg partitioning between olivine and spinel could be expressed by an equation which related the olivine and spinel end-members:

(1) $\frac{1}{2}Fe_2SiO_4 + Y^{sp}_{Cr}MgCr_2O_4 + Y^{sp}_{Al}MgAl_2O_4 + Y^{sp}_{Fe^{3+}}MgFe_2O_4 =$

$\frac{1}{2}Mg_2SiO_4 + Y^{sp}_{Cr}FeCr_2O_4 + Y^{sp}_{Al}FeAl_2O_4 + Y^{sp}_{Fe^{3+}}Fe_3O_4$ (d)

where $Y^{sp}_i = \frac{i}{Cr + Al + Fe^{3+}}$ in spinel and $Y^{sp}_{Cr} + Y^{sp}_{Al} + Y^{sp}_{Fe^{3+}} = 1$.

Assuming ideal solid solution among end-members, the equilibrium constant for this equation at equilibrium can be written (Irvine, 1965) -

$$K_d = \frac{X^{ol}_{mg} \cdot X^{sp}_{Fe^{2+}}}{X^{ol}_{Fe^{2+}} \cdot X^{sp}_{Mg}}$$

$$= \ln K_b + Y^{sp}_{Cr} \ln K_e + Y^{sp}_{Fe^{3+}} \ln K_f$$

where X^{ol}_{Mg} = mole fraction Mg/(Mg+Fe) in olivine, etc. and K is the equilibrium constant for the corresponding exchange reaction;

$$\frac{1}{2}Fe_2SiO_4 + MgAl_2O_4 = \frac{1}{2}Mg_2SiO_4 + FeAl_2O_4 \quad (b)$$

$$MgCr_2O_4 + FeAl_2O_4 = MgAl_2O_4 + FeCr_2O_4 \quad (e)$$

$$MgFe_2O_4 + FeAl_2O_4 = MgAl_2O_4 + Fe_3O_4 \quad (f)$$

Irvine (1965) showed that, if solid solution behaviour is ideal, olivine and spinel at equilibrium should define a plane in $\ln K_d - Y^{sp}_{Cr} - Y^{sp}_{Fe^{3+}}$ space at constant T. Where $Y^{sp}_{Fe^{3+}}$ is approximately constant a linear relationship should exist between $\ln K_d$ and Y^{sp}_{Cr}, the slope of which, $\ln K_e$, is dependent on temperature. The value of $\ln K_e$ will be greater than 1 for natural assemblages and will approach unity with increasing temperature (Irvine, 1965). Pressure effects are expected to

be very small since Δv's for the olivine-spinel exchange reactions are negligible for Al-rich assemblages and only slightly greater for higher Y_{Cr}^{sp} (Irvine, 1965; Robie & Waldbaum, 1968). Since $Y_{Fe}^{sp}3+$ is low in the Marum harzburgite spinels, olivines and spinels, if equilibrated at the same temperature, should display a near-linear relationship in a plot of $\ln K_d$ versus Y_{Cr}^{sp}.

Olivine and spinel data from Tables 1-1 and 1-4 have been plotted in the $\ln K_d$ versus Y_{Cr}^{sp} diagram (Fig. 1-10). Despite the restricted range of Y_{Cr}^{sp} values, olivine and spinel cores from the harzburgites approximate a linear relationship, suggesting an approach to equilibrium under similar temperatures. Rim compositions for harzburgite olivine-spinel pairs, and olivine-spinel pairs from the dunites, are displaced to higher $\ln K_d$ values, indicating equilibration at lower temperatures. Olivine inclusions in chrome spinel indicate final equilibration under even lower temperatures. The range of Mg and Fe^{2+} partitioning between olivine and spinel cores, rims and inclusions, and preservation of the $\ln K_d$ versus Y_{Cr}^{sp} relationship between cores, is evidence that partial re-equilibration has occurred under varying temperatures, and that equilibrium partitioning of Mg and Fe^{2+} under the final P-T conditions has been achieved only locally.

There is considerable uncertainty in estimating actual equilibration temperatures. Jackson (1969), following Irvine (1965) assembled thermochemical data to enable calibration of the Fe^{2+}-Mg partitioning between olivine and spinel as a geothermometer but noted that, because of the nature of the thermochemical data, uncertainty in the calibration may be as high as 300°C. Subsequent use of the geothermometer has yielded temperature estimates for a number of alpine peridotites which were in apparent agreement with temperature estimates based on other geothermometers (e.g. Medaris, 1972; Sinton, 1977; Varne & Brown, 1978) but resulted in excessively high temperature estimates for

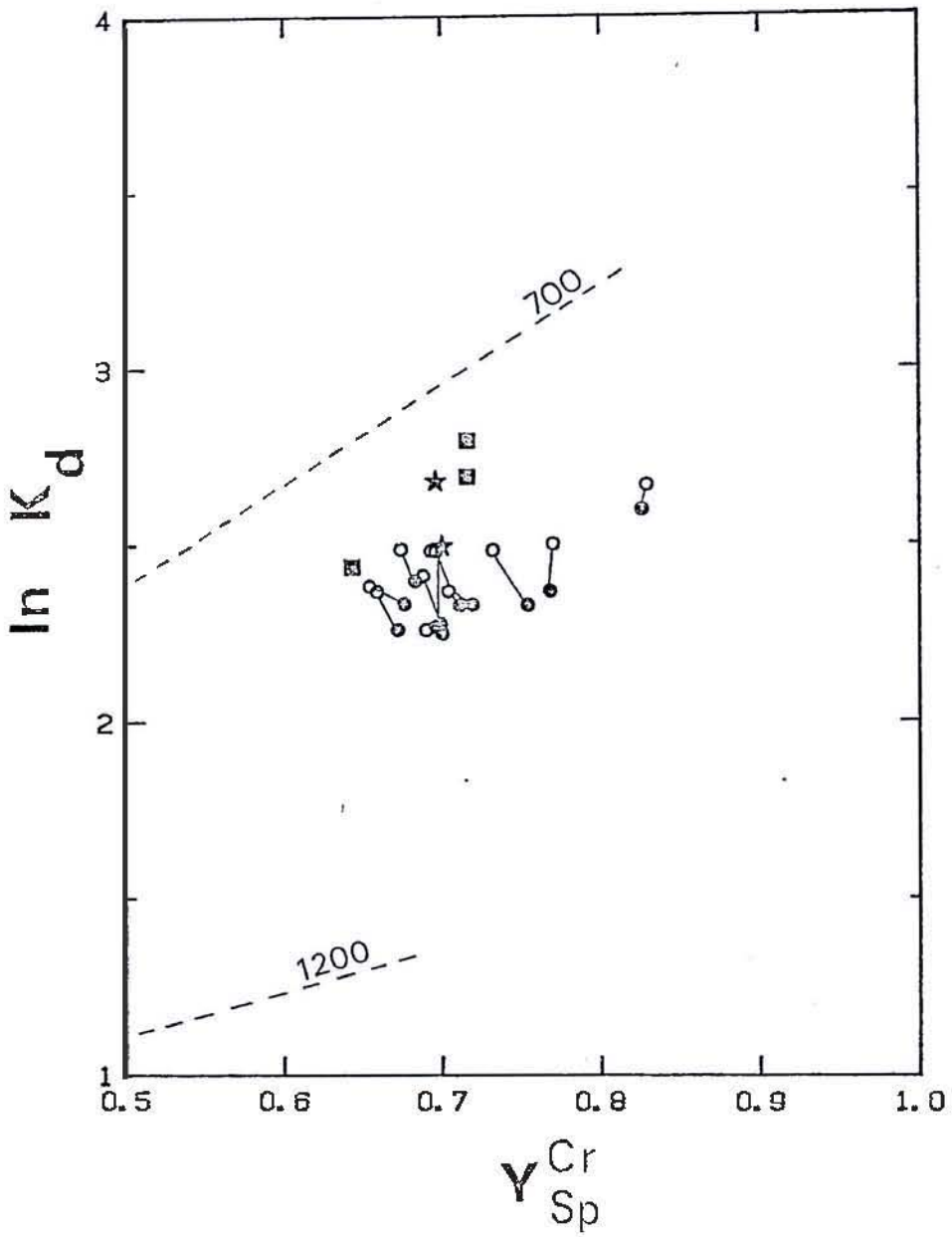

Fig. 1-10. Plot of $\ln K_d$ versus Y_{Sp}^{Cr} for olivine-spinel pairs from Marum tectonite peridotites. Tie lines join mineral cores (closed circles) and rims (open circles) of harzburgites, squares = dunite, star = pyroxenite. Dashed lines labelled 700 and 1200 refer to the 700°C and 1200°C isotherms of Evans & Frost (1975).

volcanic rocks (e.g. Evans & Wright, 1972). Evans & Frost (1975) claimed that the temperature dependence of $\ln K_d$ is probably greater than implied by Jackson's (1969) calibration and proposed a semi-empirical recalibration of the geothermometer. Comparison of the Marum data with the isothermal surfaces for olivine-spinel equilibria obtained by Medaris (1975) using the thermochemical data of Jackson (1969) would suggest quasi-magmatic equilibration temperatures ($\sim$ 1200-1250°C), whereas much lower temperatures are implied by comparison with the semi-empirical isotherms of Evans & Wright (1975).

Roeder & others (1979) have recently re-evaluated the geothermometer and shown that more realistic temperature estimates can be obtained for volcanic rocks by using alternative free energy values for $FeCr_2O_4$. Use of these lower ΔG_f^o values also results in substantially lower nominal equilibration temperatures for olivine-spinel pairs from plutonic rocks and alpine peridotites which Roeder & others (1979) suggest are a reflection of extensive subsolidus re-equilibration.

Nominal equilibration temperatures for olivine-spinel pairs using both Jackson's (1969) equation and Roeder & others' (1979) revised geothermometer are presented in Table 1-5. Equilibration temperatures for the core compositions range between 1150 and 1290°C (mean = 1236$\pm$43°C) using Jackson's (1969) equation, and much lower temperatures, 650-710°C ($\bar{x}$ = 684$\pm$20°C) using Roeder & others' (1979) revised equation. Nominal equilibration temperatures obtained for the rims were lower, 1090-1200°C ($\bar{x}$ = 1150°C) or 600-650°C ($\bar{x}$ = 640°C) using the respective equations. Similar or slightly lower temperatures were obtained from inclusions within spinel. Nominal temperatures obtained for olivine-spinel pairs in the dunite are also similar to, or lower than, those obtained for the mineral rims in the harzburgite.

The very low equilibration temperatures suggested by Roeder & others' (1979) equation imply extensive re-equilibration of both cores and

TABLE 1-5. NOMINAL EQUILIBRATION TEMPERATURES FOR CO-EXISTING OLIVINE-SPINEL PAIRS FROM THE TECTONITE PERIDOTITES.

Sample No.	Roeder[1]		Jackson[2]	
	core	rim	core	rim
	Harzburgite			
087	655	634	1245	1205
490	695	639	1276	1157
488	678	615	1217	1087
492	697	659	1290	1216
425	708	690	1271	1218
425*	-	622	-	1110
423	701	-	1250	-
423*	-	627	-	1120
473	697	648	1239	1138
418	698	643	1253	1141
489	682	608	1230	1181
474	662	641	1169	1122
046	649	617	1153	1091
	Dunite			
410	603		1111	
411	575		1061	
414	637		1123	

1. Roeder refers to temperatures calculated following Roeder & others, (1979).

2. Jackson refers to temperatures calculated following Jackson (1969).

* Indicates olivine inclusion in chrome spinel.

rims at temperatures well below the solidus. These temperatures are substantially lower than those suggested by the pyroxene solvus method for kink-controlled exsolution of pyroxene which clearly occurred during plastic deformation of the protogranular-textured harzburgite. Co-existing orthopyroxene and exsolved clinopyroxene in harzburgites 492, 488 and 425 indicate equilibration temperatures of 891, 896 and 934°C respectively using Wells' (1977) recalibration of Wood & Banno's (1973) two-pyroxene solvus to include data for Mg-rich pyroxenes in multicomponent systems. If the nominal equilibration temperatures indicated by Roeder & others' (1979) modified geothermometer are correct then they must indicate partial re-equilibration in response to cooling. At such low temperature however, assumptions regarding ideality of solid solutions might no longer be valid.

Pyroxene-spinel

The solubility of Al_2O_3 in pyroxene in equilibrium with spinel is dependent on T and P (e.g. O'Hara, 1967; Green & Ringwood, 1970; MacGregor, 1974). The Al_2O_3 content of orthopyroxene (opx) can be expressed as $MgAl_2SiO_6$ (Mg-Tschermak's component of opx solid solution), and, when in equilibrium with olivine and spinel, the following reaction can be written:

(2) $Mg_2Si_2O_6$ (opx$_{ss}$) + $MgAl_2O_4$ (spinel) = $MgAl_2SiO_6$ (opx$_{ss}$) + Mg_2SiO_4 (olivine)

At equilibrium the standard Gibbs free energy is

$$\Delta G^{o}_{P,T} = -RT \ln \frac{a^{opx}_{MgAl_2SiO_6} \cdot a^{ol}_{Mg_2SiO_4}}{a^{opx}_{Mg_2Si_2O_6} \cdot a^{sp}_{MgAl_2O_4}}$$

where a^j_i is the activity of component i in phase j.

---

* Activity-composition relationships used are defined in Appendix 1.

In the simple system $MgO - Al_2O_3 - SiO_2$ the Al_2O_3 content of orthopyroxene in equilibrium with olivine and spinel is fixed at any particular T and P, and MacGregor (1974) defined Al_2O_3 isopleths for orthopyroxene as a function of P and T. More recent experimental studies and thermodynamic considerations of reactions involving pyroxene in the $MgO - Al_2O_3 - SiO_2$ and $CaO - MgO - Al_2O_3 - SiO_2$ systems have shown that Al_2O_3 solubility in spinel peridotite is much lower than originally claimed (e.g. Presnall, 1976; Obata, 1976). Stroh (1976) has shown that addition of Cr and Fe to the simple system drastically affects the activities of phases at equilibrium.

Considering the simple system for complete coupling of tetrahedral and octahedral substitution, AlAl = MgSi, the amount of Tschermak's component in pyroxene can be approximated by Al/2 for 6 oxygens per formula unit. Sinton (1977) used this approach to show that a strong linear relationship exists between the Al content of co-existing pyroxenes and spinels from the Red Mountain peridotite. The cores of pyroxenes and spinels from the Marum harzburgites show a similar linear relationship between Al in pyroxene and spinel (Fig. 1-11), despite the fact that the analyses in Table 1-2 suggest a strong site preference of Al for the tetrahedral position, as do most orthopyroxenes from alpine peridotites (Stroh, 1976). This linear relationship, indicating constancy of partitioning between pyroxene and spinel, suggests equilibration under similar P, T conditions. Figure 1-11 also clearly shows the enhanced partitioning of Al into spinel from pyroxene exhibited by the mineral rims. Experimental studies show that preferential partitioning of this nature is favoured by a decrease in temperature (e.g. MacGregor, 1974; Herzberg & Chapman, 1976). It is also apparent that the more Al-rich pyroxenes in the least deformed protogranular harzburgites lie displaced from the general linear trend, and that the pyroxene-spinel rims of these peridotites show enhanced partitioning to more Al-rich spinels

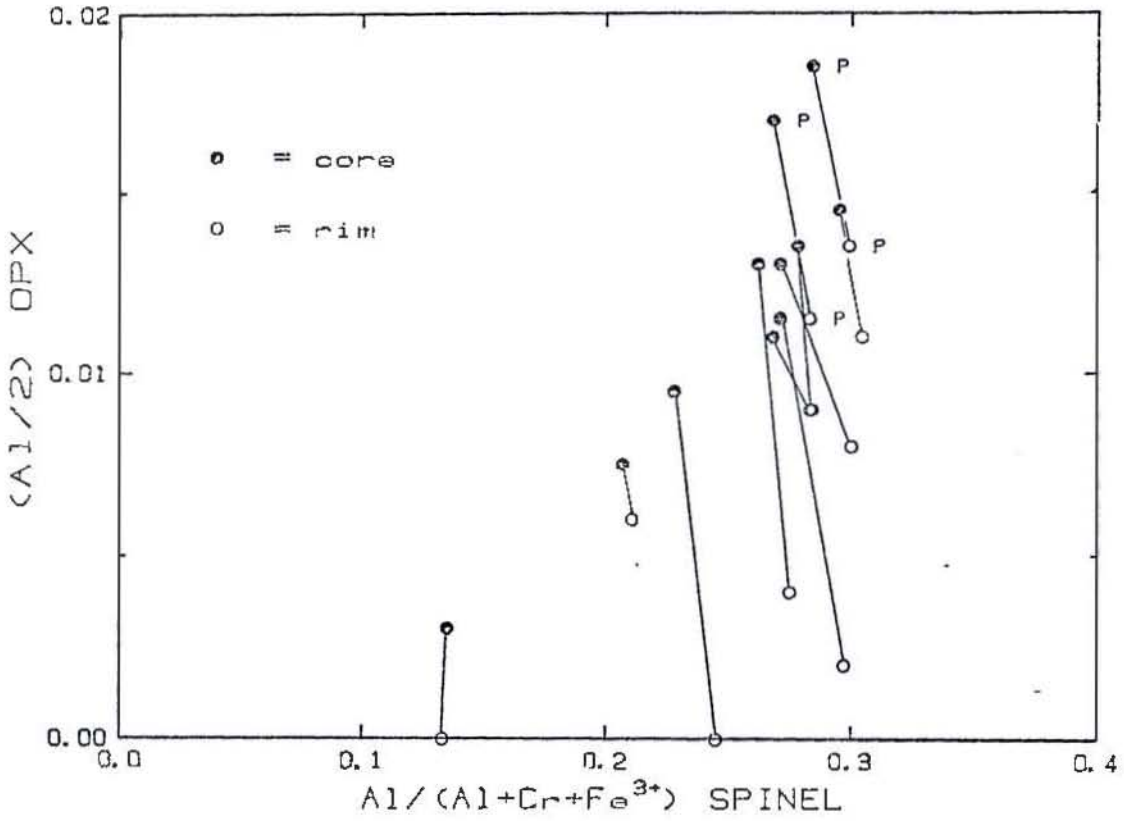

Fig. 1-11. Plot of $Al/(Al+Cr+Fe^{3+})$ in spinel versus (Al/2) in orthopyroxene for Marum harzburgites. Tie lines join mineral cores (solid circle) to rims (open circles). P = least deformed, protogranular harzburgites. Note the trend of increase in Al in spinel and decrease in pyroxene in rims relative to cores, and in the least deformed protogranular harzburgites relative to the bulk of the samples.

and Al-poor pyroxenes of similar composition to the pyroxene-spinel cores of the other harzburgites. In view of the fact that the bulk compositions of these least-deformed protogranular harzburgites are not markedly more aluminous than those containing less aluminous pyroxene (see Table 1-6) these peridotites are considered to preserve a mineral assemblage which indicates equilibration at higher temperatures than the bulk of the harzburgites. This is discussed further below.

Stroh (1976) derived an equation for calculating pressures of equilibration of reaction (2) using a simple mixing model of olivine, aluminous orthopyroxene and spinel based on that of Wood & Banno (1973), and the experimental data of MacGregor (1974). Equilibration temperatures must be known or calculated independently. Application of Stroh's (1976) equation to the Marum harzburgites using data from Tables 1-1, 2, 4 for mineral cores results in pressure estimates of several hundred bars, assuming the equilibration temperatures obtained from olivine-spinel pairs using Roeder & others (1979) equation, or, up to 1.5 kb assuming the higher equilibration temperatures derived using Jackson's original geothermometer. Nominal equilibration pressures of 0.4, 0.7 and 0.8 kb were obtained for peridotites 488, 425 and 492 respectively assuming equilibration temperatures of 900°C based on co-existing pyroxenes. These nominal equilibration pressures are very low but are in keeping with the low pressure style of deformation in the harzburgites.

Varne & Brown (1978), following Stroh (1976), constructed a plot of lnK versus P and T for reaction (2). Comparison of calculated $\ln K_{(2)}$ values for the Marum harzburgites within the P-T grid suggests that the more deformed harzburgites apparently equilibrated at temperatures below 1000°C. The less deformed harzburgites with the more Al-rich pyroxenes, however, apparently equilibrated at much higher temperatures (and possibly pressures), mostly in the range 1200-1300°C, depending on pressure. A much lower $\ln K_{(2)}$ for harzburgite 473 suggests equilibration

at even higher temperatures, 1400-1500°C.

The above considerations therefore point to a high temperature (1200-1300°C) origin for the Marum harzburgites which is recorded by the pyroxenes and spinels in the least deformed protogranular peridotites. Superimposed on the high temperature origin is a subsolidus history involving varying degrees of deformation, and re-equilibration. This subsolidus history is recorded in the different cation exchange equilibria between co-existing phases which show a range of equilibration temperatures. This range of equilibration temperatures is considered to represent the *temperatures of closure to effective cation exchange* of each equilibria, which probably depends on relative diffusion rates. Thus, geothermometers based on Ca and Al partitioning record the highest equilibration temperatures whereas those based on Fe-Mg partitioning between olivine and spinel record progressive re-equilibration (cooling) to very low temperatures. The final local re-equilibration (cooling) between the Marum spinel and olivine rims took place at very low temperatures, possibly $\sim$ 600°C.

2-4. Geochemistry

Major and trace elements have been determined for 7 harzburgites, a dunite, and an enstatite dyke from the tectonite peridotites (Table 1-6). All elements except Na and K (atomic absorption spectroscopy) and H_2O^+ and FeO (wet chemistry) were determined by X-ray fluorescence spectrometry. Analytical methods are described in Appendix 1.

Major elements

The harzburgites are extremely magnesian and strongly depleted in lithophile elements. Bulk rock *mg* (*mg* = 100Mg/(Mg+ΣFe)* (see page 31 for explanation) values are in close agreement with olivine Fo contents, indicating that the Fe_2O_3 contents shown in Table 1-6 are the result of

TABLE 1-6. CHEMICAL ANALYSES OF TECTONITE PERIDOTITES

Analysis Sample	1 057	2 488	3 490	4 492	5 489	6 423	7 473	8 414	9 257
SiO_2	41.12	41.53	41.27	41.42	42.69	42.51	43.97	39.63	56.63
TiO_2	<0.002	<0.002	<0.002	<0.002	0.003	0.002	0.002	0.004	0.02
Al_2O_3	0.03	0.22	0.09	0.17	0.24	0.24	0.33	0.30	0.45
Fe_2O_3	0.78	1.35	0.91	1.46	1.15	0.93	0.36	2.03	0.98
FeO	5.32	5.56	6.29	5.65	5.96	6.31	6.93	7.00	4.92
MnO	0.10	0.12	0.12	0.12	0.12	0.12	0.12	0.15	0.17
MgO	50.27	46.04	47.84	45.83	45.13	46.37	46.18	48.17	34.01
CaO	0.05	0.16	0.09	0.18	0.50	0.18	0.25	0.19	1.38
Na_2O	0.005	0.006	0.007	0.006	0.009	0.003	0.004	0.003	0.02
K_2O	(2)*	(4)	(5)	(2)	(7)	(4)	(4)	(3)	0.001
P_2O_5	<0.001	<0.001	<0.001	<0.001	<0.001	<0.001	<0.001	<0.001	0.001
S	<0.01	<0.01	<0.01	<0.01	<0.01	<0.01	<0.01	<0.01	<0.01
H_2O^+	2.83	4.69	3.06	5.07	3.80	2.90	2.06	2.15	1.53
Total	100.50	99.68	99.68	99.91	99.67	100.21	100.21	99.63	100.11
100 Mg/(Mg+ΣFe)	93.7	92.4	92.3	92.1	92.0	92.0	91.9	90.7	91.3
Trace elements (ppm)									
Rb	<0.1	<0.1	<0.1	<0.1	<0.1	<0.1	<0.2	<0.1	0.1
Sr	<0.1	<0.1	<0.1	<0.1	<0.1	<0.1	<0.2	<0.1	0.8
Zr	<1	<1	<1	<1	1.0	<1	1	<1	<1
Nb	<1	<1	<1	<1	<1	<1	1	<1	1
Y	<1**	<1	<1	<1	<1	<1	<1	<1	<1
Sc	2	6	4	6	8	6	7	6	13
V	4	8	5	15	17	11	19	14	16
Cr	2140	1790	1490	2390	2420	2210	2560	4460	2220
Ni	2710	2540	2680	2630	2400	2500	2410	1850	187
Cu	4	3	6	3	4	4	3	5	9
Zn	38	44	46	44	46	45	48	47	46
Ti	10	12	8	7	21	13	17	30	107

H_2O^+ determined as loss-on-ignition. All Ba <10, La <2, Ce <3, Nd <2 ppm.

* Values in parenthesis are elemental abundances in ppm.

** Spark source mass spectrometer values; Y = 0.07, La = 0.013, Ba = 0.14 ppm, Zr = 0.34 ppm.

Analyses 1-7 = harzburgite; 8 = dunite; 9 = enstatite-rich dyke.

surficial oxidation and/or oxidation accompanying serpentinization. This conclusion is also supported by the direct correlation of Fe_2O_3 and H_2O^+ contents. Al_2O_3 and CaO contents are very low and correlate directly with the modal abundance of pyroxene and, to a lesser extent, bulk rock *mg* (Fig. 1-12); the lowest Al_2O_3 and CaO contents are associated with the highest bulk rock *mg* and most Al- and Ca-poor pyroxene. TiO_2 and alkali contents are extremely low (< 100 ppm), and clearly indicate the highly depleted nature of these peridotites.

The enstatite-rich dyke is highly magnesian but contains appreciably higher contents of all lithophile elements. CaO and alkalies are markedly higher than the harzburgites and dunites, and the bulk composition has pyroxene stoichiometry.

Trace elements

The Marum harzburgites and dunites are marked by extreme depletion in all large-ion-lithophile (LIL) elements and high valence cations (Table 1-6). Ni and Cr contents are high, reflecting the highly refractory mineralogy. Ni shows a positive correlation with bulk rock *mg* (and increasing abundance of olivine), whereas Cr varies with modal abundance of chrome spinel and pyroxene. Ti and V contents show an overall positive correlation with modal abundance of orthopyroxene and negative correlation with the bulk rock *mg* (Fig. 1-12). Rare earth element (REE) abundances in the harzburgites are extremely low; incomplete

---

* The ratio *mg* = Mg/(Mg+ΣFe) where ΣFe is total iron calculated as Fe^{2+} is used for ultramafic rocks since the Mg^{2+} of these rocks is very high and the original Fe^{3+} is very low but unknown. For basaltic compositions Mg-value (= 100Mg/Mg+Fe^{2+}) is more appropriate since the Fe^{3+} content is much greater and is important in consideration of Fe-Mg partitioning between crystals and liquid.

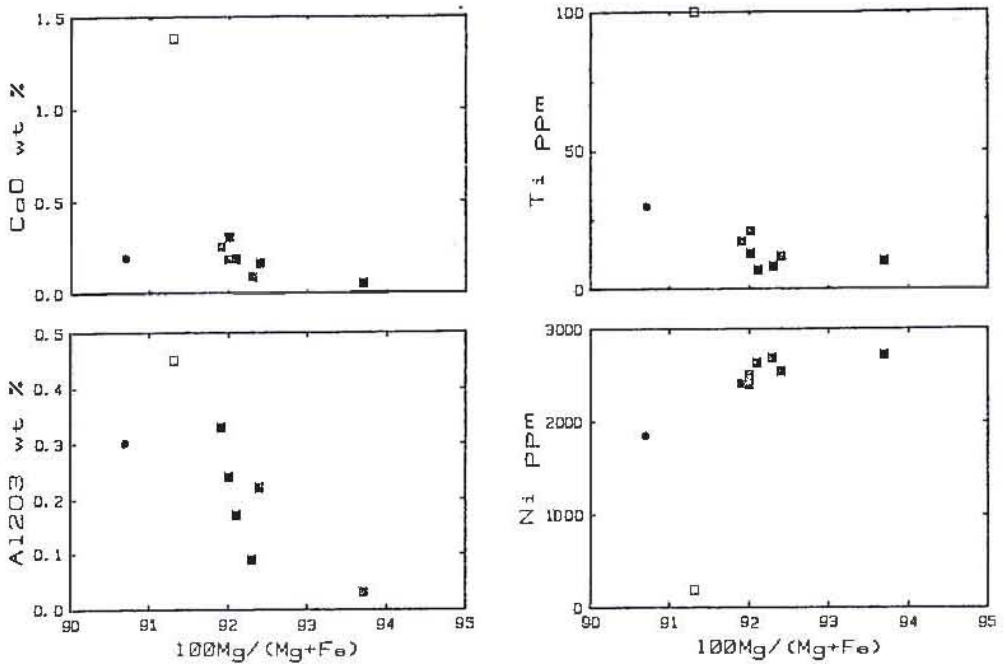

Fig. 1-12. Variation in CaO, Al_2O_3, Ni and Cr with 100Mg/(Mg+ΣFe) for Marum tectonite peridotites. Closed squares = harzburgite, circle = dunite, open square = pyroxenite.

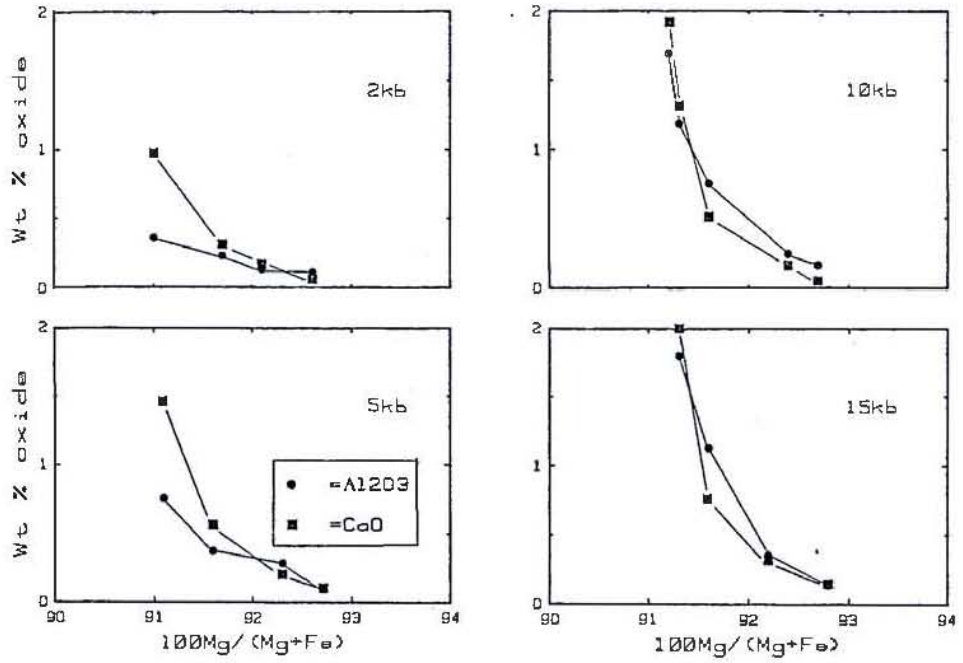

Fig. 1-13. Chemical trends of harzburgitic residues from partial melting of spinel lherzolite with varying degrees of partial melting (shown by increasing 100Mg/(Mg+ΣFe) ratio) at 2,5,10 and 15 kb pressure. Note the similarity of the CaO and Al_2O_3 variation with increasing *mg* shown by the Marum harzburgites (Fig. 1-12) with that of low pressure melting of peridotite.

spark source data for harzburgite 087 suggest a relatively unfractionated pattern at about 0.04 times (x) chondritic abundance or less.

Abundances of all incompatible elements* are higher, and Ni contents lower, in the pyroxenite dyke than the harzburgites and dunites (Fig. 1-12). The clear displacement of the pyroxenite dyke from the harzburgite trends on the CaO versus *mg*-number and Ni versus *mg*-number diagrams (Fig. 1-12) strongly suggests a separate origin, consistent with the field evidence for late emplacement.

Comparisons

Harzburgite-subtype alpine peridotites (Jackson & Thayer, 1972) and harzburgite-dunite masses in ophiolites are highly depleted in lithophile elements compared to present estimates of the upper mantle (e.g. Ringwood, 1975, 1979; Harris & others, 1967; Maaloe & Aoki, 1977; see also PART 3), and are generally interpreted as the residue remaining after extraction of a basaltic melt fraction (e.g. Green & Ringwood, 1967a; Dickey, 1970; England & Davies, 1973; Himmelberg & Loney, 1973; Menzies & Allen, 1974; Coleman, 1977, and others). The Marum harzburgites are decidedly more magnesian and more depleted in lithophile elements than alpine peridotites, and are also more refractory than most harzburgites from other ophiolites (cf. Irvine & Findlay, 1972; Montigny & others, 1973; Menzies & Allen, 1974; Coleman, 1977 p. 33), with the exception of the Papuan Ultramafic Belt (see PART 2). In particular, the higher ferrosilite and Ca-Tschermak's (and jadeite) components of pyroxenes in alpine-type peridotites (particularly lherzolite-subtype peridotites) are reflected by higher FeO, Al_2O_3 and CaO contents in the bulk rock chemistry.

---

* Incompatible elements are those whose ionic radius and/or valance does not readily permit substitution in the major phases of the mantle and are strongly partitioned into any co-existing melt.

The high *mg*-numbers and extreme depletion in lithophile elements clearly sets the Marum harzburgites aside from the overlying pyroxene-bearing cumulates. However, the field relations, the overlap in olivine compositions and trace element correlations (e.g. Ti-V, Fig. 1-38; Ni-Ti, etc) suggest a genetic relationship between the cumulate and non-cumulate peridotites.

2-5. Marum harzburgites as the residue from partial melting

The protogranular textures, lack of cumulus textures and the uniform, highly refractory mineralogy and chemistry of the Marum harzburgites suggest an origin as the residue from partial melting of a less refractory peridotite. The mineralogy of the harzburgites is unlike the overlying cumulate peridotites which range from dunite and chromitite upwards through wehrlite, lherzolite to plagioclase lherzolite. The composition of pyroxenes in the cumulate peridotites is unlike those in the harzburgites, being distinctly richer in Fe, Al and Ca (Chapter 3) and, unlike the olivine compositions, do not overlap those of the harzburgite. The highly magnesian olivine and orthopyroxenes with low Al_2O_3 content of the harzburgites are unlike olivine and orthopyroxenes crystallized from basaltic melts. Moreover, low pressure crystallization of magnesian olivine and orthopyroxene in the ratio 85:15 would seem to be precluded by the olivine-orthopyroxene reaction relationship; as observed by Irvine & Findlay (1972), cumulates of this constitution are not abundant in any of the documented stratiform intrusions.

Harzburgite with magnesian olivine and orthopyroxene in this proportion occurs as residue from partial melting of peridotite (PART 3). Melting of peridotite results in progressive elimination of residual phases with increasing degrees of melting (Fig. 3-1). At about 75-100°C above the peridotite solidus (∿ 10-20% melting) clinopyroxene is exhausted, and the residual phases are olivine, orthopyroxene and chrome spinel. With increasing temperature and degree of melting orthopyroxene

is progressively melted until a dunitic residue is reached at about 150-200°C above the solidus, corresponding to more than about 35% melting, depending on the composition of the peridotite and the pressure at which melting occurs. Data obtained on the compositions of residual phases (PART 3, Tables 3-4 to 3-8) show that residual phases become increasingly more refractory with increasing degrees of partial melting; olivine, orthopyroxene and spinel become more magnesian, chrome spinel more chrome-rich, and pyroxene progressively poorer in Al_2O_3 and CaO (Figs. 3-4, 5, 6). The compositions of the residual phases from melting of spinel lherzolite at low pressure are very similar to those of the least deformed protogranular harzburgites in terms of both the low Al_2O_3 content of the pyroxenes, and the high Mg of the phases. Differences exist in terms of the high chrome content in the pyroxenes (due to the high Cr content of the experimental peridotite compositions), and the higher Fe^{3+} content in the experimental spinels.

In addition to similarity of mineral compositions, similarity between the Marum harzburgites and the harzburgitic residues formed during experimental melting of peridotite is apparent in the compositions of the harzburgitic residues (Table 1-7), and the compositional trends shown by the residues. Data for the harzburgitic residues from partial melting of peridotite plotted in Figure 1-13 show that with increasing degrees of partial melting the bulk compositions of the residues become progressively more magnesian and depleted in CaO and Al_2O_3. At comparatively higher pressures (10-15 kb) the residue at low to moderate degrees of melting retains high Al_2O_3 and CaO content (due to the higher proportion of orthopyroxene to olivine and higher CaO and Al_2O_3 content of the orthopyroxene). The trend of residual compositions formed during experimental melting of peridotite at *low pressure* are very similar to those of the Marum harzburgites. These features suggest that the Marum harzburgites represent the residues of extensive degrees of partial melting

TABLE 1-7. COMPARISON OF MARUM AND PAPUAN HARZBURGITES WITH HARZBURGITIC RESIDUES FROM PARTIAL MELTING OF PERIDOTITE (PART 3)

	1	2	3	4	5
SiO_2	43.6 (1.2)	44.0 (0.2)	42.0	42.7	43.1
TiO_2	-	-	0.01	0.02	0.01
Al_2O_3	0.2 (0.1)	0.05 (0.01)	0.13	0.29	0.25
FeO*	7.2 (0.4)	6.9 (0.25)	7.6	7.3	7.2
MnO	0.12 (0.01)	0.12	0.16	0.16	0.16
MgO	48.7 (1.17)	48.9 (0.4)	50.0	49.3	49.0
CaO	0.2 (0.1)	0.04 (0.01)	0.17	0.21	0.17
Na_2O	-	-			
$\frac{100\ Mg}{Mg + Fe}$	92.3	92.7	92.1	92.3	92.4

1. Average 7 Marum harzburgites (1σ deviation)
2. Average 4 Papuan harzburgites
3. Harzburgitic residue, partial melting of Tinaquillo lherzolite 2 kb 1300°C.
4. Harzburgitic residue, partial melting of Tinaquillo lherzolite 5 kb 1350°C.
5. Harzburgitic residue, partial melting of Tinaquillo lherzolite 10 kb 1400°C.

* Total iron as FeO.

of mantle lherzolite under high temperatures and shallow depths ($\leq$ 5 kb) which have subsequently re-equilibrated at lower temperatures and suffered mild plastic deformation.

Dunite bodies intercalated with the harzburgites differ from the harzburgites in terms of their more Fe-rich olivine compositions and the higher Fe^{3+} of their chrome spinels. Olivines in the dunite lenses overlap the compositions of olivine in the overlying cumulate dunites. This and the apparent increase in abundance of dunite lenses towards the overlying cumulates suggests that the dunite lenses might form from olivine precipated from magmas feeding the overlying cumulates, and concentrated by crystal settling or filter-pressing within the subjacent harzburgite. An origin of this nature appears plausible for some but not all of the dunite lenses. Some of the dunites contain chrome spinel with higher Fe^{3+} contents than spinel in the overlying cumulates, and define a trend toward Fe^{3+} - Al enrichment distinct from the predominant Cr-Al trend shown by the cumulate spinels (Figs. 1-8, 17).

Formation of the pyroxenite dykes clearly post-dates formation of the foliation and banding in the harzburgites and, judging by the coarse grain-size and lack of chilled margins, must have formed at comparatively high temperatures. The bulk rock compositions (see later) show higher abundances of lithophile elements than the harzburgites, and it is suggested that the pyroxenites might represent material sweated out from less depleted harzburgite, possibly in the presence of a hot fluid phase.

2-6. Conclusions

Weakly foliated harzburgite with interfingering lenses and tabular masses of dunite underlie the thick sequence of ultramafic and mafic cumulates, and are intruded by narrow, coarse-grained pyroxenite dykes which post-date the foliation in the harzburgites.

The harzburgites are characterized by highly refractory, uniform mineralogy - olivine Mg_{92}, enstatite Mg_{93}, and chrome-rich spinel - and chemistry, with marked depletion in all lithophile elements. Partitioning between olivine, pyroxene and spinel, coupled with the widespread protogranular textures suggest an origin at high temperatures ($\sim$ 1200-1300°C) and low pressures. The harzburgites have subsequently re-equilibrated at lower temperature ($\sim$ 900°C and lower, possibly to $\sim$ 600°C), and undergone limited plastic deformation prior to solid-state emplacement. The textures, uniform mineralogy, and highly depleted chemistry of the harzburgites are consistent with an origin as a refractory residue formed by large degrees of partial melting of mantle peridotite at low pressure.

The lenses of dunite within the harzburgite appear genetically distinct from the harzburgites; some appear to represent small segregations of cumulate olivine from magma associated with the overlying cumulate dunite and chromitite. Pyroxenite dykes intruding the harzburgite postdate the foliation, and are inferred to have formed at high temperatures, possibly by sweating out of material from less depleted harzburgite in the presence of a hot fluid phase.

CHAPTER 3

PETROLOGY OF THE CUMULATE PERIDOTITES AND GABBROS

3-1. Stratigraphy of the layered sequence

A diagrammatic representation of the stratigraphy of the sequence of layered cumulates directly overlying the harzburgite-dunite is presented in Figure 1-14.

Dunite unit (olivine, chrome spinel cumulates) - (Sample Nos. 567, 497, 421, 221, 477, 1046, 092, 428, 059, 504)

Relatively undeformed dunite some 300-500 m thick with minor chromitite layers overlies the harzburgite. Apart from zones of faulting or strong jointing the degree of serpentinization is low and fresh dunite is exposed in river sections. Chromitite layers are thin (mostly 0.5 to 2.5 cms, rarely up to 10 cms thick) and commonly show fine-scale rhythmic, mineral-graded* and size-graded layering (grainsize 0.5-1 mm) conformable with rhythmic layering in overlying cumulate peridotite (Fig. 1-15A). Reverse mineral-graded layering found in several localities is thought to reflect settling overlap (cf. Goode, 1976) rather than overturning of strata.

---

* The terminology used to describe cumulus structures and layering follows Jackson (1967).

Mineral-graded layering - a layer characterized by a gradual stratigraphic change in proportions of two or more cumulus phases.

Isomodal layer - a layer characterized by a uniform proportion of one or more cumulus minerals.

Size-graded layering - a layer characterized by a gradual stratigraphic change of grain size of one or more cumulus minerals.

Phase contact - a horizon (former surface of deposition) marked by the appearance or disappearance of a cumulus mineral

Ratio contact - a horizon marked by a sharp change in the proportion of two cumulus minerals.

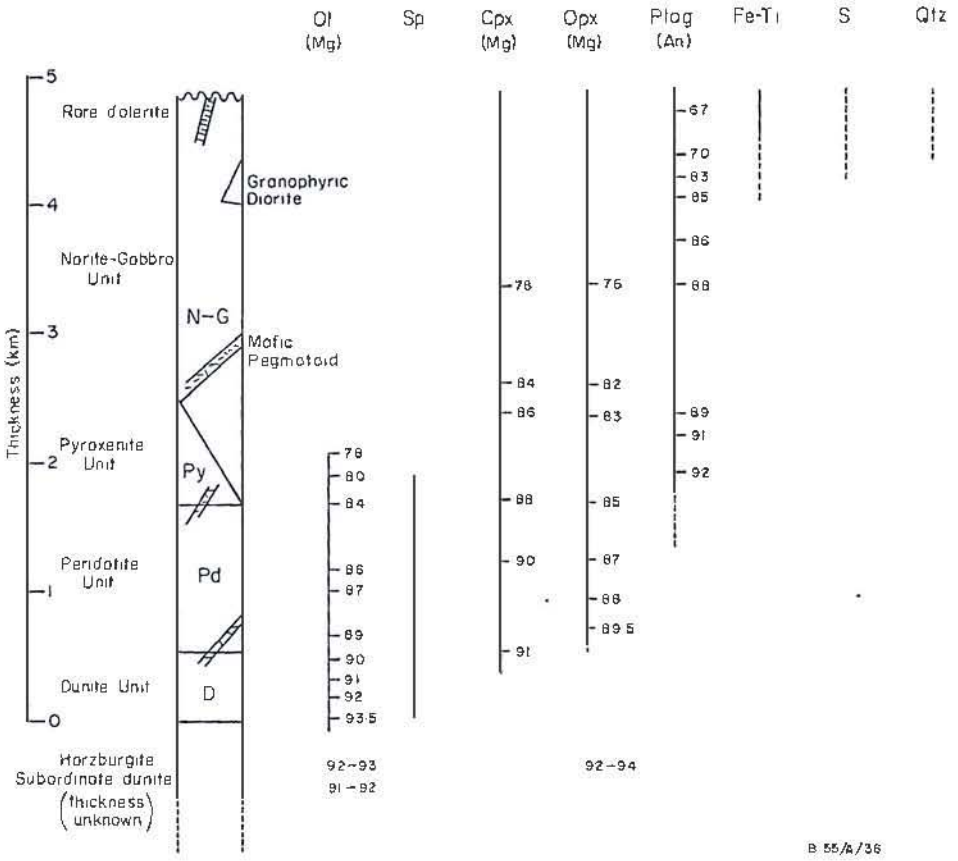

Fig. 1-14. Diagrammatic representation of the stratigraphy of the Marum layered sequence showing range of mineral compositions (schematic only). Solid lines indicate presence as a cumulus phase, dashed lines as postcumulus. Ol = olivine, Sp = spinel, Cpx = clinopyroxene, Opx = orthopyroxene, Plag = plagioclase, Fe-Ti = Fe-Ti oxides, S = sulphides, Qtz = quartz.

Fig. 1-15. Structures and textures in the cumulate sequence.

A. Fine-scale rhythmic layering of chromitite in dunite, tributary to Baia River, $5^{o}37'S$, $145^{o}15'E$.

B. Rhythmic layering of pyroxene-rich (dark) and pyroxene-poor (lighter) bands in norite-gabbro, tributary to Nep River, $5^{o}28'S$, $144^{o}53'E$. Note mineral-graded layering and small-scale sedimentary-type structures.

C. River boulder showing isomodal, rhythmic layering of olivine (dark) and plagioclase (light) in troctolite.

D. Streaky layering resembling flow-layering in norite-gabbro, Yomi River, $5^{o}33'S$, $145^{o}01'E$. Note extensive fracturing and secondary veining at high angle to layering in this outcrop.

E. Photomicrograph showing allotriomorphic granular-textured norite-gabbro. Note exsolution lamellae (orthopyroxene) in clinopyroxene host. Sample 010. Crossed polarizers, x 12.

F. Contact between two small cyclic units, marked 1 and 2, in tributary to Baia River, $5^{o}39'S$, $145^{o}15'E$. Rhythmically layered norite-gabbros (ng) of unit 1 are overlain by dunite (d) of unit 2 which passes upwards through wehrlite (w), lherzolite (l), plagioclase lherzolite (pl), and troctolitic norite-gabbro (t) to rhythmically layered norite-gabbro.

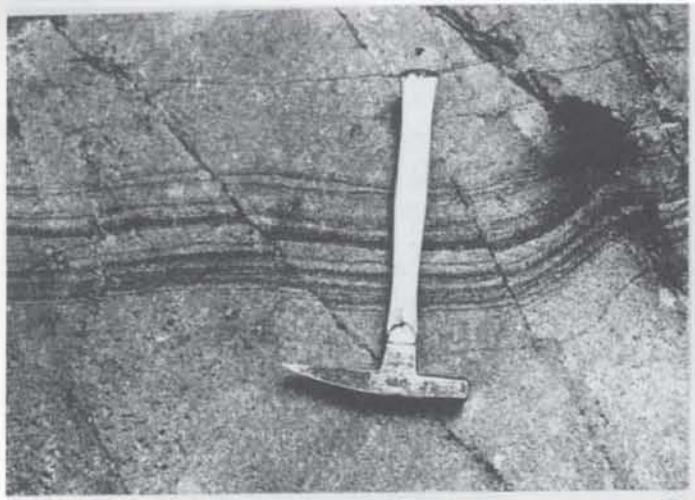

A

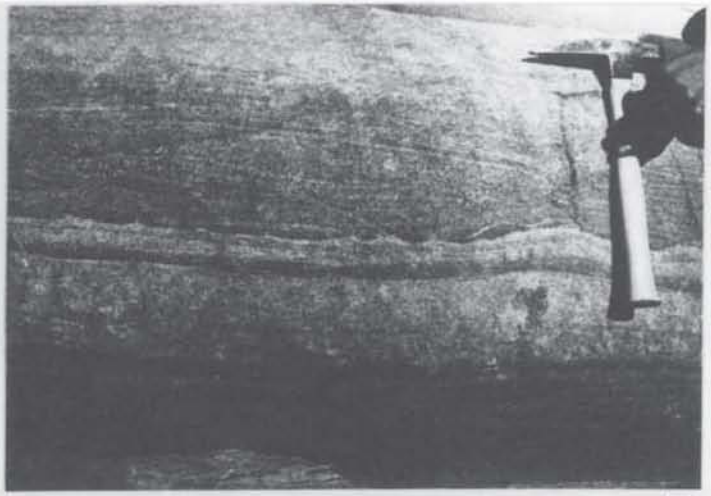

B

C

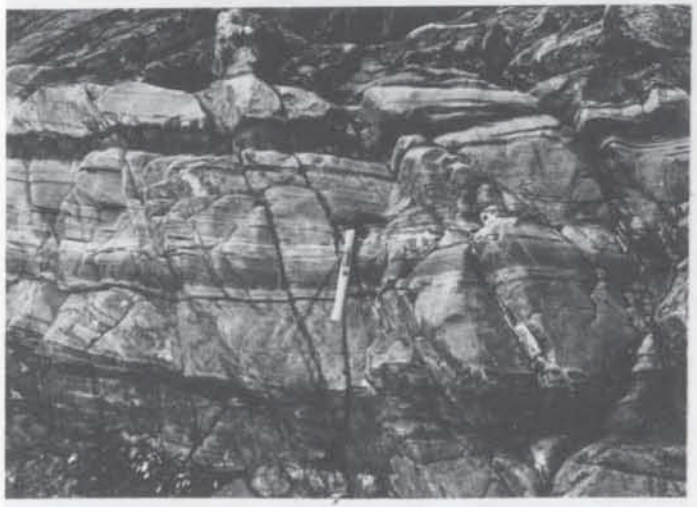

D

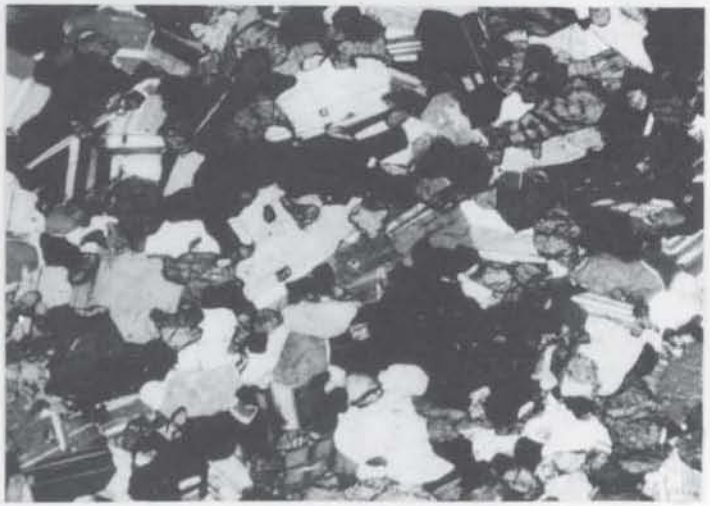

E

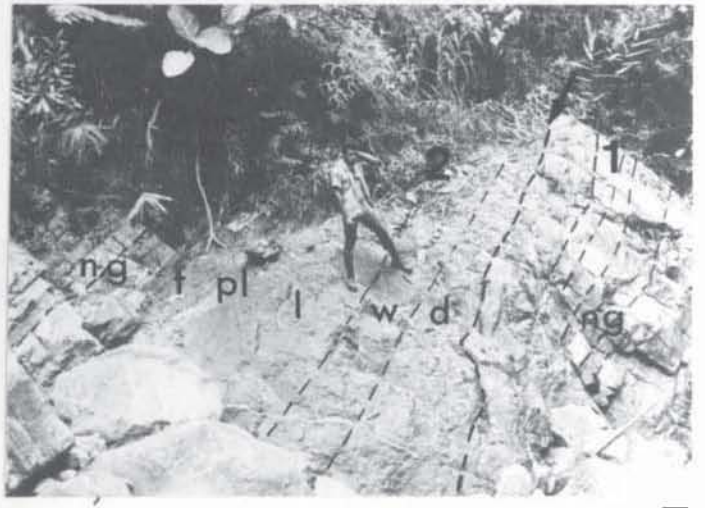

F

The dunite is an isomodal olivine adcumulate, consisting of xenoblastic olivine (Mg_{90-93}) 3-5 mm across and smaller allotriomorphic granular subgrains and neoblasts, and a small amount (1-5%) of subhedral to euhedral chrome spinel. Chromitite layers consist of coalesced chrome spinel grains, commonly partially rounded with interstitial olivine altered to serpentine and/or kammererite. Secondary magnetite rims chrome spinel grains in strongly serpentinized dunite and olivine chromitite.

Postcumulus poikilitic calcic pyroxene ($Mg_{48-50}Ca_{47-50}Fe_{1-3}$), is present in small amounts in the uppermost portion of the dunite unit (olivine Mg_{90}) enclosing olivine and spinel.

Peridotite unit (olivine, chrome spinel, clinopyroxene, orthopyroxene cumulate) - (Sample Nos. 186, 415, 189, 238, 502, 503, 168, 166, 271, 441, 203)

Layered olivine-pyroxene cumulates directly overlie the dunite, separated by a phase contact with the appearance of cumulus pyroxene. In most sections olivine-clinopyroxene cumulate (wehrlite) is overlain by lherzolite in which orthopyroxene (bronzite) is first a postcumulus and later a cumulus phase. Postcumulus bronzite commonly forms poikilitic grains up to 5 cm diameter enclosing resorbed and embayed cumulus olivine, and, to a lesser extent, cumulus clinopyroxene. In a number of outcrops the postcumulus bronzite grains are nearly spherical and have marked relief on weathered surfaces.

Plagioclase lherzolite i.e. olivine-clinopyroxene-orthopyroxene cumulate with postcumulus anorthitic plagioclase (An_{92-97}) occurs in the upper portion of the peridotite unit. The plagioclase commonly forms poikilitic plates enclosing, or aggregates of interstitial crystals between, subhedral to euhedral cumulus olivine and pyroxene.

Throughout the unit cumulate textures are well preserved and, except where a reaction relationship exists, cumulus phases are mostly subhedral to euhedral. Postcumulus material apparently formed by two means; 1) by crystallization from an intercumulus liquid (clinopyroxene, plagioclase); 2) by reaction of cumulus olivine with the intercumulus liquid (orthopyroxene and to a lesser extent clinopyroxene).

Pyroxenite unit (bronzite, augite ± olivine, plagioclase cumulate) - (Sample Nos. 051, 249, 264)

A unit of pyroxene-rich cumulates of variable thickness discontinuously overlies the cumulate peridotite: with increasing plagioclase content pyroxenite grades upwards into norite-gabbro. Two-pyroxene pyroxenite (websterite) predominates; olivine and plagioclase are additional cumulus phases. Pyroxenite is commonly interlayered with olivine-rich pyroxenite near the base of the unit and plagioclase-rich pyroxenite and gabbro near the top. Isomodal and mineral-graded layering, and rhythmic layering with layers 10-15 cms thick, is common; some show sedimentary-type structures such as load casts and slumping. The pyroxenite is mostly allotriomorphic granular in texture with a grainsize of about 1 mm.

Norite-gabbro unit (plagioclase, augite, bronzite ± olivine, magnetite, ilmenite cumulate) - (Sample Nos. 191, 225, 073, 1020, 008, 123, 163, 128, 148, 162, 131, 129)

The norite-gabbro unit, defined by the presence of cumulus plagioclase, has a phase contact with the peridotite and a transitional contact with the pyroxenite unit. The thickness of the unit probably exceeds 2.5 km. The lower portion is well layered with rhythmic isomodal and mineral-graded layers of pyroxene and plagioclase ± olivine ranging from several centimetres to more than a metre in thickness (Fig. 1-15B). Rhythmic pyroxene-rich layers (mostly websterite, some bronzite and clino-pyroxenite) are typically interlayered with plagioclase-rich layers

(leucogabbro and anorthosite) which become more abundant higher in the sequence.

Isomodal, and near-isomodal, olivine-rich layers (troctolite) are interlayered with plagioclase-rich layers (anorthosite) in some horizons forming fine-scale rhythmic layering (Fig. 1-15C). Lenticular bands, load-casts and slumped blocks of pyroxene-rich rocks into plagioclase-rich bands are relatively common. High in the norite-gabbro unit layering becomes streaky and lenticular (Fig. 1-15D), and resembles the 'flow layering' described by Thayer (1963, 1967) from alpine peridotite-gabbro complexes.

Magnetite and ilmenite occur as cumulus phases in the upper part of the unit commonly forming mineral-graded layers.

Textures in the norite-gabbro unit are mostly allotriomorphic granular (grainsize mostly $\leq$ 1 mm) with no interstitial material (Fig. 1-15E), suggesting extensive adcumulus growth and/or secondary recrystallization (see later). Cumulus textures are only poorly developed; in some norite-gabbro elongated plagioclase defines a weak lamination. Gabbros with streaky or flow-type layering have a marked foliation and some have a lineation in the plane of the foliation. Other gabbros have a marked tectonite fabric (see later).

Non-cumulus rocks

Granular microgabbro-dolerite. Fine-grained hypidiomorphic granular to subophitic quartz microgabbro and quartz dolerite occur in several localities in the upper part of the cumulate sequence. In at least two areas quartz dolerite occurs as narrow dykes discordant to the layering in norite-gabbro. Both the microgabbro and dolerite have undergone low temperature alteration; plagioclase is commonly albitized, Fe-Ti oxide altered to leucoxene and pyroxene partly uralitized.

Mafic pegmatite (Sample Nos. 150, 431, 543). Narrow (mostly 0.2-0.5 m) dykes and veins of very coarse grained (1-5 cm) mafic, iron-rich pegmatoid intrude all units of the cumulate sequence. Contacts between pegmatoid and ultramafic cumulates are sharp, and the pegmatoid dyke or vein is generally surrounded by a zone of serpentinization and Ca metasomatism. Some pegmatoids have a fluidal fabric at the margin and a coarser-grained, pegmatitic texture at the centre of the dyke or vein. In many cases crystals are orientated perpendicular to the margin of the dyke. Contacts with the norite-gabbro, particularly the upper levels of the unit, are commonly diffuse and gradational. The pegmatoids consist of calcic plagioclase (An_{92-96}, commonly altered to clinozoisite), hypersthene Mg_{60-65}, augite $Mg_{38-40}Ca_{40-46}Fe_{14-19}$ (commonly altered to actinolite $Ca_{26}Mg_{53}Fe_{21}$), and titanomagnetite or magnetite with 'exsolved' ilmenite.

Granophyric diorite (Sample No. 578). Minor granophyric-to pegmatitic-textured orthopyroxene-plagioclase-actinolitic hornblende-quartz-magnetite dykes and veins occur sporadically in the upper part of the norite-gabbro. Relations with the cumulate sequence are both concordant and discordant with contacts ranging from sharply intrusive to gradational. Although these rocks bear some similarities with the more mafic examples of the plagiogranite suite of other ophiolites (Coleman & Peterman, 1975) they are not end-stage differentiates and more likely result from filter pressing of trapped intercumulus liquid from the cumulate pile.

3-2. Primary structures

Cyclic units

Superimposed on the gross layering of the cumulate sequence (i.e. dunite - peridotite - pyroxenite - norite-gabbro) are at least three major cyclic units or macrocycles of crystallization (terminology of Campbell, 1977), and an undetermined number of smaller cyclic units (Fig. 1-15F). The cyclic units occur at all levels above the dunite unit and are essentially

conformable with thicknesses ranging from several hundred metres to about 10 metres. The crystallization sequence in each of the cyclic units is essentially the same, commencing with olivine cumulates at the base and passing upwards through pyroxene- to plagioclase-rich cumulates. Cyclic units are well documented in stratiform intrusions (e.g. Jackson, 1970; Irvine, 1970) and have also been recognized in other ophiolites (Jackson & others, 1975, Church & Riccio, 1977). Formation of cyclic units is generally believed to result from periodic influxes of fractionating batches of magma. However, the absence of truncated units or of disruption of underlying cycles suggests that if the Marum cyclic units result from influxes of magma, such influxes were only of small volume compared to the size of the magma chamber. Alternatively some of the smaller cyclic units might represent convective overturn in a magma chamber as suggested by Wager & Brown (1968).

Crystallization Sequence

The crystallization sequence both in the gross layering and in the cyclic units is: olivine (ol) + Cr spinel; ol + clinopyroxene (cpx) + Cr spinel; ol + cpx + orthopyroxene (opx) + Cr spinel; ol + opx + cpx + plagioclase (plag); plag + cpx + opx; plag + cpx + opx + Fe-Ti oxide ($\pm$ quartz). The crystallization interval ol + cpx : ol + cpx + opx is brief, and in at least one of the minor cyclic units is reversed. The main crystallization sequence is very similar to that deduced for the Troodos ophiolite by Greenbaum (1972), and to that found in the Papuan ophiolite except that in the latter it appears that orthopyroxene may have preceded clinopyroxene (Davies, 1971). The Marum cumulate sequence differs from that documented in a number of other ophiolites (cf. Church & Riccio, 1977; Jackson & others, 1975; Hopson & others, 1975 cited by Coleman, 1977) with respect to the relative order of appearance of clinopyroxene, orthopyroxene, and plagioclase.

Layering

Small-scale rhythmic layering is common throughout the cumulate sequence with individual layers ranging from 0.5 cm thick chromitite layers in dunite to pyroxene-rich and olivine-rich layers tens of centimetres thick in pyroxenite and norite-gabbro. Small-scale layering in the dunite unit consists of sparse, thin, mineral-graded and size-graded layers of chromitite. In the peridotite unit layering commonly consists of rhythmic, isomodal and mineral-graded layering with ratio contacts. Layering in the pyroxenite and norite-gabbro units consists of alternating conformable pyroxene-rich and plagioclase-rich layers. Thin mineral-graded, rhythmic layers of olivine-rich cumulates, some with sharp ratio or phase contacts, occur at the base of each unit. In the norite-gabbro unit small-scale layers may be either mineral-graded or isomodal. Contacts between some plagioclase-rich layers (anorthosite in places) and the overlying pyroxene-rich bands range from sharp ratio or phase contacts to graded contacts. Layered Fe-Ti oxide-bearing cumulates commonly show strong mineral and size-grading, and the top of the oxide layer commonly has a sharp ratio or phase contact with the overlying oxide-free norite-gabbro.

Additional depositional structures observed include slumping resulting in rocks resembling sedimentary-type breccia, load casts, settled blocks, scour structures, and, rarely, small angular unconformities.

Cumulus textures and igneous layering, together with many of the other features described above, are commonly ascribed to gravitational settling of crystals in a magma chamber (e.g. Wager & Brown, 1968). The prime role of gravitational settling in the differentiation of layered intrusions has recently been questioned. Campbell (1978) has shown that it is unlikely that plagioclase will sink in Fe-rich tholeiitic liquids and has suggested that features such as small-scale rhythmic layering result from *in situ* rhythmic crystallization from a super-cooled liquid at the

floor of the magma chamber. Maaloe (1978) has also proposed that rhythmic layering is due to rhythmic nucleation in a slightly supersaturated magma where crystallization of one primocryst phase in turn modifies the magma composition and influences the nucleation rates of other primocrysts. McBirney & Noyes (in press), in a recent detailed review of crystallization and layering of the Skaergaard Intrusion, have also rejected gravitational settling as the prime agent of differentiation in favour of *in situ* nucleation and crystallization in a static boundary layer that was normally outside a zone in which the magma moved by laminar flow. They ascribe layering to an oscillatory process dependent on relative rates of thermal and chemical diffusion. Irvine (1978), on the other hand, has suggested from experiments involving flow structure that layer formation may be due to current deposition.

While many of the primary structures of the Marum ophiolite, particularly those in the lower part of the sequence, are not inconsistent with an origin by gravity settling, the thick sequence of rhythmically layered gabbros is probably best explained by *in situ* rhythmic crystallization. The extent to which magmatic current activity influenced differentiation is not known: the presence of magmatic currents in some parts of the Marum cumulate succession is suggested by strong igneous lamination in some feldspar-rich cumulates, and by the local disruption and scouring of individual layers by succeeding horizons. It would appear that the primary small-scale structures in the Marum sequence are best explained by a combination of all three mechanisms, gravity settling, rhythmic nucleation and, to a lesser extent, magmatic currents.

3-3. Secondary deformation

Superimposed on the primary textures is a variable but mostly weak metamorphic fabric. Almost all rocks show some evidence of secondary recrystallization, and most gabbros and pyroxenites have been recrystal-

lized to equigranular granoblastic textures. Many of the dunites have a weak foliation defined by a preferred orientation of olivine grains which commonly show undulose extinction and kink-banding. Olivine grains in more strongly deformed dunite commonly have a preferred orientation which defines a weak foliation and lineation; this preferred orientation locally reflects that of former large olivine grains. The size of the neoblasts and subgrains suggest extensive recrystallization under low pressure, possibly only several hundred bars (A. Nicolas, pers. comm. 1977). Some transitional dunites show two phases of deformation; a high temperature phase characterized by slow strain rates overprinted by a low temperature, fast strain rate deformation which is presumed to be related to emplacement of the ophiolite (P. Chopra, pers. comm. 1979).

In layered pyroxenites, norite-gabbros and gabbros a weak foliation, approximately parallel to the primary layering, has resulted in a streaky foliation, commonly with boudins of pyroxenite. This layering closely resembles the flow layering described by Thayer (1969), and is interpreted as resulting from high temperature deformation involving flow of the cumulate pile.

Despite their well developed layering the bulk of the pyroxenites and norite-gabbros have a granoblastic texture and cumulus textures have commonly been obliterated.

Adcumulus textures resembling those of high grade granulites are not uncommon in layered basic intrusions (e.g. Jackson, 1961; Weedon, 1965; Cameron, 1969; Vernon, 1970) and are commonly ascribed to post-cumulus addition of intercumulus material involving diffusion of elements between the intercumulus liquid and the overlying magma (Hess, 1960; Wager & Brown, 1968). The extremely low abundances of incompatible elements in the Marum cumulates (Chapter 4) requires continued pore connection and extremely efficient diffusion throughout the layered sequence for this mechanism to be a viable means of producing the granoblastic textures in

the Marum sequence. This seems unlikely and an alternative explanation, sintering of the cumulus phases in the solid state and expulsion of the interstitial liquid (Voll, 1960; Vernon, 1970), is preferred. In this process, essentially static annealing, the grains would grow together under the influence of interfacial free energy, and annealing would occur by diffusion at grain boundaries. Heat required for this process would be provided by the slow cooling of the thick cumulate pile, periodic injections of fresh magma, and possibly, from subjacent mantle diapirism and partial melting.

In several localities small mesoscopic folds (amplitude less than 50 cms) are developed in layered norite-gabbro and gabbro. *Flaser gabbro* formed in the folded rocks passes directly into streaky gabbro with lenticular flow-layering and then into regularly layered gabbro. The flaser gabbro has a gneissic texture with augen of plagioclase in a recrystallized matrix of plagioclase, pyroxene, and commonly, magnetite, ilmenite and quartz. Foliation in the tectonite gabbro is generally parallel to the primary layering suggesting stress and flow in the plane of the primary layering.

More strongly tectonized gabbro - *mylonite gabbro* - has a well developed mortar texture and the same anhydrous mineral assemblage, commonly with strained quartz, feldspar or pyroxene porphyroclasts in a granulated matrix. These features are indicative of high temperature anhydrous cataclasis.

It is concluded that while mesoscopic and macroscopic primary features, e.g. rhythmic layering, are preserved, the development of secondary textures and structures (including flow layering) indicate extensive subsolidus recrystallization under anhydrous conditions at high temperatures. Superimposed on the subsolidus recrystallization is a weak, sporadically developed low grade (greenschist) metamorphism which has resulted in incipient saussuritization of feldspar, uralitization of

pyroxene, and serpentinization of olivine.

3-4. Mineral Chemistry

Approximately 2500 complete mineral analyses from some 50 representative rock samples from the cumulate sequence were obtained by energy dispersive TPD electron microprobe. Selected bulk pyroxene analyses (host plus lamellae) were obtained by rapid, reduced-area scans (100-250μ) using a JEOL JX 50A microprobe-scanning electron microscope with EDAX energy dispersive system (Appendix 1). Representative analyses of phases are presented in Tables 1-8 to 1-16, and sample descriptions and localities given in Appendix 2. Unless otherwise stated all iron is reported as FeO.

Olivine

Olivine compositions (Table 1-8) vary with lithology and range from Mg_{97} in olivine chromitite to Mg_{78} in olivine-bearing norite-gabbro (Fig. 1-14). Compositions are mostly homogeneous ($\pm$ 1 mol. %) although some grains, particularly within olivine chromitite, show reverse zoning of 2 to 3 mol. %. Olivine compositions in the dunite unit lie in the range $Mg_{90-93.5}$ and average $Mg_{91.5}$. The most magnesian olivine $Mg_{96.8}$ is likely to reflect subsolidus re-equilibration within the olivine chromitite rather than a primary liquidus composition since Irvine (1965, 1967) has shown that not only is the Fe-Mg partitioning between olivine and chrome spinel dependent on temperature (the Fe/Mg ratio of olivine decreases while that of chrome spinel increases with falling temperature), but the final composition of olivine and spinel depends upon their modal proportions in the rock as well as the original compositions. The most magnesian primary cumulus olivine composition in the dunite unit is Mg_{92} but more magnesian olivine, $Mg_{93.5}$, occurs in dunite transitional to tectonite peridotite. These compositions are more magnesian than olivine from the base of cumulate stratiform intrusions such as the Bushveld and Stillwater intrusions (cf. Wager & Brown, 1968) but similar to olivine in basal

TABLE 1-8. REPRESENTATIVE ANALYSES OF CUMULUS OLIVINE

	DUNITE								PERIDOTITE								GABBRO				
	221[1]	497[1]	567	421	1046	428	504[2]	059[2]	209	186	415	180	592	271	238	166	191	051	073	225	162
SiO_2	41.76	41.22	41.30	41.13	40.88	40.81	40.67	40.44	40.67	40.52	40.27	39.77	40.15	39.95	39.69	39.34	40.06	39.63	38.85	38.69	38.39
FeO	4.49	5.75	6.51	7.92	8.72	9.09	9.59	9.72	9.93	10.57	11.85	11.76	13.08	12.97	13.19	15.22	13.55	15.74	19.23	19.23	19.90
MnO	<0.09	<0.09	<0.09	<0.09	<0.09	<0.09	<0.09	<0.09	<0.09	<0.09	<0.09	0.11	<0.09	0.13	<0.09	<0.09	<0.09	<0.09	0.21	0.14	0.21
MgO	53.72	52.65	52.24	50.95	50.57	50.01	50.04	49.40	49.16	48.70	47.89	47.70	47.32	47.08	46.91	45.08	46.68	45.03	41.88	41.75	41.25
Total	99.97	99.62	100.05	100.49	100.17	99.91	100.30	99.56	99.76	99.79	100.01	99.34	100.55	100.13	99.90	99.64	100.29	100.40	100.18	99.81	99.75
									Cations on the basis of 4 oxygens												
Si	0.998	0.995	0.996	0.998	0.994	0.997	0.992	0.995	0.999	0.998	0.995	0.991	0.993	0.992	0.992	0.992	0.995	0.994	0.994	0.993	0.990
Fe	0.090	0.116	0.131	0.161	0.178	0.186	0.196	0.200	0.204	0.218	0.245	0.245	0.271	0.270	0.275	0.321	0.281	0.330	0.412	0.413	0.429
Mn	-	-	-	-	-	-	-	-	-	-	-	0.002	-	0.003	-	-	-	-	0.005	0.003	0.005
Mg	1.914	1.894	1.877	1.843	1.834	1.821	1.820	1.811	1.799	1.787	1.764	1.771	1.744	1.743	1.742	1.695	1.728	1.683	1.597	1.598	1.586
Total	3.002	3.005	3.004	3.002	3.006	3.003	3.008	3.005	3.001	3.002	3.005	3.009	3.007	3.008	3.008	3.008	3.005	3.007	3.006	3.007	3.010
100 Mg/Mg+Fe	95.5	94.2	93.5	92.0	91.2	90.7	90.3	90.1	89.8	89.2	87.8	87.8	86.6	86.6	86.4	84.1	86.0	83.6	79.5	79.5	78.7
Ni ppm	2500		2490	3540		1960			2200	2530	1940	1570	2560	2100	1200	1930	1090	1360			

All CaO, Al_2O_3 and TiO_2 contents <0.07%

1. Olivine in chromitite layer

2. Rock contains poikilitic clinopyroxene

cumulates from other ophiolites (e.g. England & Davies, 1973; Jackson & others, 1975; Irvine & Findlay, 1972; Church & Riccio, 1977; Malpas, 1978).

The cumulus olivine compositions overlap those from the non-cumulus peridotite which lie in the range $Mg_{91.6-93.8}$ (Chapter 2). The overlap in the Marum olivine compositions contrasts with the Papuan ophiolite in which England & Davies (1973) found a compositional hiatus between cumulus and non-cumulus olivine.

Olivine in cumulus peridotite overlying the dunite unit ranges from $Mg_{89.8}$ to $Mg_{83.5}$ and are thus more iron-rich than olivine in the dunite unit. Olivine in dunite horizons at the base of cyclic units are of similar composition to the most magnesian olivine at the base of the peridotite unit ($Mg_{89-89.5}$) and also more iron-rich than olivine in the dunite unit. Olivine in olivine pyroxenite, troctolite and olivine norite-gabbro is more iron-rich, of smaller grainsize and strongly embayed or resorbed indicating extensive olivine-liquid reaction.

Minor element concentrations are low. CaO contents are all less than 0.07%, typical of olivine equilibrated at low temperature. MnO content increases with Fa component from less than 0.09% to 0.2% (Table 1-8). Ni concentrations range from about 3500 ppm in Fo-rich olivine in the dunite unit to about 2000 ppm in the peridotite unit to about 1000 ppm in olivine norite-gabbro. This overall progressive decrease in Ni content with increasing Fa content of olivine is typical of fractional crystallization occurring in stratiform intrusions. In detail however Ni contents do not decrease regularly with Fa content of olivine, and olivines of similar Mg from different levels in the sequence commonly have different Ni contents.

The most iron-rich olivine $Mg_{78.5}$, from an olivine-bearing norite-gabbro, is replaced or partially replaced by orthopyroxene-magnetite symplectites in which magnetite forms intricate patterns. Cumulus olivine

in this rock lies in the range $Mg_{78.5-80}$ and cumulus orthopyroxene $Mg_{77.6-80.0}$. Orthopyroxene in the symplectite is slightly more magnesian, $Mg_{80.9}$, and in equilibrium with the symplectite olivine, $Mg_{80.0}$. The co-existing magnetite is characterized by a high Fe_2O_3 content. The textural evidence strongly suggests that the replacement of olivine by orthopyroxene-magnetite symplectites occurred as a result of olivine-liquid reaction rather than by subsolidus oxidation as suggested by Goode (1974). The small difference in composition between cumulus and symplectite orthopyroxene also argues against an oxidation origin since orthopyroxene produced by oxidation should be more magnesian due to oxidation of the Fa molecule of the cumulus olivine. Moreover the occurrence of intercumulus magnetite indicates that the intercumulus liquid was capable of crystallizing both orthopyroxene (inferred from the adcumulate texture) and magnetite of similar composition to the symplectite phases. The preferred explanation of the symplectite is that it is a eutectic-like texture due to simultaneous crystallization of orthopyroxene and magnetite as a result of reaction of cumulus olivine with a silica and iron (including Fe^{3+}) enriched intercumulus liquid.

Chrome Spinel

Chrome spinel is a minor cumulus phase comprising about 1-3 vol. % in the dunite and peridotite units. Discrete chromitite layers, mostly 0.5-2.5 cms thick, are restricted to the lower sections of the dunite unit; elsewhere chrome spinel is present as a disseminated accessory.

Textural relations indicate that olivine and spinel were co-liquidus phases. Grainsize decreases with stratigraphic height, and with decreasing 100Mg/(Mg + Fe) ratio of both the bulk rock and co-existing olivine within the cumulate sequence. Grainsize decreases from 0.5-1.5 mm diameter in chromitite layers to 250-500 μ for disseminated spinel in dunite, to less than 250 μ (commonly less than 100 μ) in spinel-bearing peridotite. The decrease in grainsize probably reflects a decreasing Cr

TABLE 1-9. REPRESENTATIVE ANALYSES OF CUMULUS CHROME SPINEL

	DUNITE									PERIDOTITE									
Sample No.	567	059	221*	421	092	497*	428	504	1066	415	186	189	238	271	203	441	166	168	107
TiO_2	<0.07	<0.07	0.14	<0.07	<0.07	0.13	<0.07	0.19	0.15	0.34	0.44	0.41	0.21	0.31	0.42	0.41	0.27	0.25	0.47
Al_2O_3	5.95	7.45	8.52	9.21	9.87	10.29	11.75	12.89	21.21	14.56	17.93	16.52	18.20	22.34	23.08	24.49	24.65	23.21	9.50
Cr_2O_3	63.31	58.62	60.66	58.85	57.95	59.55	52.75	48.03	41.00	46.52	41.65	37.42	36.10	35.78	32.27	34.28	33.17	34.38	36.33
Fe_2O_3	3.16	4.59	4.15	3.87	3.64	3.79	6.39	9.61	8.69	8.46	9.90	15.38	15.09	10.61	13.24	10.00	11.37	10.69	22.72
FeO	16.08	21.13	14.35	18.17	18.26	13.92	20.97	21.31	17.21	23.00	21.19	23.49	23.66	23.73	23.53	22.28	21.60	23.18	29.12
MnO	0.36	<0.09	<0.09	0.25	<0.09	<0.09	<0.09	0.66	<0.09	0.24	0.53	0.34	0.60	<0.09	0.73	<0.09	0.58	0.38	0.50
MgO	10.62	7.72	12.32	9.83	9.94	12.87	8.45	7.90	12.10	7.23	8.48	7.01	6.93	7.69	7.53	8.83	8.94	7.66	2.56
CaO	0.15	0.11	0.20	0.07	<0.07	0.24	0.07	0.11	0.14	0.07	0.13	0.12	0.11	0.11	<0.07	0.10	0.15	0.26	0.09
Total	99.63	99.62	100.34	100.25	99.68	100.79	100.38	100.70	100.50	100.42	100.25	100.35	100.90	100.57	100.80	100.39	100.73	100.02	101.29
										Cations on the basis of 4 oxygens									
Ti	-	-	0.003	-	-	0.003	-	0.005	0.004	0.009	0.011	0.010	0.005	0.008	0.010	0.009	0.007	0.006	0.012
Al	0.236	0.300	0.328	0.361	0.388	0.391	0.459	0.502	0.780	0.566	0.683	0.639	0.697	0.838	0.864	0.905	0.907	0.872	0.390
Cr	1.684	1.582	1.568	1.543	1.522	1.515	1.382	1.254	1.012	1.214	1.065	0.971	0.929	0.900	0.810	0.850	0.819	0.866	1.081
Fe^{3+}	0.080	0.118	0.102	0.096	0.091	0.092	0.159	0.239	0.204	0.210	0.241	0.380	0.369	0.254	0.316	0.236	0.267	0.256	0.596
Fe^{2+}	0.452	0.603	0.392	0.504	0.507	0.375	0.580	0.589	0.434	0.635	0.573	0.643	0.643	0.632	0.625	0.584	0.564	0.617	0.849
Mn	0.010	-	-	0.007	-	-	-	0.018	-	0.007	0.015	0.010	0.017	-	0.019	-	0.015	0.011	0.015
Mg	0.533	0.393	0.600	0.486	0.492	0.617	0.417	0.389	0.562	0.356	0.408	0.343	0.336	0.364	0.356	0.413	0.416	0.363	0.133
Ca	0.006	0.004	0.007	0.003	-	0.007	0.003	0.004	0.005	0.003	0.004	0.004	0.004	0.004	-	0.003	0.005	0.009	0.004
100 $Mg/(Mg+Fe^{2+})$	54.1	39.4	60.5	49.1	49.3	62.2	42.0	39.8	56.4	35.9	41.6	34.8	34.3	36.6	36.3	41.4	42.4	37.0	13.5
$Cr/(Cr+Al)$	0.877	0.841	0.827	0.811	0.797	0.795	0.751	0.714	0.565	0.682	0.609	0.603	0.571	0.518	0.484	0.484	0.475	0.498	0.720
$Cr/(Cr+Al+Fe^{3+})$	0.842	0.791	0.785	0.771	0.761	0.785	0.691	0.629	0.507	0.610	0.533	0.488	0.466	0.452	0.407	0.427	0.411	0.434	0.504
$Al/(Cr+Al+Fe^{3+})$	0.118	0.150	0.164	0.180	0.194	0.196	0.230	0.251	0.391	0.284	0.346	0.321	0.349	0.421	0.434	0.454	0.455	0.437	0.196
$Fe^{3+}/(Cr+Al+Fe^{3+})$	0.040	0.059	0.051	0.048	0.045	0.046	0.079	0.120	0.102	0.106	0.121	0.191	0.185	0.127	0.159	0.119	0.134	0.129	0.300
Co-existing olivine (Mg)	93.5	90.0	95.0	92.0	93.3	96.0	90.6	90.3	91.2	87.9	89.2	87.8	86.4	86.7	86.4	84.4	83.6	84.3	-

Fe determined as FeO; Fe^{3+} and Fe_2O_3 calculated from ideal $R^{2+}O.R_2^{3+}O_3$ spinel formula

* Chromitite

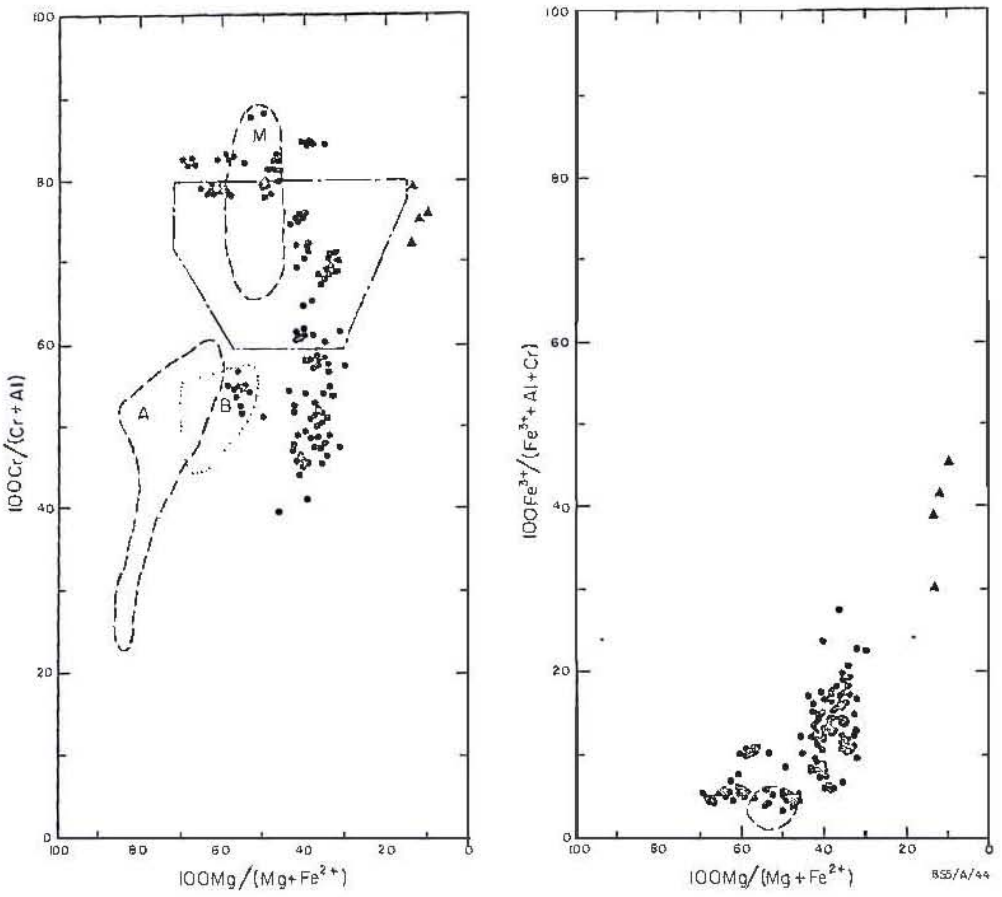

Fig. 1-16. Compositional variation of Marum cumulus spinels in terms of $100Cr/(Cr+Al)$ and $100Fe^{3+}/(Fe^{3+}+Al+Cr)$ versus $100Mg/(Mg+Fe^{2+})$ compared to spinel from Marum harzburgites (dashed line, M), stratiform intrusions (long dashes, dots) after Irvine & Findlay (1972), and spinels from Mid-Atlantic Ridge basalts. A = MAR (Sigurdsson & Schilling, 1976) B = FAMOUS basalts (Dick, 1979). Triangles are for orthopyroxenite sample 107.

content in the liquid and, correspondingly, an increasingly large liquid/spinel volume ratio required for crystallization due to the very high partition coefficient (D), equal to (Cr in spinel)/(Cr in liquid).

The cumulus spinels show a much wider range in composition than those from the underlying non-cumulate harzburgite. Representative analyses are given in Table 1-9, and the data plotted in Figure 1-16. Early formed spinels are highly Cr-rich (picrochromite) containing 62-64% Cr_2O_3 with $Cr/(Cr + Al + Fe^{3+})$ ratios of 0.80-0.84 and $100Mg/(Mg + Fe^{2+})$ ratios of 60, and overlap the non-cumulus spinel compositions. $Fe^{3+}/(Fe^{3+} + Al + Cr)$ ratios in these spinels are low - 0.05 or less - and Ti and Ca contents are also low. Spinel at the top of the dunite unit is less chrome-rich, with $Cr/(Cr + Al + Fe^{3+})$ ratios $\sim$ 0.65 and $100Mg/(Mg + Fe^{2+})$ ratios of 40-45. The $100Mg/(Mg + Fe^{2+})$ and $Cr/(Cr + Al + Fe^{3+})$ ratios show a sympathetic decrease in the overlying cumulate peridotite to approximately 30-35, and 0.40 respectively. The most aluminous spinels have $Cr/(Cr + Al + Fe^{3+})$ ratios $\sim$ 0.3 - 0.4 ($Al/(Cr + Al + Fe^{3+})$ = 0.5 - 0.6), and occur as small (25 μ) disseminated grains in a lherzolite containing olivine Mg_{84}.

$Fe^{3+}/(Fe^{3+} + Al + Cr)$ ratios increase during fractionation as shown by the trend from the Cr apex to the $Al-Fe^{3+}$ join on the ternary trivalent ion plot (Fig. 1-17). The most Al-rich spinels have $Fe^{3+}/(Fe^{3+} + Al + Cr)$ ratios $\sim$ 0.16. Small (<50μ) Fe-rich spinels, ferrochromite ($100Mg/Mg + Fe^{2+}$ = 10-14), from a bronzite cumulate, have a higher $Fe^{3+}/(Fe^{3+} + Al + Cr)$ ratio and lie displaced from the cumulate trend suggesting higher P_{O_2} conditions than the main series. The chrome-rich nature of these spinels probably results from $Fe^{3+} - Al^{3+}$ substitution rather than Fe^{3+} - Cr substitution, due to the large octahedral site preference energy of Cr^{3+}. The trend to Al and Fe^{3+} enrichment of spinel with stratigraphic height shown by the cumulate ultramafics contrasts with that of the tectonite harzburgites which show no increase in Fe^{3+} (Fig. 1-17 Chapter 2).

Spinels from the Marum ophiolite show a much greater range in Cr-Al substitution than spinels from most stratiform intrusions, as shown in Figure 1-16. Cessation of spinel crystallization in stratiform intrusions is generally believed to be due to the peritectic reaction between chrome spinel and pyroxene (Irvine, 1967), however in the Marum ophiolite spinel and pyroxene co-exist over a short interval. The high Cr_2O_3 content of early crystallizing cumulus clinopyroxene in the Marum sequence ($\sim$ 1%) necessitates rapid depletion of Cr in the magma due to the high partition coefficient (Cr in clinopyroxene/Cr in liquid). Chrome spinel co-existing with cumulus clinopyroxene is markedly more Al-rich and of much smaller grainsize than spinel co-existing with dunite. The presence of spinel in olivine-pyroxene cumulates (some containing postcumulus plagioclase) but absence of spinel-plagioclase cumulates suggests that cessation of spinel crystallization might ultimately have been due to the peritectic reaction which exists between plagioclase, and olivine and spinel (Osborn & Tait, 1952). However, as pointed out by Irvine (1967), this relationship could only be expected to terminate precipitation of Cr-rich spinel in situations where it was forming in only very small amounts; the small volume and very small grainsize of the spinel in the uppermost cumulate peridotites in the Marum appear consistent with this requirement.

Spinels from the Marum cumulate sequence range to more Cr-rich compositions than spinels from presently sampled ocean floor peridotites and gabbros (e.g. Hodges & Papike, 1976; Sigurdsson, 1976; Prinz & others, 1976; Dick & Bryan, 1979; Sinton, 1979) and ocean floor basalts (Sigurdsson & Schilling, 1976; Dick, 1979; Frey & others, 1974; Donaldson & Brown, 1977). In addition the Marum spinels are more iron-rich than spinels with similar Cr/(Cr + Al) ratios from peridotites and basalts from the Mid-Atlantic Ridge (Fig. 1-16), probably reflecting a greater degree of subsolidus re-equilibration. The available data for cumulus spinel in ophiolites show both Cr-Al and Cr-Fe variation (Menzies, 1975). Menzies (1975) suggested

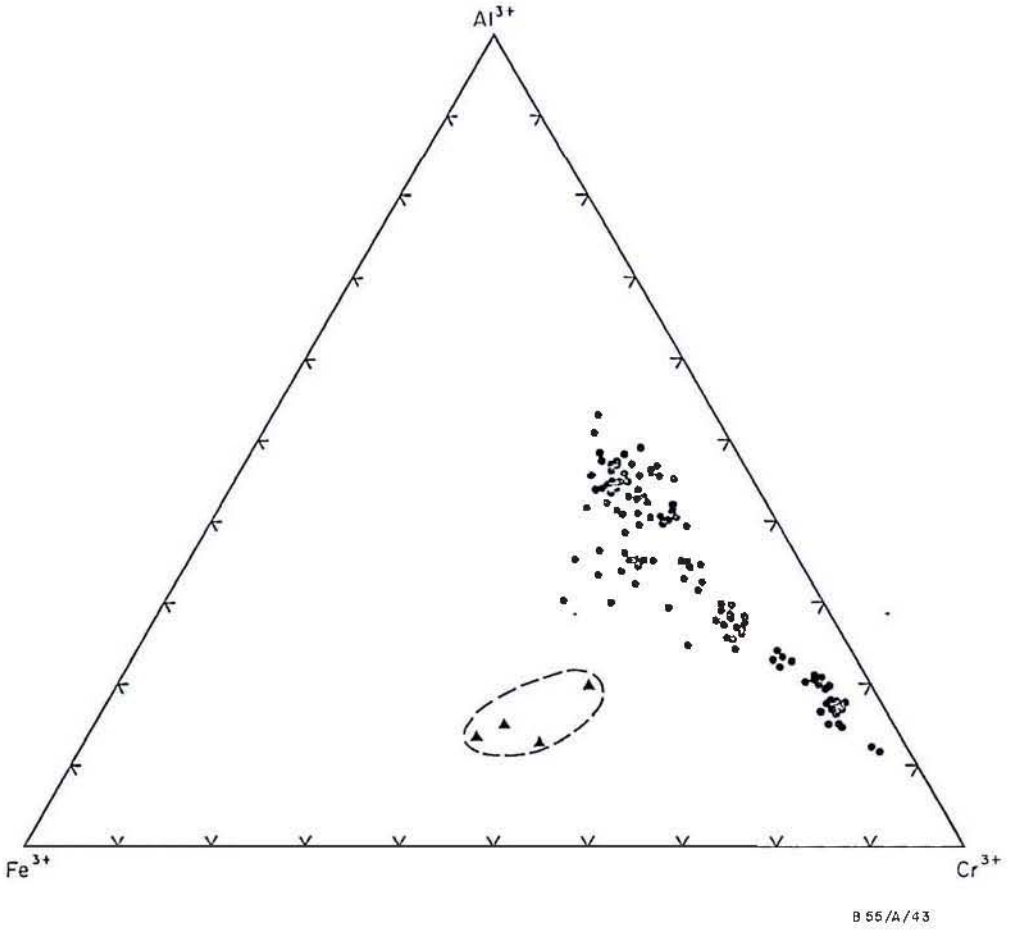

Fig. 1-17. Ternary plot showing variation in trivalent cations of spinel from Marum cumulates. Note the Fe^{3+}-rich spinels of orthopyroxene sample 107 (triangles).

that the variation in cumulus spinel compositions from the Othris ophiolite resulted from reaction with co-existing silicates (Cr-Al) or intercumulus liquid (Cr-Fe). It would seem however by comparison with the Marum spinels that the Cr-Al variation could equally be caused by fractionation of pyroxene.

Pyroxenes

Pyroxene is a cumulus phase in the sequence above the dunite unit. Pyroxene compositions from the cumulate rocks form two series: a *primary solidus* or high temperature crystallization trend, and a *subsolidus* trend where clinopyroxenes lie on the calcic side of the solidus and orthopyroxenes are less calcic than solidus orthopyroxene. Most pyroxene compositions lie between the solidus and subsolidus trends indicating progressive re-equilibration at lower temperatures.

Microprobe analyses of solidus pyroxenes are given in Tables 1-10 and 1-11, and of co-existing subsolidus pairs in Table 1-12. The Al_2O_3 contents of both solidus and subsolidus pyroxenes are low and typical of tholeiitic pyroxenes which have crystallized at crustal levels (e.g. Brown, 1967). Contents of TiO_2 and Na_2O are particularly low, comparable with those of pyroxenes in other ophiolites (e.g. Church & Coish, 1976; PART 2 Chapter 2) and ocean-floor peridotite and gabbro (e.g. Hodges & Papike, 1976). Cumulus orthopyroxene is compositionally distinct from non-cumulus orthopyroxene: the most magnesian cumulus orthopyroxene is $Mg_{89.5}$ and more iron rich than the tectonite enstatites, $Mg_{92.2-94.5}$ which also have much lower Al_2O_3 and CaO contents (Chapter 2).

Primary low calcium pyroxenes in the peridotite and norite-gabbro units are of the Bushveld-type. Exsolution lamellae (100) of calcic pyroxene are generally thin or diffuse, and, in re-equilibrated grains, absent. No inverted low-calcium pyroxenes of the pigeonite series were found. Point analyses of relic primary hosts and bulk pyroxene (host plus lamellae) analyses obtained by rapid reduced-area scanning partially define a high temperature solidus trend with approximately 4 mol % Wo (Fig. 1-18).

TABLE 1-10. REPRESENTATIVE ANALYSES OF PRIMARY ORTHOPYROXENE

Sample	PERIDOTITE 186	415	238	502	166	503	GABBRO 051	191	174	073	1020
SiO_2	55.62	56.11	56.06	55.14	54.82	53.69	56.09	55.03	55.66	54.83	54.42
Al_2O_3	1.37	1.22	1.17	2.66	2.14	2.85	0.48	1.98	1.07	1.47	1.24
Cr_2O_3	0.46	0.45	0.58	0.60	0.51	0.61	0.13	0.11	0.08	<0.07	0.22
FeO	6.79	7.67	8.38	8.12	9.53	9.40	10.13	9.88	11.29	11.34	15.72
MnO	<0.09	<0.09	<0.09	<0.09	<0.09	<0.09	0.12	<0.09	0.18	0.20	0.21
MgO	32.65	32.74	31.62	30.74	30.42	29.85	31.88	30.76	30.20	28.95	27.30
CaO	1.78	1.46	2.42	2.36	2.53	2.15	1.42	1.69	2.14	2.24	1.37
Total	98.67	99.65	100.23	99.62	99.95	98.55	100.25	99.45	100.62	99.03	100.48
	Cations on the basis of 6 oxygens										
Si	1.958	1.961	1.960	1.937	1.935	1.920	1.972	1.947	1.962	1.965	1.958
Al^{IV}	0.042	0.039	0.040	0.063	0.065	0.080	0.020	0.053	0.038	0.035	0.042
Al^{VI}	0.015	0.011	0.008	0.047	0.024	0.040	-	0.030	0.006	0.027	0.011
Cr	0.013	0.012	0.016	0.017	0.014	0.017	0.004	0.003	0.002	-	0.006
Fe	0.200	0.224	0.245	0.239	0.281	0.281	0.298	0.292	0.333	0.340	0.473
Mn	-	-	-	-	-	-	0.004	-	0.005	0.006	0.006
Mg	1.713	1.705	1.647	1.609	1.599	1.591	1.665	1.622	1.586	1.546	1.464
Ca	0.067	0.055	0.091	0.089	0.096	0.082	0.054	0.064	0.081	0.086	0.053
Total	4.007	4.008	4.008	4.000	4.014	4.011	4.016	4.010	4.014	4.004	4.013
Ca	3.4	2.8	4.5	4.6	4.8	4.2	2.7	3.2	4.1	4.4	2.7
Mg	86.5	85.9	83.1	83.1	80.9	81.4	82.5	82.0	79.3	78.4	73.6
Fe	10.1	11.3	12.4	12.3	14.2	14.4	14.8	14.8	16.6	17.2	23.7
100 Mg/Mg+Fe	89.5	88.4	87.1	87.1	85.1	85.0	84.8	84.7	82.7	82.0	75.6

All TiO_2 <0.07%, Na_2O <0.20%.

TABLE 1-11. REPRESENTATIVE ANALYSES OF PRIMARY CLINOPYROXENE

Sample No.	PERIDOTITE										GABBRO					
	059*	209	186	415	238	502	180	166	271	503	191	051	174	073	264	1020
SiO_2	54.46	52.55	53.16	53.01	53.14	52.58	54.36	53.80	53.01	52.15	52.66	54.57	52.45	53.05	52.77	52.72
TiO_2	<0.07	<0.07	<0.07	<0.07	<0.07	<0.07	<0.07	<0.07	<0.07	<0.07	<0.07	<0.07	0.13	<0.07	<0.07	0.13
Al_2O_3	0.16	2.62	2.54	2.33	1.46	3.23	1.51	2.18	2.15	3.94	2.22	0.61	2.64	2.64	1.79	2.55
Cr_2O_3	0.80	0.89	0.85	1.35	0.95	0.87	0.64	0.94	1.05	1.10	0.43	0.41	0.26	0.32	0.30	0.27
FeO	1.40	2.79	3.29	3.39	3.62	3.70	3.93	3.94	4.44	4.68	4.41	4.85	5.67	5.96	7.96	9.25
MnO	<0.09	<0.09	<0.09	<0.09	<0.09	<0.09	<0.09	<0.09	<0.09	<0.09	<0.09	<0.09	<0.09	<0.09	0.10	0.10
MgO	17.35	18.12	19.40	18.23	19.18	19.21	19.62	18.40	18.79	17.90	18.77	19.66	18.78	17.95	17.99	18.62
CaO	24.84	22.10	20.56	21.29	20.77	19.91	20.45	20.92	20.49	20.30	20.23	20.11	18.72	20.06	18.91	16.96
Total	99.00	99.07	99.80	99.57	99.12	99.50	100.51	100.18	99.93	100.07	98.73	100.21	98.65	99.98	99.82	100.60
Cations on the basis of 6 oxygens																
Si	1.995	1.925	1.927	1.933	1.946	1.912	1.958	1.948	1.931	1.897	1.937	1.977	1.932	1.936	1.944	1.926
Al^{IV}	0.005	0.075	0.073	0.067	0.054	0.088	0.042	0.052	0.069	0.103	0.063	0.023	0.068	0.064	0.056	0.074
Al^{VI}	0.002	0.036	0.036	0.033	0.009	0.051	0.022	0.041	0.023	0.066	0.033	0.003	0.047	0.050	0.022	0.036
Ti	-	-	-	-	-	-	-	-	-	-	-	-	0.004	-	-	0.004
Cr	0.023	0.026	0.024	0.039	0.028	0.025	0.018	0.027	0.030	0.032	0.013	0.012	0.008	0.009	0.009	0.008
Fe	0.043	0.085	0.100	0.103	0.111	0.113	0.118	0.119	0.135	0.142	0.136	0.147	0.175	0.182	0.245	0.283
Mn	-	-	-	-	-	-	-	-	-	-	-	-	-	-	0.003	0.003
Mg	0.947	0.989	1.048	0.991	1.047	1.041	1.053	0.994	1.020	0.971	1.029	1.062	1.031	0.977	0.988	1.014
Ca	0.975	0.867	0.799	0.832	0.815	0.776	0.789	0.811	0.800	0.791	0.797	0.781	0.739	0.784	0.746	0.664
Total	3.990	4.006	4.006	3.998	4.009	4.006	4.001	3.992	4.008	4.002	4.008	4.004	4.003	4.002	4.013	4.011
Ca	49.6	44.7	41.0	43.2	41.3	40.2	40.3	42.2	40.9	41.5	40.6	39.2	38.0	40.4	37.7	33.9
Mg	48.2	50.9	53.8	51.4	53.1	54.0	53.7	51.6	52.2	51.0	52.4	53.4	53.0	50.3	49.9	51.7
Fe	2.2	4.4	5.2	5.4	5.6	5.8	6.0	6.2	6.9	7.5	6.9	7.4	9.0	9.3	12.4	14.4
$\frac{100\ Mg}{Mg+Fe}$	95.7	92.0	91.3	90.6	90.4	90.2	89.9	89.3	88.3	87.2	88.3	87.8	85.5	84.3	80.1	78.2

All Na_2O <0.20%

* Poikilitic intercumulus pyroxene

Compositions range from bronzite $Mg_{89.5}$ co-existing with olivine Mg_{89} through to hypersthene Mg_{60}. Compositions more iron-rich than Mg_{72} lie on the iron-rich side of the orthopyroxene-pigeonite inversion point in the Bushveld and Skaergaard Intrusions (Wager & Brown, 1968) and, although some have up to 4 mol % Wo, are considered to represent subsolidus rather than solidus pyroxene.

Primary calcic pyroxene ranges from diopsidic augite to augite, and commonly have narrow (100) exsolution lamellae of orthopyroxene. Point analyses of relic cores and bulk pyroxene analyses define a portion of the diopside limb of the primary pyroxene solvus (Fig. 1-18). The miscibility gap defined by the primary pyroxenes is narrower than that defined by primary pyroxenes from layered stratiform intrusions such as the Bushveld and Skaergaard Intrusions (Atkins, 1969; Wager & Brown, 1968; Nwe, 1976) indicating higher crystallization temperatures. The first-formed orthopyroxene from the Marum cumulate sequence is more magnesian than the lowermost orthopyroxenes found in stratiform intrusions, which is rarely more magnesian than Mg_{85} (e.g. Wager & Brown, 1968; Atkins, 1969; Nwe, 1976; Cameron, 1978; Campbell & Borley, 1974) but comparable to the most magnesian orthopyroxenes from cumulus ocean-floor peridotite (Hodges & Papike, 1976).

Subsolidus pyroxenes, the vast majority of the pyroxenes examined, are either optically homogeneous or have only weak, diffuse exsolution lamellae. Both point and bulk pyroxene analyses show a spread of Ca contents defining a trend of decreasing Ca content in orthopyroxene, and increasing Ca content in clinopyroxene from the solidus (Fig. 1-19). The subsolidus trend, defined by compositions farthest displaced from the solidus, roughly parallels the Di-Hd and En-Fs joins, and coincides with the subsolidus trend defined by exsolved pyroxenes (Fig. 1-20). The extreme phase separation of the subsolidus pyroxenes indicates re-equilibration at low temperature. The subsolidus solvus lies on the low temperature side of the 810°C solvus defined by Lindsley & others (1976) and very close to the 800°C solvus of

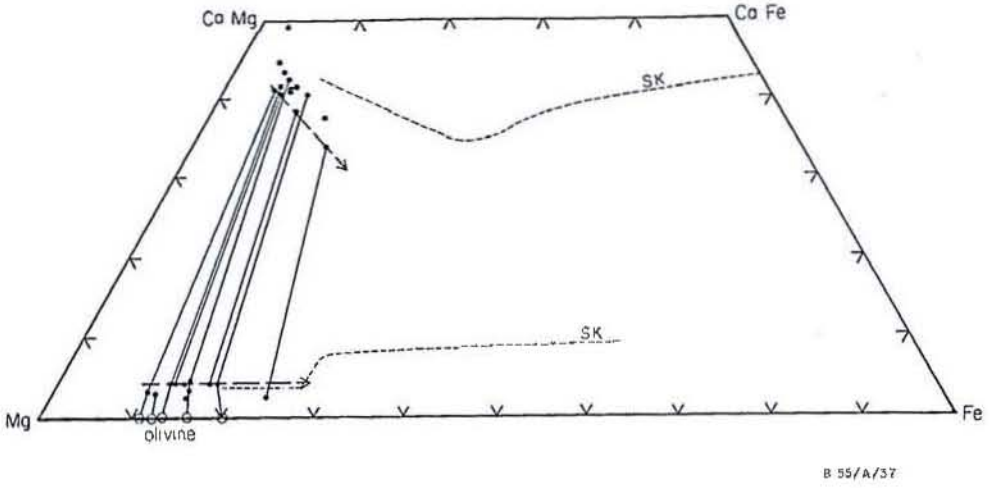

Fig. 1-18. Pyroxene quadrilateral showing primary pyroxene compositions (solid circles) and co-existing olivine (open circles). Dashed line SK is the trend for pyroxenes from the Skaergaard Intrusion (Nwe, 1976).

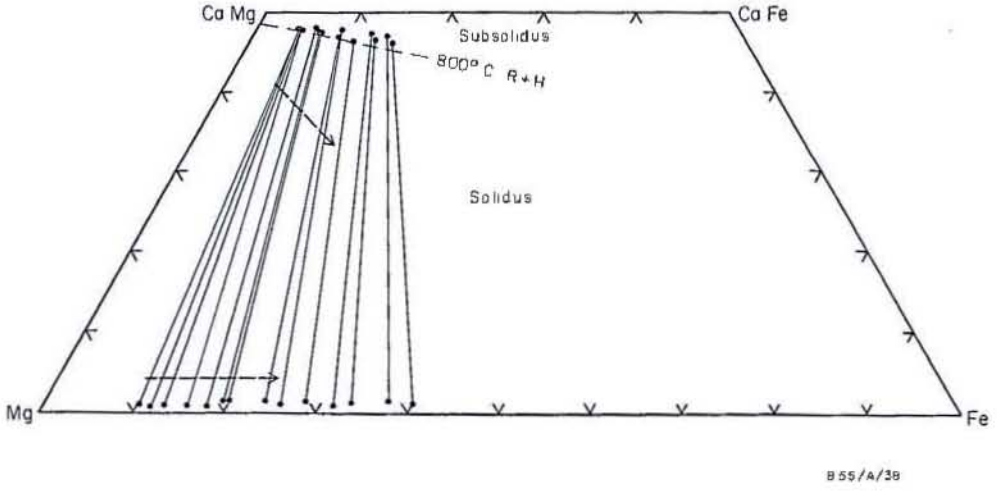

Fig. 1-19. Pyroxene quadrilateral showing composition of co-existing subsolidus pyroxenes. Heavy dashed line (solidus) is trend for primary pyroxenes. Dashed line 800°C R+H is the 800°C pyroxene solvus of Ross & Huebner (1975).

TABLE 1-12

Representative analyses of coexisting subsolidus pyroxenes

Sample No.	186		180		238		191		225		073		249		264		1020		008		123		163		431		128	
	opx	cpx	opx	cpx	opx	cpx	opx	cpx	opx	cpx	opx	cpx	opx	cpx	opx	cpx	opx	cpx	opx	cpx	opx	cpx	opx	cpx	opx	cpx	opx	cpx
SiO_2	56.31	52.52	56.11	54.02	57.49	52.87	55.92	53.61	55.45	53.19	55.48	53.46	55.52	53.58	54.53	52.51	53.87	52.45	53.59	52.60	52.62	52.04	53.51	52.97	52.21	52.61	52.01	52.44
TiO_2	<0.07	<0.07	<0.07	<0.07	<0.07	<0.07	<0.07	<0.07	<0.07	<0.07	<0.07	<0.07	<0.07	<0.07	<0.07	0.12	<0.07	0.17	<0.07	<0.07	<0.07	<0.07	<0.07	0.14	<0.07	<0.07	<0.07	<0.07
Al_2O_3	1.37	2.10	1.61	1.56	0.95	1.35	1.05	1.35	1.19	1.94	1.40	1.80	0.47	0.64	1.12	1.82	1.42	1.60	0.79	2.26	0.59	1.32	0.71	1.23	1.03	1.09	0.31	1.08
Cr_2O_3	0.39	1.10	0.29	0.68	0.22	0.73	<0.07	0.51	0.15	0.59	<0.07	0.34	<0.07	0.34	<0.07	0.31	<0.07	0.37	<0.07	<0.07	<0.07	0.27	<0.07	0.23	<0.07	0.20	<0.07	0.16
FeO	7.01	2.73	8.10	2.74	8.99	2.99	10.43	2.95	11.87	4.12	12.93	4.11	13.28	4.54	15.96	6.08	16.97	5.66	18.30	7.12	20.30	7.99	21.62	8.29	23.99	8.89	25.60	9.49
MnO	<0.09	<0.09	<0.09	<0.09	0.11	<0.09	0.20	<0.09	0.18	<0.09	0.19	<0.09	0.19	<0.09	0.22	<0.09	0.30	0.15	0.38	<0.09	0.55	0.21	0.38	<0.09	0.38	<0.09	0.60	0.19
MgO	33.90	16.81	33.33	17.34	33.18	17.13	31.55	17.20	30.57	16.31	29.86	16.30	29.92	16.61	28.03	15.74	26.95	15.51	25.59	15.04	24.44	14.19	23.96	14.38	22.09	13.90	21.11	13.79
CaO	0.41	23.50	0.33	24.48	0.51	23.91	0.48	24.19	0.44	23.84	0.62	23.57	0.68	23.54	0.63	22.89	0.59	23.30	0.63	22.52	0.50	22.93	0.71	22.67	0.71	23.19	0.47	22.56
Na_2O	<0.17	<0.17	<0.17	<0.17	<0.17	<0.17	<0.17	<0.17	<0.17	<0.17	<0.17	<0.17	<0.17	<0.17	<0.17	<0.17	<0.17	<0.17	<0.17	0.17	<0.17	<0.17	<0.17	0.17	<0.17	<0.17	<0.17	<0.17
Total	99.39	98.76	99.77	100.82	101.35	99.98	99.63	99.81	99.85	99.30	100.48	99.58	100.06	99.25	100.49	99.47	100.04	99.21	99.65	99.71	99.00	99.01	100.89	100.00	100.61	99.87	100.10	99.71
	Cations on the basis of 6 oxygens																											
Si	1.961	1.938	1.955	1.953	1.977	1.951	1.972	1.959	1.965	1.902	1.963	1.962	1.978	1.979	1.959	1.947	1.954	1.950	1.966	1.950	1.965	1.959	1.958	1.969	1.954	1.968	1.969	1.969
Al^{IV}	0.039	0.062	0.045	0.047	0.023	0.049	0.028	0.041	0.035	0.038	0.037	0.038	0.020	0.021	0.041	0.053	0.046	0.050	0.034	0.050	0.026	0.041	0.031	0.031	0.045	0.032	0.014	0.031
Al^{VI}	0.017	0.030	0.021	0.020	0.016	0.009	0.015	0.017	0.016	0.021	0.022	0.040	-	0.007	0.006	0.026	0.015	0.020	-	0.049	-	0.018	-	0.023	-	0.006	-	0.017
Ti	-	-	-	-	-	-	-	-	-	-	-	-	-	-	-	0.003	-	0.005	-	-	-	-	-	0.008	-	-	-	-
Cr	0.011	0.032	0.008	0.019	0.006	0.021	-	0.015	0.004	0.015	-	0.010	-	0.010	-	0.009	-	0.011	-	-	-	0.008	-	0.007	-	0.006	-	0.005
Fe	0.204	0.084	0.236	0.083	0.256	0.092	0.308	0.090	0.352	0.127	0.383	0.126	0.395	0.140	0.479	0.188	0.515	0.176	0.563	0.221	0.634	0.252	0.665	0.258	0.751	0.278	0.810	0.298
Mn	-	-	-	-	0.003	-	0.006	-	0.006	-	0.006	-	0.006	-	0.007	-	0.009	0.005	0.012	-	0.018	0.007	0.012	-	0.012	-	0.019	0.006
Mg	1.759	0.924	1.731	0.934	1.700	0.942	1.659	0.937	1.615	0.897	1.575	0.892	1.588	0.915	1.501	0.870	1.457	0.859	1.396	0.831	1.360	0.796	1.319	0.797	1.232	0.775	1.192	0.772
Ca	0.015	0.929	0.013	0.948	0.017	0.945	0.018	0.947	0.017	0.942	0.023	0.927	0.026	0.932	0.025	0.909	0.021	0.929	0.025	0.895	0.020	0.927	0.028	0.909	0.029	0.930	0.019	0.908
Fe	-	-	-	-	-	-	-	-	-	-	-	-	-	-	-	-	-	-	-	0.019	-	-	-	0.012	-	-	-	-
Total	4.006	4.000	4.008	4.004	4.000	4.010	4.006	4.005	4.008	4.002	4.008	3.995	4.013	4.003	4.018	4.006	4.016	4.005	4.016	4.009	4.022	4.006	4.017	4.006	4.023	4.005	4.024	4.005
Ca	0.8	48.0	0.6	48.2	1.0	47.8	0.9	48.0	0.8	47.9	1.2	47.7	1.3	46.9	1.2	46.2	1.0	47.3	1.2	46.0	1.0	46.9	1.4	46.1	1.4	46.9	0.9	45.9
Mg	88.9	47.7	87.5	47.5	86.0	47.6	83.6	47.4	81.4	45.6	79.5	45.9	79.0	46.0	74.9	44.2	73.1	43.8	70.7	42.7	67.5	40.3	65.5	40.7	61.3	40.0	59.0	39.0
Fe	10.3	4.3	11.9	4.2	13.0	4.7	15.5	4.6	17.7	6.5	19.3	6.5	19.7	7.1	23.9	9.5	25.8	9.0	28.1	11.3	31.5	12.7	33.1	13.2	37.3	14.4	40.1	15.1

opx = orthopyroxene, cpx = clinopyroxene

Ross & Huebner (1975). Compared to the solidus calcic pyroxenes, subsolidus compositions have lower Al_2O_3 contents, consistent with recrystallization at lower temperature (Herzberg & Chapman, 1976).

Re-equilibrated subsolidus pyroxenes do not lie on the low temperature extension of the tie lines defined by the primary pairs but show a counter-clockwise rotation about the solidus compositions, as does pyroxene exsolved from the primary phases. This rotation, shown by exsolved orthopyroxene compared to primary orthopyroxene (Fig. 1-20), reflects stronger partitioning of iron into orthopyroxene at lower temperature, and has previously been noted in pyroxenes from DSDP Leg 37 site 334 peridotites and gabbros by Hodges & Papike (1976).

Most iron-rich pyroxenes, orthopyroxene Mg_{60}, occur in deformed quartz-bearing ferrogabbros. Pyroxene in gabbro pegmatoid is also more iron-rich than pyroxene in most of the layered rocks. Pyroxenes from granophyric diorite are more mafic than those from the gabbro pegmatoids and ferrogabbros.

Minor elements show a systematic variation with stratigraphic height in the sequence and bulk rock *mg*-value; Mn, Ti and Na increase, and Cr decreases, with height. Cr_2O_3 contents of the first cumulate pyroxenes are comparatively high, 0.5 % Cr_2O_3 in orthopyroxene and $\sim$ 1% in clinopyroxene. Mn is preferentially partitioned into orthopyroxene whereas Ti and Cr contents are higher in clinopyroxene than orthopyroxene (Table 1-12).

Plagioclase

Plagioclase occurs as a postcumulus phase in the peridotite unit and is a cumulus phase throughout the remainder of the sequence. Postcumulus plagioclase (commonly altered to clinozoisite) ranging in composition from An_{84} to An_{97} occurs in plagioclase lherzolite co-existing with olivine Mg_{89-84}; core compositions are mostly less calcic than An_{96} and, commonly, An_{92}. Cumulus plagioclase compositions range from approximately

TABLE 1-13. REPRESENTATIVE ANALYSES OF CLINOPYROXENE HOST AND ORTHOPYROXENE EXSOLUTION LAMELLAE.

Sample No.	238 Host-lamellae		051 Host-lamellae		174 Host-lamellae		1020 Host-lamellae	
SiO_2	53.32	56.31	53.95	56.68	53.20	55.24	51.71	53.67
Al_2O_3	1.05	1.08	0.60	0.47	1.27	1.12	1.99	1.42
Cr_2O_3	0.83	0.30	0.55	<0.09	0.31	<0.09	0.44	0.14
FeO	2.81	9.07	3.35	10.46	4.01	12.78	6.18	17.29
MnO	<0.09	<0.09	<0.09	0.16	<0.09	0.16	<0.09	0.17
MgO	17.23	32.74	17.21	32.24	16.38	29.95	15.24	26.85
CaO	24.16	0.52	24.04	0.75	24.13	0.61	22.74	0.58
Total	99.40	100.03	99.70	100.76	99.30	99.85	98.30	100.12
Si	1.958	1.966	1.976	1.978	1.963	1.966	1.943	1.948
Al^{IV}	0.042	0.034	0.024	0.019	0.037	0.034	0.057	0.052
Al^{VI}	0.003	0.012	0.002	-	0.018	0.013	0.031	0.009
Cr	0.024	0.008	0.016	-	0.009	-	0.013	0.004
Fe	0.086	0.265	0.103	0.305	0.124	0.380	0.194	0.525
Mn	-	-	-	0.005	-	0.005	-	0.005
Mg	0.943	1.704	0.940	1.677	0.901	1.589	0.853	1.453
Ca	0.951	0.019	0.943	0.028	0.954	0.023	0.915	0.023
Total	4.007	4.007	4.003	4.012	4.005	4.010	4.007	4.019
Ca	48.0	1.0	47.3	1.4	48.2	1.2	46.6	1.1
Mg	47.6	85.7	47.5	83.4	45.5	79.7	43.5	72.6
Fe	4.4	13.3	5.2	15.2	6.2	19.1	9.9	26.2
$\frac{100\ Mg}{Mg+Fe}$	91.6	86.5	90.1	84.6	87.9	80.7	81.5	73.5

TiO_2 and Na_2O all less than 0.07 and 0.20% respectively

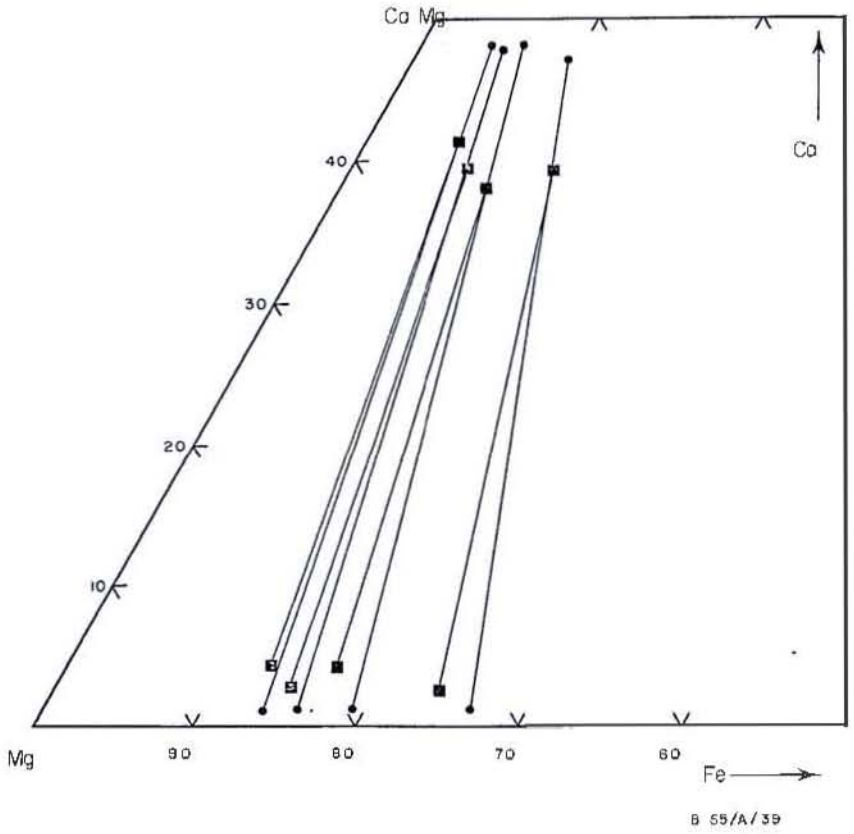

Fig. 1-20. Portion of pyroxene quadrilateral showing the counter-clockwise rotation of tie lines for exsolved orthopyroxene compared to primary host pyroxene compositions (squares) and subsolidus clinopyroxene.

An_{92} in olivine norite gabbro to An_{63} in magnetite-rich norite gabbro. The most calcic cumulus plagioclase, An_{92}, occurs in a troctolite co-existing with olivine Mg_{86}. Representative analyses are presented in Table 1-14. Compositional variation is common both among cores of grains, and between core and rim compositions. In most gabbros the rims are more calcic, some by as much as 10 mol %, particularly where plagioclase is adjacent to pyroxene; in some gabbros and the pyroxene diorite zoning is in a normal sense. The extent of the zoning is shown in Figure 1-21 where core and rim compositions are plotted against the 100Mg(Mg + Fe) ratio of co-existing orthopyroxene. The more sodic compositions are mostly restricted to the cores of larger grains (primocrysts?) whereas small recrystallized plagioclase grains have similar composition to the calcic rims. This fact suggests that the strong reverse zoning may be due to subsolidus re-equilibration (see later). K_2O contents in the layered rocks are extremely low (mostly <0.1%) and all plagioclase grains analysed plot on the Ab-An join in the ternary system Ab-An-Or. Plagioclase from the pyroxene diorite is strongly zoned from An_{82} at the core to An_{55} at the rim; K_2O contents are higher (0.2%, 1 mol % Or) than cumulate plagioclase. FeO in plagioclase shows a direct correlation with An content and bulk rock *mg*-value, and FeO contents range up to 0.4 % in the magnetite-bearing gabbros.

Plagioclase compositions in the iron-rich gabbro pegmatites are very calcic, commonly An_{92-94} with some as calcic as An_{97}, which is at variance with the overall increase in Ab content with stratigraphic height, and increase in $\frac{100Mg}{Mg + Fe}$ of co-existing pyroxene (Fig. 1-21) and bulk rock *mg*-value, and that expected from a differentiating body of magma (cf. Wager & Brown, 1968). A possible explanation may be increased P_{H_2O} in residual liquids. Johannes (1978), in a study of the melting of plagioclase in the Ab-An-H_2O and Qz-Ab-An-H_2O systems at 5 kb water pressure, has shown that plagioclase crystallizing under high water pressure is more calcic than

TABLE 1-14. REPRESENTATIVE PLAGIOCLASE ANALYSES

	PERIDOTITE				GABBRO														
	203	271	186	238	131	148	191c	191r	162c	162r	264	123	1020c	1020r	128	163c	163r	431[1]	578c[2]	578r
SiO_2	45.35	44.45	45.27	46.28	44.51	44.55	45.75	44.63	45.29	44.72	45.86	46.48	47.80	46.06	48.83	50.43	49.14	44.13	46.86	53.58
Al_2O_3	35.15	35.39	35.49	34.42	35.86	35.30	35.22	36.10	35.18	35.29	35.12	34.19	33.09	34.99	32.87	31.35	32.63	36.18	34.25	29.57
FeO	<0.07	0.16	<0.07	<0.07	0.27	0.20	0.13	<0.07	0.21	0.24	0.15	0.15	0.16	0.13	<0.07	0.23	0.27	0.29	0.26	0.15
CaO	19.05	18.52	18.04	17.89	18.85	18.25	18.07	19.11	18.00	18.43	18.05	17.27	16.58	18.18	15.15	13.66	15.28	19.37	16.96	11.36
Na_2O	0.83	1.00	1.14	1.80	0.80	1.08	1.21	0.76	1.26	0.96	1.43	1.84	2.14	1.43	2.87	3.65	2.69	0.59	2.00	5.03
K_2O	0.08	<0.06	<0.06	0.07	0.10	<0.06	0.09	0.07	0.08	<0.06	0.08	0.10	<0.06	<0.06	0.09	0.13	<0.07	0.07	0.16	0.20
Total	100.46	99.52	99.94	99.76	100.39	99.38	100.47	100.67	100.02	99.64	100.69	100.02	100.61	100.79	99.81	99.45	100.01	100.63	100.49	99.89
	Cations on the basis of 8 oxygens																			
Si	2.084	2.063	2.085	2.132	2.050	2.069	2.098	2.048	2.088	2.071	2.100	2.138	2.197	2.106	2.234	2.309	2.244	2.031	2.146	2.425
Al	1.904	1.935	1.926	1.870	1.947	1.932	1.904	1.953	1.912	1.927	1.896	1.854	1.793	1.886	1.772	1.692	1.757	1.963	1.849	1.577
Fe	-	0.006	-	-	0.010	0.008	0.005	-	0.008	0.009	0.006	0.006	0.006	0.005	-	0.009	0.010	0.011	0.010	0.006
Ca	0.938	0.921	0.890	0.849	0.930	0.908	0.888	0.939	0.889	0.915	0.885	0.851	0.816	0.891	0.743	0.670	0.747	0.955	0.832	0.551
Na	0.074	0.090	0.102	0.162	0.072	0.097	0.108	0.067	0.113	0.086	0.127	0.164	0.191	0.127	0.255	0.324	0.239	0.053	0.177	0.442
K	0.005	-	-	0.004	0.006	-	0.005	0.004	0.005	-	0.005	0.006	-	-	0.005	0.008	-	0.004	0.010	0.012
Total	5.004	5.015	5.003	5.016	5.015	5.014	5.007	5.011	5.015	5.008	5.018	5.020	5.003	5.015	5.010	5.011	4.997	5.016	5.023	5.013
An	92.3	91.1	89.8	83.7	92.3	90.3	88.7	92.9	88.3	91.4	87.0	83.3	81.0	87.5	74.0	66.8	75.8	94.4	81.7	54.9
Ab	7.3	8.9	10.2	15.9	7.1	9.7	10.8	6.7	11.2	8.6	12.5	16.1	19.0	12.5	25.4	32.4	24.2	5.2	17.4	44.0
Or	0.4	-	-	0.4	0.6	-	0.5	0.4	0.5	-	0.5	0.6	-	-	0.6	0.8	-	0.4	0.9	1.1

All MnO, MgO 0.09%. c = core, r = rim. All other analyses of core composition.

1. Mafic pegmatoid

2. Granophyric diorite

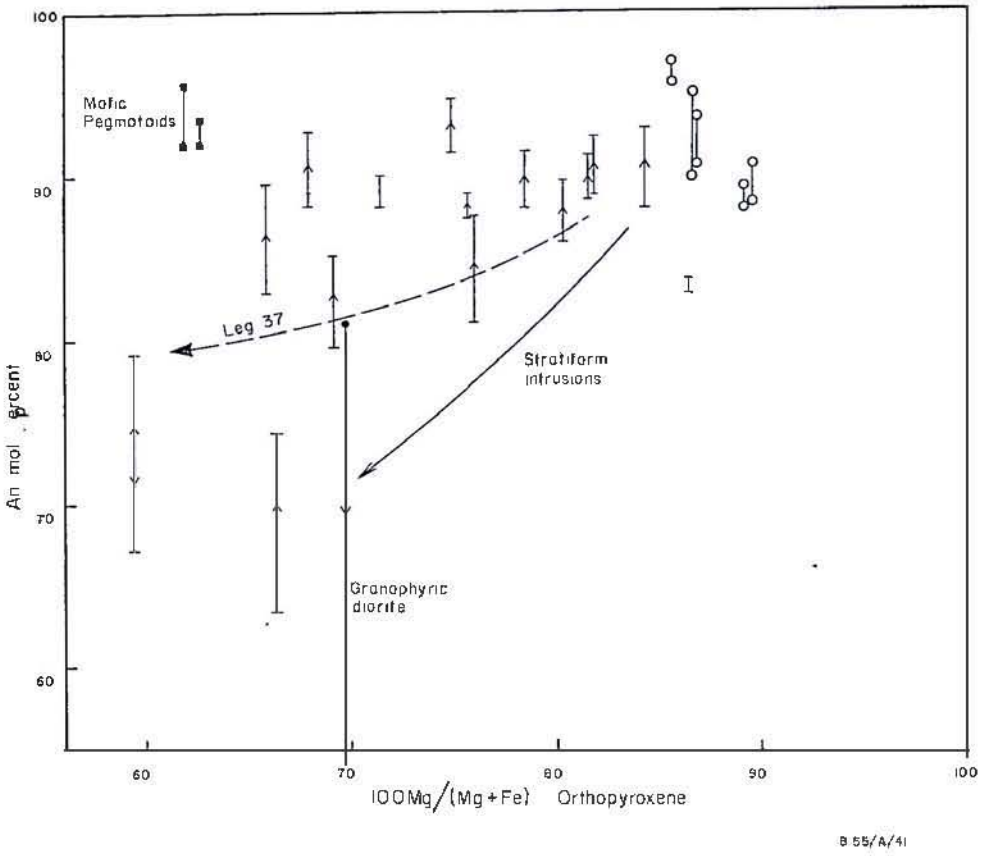

Fig. 1-21. Plot of An in plagioclase versus 100Mg/(Mg + Fe) in co-existing orthopyroxene for Marum cumulates. Open circles are for postcumulus plagioclase. Bars and arrows indicate the extent and direction of compositional zoning in plagioclase. Trends for Leg 37 site 334 and stratiform intrusions from Hodges & Papike (1976). Note the extremely calcic plagioclase in the mafic pegmatoids (squares).

that crystallizing under anhydrous conditions, and that this effect is most marked in the system Qz-Ab-An-H_2O where the configuration of the plagioclase loop changes markedly. High activities of both silica and water in the late-stage magmatic liquids is implied by quartz-feldspar eutectic intergrowths and the extensive deuteric alteration of pyroxene to amphibole.

The plagioclase of the cumulate rocks is extremely calcic and, unlike stratiform bodies such as Skaergaard and the Bushveld, the Marum cumulate sequence exhibits only limited compositional change with differentiation as marked by decreasing 100Mg/(Mg + Fe) ratios of ferromagnesian phases (Fig. 1-21). Similar highly calcic plagioclase has been observed in the Papuan Ultramafic Belt (Davies, 1971; PART 2) and other ophiolites (Coleman, 1977), and early cumulus plagioclase in ophiolites is commonly up to 10 mol % richer in An than plagioclase in stratiform tholeiitic intrusions (Wager & Brown, 1968). The relatively slow decrease in An content of the Marum plagioclase is similar to that observed by Hodges & Papike (1976) in the DSDP Leg 37 site 334 gabbros (Fig. 1-21). A possible explanation of the slow increase in Ab is that periodic influxes of of fresh magma into the magma chamber may have prevented significant enrichment of Ab component in the residual liquids.

Fe-Ti oxides

A minor amount of interstitial magnetite is present in some plagioclase-rich norite-gabbros and gabbros. Cumulus ilmenite and magnetite occurs in ferrogabbros in the upper part of the norite-gabbro unit and these plag-cpx-opx-Fe-Ti oxide cumulates commonly show mineral-graded layering. Magnetite and ilmenite also occur in gabbro pegmatoid, intergrown with quartz, plagioclase and pyroxene. Ti-poor magnetite ($\leq$1% TiO_2) occurs alone in some anorthositic norite-gabbro, and appears, on the basis of pyroxene and bulk rock Mg-values, to have crystallized before more Ti-rich magnetite and titaniferous magnetite-ilmenite pairs.

TABLE 1-15. REPRESENTATIVE ANALYSES OF TITANIFEROUS MAGNETITE AND FERRIAN ILMENITE

	Cumulus										Non-cumulus					
Magnetite	128c	128r	128	128[1]	128[2]	148[3]	163[4]	163	129c	129r	543[5]	543[6]	150[7]	431	431c	431r
SiO_2	<0.10	<0.10	0.10	<0.10	<0.10	0.36	0.12	0.30	<0.10	0.10	0.24	0.27	0.25	<0.10	<0.10	<0.10
TiO_2	4.55	2.16	6.97	2.47	1.21	1.80	2.75	6.25	5.30	9.58	1.24	1.74	1.71	7.62	18.47	13.98
Al_2O_3	1.14	1.01	1.94	1.27	0.95	1.10	1.77	0.63	1.39	1.42	2.47	3.78	2.38	4.79	6.63	2.08
Cr_2O_3	0.28	0.32	0.28	0.35	0.27	0.19	0.27	0.43	0.66	0.62	0.46	0.45	<0.08	0.37	0.33	0.37
Fe_2O_3	59.49	64.31	53.82	62.19	65.96	62.60	60.95	55.47	56.86	47.90	62.58	61.18	63.03	49.77	15.90	40.47
FeO	35.74	33.53	37.71	32.92	32.65	31.86	33.64	36.17	35.95	38.31	31.36	32.71	32.53	36.91	56.61	43.16
MnO	0.14	<0.09	0.33	<0.09	<0.09	<0.09	0.16	0.89	<0.09	0.48	<0.09	<0.09	0.21	0.29	0.72	0.51
MgO	<0.10	<0.10	0.15	0.20	<0.10	0.64	0.13	0.14	0.16	0.82	0.82	0.75	0.54	1.37	2.01	0.74
CaO	<0.07	0.12	0.12	0.16	<0.07	0.10	0.07	0.19	0.13	0.08	0.08	0.10	<0.07	<0.07	<0.07	<0.07
Total	101.34	101.45	101.42	99.56	101.04	98.65	99.79	100.47	100.45	99.31	99.25	100.98	100.65	101.12	100.67	101.31
Mol % ulvöspinel	13.0	6.2	20.2	7.2	3.5	6.7	8.5	19.1	15.3	28.0	4.5	6.0	5.9	21.7	51.5	39.4

Ilmenite	128	128[1]	128[2]	148[3]	163[4]	543[5]	543[6]	150[7]
SiO_2	<0.10	<0.10	<0.10	0.41	0.26	<0.10	0.27	0.22
TiO_2	48.78	50.62	48.24	50.92	50.16	43.63	49.62	50.02
Al_2O_3	0.13	<0.10	<0.10	0.33	<0.10	0.89	0.35	0.20
Cr_2O_3	<0.08	<0.08	<0.08	<0.08	<0.08	0.26	0.63	<0.08
Fe_2O_3	8.10	5.51	9.95	4.28	3.65	16.60	4.61	4.96
FeO	42.90	41.85	41.44	39.10	37.74	37.31	42.54	40.37
MnO	0.51	0.90	0.65	1.56	7.48	0.98	1.40	1.91
MgO	0.16	1.45	0.72	3.00	<0.10	0.47	0.55	1.65
CaO	0.13	0.14	<0.07	0.20	0.08	0.08	<0.07	<0.07
Total	100.71	100.47	101.00	99.80	99.37	100.22	99.98	99.33
Mol % R_2O_3	7.8	5.2	9.4	4.2	3.5	16.7	5.0	4.8
T°C	675	580	<600	<600	<600	<600	<600	<600
-log f_{O_2}	17.7	20.9	<20	<20	<20	<20	<20	<20

*Total iron determined as FeO; Fe_2O_3 and mol % ulvöspinel and R_2O_3 calculated following Carmichael (1967).

Superscripts 1,2,3 etc indicate ilmenite lamellae - magnetite pair; analyses without superscripts are of discrete grains.
c = core, r = rim.

Titaniferous magnetite occurs as an optically homogeneous anhedral phase commonly interstitial to the silicates and ranges in size to 1 mm. *Ferrian ilmenite* occurs mainly as granules adjacent to, or forming rims on, magnetite grains, or as broad irregular lamellae in titaniferous magnetite and, less commonly, as discrete grains (sample 128). More regular lamellae, parallel to one or more of the octahedral (111) planes in titanomagnetite, occur in some gabbro pegmatoids. Ilmenite intergrown with or rimming magnetite probably results from unmixing of a single phase titaniferous magnetite (Buddington & Lindsley, 1964) whereas discrete ilmenite grains may have either crystallized contemporaneously with magnetite, as commonly observed in stratiform bodies (e.g. Mathieson, 1975; Himmelberg & Ford, 1976) or, alternatively, may also be due to 'exsolution'. The textures observed are similar to 'type 5' or 'external granule 'exsolution' ' of Buddington & Lindsley (1964), and indicate extensive diffusion and oxidation and, for the cumulate rocks, probably extensive recrystallization.

Representative analyses of Fe-Ti oxides are presented in Table 1-15, and plotted in terms of molecular percent ulvöspinel and R_2O_3 in Fig. 1-22. Fe_2O_3 and FeO contents and mol % ulvöspinel and R_2O_3 in magnetite and ilmenite respectively were calculated following the method of Carmichael (1967). Temperatures and oxygen fugacities (Table 1-15) for co-existing ilmenite-magnetite pairs were determined using the T-f_{O_2}-X curves of Buddington & Lindsley (1964).

The mol % of ulvöspinel in titaniferous magnetite varies greatly and is very low in grains with ilmenite 'exsolution' lamellae. These compositions clearly reflect subsolidus conditions. Titaniferous magnetite in sample 431 contains up to 18.5% TiO_2 and thus may represent a primary composition; there is no co-existing ilmenite. Compositional zoning is apparent in many titaniferous magnetite grains, commonly from more Ti- and Al-rich cores to Fe-rich rims, although magnetites in sample 129 show the reverse. The R_2O_3 content of ilmenites is variable and probably reflects

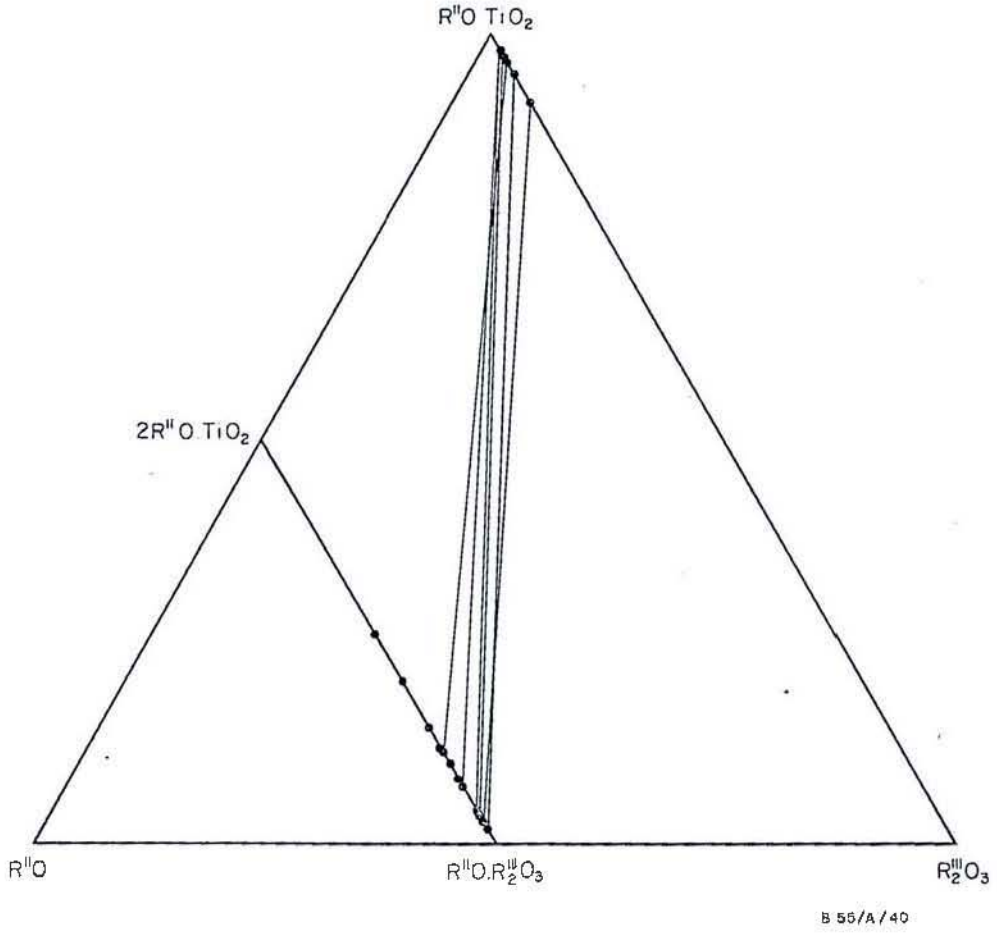

Fig. 1-22. Ternary plot showing compositions of titaniferous magnetite and ferrian ilmenite in the Marum layered sequence in terms of R''O, $R_2'''O_3$ and R''O.TiO_2. Tie lines join co-existing oxide pairs.

varying degrees of oxidation, particularly as some ilmenite has associated traces of rutile.

A feature of the Marum ilmenites is their relatively high MnO content which ranges up to 7.48% in ilmenite lamellae in sample 163, a quartz-bearing oxide-rich norite-gabbro (Table 1-15). MnO contents are generally variable from grain to grain but high (> 1%) MnO contents are restricted to ilmenite which has clearly 'exsolved' from magnetite, the magnetite host being depleted in MnO relative to the assumed original titaniferous magnetite. Strong enrichment of MnO in ilmenite and increasing MnO_{il}/MnO_{mag} ratio between co-existing oxides typically occurs in more fractionated members of plutonic suites (e.g. Buddington & Lindsley, 1964); very high MnO contents are generally restricted to silicic rocks (e.g. Buddington & Lindsley, 1964; Neumann, 1974). K_D $(^{Mn}/_{Fe})_{il}$ / $(^{Mn}/_{Fe})_{mag}$ for oxide pairs varies from about 8 to over 40.

Amphibole

Amphibole is not a primary phase but pale green tremolite-actinolite occurs as an alteration product of pyroxene, predominantly clinopyroxene. Alteration commonly commences in cleavage traces and along exsolution lamellae. Representative analyses are presented in Table 1-16 and are classified mostly as tremolite-actinolite but some are tremolitic-hornblendes, using Leake's (1978) classification. The amphibole composition directly reflects that of the replaced pyroxene: magnesian tremolite in plagioclase lherzolite 186 is chrome-rich and poor in TiO_2 whereas actinolite in more differentiated cumulates (e.g. sample 123), is richer in TiO_2 and poor in Cr_2O_3. The Na_2O content of all amphiboles is very low, in keeping with the Na-poor nature of the replaced pyroxenes.

Additional phases

Quartz is present in some plagioclase - 2 pyroxene - Fe-Ti oxide cumulates, in deformed gabbro (flaser gabbro) and in gabbro pegmatoid and

TABLE 1-16. REPRESENTATIVE AMPHIBOLE ANALYSES

Sample No.	186	107	008	578	123	431
SiO_2	54.79	54.59	53.08	50.40	52.17	50.03
TiO_2	<0.07	<0.07	0.15	0.50	0.36	0.29
Al_2O_3	3.11	3.44	4.59	5.79	4.48	6.08
Cr_2O_3	0.71	0.49	0.08	<0.08	0.15	<0.08
FeO	2.57	4.89	9.10	10.67	11.25	11.94
MnO	<0.09	<0.09	<0.09	<0.09	<0.09	<0.09
MgO	22.18	21.32	18.89	17.36	17.04	16.36
CaO	13.02	12.50	12.07	11.26	12.60	11.54
Na_2O	0.32	0.53	0.39	0.91	0.48	0.50
K_2O	<0.06	<0.06	<0.06	<0.06	<0.06	<0.06
Total	96.72	97.76	98.27	96.88	98.59	96.75
	Cations on the basis of 23 oxygens					
Si	7.619	7.581	7.459	7.266	7.418	7.261
Al^{IV}	0.381	0.419	0.541	0.734	0.582	0.739
Al^{VI}	0.129	0.144	0.219	0.250	0.170	0.301
Ti	-	-	0.016	0.054	0.038	0.032
Cr	0.078	0.054	0.009	-	0.017	-
Fe	0.299	0.568	1.069	1.287	1.338	1.449
Mn	-	-	-	-	-	-
Mg	4.597	4.413	3.956	3.730	3.611	3.539
Ca	1.940	1.441	1.817	1.739	1.920	1.795
Na	0.086	0.143	0.106	0.255	0.133	0.141
K	-	-	-	-	-	-
Total	15.130	14.763	14.653	14.581	14.645	14.518
Ca	28.4	27.2	26.6	25.7	27.9	26.5
Mg	67.2	64.5	57.8	55.2	52.6	52.2
Fe	4.4	8.3	15.6	19.0	19.5	21.4

pyroxene diorite. In the cumulates the quartz is anhedral to allotriomorphic granular and is considered to be re-textured intercumulus material. In the deformed cumulates the quartz is highly strained, granoblastic, and commonly mortar-textured. Quartz in granophyric rocks forms a eutectic intergrowth with plagioclase and Fe-Ti oxide.

Pyrite and CuFe sulphide (mainly chalcopyrite with some pyrrhotite) occur as globules in trace amounts in some Fe-Ti oxide-bearing cumulates and in gabbro pegmatoids.

3-5. Conditions of crystallization

Temperature estimates

Olivine-spinel. The basis of the temperature dependence of the partitioning of Fe and Mg between olivine and spinel, and the uncertainties in the present calibration of the geothermometer are discussed in Chapter 2.

Temperature estimates using Jackson's (1969) equation for 25 olivine-spinel pairs from the dunite unit range from 1100-1340°C, averaging 1170 ± 80°C for the core compositions. The highest temperatures were obtained for dunites at the base of the unit. Lower temperatures 950-1100°C (average 1050°C), were obtained for the rims of contacting olivine-spinel pairs. Substantially lower temperatures, well below the solidus, were obtained using Roeder & others (1979) revised calibration: spinel cores from the dunite unit yielded nominal temperatures in the range 600-720°C (average 670 ± 40°C). Lower temperatures were obtained from the rims (550-680°C), confirming that even if the absolute values obtained by Jackson's equation are in error the relative sense of temperature changes indicated are correct.

Irvine (1967) suggested that original temperatures of crystallization can be approximated by using spinel and olivine from adjacent layers in the same sequence where they are at their maximum concentration thus minimizing the effect of bulk composition-dependent changes of

subsequent re-equilibration. Nominal temperatures obtained using Jackson's equation for olivine-spinel pairs in adjacent dunite and chromitite layers in the dunite unit are considerably higher than those obtained for co-existing pairs, 1170-1550°C (average 1350 ± 90°C). Much lower temperatures (730-815°C) are obtained using Roeder & others (1979) equation which, if it yields a true estimate of equilibration, clearly indicates extensive subsolidus re-equilibration at comparatively low temperatures, and imply that no estimate of magmatic conditions may be obtained by the olivine-spinel geothermometer even for alternating layers.

Pyroxene solvus. Nominal crystallization temperatures have been calculated for primary pyroxene pairs using the semi-empirical orthopyroxene-clinopyroxene geothermometer proposed by Wood & Banno (1973) and recalibrated to include more recent data for Mg-rich pyroxenes by Wells (1977). Nominal temperatures are given in Table 1-17. Estimates using Well's (1977) recalibration differ by up to 60°C from temperatures obtained from the Wood & Banno (1973) equation. Nominal temperatures range between 1100° and 1200°C indicating higher crystallization temperatures than most stratiform intrusions. No systematic decrease in temperature with stratigraphic height in the succession is apparent.

Cr-Al in pyroxenes. Mysen & Boettcher (1975) proposed an impirical geothermometer for co-existing pyroxenes based on the partitioning of Cr and Al. Application of their equation to primary pyroxene pairs from the cumulate peridotites yielded nominal temperatures which were mostly lower than those obtained by the pyroxene solvus method, ranging between 930° and 1210°C. The solvus temperature estimates are preferred to those obtained from this geothermometer due to the uncertainties in determination of Al^{VI}, the relatively poor precision of Cr analyses at low levels by energy dispersive microprobe, and the unsatisfactory calibration of the geothermometer at high temperatures.

TABLE 1-17. NOMINAL EQUILIBRATION TEMPERATURES
BASED ON CO-EXISTING PYROXENES

Sample No	Solidus		Subsolidus		Exsolution	
	W&B (1973)	W(1977)	W&B (1973)	W(1977)	W&B (1973)	W (1977)
186	1208	1155	1005	904		
415	1150	1093	962	862		
238	1173	1139	953	863	934	844
502	1212	1191	-	-		
503	1157	1140	995	924		
180	-	-	952	854		
166	1148	1127	969	898		
191	1157	1143	931	855		
051	1169	1159	937	857	940	864
174	1175	1190	940	876	945	849
225	-	-	931	871		
073	1131	1136	937	889		
249	-	-	929	882		
264	-	-	933	915		
1020	1175	1190	906	890	980	937
008	-	-	926	930		
123	-	-	844	836		
163	-	-	858	863		
431	-	-	827	838		
128	-	-	846	875		
107	-	-	935	874		

W&B (1973) refers to Wood & Banno (1973),
W (1977) refers to Wells (1977)

Pressure

The thermodynamic equations expressing the solubility of Al_2O_3 in pyroxene in equilibrium with olivine and spinel in terms of P-T dependence are summarized in Chapter 2. Recent experimental studies and thermodynamic considerations of reactions involving pyroxenes in the $CaO-MgO-Al_2O_3-SiO_2$ and $MgO-Al_2O_3-SiO_2$ systems have shown that Al_2O_3 solubility in orthopyroxene in spinel peridotite is much lower than originally claimed (e.g. Presnall, 1976; Obata, 1976). Stroh (1976) has shown that the addition of Cr and Fe to the simple system drastically affects the activity of phases involved in the equilibrium $Mg_2SiO_4 + MgAl_2SiO_6 \rightleftarrows MgAl_2O_4 + Mg_2Si_2O_6$. Application of Stroh's(1976) equation (b) to three cumulate spinel lherzolites (186, 415, 166), using the compositions of primary pyroxenes and assuming a crystallization temperature of 1200°C, gives nominal pressure estimates of 1 kb or less, 0.7, 0.5 and 1 kb respectively.

Herzberg (1978), applying thermodynamic mixing models of clinopyroxenes to experimentally determined clinopyroxene compositions involved in a number of reactions, has constructed a P-T grid for plagioclase and spinel lherzolite, and spinel gabbro analogues in the $CaO-MgO-Al_2O_3-SiO_2$ system. Comparison of primary pyroxene compositions from cumulate plagioclase lherzolites and olivine gabbros with his P-T grid mostly results in negative pressure estimates, suggesting that either the primary phases were not at equilibrium, or that the grid does not adequately provide for the effect of other components, notably FeO and Cr_2O_3.

P-T conditions of crystallization can also be calculated from the variation of silica activity with P and T for a number of silica buffers (e.g. Carmichael & others, 1974), given the composition of co-existing phases, and appropriate thermodynamic data and crystal solution models. Two such equations are

1) $Mg_2SiO_4 + SiO_2 = Mg_2Si_2O_6$

in olivine in melt in orthopyroxene

2) $CaAl_2SiO_6$ + SiO_2 = $CaAl_2Si_2O_8$

in cpx in melt in plag

At equilibrium these can be written as

1') $\Delta G^o_{r,1} = -RT \ln K_1 = -RT \ln \dfrac{(a^{opx}_{Mg_2Si_2O_6})}{(a^{ol}_{Mg_2SiO_4})\,(a^{melt}_{SiO_2})}$

2') $\Delta G^o_{r,2} = -RT \ln K_2 = -RT \ln \dfrac{(a^{plag}_{CaAl_2Si_2O_8})}{(a^{cpx}_{CaAl_2SiO_6})\,(a^{melt}_{SiO_2})}$

where a^j_i = activity of component i in phase j.

Arculus & Wills (in press) have used the thermodynamic data of Robie & others (1978) to derive the following equations

1'') $-\ln (a^{melt}_{SiO_2}) = \dfrac{17230-6.79T+0.818P}{8.3144T} - \ln (a^{opx}_{Mg_2Si_2O_6}) + \ln (a^{ol}_{Mg_2SiO_4})$

2'') $-\ln (a^{melt}_{SiO_2}) = \dfrac{59640-4.1T-1.002P}{8.3144T} - \ln (a^{plag}_{CaAl_2Si_2O_8}) + \ln (a^{cpx}_{CaAl_2SiO_6})$

where P is in bars and T in degrees Kelvin.

Following Arculus & Wills (in press) curves of $-\ln a^{melt}_{SiO_2}$ versus T at constant P can be drawn for a given assemblage and the intersection of these curves defines the locus of variation of $-\ln a^{melt}_{SiO_2}$ with P and T. If either P,T or $\ln a^{melt}_{SiO_2}$ can be determined by independent method (or alternatively by additional equilibria) unique P-T-$\ln a^{melt}_{SiO_2}$ conditions of equilibration can be determined.

Compositional data for the solidus phases of a plagioclase lherzolite (186) and an olivine gabbro (191) have been inserted into equations 1'') and 2'') to construct P-T-$\ln a^{melt}_{SiO_2}$ diagrams (Fig. 1-23). If the crystallization temperature estimates ($\sim 1200^oC$) obtained from co-existing solidus pyroxenes are accepted crystallization pressures of $\sim$ 2 and 1 kb respectively are obtained. These estimates are in good agreement

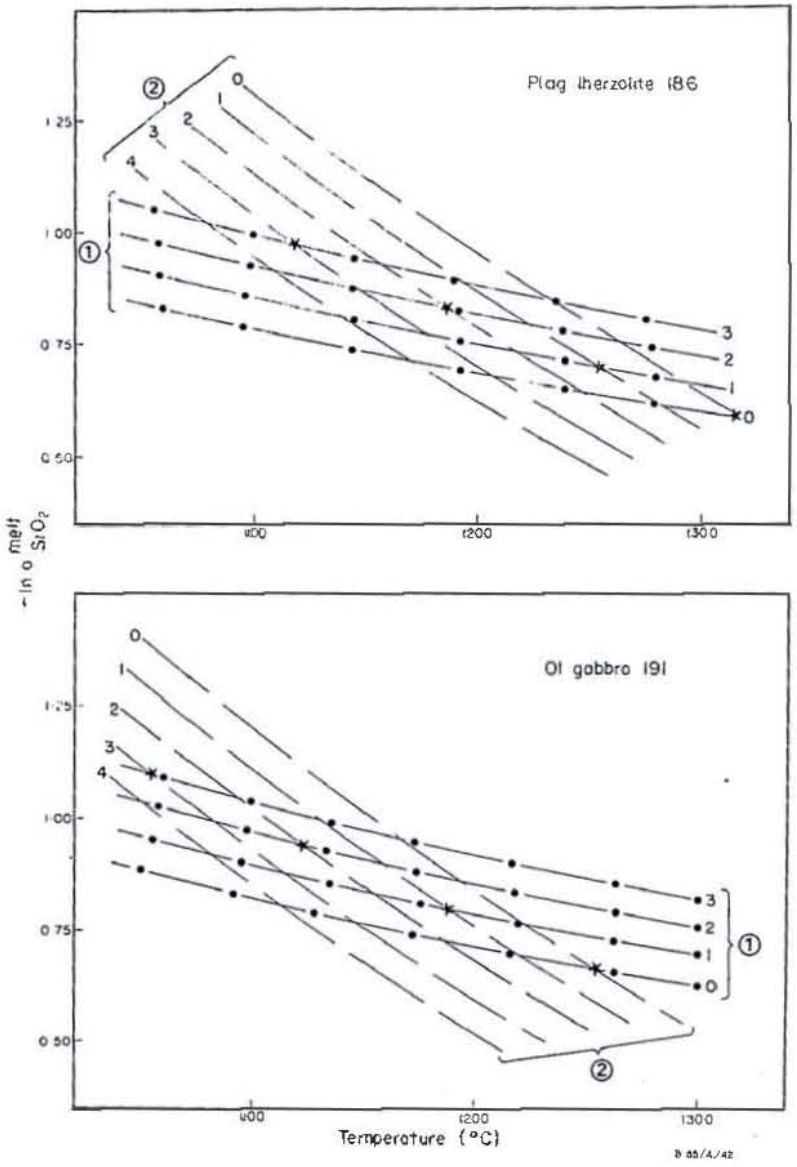

Fig. 1-23. Variation of $-\ln a^{melt}_{SiO_2}$ versus temperature at specified pressures (0,1,2,3 etc) defined by reactions 1) and 2) (see text) for selected Marum cumulates. Stars define locus of $-\ln a^{melt}_{SiO_2}$ variation in P-T space.

with the low pressures estimated from other geobarometers and inferred from field relations.

Water content and oxygen fugacity

P_{O_2} in a magma is largely controlled by dissociation of water according to the reaction $2\ H_2O = H_2 + O_2$ at high temperatures and pressures (Hamilton & Anderson, 1967), and is therefore a function of water content and temperature of the magma. Under anhydrous conditions the P_{O_2} will be dependent on redox reactions involving crystallizing phases (each with its own intrinsic f_{O_2}) and the magma, and the fugacity of magmatic gases.

The anhydrous primary mineral assemblage, late crystallization of Fe-Ti oxides, and relatively early crystallization (intercumulus) of plagioclase, all imply a low P_{H_2O} during crystallization of the cumulate sequence. A comparatively low f_{O_2} (but probably increasing with fractionation) is suggested by the Fe^{3+} contents of the early cumulate pyroxenes, although calculation and direct comparison of Fe^{3+} contents is hindered by the lack of precision in determination of minor elements at low levels. Early-formed cumulate pyroxenes commonly have $Fe^{3+}/(Fe^{3+} + Fe^{2+})$ values < 0.2, commonly $\sim$ 0.1. More iron-rich pyroxene pairs generally have slightly higher Fe^{3+} contents.

Irvine (1965) has shown that f_{O_2} is related to the compositions of co-existing spinel, olivine and pyroxene by the expression

$$f_{O_2} = \frac{(a_{Mt}^{sp})^2 \quad (a_{Fs}^{opx})^6}{K\ (a_{Fa}^{ol})^6}$$

and has contoured the spinel prism with a set of surfaces representing possible compositions for different f_{O_2} at constant P and T. Chrome-rich spinels from the dunite unit form a linear trend resembling an oxygen-fugacity isobar on the $Fe^{3+}/(Fe^{3+} + Cr + Al)$ versus $Mg/(Mg + Fe^{2+})$ projection of the spinel prism (Fig. 1-16). Since in the absence of pyroxene the inferred f_{O_2} probably represents a maximum (Irvine, 1967), and,

if it is assumed that subsequent re-equilibration is more likely to have occurred under f_{O_2} conditions equal to or higher than original magmatic conditions then it may be inferred that the initial cumulates crystallized under low f_{O_2} conditions from a magma with a high Fe^{2+}/Fe^{3+} ratio (cf. Hill & Roeder, 1974). The trend toward higher $Fe^{3+}/(Fe^{3+} + Cr + Al)$ ratios defined by the more Al-rich spinels of the peridotite unit may represent either primary crystallization, or subsequent re-equilibration under a higher f_{O_2}.

3-6. Subsolidus re-equilibration

The metamorphic textures (allotriomorphic granular to granoblastic) of many of the layered gabbros, the paucity of exsolution in pyroxenes, and the subsolidus pyroxene compositions all indicate extensive subsolidus re-equilibration.

Temperature

Nominal temperatures obtained from olivine-spinel rims in dunite, olivine in chromitite and chromite inclusions in olivine suggest equilibration temperatures in the range 990-1260°C (average 1050°C) using Jackson's (1969) equation, or much lower temperatures, 570-680°C using Roeder & others' (1979) equation. Temperature estimates from inclusions, mainly olivine in spinel, suggest that local equilibrium was achieved at even lower temperatures, 560-600°C. Lower temperatures were obtained from the finer-grained, sparsely disseminated, more Al-rich spinels in the cumulate lherzolites, some 40 olivine-spinel pairs averaging 935 ± 75°C (Jackson's equation), or much lower temperatures, 590 ± 60°C, using Roeder & others' equation. The latter results agree with the nominal temperatures obtained from inclusions in dunite and chromitite.

Re-equilibration temperatures for 20 pairs of co-existing subsolidus pyroxenes averaged 926 ± 48°C using Wood & Banno's (1973) equation,

and 878 $\pm$ 26°C using Well's (1977) equation. Temperature estimates for exsolved pyroxene pairs are similar to the subsolidus average. Nominal equilibration temperatures based on Cr-Al partitioning are generally lower, 725-978°C, averaging 843 $\pm$ 80°C.

Co-existing magnetite-ilmenite pairs indicate even lower temperatures, 675°C and below, which may reflect either final cooling and/or superimposed low-grade greenschist metamorphism.

Pressure

The stability of plagioclase in the presence of olivine indicates re-equilibration pressures $\leq$ 9 kb (e.g. Green & Hibberson, 1970). An estimate of P-T conditions of equilibration for the assemblage olivine, plagioclase, orthopyroxene and clinopyroxene can be obtained by combination of equations 1) and 2) to give

3) $\underset{\text{in ol}}{Mg_2SiO_4} + \underset{\text{in plag}}{CaAl_2Si_2O_8} = \underset{\text{in opx}}{Mg_2Si_2O_6} + \underset{\text{in cpx}}{CaAl_2SiO_6}$

Rearrangement of equations 1"') and 2"') gives an expression relating P and T to the activities of the relevant components in their respective phases. Substitution of the data for the subsolidus assemblages of 5 olivine-orthopyroxene-clinopyroxene-plagioclase cumulates and assuming equilibration temperatures based on the pyroxene solvus gave nominal equilibration pressures ranging from less than 1 kb to 6 kb. Both plagioclase lherzolite 186 and olivine gabbro 191 yielded higher nominal equilibration pressures for the subsolidus assemblage than for the primary assemblage (6.1 and 2.3 kb respectively). This might indicate subsolidus equilibration under slightly higher pressures than which they accumulated (perhaps due to thickening and subsidence of the crust with cooling and distance from the zone of spreading), or perhaps, that the compositions used in the calculations do not constitute an equilibrium assemblage. However the calculations are particularly dependent on the Ca-Tschermak's component of clinopyroxene which in the subsolidus pyroxenes is generally very low, and it is possible

that the apparent discrepancy may be due to departures from the assumed activity-composition relationship at these low levels.

Equilibration pressures may be calculated from equation 2) which, when applied to quartz-bearing gabbros results in the following exchange reaction

4) $CaAl_2Si_2O_8$ (in plag) = $CaAl_2SiO_6$ (in cpx) + SiO_2 (in quartz)

for which

4') $\Delta G^{o}_{r,4} = -RT \ln K_4$ where K_4 reduces to

$$K = \frac{a^{plag}_{CaAl_2Si_2O_8}}{a^{cpx}_{CaAl_2SiO_6}} \quad \text{since} \quad a^{quartz}_{SiO_2} = 1$$

Ellis (1979) has pointed out that because of the large ΔV and small ΔS this reaction is potentially a useful geobarometer, and used the data of Robie & Waldbaum (1968) to derive the following equation expressing ln K in terms of P and T

4") $-RT \ln K = 5359.8 + 2.9876\ T\ (^{o}K) - 0.349\ P\ (bars)$

Application of this equation to quartz-bearing gabbros 128, 129 and 163, assuming the subsolidus equilibration temperatures obtained from the pyroxene solvus, yielded pressures of -0.4, 0.2 and 1.85 kb respectively. Slightly higher pressures, 0.3, 0.6 and 2.3 kb respectively, were obtained using the more complex equation derived by Ellis (1979) to account for non-ideal solution in plagioclase and clinopyroxene. Significantly, both equations resulted in negative pressure estimates for the subsolidus assemblage of gabbroic pegmatoid 431 which has extremely low CaTs content, suggesting departures from the solution model at these low CaTs levels.

These low equilibration pressures are also supported by comparison with Herzberg's (1978) P-T grids which suggest equilibration pressures < 3.5 kb (some negative) and temperatures in the range 950-1100°C.

Oxygen fugacity

The available oxygen fugacity estimates from magnetite-ilmenite pairs indicate a comparatively low f_{O_2}, possibly near the Ni-NiO buffer. The variable R_2O_3 content of ferrian ilmenite suggests that subsolidus re-equilibration was not a result of simple cooling along an ilmenite isopleth such as observed in some stratiform intrusions (e.g. Himmelberg & Ford, 1976). It is suggested that the Fe-Ti oxide compositions reflect a more complex history involving high temperature re-equilibration (annealing), low grade metamorphism and final cooling.

The Fe^{3+} contents of subsolidus pyroxenes are comparable to that of the solidus pyroxenes although the more iron-rich orthopyroxenes generally show higher calculated Fe^{3+} contents, which may reflect higher primary Fe^{3+} contents due to higher f_{O_2} during crystallization of the more fractionated rocks or, equally, a higher f_{O_2} during subsolidus re-equilibration.

3-7. Composition of the parent magma

The very low abundances of TiO_2, Na_2O and K_2O in the cumulate phases indicate a distinctly sub-alkaline magma type. In particular the extremely Ti- and Na-poor pyroxenes are unlike pyroxenes crystallized from tholeiitic magmas in stratiform intrusions such as Skaergaard, Bushveld, etc, and require a magma with very low abundances of these elements. Bulk rock analyses show very low concentrations of incompatible trace elements (Ba, Rb, Sr, REE, etc) and imply a parent magma depleted in incompatible elements (Chapter 4).

The $100Mg/(Mg+Fe^{2+})$ ratio of the parent magma can be estimated from the composition of the first-formed cumulus olivine since the Fe^{2+}/Mg partitioning between olivine and liquid has been shown to be nearly constant over a range of temperatures and magma compositions (Green & Ringwood, 1967a; Roeder & Emslie, 1970). Assuming the applicability of the experimentally

determined equilibrium distribution coefficient, K_D^{ol}/liquid = 0.30 - 0.33 (Roeder & Emslie, 1970), liquid in equilibrium with olivine (Mg_{92}) in the dunite unit, would have had a 100Mg/(Mg + Fe^{2+}) ratio ∿ 77-79. Liquid in equilibrium with more magnesian olivine ($Mg_{93.5}$) in dunite transitional to tectonite peridotite would have had a 100Mg/(Mg + Fe^{2+}) ratio greater than 80. For lower K_D values (0.27) such as found for glass-microphenocryst pairs in the more 'primitive' MORB (e.g. Bryan & Moore, 1977; Rhodes & others, 1979) the parent liquid would have had an Mg ∿ 76. Clearly the Marum parent magma was highly mafic with a 100Mg/(Mg + Fe^{2+}) ratio of 78 ± 2.

The occurrence of modal quartz in more fractionated gabbros, the abundance of cumulus orthopyroxene and the olivine-liquid reaction relationship all point to a strongly hypersthene-normative magma either saturated or oversaturated in silica. A qualitative estimate of the degree of silica saturation can be obtained from the range of olivine compositions since cessation of olivine crystallization in a fractionating basaltic magma is ultimately governed by the reaction

$$(MgFe)_2SiO_4 + SiO_2 = (MgFe)_2Si_2O_6.$$

Cessation of olivine crystallization in the Marum sequences occurs at a point equivalent to olivine Mg_{78} which is at an earlier stage than tholeiitic stratiform intrusions such as Skaergaard - Mg_{53} - (Wager & Brown, 1968), Hawaiian tholeiites - Mg_{65} - (Moore & Evans, 1967), and ocean floor basalts- Mg_{60} - (Hodges & others, 1976) suggesting a higher activity of silica in the Marum parent magma than for these other tholeiitic magmas. In theory an estimate of silica activity and thereby silica content in the magma should be provided by reactions 1) and 2). From the -ln $a^{melt}_{SiO_2}$-P-T diagram (Fig. 1-23) the ($a^{melt}_{SiO_2}$) 1200°C, 1 kb for the parent magma (i.e. at the point of equilibration of the cumulate peridotites and gabbros) is estimated to be approximately 0.45-0.46, which, in terms of $a^{melt}_{SiO_2}$ versus

T diagrams (e.g. Carmichael & others, 1974, p. 52), appears to lie below the ol-opx reaction boundary. Arculus (1979) has recently criticized use of the ol-opx-melt buffer for classification of basalts and pointed out that such reactions in natural rocks would be characterized by a band or zone rather than a line in $a_{SiO_2}^{melt}$ - T space. No direct estimate of the SiO_2 content of the parent magma can be made since activity - composition relationships for silicate liquids are at present unknown.

The highly calcic cumulus plagioclase indicates a parent magma with low Na_2O content and a high CaO/Na_2O ratio. Comparison with experimental data for plagioclase crystallizing from basaltic magma under anhydrous conditions (Green & others, 1979; Green & others, 1975a; PART 4; Bender & others, 1978) suggests that a liquid capable of crystallizing calcic plagioclase comparable to cumulus plagioclase in the Marum sequence, $\geq An_{90}$, must have a CaO/Na_2O ratio > 13, probably 14-15. While it has been recently shown that water affects the composition of the liquidus plagioclase (Johannes, 1978) this effect is thought not to be important since the anhydrous primary assemblage and late crystallization of Fe-Ti oxides suggests a low P_{H_2O}.

The chrome-rich early spinels of the Marum ophiolite have very low TiO_2 and R_2O_3 content implying a Ti-poor chrome-rich parent magma. As noted, the spinels of the lower part of the dunite unit are more chrome-rich than spinels from stratiform intrusions (e.g. Irvine & Smith, 1967; Jackson, 1969; Cameron, 1978). Basalt crystallization studies have shown that spinel crystallizing at low pressure on the liquidus of basalts containing 800 to 1100 ppm contains between 30 and 37% Cr_2O_3 (Cr/(Cr + Al) ratios = 37-46), and that the spinel becomes increasingly aluminous at higher pressure (PART 4). These experiments are in agreement with those of Hill & Roeder (1974) who found that spinel crystallizing from a basalt containing 500 ppm Cr under varying temperatures and f_{O_2} at 1 atmosphere pressure contained a maximum of 40% Cr_2O_3. Spinels of this composition are

comparable to those found in the more primitive ocean floor tholeiites which contain less than 1000 ppm Cr (e.g. Frey & others, 1974; Sigurdsson & Schilling, 1976; Donaldson & Brown, 1977; Dick, 1979). Liquid capable of crystallizing the highly chrome-rich spinels at the base of the Marum sequence clearly contained appreciably more than 1000 ppm Cr, possibly 1500-2000 ppm, and crystallized at very low pressure.

Similarly the high Ni concentrations in olivine of the dunite unit imply a Ni-rich parent magma. Assuming an olivine Ni partition coefficient between 6 and 10 for the most magnesian olivine crystallizing from a mafic magma with, say, 12-15% MgO at about 1300°C (Hart & Davis, 1978) the parent magma would have contained at least 300, and possibly as much as 600 ppm Ni. For lower Ni partition coefficients, such as those found for komatiites by Arndt (1977b), the parent magma may be inferred to be even richer in Ni.

The comparative rarity of ilmenite and its absence as a primary phase co-precipitating with titanomagnetite implies a parent magma with lower TiO_2 content than those associated with stratiform intrusions. The roles of ilmenite and titanomagnetite imply undersaturation in TiO_2 for the temperature and f_{O_2} conditions at which the oxide phase crystallized (Buddington & Lindsley, 1964). Calculations using published partition coefficients for the cumulus phases and trace element data from cumulate gabbros and peridotites suggest that the TiO_2 content of the parent magma was less than 0.6% and may have been as low as 0.3% (Chapter 4).

These compositional requirements appear to exclude as candidate parent magmas even the most primitive mid-ocean ridge-type high-alumina olivine tholeiites such as those of DSDP Leg 3-14, 18 (Frey & others, 1974), Leg 37 and the FAMOUS area (Langmuir & others, 1977; Bryan & Moore, 1977; Bryan & Thompson, 1977), and compositions akin to the melt inclusions contained in phenocryst phases of some of the more mafic MORB (Donaldson & Brown, 1977; Dungan & Rhodes, 1978; Rhodes & others, 1979).

Crystallization studies of the more primitive of these compositions (Green & others, 1979; Bender & others, 1978; PART 4) have shown that low pressure accumulates from such liquids are dominated by olivine, plagioclase and calcic clinopyroxene. Green & others (1979) have argued that low pressure cumulate sequences (such as the Marum) containing magnesian orthopyroxene (> Mg_{87}) are formed from more silica-rich magmas with high MgO content.

Magmas with the above characteristics are found among the Ti-poor magnesian olivine-poor tholeiites of the Upper Pillow Lavas of the Troodos ophiolite (Smewing & others, 1975; Smewing & Potts, 1976) and the Arakapas Fault Belt area (Simonian & Gass, 1978). Lavas of similar composition also occur in the Newfoundland, Baer-Bassit (Syria) and Kan-Taishir (Mongolia) ophiolites (Church & Coish, 1976; Gale, 1973; Parrot, 1977; Zonenshain & Kuzmin, 1978). The more magnesian of the Troodos lavas contain phenocrysts of magnesian olivine Mg_{90-80}, chrome spinel, orthopyroxene ($\sim Mg_{89}$), and clinopyroxene ($Ca_{41}Mg_{51}Fe_8$), the crystallization sequence being chromite, olivine, orthopyroxene or clinopyroxene followed by plagioclase (Simonian & Gass, 1978) which is similar to that of the layered cumulates of the Troodos plutonic suite (Greenbaum, 1972). The more primitive of these lavas have very low TiO_2 contents ($\sim$ 0.2-0.3%), Mg-values > 70, high Ni and Cr contents, and many have very high CaO/Na_2O ratios (Table 1-18).

Lavas with these characteristics are also found among basaltic members of the komatiite suite of Archaean greenstone belts (e.g. Viljoen & Viljoen, 1969; Williams, 1972; Hallberg & Williams, 1972; Nesbitt & Sun, 1976; Arndt & others, 1977), and also typify high-Mg andesites or boninites found in Cainozoic island-arcs in the western Pacific (e.g. Dallwitz, 1968; Kuroda & Shiraki, 1975; Dietrich & others, 1978; Cameron & others, 1979). Williams & Hallberg (1973) have shown that the high-Mg basalts or basaltic komatiites of the Eastern Goldfields region of Western Australia are

TABLE 1-18. COMPARISON OF INFERRED MAGMA COMPOSITION WITH OTHER PRIMITIVE BASALTS

	1	2	3	4	5	6
SiO_2	52.3	54.6	51.7	52.5	57.5	48.4
TiO_2	0.3	0.19	0.36	0.4	0.3	0.60
Al_2O_3	11.7	11.4	11.8	10.0	8.9	13.7
FeO	8.4	8.4	9.5	9.7	9.5	7.9
MnO	0.15	0.17	0.16	0.2	0.2	0.12
MgO	15.8	13.5	16.8	16.7	17.5	16.7
CaO	10.7	10.7	8.3	9.2	4.8	10.9
Na_2O	0.7	0.71	1.1	1.0	0.8	1.65
K_2O	0.1	0.29	0.19	0.3	0.3	0.01
P_2O_5	-	0.04	0.06	-	0.1	-
$\frac{100\ Mg}{(Mg+\Sigma Fe)}$	77.0	74.0	75.9	74.7	76.7	79.0
CIPW Norm						
Qz	-	5.1	-	-	8.6	-
Or	0.6	1.7	1.1	1.8	1.8	tr
Ab	5.9	6.0	9.3	8.5	6.8	14.0
An	28.5	27.0	26.7	21.9	19.8	29.9
Di	19.8	21.0	11.3	19.1	2.7	19.5
Hy	44.7	38.6	43.5	43.2	59.2	8.3
Ol	tr	-	7.0	4.5	-	27.1
Il	0.6	0.4	0.7	0.8	0.6	1.1
Ap	-	0.1	0.1	-	0.2	-

Total iron as FeO. All analyses recalculated volatile free to 100%.

1. Inferred parental magma composition for Upper Pillow Lavas, Troodos (Duncan & Green, 1979).
2. Basalt 8946, Arakapas Fault Belt, Cyprus (Simonian & Gass, 1978)
3. Average parent composition for 4 Archaean high-Mg layered sills, Yilgarn Block, W. Australia (Williams & Hallberg, 1973).
4. Spinifex-textured basalt (basaltic komatiite), Pilbara block, W. Australia (Sun & Nesbitt, 1978b).
5. Average of 6 high-Mg andesites, Cape Vogel, Papua New Guinea (Dallwitz, 1968).
6. Inferred parent magma for DSDP 3-18 basalt (Green & others, 1979).

associated with layered sills characterized by cumulate sequences similar to the Stillwater Complex where the crystallization sequence is ol, ol + opx, opx, opx + plag, opx + plag + cpx, plag + cpx. This accumulate sequence differs from that of the Marum and Troodos ophiolites by virtue of the paucity of cumulate orthopyroxenites and harzburgites, and the early crystallization of clinopyroxene in the ophiolites. Comparison of the inferred parental magma compositions (Table 1-18) shows that the high-Mg basalts are characterized by lower normative diopside compared to the Troodos compositions, and this difference is manifested by later crystallization of calcic pyroxene relative to low Ca-pyroxene in low pressure accumulates in the Archaean layered sills compared to the Troodos plutonic suite. Consequently this magma is not considered a suitable candidate parent magma for the Marum sequence. Sun & Nesbitt (1978a) and Cameron & others (1979) have suggested an association between the high-Mg andesite or boninite suite and ophiolite sequences such as Troodos. Inspection of typical high-Mg andesite or boninite compositions (Table 1-18, and compilations by Sun & Nesbitt, 1978a; Cameron & others, 1979) shows that these rocks are typically oversaturated in silica and have very low contents of CaO (5-8%) and normative diopside. By analogy with the Archaean komatiites low pressure accumulate sequences would also be expected to contain a preponderance of magnesian low Ca-pyroxene. Moreover, since boninites commonly contain water-rich glass and are thought to result from water-saturated melting of peridotite (Green, 1973, 1976a), differentiates might be reasonably expected to contain primary hydrous phases.

It is concluded therefore that parental magmas to the Marum cumulate sequence most closely resemble the more primitive basalts of the Upper Pillow Lavas of the Troodos ophiolite. Duncan & Green (1979) have identified a possible parental magma in the Upper Pillow Lavas (Table 1-18) and suggested that magmas of this composition, magnesian olivine-poor tholeiite, may be parental to ophiolites with cumulate sequences similar to

Troodos. Crystallization studies on a synthetic glass of this composition have shown that, at 1 atmosphere, olivine $Mg_{91.6}$ is the liquidus phase at 1340°C, and is jointed by pyroxene at 1220°C and plagioclase An_{90} at 1190°C (R.A. Duncan, pers. comm. 1979). The roles of orthopyroxene, protopyroxene, pigeonite and diopside are complex at these temperatures at low pressure, and apart from demonstrating that low calcium pyroxene crystallizes before plagioclase, the data are as yet incomplete. However, the available data clearly show that the crystallization sequence and temperatures of this magma composition are very similar to those inferred for the Marum cumulates - olivine and chrome spinel (1300-1350°C) followed by clinopyroxene, orthopyroxene (∿ 1200°C) and then plagioclase -, and provide good evidence that the layered peridotites and gabbros of the ophiolite accumulated from a magma of very similar composition.

3-8. Conclusions

The plutonic suite of the Marum ophiolite complex comprises a thick (3-4 km) sequence of layered cumulates ranging from dunite at the base upwards through lherzolite, plagioclase lherzolite, pyroxenite, plagioclase pyroxenite, and olivine norite-gabbro to norite-gabbro, ferro-gabbro and anorthositic gabbro at the top. Well-preserved igneous layering, igneous structures, and cumulate textures indicate an origin by magmatic crystallization in a large magma chamber by cumulus processes combined with in-situ rhythmic crystallization from a mafic magma of evolving composition. Cyclic units superimposed on the gross stratification suggest periodic influxes of fresh magma to the chamber. Most rocks show textural and mineralogical evidence of subsolidus re-equilibration and some are overprinted by sporadic, incipient low grade (greenschist facies) metamorphism.

The accumulate sequence in the layered rocks is: ol + Cr spinel (cr); ol + cr + cpx; ol + cr + cpx + opx; ol + cpx + opx + plag;

plag + cpx + opx; plag + cpx + opx + Fe-Ti oxide ($\pm$ quartz). The crystallization interval between clinopyroxene and orthopyroxene is small. This sequence is similar to that deduced for the Troodos and Papuan ophiolites where orthopyroxene is also a prominent cumulus phase, and differs from that of some other ophiolites, such as Vourinos, where orthopyroxene cumulates are relatively minor and form late in the sequence.

Early formed cumulus olivine is extremely magnesian, (Mg_{92}), and the spinel is rich in Cr (62-64% Cr_2O_3, $Cr/(Cr + Al + Fe^{3+}) \sim 80$). Both exhibit cryptic variation, olivine progressively changing to Mg_{78} and spinel becoming increasingly aluminous. Plagioclase is highly calcic, An_{94-67}, and commonly shows reverse zoning. Analyses of relic primary grains and bulk pyroxenes (host plus lamellae) partially define a high temperature pyroxene solidus with a narrower miscibility gap than found in pyroxenes from stratiform intrusions. Early formed pyroxenes are also more magnesian than generally found in stratiform intrusions, and include orthopyroxene as magnesian as $Mg_{89.5}$. Most pyroxenes, however, have re-equilibrated under subsolidus conditions and have compositions which lie between the solidus and subsolidus solvii.

Various geothermometers and geobarometers based on pyroxene-pyroxene and olivine-pyroxene-spinel equilibria, together with thermodynamic calculations using silica buffers, suggest that the pyroxene-bearing cumulates crystallized at about 1200°C and about 1 to 2 kb pressure under low f_{O_2} conditions. The underlying dunites and chromitites crystallized at higher temperatures, possibly as high as 1300-1350°C. Subsequently the ophiolite has recrystallized under subsolidus conditions at about 850-900°C (as recorded by co-existing pyroxenes) and pressures similar to the primary crystallization pressures, and slowly cooled. Partitioning of Fe and Mg between olivine and spinel records cooling temperatures to about 600°C. Co-existing magnetite-ilmenite pairs record final cooling and/or low grade greenschist metamorphism at temperatures below 600°C.

The crystallization sequence and the composition of the cumulus phases points to a highly magnesian ($Mg_{78\pm2}$) olivine-poor or quartz tholeiite parent magma(s) rich in Ni (300-600 ppm) and Cr, and poor in TiO_2 and alkalies. This magma(s) probably most closely resembles the more primitive lavas found in the Upper Pillow Lavas of the Troodos ophiolite.

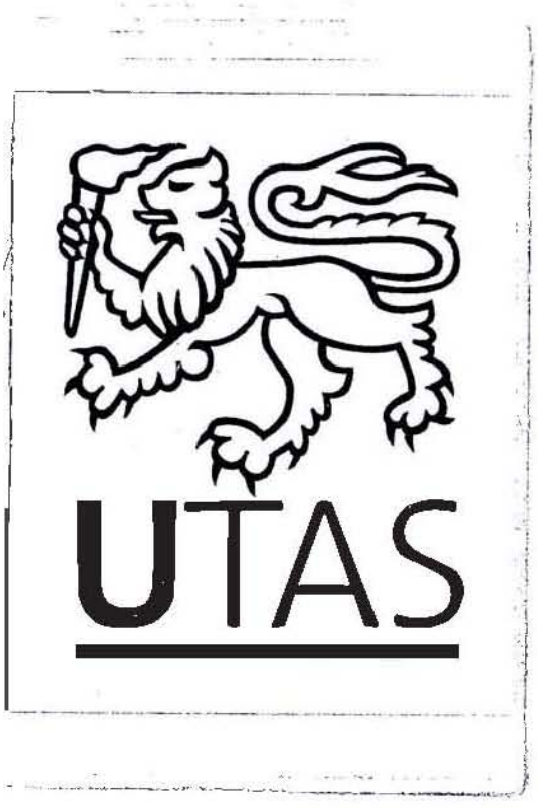

CHAPTER 4

GEOCHEMISTRY OF CUMULATE PERIDOTITES AND GABBROS

4-1. Analytical methods

Chemical analyses of 23 cumulate peridotites and gabbros, 4 non-cumulus gabbro pegmatoids and a granophyric diorite are presented in Table 1-19. Also presented are 3 analyses of quartz microgabbro and quartz dolerite dykes intruding the gabbros. Analyses were by XRF spectrometry except for Na and K (atomic absorption spectroscopy) and FeO and H_2O^+ (wet chemical methods). Details of the analytical techniques are given in Appendix 1. Major elements for samples 128, 543 and 541 were determined by electron microprobe after fusion on an iridium strip and P_2O_5, MnO and TiO_2 in these samples were determined by XRF on pressed powder pellets. All trace elements were determined by XRF on pressed powder pellets following Norrish & Chappell (1977). Where available values determined by spark source mass spectrometry are given in parenthesis for trace elements present at levels below the XRF limit of detection. Rb and Sr were determined at low levels by the method of Chappell & others (1969).

4-2. Major elements

Major element chemistry directly reflects the modal mineralogy of the cumulates. The cumulates range from highly magnesian (*mg* > 90) dunite compositions with very low abundances of lithophile elements, through less magnesian peridotites and pyroxenites (*mg* ∿ 83-90) with higher abundances of CaO and Al_2O_3 and cumulate norite-gabbros with high CaO and Al_2O_3 contents to ferrogabbro (*mg* ∿ 40) containing ∿ 19% FeO (total iron as FeO) and anorthosite containing ∿ 31% Al_2O_3. A feature of the cumulates is their extremely low TiO_2, Na_2O, K_2O, MnO and P_2O_5 contents. These oxides increase with increasing differentiation (shown by decreasing *mg*) but, even in the more fractionated rocks, abundances of TiO_2, Na_2O, K_2O

TABLE 1-19. CHEMICAL ANALYSES OF CUMULATE PERIDOTITES AND GABBROS

Analysis	1	2	3	4	5	6	7	8
Sample	567	220	1046	180	227	415	51	271
SiO_2	39.80	37.02	38.31	50.21	49.02	39.55	54.11	39.95
TiO_2	<0.002	0.003	<0.002	0.03	0.03	0.01	0.05	0.02
Al_2O_3	0.04	0.28	0.38	1.77	2.33	0.32	0.80	4.08
Fe_2O_3	0.71	2.38	1.55	0.85	1.04	2.56	1.14	3.04
FeO	5.87	5.45	7.20	3.85	3.99	8.49	5.09	7.80
MnO	0.11	0.13	0.15	0.14	0.14	0.18	0.20	0.18
MgO	49.93	46.00	47.10	22.72	23.91	42.14	23.12	35.85
CaO	0.05	0.16	0.19	17.70	16.59	1.95	15.24	4.62
Na_2O	0.002	0.003	0.002	0.09	0.09	0.010	0.07	0.11
K_2O	<0.0005	0.0005	<0.0005	0.001	0.005	<0.0005	0.001	0.002
P_2O_5	<0.001	<0.001	<0.001	0.005	0.007	<0.001	0.006	0.004
S	<0.01	<0.01	<0.01	0.02	0.01	<0.01	0.01	0.02
loss	2.52	7.07	4.22	2.06	3.13	4.50	0.73	4.33
rest	0.94	1.13	0.82	0.54	0.58	0.72	0.36	0.65
				99.99				100.66
O=S				0.01				0.01
Total	99.97	99.63	99.92	99.98	100.87	100.43	100.93	100.65
Mg #	93.2	91.5	90.7	89.8	89.6	87.4	87.1	85.8
Trace elements (ppm)								
Ba	<10	<10	<10	<10	<10	<10	<10 (0.3)	<10 (0.3)
Rb	<0.1	<0.1	<0.1	<0.1	<0.1	<0.1	0.2	0.1 (0.08)
Sr	<0.1	0.2	<0.1	6.6	6.0	0.9	5.6	21.0
Zr	<1	<1	<1	1	1	<1	1 (0.66)	<1 (0.5)
Nb	<1	<1	<1	<1	1	<1	1 (0.39)	<1 (0.30)
Y	<1	<1	<1	1	1	<1	1 (0.90)	1
La	<2	<2	<2	<2	<2	<2	<2	<2
Ce	<3	<3	<3	<3	<3	<3	<3	<3
Nd	<2	<2	<2	<2	<2	<2	<2	<2
Sc	2	4	5	50	49	10	49	13
V	5	15	12	85	77	26	70	37
Cr	4210	5750	3950	3130	3360	3520	2040	3120
Ni	2520	2210	1860	400	480	1540	250	1360
Cu	4	4	2	5	1	6	1	31
Zn	40	38	47	26	24	55	34	73
Ti	12	22	11	193	192	59	294	111

$Mg^{\#}$ = 100Mg/(Mg + ΣFe). Analyses 1-3 = dunite; 4,5,7 = Wehrlite and olivine pyroxenite; 6 = lherzolite; 8 = plagioclase lherzolite.

TABLE 1-19. CONTINUED

Analysis Sample	9 191	10 174	11 1104	12 225	13 1040	14 120	15 264	16 162
SiO_2	47.57	47.96	43.46	48.88	54.48	46.74	52.70	48.08
TiO_2	0.04	0.08	0.07	0.10	0.06	0.05	0.19	0.13
Al_2O_3	17.82	16.16	13.37	15.79	1.28	19.62	2.76	13.34
Fe_2O_3	0.50	0.69	1.75	0.77	0.82	0.59	1.04	1.76
FeO	2.55	3.01	5.02	3.47	9.98	3.75	8.02	5.04
MnO	0.08	0.10	0.13	0.11	0.25	0.11	0.24	0.16
MgO	11.75	11.65	19.67	11.82	29.35	11.08	19.20	13.62
CaO	18.19	17.31	10.66	18.09	2.49	16.32	15.47	15.66
Na_2O	0.43	0.68	0.71	0.48	0.03	0.49	0.17	0.47
K_2O	0.002	0.010	0.002	0.002	0.001	0.02	0.002	0.003
P_2O_5	0.011	0.013	0.004	0.005	0.004	0.01	0.012	0.004
S	0.05	0.04	0.05	0.01	0.01	0.06	0.02	0.05
loss	1.41	2.66	5.07	1.08	0.96	1.62	0.87	1.88
rest	0.18	0.17	0.37	0.21	0.61	0.22	0.19	0.16
	100.58	100.53	100.34			100.68	100.88	100.36
O=S	0.02	0.02	0.02			0.03	0.01	0.02
Total	100.56	100.51	100.32	100.82	100.33	100.65	100.87	100.34
Mg #	87.5	85.1	84.2	83.5	83.0	82.2	79.3	78.6
Trace elements (ppm)								
Ba	<10	<10	<10	<10(0.7)	<10	<10	<10	<10
Rb	0.1	0.3	0.1	<0.1	<0.1	0.9	<0.1	<0.1
Sr	63	74	51	64	1.6	109	17.5	65
Zr	<1	1	1	1(1.52)	1	1	3	1
Nb	<1	<1	<1	<1(0.53)	1	1	<1	1
Y	1	3	3	3(2.72)	1	1	6	4
La	<2	<2	<2	<2	<2	<2	<2	<2
Ce	<3	<3	<3	<3	<3	<3	4	<3
Nd	<2	<2	<2	<2	<2	<2	2	<2
Sc	37	41	28	42	32	28	85	46
V	66	93	74	101	76	60	198	126
Cr	905	600	1640	1090	3500	935	750	565
Ni	185	193	735	154	540	210	186	190
Cu	18	204	75	4	12	211	10	45
Zn	12	24	37	20	91	39	57	41
Ti	221	415	375	585	320	253	1030	765

Analyses 9,10,12,14,16 = olivine norite-gabbro; 11,13,15 = websterite, plag websterite.

TABLE 1-19. CONTINUED

Analysis	17	18	19	20	21	22	23
Sample	1020	128	131	129	123A	123B	148
SiO_2	50.33	47.72	47.92	47.08	45.80	46.49	39.83
TiO_2	0.15	0.06	0.06	0.20	0.04	0.11	0.76
Al_2O_3	12.72	19.98	20.08	18.02	31.28	26.52	16.96
Fe_2O_3	0.83	1.10	1.56	3.92	0.66	1.46	9.94
FeO	6.19	5.05	4.73	5.93	1.00	3.13	9.70
MnO	0.17	0.13	0.13	0.21	0.03	0.09	0.19
MgO	13.66	9.45	9.47	9.44	1.16	4.09	7.16
CaO	14.75	15.27	15.41	13.61	17.35	16.03	13.75
Na_2O	0.57	0.42	0.42	0.76	1.37	0.83	0.43
K_2O	0.002	0.004	0.004	0.006	0.03	0.02	0.01
P_2O_5	0.01	0.01	0.01	0.007	0.02	0.02	0.02
S	0.09	<0.01	0.01		0.01	0.01	0.07
loss	0.89	1.27	0.88	0.91	1.34	1.26	1.01
rest	0.22	0.08	0.08	0.13	0.05	0.08	0.28
	100.58						100.11
O=S	0.04						0.03
Total	100.54	100.54	100.76	100.22	100.14	100.14	100.08
Mg #	77.8	73.6	73.3	64.0	56.5	62.1	40.6
Trace elements (ppm)							
Ba	<10(1)	<10(2)	<10	<10	<10	<10	<10
Rb	<0.1 (.06)	<0.1(.03)	0.1	<0.1	0.6	0.3	<0.1
Sr	59(53)	135	133	188	259	216	120
Zr	2(1.77)	2	1	2	2	1	1
Nb	1(0.39)	<1(0.2)	1	1	1	<1	<1
Y	5(5.08)	1	1	2	<1	1	1
La	<2	<2	<2	<2	<2	<2	<2
Ce	<3	<3	<3	<3	<3	<3	<3
Nd	<2	<2	<2	<2	<2	<2	<2
Sc	50	36	36	44	5	19	55
V	140	96	97	238	28	95	955
Cr	765	179	169	157	76	172	80
Ni	182	71	68	59	9	26	16
Cu	292	2	3	115	9	7	525
Zn	44	28	35	65	10	28	73
Ti	865	330	340	1210	213	610	4550

Analyses 17-20 = norite-gabbro; 21-22 = felsic and mafic bands in anorthosite; 23 = ferronorite-gabbro.

TABLE 1-19. CONTINUED

Analysis	24	25	26	27	28	29	30	31
Sample	578	543	431	150	541	545	576	169
SiO_2	56.08	42.00	41.07	39.59	38.28	50.08	50.67	52.15
TiO_2	0.42	0.39	0.33	0.75	0.82	2.04	1.06	1.21
Al_2O_3	15.38	20.95	23.27	17.83	25.42	14.19	14.85	15.07
Fe_2O_3	1.69	2.97	4.89	10.09	1.89	1.37	3.72	3.72
FeO	4.66	7.78	6.11	9.99	7.82	9.18	7.93	7.51
MnO	0.20	0.18	0.15	0.20	0.14	0.19	0.23	0.21
MgO	7.86	6.63	5.06	5.92	2.62	7.72	4.12	3.90
CaO	9.65	14.95	14.28	12.62	16.81	12.08	9.14	7.52
Na_2O	2.05	0.56	0.79	0.76	0.54	2.63	2.18	3.70
K_2O	0.09	0.05	0.34	0.01	0.28	0.32	0.50	0.81
P_2O_5	0.04	0.01	0.01	0.016	0.29	0.12	0.22	0.26
S	0.01		0.01	0.35			0.14	
loss	2.11	3.66	4.09	2.54	5.37		5.43	4.44
rest	0.13	0.16	0.20	0.19	0.54	0.19	0.15	0.16
				100.86			100.34	
O=S				0.17			0.07	
Total	100.37	100.29	100.60	100.69	100.82	100.11	100.27	100.66
Mg #	69.4	53.1	46.2	35.6	32.9	56.9	39.4	39.0
Trace elements (ppm)								
Ba	<10	<10	<10	<10	170	40	150	240
Rb	1.0	1.0	7.0	0.2	6.8	4.6	10.5	15.5
Sr	135	334	494	183	3520	202	259	240
Zr	38	2	2	3	16	73	56	98
Nb	3	1	<1	<1	1	5	2	4
Y	7	1	<1	2	1	19	21	26
La	<2	<2	<2	<2	<2	6	8	8
Ce	5	<3	<3	<3	4	19	24	25
Nd	<2	<2	<2	<2	<2	11	11	13
Sc	39	39	32	48	19	38	27	29
V	141	383	606	621	288	268	304	280
Cr	277	110	73	57	137	477	53	54
Ni	83	113	44	7	52	43	6	12
Cu	91	29	8	197	59	30	30	65
Zn	80	68	60	112	84	64	96	86
Ti	2500	2400	1975	4500	5000	12250	6400	7500

Analyses 24 - granophyric diorite; 25-28 = gabbro pegmatoid; 29-31 = quartz dolerite and microgabbro.

and P_2O_5 are very low compared to gabbroic cumulates in stratiform intrusions (cf. Wager & Brown, 1968) which typically contain appreciable intercumulus material. The non-cumulus rocks are characterized by high Al_2O_3 and FeO contents, and markedly higher contents of TiO_2, alkalies and P_2O_5 than the cumulates. The gabbro pegmatoids have comparatively low SiO_2 content compared to both the cumulate gabbros and the granophyric diorite. The quartz microgabbro and dolerites are highly fractionated and have low MgO and high FeO contents; alkali contents are appreciably higher than for the gabbroic rocks.

The overall differentiation trends from magnesian cumulates to CaO-rich cumulates (*wehrlite-lherzolite*) to Fe-rich and Al_2O_3-rich cumulates (*gabbro*) is clearly shown on the CaO-FeO-MgO and CaO-Al_2O_3-MgO diagrams (Fig. 1-24a, b). The early magnesian cumulates overlap the non-cumulus peridotites, whereas the non-cumulus gabbros lie at the Fe-Al-rich end of the cumulate trend supporting the interpretation of these rocks as late-stage differentiates. On an AFM (Fig. 1-24c) the low alkali contents of all the Marum rocks is reflected in a strong linear trend toward Fe enrichment. The higher alkali contents of the quartz microgabbro and quartz dolerites are reflected in the displacement of these rocks towards the alkali apex.

4-3. Trace elements (excluding REE)

Trace element abundances vary with both the modal mineralogy (including the amount of postcumulus material) and the *mg* number of the rock. Ni and Cr contents decrease markedly from very high values in the dunites ($\sim$ 2000 ppm Ni, $\sim$ 4000 ppm Cr) to much lower values in the gabbros ($\leq$ 200 ppm Ni), and very low values ($\leq$ 50 ppm) in the more differentiated, iron-rich mafic pegmatoids. Sc, Ti and V abundances in the cumulates vary with the modal abundance of clinopyroxene, and, in the more differentiated cumulates, with the modal abundance of Fe-Ti oxide (Ti, V). Sr contents increase regularly with decrease in *mg*, primarily reflecting the increase

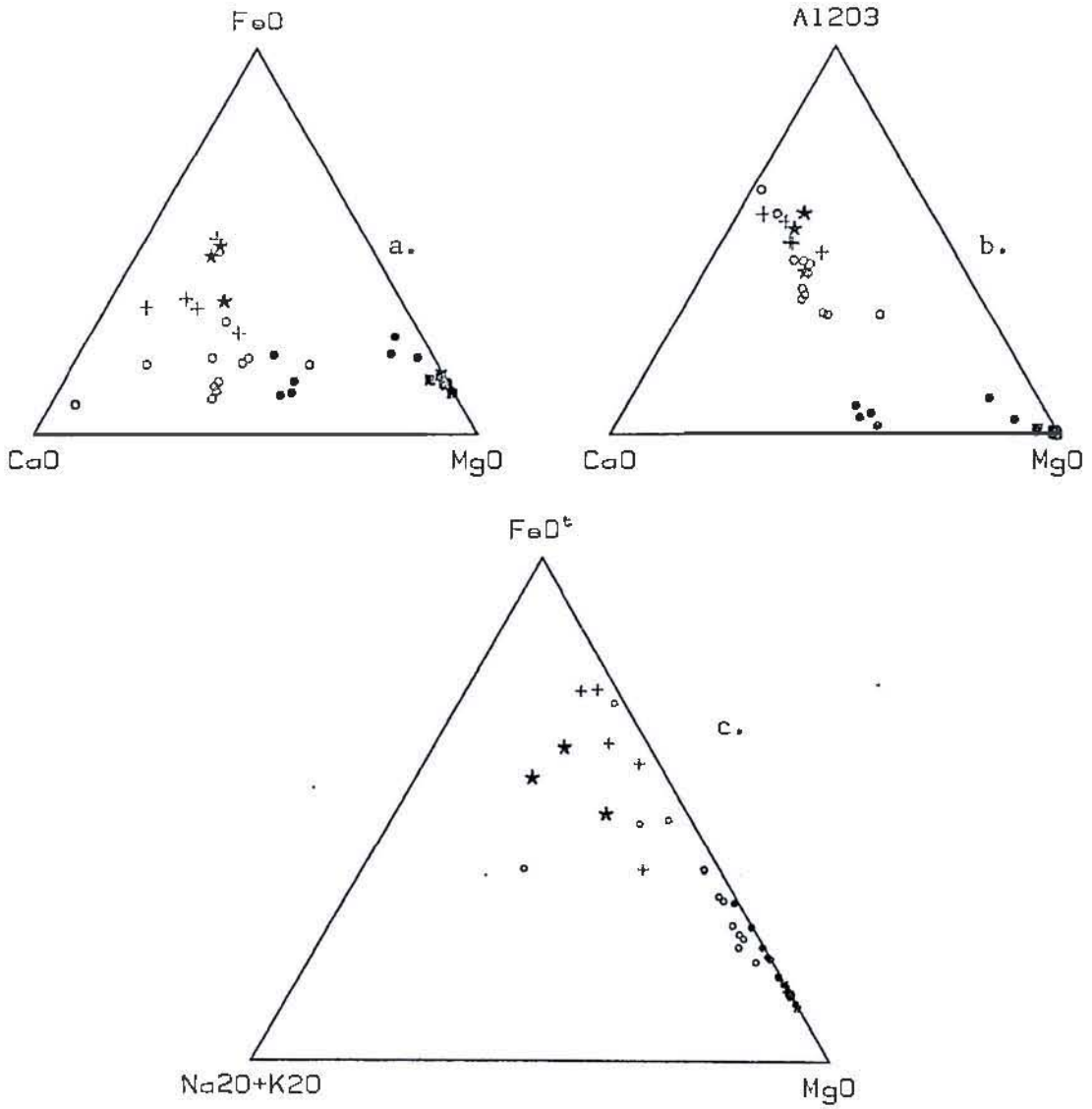

Fig. 1-24. Compositional variation of Marum layered rocks in terms of a) CaO-FeO-MgO, b) $CaO-Al_2O_3-MgO$, c) $Na_2O+K_2O-FeO-MgO$ compared to the tectonite peridotites (squares). Closed circles = cumulate peridotite, open circle = cumulate gabbro, crosses = pegmatoids, stars = dolerites.

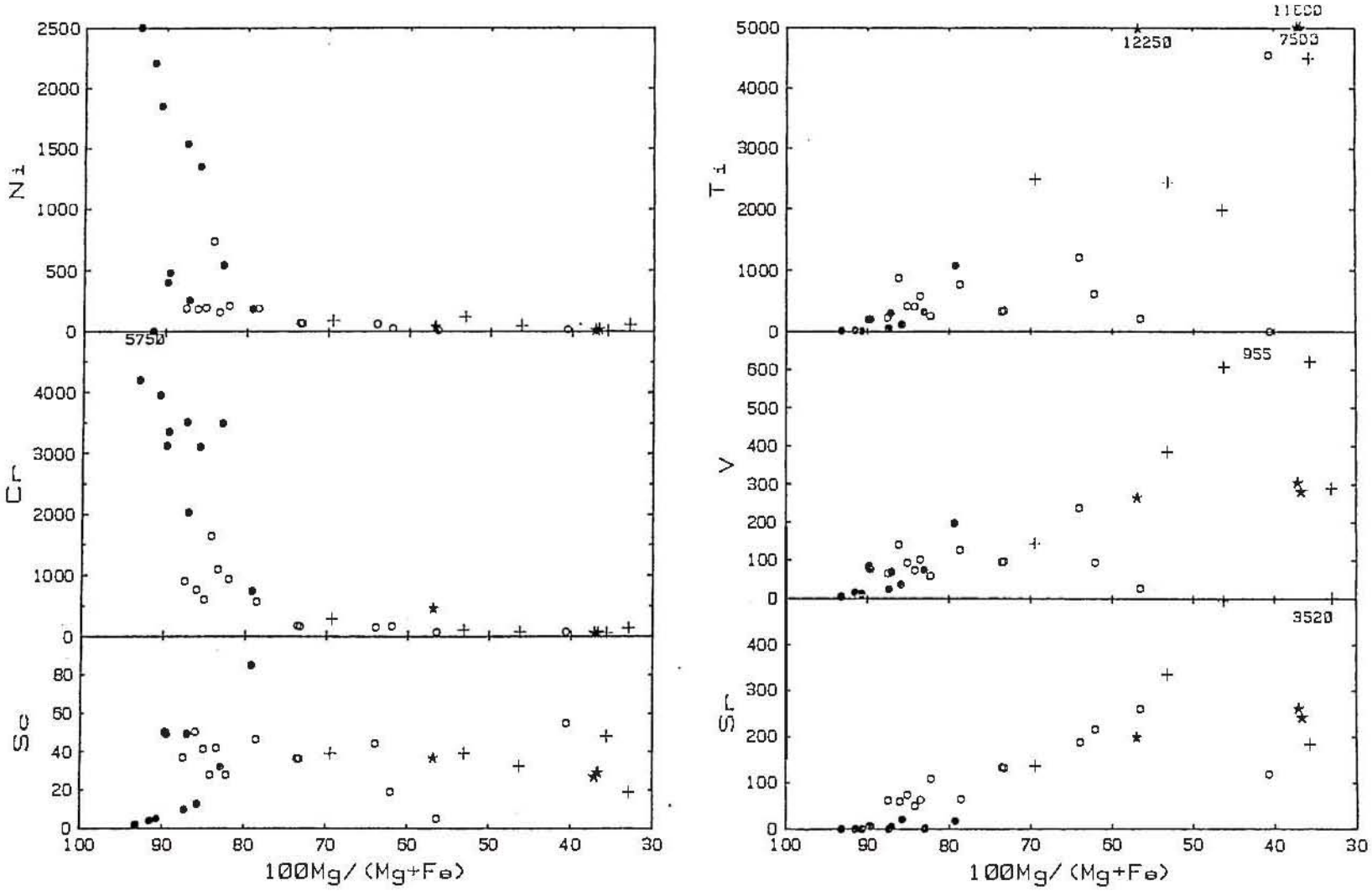

Fig. 1-25. Variation in trace elements with 100Mg/(Mg+ΣFe) of Marum layered sequence. Symbols as for Fig. 1-24.

in modal abundance of plagioclase, and reach a peak of 260 ppm in anorthosite (Fig. 1-25). The most iron-rich mafic pegmatoid contains extremely high abundances of Sr (3520 ppm), Rb and Ba suggesting that this rock is a residual liquid into which the incompatible elements have been partitioned. Zr, Nb, Y, Ba and Rb abundances in the cumulates are very low, and appreciably higher in all the non-cumulus rocks.

The extremely low abundances of incompatible elements, and the high abundances of the compatible elements Ni, Cr in the early cumulates confirms the petrologic interpretation of the layered rocks as cumulates which contain virtually no intercumulus melt. The quartz microgabbro and quartz dolerites have similar Ni, Cr and V but far higher Ti, Zr, Y and REE than gabbroic rocks of comparable *mg*-value.

4-4. REE

REE and additional trace elements U, Th, Pb, Hf, Cs were determined by spark source mass spectrometry (Appendix 1) for 5 cumulate rocks, a granophyric diorite, and a microgabbro-dolerite dyke which intrudes the layered sequence. Analyses are presented in Table 1-20 and the chondrite-normalized * REE patterns shown in Figure 1-26.

The REE abundances in a cumulate rock may be expected to vary according to the amount of interstitial material (Kay & Senechal, 1976) and the degree of differentiation of the magma (Montigny & others, 1973). The Marum cumulates have chondrite-normalized REE patterns which are depleted in LREE but the overall level of REE varies by almost a factor of 10 (Fig. 1-26). In the Marum cumulates the level of LREE-depletion and the absolute abundance of REE correlate primarily with the modal abundance of pyroxene, and, to a lesser extent, with the degree of differentiation of

---

* All REE data have been normalized to the chondrite-normalizing values of Taylor & Gorton (1977) (Appendix 1).

TABLE 1-20. REE ABUNDANCES IN MARUM CUMULATES

	271	051	225	1020	128	578*	576**
La	0.04	0.04	-	-	-	0.85	7.76
Ce	-	-	0.03	0.42	0.18	2.11	19.95
Pr	-	-	0.05	0.08	0.03	0.36	2.56
Nd	0.085	0.21	0.33	0.56	0.14	1.90	11.36
Sm	0.03	0.09	0.16	0.29	0.05	0.63	2.70
Eu	0.023	0.033	0.10	0.15	0.04	0.21	0.90
Gd	0.05	0.13	0.30	0.51	0.10	0.85	3.05
Tb	0.01	0.025	0.07	0.10	-	0.16	0.52
Dy	-	0.16	0.45	0.73	0.11	1.15	10.34
Ho	-	-	0.11	0.18	0.02	0.27	0.74
Er	0.05	0.10	0.31	0.53	-	0.82	2.12
Tm	-	-	-	-	-	-	-
Yb	0.06	0.095	0.29	0.54	0.075	0.77	2.05
La_N/Sm_N	0.81	0.27	(0.36)	(0.25)	(0.81)	0.82	1.75
La_N/Yb_N	0.44	0.26	(0.22)	(0.14)	(0.58)	0.73	2.50
Eu/Eu*	1.71	0.90	1.43	1.24	1.61	0.91	0.97
Cs	-	0.01	-	-	-	0.03	0.16
Pb	0.09	0.13	0.16	0.29	0.18	0.65	3.5
Th	-	-	-	-	-	0.14	2.07
U	-	-	-	-	-	0.11	0.45
Hf	-	-	0.07	0.10	-	0.62	1.50

Values in parentheses are interpolated from Ce values and the REE profile.

* Non-cumulus granophyric diorite.

** Quartz microgabbro dyke intruding cumulate sequence.

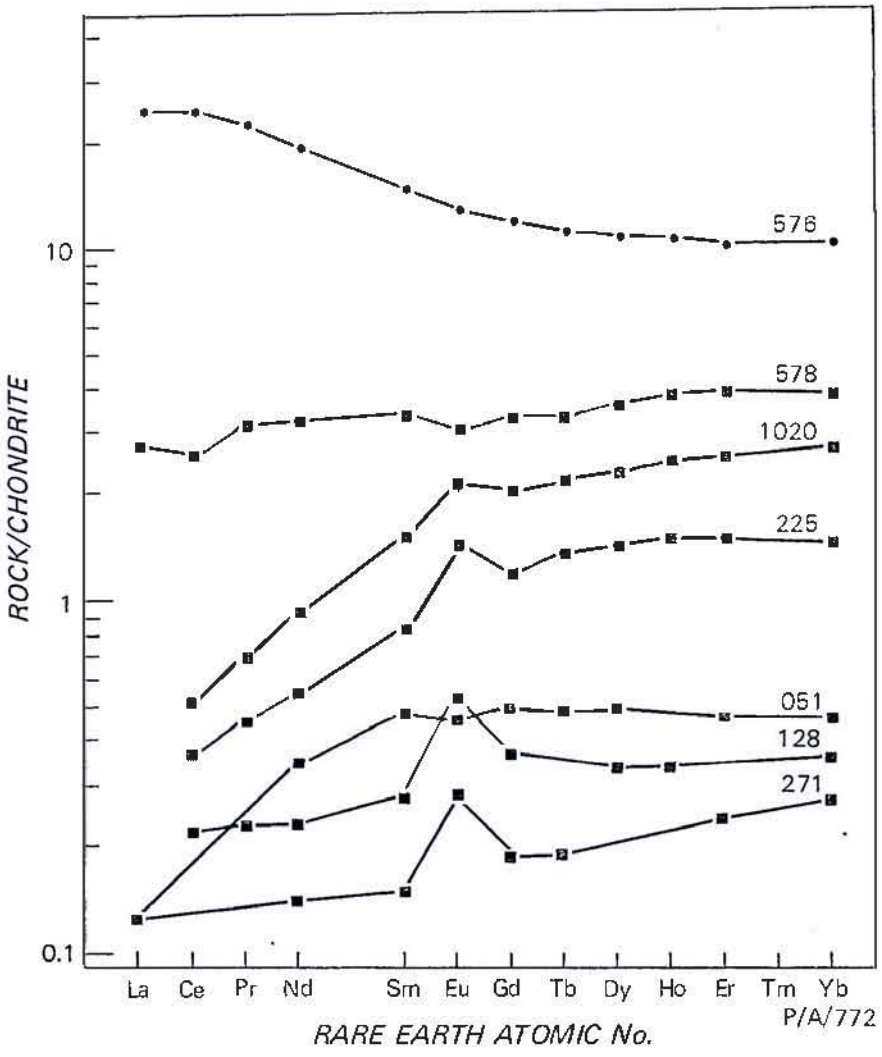

Fig. 1-26. Chondrite-normalized REE patterns for Marum peridotites and gabbros (squares) and microgabbro (576). Sample 271 = plagioclase lherzolite, 051 = olivine websterite, 128 = deformed quartz-magnetite-norite-gabbro, 225 = olivine norite-gabbro, 1020 = norite-gabbro, 578 = granophyric diorite.

the cumulate (bulk rock *mg*). Olivine pyroxenite 051 has a chondrite-normalized REE pattern which is typical of clinopyroxene, being strongly depleted in LREE and slightly depleted in HREE (heavy REE) relative to MREE (middle REE), i.e. $Gd_N/Yb_N = 1.10$). The variation in REE profile and abundance of REE in the cumulates with the modal abundance of clinopyroxene implies that the slope of the REE pattern directly reflects the fractionation of REE between clinopyroxene and basaltic liquid. The plagioclase cumulates have positive Eu anomalies consistent with accumulation of calcic plagioclase. The magnitude of the Eu anomaly decreases with increase in overall abundance of REE (modal abundance of clinopyroxene) and, to a lesser extent, with decrease in *mg* number of the rock. The low absolute abundances of REE in gabbro 128 are diluted by the presence of modal quartz and Fe-Ti oxide.

The Marum cumulates are strikingly similar to cumulate gabbros from other ophiolites, such as the Troodos (Kay & Senechal, 1976), Pindos (Montigny & others, 1973), Bay of Islands (Suen & others, in press), Papua (PART 2), and from the ocean floor (Masuda & Jibiki, 1973; Dostal & Muecke, 1978). All are characterized by LREE-depleted patterns and low overall abundances of REE, and contrast markedly with cumulate gabbros from the Sarmiento ophiolite (Saunders & others, 1979) both in terms of La_N/Sm_N ratios and overall abundance of REE.

Granophyric diorite 578 has a higher level of REE than the cumulates, and has a chondrite-normalized REE pattern with distinct negative Eu and Ce anomalies (Fig. 1-26). The Eu anomaly undoubtedly reflects extensive plagioclase fractionation in the gabbros lower in the cumulate pile. The Ce anomaly might reflect a high f_{O_2} in residual intercumulus liquids derived from the cumulate pile: this interpretation is supported by the extensive deuteric alteration of pyroxene to amphibole, however the Fe_2O_3 content of the rock is not unduly high. The REE content of the granophyric diorite differs considerably from that of felsic differentiates found in other ophiolites and stratiform intrusions (e.g. Coleman &

Peterman, 1975; Coleman, 1977; Saunders & others, 1979; Haskin & Haskin, 1968). Felsic differentiates broadly of trondhjemitic composition in ophiolites, generally referred to as oceanic plagiogranites (Coleman & Peterman, 1975), typically have chondrite-normalized REE patterns similar to those of the underlying cumulates but the absolute level of REE (and Zr, Y, Nb, P, etc.) is markedly higher due to extensive fractionation of olivine, pyroxene and plagioclase. Such differentiates typically have marked negative Eu anomalies consistent with extensive plagioclase fractionation.

Microgabbro 576 has a markedly different REE pattern to that of the cumulates (Fig. 1-26). The pattern is enriched in LREE (La_N/Sm_N = 1.75) at ∿ 20 x chondritic abundance, similar to the Tumu River basalts (Chapter 5) but overall abundances of REE, Zr and Y are very low for such a differentiated rock (*mg* = 39). The difference in REE pattern together with both the microgabbro and dolerites compared to the gabbro pegmatoids suggest that the dyke rocks are not genetically related to the layered sequence. This is also suggested by the poor correlation of these rocks with those of the layered sequence on Ti-V (Fig. 1-38) and other trace element (e.g. Ti-Zr, Zr-Y) diagrams.

4-5. Strontium isotope ratios

$^{87}Sr/^{86}Sr$ ratios have been determined for 4 gabbros from the Marum layered sequence by Dr. R.W. Page (Appendix 1). The values range from 0.7031 to 0.7038 and are very similar to values obtained for gabbros from the Papuan ophiolite (PART 2), and comparable (although slightly lower than) the average ratio found for calc-alkaline intrusives in the Papua New Guinea highlands (Page, 1976). The ratios are thought to be close to primary values since the samples are unaltered and show no evidence of Rb enrichment. These ratios are slightly higher than commonly found for fresh MORB and more in line with values obtained for island-arc volcanic rocks

(see PART 2, Chapter 3). Like most MORB the Rb/Sr ratio of the Marum rocks is too low to support their present $^{87}Sr/^{86}Sr$ ratio. Similar values have been reported from the Troodos (Peterman & others, 1971; Kay & Senechal, 1976; Spooner & others, 1977) and Mediterranean ophiolites (Allegre & others, in press).

The data, although limited, appear to show a correlation between $^{87}Sr/^{86}Sr$ ratio and Rb/Sr ratio, and bulk rock *mg* (Fig. 1-27). Further work is needed to examine this apparent relationship which, if substantiated, is highly significant in making comparisons with common MORB since the Marum gabbros (like many other gabbros from ophiolites for which Sr isotopes have been determined) are differentiated compared to commonly sampled MORB. For example, the most magnesian Marum cumulate analysed (for $^{87}Sr/^{86}Sr$ ratio) contains olivine Mg_{80} which, from the Fe-Mg partitioning between olivine and liquid (Roeder & Emslie, 1970), implies a co-existing basalt of Mg_{55}.

4-6. Trace element content of the parent magma

The trace element content of a liquid in equilibrium with a cumulus phase(s) can be calculated from the Nernst equation ($D^{i} = \frac{c^{i}_{\alpha}}{c^{i}_{1}}$ where D^{i*} = the partition coefficient for element i, c^{i}_{α} = the concentration of element i in phase α, c^{i}_{1} = concentration of i in the liquid) if equilibrium exists between the entire separated solid and the melt. Partitioning of this type (*total equilibrium*) is probably restricted to plutonic crystallization and is not applicable to shallow level fractionation or closed system fractionated during crystallization of a lava, where equilibrium is obtained only between the surface of the solid and the liquid (*surface or logarithmic equilibrium*). Under surface equilibrium partitioning of trace elements follows the Rayleigh (logarithmic) equation $c^{i}_{1} = c^{i}_{o} \; F^{(D-1)}$

---

* For crystal aggregates, i.e. cumulate rocks, the bulk distribution coefficient $\overline{D}$ is used, where $D^{-i} = D^{i}x_{\alpha} + D^{i}x_{\beta} + D^{i}x_{\psi}$ + etc, and x_{α}, x_{β} etc. are the weight fractions of phases α, β, ψ, etc.

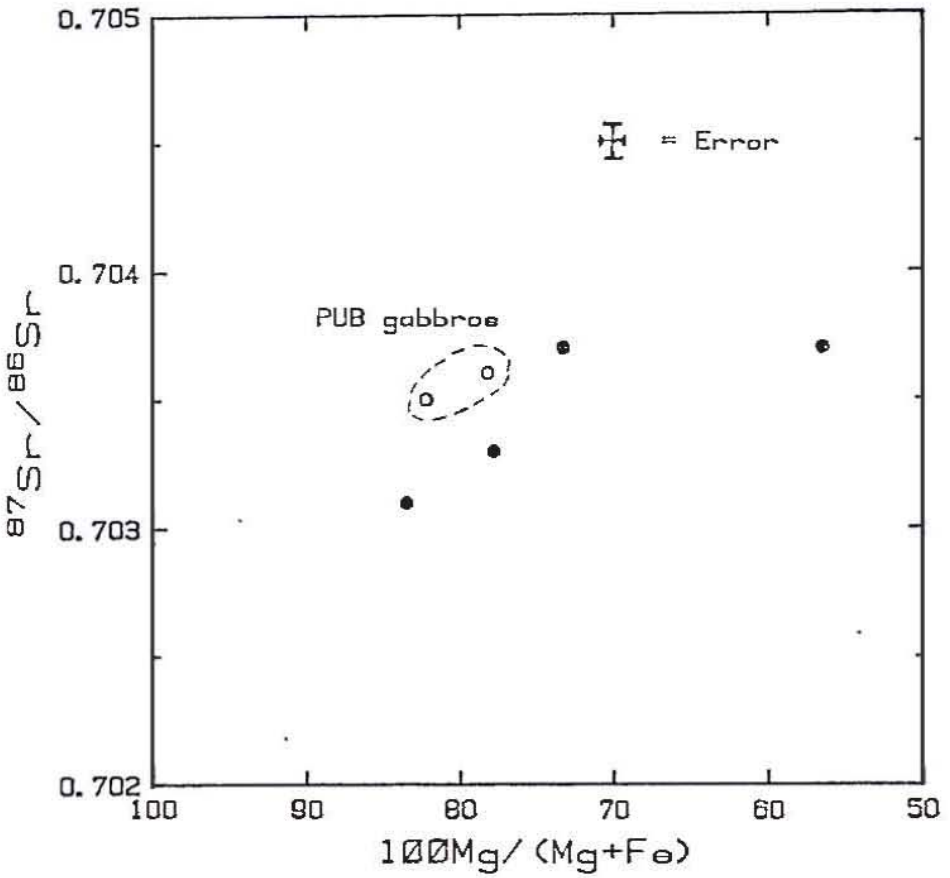

Fig. 1-27. Plot of $^{87}Sr/^{86}Sr$ versus 100Mg/(Mg+ΣFe) for Marum gabbros (closed circles) and Papuan Ultramafic Belt gabbros (open circles).

where c_o^i = the concentration of element i in the initial liquid, F = the fraction of liquid remaining.

Paster & others (1974) showed that the partitioning of trace elements during crystallization of the cumulate gabbros of the layered series of the Skaergaard Intrusion most closely followed a surface equilibrium model, and derived the following equation to describe the partitioning of trace elements between the solid and the co-existing liquid at any point during crystallization of the liquid:

$$c_s^i = c_o^i \left\{ \frac{1 - (1-X)^{\bar{D}}}{X} \right\}$$ where c_s^i = concentration of i in solid s, c_o^i = the concentration of i in the initial liquid, X = fraction of solidification, $\bar{D}$ = the bulk partition coefficient of the solid. Haskin & Korotev (1977) showed that this equation describes the partitioning behaviour of trace elements during closed-system crystallization of silicate melts in general. They also showed that application of total equilibrium models (using published partition coefficients) to cumulate rocks containing interstitial melt or postcumulus material, or where crystals are strongly zoned with respect to trace elements, can lead to gross over-estimation of the abundances of incompatible elements, and under-estimation of compatible elements, in the co-existing liquid. In practice, the trace element partitioning in most cumulate rocks may be expected to lie between the two extremes of surface and total equilibrium, since most cumulates consist of primocrysts and variable amounts of postcumulus or intercumulus material.

The extremely low abundances of incompatible elements, the allotriomorphic granular texture, and lack of interstitial phases or mesostasis in the Marum cumulates are more consistent with *total* rather than surface equilibrium partitioning. These features also characterize gabbroic cumulates from the Papuan (PART 2), Troodos (Kay & Senechal, 1976), and other ophiolites (e.g. Coleman, 1977), and from the ocean floor

(e.g. Hodges & Papike, 1976; Dostal & Muecke, 1978), and suggest that total equilibrium may have been closely approached in these large magma chambers which periodically received fresh influxes of basaltic magma.

On this basis the REE content of the liquid co-existing with Marum gabbros 225 and 1020 has been calculated assuming total equilibrium between crystals and melt using the modal abundance of the cumulus phases (determined by mixing models using the compositions of constituent phases obtained by microprobe and the bulk composition) and published partition coefficients (Appendix 1). The chondrite-normalized REE patterns for the calculated equilibrium liquids are shown in Figure 1-28 together with the range of REE abundances found for MORB (Bryan & others, 1976), and for the Tumu River basalts (Chapter 5). Also shown is the average REE pattern for the highly LREE-depleted 'primitive' basalts from DSDP Leg 3 (Frey & others, 1974). The liquids calculated for the gabbros have LREE-depleted patterns (La_N/Sm_N = 0.5) similar to the gabbro cumulates (but with strong negative Eu anomalies) at 11-25 x chondritic abundance (HREE). The calculated REE abundances in the equilibrium liquids are considered to be a *maximum* because the partition coefficients used in the calculations (particularly for ferromagnesian phases) are probably minimum values (Frey & others, 1978) and because the presence of adcumulus material in the gabbros will result in over-estimation of the equilibrium liquid abundances (Haskin & Korotev, 1977). By similar reasoning, the degree of depletion of the LREE in the calculated equilibrium liquid can be taken as a minimum. The calculations therefore suggest that the mafic liquids parental to the cumulate gabbros were strongly depleted in LREE (and other LIL elements), similar to the strongly depleted basalts from DSDP Leg 3. However, since the cumulate gabbros are fractionated relative to the underlying peridotite cumulates the level of REE in the parent magma(s) must have been appreciably lower, and thus lower than exhibited by MORB sampled to date.

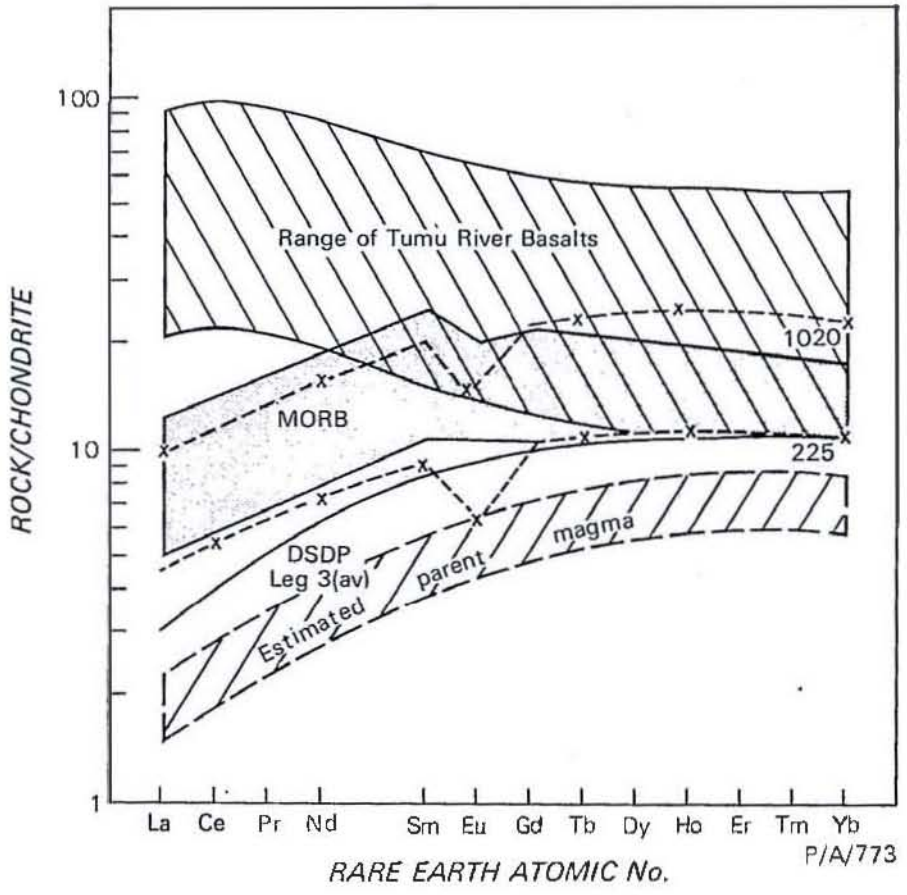

Fig. 1-28. Chondrite-normalized REE patterns of calculated equilibrium liquids for cumulate gabbros 1020 and 225 (dashed lines) compared to the range for MORB (Frey & others, 1974) and the Tumu River basalts (Chapter 5). Solid line = average of DSDP Leg 3 basalts (Frey & others, 1974). Estimated parent magma for Marum cumulates has ∿ 6-9 x chondrites (HREE) - see text.

The REE content was also calculated by similar method for the liquid in equilibrium with cumulate pyroxenite 051. The calculated equilibrium liquid in this case is LREE-enriched (La_N/Sm_N = 1.9) with HREE ∿ 4 x chondritic. Taken at face value this implies the existence of additional parent magmas of markedly different trace element abundances to those inferred above. However, as earlier pointed out, modelling of this type is critically dependent on the choice of partition coefficients, and the very low partition coefficients used will over-estimate both the absolute abundance of REE and the degree of LREE enrichment. In order to relate pyroxenite 051 to a strongly LREE-depleted magma similar to that parental to the other cumulates the bulk REE partition coefficients must have similar form to the REE pattern of the pyroxenite itself and have La_N/Sm_N ∿ 0.5 and La_N/Yb_N ∿ 0.6. Such a pattern is broadly consistent with pyroxene domination but the clinopyroxene REE partition coefficients must more closely resemble the values used by Kay & Gast (1973) rather than the very low values used in the calculations. The inferred higher partition coefficients may be due to the presence of adcumulus material with higher REE content; this explanation is consistent with the petrographic evidence of zoning in the pyroxenes. The apparent discrepancy in the degree of LREE depletion among the calculated parent magmas therefore seems more likely to be due to the use of inappropriate partition coefficients rather than to the existence of a LREE-enriched parent magma.

Abundances of Ti and Zr in the liquid which equilibrated with olivine gabbro 225 have been estimated by a similar approach using the partition coefficients in Appendix 1. If the lowest partition coefficients are used the equilibrium liquid is estimated to contain ∿ 5000 ppm Ti and ∿ 60 ppm Zr, whereas considerably lower abundances ∿ 3500 ppm Ti and ∿ 30 ppm Zr are obtained if intermediate values for the partition coefficients are used. Since cumulate gabbro 225 (*mg* ∿ 84, olivine Mg_{80}) is differentiated compared to the underlying cumulate peridotites (*mg* ∿ 90, olivine Mg_{90})

the primary parent magmas can be inferred to have contained appreciably lower abundances of Ti and Zr. Assuming that cumulate gabbro 225 represents, say, 20% crystal fractionation, then the primary parent magma can be inferred (from the equation for total equilibrium fractionation, i.e. $\frac{c_l}{c_o} = \frac{1}{F+D(1-F)}$) to have contained a maximum of 4000 ppm Ti and 50 ppm Zr. Similarly the abundance of HREE in the primary parent magma can be estimated to be less than 10 x chondritic, probably ∿ 6-9 x (Fig. 1-28). These low abundances of high valence cations are in keeping with the inferences made from the petrology of the cumulates (Chapter 3) and with calculations for pyroxenites and peridotites which suggest that the Ti content of the parent magma may have been as low as 2000-2500 ppm.

These calculations, and the conclusions drawn from the petrology of the cumulates, point to a highly magnesian olivine-poor tholeiite or quartz tholeiite parent magma with high Ni (300-600 ppm) and Cr (1500-2000 ppm) contents, very low abundances of LIL elements (including LREE, Ti, Zr, Nb), and depleted in LREE (La_N/Sm_N ∿ 0.5) with an overall HREE abundance of 6-9 x chondritic. Modern examples of such magmas are not readily apparent. These abundances of Ti, Zr, Hf, Y and HREE are lower than found in even the most depleted primitive MORB, such as DSDP 3-14, 18 (Frey & others, 1974). Low abundances of REE, Ti, Zr, Y are a feature of the island-arc tholeiite suite but arc tholeiites typically have low Ni and Cr contents (Jakeš & Gill, 1970; Gill, 1976; Ewart & others, 1977). High-Mg andesites or boninites typically have low abundances of Ti, Zr, HREE and high Ni and Cr contents, but are enriched in LREE (Sun & Nesbitt, 1978a: Dietrich & others, 1978; F.A. Frey, pers. comm. 1979). Komatiites of Archaean greenstone belts are also characterized by low Ti, Zr, Y and HREE, and high Ni and Cr contents compared to MORB (e.g. Arndt & others, 1977; Hawkesworth & O'Nions, 1977; Arth & others, 1977; Nesbitt & Sun, 1976; Sun & Nesbitt, 1978b). Basaltic members of the komatiite suite, however, exhibit considerable variation in the level of LIL elements, and many are enriched in LREE (Sun & Nesbitt, 1978b).

Lavas with trace element abundances most closely resembling those inferred for the Marum parent magma are well represented in the Upper Pillow Lavas of the Troodos ophiolite which typically have low Ti (∿ 3300 ppm), Zr (∿ 31 ppm) and Y (∿ 15 ppm), and high Cr (Smewing & others, 1975), and are strongly depleted in LREE with HREE abundances ranging from 5-12 x chondritic (Smewing & Potts, 1976; Kay & Senechal, 1976).

4-7. Conclusions

The geochemistry of the layered peridotites and gabbros supports the petrologic interpretation of these rocks as cumulates from a highly magnesian melt with low abundances of LIL elements. The cumulates range from highly magnesian compositions with extremely low abundances of lithophile elements through CaO-MgO-rich cumulates to CaO-Al_2O_3-rich cumulates enriched in Fe. Ni and Cr contents decrease with decreasing modal abundance of olivine and rock *mg*; Sc, V and Ti abundances vary with the modal abundance of pyroxene (and Fe-Ti oxides in the ferrogabbros), and, to a lesser extent, rock *mg*. Abundances of Ti, Zr, Y, Nb, Ba, Rb and K are very low in all the Marum rocks but are enriched in the non-cumulate rocks over the cumulates, consistent with the petrologic and major element evidence that these rocks represent residual liquids formed by differentiation.

The textures and very low abundances of incompatible elements of the cumulates suggest a close approach to total equilibrium partitioning of trace elements during crystallization. Calculations based on a total equilibrium model, using the modal proportions of cumulus phases and published partition coefficients, suggest that the parent magma(s) to the cumulate sequence contained < 4000 ppm Ti and < 50 ppm Zr (possibly as low as 2500 ppm Ti) and were strongly depleted in LREE (La_N/Sm_N ∿ 0.5) with ∿ 6-9 x chondritic abundance of HREE. These characteristics, together with the high Ni and Cr contents (300-600 ppm Ni, 1500-2000 ppm Cr) inferred from the petrology of the cumulates, point to a parent magma(s) similar in composition to the more 'primitive' basalts of the UPL of the Troodos ophiolite.

CHAPTER 5

ASSOCIATED BASALTS AND SEDIMENTS *

5-1. Petrography of the Tumu River basalts

The Tumu River basalts consist mainly of basaltic pillow lava and lava, with minor aquagene breccia and some dolerite dykes. Most of the lavas have undergone low-grade (zeolite facies) metamorphism and petrographically are spilites. Secondary minerals - chlorite, smectite, epidote, calcite, zeolite, sphene and leucoxene - occur in variable amounts in the groundmass of most lavas. Prehnite and rare pumpellyite occur in some breccias and tuff. Greenschist facies metabasites occur near the thrust separating the basalts from the peridotite-gabbro massif, and range from actinolite-chlorite ($\pm$ epidote, albite, sphene) schists through weakly and incipiently metamorphosed greenschist to spilite with increasing distance from the imbricate zone.

The dominant primary mineral assemblage is plagioclase, clinopyroxene and Fe-Ti oxide (titanomagnetite, some ilmenite). Most lavas are classified as augite tholeiites, and have plagioclase (now mostly albite Ab_{96-98}) and augite ($Ca_{42-40}Mg_{44-39}Fe_{14-22}$) microphenocrysts seriate to a fine-grained intergranular, intersertal or pilotaxitic groundmass containing delicate microlites and variolites of plagioclase and/or clinopyroxene, or, in the more fractionated rocks, of skeletal Fe-Ti oxide. Textural evidence indicates that the crystallization order was plagioclase, augite, and Fe-Ti oxide. Many lavas show evidence of a cotectic relationship between plagioclase and pyroxene. No lavas bearing fresh olivine were found but olivine psuedomorphs occur in altered glass with quench clinopyroxene in the most magnesian basalts. Ferrobasalts with high FeO^t (total

---

* This chapter has already been published: Jaques & others (1978).

iron as FeO) - > 15% - and TiO_2 (2-4%) contents have textures suggesting simultaneous crystallization of plagioclase, augite and Fe-Ti oxide.

In general, the paucity of mafic phenocrysts (particularly olivine), plagioclase-pyroxene relationships and an abundance of Fe-Ti oxide indicate crystallization from evolved, fractionated liquids.

Pyroxene

Clinopyroxene (augite) is preserved in all rocks except the schistose metabasalts. Microprobe analysis shows that the pyroxenes are of augite composition, and range from quartz-normative to olivine-hypersthene normative types. On a normative Di-Ol-Hy diagram the Tumu River basalt pyroxenes plot near the Di apex and define a trend away from the Di-Ol join toward silica saturation, indicating a non-alkaline magma type (Coombs, 1963).

The augites are commonly zoned (both concentric and sector zoning) and show Fe enrichment, and Ca depletion trends (Fig. 1-29). Microphenocrysts are distinguishable from groundmass pyroxene by higher Mg-values and Cr contents (commonly 0.3 - 0.4% Cr_2O_3, compared to $\sim$ 0.1 in the groundmass), and lower Ti and Al contents. These features, together with the trends in Figure 1-29 and the high TiO_2 and Al_2O_3 contents of pyroxene rims (up to 3% TiO_2, 4% Al_2O_3) relative to cores (< 1% TiO_2, 1.5% Al_2O_3), suggest quench or metastable growth (e.g. Smith & Lindsley, 1971). Similar trends have been observed in a number of DSDP basalts (e.g. Ayuso & others, 1976).

5-2. Geochemistry

Low temperature alteration - weathering, low grade metamorphism (including spilitization), and interaction with sea water, can have considerable effects on bulk rock composition (e.g. Smith, 1968; Cann, 1969; Hart, 1970; Aumento & others, 1976) and significantly change the abundance of certain trace elements (Hart, 1969; Cann, 1970). Despite the

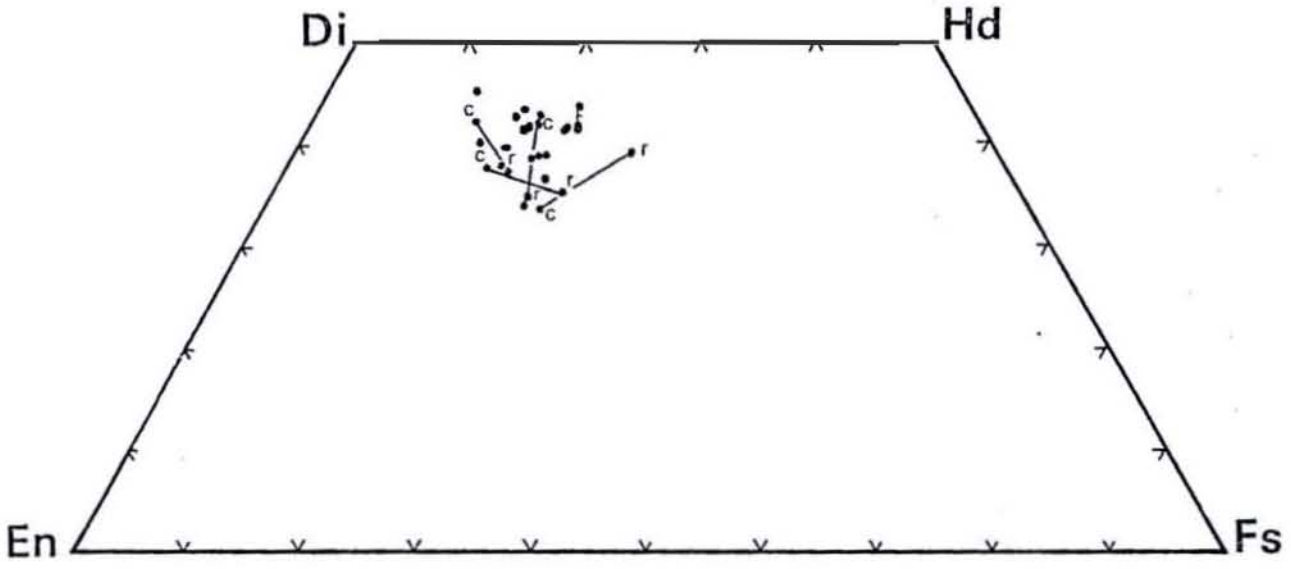

Fig. 1-29. Pyroxene quadrilateral showing compositions of analysed clinopyroxenes in Tumu River basalts. Tie lines join mineral cores (c) to rims (r).

secondary mineral assemblage, high volatile contents and moderately high Fe_2O_3/FeO ratios of the Tumu River basalts, a good correlation still exists between the mineral mode and major element compositions, and indicator trace elements such as Ni, Cr, V and Zr. SiO_2 and Al_2O_3 contents mostly lie within the range of basaltic compositions. However, the spilitic basalts have significantly lower CaO and higher Na_2O than appropriate for their Al_2O_3 contents, and it seems likely that in common with other described spilites (e.g. Cann, 1971; Vallance, 1974) there has been a loss in CaO and a gain in Na_2O and H_2O.

The effect of alteration on LIL trace elements was tested by examining the correlation with Zr, a LIL element known to be relatively insensitive to the effects of low-grade metamorphism (Pearce & Cann, 1971, 1973; Smith & Smith, 1976). Rb, Cs, Sr, K, U and Th showed very poor correlation, indicating a high mobility during alteration. Y showed excellent correlation (Fig. 1-30) apart from four samples (549, 550, 080, 083) which deviated appreciably. These samples have low CaO/Al_2O_3, low Y/Nb (< 3), appreciably higher P_2O_5 and, in some cases, Rb, Ba, Sr than the other metabasalts, and are thought to be chemically altered. La_N/Y_N * ratios in these rocks are also high (see later). Significantly three of the four rocks were originally glass-bearing, and alteration of glass is known to result in greater chemical mobility than alteration of crystalline rocks. It is concluded that although changes in Ca, Na, K, Rb, Sr, Ba contents have occurred in many of the samples consistency in the ratios of the more insensitive LIL elements Ti, P, Zr, Hf, Y indicates that, in general, little change in the abundances of these elements has occurred. In addition, the abundances of a number of other trace elements (Ni, Cr, V, Zn), and some major element abundances have not changed markedly during alteration.

---

* La and Y normalized to the chondrite abundances of Taylor & Gorton (1977). Y behaves as a HREE with ionic radius intermediate between Dy and Ho.

TABLE 1-21. CHEMICAL ANALYSES OF TUMU RIVER BASALTS

	1 143	2 524	3 522	4 1007	5 521	6 1057	7 036	8 081	9 549
SiO_2	51.42	49.91	50.97	47.52	51.02	46.17	50.60	51.22	47.65
TiO_2	1.35	1.66	1.71	2.11	1.80	2.01	2.19	1.89	3.02
Al_2O_3	11.90	13.11	14.40	16.17	15.23	16.03	14.37	14.11	16.84
Fe_2O_3[a]	1.34	1.34	1.31	1.53	1.22	1.39	1.48	1.54	1.62
FeO	8.95	8.91	8.68	10.19	8.09	9.24	9.84	10.28	10.83
MnO	0.18	0.11	0.16	0.19	0.16	0.19	0.25	0.19	0.63
MgO	12.40	10.97	8.24	9.37	7.17	7.38	7.30	7.61	8.00
CaO	9.51	10.51	9.95	7.90	11.10	14.76	8.78	8.56	6.80
NaO	2.47	2.79	3.98	3.32	3.68	2.53	4.86	4.43	3.85
K_2O	0.24	0.12	0.08	0.83	0.06	0.23	0.10	0.23	0.31
P_2O_5	0.12	0.13	0.17	0.32	0.14	0.31	0.27	0.18	0.54
Mg-value	71.2	68.0	62.9	62.1	61.2	58.7	56.9	56.9	56.8
LOI	4.17	3.73	2.87	5.87	2.83	5.70	4.07	3.82	5.60
Original $\frac{Fe_2O_3}{FeO}$	0.21	0.66	0.86	0.38	0.80	0.63	0.62	0.44	0.52
p.p.m.									
Sc	25	34	35	27	37	34	38	32	25
V	184	223	237	236	267	264	277	267	233
Cr	875	685	520	209	565	282	173	179	54
Ni	420	340	184	147	152	110	32	94	40
Cu	67	45	79	45	90	58	68	56	32
Zn	97	102	98	111	93	94	116	105	113
Ba	51[b]	28[b]	30	50	20	20	70	40	195[b]
Rb	2.2	0.5	0.2	8.8	0.3	2.8	3.8	1.6	2.6
Sr	119	229	139	150	133	104	277	217	361
Y	19	20	23	36	22	32	35	21	26
Zr	80	97	106	154	102	158	173	106	209
Hf	2.68	2.8							5.9
Nb	6	6	6	9	5	10	11	10	28
Th	1.18	0.9							2.69
U	0.27	0.2							0.81
La	7	5		9	5	10	11	9	20
Ce	19	20		27	16	31	31	27	51
Nd	10	10		15	10	17	19	14	24
La_S/Y_S	2.34	1.59		1.59	1.44	1.98	2.0	2.72	4.88
Zr/Nb	13	16	18	17	20	16	16	11	8
K/Rb	905	1990	2350	780	1660	680	655	1190	990

	10 566	11 563	12 465	13 035	14 508	15 080	16 539	17 468	18 561
SiO_2	49.92	47.63	49.26	49.93	49.04	48.22	47.13	47.81	49.09
TiO_2	1.99	2.21	1.49	1.62	1.93	2.79	3.39	3.90	3.85
Al_2O_3	14.17	14.88	17.66	13.42	15.03	13.30	13.56	12.45	12.75
Fe_2O_3[a]	1.57	1.60	1.16	1.37	1.63	1.91	1.96	2.09	2.14
FeO	10.48	10.70	7.72	9.16	10.90	12.72	13.02	13.90	14.26
MnO	0.20	0.25	0.17	0.20	0.23	0.27	0.25	0.23	0.21
MgO	7.40	7.27	5.18	6.00	6.79	7.46	5.94	5.87	5.57
CaO	9.77	11.56	13.12	13.03	10.51	8.81	9.41	9.05	7.52
Na_2O	3.99	3.07	4.07	4.31	3.97	4.19	4.17	4.41	4.32
K_2O	0.54	1.04	0.27	0.28	0.11	0.28	0.32	0.05	0.17
P_2O_5	0.22	0.23	0.18	0.15	0.16	0.30	0.45	0.50	0.40
Mg-value	55.7	54.8	54.5	53.9	52.6	51.1	44.8	42.9	41.0
LOI	4.35	5.66	5.61	6.04	4.36	4.18	4.88	3.85	3.97
Original $\frac{Fe_2O_3}{FeO}$	0.40	0.51	0.35	0.63	0.41	0.52	0.49	0.44	0.57
p.p.m									
Sc	35	34	32	35	51	35	43	44	43
V	264	275	208	263	347	419	364	437	413
Cr	128	116	246	246	161	78	99	84	63
Ni	42	45	41	75	60	63	34	33	30
Cu	65	66	58	53	77	194	37	58	37
Zn	105	118	82	91	113	137	141	159	145
Ba	160	20	40	40	32[b]	70	60	20	40
Rb	5.6	19.5	3.2	6.6	0.8	3.2	4.2	0.8	1.2
Sr	174	80	226	152	108	311	191	88	117
Y	28	31	24	32	38	29	59	65	63
Zr	137	151	115	117	119	172	256	283	257
Hf					2.7				
Nb	9	9	6	5	5	20	13	16	13
Th					0.36				
U					0.13				
La	9	9	6	7	6	18	13	16	12
Ce	24	27	20	17	21	50	45	48	43
Nd	14	16	13	12	12	22	28	28	26
La_S/Y_S	2.0	1.73	1.59	1.39	1.05	3.94	1.40	1.56	1.21
Zr/Nb	15	17	19	23	24	9	20	18	20
K/Rb	800	440	700	350	1140	725	650	520	1180

Analyses 29-35 are of lower Ti-group. Analyses 29, 33, 34 are for dolerites from Marum gabbros. All trace elements except Th, U, Hf by XRF; Th, U, Hf by spark source mass spectrometry (Taylor, 1965, 1970; Taylor & Gorton, 1977).

[a] Standardised to $\frac{Fe_2O_3}{FeO}=0.15$.

[b] Ba by spark-source mass spectrometry.

TABLE 1-21. CONT.

	19 550	20 438	21 558	22 562	23 083	24 565	25 540	26 560	27 435
SiO_2	48.54	48.68	50.46	47.31	53.82	48.80	49.52	51.06	48.34
TiO_2	3.48	3.60	3.70	3.75	3.00	3.55	3.34	2.72	2.71
Al_2O_3	14.12	12.71	12.51	12.45	11.74	12.32	13.38	13.57	13.72
Fe_2O_3[a]	2.01	1.92	1.89	2.38	1.88	2.20	2.09	2.00	1.98
FeO	13.37	12.78	12.57	15.85	12.54	14.64	13.94	13.37	13.21
MnO	0.20	0.28	0.28	0.28	0.20	0.28	0.30	0.31	0.29
MgO	5.04	4.82	4.74	5.78	4.22	4.55	4.31	3.66	3.15
CaO	7.50	10.21	8.30	7.59	8.07	7.88	7.15	7.05	10.95
Na_2O	4.80	4.60	4.67	4.36	2.31	4.66	5.23	5.54	4.50
K_2O	0.34	0.16	0.26	0.08	1.76	0.07	0.32	0.08	0.09
P_2O_5	0.87	0.38	0.48	0.45	0.75	0.55	0.69	0.89	1.32
Mg-value	40.2	40.2	40.2	39.4	37.5	35.6	35.5	32.8	29.8
LOI	5.28	3.69	3.05	4.12	2.67	3.31	3.30	3.18	3.68
Original $\frac{Fe_2O_3}{FeO}$	0.56	0.64	0.63	0.53	0.52	0.56	0.49	0.44	0.65
p.p.m.									
Sc	30	39	45	41	29	37	39	32	31
V	274	395	408	378	236	330	196	94	59
Cr	27	65	76	30	60	33	41	35	19
Ni	46	22	21	10	17	10	2	3	2
Cu	26	39	40	32	28	17	18	14	13
Zn	156	163	159	171	200	164	195	192	212
Ba	80	10	40	20	900	26[b]	80	<10	<10
Rb	3.4	0.7	1.6	0.3	27	0.3	2.4	0.3	0.4
Sr	136	118	132	91	254	53	152	58	75
Y	42	66	71	77	49	77	99	111	116
Zr	279	282	299	276	313	293	429	438	467
Hf						6.8			
Nb	21	14	15	14	20	16	21	19	22
Th						1.10			
U						0.36			
La	21	13	15	17	24	18	21	24	25
Ce	61	45	47	52	65	52	70	79	83
Nd	31	28	30	30	32	32	42	47	53
La_S/Y_S	3.17	1.25	1.34	1.40	3.11	1.60	1.35	1.37	1.37
Zr/Nb	13	20	20	20	16	18	20	23	21
K/Rb	830	1355	1350	2210	540	1720	1100	2210	1870

	28 1030	29 545	30 034	31 553	32 434	33 576	34 169	35 1053
SiO_2	51.54	50.08	52.22	49.57	52.87	53.55	54.55	53.92
TiO_2	1.23	2.04	1.11	0.99	1.40	1.12	1.25	1.93
Al_2O_3	14.01	14.19	16.50	15.73	15.32	15.70	15.76	15.60
Fe_2O_3[a]	1.49	1.37	1.12	1.28	1.67	1.58	1.50	1.68
FeO	9.94	9.18	7.48	9.33	11.14	10.56	10.01	11.17
MnO	0.20	0.19	0.17	0.20	0.21	0.24	0.21	0.25
MgO	7.67	7.72	6.19	6.01	4.62	4.34	4.08	3.74
CaO	9.76	12.08	9.77	11.10	6.59	9.67	7.87	7.96
Na_2O	3.85	2.63	5.36	4.59	5.43	2.31	3.87	3.01
K_2O	0.43	0.32	0.15	0.09	0.72	0.53	0.85	0.21
P_2O_5	0.11	0.12	0.10	0.48	0.27	0.23	0.28	0.37
Mg-value	62.8	60.0	59.6	53.4	42.5	42.3	42.1	37.4
LOI	3.35	2.62	5.20	4.15	3.85	5.57	4.57	3.43
Original $\frac{Fe_2O_3}{FeO}$	0.44	0.36	0.58	0.53	0.36	0.48	0.49	0.50
p.p.m.								
Sc	47	38	34	26	30	27	29	32
V	325	268	224	336	333	304	280	202
Cr	248	477	311	86	39	53	54	59
Ni	89	43	72	32	13	6	12	10
Cu	135	30	54	159	110	30	65	21
Zn	87	64	74	92	114	96	86	83
Ba	50	40	70	515	250	190[b]	240	60
Rb	5.6	4.6	1.2	0.8	9.8	10.5	15.5	1.6
Sr	303	202	246	402	670	259	240	222
Y	21	19	20	16	28	21	26	41
Zr	63	73	74	78	118	56	98	149
Hf						1.50		
Nb	3	5	5	3.5	2	2	4	7
Th						2.07		
U						0.45		
La	3	6	5		9	8	8	10
Ce	12	19	12		29	24	25	28
Nd	7	11	8		15	11	13	18
La_S/Y_S	0.91	2.01	1.59		2.04	2.42	1.95	1.55
Zr/Nb	21	15	15	22	10	28	25	21
K/Rb	640	580	1040	930	610	420	460	1090

Major and trace element analyses of 32 samples of basalt and dolerite of the Tumu River basalts are presented in Table 1-21. Sample descriptions and localities are presented in Appendix 2. Major elements were determined by microprobe after fusion on an iridium strip heater and trace elements by XRF and spark source mass spectrometry (Appendix 1). Also presented are analyses of three dolerite dykes which intrude the uppermost gabbros in the peridotite-gabbro massif. In view of the inferred Ca loss and Na gain during spilitization normative classification is unlikely to be reliable but significantly the least altered lavas are *ol - hy* normative and plot within the olivine tholeiite field. This, together with the low K_2O and P_2O_5 contents, suggest a subalkaline or tholeiitic type.

Compositions range from relatively unfractionated magnesia-rich types with Mg-values* $\sim$ 70 to the highly fractionated TiO_2-rich ferro-basalts and dolerites with Mg-values $\sim$ 30. Oxide - Mg-value variation diagrams (Fig. 1-31) define differentiation trends of strong iron enrichment, and enrichment in TiO_2 and P_2O_5. Strong iron enrichment typical of tholeiitic suites is also apparent on an AFM diagram.

Trace elements Ni, Cr, V and Zr, (and Y and Zn) show well-defined differentiation trends when plotted against Mg-value (Fig. 1-32); Ni and Cr are rapidly depleted from 'primitive' values (300 ppm Ni; 600 ppm Cr) to extremely low values (< 5 ppm Ni, 50 ppm Cr) in the ferro-basalts. The marked increase in abundance of incompatible elements (Zr, Zn, Y) during fractionation (more than a five-fold increase in Y) is also indicative of strong fractional crystallization. The trend shown by V of increasing abundance in the early and middle stages of differentiation followed by depletion in later liquids, is typical of tholeiitic iron enrichment fractionation patterns.

---

* Mg-value $= \frac{100\ Mg}{Mg + Fe^{2+}}$; Fe_2O_3/FeO standardized to 0.15.

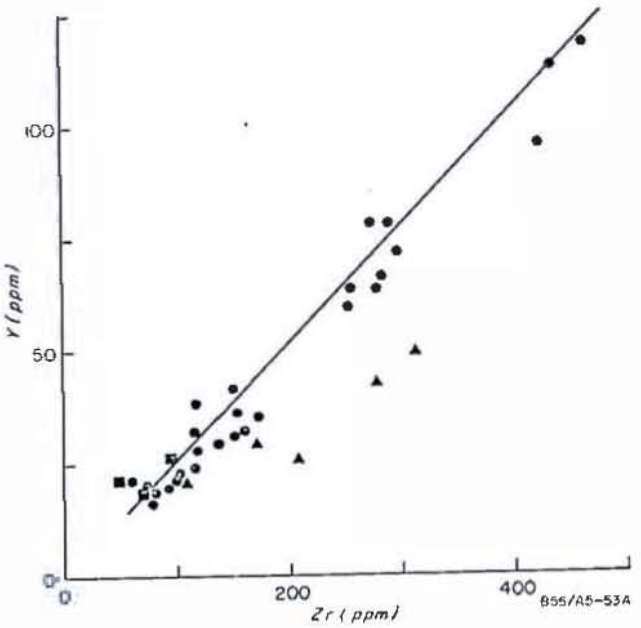

Fig. 1-30. Zr-Y diagram for Tumu River basalts (closed circles). Squares = dolerites in cumulate sequence, triangles are for those rocks recognized as chemically altered.

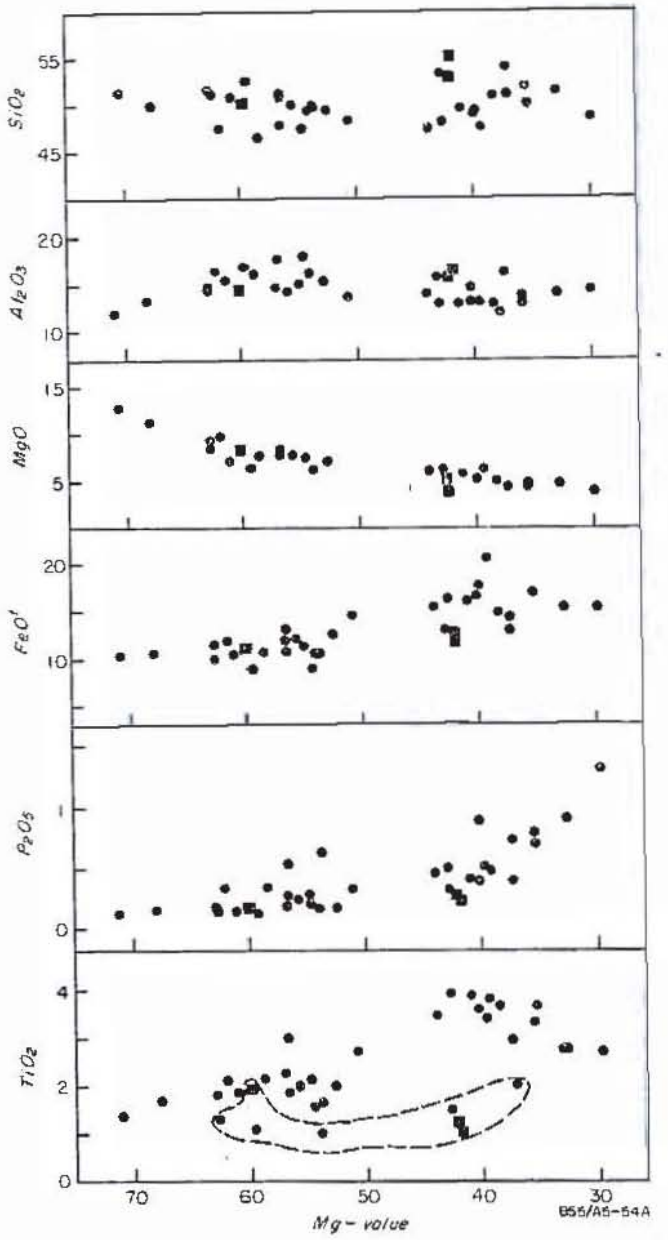

Fig. 1-31. Variation of oxides (wt %) versus $100Mg/(Mg+Fe^{2+})$ diagram for Tumu River basalts. Symbols as for Fig. 1-30. $Fe_2O_3/$

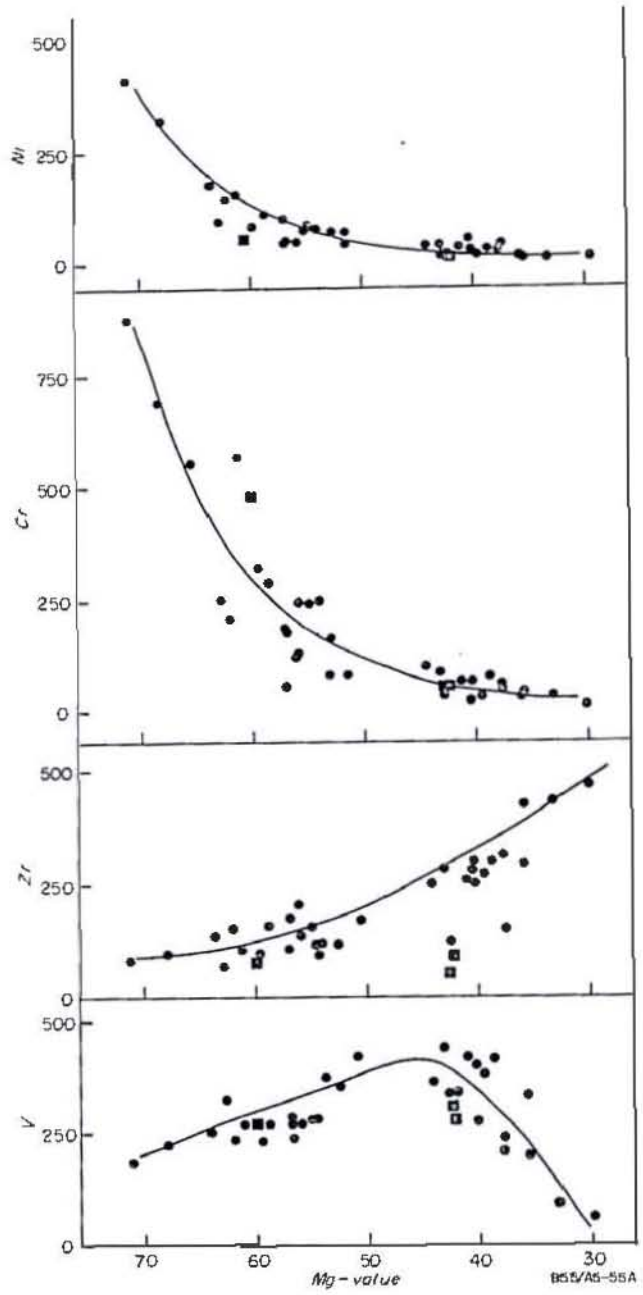

Fig. 1-32. Variation of trace elements with Mg-value. Symbols as for Fig. 1-30.

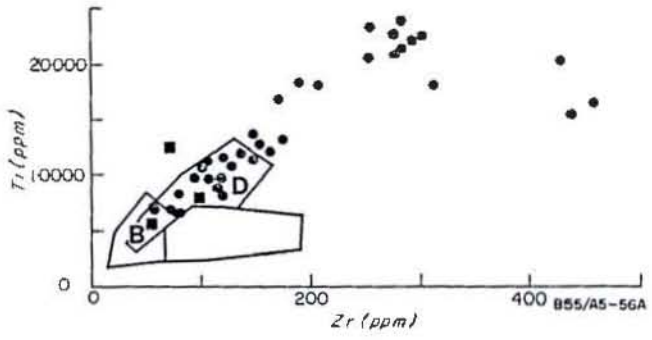

Fig. 1-33. Ti-Zr diagram for the Tumu River basalts. B,D = fields of ocean floor tholeiites (Pearce & Cann, 1973).

5-3. Chemical affinities

Analyses 1-26 in Table 1-21 of the Tumu River basalts form a continuous series from magnesian tholeiite to ferrotholeiite characterized by high FeO^t, TiO_2 and P_2O_5 contents, and high levels of LIL elements (especially Zr). A smaller group of basalts, together with the three dolerites from the gabbro massif (analyses 28-35) are characterized by lower TiO_2, P_2O_5 and Zr contents for comparable Mg-values. The higher Ti group of the Tumu River basalt sequence bear similarities with tholeiites described from Iceland (e.g. Sigvaldson, 1974; Bailey & Noe-Nygaard, 1976; Wood, 1976) and Galapagos Islands (McBirney & Williams, 1969) which range to highly differentiated lavas, ferrobasalts and andesites. Ferrobasalts also occur at aseismic ridges e.g. Ninety East Ridge (Hekinian, 1973), and at some mid-ocean ridges e.g. Juan de Fuca Ridge (Kay & others, 1970; Vogt & Byerly, 1976), the East Pacific Rise (Clague & Bunch, 1976) and the Galapagos Spreading Centre (Byerly & others, 1976).

Classification of tholeiites

Tholeiites of similar major element composition show a considerable range in abundance of incompatible elements (e.g. LREE, Ba, Rb, K, P, Th, U) ranging from the LREE-depleted MORB (Group 1 basalts of Bryan & others, 1976) with La_N/Sm_N ratios of 0.6 - 0.8 (e.g. Schilling, 1971, 1975; Kay & others, 1970; Bryan & others, 1976) to the LREE-enriched tholeiites of oceanic islands e.g. Hawaii, Azores, Iceland, with La_N/Sm_N ratios of 2-3 (e.g. Schilling, 1973, 1975). Continental tholeiites are generally even more enriched in LIL elements. Another group of tholeiites with transitional LREE enrichment (Group II basalts of Bryan & others, 1976) have been found in a variety of localities in the ocean basins; in the vicinity of oceanic islands, at seamounts, fracture zones, aseismic ridges, at several DSDP sites on the ocean floor, at the Mid-Atlantic ridge in the FAMOUS area (e.g. White & Bryan, 1977; Langmuir & others, 1977), and

in some marginal basins (Gill, 1976; Tarney & others, 1977; Weaver & others, 1979).

These and other studies show the fractionation among REE in tholeiites, and it is clear that source regions with different REE abundances exist in the earth's mantle (e.g. Gast, 1968; Schilling, 1973, 1975; Frey & others, 1978).

The various tholeiites are referred to simply on the basis of the level of enrichment of LREE (La) relative to HREE (Yb). *Depleted* tholeiites have $La_N/Yb_N \leq 0.8$ and low abundances of LIL elements; most MORB fall in this group. *Chondritic* tholeiites have flat, chondritic or near-chondritic REE patterns with $La_N/Yb_N = 0.8 - 2$. Basalts with 'transitional' LREE enrichment such as found at 37^{o}-45^{o}N, and many of the Group 11 basalts of Bryan & others (1976) fall in this group. *Enriched* tholeiites have $La_N/Yb_N > 2$, and include the oceanic island tholeiites of Hawaii, Azores, Iceland, and continental tholeiites (e.g. S.E. Australia, Deccan Plateau, Ferrar Dolerite).

K, Rb, Cs, Ba, Sr, U, Th

The abundances of these LIL elements have provided a useful discrimination among magma types (e.g. Gast, 1968; Hart, 1969; Kay & others, 1970). However, as already noted, these elements are very susceptible to alteration; altered samples commonly show increased abundances of Rb, Ba, etc. and decreased K/Rb, K/Ba, etc. ratios (Hart, 1970). Although the alteration of the Tumu River basalts precludes confident use of these elements as petrogenetic indicators it is noteable that the bulk of the basalts (excluding those recognized as chemically altered) have low K_2O contents ($\leq$ 0.4%), low Rb ($\leq$ 2.5 ppm) and low Ba ($\leq$ 50 ppm). K/Rb and K/Ba ratios in least altered rocks are moderate to high, 500 -1500 and 20 - 50 respectively. Sr contents are variable but most lie in the 75 - 225 ppm range. These abundances are similar to, or higher than,

those commonly found in depleted tholeiites, MORB (e.g. Hart, 1969; Kay & others, 1970). U and Th abundances are low, and Th/U ratios are in the range 3 - 4 which is higher than MORB (1.5 - 2) and similar to ocean island tholeiites. Sample 549 (judged to be chemically altered) has significantly higher abundances.

Ti, Zr, Y, Nb, P, Hf

Several schemes for discriminating among magma types have been proposed using these elements which are widely regarded as insensitive to alteration (e.g. Cann, 1970, 1971; Pearce & Cann, 1973; Smith & Smith, 1976).

Y/Nb ratios for the Tumu River basalts are mostly in the range 4 - 7, typical of tholeiitic rather than alkalic basalts; this range is somewhat lower than that exhibited by most MORB which commonly have ratios greater than 8 (Erlank & Cable, 1976). Zr/Nb ratios are intermediate between those of depleted tholeiites, ($\sim$ 37), and alkali basalts ($\sim$ 6.5) (Erlank & Cable, 1976) suggesting a transitional nature. On a Ti-Zr diagram (Fig. 1-33) the basalts form a strongly linear trend which extends through and well beyond the field specified for ocean floor basalts by Pearce & Cann (1973). The trend defined is typically tholeiitic: Ti, like Zr, is strongly partitioned into the liquid during the early and middle stages of differentiation but late-stage liquids become depleted in Ti due to the formation of Fe-Ti oxide.

The overall abundances of Ti, Zr, Hf, Y and Nb are significantly higher than for average depleted tholeiites of comparable Mg-value and Ni content. Fractionated DSDP basalts showing LIL element depletion described by Ayuso & others (1975), Frey & others (1974), and Thompson & others (1975) with comparable Mg- values commonly have about half the TiO_2, Zr, Nb, Hf contents of the Tumu River basalts.

The higher abundances of Ti, P, Zr, Nb and Hf of the Tumu River basalts are similar to those of oceanic island tholeiites of Hawaii (MacDonald & Katsura, 1964; Murali & others, in press), Iceland (Sigvaldson,

1974; Bailey & Noe-Nygaard, 1976; Wood, 1976), and Galapagos (McBirney & Williams, 1969). Relatively unfractionated tholeiites of these localities (Mg-value $\geq$ 68, Ni $\geq$ 200 ppm) contain $\sim$ 1-2% TiO_2, $\sim$ 0.1 - 0.15% P_2O_5, > 75 ppm Zr and > 2 ppm Hf, all higher than depleted tholeiites. The abundances of Ti, P, Zr, Nb and Hf in analyses 29-35 in Table 1-21 are considerably lower than in the 'oceanic island'-type series and more closely resemble depleted tholeiites, but abundance ratios Zr/Nb, Y/Nb, etc. are more like those of enriched tholeiites from oceanic islands.

REE

REE are commonly regarded as the most insensitive of LIL elements to low temperature alteration and have been widely used as a petrogenetic indicator even for altered rocks. Frey & others (1974) suggested from studies of DSDP basalts that glass may decrease in REE abundance (except for Ce) following alteration, and crystalline samples may increase in LREE (and Sr, Ba) and decrease in HREE (and Y, Sc, Nb, Ni) following alteration. Hellman & Henderson (1977) have shown that progressive spilitization of a tholeiitic basalt can result in both an increase in absolute REE abundance and La/Sm and La/Yb ratios. Wood & others (1976) suggest that zeolite facies metamorphism can result in mobility of LREE, with the degree of mobility increasing with ionic radius. Data from the Cliefden Outcrop (Hellman & others, 1977), however, show little fractionation among REE although the absolute level of abundance of REE varies considerably.

In addition to the La, Ce, Nd and Y values determined by XRF, 5 basalts and 1 microgabbro have been analysed for REE by spark source mass spectrometry (Table 1-22). The effect of alteration of REE in the Tumu River basalts has been examined in Figure 1-34 where LREE (Σ La, Ce, Nd) are plotted against Zr. The excellent correlation (r = 0.97) obtained suggests that most LREE abundances have not changed. However, those basalts judged on the basis of their poor Zr-Y correlation to be altered also show a poor LREE-Zr correlation, and have higher La_N/Y_N ratios and

TABLE 1-22. REE DATA FOR TUMU RIVER BASALTS

Sample	143	524	549	508	565	576
ppm						
La	8.43	7.27	21.38	6.27	20.96	7.76
Ce	19.80	20.0	42.99	18.65	50.42	19.95
Pr	2.51	2.65	6.24	2.61	7.56	2.56
Nd	11.83	14.25	29.31	12.22	34.65	11.36
Sm	3.21	3.93	6.78	3.45	9.89	2.70
Eu	1.16	1.42	2.28	1.33	3.31	0.90
Gd	-	-	-	-	11.42	3.05
Tb	0.75	0.79	1.17	0.92	1.97	0.52
Dy	4.55	4.74	6.70	6.24	13.26	10.34
Ho	0.91	0.95	1.23	1.43	2.94	0.74
Er	2.52	2.72	3.24	3.98	8.56	2.12
Tm	-	-	0.41	-	1.18	-
Yb	2.05	2.13	2.56	3.84	8.76	2.05
La_N/Sm_N	1.60	1.13	1.92	1.11	1.29	1.75
La_N/Yb_N	2.72	2.25	5.51	1.08	1.58	2.50

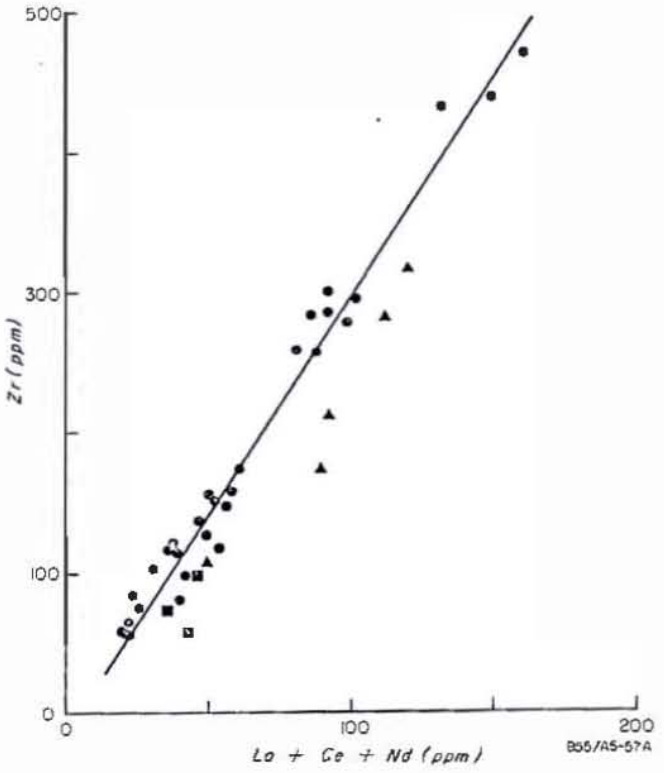

Fig. 1-34. ΣLREE (La+Ce+Nd) versus Zr. All data in ppm. Symbols as for Fig. 1-30.

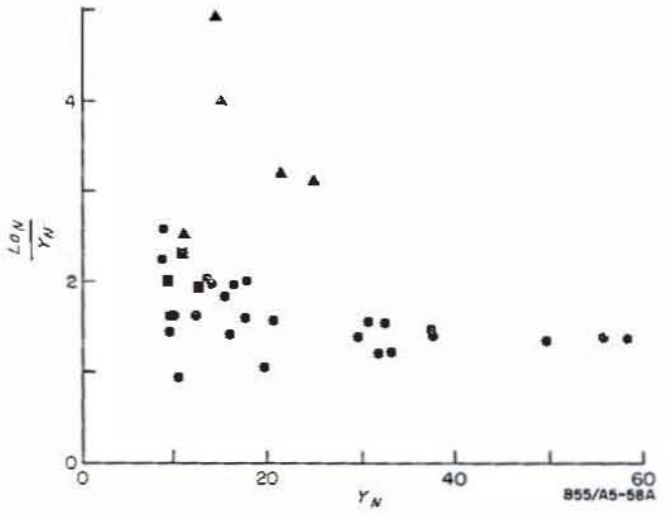

Fig. 1-35. Chondrite-normalized La_N/Y_N versus Y_N plot showing increasing absolute level of REE (10-60 x), and variation in degree of LREE enrichment of the Tumu River basalts. Symbols as for Fig. 1-30.

lower Y/Nb ratios than the bulk of the samples which have La_N/Y_N ratios of about 1.2 - 1.6 (Fig. 1-35). The REE pattern for sample 549 (Fig. 1-36) shows a smooth curve with no significant relative fractionation among REE except Ce which has a marked negative anomaly. Ce anomalies are also apparent in strongly altered DSDP basalts (Frey & others, 1974) and the spilitized Bhoiwada Basalt (Hellman & Henderson, 1977). It appears, therefore, that strong alteration, spilitization especially, can produce an increase both in absolute REE abundance and in degree of LREE enrichment.

Total REE abundances of the Tumu River basalts, shown by the range in Y contents in Figure 1-35 and the six REE patterns in Figure 1-36, range from 10 to 60 times chondritic. The chondrite-normalized REE profiles are all characterized by slight LREE enrichment. Strongly fractionated ferrobasalt 565 (Mg = 36) has a generally similar pattern (although a slightly flatter profile) and similar La_N/Sm_N ratio to relatively unfractionated samples 143 and 524 (Mg = 71 and 68) and dolerite 576 but the absolute level of REE is nearly four times higher. LREE and Y data for the most evolved ferrobasalt (Mg = 30) show a similar pattern with HREE at 60 x chondritic. Significantly ferrobasalt 565 has no apparent negative Eu anomaly, unlike other highly fractionated ferrobasalts (e.g. Vogt & Byerly, 1976). Lack of a negative Eu anomaly does not preclude plagioclase fractionation since only a small Eu anomaly results from extensive plagioclase removal (10% increase in Sm/Eu if 50% of system is removed as plagioclase: Frey & others, 1974). Dolerite 576 from the Marum gabbros has a flat pattern for HREE with LREE enrichment (La_N/Sm_N = 2.5) similar to the Tumu River basalts. However, the absolute level of REE is lower than the most Mg-rich basalt, indicating that the parent liquid for dolerite 576 (Mg = 42) had a very low level of REE. Sample 508 has a flat pattern with very slight depletion in MREE, and slight LREE enrichment. Th/U ratios are slightly lower than, but Zr/Hf, La/Ce and Zr/Nb ratios are similar to, the other analysed samples (except the altered sample 549).

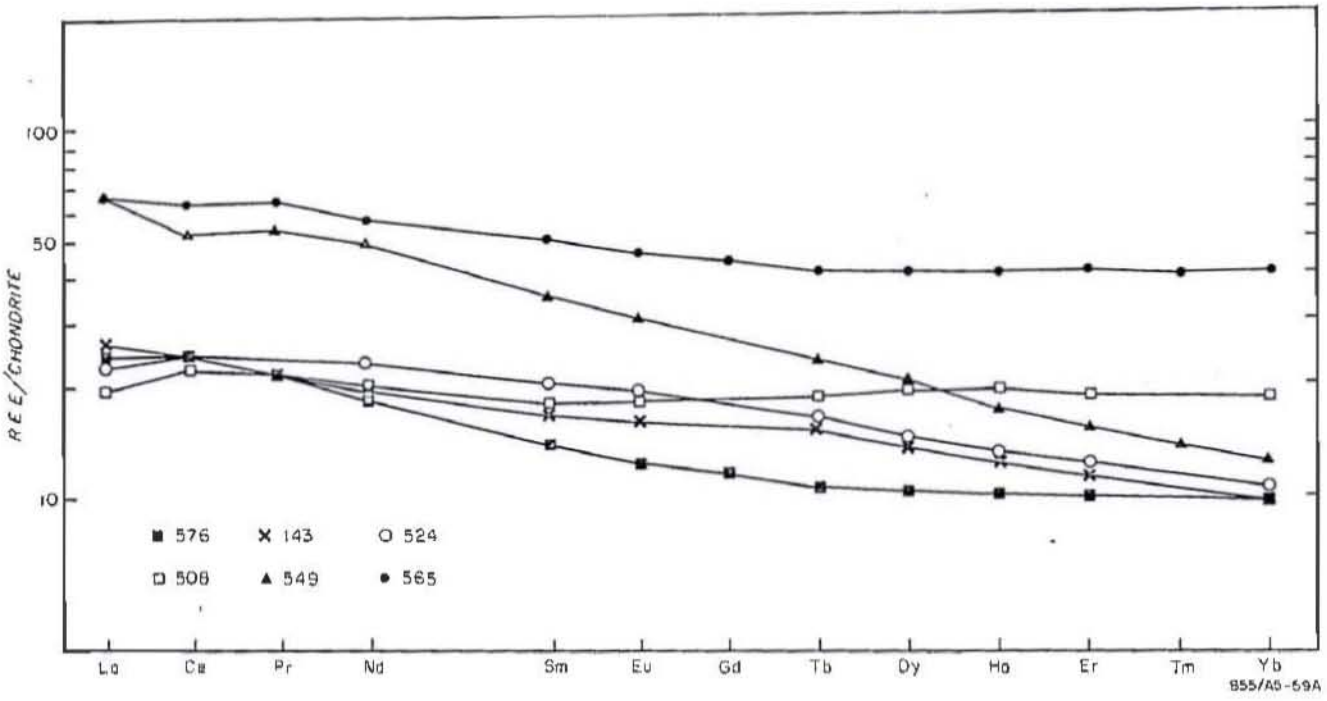

Fig. 1-36. Chondrite-normalized REE patterns of selected Tumu River basalts, and microgabbro 576 in cumulate sequence.

The Tumu River basalts have La_N/Sm_N ratios intermediate between the depleted tholeiites with La_N/Sm_N ratios of 0.6 - 0.8, and the enriched tholeiites of oceanic islands with La_N/Sm_N ratios of 2 - 3. La_N/Yb_N ratios are mostly greater than 2, except for 508 and 565 which have near chondritic ratios, indicating affinities with the enriched tholeiites.

5-4. Petrogenesis

Fractionation

The differentiation trends shown by both major and trace elements, and the similarity in incompatible element ratios suggests that the bulk of the Tumu River basalts may be related by fractional crystallization from a common parent magma. Quantitative modelling of possible fractionation processes by least squares mixing involving major elements is precluded by the chemical changes of spilitization. However, trace elements permit evaluation of fractionation processes if crystal fractionation follows the Rayleigh Law. Allegre & others (1977) have demonstrated that, in practice, the bulk partition coefficient, D, for many trace elements in a fractionation sequence (or parts of a sequence) are more or less constant, and that these D values may, on the basis of a re-written form of the standard Rayleigh fractionation equation, be obtained by plotting on log scales the concentrations of a trace element in a sequence of rocks against the concentrations of an element, such as Zr, which has solid-liquid partition coefficients substantially less than unity. A line of best fit is drawn through the data points, and the slope of this line is 1-D (if D is less than 1) or D-1 (if D is greater than 1).

Trace elements for the Tumu River basalts are plotted in log form against Zr in Figure 1-37. The bulk partition coefficients obtained by least squares treatment for these elements are presented in Table 1-23, and are constant except for V, Ti and Sc. The bulk partition coefficients for these elements change markedly from less than 1 to significantly greater

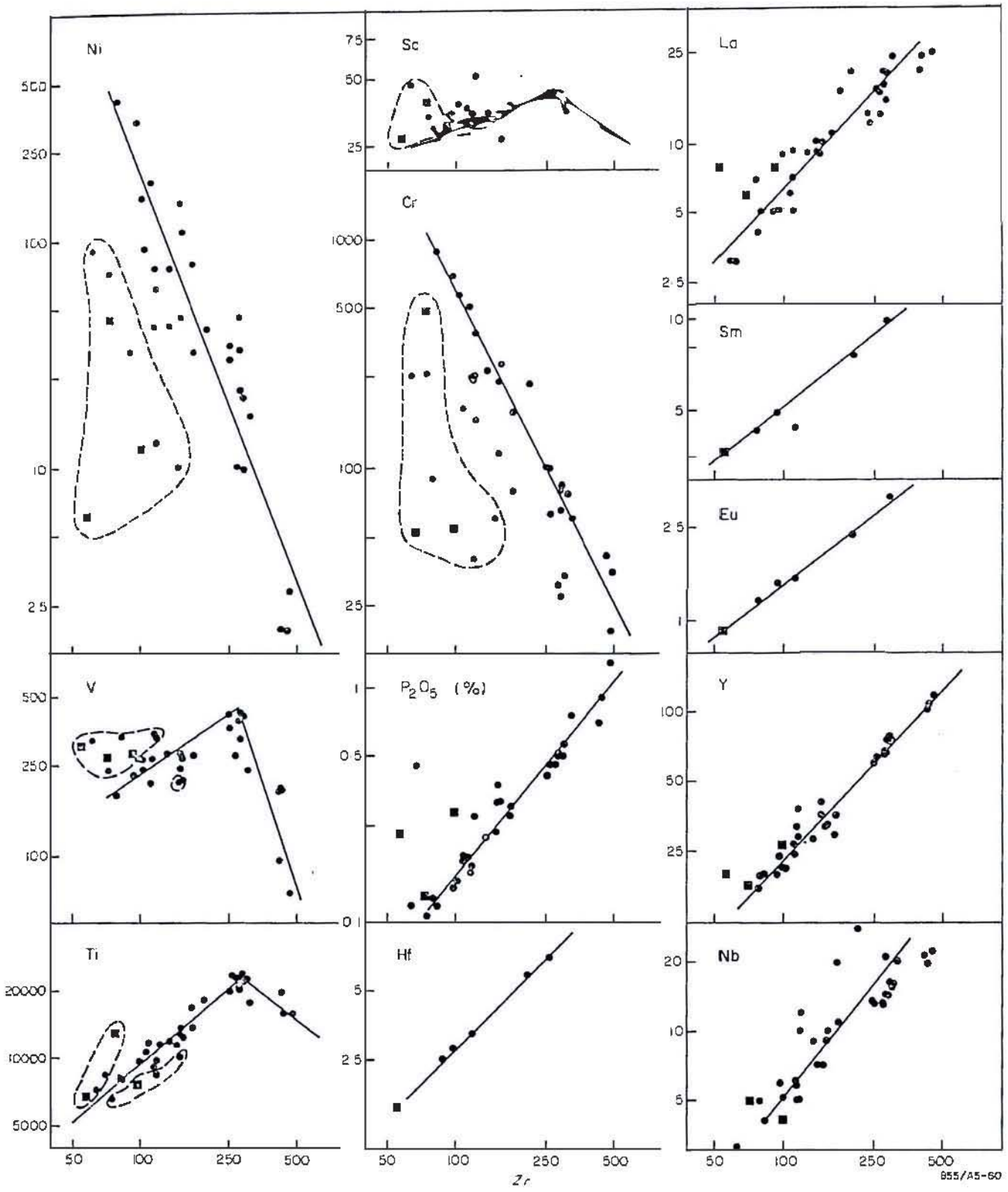

Fig. 1-37. Logarithmic plot of selected elements against Zr for Tumu River basalts (closed circles) and dolerites from the Marum gabbro sequence (squares). Lines of best fit define bulk partition coefficients (see text). Dashed lines outline the lower Ti group. Note change in bulk partition coefficients for V, Ti and Sc at about 270 ppm Zr marking titanomagnetite and ilmenite fractionation.

than 1 at a point late in the differentiation sequence equivalent to 260-280 ppm Zr, as a result of crystallization of Fe-Ti oxide.

An initial Zr concentration of 77 $\pm$ 5 ppm was estimated assuming a Ni concentration of 300 - 450 ppm in the primary magma (Allegre & others, 1977). Initial concentrations for all other trace elements were then calculated using the rewritten Rayleigh equation of Allegre & others (1977): these are presented in Table 1-23. The D^{Ni} obtained for the Tumu River basalts (3.6) is slightly lower than that suggested by Allegre & others (1977) as typical of primitive sequences (i.e. > 4), and it is possible that the initial concentrations obtained may not be the most primitive; on the other hand the high Ni and Cr contents of the calculated initial composition imply little fractionation. The calculated abundances (Table 1-23) closely match high-Mg basalt 143 which is the least fractionated of the sequence. Rayleigh fractionation calculations using the D values in Table 1-23 indicate that 4-6% fractional crystallization is required to derive sample 143 from the calculated initial liquid composition, whereas the most evolved ferrotholeiites require extremely high degrees, about 85%, of crystallization. A major break in the differentiation sequence occurs at about f = 0.3, due to the formation of Fe-Ti oxide as a fractionating phase. The extremely high degree of fractionation invoked is not unique: Clague & Bunch (1976) estimate using both major element mixing models and phosphorus calculations that the ferrobasalts of the East Pacific mid-ocean spreading centres result from up to 74% fractional crystallization.

An estimate of the mineralogical composition and proportions of the cumulate phases involved in the fractionation can also be derived from the trace element abundances. The rapid depletion of Ni indicates fractionation of olivine: a similar depletion of Cr probably indicates fractionation of a very small amount of chrome spinel. The phenocryst

assemblage and behaviour of Ti and V suggests additional fractionating phases in the first sequence were plagioclase and clinopyroxene. Phases involved in the second sequence are likely to have been plagioclase, clinopyroxene, ilmenite and titanomagnetite.

Insertion of published mineral/liquid partition coefficients (Allegre & others, 1977; Frey & others, 1978; Irving, 1978) into equations defining the bulk partition coefficient in terms of proportions of phases fractionating for trace elements Ni, Cr, V, Ti yields a set of simultaneous equations e.g. $D_{Ni} = 13X_{ol} + 4X_{cpx}$ etc. Solution of the equations suggests fractionation in the approximate proportions - olivine 0.15, clinopyroxene 0.4 and plagioclase 0.45. Fractionation of a small percentage ($\sim$ 1%) of chrome spinel is also likely. Sc appears anomalous; published Sc partition coefficients for clinopyroxene are high (3 according to Frey & others, 1978) and a sequence in which clinopyroxene is a significant fractionating phase should show marked decreases in Sc abundances. However, the available Sc data for MORB in the literature do not appear to show a correlation with decreasing Mg-value, yet significant clinopyroxene fractionation is commonly invoked in mixing models. The D^{Sc} for the Tumu River basalts requires a D^{Sc}_{cpx} of less than 1.5 if the fractionation model is correct. The decrease in Sc abundances in sequence 2 (Fig. 1-37) suggests that clinopyroxene fractionation is more important and/or that Sc partition coefficients for Fe-Ti oxides are appreciably higher than unity. Quantitative modelling for sequence 2 is not possible because the partition coefficients of Ti and V for Fe-Ti oxides are poorly known.

Not all the Tumu River basalts can be related by crystal fractionation: the lower Ti group, particularly dolerites 576 and 169, are chemically distinct. Similarly, the REE pattern of basalt 508 precludes a simple relationship with the other basalts. The low degree of LREE enrichment of this basalt may be explained by derivation from an increasingly

TABLE 1-23. BULK PARTITION COEFFICIENTS AND INITIAL COMPOSITION FOR TUMU RIVER BASALTS

ppm	Sequence 1	Sequence 2	Initial composition
Ni	3.6	—	450
Cr	3	—	900
Sc	0.6	1.65	24
Ti	0.15	1.75	7750
V	0.56	4.3	180
Y	0	—	18
Zr	0	—	77±5
Nb	0	—	4.8
Hf	0	—	2.4
P_2O_5 (wt%)	0	—	0.12
La	0	—	5.8
Sm	0	—	3
Eu	0.23	—	1.1
Yb	0.09	—	1.9

TABLE 1-24. COMPARISON OF CALCULATED PARENT MAGMA WITH LEAST FRACTIONATED LAVAS FROM OCEANIC ISLANDS AND AVERAGE MORB.

	Chondritic				Enriched					Depleted		
	1	2	3	4	5	6	7	8	9	10	11	12
Sc	24	28						28		39	40	
Ti	7750	6480	5935	8940	9240	6540	1810	13900	11750	4200	9000	620
V	180	190			270	350		292		190		64
Cr	900	560		355	760	505	480	445	770	900	250	
Ni	450	239		199	190	213		211		320		
Y	18	28	17.5	23	26	15	34		23	20	30	2
Zr	77	58	49	77	115	76	182	113	148	35	90	6
Hf	2.4	1.71	1.26	2.3				3.1		1.16		
Nb	4.5	7.9	7.5	10			22		11		2.5	0.39
P_2O_5	0.12			0.19	0.12	0.09		0.25				
La/Sm EF	1.2	1.23	1.37	1.04				1.48		0.4	0.4-0.7	1
Ti/V	43	34			34	19		48		22	22-29	9
Ti/Y	450	230	340	389	355	436	532		510	210	285	256
Ti/Zr	100	112	121	116	80	86	100	123	79	120	100	102
Zr/Hf	34	34	39	33				36.5		30		44
Zr/Nb	16	7	6.5	7.7			8.3		13.5		30-40	16
Zr/Y	4.5	2.1	2.8	3.35	4.4	5.06			6.4	1.75		2.5
TiO_2/P_2O_5	11			7.8	12.8	11.4		9.3			11	10
V/Zr	2.3	3.3			2.4	4.6				5		11.5
Y/Nb	3.75	3.5	2.3	2.3								5
Ti/Sc	320	230						500		110	225	

1. Tumu River basalt—calculated parental magma composition. 2. FAMOUS basalt 529-4 (Langmuir & others, 1977). 3. Leg 37-332 A (Bence & Taylor, 1977). 4. Iceland basalt (Wood, 1976). 5. Iceland basalt NAL 19 (Sigvaldson, 1974). 6. Iceland basalt NAL 13 (Sigvaldson, 1974). 7. Galapagos basalt (Pearce, 1975). 8. Hawaii, 1840 Kilauea (Murali & others, in press). 9. Hawaii (Pearce, 1975). 10. Leg 3-14 (Frey & others, 1974). 11. 'Average' MORB (Smewing & others, 1975). 12. Chondritic (Nesbitt & Sun, 1976; Sun & Nesbitt, 1977).

TABLE 1-25. CALCULATED MODEL SOURCE ABUNDANCES FOR TUMU RIVER BASALTS

	La	Sm	Eu	Yb	Y	Zr	TiO_2	Hf	Nb	V	Sc	P_2O_5
20%;ol,opx*	1.16	0.61	0.22	0.39	3.65	16	0.27	0.5	0.96	55	13	0.03
30%;ol,opx	1.74	0.90	0.33	0.58	5.5	24	0.40	0.75	1.44	70	14	0.04

* 80% olivine, 20% orthopyroxene

depleted source, or, perhaps, by a process of 'dynamic melting' as suggested by Langmuir & others (1977). In this model partial melting is a continuous process in which some of the melt always remains in the residue. Continuous incremental melting can result in highly variable trace element abundances, and this model is able to explain the variable LREE enrichment and lack of correlation between LREE enrichment and HREE abundance (i.e. crossing REE patterns such as in Figure 1-36) exhibited by basalts from the FAMOUS area (Langmuir & others, 1977).

Comparison of initial magma composition with other primitive basalts

The calculated initial abundances and abundance ratios for the Tumu River basalt sequence are compared with values for relatively unfractionated sea-floor and oceanic island tholeiites in Table 1-24. Most MORB have undergone some degree of crystal fractionation, at least of olivine and, commonly, of plagioclase and, to a lesser extent, of pyroxene (e.g. Miyashiro & others, 1969; Frey & others, 1974; Hekinian & others, 1976; Bryan & others, 1976; Bryan & Moore, 1977). Relatively primitive basalts have been found at DSDP sites 3-14 and 3-18 (Frey & others, 1974), and more recently in the rift valley of MAR in the FAMOUS area (Bryan & Moore, 1977; Hekinian & others, 1976; Langmuir & others, 1977) and at several Leg 37 DSDP sites (Bence & Taylor, 1977; Blanchard & others, 1976). The Tumu River basalt initial composition has about twice the Ti, Zr, Nb, Hf (P_2O_5) contents of these 'primitive' depleted tholeiites, and has higher Ti/Y, Ti/Sc, Ti/V and Zr/Y ratios than most LREE-depleted MORB but comparable (i.e. close to chondritic) Ti/Zr, Zr/Hf, TiO_2/P_2O_5, and Zr/Nb ratios. LREE-enriched basalts are commonly strongly differentiated, some to FeTi-rich basalts with high levels of LIL elements. However, not all LREE-enriched basalts are characterized by high levels of Ti, Zr, Hf etc. The relatively primitive slightly LREE-enriched leg 37-332 basalts (Bence & Taylor, 1977) have similar La_N/Sm_N ratios but much lower (about half)

abundances of Ti, Zr and Hf compared to the Tumu River basalts.

Abundances of Ti, Zr, Hf and P in the Tumu River basalts, therefore, most closely resemble the Icelandic tholeiites. REE and major element chemistry also suggests affinities with basalts from oceanic islands and aseismic ridges, which range to highly fractionated ferro-basalts.

Abundances in the source region

Experimental studies of model mantle compositions (Green & Ringwood, 1967; Green, 1971; PARTS 3 & 4) indicate that olivine tholeiite liquids may be produced by large degrees, 20-30%, of partial melting leaving a harzburgite residue. Green & others (1979) also invoke large degrees, approximately 25%, of melting to leave an olivine, enstatite ± spinel residue in an experimental study of DSDP basalt 3-18.

During equilibrium melting of a mantle source the enrichment of a trace element in the melt relative to the original source concentration can be expressed by the partial melting equation;

$$\frac{Cl}{Co} = \frac{1}{D + F(1-D)}$$

where D = bulk partition coefficient, Cl = concentration in melt, Co = concentration in source, and F = fraction of melt (Shaw, 1970). If the degree of partial melting and nature of the residue is specified source abundances can be calculated using appropriate partition coefficients. (The partition coefficients of Frey & others, 1978 were used in the following calculation; see Appendix 1).

For 20-30% melting leaving olivine (80%) and orthopyroxene (20%) as residual phases the model mantle source for the parent Tumu River basalt has LREE = 3.5 - 5.5 x chondrites, HREE, Y, Zr, Nb = 1.8 - 2.8 x, Hf = 2 - 4 x, Ti = 2 - 3 x, Sc = 2 - 2.5 x, V = 1 x, and P_2O_5 = 2 - 3 x chondrites (Table 1-25). These values are similar to those obtained by Frey & others (1978) for continental tholeiites from S.E. Australia, and

suggest that the source for the Tumu River basalts had not experienced a previous melting event, unlike the source regions for depleted tholeiites. The level of HREE (1.5 - 3 x chondrites) is in agreement with other conclusions that the upper mantle has HREE abundances equal to 2 - 4 x chondrites (e.g. Gast, 1968; Kay & Gast, 1973; Frey & others, 1978). The LREE, at 3 - 5 x chondrites, are slightly enriched relative to HREE. The abundances of REE, and Nb, Hf, Zr, Y, Ti, and P_2O_5 etc. in the source region are therefore similar to abundances in the source regions for both oceanic island basalts and continental tholeiites. These data accord with the detailed integrated modelling of Frey & others (1978) who showed that the source for continental and oceanic island basalts has been enriched in the strongly incompatible elements (Ba, Sr, Th, U, LREE) at 6 - 9 x chondrites. This they infer to be the result of migration of a LIL element-enriched melt or fluid depleting some mantle regions and enriching others, an interpretation consistent with the concept of a chemically zoned upper mantle (Green, 1971; Green & Lieberman, 1976).

5-5. Relationship with the cumulate peridotites and gabbros

The spatial association of the field (although separated by thrust faults) suggests a genetic (cumulate - liquid) relationship between the Tumu River basalt and the cumulate peridotites and gabbros. The petrologic and geochemical evidence however militate against such a relationship, and provide evidence for a markedly different magma composition from that which gave rise to the cumulates. Evidence against a genetic relationship includes;

1) lack of orthopyroxene phenocrysts in the lavas. The paragenetic sequence in the Tumu River basalts is ol (+ Cr spinel), plag, plag + cpx, plag + cpx + Fe-Ti oxide which contrasts sharply with that of the cumulates (Chapter 3). The parent magma composition inferred for the cumulate sequence is decidedly richer in normative

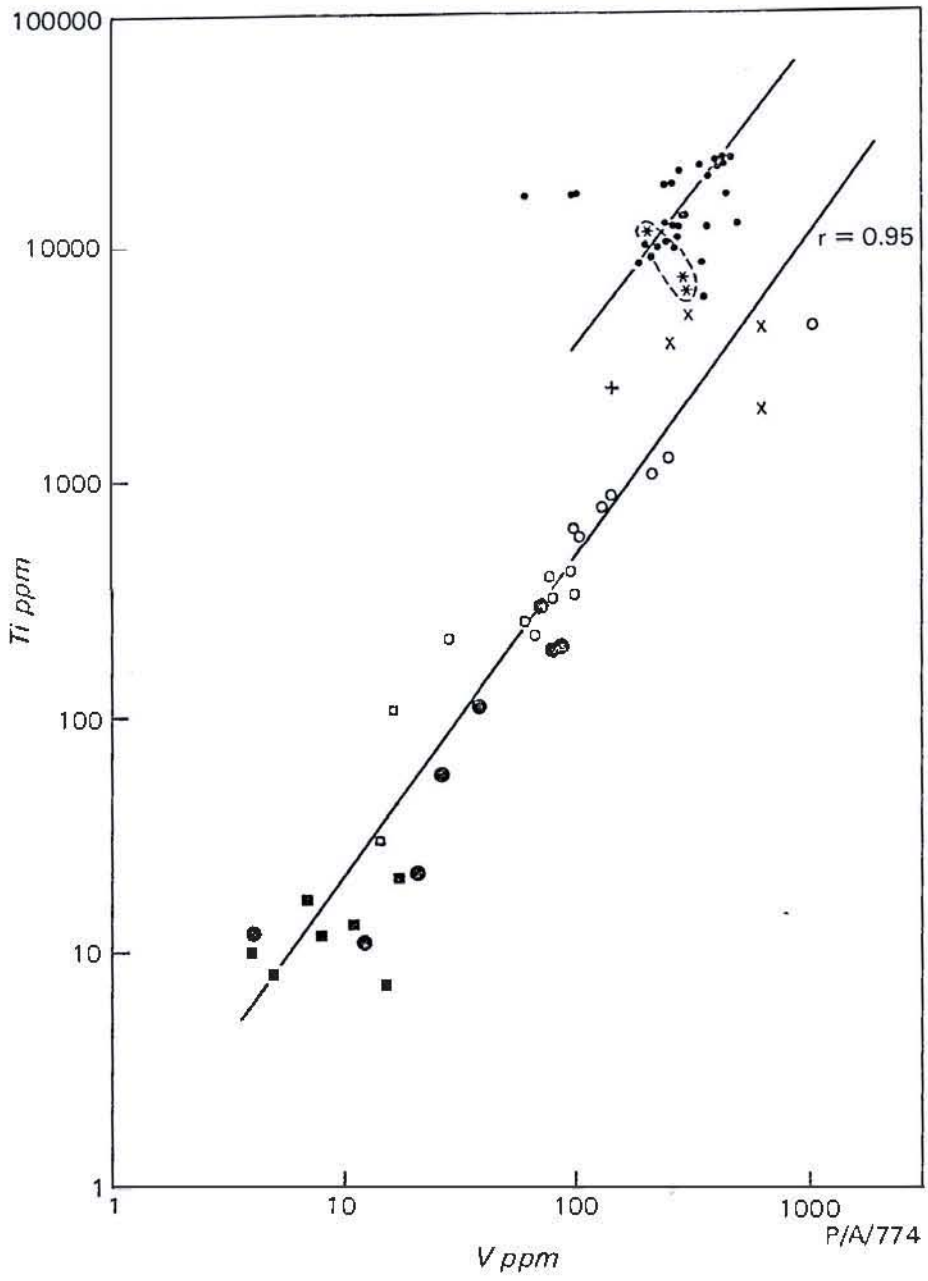

Fig. 1-38. Ti-V diagram for Tumu River basalts (small dots), and Marum peridotites and gabbros. Closed squares = tectonite harzburgite and dunite, open squares = enstatite-rich dykes, closed circles = cumulate peridotites, open circles = cumulate gabbros, + = granophyric diorite, x = mafic pegmatoids, stars = dolerites in layered sequence. Note good correlation of all peridotites and gabbros but poor correlation with Tumu River basalts.

hypersthene, and poorer in normative diopside and olivine than the magma parental to the Tumu River basalts.

2) the high abundances of Ti, Zr, Nb, Y, P and the LREE-enriched REE patterns of the Tumu River basalts. Evidence from the cumulates points to a parent magma strongly depleted in LREE and other incompatible elements (Chapter 4).

3) the Ti-V relationship exhibited by the cumulates differs from that of the Tumu River basalts, which have markedly higher Ti contents for similar V contents (Fig. 1-38). This lack of correlation between the Tumu River basalts and the peridotites and gabbros is also borne out in other trace element plots.

It is therefore concluded that the Tumu River basalts bear no genetic relationship with the cumulate peridotite-gabbro massif. The present spatial association results from tectonic emplacement, and the basalts parental to the cumulates have been either removed by dismembering on emplacement and/or erosion following regional uplift in the late Neogene.

5-6. Sediments

The Tumu River basalts are overlain by finely bedded, red-brown radiolarian argillite, radiolarite, chert and mudstone. These sediments grade upwards into fine-grained, bedded, green-brown volcanolithic siltstone and sandstone. Chemical analyses of 5 representative sediments are given in Table 1-26.

The radiolarian argillite typically consists of fine quartz, feldspar, and replaced outlines of radiolaria tests in a fine-grained amorphous Fe-oxide rich matrix. Chemically the argillites are characterized by high SiO_2 and low CaO, MnO and Na_2O (Table 1-26, analyses 1, 2) compared to the 'average deep sea clay' of Turekian & Wedepohl (1961). Abundances of Ni, Cu, Zn, Ba and REE are also considerably lower than Turekian & Wedepohl's (1961) average. These differences may be due to dilution by siliceous organisms. The Marum

TABLE 1-26. CHEMICAL ANALYSES OF MARUM SEDIMENTS

	1	2	3	4	5	6	7
SiO_2	69.10	64.67	87.34	61.44	61.20	54.0	73.0
TiO_2	0.58	0.70	0.14	0.83	0.85	0.8	0.5
Al_2O_3	14.31	15.91	4.09	15.74	15.84	16.2	9.5
Fe_2O_3	5.30	7.57	0.37	2.80	3.44	-	-
FeO	1.00	0.80	3.59	6.24	5.78	8.5	6.6
MnO	0.24	0.05	0.05	0.65	0.56	0.9	1.4
MgO	2.16	1.66	3.32	3.69	3.25	3.5	2.7
CaO	0.98	1.04	0.60	4.60	6.59	7.3	1.0
Na_2O	2.54	4.47	0.05	3.10	1.17	5.5	-
K_2O	3.64	3.01	0.07	0.67	1.11	3.0	1.5
P_2O_5	0.16	0.12	0.37	0.23	0.21	0.3	-
(H_2O^+)	(3.67)	(2.94)	(2.53)	(4.44	(11.14)	-	-
Trace elements							
Sc	21	22	4	26	24	19	
V	114	147	40	136	128	120	98
Cr	68	71	180	35	27	90	38
Ni	49	45	12	13	11	225	71
Cu	33	64	9	86	78	250	142
Zn	103	111	67	130	118	165	222
Ba	230	250	<10	590	1060	2300	80
Rb	95	99	3.2	11	28.5	110	
Sr	91	141	31.5	885	3490	180	217
Y	33	32	13	34	31	90	
Zr	140	154	27	132	129	150	56
Nb	6	7	2	2	2	14	
La	24	32	8	18	16	115	
Ce	46	75	17	46	38	345	
Nd	25	30	8	22	17	140	
Pb	17	17		17	16	80	53

1. Radiolarian argillite, 544
2. Radiolarian argillite, 512
3. Chert, 469
4. Volcanolithic siltstone, 527
5. Volcanolithic siltstone, 528
6. Average deep sea clay, normalized to 100% (Turekian & Wedepohl, 1961)
7. Average of 15 radiolarian mudstones and radiolarites (Robertson & Hudson, 1973)

argillites are similar in composition to radiolarian mudstone and radiolarite from the Troodos ophiolite (Robertson & Hudson, 1973) apart from Al_2O_3 and MnO which are higher and markedly lower respectively in the Marum sediments.

The argillite grades upwards into fine to medium grained volcanolithic siltstone and sandstone containing angular plagioclase, pyroxene and quartz detritus in a highly chloritized matrix. Compared to the argillites the volcanolithic sediments have appreciably higher MgO, CaO, FeO and lower SiO_2 contents (Table 1-26 analyses 3, 4), reflecting the detrital volcanic component. Ba and Sr contents are markedly higher, and Ni and Cr contents lower, in the volcanolithic sediments than the argillites. The abundance of volcanic detritus in the upper part of the sedimentary sequence indicates contemporaneous volcanism in the ?mid to late Eocene. This age is consistent with the commencement of volcanism in the island-arc to the north and northeast of the ophiolite (Jaques & Robinson, 1977; Appendix 3; see Chapter 6).

5-7. Tectonic implications

The LIL element - enriched chemistry of the Tumu River basalts differs markedly from that of basalts in the Papuan (PART 2), Troodos, Pindos and other ophiolites which are commonly characterized by LREE depletion and low abundances of LIL elements similar to MORB (e.g. Montigny & others, 1973; Kay & Senechal, 1975; Smewing & others, 1975; Smewing & Potts, 1976; Menzies & others, 1977). However, basalts with slight LREE-enrichment similar to the Tumu River basalts occur in the Sarmiento ophiolite (Saunders & others, 1979), and in the Smartville (Menzies & Blanchard, 1977) and Betts Cove ophiolites (G.A. Jenner, pers. comm. 1977) where they overlie LREE-depleted tholeiites. Basalts from the Chilean ophiolites which are believed to have formed in an ensialic marginal basin (Saunders & others, 1979) share many of the chemical features

of the Tumu River basalts (such as high Ti, Zr, Nb, etc.) but have slightly higher abundances of Ba and Rb, and higher La_N/Sm_N ratios and lower K/Rb ratios, than the Tumu River basalts.

LIL element - enriched tholeiites occurring in the ocean basins are commonly interpreted as the result of mantle 'plumes' or 'hot spots' (e.g. Schilling, 1973, 1975). However, as noted by Bryan & others (1976), LREE-enriched basalts occur in areas where there is no evidence of structural, bathymetric or geophysical anomalies associated with a 'plume'. Moreover, basalts with LREE-enrichment similar to the Tumu River basalts have also been described from marginal basins (Gill, 1976; Tarney & others, 1977; Weaver & others, 1979; Saunders & Tarney, 1979). Although marginal basin basalts sampled to date embrace the spectrum of compositions established for MORB, most are characterized by higher abundances of LIL elements than common MORB. Basalts erupted immediately behind an active island-arc commonly have features transitional with island-arc volcanics.

Basalts with transitional LREE-enrichment do not therefore appear to be characteristic of any particular geologic setting in the ocean. Rather, it seems that although different levels of abundance and different degrees of enrichment of LIL-elements in olivine tholeiite basalts may in some cases arise by the process of dynamic melting as outlined by Langmuir & others (1977), and by variations in the degree of partial melting, the most important factor is mantle heterogeneity. Basalts in various tectonic environments may tap different source regions in a chemically zoned upper mantle (Green, 1971). Apparent geochemical-tectonic correlations (e.g. Pearce & Cann, 1971, 1973) may be a consequence of such a vertically zoned upper mantle: pre-rifting basalts may tap a shallow, enriched source while basalts associated with deep rifting tap a deeper, depleted source region (Green, 1971; Green & Lieberman, 1976). Olivine tholeiite basalts erupted in marginal basins with a long history of extension and well-removed from a volcanic arc and any

influence of subducting lithosphere may be expected to show depleted source characteristics. Marginal basin basalts erupted close to an active volcanic arc show chemical features suggesting addition of LIL element - enriched fluids derived from the dehydrating, subducting lithosphere.

The Tumu River basalt volcanism therefore cannot, on the basis of geochemistry alone, be confidently ascribed to any particular tectonic setting within the ocean basin (such as anomalous ridge segment, fracture zone or marginal sea) which the regional geology suggests lay to the north of the Australian continent in Cretaceous to earliest Tertiary times. Sediments overlying the Tumu River basalts are consistent with a deep water origin but pass upwards into volcanolithic sediments indicating contemporaneous volcanism in the ?mid to late Eocene. The relatively short time span between formation of the Tumu River basalts and their emplacement as an allochthonous wedge would seem more consistent with a marginal basin origin (see Chapter 6).

CHAPTER 6

ORIGIN OF THE MARUM OPHIOLITE COMPLEX

6-1. Tectonic framework

The present disposition of the Marum ophiolite as allochthonous thrust sheets at the deformed outer margin of the continental mass dipping northwards towards (and possibly underlying) the Tertiary island-arc rocks of the north coast ranges provides compelling evidence that the ophiolite was emplaced as the result of continent-arc collision. Details of the collision event and the subsequent tectonic evolution of northern Papua New Guinea are described by Jaques & Robinson (1977) (Appendix 3).

The northern coastal ranges form part of the outer Melanesian Arc (Robinson, 1973) which is generally regarded as having formed an extended, fractured island-arc system in response to early Tertiary interaction between the northward-moving Australian and westward-moving Pacific plates. The simplest interpretation of the early Tertiary tectonic history of northern Papua New Guinea is that the Paleogene arc formed by subduction of the leading edge of the Australian plate beneath the Pacific plate. This interpretation requires that the Marum ophiolite represents a segment of Pacific ocean floor, since the geology indicates that the ophiolite has been thrust from the fore-arc region over the collision zone. In this model the age of the Marum complex would be expected to be *as old*, or *older than*, the adjacent segment of Pacific plate. The map of Heezen & Fornari (1975) shows that the oldest part of the Pacific plate lies in the western Pacific, and that the sea-floor to the north and east of New Ireland and Bougainville is of early Cretaceous age. The somewhat equivocal age data available for the Marum ophiolite suggests that the ophiolite might be younger than this.

Examination of the late Mesozoic-early Tertiary geology in both the North Sepik region to the northwest and of the orogenic belt to the southwest of the ophiolite suggests that the tectonic history of northern Papua New Guinea may be more complex than previously supposed. Regional mapping of the North Sepik region has revealed the existence of Cretaceous volcanics and co-magmatic intrusives of island-arc affinities in addition to a Paleogene island-arc sequence like that of the Adelbert and Finisterre Ranges further east (Hutchison, 1975). An additional complicating factor is the occurrence of granitoids of Permian age in the North Sepik region near the Irian Jaya border (Hutchison, 1975). Cretaceous andesitic rocks also occur in the Bismarck and Schrader Ranges to the south and west of the Marum ophiolite, and appear to have been erupted in a volcanic arc peripheral to the continental margin which shed volcanic detritus to the Cretaceous-Eocene sediments of the central orogenic belt (Brown & others, in press). The Cretaceous volcanics are of island-arc affinity and thus imply the existence of an arc-trench system at the continental margin in the late Mesozoic. Jaques & Robinson (1977) pointed out that changes in the style and type of sedimentation at the continental margin implied evolution from a convergent-type margin in the early or middle Cretaceous to a divergent-type in the late Mesozoic-early Tertiary, which was then followed by plate convergence again in the late Eocene-Oligocene.

The rapid changes in tectonic style at the continental margin, repetition of arc-trench type magmatism during the late Mesozoic-earliest Tertiary and the apparently short time span between formation of the ophiolite, its association with arc-trench type magmatism, and subsequent emplacement argue for a tectonic history more complex than simple subduction of the leading edge of the Australian plate in the Paleogene. Some of the apparent discrepancies outlined above can be more readily reconciled by models in which formation of the Marum ophiolite is ascribed to a

marginal basin peripheral to the continental margin. Such an interpretation is in general accord with the present tectonic regime in the western Pacific where the continental margin is bordered by Tertiary marginal basins and fringing arcs.

6-2. A marginal basin model

Cretaceous andesitic magmatism at the northern margin of the orogenic belt seems likely to be related to a period of southward underthrusting beneath the continental margin (Johnson & others, 1979). Hutchison (1975), on the other hand, suggested that the Cretaceous magmatism in the North Sepik region might be related to northward or northeastward subduction. An alternative interpretation is that the Cretaceous igneous rocks of both the North Sepik region and of the orogenic belt formed in a continuous, or at least contiguous, magmatic arc at the continental margin which subsequently evolved to form frontal (North Sepik) and remnant (orogenic belt) arcs by formation of an inter-arc basin. With continued extension the inter-arc basin evolved into a marginal sea. In this model, similar to that proposed by Brown & others (in press), the Permian granitoids comprise a rifted segment of the continental margin separated from the continent by younger oceanic crust, represented by the ophiolite belt. Volcanism and marginal basin extension ceased in the early Tertiary, and northward movement of the Australian plate in the Eocene resulted in formation of a northward or northeastward-dipping subduction zone and the Paleogene volcanic arc now exposed in the northern coastal ranges. Continued subduction resulted in closure of the marginal basin, and collision between the continent (and remnant arc) and the Paleogene volcanic arc in the late Oligocene-early Miocene.

While this interpretation is broadly consistent with the known geology uncertainties remain. The model requires that the ophiolites be not older than the age of the volcanism in the associated arc i.e. late

Cretaceous. It also predicts the existence of a Cretaceous volcanic arc assemblage beneath the Tertiary arc sequence of the northern coastal ranges, i.e. that the Tertiary (Paleogene) arc be superimposed on an older arc, as is apparently the case in the North Sepik region (Hutchison, 1975). No evidence for an older arc has been found in the Adelbert-Finisterre-Huon region, although it is conceivable that this might be due to lack of exposure since uplift is younger in the east than the west and the level of erosion correspondingly less. Alternatively, the Cretaceous arc, if once present, might have been displaced westward by early Tertiary sinistral transcurrent faulting.

Petrological evidence from the ophiolite does not discriminate between a marginal basin and a mid-ocean ridge origin. The geochemistry of the Tumu River basalts is equally consistent with an origin in a marginal basin behind an arc fringing the continental margin as with an origin in a LREE-enriched segment of a major ocean basin. On the other hand, the cumulate peridotites and gabbros are genetically unrelated to the Tumu River basalts and formed from mafic lavas more strongly depleted in LIL and associated elements than common MORB. This implies that, if the ophiolite formed in a marginal basin, spreading was sufficiently extensive for deep rifting and tapping of depleted mantle sources free from the influence of sialic crust or dehydrating, underthrust lithosphere.

The most important factor in discriminating between a marginal basin and a mid-ocean ridge origin for the Marum ophiolite seems to be *the age of formation of the ophiolite.* If the ophiolite is of Jurassic or early Cretaceous age (as suggested by K-Ar dating of the cumulates) an origin as a trapped segment of Pacific plate seems likely. On the other hand, if the age of formation of the ophiolite ranges into the earliest Tertiary, as suggested by the K-Ar date obtained from the granophyric diorite, a marginal basin origin is more plausible. Discrimination between the two models clearly requires more accurate dating of the ophiolite.

PART 2

PETROLOGY AND GEOCHEMISTRY OF THE PAPUAN ULTRAMAFIC BELT

Contents

			page
SUMMARY			111
CHAPTER	1.	GEOLOGY	113
	2.	PETROLOGY	116
	3.	GEOCHEMISTRY	127
	4.	ORIGIN OF THE PAPUAN ULTRAMAFIC BELT	142

SUMMARY

The Papuan Ultramafic Belt is a classic ophiolite suite in southeast mainland Papua New Guinea which is believed to have been emplaced when sialic crust of the Australian continent choked a northeastward-dipping subduction zone in the early to middle Tertiary.

Petrologic and geochemical data obtained for the tectonite peridotites at the base of the ophiolite show that these rocks have extremely refractory, uniform mineralogy (consisting mainly of olivine Mg_{92-94}, enstatite Mg_{93-94} and chrome-rich spinel, $Cr/Cr + Al > 0.9$), and are exceptionally depleted in lithophile elements. These features, together with the marked plastic deformation, are consistent with an origin as depleted upper mantle, residual after extensive degrees of partial melting at low pressure.

The tectonite peridotites are overlain by a thick sequence of layered ultramafic and mafic cumulates containing olivine, orthopyroxene, clinopyroxene and plagioclase as the major cumulus phases. Early cumulates are characterized by highly magnesian olivine Mg_{90}, orthopyroxene Mg_{90} and calcic plagioclase An_{86}, and exhibit cryptic variation towards more iron-rich and sodic compositions. Abundances of LIL elements in the cumulates are extremely low, which, together with the nature of the cumulate phases, points to a magnesian olivine-poor tholeiite or magnesian quartz tholeiite parent magma(s) strongly depleted in LIL elements and high valence cations. Highly fractionated iron-rich examples of this parent magma type are represented by the LREE-depleted lavas in the overlying basalt sequence which, although resembling the most depleted MORB in terms of their very low abundances of LIL elements have higher abundances of transition metals and lower abundances of Ti, HREE and other high valence cations compared to common MORB of similar $Mg/(Mg + \Sigma Fe)$ ratio. Also present are LREE-enriched rocks whose relationship with the LREE-depleted cumulates and

basalts is not clear. The existence of these rocks, together with differences in stratigraphy of various cumulate sections in the ophiolite and the irregular variation in plagioclase compositions points to the existence of several stratiform sequences associated with compositionally distinct parent magmas.

Eocene tonalites intruding the PUB are genetically unrelated to the ophiolites. These rocks appear to be related by crystal fractionation to the Ti-poor high-Mg andesites of Cape Vogel, and similar andesites and dacites at the northern end of the PUB. This suite is considered to represent the early stages of island-arc magmatism associated with a north-eastward-dipping subduction zone in the early Eocene immediately prior to emplacement of the PUB. The high-Mg andesite parent magmas are believed to result from water-saturated melting of highly refractory peridotite due to dehydration of the underlying, downgoing lithospheric slab, and subsequently underwent extensive fractionation of olivine and pyroxene at shallow depth.

CHAPTER 1

GEOLOGY

1-1. Introduction

The Papuan Ultramafic Belt is a classic ophiolite complex which extends in a 400 km long belt along the northern side of the Owen Stanley Range in southeast mainland Papua New Guinea between 7 and 10°S, and 147 and 149°E (Fig. 2-1). Davies (1971) has shown that the ophiolite comprises a simple layered sequence consisting of an ultramafic zone (4-8 km thick) overlain by gabbro (4 km) and basalt (4 km) layers which dip at angles of 10 to 40° in a general northeasterly direction towards the coast. Davies (1977) and Davies & Smith (1971) have proposed that the Papuan Ultramafic Belt (PUB) represents an overthrust slab of Jurassic-Cretaceous oceanic crust and mantle which was emplaced as a result of a continent/island-arc collision. This collision is believed to have occurred when sialic crust carried by the northward-moving Australian lithospheric plate encountered a southwest-facing arc-trench system in the Eocene (or, possibly, Oligocene: see later).

While the notion of the PUB as an overthrust slab of crust of oceanic affinity seems clearly established and, indeed, geophysical surveys indicate that the layers of the ophiolite are continuous northeastwards with the crust and upper mantle layers of the Solomon Sea (Finlayson & others, 1976, 1977), doubt has been expressed as to whether the PUB actually represents a segment of oceanic crust generated at a mid-ocean ridge. Karig (1972), Milsom (1973) and Finlayson & others (1977) have all suggested that the PUB may have formed in a marginal basin rather than at a mid-ocean ridge spreading centre.

This study presents new petrologic and geochemical data (including trace elements and $^{87}Sr/^{86}Sr$ ratios) on a suite of representative rock samples collected in collaboration with H.L. Davies (GSPNG) in November 1975 in an attempt to further elucidate the nature and origin of

one of the largest and best preserved ophiolites in the world (cf. Coleman, 1977).

1-2. Geology

Present knowledge of the geology of the Papuan Ultramafic Belt is based on the updated account given by Davies (1977). The geological map of the region presented in Figure 2-1, based on the revised map of Davies (1977), shows the distribution of the peridotite, gabbro and basalt layers. Details of the geology of eastern Papua are given in Davies & Smith (1971) and Smith & Davies (1976), and the various explanatory notes accompanying 1:250 000 scale maps of the region.

Rocks of the ultramafic zone are of two types: 1) tectonite peridotite, mostly harzburgite with minor dunite and orthopyroxenite, with a marked metamorphic fabric, and 2) layered peridotite with cumulus texture (Davies, 1971: England & Davies, 1973). England & Davies (1973) showed that the tectonite peridotites are of extremely refractory and uniform composition, consisting almost entirely of forsteritic olivine, enstatite and chrome spinel. According to Davies (1971, 1977) the cumulate ultramafics form only a small component of the ultramafic mass and contain cumulus olivine, orthopyroxene, clinopyroxene and chrome spinel with minor postcumulus plagioclase.

The cumulate peridotites pass upwards into a thick (4 km) sequence of cumulate gabbro with olivine, orthopyroxene, clinopyroxene and plagioclase as the major cumulus phases (Davies, 1971).. The cumulus-textured gabbro is overlain by granoblastic-textured gabbro containing calcic plagioclase and pyroxenes which passes upwards into ophitic-textured microgabbro with an overall thickness of about 1 km. Ophitic-textured gabbro is overlain by the basalt layer which consists of basaltic lavas and pillow lavas some 4 km thick. A sheeted dyke complex is developed between the ophitic gabbros and the basalt in places (Davies, 1977).

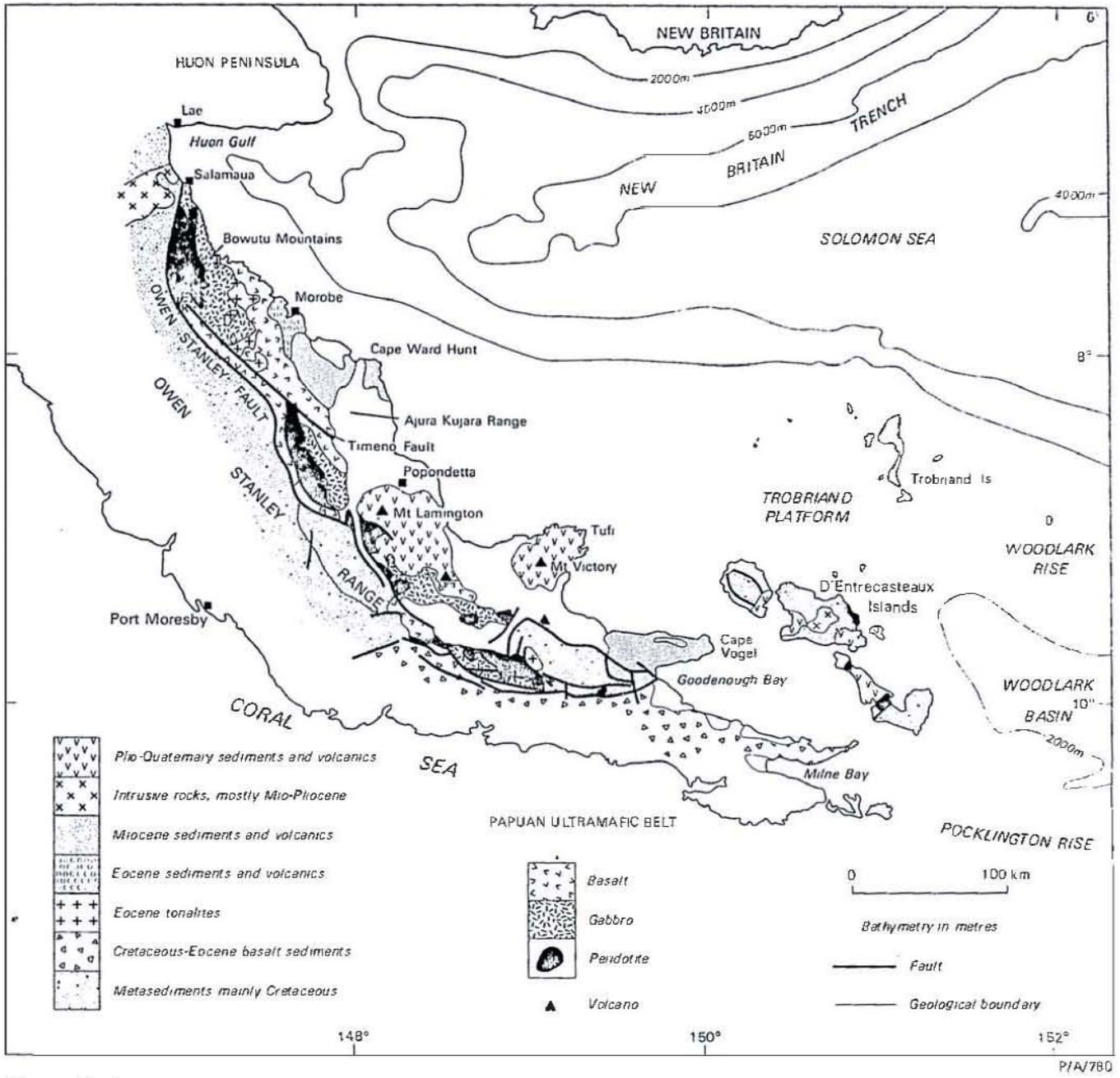

Fig. 2-1. Simplified geology of the Papuan Ultramafic Belt.

The upper part of the ophiolite is intruded by high level tonalitic stocks of Eocene age (Davies, 1971; Davies & Smith, 1971), and Eocene andesite and dacites (largely pyroclastic) unconformably overlie the basalt at the northern end of the ophiolite. Farther south the ophiolite is overlain by Neogene volcanics and sediments.

The ophiolite is bounded to the west by the Owen Stanley Fault which separates the ophiolitic rocks from metamorphosed pelitic sediments of mainly Cretaceous age (Owen Stanley Metamorphics, Pieters, 1978) in the north, and metamorphosed submarine basalt of Cretaceous to Eocene age in the southeast (Smith & Davies, 1976). Slices of granulite and amphibolite facies metamorphics occur in places immediately above the bounding fault, whereas underlying metamorphic rocks are of blueschist or greenschist facies (Davies, 1977; Pieters, 1978).

The age of formation of the Papuan Ultramafic Belt is believed to be (?) Jurassic to Cretaceous. Evidence for this age is based on the occurrence of Maestrichtian planktonic foraminifera in marls intercalated in basalt near the basal thrust, and K-Ar ages of 117 m.y. obtained on a pyroxene from a basalt, and 147-150 m.y. from gabbros (Davies & Smith, 1971; Davies, 1977). However, in view of the very low K contents of the gabbros, and the fact that dating of similar gabbros from the Marum ophiolite showed that the apparent age determined depended on the K content of the sample (PART 1 Chapter 1), the Jurassic ages must be regarded as maximum ages and are open to question.

The age of emplacement is thought to be Eocene (Davies, 1977), based on K-Ar ages of 52-42 m.y. obtained from hornblende in granulites (Davies, 1977). However, if the metamorphism and deformation of the Cretaceous to Eocene strata of the Papuan mainland are directly related to emplacement of the ophiolite as is generally supposed, emplacement may have occurred later than this, possibly late Eocene or Oligocene (Pieters, 1978).

CHAPTER 2

PETROLOGY

2-1. Tectonite Peridotites (Samples 714, 715, 716, 720, 718, 722, 725)

Textures

The harzburgites have been plastically deformed and have a marked tectonite fabric. Most have a porphyroclastic texture characterized by porphyroclasts (augen) of enstatite up to 1 cm long in a matrix of xenoblastic olivine and accessory, subhedral chrome spinel (Fig. 2-2A, B). Olivine grains have marked undulatory extinction, kink-bands and deformation lamellae; many of the larger xenoblastic grains have recrystallized along kink-band boundaries to form subgrains whose grain boundaries form triple junctions. Smaller strain-free neoblasts occur at the granulated margins of enstatite porphyroclasts. Enstatite porphyroclasts have a marked foliation parallel to (010) or (100) directions with numerous kink-bands and pronounced undulatory extinction. Kink-band boundaries are typically at right angles to the foliation. Many of the enstatite porphyroclasts have been disrupted and dismembered into strips along (010) or (100) planes (Fig. 2-2C,D) similar to those described by Nicolas & others (1971), and contain elongate olivine inclusions or 'stringers' (Fig. 2-2B). Chrome spinel grains show both cuspate and sub-to euhedral forms. Compared to the Marum harzburgites the PUB tectonites are appreciably more deformed. Grain size comparisons suggest deformation pressures significantly greater than for the Marum peridotites.

The enstatite-rich pyroxenite dykes consist of xenomorphic granular to xenoblastic pyroxene with interstitial olivine and accessory, tiny euhedra of chrome spinel enclosed in pyroxene. The enstatite typically shows marked undulatory extinction and kink-banding. Some enstatites show spectacular flexures (marked by (010) or (100) cleavage) with numerous closely spaced kink-bands at right angles to the slip plane,

Fig. 2-2. Textures in tectonite peridotites from the PUB.

A. Porphyroclastic harzburgite (725) showing deformed augen of enstatite (OPX) in matrix of recrystallized olivine. Note strong kink-banding in enstatite porphyroclast with kink-band boundaries oriented perpendicular to the foliation. Cross polarizers, x 12.

B. Porphyroclastic harzburgite (720) with strongly deformed augen of enstatite (OPX) in process of being dismembered. Note 'stringers' of olivine. Crossed polarizers, x 12.

C. Porphyroclastic harzburgite (725) with dismembered strips of enstatite (OPX) surrounded by olivine. Crossed polarizers, x 12.

D. Porphyroclastic harzburgite (720) with dismembered strips of enstatite in matrix of recrystallized olivine (OL) and euhedral chrome spinel (SP). Note olivine inclusions in chrome spinel. Crossed polarizers, x 12.

E. Spectacular flexuring (simple shear) and kink-banding of enstatite in enstatolite dyke (718). Small dark euhedra are chrome spinel. Crossed polarizers, x 15.

F. Similar to E. Cross polarizers, x 15.

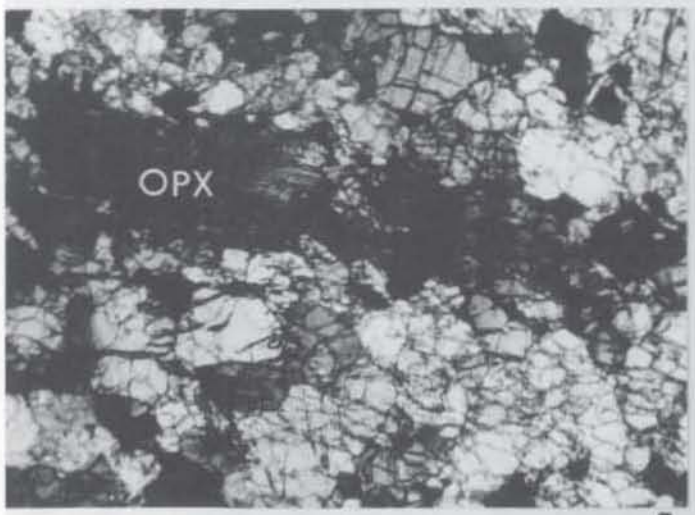

A

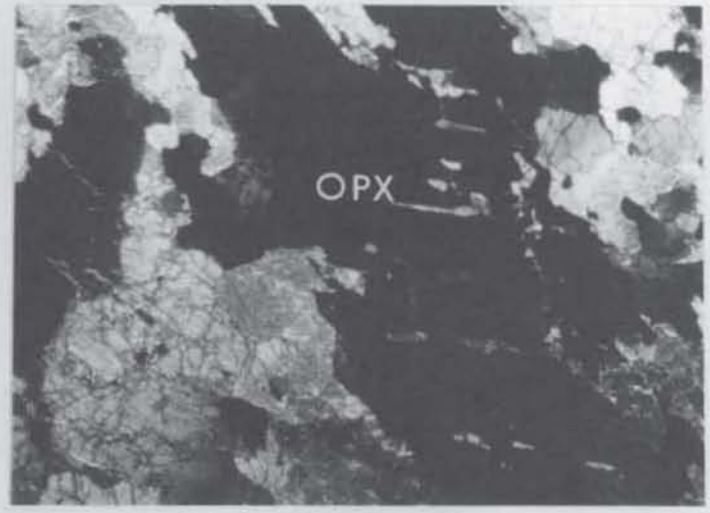

B

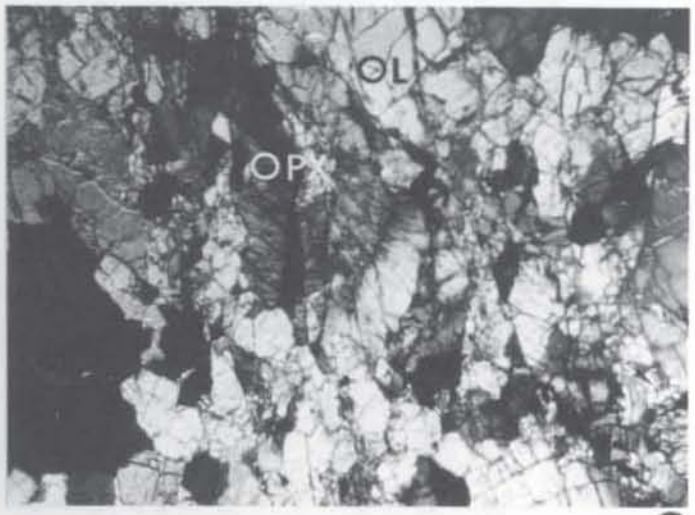

C

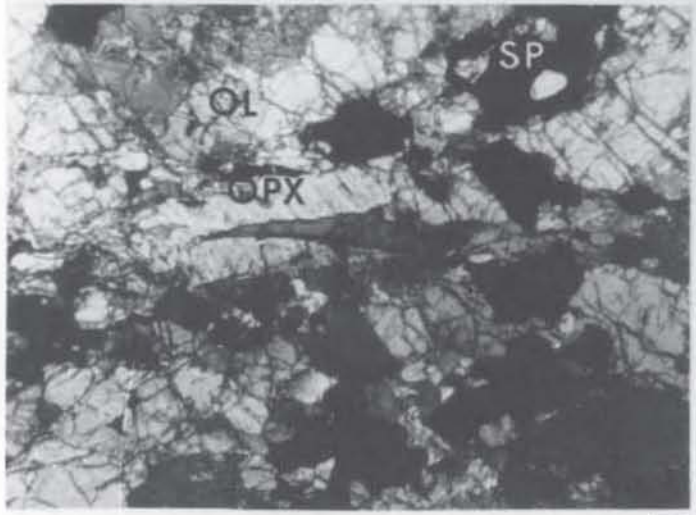

D

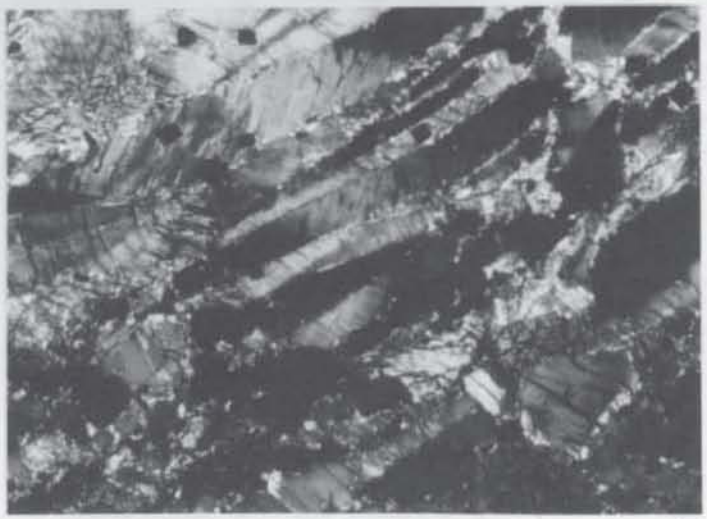

E

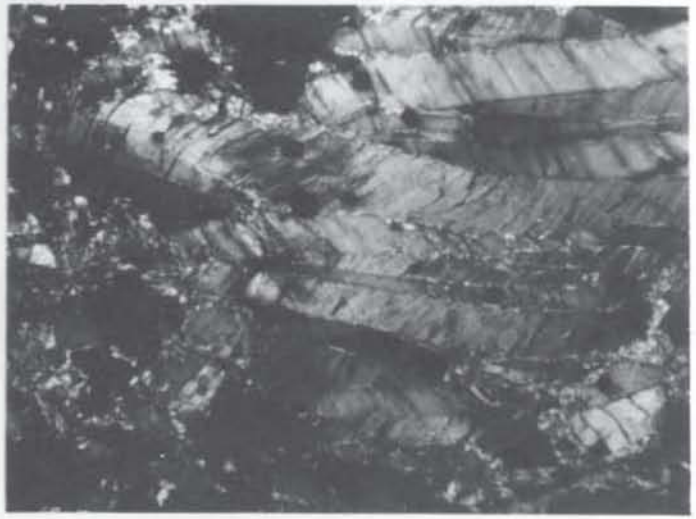

F

commonly with a mylonitised zone at the kink-band boundaries (Fig.2-2E,F) Such textures are indicative of solid state deformation and probably result from intracrystalline glide (Nicolas & others, 1971).

Although the fabrics of the harzburgites indicate extensive plastic deformation relics of a pre-existing fabric are preserved in the form of curvilinear and interlocking cuspate grain-boundaries. The effect of plastic deformation has been a reduction in grainsize and development of subgrains with straight grain-boundaries which intersect at triple junctions. The relic curvilinear grain-boundaries and the inferred very large grainsize of the former xenoblasts (up to 8-10 mm) are interpreted to indicate a former protogranular texture, which has subsequently been plastically deformed to yield porphyroclastic textures.

Mineralogy

Quantitative analyses were obtained by TPD electron microprobe by energy dispersive analysis following the method of Reed & Ware (1973, 1975) (See Appendix 1).

Olivine. The tectonites are characterised by extremely magnesian olivine (Table 2-1). Coarse-grained, xenoblastic olivines are of restricted composition - Mg_{92} to $Mg_{93.4}$ - and lie in the range of compositions found by England & Davies (1973), $Mg_{91.6-93.6}$. Recrystallised subgrains and neoblasts adjacent to chrome spinel are more magnesian (up to $Mg_{94.4}$) reflecting the effects of Fe-Mg partitioning between olivine and spinel with falling temperature (Irvine, 1965, 1967; Roeder & others, 1979). NiO contents are comparatively high, consistent with the highly magnesian character of the olivine. Analyses by wavelength-dispersive probe gave higher NiO contents than those obtained by energy-dispersive probe (0.19-0.33%), and are comparable with NiO values (0.4%) obtained by England & Davies (1973). Cr_2O_3, MnO and CaO were not detected.

The highly magnesian olivine compositions of the tectonites are more magnesian than olivine from tectonite harzburgite in other

TABLE 2-1. REPRESENTATIVE OLIVINE ANALYSES FROM PUB TECTONITE PERIDOTITES

	725	725[1]	716	716[2]	720	720[3]	715	715[4]	714	714[5]
SiO_2	41.19	41.42	41.57	41.49	41.13	41.57	41.58	41.57	41.30	41.55
FeO	6.60	6.25	6.63	5.99	7.02	5.54	7.16	5.87	7.73	6.19
NiO	0.19	0.33	0.22	0.20	0.26	0.26	0.19	0.21	0.27	0.21
MnO	<0.09	<0.09	<0.09	<0.09	<0.09	<0.09	<0.09	<0.09	<0.09	<0.09
MgO	51.55	51.77	51.94	52.31	51.12	52.22	51.57	52.27	50.78	52.19
Total	99.53	99.77	100.36	99.99	99.53	99.59	100.50	100.00	100.08	100.13
			Cations per 4 oxygens							
Si	0.999	1.001	1.000	0.999	1.000	1.003	1.001	1.001	1.001	1.000
Fe	0.134	0.126	0.133	0.121	0.143	0.112	0.144	0.118	0.157	0.124
Ni	0.004	0.006	0.004	0.004	0.005	0.005	0.004	0.004	0.005	0.004
Mn	-	-	-	-	-	-	-	-	-	-
Mg	1.864	1.865	1.862	1.877	1.852	1.877	1.850	1.876	1.835	1.872
Total	3.001	2.999	3.000	3.001	3.000	2.997	2.999	2.999	2.999	3.000
100Mg/(Mg+Fe)	93.4	93.7	93.3	94.0	92.8	94.4	92.8	94.1	92.1	93.8
Ni ppm			2890		2740				2590	

All CaO <0.07, Al_2O_3 <0.09%. Superscripts 1, 2, 3 indicate rim compositions of olivine subgrains adjacent to chrome spinel rims (Table 2-3) with same superscript. Ni analyses in ppm by wavelength dispersive probe.

TABLE 2-2. REPRESENTATIVE ANALYSES OF ORTHOPYROXENE FROM TECTONITE PERIDOTITES

	Harzburgite							Enstatolite
	725	725*	716	716*	720	715	714	718
SiO_2	58.68	58.40	58.48	58.08	58.51	58.66	58.84	57.69
Al_2O_3	<0.09	<0.09	<0.09	<0.09	<0.09	<0.09	<0.09	<0.09
Cr_2O_3	0.08	0.23	<0.08	0.13	0.09	<0.08	<0.08	<0.08
FeO	4.31	4.34	4.47	4.42	4.50	4.35	4.81	7.25
MnO	<0.09	<0.09	<0.09	<0.09	<0.09	<0.09	<0.09	<0.09
MgO	36.87	36.65	36.85	36.81	36.60	37.18	36.51	34.40
CaO	0.15	0.08	<0.07	<0.07	0.08	<0.07	<0.07	0.14
Total	100.09	99.70	99.80	99.44	99.78	100.19	99.86	99.48
	Cations per 6 oxygens							
Si	1.999	1.998	1.998	1.992	2.000	1.996	2.001	2.002
Al	-	-	-	-	-	-	-	-
Cr	0.002	0.006	-	0.003	0.002	-	-	-
Fe	0.123	0.124	0.128	0.126	0.129	0.124	0.138	0.210
Mn	-	-	-	-	-	-	-	-
Mg	1.871	1.868	1.876	1.883	1.865	1.885	1.860	1.780
Ca	0.005	0.003	-	-	0.003	-	-	0.005
Total	4.000	3.999	4.002	4.004	3.999	4.004	3.999	3.998
100Mg/(Mg+Fe)	93.8	93.8	93.6	93.7	93.5	93.8	93.1	89.4

All TiO_2 <0.07%

* inclusion in chrome spinel

ophiolites such as Marum (Table 1-1), Troodos (Menzies & Allen, 1974), Vourinos (Jackson & others, 1975), Bay of Islands (Irvine & Findlay, 1972; Malpas, 1978), and from harzburgite-subtype alpine peridotites (e.g. Loney & others, 1971; Himmelberg & Loney, 1973; Dick, 1977).

Orthopyroxene. Representative analyses of orthopyroxene are presented in Table 2-2. The orthopyroxenes are highly magnesian, and extremely low in CaO and R_2O_3 content, being essentially enstatite-ferrosilite solid solutions. Although of similar Mg-value, orthopyroxenes analysed by England & Davies (1973) have significantly higher CaO and Al_2O_3 contents (up to 1.5%) than those reported here. The restricted range of compositions exhibited by the tectonite orthopyroxenes is shown in Figure 2-4.

Compared to orthopyroxenes from alpine peridotites and other ophiolites, the PUB orthopyroxenes are decidedly more magnesian and poorer in CaO and R_2O_3, and plot at the Al-poor extremity of the Al_2O_3 versus Mg trend (Fig. 1-5).

Chrome spinel. Chrome spinels from the harzburgites are extremely chrome-rich containing 66-69% Cr_2O_3 with Cr/(Cr+Al) ratios $\geq$ 0.9. Both TiO_2 and calculated Fe_2O_3 contents are very low. Spinels from harzburgite 714 are noticeably more aluminous than spinels from the other harzburgites which are of uniform composition and show only very small variations in Cr-Al and Mg-Fe^{2+} (Fig. 2-3). Small differences exist between cores and rims in many spinel grains: rims commonly have lower Mg/(Mg+Fe^{2+}), and slightly higher Al and Fe^{3+} than the cores. Spinel from the enstatolite dyke is significantly more iron rich than the harzburgite spinels, and has markedly higher Fe^{3+}.

The chrome-spinels in the harzburgites are decidedly more chrome-rich than spinel in the overlying cumulates (Table 2-3), and are also more chrome-rich than spinel in alpine peridotite and harzburgite from other ophiolites (e.g. Himmelberg & Loney, 1973; Dick, 1977; Menzies, 1975; Rodgers, 1973; Malpas & Strong, 1975).

TABLE 2-1. REPRESENTATIVE CHROME SPINEL ANALYSES

	Harzburgite										Enstatolite	Lherzolite
	725	725[1]	716	716[2]	720	720[3]	715	715[4]	714	714[5]	718	736
TiO_2	<0.07	<0.07	<0.07	<0.07	<0.07	<0.07	<0.07	<0.07	<0.07	<0.07	0.12	0.20
Al_2O_3	2.74	2.64	2.60	2.61	2.62	2.64	2.60	2.76	5.47	5.07	3.27	11.89
Cr_2O_3	68.22	68.03	68.06	68.52	68.61	68.72	68.70	68.23	66.08	66.75	61.11	55.13
Fe_2O_3	0.96	1.82	1.35	1.44	1.48	1.38	1.40	1.37	0.95	0.44	6.05	3.67
FeO	17.77	18.08	17.71	18.26	17.76	18.02	18.10	18.73	16.90	18.68	23.96	20.07
MnO	0.54	0.58	0.43	0.41	0.66	0.72	0.57	0.53	0.56	0.33	0.64	<0.09
MgO	9.14	9.08	9.24	9.09	9.26	9.10	9.12	8.73	10.14	9.16	5.26	9.03
CaO	<0.07	<0.07	<0.07	<0.07	<0.07	<0.07	<0.07	<0.07	<0.07	<0.07	<0.07	<0.07
Total	99.37	100.23	99.39	100.33	100.39	100.58	100.49	100.35	100.10	100.43	100.41	99.99
	Cations per 4 oxygens											
Ti	-	-	-	-	-	-	-	-	-	-	0.003	0.005
Al	0.112	0.106	0.106	0.105	0.106	0.106	0.015	0.112	0.127	0.203	0.136	0.463
Cr	1.863	1.847	1.859	1.857	1.856	1.858	1.859	1.853	1.759	1.786	1.701	1.441
Fe^{3+}	0.025	0.047	0.035	0.037	0.038	0.036	0.036	0.035	0.024	0.011	0.160	0.091
Fe^{2+}	0.513	0.519	0.511	0.524	0.508	0.515	0.518	0.538	0.476	0.529	0.705	0.555
Mn	0.016	0.017	0.013	0.012	0.019	0.021	0.017	0.015	0.016	0.009	0.019	-
Mg	0.471	0.464	0.476	0.464	0.472	0.464	0.465	0.447	0.508	0.462	0.276	0.445
Ca	-	-	-	-	-	-	-	-	-	-	-	-
$100Mg/(Mg+Fe^{2+})$	47.8	47.2	48.2	47.0	48.2	47.4	47.3	45.4	51.6	46.6	28.1	44.5
$\frac{Cr}{(Cr+Al+Fe^{3+})}$	0.932	0.924	0.930	0.929	0.928	0.929	0.930	0.926	0.880	0.893	0.852	0.722
$\frac{Al}{(Cr+Al+Fe^{3+})}$	0.056	0.053	0.053	0.053	0.053	0.053	0.052	0.056	0.109	0.101	0.068	0.232
$\frac{Fe^{3+}}{(Cr+Al+Fe^{3+})}$	0.012	0.024	0.018	0.019	0.019	0.018	0.018	0.018	0.012	0.005	0.080	0.046
$\frac{Cr}{(Cr+Al)}$	0.943	0.946	0.946	0.946	0.946	0.946	0.947	0.943	0.890	0.898	0.926	0.757

Total iron determined as FeO; Fe_2O_3 calculated assuming ideal $R^{2+}O.R_2^{3+}O_3$ spinel formula.
Superscripts [1,2] etc refer to coexisting olivine subgrains (Table 2-1)

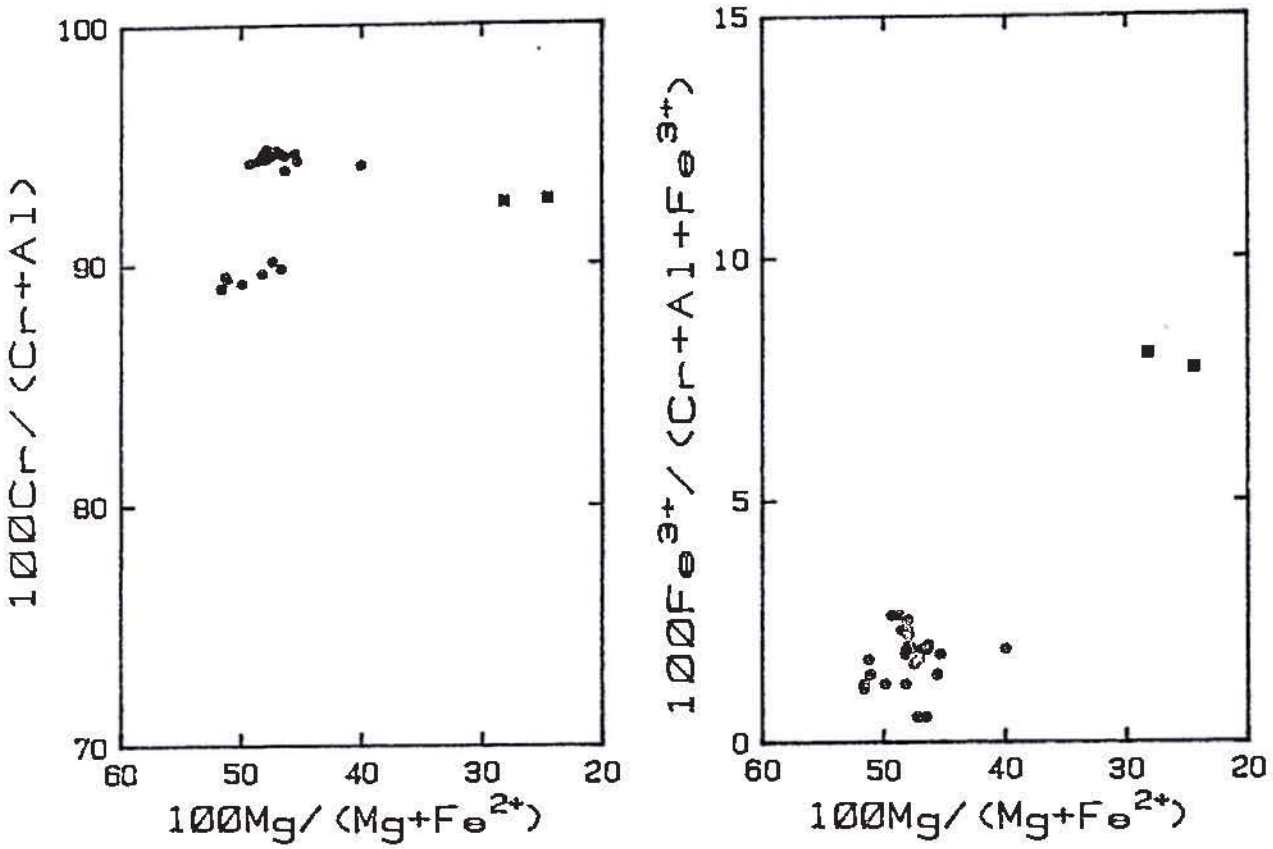

Fig. 2-3. Variation in composition of spinel from PUB tectonite peridotites. Circles = harzburgites, square = enstatolite dykes.

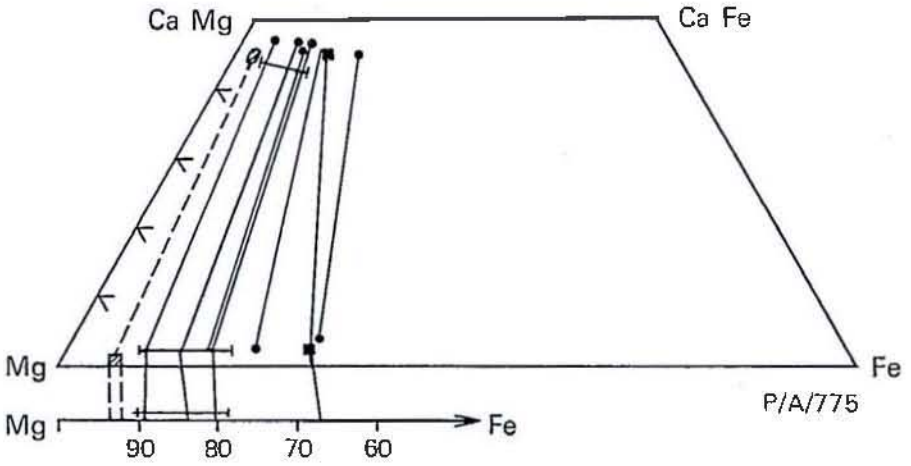

Fig. 2-4. Pyroxene quadrilateral showing compositions of co-existing olivines and pyroxenes from tectonites (hatched) and cumulate peridotites and gabbros (dots). Bars indicate range of cumulus compositions found by England & Davies (1973). Squares = hornblende granulite.

Olivine-spinel equilibria

The markedly higher Mg/(Mg+Fe) ratio of olivine subgrains adjacent to spinel and the higher Fe^{2+} of spinel rims is consistent with re-equilibration of Mg and Fe^{2+} between olivine and spinel with falling temperature (Irvine, 1965; Roeder & others, 1979; see PART 1 Chapter 2 for discussion). Olivine and spinel equilibrated under the same temperature (and pressure) conditions should define a linear relationship on a ln K_d versus Y_{Cr}^{sp} diagram, where

$$K_d = \frac{X_{Mg}^{ol} \cdot X_{Fe}^{sp\,2+}}{X_{Fe}^{ol\,2+} \cdot X_{Mg}^{sp}}$$

The restricted range of Y_{Cr}^{sp} for the PUB harzburgites precludes any meaningful interpretation of attainment of equilibrium between olivine and spinel cores. It is noteable, however, that rims have variable, although consistently higher, ln K_d values than the cores, suggesting attainment of equilibrium on a local scale only. Quasi-magmatic (1200-1400°C) nominal equilibration temperatures were obtained using Jackson's (1969) calibration of the olivine-spinel geothermometer for olivine-spinel cores, and slightly lower temperatures (1100- 1200°C) were obtained for the rim compositions. Markedly lower nominal equilibration temperatures were obtained using Roeder & others (1979) revised equation using lower $\Delta^{o}G$ $FeCr_2O_4$ values: olivine-spinel cores gave temperatures in the range 650-740°C ($\bar{x}$ = 680 $\pm$ 30°C) whereas adjacent rims and subgrains gave lower nominal temperatures 580-630°C ($\bar{x}$ = 600 $\pm$ 20°C). These low temperatures indicate extensive subsolidus re-equilibration (possibly cooling) and provide no information on the high temperature equilibration history of the peridotites.

2-2. Cumulate peridotites and gabbros (Samples 719, 728-733, 736).

Petrography

Ultramafic cumulates directly overlie the ultramafic tectonites,

and consist of cumulus olivine, orthopyroxene, clinopyroxene and chrome spinel with post-cumulus pyroxene (Davies, 1971). The samples of cumulate ultramafics studied range from lherzolite through olivine pyroxenite to plagioclase lherzolite. The lherzolite (736) consists of cumulus, embayed olivine Mg_{89}, subhedral bronzite Mg_{90}, subordinate diopside, and accessory chrome spinel. Olivine pyroxenite consists of xenoblastic pyroxene, subordinate embayed olivine, and disseminated euhedra of chromian spinel. Plagioclase lherzolite (733) consists of cumulus olivine Mg_{83-84} (commonly resorbed), sub-to euhedral plagioclase An_{81-86}, subhedral diopside, and minor chrome spinel enclosed in poikilitic orthopyroxene Mg_{85}. The cumulate peridotites commonly show evidence of deformation, generally kink-banding and undulose extinction, but the degree of deformation is markedly less than that in the tectonite peridotites. The extent of secondary alteration is variable. Typically olivine is partially serpentinized, pyroxene altered in part to bastite $\pm$ talc, and, where enclosing olivine, cut by serpentine-filled expansion fissures. Plagioclase is altered in part to saussurite.

Cumulus peridotite is overlain by layered troctolite (732) containing embayed cumulus olivine Mg_{80-81} and cumulus sub-to euhedral plagioclase An_{86-87} enclosed in poikilitic augite and/or hypersthene, and olivine-poor norite-gabbro. Layered norite-gabbros (728-731) are more differentiated, consisting entirely of allotriomorphic granular plagioclase An_{81-93}, augite and hypersthene, and have little secondary alteration. These rocks, interpreted as modified adcumulates, comprise the bulk of the cumulate sequence.

The fine-grained high-level granular textured microgabbro examined here (727) consists of plagioclase euhedra enclosed in poikilitic augite and/or hypersthene (commonly replaced by amphibole) with a matrix of granular plagioclase, quartz, magnetite, ilmenite and apatite. The abundance of quartz and Fe-Ti oxides, and the composition of the pyroxenes

suggests crystallization from an evolved silica and iron-rich liquid.

Mineralogy

Olivine. Olivine compositions from the cumulate sequence range from $Mg_{89.3}$ to $Mg_{80.6}$, and lie within the range of 89.6-78.3 found for cumulus olivine by England & Davies (1973). These compositions are markedly less magnesian than olivine from the tectonite peridotites (Fig. 2-4). NiO contents are comparatively low, and decrease with increase in Fo content, typical of olivine crystallizing from a differentiating basaltic magma.

Pyroxenes. Pyroxene compositions analysed here extend the range of compositions observed by England & Davies (1973) to appreciably more iron-rich compositions as shown in Figure 2-4. Representative analyses are given in Table 2-4. Ca contents of the co-existing pyroxenes are variable and reflect varying degrees of subsolidus re-equilibration. Orthopyroxene compositions range from $\sim Ca_4$ (solidus) to $\sim Ca_1$ (subsolidus) in exsolved lamellae in augite. Clinopyroxenes show a similar range from near-solidus to subsolidus compositions ($\sim Ca_{48}$). Al_2O_3 contents are low, typical of pyroxenes crystallized from tholeiitic magma at shallow crustal levels, and decrease with increase in Wo content in clinopyroxene and with decreasing Wo content in orthopyroxene. Na_2O and TiO_2 contents are extremely low, and indicate a parent magma with low levels of these elements. MnO contents increase and Cr_2O_3 contents decrease with increase in Fs component.

Equilibration temperatures for co-existing pyroxene pairs estimated from the pyroxene solvus (Wells, 1977) lie in the range 900-1000°C which suggests that all have re-equilibrated under subsolidus conditions. Slightly lower temperatures, 900-930°C, were estimated from pyroxene host-lamellae pairs.

Spinel. Chrome spinel occurs as small euhedra in the lowermost cumulate peridotites. A representative analysis of cumulus spinel from lherzolite

TABLE 2-4. REPRESENTATIVE ANALYSES OF CUMULUS OLIVINE AND PYROXENE

	OLIVINE				PYROXENE													
	736	733	732	723*	736		733		730		732	728		727		723*		705**
					opx	cpx	opx	cpx	opx	cpx	opx	cpx	opx	cpx	opx	cpx	opx	cpx	opx
SiO_2	40.66	39.51	39.17	36.87	56.90	54.33	56.14	52.35	55.75	52.66	55.59	52.64	54.59	52.55	52.33	52.41	53.39	51.47	53.27
Al_2O_3	<0.10	<0.10	<0.10	0.14	<0.07	<0.07	<0.07	<0.07	<0.07	0.14	<0.07	<0.07	<0.07	0.12	<0.07	0.11	0.41	0.70	<0.07
FeO	10.45	15.65	18.22	29.08	0.71	0.91	1.38	2.27	1.38	2.60	1.27	1.94	1.01	1.67	0.48	0.65	1.67	2.72	1.32
NiO	0.19	0.22	<0.15	0.27	0.27	0.61	0.13	0.83	<0.07	0.18	<0.07	0.28	<0.07	0.11	<0.07	<0.07	<0.07	<0.07	<0.07
MnO	<0.09	0.18	<0.09	0.27	6.59	2.17	9.84	4.39	11.93	5.38	11.98	5.29	15.23	6.46	24.88	9.64	17.60	8.55	19.75
MgO	49.05	44.20	42.37	33.40	<0.09	<0.09	0.22	<0.09	0.18	<0.09	0.28	<0.09	0.35	<0.09	0.45	<0.09	0.32	0.19	0.56
CaO	<0.07	<0.07	<0.07	<0.07	33.87	18.40	32.12	16.52	29.84	16.75	29.89	16.22	27.39	15.80	21.38	14.28	25.38	15.61	23.60
Total	100.35	99.76	99.76	100.03	1.42	23.71	0.66	22.82	1.52	22.24	1.37	22.62	1.41	22.65	0.64	22.50	1.28	20.09	1.58
					<0.15	<0.15	<0.15	<0.15	<0.15	<0.15	<0.15	<0.15	<0.15	<0.15	<0.15	<0.15	<0.15	0.18	<0.15
	Cations per 4 oxygens				99.76	100.13	100.49	99.18	100.60	99.95	100.37	99.00	99.96	99.36	100.15	99.59	100.05	99.51	100.08
Si	0.996	0.998	1.000	0.993															
Al	–	–	–	0.004							Cations per	6 oxygens							
Fe	0.214	0.331	0.389	0.655	1.975	1.968	1.960	1.934	1.966	1.928	1.966	1.951	1.969	1.951	1.972	1.970	1.947	1.917	1.964
Ni	0.004	0.004	–	0.006	0.025	0.032	0.040	0.066	0.034	0.072	0.034	0.049	0.031	0.049	0.021	0.029	0.053	0.083	0.036
Mn	–	0.004	–	0.006	0.004	0.007	0.017	0.033	0.023	0.040	0.019	0.036	0.012	0.024	–	–	0.019	0.036	0.021
Mg	1.790	1.664	1.612	1.341	–	–	–	–	–	0.004	–	–	–	0.003	–	0.003	0.011	0.020	–
Ca	–	–	–	–	0.007	0.017	0.004	0.024	–	0.005	–	0.008	–	0.003	–	–	–	–	–
Total	3.004	3.002	3.000	3.005	0.191	0.066	0.287	0.136	0.352	0.165	0.354	0.164	0.459	0.201	0.784	0.303	0.537	0.266	0.609
					–	–	0.007	–	0.005	–	0.008	–	0.011	–	0.014	–	0.010	0.006	0.017
100 Mg / Mg+Fe	89.3	83.4	80.6	67.2	1.752	0.993	1.671	0.909	1.568	0.914	1.575	0.896	1.473	0.874	1.201	0.800	1.379	0.866	1.297
					0.053	0.920	0.025	0.903	0.057	0.880	0.052	0.898	0.055	0.901	0.026	0.907	0.050	0.802	0.062
					–	–	–	–	–	–	–	–	–	–	–	–	–	0.013	–
					4.007	4.004	4.009	4.005	4.006	4.009	4.008	4.002	4.009	4.007	4.018	4.012	4.006	4.010	4.007
					90.2	93.8	85.3	87.0	81.7	84.7	81.6	84.5	76.2	81.3	60.5	72.5	72.0	76.5	68.0
					2.7	46.5	1.2	46.3	2.9	44.9	2.6	45.8	2.8	45.6	3.2	45.1	2.5	44.8	3.2
					87.8	50.2	84.3	46.7	79.3	46.7	79.5	45.8	74.1	44.2	65.9	39.8	70.1	41.4	65.9
					9.5	3.3	14.5	7.0	17.8	8.4	17.9	8.4	23.1	10.2	30.9	15.1	27.3	13.8	30.9

* Hornblende granulite

** Relic core in hornblende from tonalite

TABLE 2-5. REPRESENTATIVE PLAGIOCLASE ANALYSES

	Cumulates								Granulite	Tonalites		
	733 core	733 rim	732	730 core	730 rim	728 core	728 rim	727	723	705 core	705 rim	703
SiO_2	46.88	46.18	46.08	45.58	44.20	47.21	47.12	55.66	46.78	47.75	55.63	57.20
Al_2O_3	33.31	34.28	34.22	34.91	35.58	33.48	33.84	28.12	33.72	33.27	28.35	27.03
FeO	0.48	0.28	0.55	0.36	0.23	0.37	0.25	0.44	<0.07	0.42	<0.07	0.29
MgO	0.21	<0.09	<0.09	<0.09	<0.09	<0.09	<0.09	<0.09	<0.09	<0.09	<0.09	<0.09
CaO	16.82	17.49	17.71	18.40	19.12	16.81	16.90	10.22	16.89	16.45	10.36	8.80
Na_2O	1.89	1.64	1.55	1.25	0.85	2.07	1.97	5.69	1.92	2.18	5.72	6.50
K_2O	<0.07	<0.07	<0.07	<0.07	<0.07	<0.07	<0.07	<0.07	<0.07	0.13	0.09	0.14
Total	99.59	99.86	100.12	100.50	99.98	99.94	100.08	100.13	99.32	100.20	100.15	99.95
	Cations per 8 oxygens											
Si	2.165	2.129	2.123	2.094	2.046	2.171	2.163	2.503	2.162	2.189	2.499	2.567
Al	1.813	1.863	1.859	1.891	1.942	1.815	1.831	1.491	1.836	1.798	1.501	1.430
Fe	0.018	0.011	0.021	0.014	0.009	0.014	0.010	0.016	-	0.016	-	0.011
Mg	0.015	-	-	-	-	-	-	-	-	-	-	-
Ca	0.832	0.864	0.874	0.906	0.948	0.829	0.831	0.492	0.836	0.808	0.498	0.423
Na	0.169	0.146	0.139	0.112	0.076	0.185	0.176	0.496	0.172	0.194	0.498	0.565
K	-	-	-	-	-	-	-	-	-	0.008	0.005	0.008
Ca	83.1	85.5	86.3	89.0	92.5	81.7	82.6	49.8	82.9	80.0	49.7	42.5
Na	16.9	14.5	13.7	11.0	7.5	18.3	17.4	50.2	17.1	19.2	49.7	56.7
K	-	-	-	-	-	-	-	-	-	0.8	0.6	0.8

736 is given in Table 2-3. The cumulate spinels are markedly more aluminous than spinels from the underlying tectonite peridotites, and have higher Fe^{3+} content. Cumulus plagioclase and spinel do not co-exist.

Plagioclase. Plagioclase occurs as an intercumulus phase in the upper portion of the peridotite unit (Davies, 1971), and is a cumulus phase throughout the gabbro zone. The plagioclases are essentially albite-anorthite solid solutions and have extremely low Or component. Plagioclase in the gabbros is commonly zoned from bytownite cores to calcic bytownite-anorthite rims (Table 2-5) with rims mostly 2-4 mol % more Ca-rich, as was found in the Marum cumulate gabbros (PART 1 Chapter 3). Plagioclase compositions show only a poor correlation with the Mg of co-existing phases and bulk-rock *mg* such as typically found in stratiform intrusions (e.g. Wager & Brown, 1968). In the PUB changes in plagioclase compositions are irregular, and early forming plagioclase is, in some cases, less calcic than plagioclase in more differentiated cumulates. These differences point to compositional differences between the various cumulate sections (see later).

Fe-Ti oxide. Ilmenite and magnetite occur only in the microgabbro. Titaniferous magnetite shows variation in TiO_2 content from 3 to 9% (Table 2-6). Comparison with the T-f_{O_2}-X curves of Buddington & Lindsley (1964), suggests equilibration at temperatures of about 720°C and $f_{O_2} = 10^{-14}$.

Amphibole. Colourless, secondary amphibole, tremolite-actinolite, is present in minor amount in many of the PUB peridotites and gabbros where it occurs as a replacement of pyroxene. Abundant actinolitic amphibole occurs in the microgabbro as deuteric replacement of primary pyroxene. The absence of primary amphibole and late formation of Fe-Ti oxides in the cumulates points to a parent magma with low water content, and crystallization under comparatively low f_{O_2}.

TABLE 2-6. REPRESENTATIVE ANALYSES OF AMPHIBOLES AND FeTi OXIDES

AMPHIBOLE

Sample No	Gabbro 727	Granulite 723	Tonalite 705c	Tonalite 705r	703
SiO_2	51.30	41.91	53.82	49.62	49.68
TiO_2	0.21	3.97	0.10	0.25	0.85
Al_2O_3	2.44	12.15	2.10	5.04	5.08
Cr_2O_3	<0.07	0.12	<0.07	<0.07	<0.07
FeO	17.03	11.28	12.32	13.50	13.83
MnO	0.30	<0.09	0.18	0.27	0.24
MgO	13.21	13.64	15.73	15.44	15.38
CaO	11.07	11.80	12.73	11.22	11.27
Na_2O	<0.15	2.80	0.28	0.88	1.09
K_2O	<0.07	<0.07	<0.07	0.32	0.08
Total	95.55	97.67	97.26	96.54	97.50
Cations per 23 oxygens					
Si	7.698	6.158	7.770	7.309	7.255
Al^{IV}	0.302	1.842	0.230	0.691	0.745
Al^{VI}	0.129	0.263	0.127	0.184	0.129
Ti	0.024	0.439	0.011	0.028	0.093
Cr	-	0.014	-	-	-
Fe	2.138	1.386	1.488	1.663	1.689
Mn	0.038	-	0.022	0.033	0.029
Mg	2.954	2.987	3.384	3.390	3.349
Ca	1.779	1.858	1.969	1.770	1.763
Na	-	0.799	0.078	0.252	0.308
K	-	-	-	0.060	0.016
Total	15.062	15.744	15.080	15.381	15.376
Ca	25.9	29.8	28.8	25.9	25.9
Mg	43.0	47.8	49.5	49.7	49.2
Fe	31.1	22.2	21.4	24.4	24.8

MAGNETITE

Sample No	Gabbro 727		Granulite 723	Tonalite 705	703
SiO_2	0.20	0.13	0.29	0.39	0.45
TiO_2	8.84	3.57	19.85	0.29	0.13
Al_2O_3	<0.09	0.16	4.57	<0.09	0.30
Cr_2O_3	0.12	0.90	2.69	0.48	0.26
V_2O_3	0.88	<0.09	0.62	0.47	0.61
Fe_2O_3*	50.88	60.68	22.30	66.98	66.96
FeO	39.01	34.57	48.35	32.04	32.06
MnO	0.44	<0.09	0.46	<0.09	<0.09
MgO	<0.09	<0.09	1.27	<0.09	<0.09
CaO	0.23	<0.07	0.11	<0.07	<0.07
Total	100.60	100.01	100.51	100.65	100.77
mol % ulvospinel	26.1	10.9	57.9	2.3	2.1

ILMENITE

SiO_2	0.11	0.45
TiO_2	48.04	51.52
Al_2O_3	<0.09	0.14
Cr_2O_3	<0.07	0.22
V_2O_3	0.37	<0.09
Fe_2O_3	8.82	1.41
FeO	41.39	43.76
MnO	1.92	2.52
MgO	<0.09	0.18
CaO	<0.07	0.11
Total	100.65	100.31
mol% R_2O_3	8.6	1.6

* Total iron determined as FeO. Fe_2O_3 and FeO, and mol% ulvospinel and R_2O_3 calculated following Carmichael (1967)

Comparison

The PUB cumulates are petrologically very similar to the cumulate peridotites and gabbros of the Marum ophiolite (PART 1), particularly in terms of the magnesian nature of the early cumulates, the abundance of cumulus orthopyroxene throughout the sequence, and the highly calcic nature of the plagioclase. The range of iron enrichment in olivine compositions is also similar, $Mg_{92-78.7}$ in the Marum compared to $Mg_{89.6-78.3}$ in the PUB. The cumulate sequence of both ophiolites is similar to the Troodos ophiolite (Greenbaum, 1972) which is also characterized by the early crystallization of cumulus orthopyroxene, and differs from ophiolites such as Vourinos, Point Sal and Bay of Islands where orthopyroxene is either a minor phase often forming late in the cumulate sequence and is appreciably more iron-rich, or is entirely lacking (Jackson & others, 1975; Coleman, 1977; Church & Riccio, 1977; Malpas, 1978). The PUB cumulates are also very similar to cumulate peridotites and gabbros described from DSDP site 334 by Hodges & Papike (1976). As discussed in PART 1 Chapter 3, low pressure crystallization of highly magnesian orthopyroxene (Mg_{90}) points to a parental magma(s) distinctly more silica-saturated than MORB-type olivine tholeiites (Green & others, 1979). Davies (1971) described bronzite cumulates from the Bowutu Mountains at the northern section of the PUB, and pointed out that some of the orthopyroxene-bearing cumulates were similar to those found in the Stillwater Complex. Williams & Hallberg (1973) showed that small layered intrusions in the Archaean Yilgarn Block of Western Australia had layered sequences very similar to that of the Stillwater Complex, and that the parent magmas for these bodies was of high-Mg basalt or basaltic komatiite composition (Mg $\sim$ 74-77) containing approximately 15-17% MgO, 50-52% SiO_2 and low normative olivine (< 5%). These compositions are very similar to the least altered, more mafic members of the Upper Pillow Lavas and the Arakapas Fault Belt basalts of Troodos (Smewing & others,

1975; Simonian & Gass, 1978; See PART 1 Chapter 3 for discussion), although the Troodos basalts have higher SiO_2 and CaO contents and are mainly quartz-normative. Although cumulate sections containing abundant orthopyroxenites do not appear to be typical of the PUB as a whole (Davies, 1971) and none were sampled in this study, the presence of such cumulates in some cumulate sections points to different parent magma compositions in the ophiolite sequence. This inference is also supported by the poor correlation of plagioclase compositions with the Mg-value of co-existing ferromagnesian phases. Overall however, the PUB cumulates are consistent with low pressure accumulation from parent magmas of magnesian olivine-poor tholeiite or even magnesian quartz tholeiite composition.

2-3. Basalts (Samples 706-710, 712)

The basalts are mainly of aphanitic pillow lava, commonly with sparse amygdales and veinlets containing secondary epidote, calcite, quartz, and/or pyrite. Pillow margins are fine-grained to glassy with variolitic texture, and grade into intergranular texture at the pillow core. Petrographically the basalts are either aphanitic or carry rare microphenocrysts of iron-rich augite ($Mg_{40-21}Ca_{35-48}Fe_{25-31}$) or plagioclase (mostly labradorite) in an intergranular to variolitic textured groundmass of plagioclase, clinopyroxene and Fe-Ti oxide which is commonly of skeletal form. Secondary minerals include chlorite-smectite, calcite epidote and albite. The cotectic crystallization of clinopyroxene and plagioclase, and, in more iron-rich lavas, of Fe-Ti oxide, clearly indicates crystallization from highly evolved Fe-rich liquids.

2-4. Tonalite (Samples 703, 704, 705)

Eocene tonalites form high-level stocks intruding the upper portion of the gabbro unit of the ophiolite. Typically they consist of sub-to euhedral phenocrysts of strongly zoned plagioclase, An_{70-34} (with some cores as calcic as An_{80}; Table 2-5), and pleochroic green

actinolitic hornblende (Table 2-6) in a matrix of anhedral quartz, more sodic plagioclase An_{50-20} and hornblende. Ti-poor magnetite, apatite and, less commonly, biotite are accessory phases. Minor amounts of secondary sphene, epidote, actinolite, albite and chlorite are also present in some samples. Hornblende phenocrysts are commonly strongly zoned from pale coloured, Al-poor cores ($\sim$ 2% Al_2O_3) to more strongly coloured rims richer in Al_2O_3, TiO_2 and Na_2O (Table 2-6) similar to the groundmass hornblende. The Al-poor hornblende appears to be a deuteric alteration product from pyroxene. Relic hypersthene Mg_{68} (Table 2-4) was found in hornblende-rich mafic inclusion in tonalite 705 enclosed in actinolitic hornblende.

2-5. Hornblende granulite (Sample 723)

Amphibolite and granulite facies rocks occur near the Timeno and Owen Stanley fault zones, and are believed to have formed during emplacement of the PUB (Davies, 1971, 1977). Some of the granulites have the unusual assemblage olivine-hypersthene-augite-brown hornblende-bytownite-magnetite-ilmenite, and have a granoblastic, equigranular texture. Representative analyses of the phases are presented in Table 2-4, 5, 6. Compared to the PUB peridotites and gabbros the olivine in the granulite is markedly more iron-rich, and the pyroxenes are distinctly richer in Al_2O_3 and, particularly, TiO_2 (approx. 6 times that in the cumulates). The $K_D^{opx-cpx}$, where $K_D = (\frac{Fe}{Mg})opx / (\frac{Fe}{Mg})cpx$, for the pyroxenes in the granulite differs considerably from that of the cumulates (Fig. 2-4), and is significantly lower (1.27) than commonly found for co-existing pyroxene pairs from high-grade metamorphic terraines, being closer to those of igneous pyroxenes (cf. Kretz, 1963). The amphibole is a strongly coloured, brown titan-pargasite approaching kaersutite in composition. The very high TiO_2 of the hornblende sets it aside from most other metamorphic hornblendes co-existing with ilmenite (e.g. Leake, 1965). The hornblende in the granulites compares most closely with the kaersutitic amphiboles described from the brown hornblende mylonites, or hornblende gabbros, of St Paul's

Rocks by Melsom & others (1972), apart from having low K_2O content.

The mineral assemblage and stable co-existence of olivine and plagioclase indicate equilibration at high temperature and low pressure ($\leq$ 9 kb e.g. Green & Hibberson, 1970). Temperature estimates for co-existing pyroxenes based on the pyroxene solvus (Wells, 1977) indicate equilibration at $\sim$1040°C. Co-existing titaniferous magnetite and ferrian ilmenite compositions plot close to the magnetite - ulvöspinel solvus and suggest equilibration at approximately 680°C and $f_{O_2} = 10^{-20}$, according to the T-f_{O_2}-X curves of Buddington & Lindsley (1964). High equilibration temperatures are also suggested by the Fe-Mg partitioning between pyroxenes, and the TiO_2-rich nature of the amphibole.

Formation of the hornblende granulites is not readily explained; the high temperature-low pressure mineralogy is at variance with the high pressure-low temperature (blueschist) assemblage in the metamorphics immediately west of the Owen Stanley fault zone, and with the postulated choked subduction zone model for emplacement of the PUB (Davies, 1977; Davies & Smith, 1971). If formed at the base of the thrust, with heat produced by friction, the granulites might be expected to have a strongly foliated, even mylonitic, fabric rather than the observed equigranular texture. Alternatively, the high equilibration temperatures of the granulites might indicate that PUB was relatively hot at the time of emplacement.

CHAPTER 3

GEOCHEMISTRY

3-1. Analytical techniques

Chemical analyses of the samples studied are presented in Table 2-7. Analyses, except for FeO, Na_2O, H_2O and CO_2, were made by X-ray fluorescence spectrometry. Major elements were analysed on fused samples (Norrish & Hutton, 1969) and trace elements were determined on pressed powder pellets (Norrish & Chappell, 1977) with corrections made for non-linear backgrounds and inter-element interferences. Details of the analytical techniques are described in Appendix 1. Accurate determination of Rb and Sr at low levels was made following the method of Chappell & others (1969).

REE and trace elements Pb, Th, U, Hf, Cs, Ba, Zr and Nb were determined by spark source mass spectrometry following the improved technique of Taylor & Gorton (1977). Details of the method are given in Appendix 1. Precision and accuracy are described in detail by Taylor & Gorton (1977) and are estimated to be REE, Th, U, Hf, Ba ($\pm$ 5%), and Zr, Y, Nb ($\pm$ 10-15%). Agreement between XRF and spark source data generally lay within the analytical precision (Appendix 1).

$^{87}Sr/^{86}Sr$ ratios determined for two fresh gabbros by R.W. Page are presented in Appendix 1. Also presented in Appendix 1 are unpublished $^{87}Sr/^{86}Sr$ ratios previously determined by P.A. Arriens on samples submitted by H.L. Davies.

3-2. Major and trace element geochemistry of the PUB

Tectonites

The highly refractory mineralogy of the harzburgite tectonites is reflected in their bulk composition. The *mg*-numbers (100 Mg/Mg + ΣFe) of the bulk rocks are high ($\sim$ 90), close to the Mg-value of the constituent olivine and orthopyroxene. CaO and Al_2O_3 contents are very low. The harzburgites are extremely depleted in lithophile elements: Ti = 3-13 ppm,

TABLE 2-7. CHEMICAL ANALYSES OF PAPUAN ULTRAMAFIC BELT ROCKS

TECTONITE PERIDOTITES

Analysis	1	2	3	4	5	6
Sample	720	715	716	714	718	722
SiO_2	43.11	43.41	43.24	42.95	55.75	55.92
TiO_2	<0.002	<0.002	<0.002	<0.002	0.01	0.01
Al_2O_3	0.03	0.06	0.04	0.05	0.17	0.20
Fe_2O_3	1.65	1.76	1.63	1.80	2.02	1.49
FeO	5.14	5.07	5.23	5.53	5.95	6.32
MnO	0.11	0.11	0.12	0.12	0.18	0.20
MgO	48.29	48.24	48.36	47.48	34.84	33.82
CaO	0.04	0.03	0.03	0.04	0.24	0.66
Na_2O	0.007	0.006	0.006	0.006	0.008	0.007
K_2O	<0.005	<0.005	<0.005	<0.005	<0.005	<0.005
P_2O_5	<0.001	<0.001	<0.001	<0.001	0.001	<0.001
S	<0.01	<0.01	<0.01	<0.01	<0.01	<0.01
H_2O+	0.83	0.91	0.78	1.26	0.33	0.37
H_2O-	0.11	0.11	0.12	0.15	0.07	0.06
CO_2	0.22	0.29	0.05	0.04	0.24	0.19
rest	0.65	0.67	0.71	0.75	0.93	0.64
O=S						
Total	100.19	100.67	100.32	100.18	100.74	99.89
Mg #	92.9	92.8	92.8	92.2	88.9	88.7
Trace elements (ppm)						
Ba	<5	<5	<5	<5	<5	<5
Rb	<0.1	<0.1	<0.1	<0.1	<0.1	<0.1
Sr	<0.1	<0.1	<0.1	<0.1	<0.1	<0.1
Zr	<1	<1	<1	<1	<1	<1
Nb	<0.5	<0.5	0.5	<0.5	<0.5	<0.5
Y	<1	<1	<1	<1	<1	<1
Sc	3	3	3	4	11	11
V	8	9	8	9	22	27
Cr	1980	2150	2410	2680	5470	3660
Ni	2790	2760	2740	2740	935	710
Cu	<1	<1	<1	<1	<1	<1
Zn	42	42	42	44	48	46
Ti	3	6	5	13	44	47

Mg# = 100Mg/(Mg + ΣFe). Analyses 1-4 = harzburgite; 5-6 = enstatolite.

TABLE 2-7. CONTINUED

CUMULATES

Analysis	7	8	9	10	11	12	13	14	15
Sample	719	736	733	732	729	730	731	728	727
SiO_2	51.80	54.53	44.25	43.64	48.63	50.03	49.73	50.55	55.83
TiO_2	0.03	0.02	0.06	0.04	0.09	0.08	0.08	0.13	0.57
Al_2O_3	1.39	3.58	7.88	20.10	17.22	15.17	17.88	15.19	15.98
Fe_2O_3	0.78	2.45	2.44	1.62	1.03	1.20	1.52	1.40	3.10
FeO	3.63	5.90	8.24	3.84	3.19	4.18	3.83	4.54	5.87
MnO	0.14	0.20	0.21	0.09	0.09	0.14	0.13	0.14	0.13
MgO	23.09	28.00	25.11	15.11	10.82	13.65	11.30	11.70	4.76
CaO	17.58	5.00	8.14	11.57	17.40	14.55	15.09	15.32	9.55
Na_2O	0.11	0.08	0.35	0.83	0.68	0.50	0.64	0.90	3.01
K_2O	0.007	<0.005	0.010	0.02	0.02	0.005	0.005	0.008	0.13
P_2O_5	0.02	0.006	0.006	0.01	0.02	0.01	0.01	0.01	0.08
S	<0.01	<0.01	<0.01	0.01	0.01	0.01	0.01	0.01	0.10
H_2O+	0.58	0.18	2.99	2.87	0.64	0.48	0.28	0.36	0.81
H_2O-	0.07	0.14	0.23	0.21	0.04	0.06	0.05	0.06	0.06
CO_2	0.17	0.08	0.25	0.26	0.28	0.10	0.01	0.11	0.33
rest	0.80	0.48	0.23	0.22	0.23	0.14	0.10	0.12	0.13
									100.44
O=S									0.05
Total	100.20	100.65	100.39	100.43	100.39	100.29	100.67	100.55	100.39
Mg #	90.5	86.0	81.1	83.6	82.4	82.2	79.5	78.2	49.5
Trace elements (ppm)									
Ba	<5	<5	<5	<5	<5	<5(2.5)	<5	<5	5
Rb	<0.1	<0.1	0.2	0.2	0.2	<0.1(.04)	0.1	<0.1	1.2
Sr	5.0	9.8	32.5	75	71	92	136	90	170
Zr	<1	<1	1	<1	2	2	<1	<1	37
Nb	<0.5	0.5	<0.5	<0.5	<0.5	1	<0.5	<0.5	2
Y	1	<1	2	<1	3	2	2	3	13
Sc	48	35	27	11	39	42	38	46	35
V	95	70	61	29	98	89	79	119	233
Cr	4930	2810	740	895	1190	545	314	414	107
Ni	424	368	730	498	189	155	139	134	35
Cu	2	2	5	17	13	2	3	21	253
Zn	18	46	63	32	22	30	26	36	32
Ti	160	110	280	220	490	430	370	660	3420

Analysis 7 = olivine pyroxenite; 8 = lherzolite; 9 = plagioclase lherzolite; 10 = troctolite; 11 = olivine norite-gabbro; 12-14 = norite-gabbro; 15 = microgabbro.

TABLE 2-7. CONTINUED

BASALTS

Analysis	16	17	18	19	20	21	22	23
Sample	723	708	707	712	709	706	710B	710A
SiO_2	44.89	49.69	50.00	49.10	48.72	49.67	46.96	46.99
TiO_2	2.29	1.30	1.30	1.92	1.32	1.29	1.35	1.31
Al_2O_3	11.19	12.75	12.79	12.75	12.89	12.68	13.39	13.11
Fe_2O_3	3.71	3.27	3.55	4.01	4.64	4.47	4.75	4.72
FeO	9.23	11.09	10.64	10.65	10.54	10.42	10.78	10.87
MnO	0.20	0.21	0.21	0.23	0.23	0.21	0.24	0.24
MgO	13.97	7.81	6.80	6.66	6.63	6.48	6.58	6.54
CaO	12.00	9.98	9.84	9.37	10.46	10.30	10.96	11.21
Na_2O	1.26	1.58	2.03	1.84	1.85	1.73	2.56	2.64
K_2O	0.06	0.04	0.04	0.11	0.03	0.04	0.04	0.06
P_2O_5	0.12	0.12	0.13	0.17	0.12	0.11	0.12	0.12
S	0.02	0.09	0.06	0.05	0.07	0.07	0.08	0.09
H_2O+	1.07	2.75	2.64	2.72	2.37	2.24	2.43	2.21
H_2O-	0.10	0.16	0.16	0.19	0.17	0.14	0.14	0.13
CO_2	0.15	0.01	0.27	0.02	0.03	0.33	0.11	0.10
rest	0.33	0.17	0.18	0.17	0.18	0.17	0.17	0.18
	100.59	100.22	100.64	99.96	100.25	100.35	100.66	100.52
O=S	0.01	0.04	0.03	0.02	0.03	0.03	0.04	0.04
Total	100.58	100.18	100.61	99.94	100.22	100.32	100.62	100.48
Mg #	66.5	47.1	46.7	45.4	44.5	44.4	43.8	43.5
Trace elements (ppm)								
Ba	<5	<5	<5	5	<5	<5	<5	<5
Rb	1.2	0.3	0.4	1.8	0.5	0.5	0.3	0.5
Sr	202	47.5	61	95	59	52	70	74
Zr	43	68	67	107	68	64	71	67
Nb	7	2.5	1.5	7	1.5	1	2	1.5
Y	19	32	30	35	33	31	33	32
Sc	39	42	45	40	43	42	49	49
V	327	466	478	435	479	463	494	498
Cr	1010	116	127	97	136	134	120	134
Ni	461	75	93	57	77	73	76	77
Cu	76	121	189	146	131	127	71	110
Zn	98	146	137	140	141	151	134	128
Ti	13750	8000	7800	11500	8000	7750	8100	7850

Analysis 16 = hornblende granulite; 17-23 = basalts. A = pillow rim, B = core.

TABLE 2-7. CONTINUED

TONALITES

Analysis	24	25	26
Sample	704	705	703
SiO_2	60.69	62.08	63.18
TiO_2	0.27	0.33	0.26
Al_2O_3	16.12	15.05	14.47
Fe_2O_3	1.40	1.71	1.92
FeO	3.62	3.38	3.89
MnO	0.10	0.09	0.11
MgO	4.74	4.23	4.62
CaO	8.91	8.24	7.12
Na_2O	2.96	2.96	3.01
K_2O	0.22	0.20	0.55
P_2O_5	0.05	0.07	0.07
S	<0.01	0.01	0.04
H_2O+	1.04	1.14	1.39
H_2O-	0.11	0.10	0.10
CO_2	0.11	0.17	0.16
rest	0.09	0.10	0.10
			100.99
O=S			0.02
Total	100.43	99.86	100.97
Mg #	63.4	60.5	59.4
Trace elements (ppm)			
Ba	35	30	45
Rb	1.2	1.2	9.4
Sr	183	184	203
Zr	39	57	45
Nb	1.5	1.5	1
Y	9	10	6
Sc	28	26	25
V	115	138	114
Cr	176	188	183
Ni	39	44	29
Cu	10	4	23
Zn	39	32	41
Ti	1620	2000	1560

$Na_2O \sim 0.006\%$, $K_2O < 0.001\%$, and Rb and Sr <0.1 ppm. The PUB harzburgites are more depleted than harzburgites described from other ophiolites (e.g. Coleman, 1977; Menzies & Allen, 1974; Beccaluva & others, 1977; PART 1 Chapter 2) and decidedly more refractory than estimates of the upper mantle capable of yielding a basaltic melt (e.g. Ringwood, 1975, 1979; Maaloe & Aoki, 1977). Such extreme depletion in lithophile elements, together with the uniformly refractory mineralogy is consistent with a proposed origin as depleted upper mantle, residual after extraction of basaltic melt (see PART 1 Chapter 2 for discussion).

The enstatite-rich dykes are also of refractory composition but less magnesian, and contain measurably higher abundances of CaO, Al_2O_3, Ti, V and Sc. Ni contents are lower and Cr contents appreciably higher than the harzburgites, consistent with their pyroxene-rich character. The enstatolites could effectively be recast as orthopyroxene analyses.

Cumulate peridotite and gabbro

The major element chemistry and abundances of indicator trace elements Sc, Ni, Cr and Sr vary according to the modal abundance of the cumulus phases. The cumulate peridotites are characterized by high *mg*-numbers, and low CaO, Al_2O_3 and Sr contents, whereas the plagioclase-rich cumulate gabbros have very high Al_2O_3 and CaO contents, and markedly higher Sr contents. These rocks, as cumulates, are clearly displaced from the liquid trend. Trace elements show a systematic variation with degree of differentiation, as indicated by decreasing bulk rock *mg*-number: Ni and Cr contents decrease whereas Ti, Zr, V increase with decreasing rock *mg*-number (Fig. 2-5).

All the cumulates have very low levels of LIL (Ba, Rb, K, etc) and other incompatible elements (Ti, Zr, Nb, REE) consistent with the petrographic observations that the cumulates contain virtually no trapped intercumulus basaltic liquid. The levels of REE in the cumulates, as judged by their Y contents, are very low, commonly less than that of

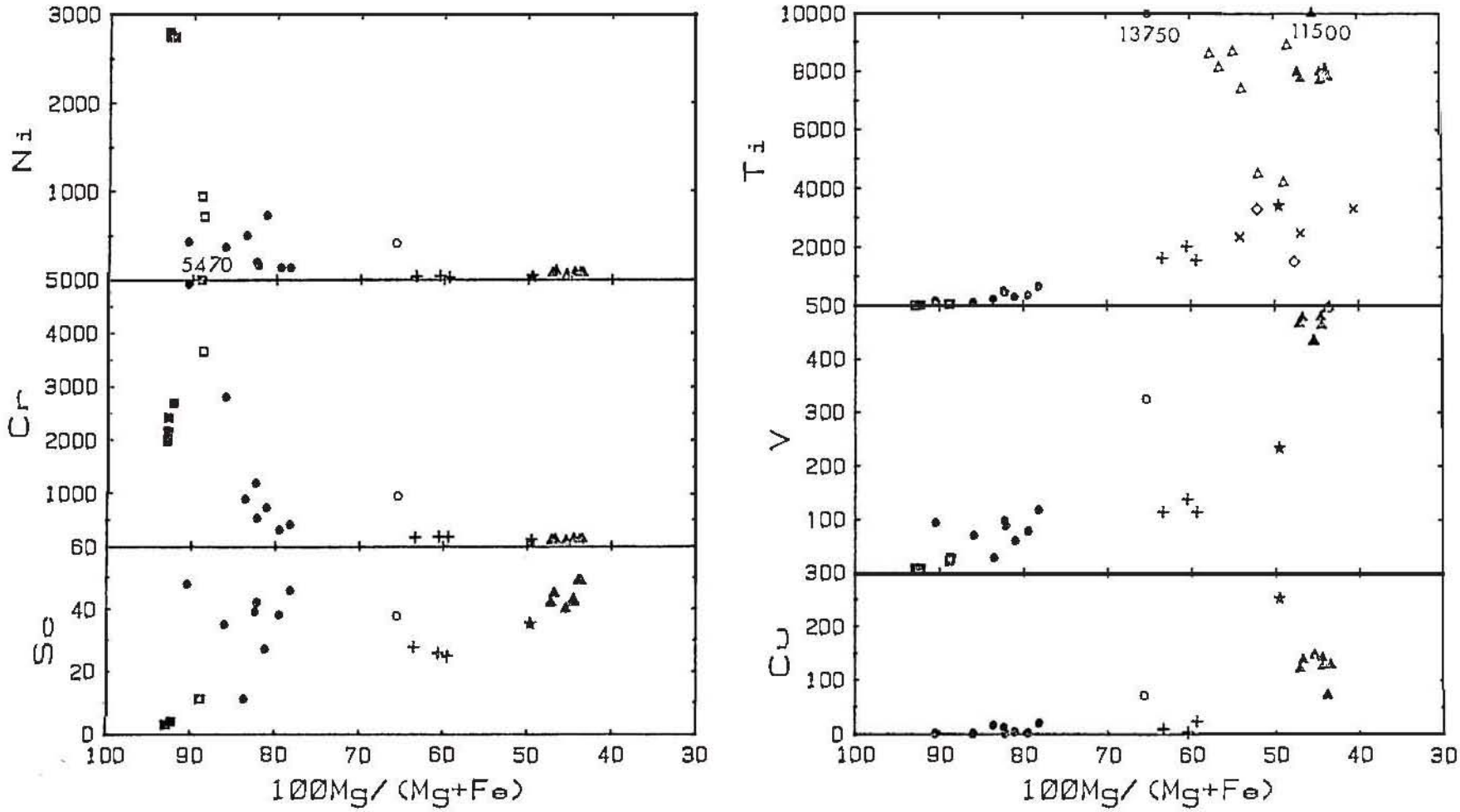

Fig. 2-5. Variation in trace elements with 100Mg/(Mg+ΣFe) for PUB rocks. Squares = tectonite peridotites, open squares = enstatolite dykes, solid circles = cumulate peridotites and gabbros, star = microgabbro, solid triangles = basalts (Table 2-7), open triangles = basalts (Davies, 1971), + = tonalites, x = tonalites (Davies, 1971), diamonds = felsic differentiates (Davies, 1971), open circles = hornblende granulite.

chondrites. REE have been determined for one of the gabbros, a bytownite-bronzite-augite cumulate (Table 2-8). The chondrite-normalized pattern, at 0.3 to 1 x chondrites is strongly depleted in LREE, and has a marked positive Eu anomaly (Fig. 2-6). Such patterns, dominated by calcic pyroxene, are typical of pyroxene-plagioclase cumulates from other ophiolites (e.g. Montigny & others, 1973; Allegre & others, 1973; Kay & Senechal, 1976; Suen & others, in press; PART 1 Chapter 4) and ocean floor gabbros (Masuda & Jibiki, 1973; Dostal & Muecke, 1978). The very low abundance of REE in these rocks provide clear evidence that they are cumulates from a mafic liquid, and that any intercumulus melt has been expelled.

Two new $^{87}Sr/^{86}Sr$ ratios have been determined for cumulate gabbros and are presented in Appendix 1 together with an earlier unpublished analysis by P.A. Arriens. The new values, 0.7036 and 0.7035, are in good agreement with values of 0.7036, 0.7039 and 0.7041 obtained by Allegre & others (in press) on additional PUB gabbro samples. These values are also in good agreement with the values obtained for the Marum ophiolite (PART 1 Chapter 4; Appendix 1), and lie in the range found for calc-alkaline intrusives in the Papua New Guinea highlands (Page, 1976) and for Quaternary island-arc volcanics in northern Papua New Guinea (Page & Johnson, 1974.) The new values determined are considered to be close to primary values since the gabbros analysed show no evidence of alteration or Rb enrichment. These values appear slighly higher than reported for fresh MORB (see later).

High-level microgabbro

The high-level microgabbro has a high silica content, and is relatively iron-rich ($mg \sim 49$), consistent with the petrologic interpretation that this rock is highly differentiated. The sample analysed here is chemically similar to the coarser grained rocks of intermediate composition (i.e. basic diorite and basic tonalite) analysed by Davies (1971), and is distinct from the mafic high-level gabbro analysed previously (Davies, 1971; Table 2, No. 144).

The microgabbro is strongly enriched in incompatible elements relative to the cumulates; TiO_2, K_2O, Ba, Rb, Sr, Zr and Y are markedly higher, and Ni and Cr considerably lower, than the cumulates. Ti, Zr and Y contents in the microgabbro are less than half that of the overlying basalts. REE abundances of the microgabbro are also markedly enriched relative to the cumulates (Table 2-8), and the chondrite-normalised REE pattern shows enrichment in LREE and a small positive Eu anomaly (Fig. 2-6). The positive Eu anomaly suggests that the microgabbro accumulated feldspar although the texture is not obviously cumulus. A possible explanation of this rock is that it crystallized near the roof of the magma chamber and contains small plagioclase crystals which floated in the highly differentiated magma. The enrichment in incompatible elements may reflect concentration in late-stage liquids, and, possibly, accumulation of intercumulus liquid dispelled from the cumulate pile lower in the magma chamber. Alternatively the microgabbro may be related to a LREE-enriched parent liquid similar to basalt 712 (see below).

Basalts

The basalts analysed here have very similar chemistry, and are characterized by high iron contents (14-15% total iron as FeO), relatively high Al_2O_3 contents and low *mg*-numbers $\sim$ 45. The high iron contents are considered to be a primary feature and not due to secondary iron sulphide since care was taken during sample preparation to exclude sulphide veins, and analysed sulphur contents are low (Table 2-7). Many of the basalts analysed by Davies (1971) have similarly high iron contents. Anhydrous silica contents range from 48 to 52%. The basalts range from olivine normative through to quartz normative-types but in view of the possibility of major element (especially SiO_2) redistribution during low temperature alteration normative classification may be unreliable. In general, the basalts analysed here are of similar composition to those analysed by Davies (1971) but more fractionated.

TABLE 2-8. RÈE ABUNDANCES IN SELECTED SAMPLES

Analysis No.	1	2	3	4	5	6
Sample No.	730	727	709	710a	712	703
La	-	3.49	2.18	2.18	7.09	3.34
Ce	0.23	8.50	7.16	7.17	19.43	8.97
Pr	0.045	1.15	1.18	1.19	2.84	1.06
Nd	0.27	5.24	6.87	6.97	14.59	4.74
Sm	0.12	1.42	2.44	2.26	4.24	1.01
Eu	0.07	0.59	0.90	0.82	1.55	0.34
Gd	0.20	1.64	3.96	3.66	5.68	1.05
Tb	0.04	0.30	0.77	0.68	0.98	0.17
Dy	0.29	2.04	5.20	4.67	6.59	0.99
Ho	0.075	0.48	1.31	1.19	1.53	0.21
Er	0.22	1.37	4.07	3.52	4.58	0.62
Tm	-	0.19	0.58	0.49	0.63	-
Yb	0.23	1.34	4.24	3.64	4.53	0.66
La_N/Sm_N	0.3 *	1.50	0.54	0.59	1.02	2.01
La_N/Yb_N	0.2 *	1.72	0.34	0.39	1.03	3.34
Cs	-	0.03	0.02	0.02	0.07	0.14
Pb	-	0.27	0.40	0.36	0.67	0.75
Th	-	0.13	0.23	0.15	0.59	0.47
U	-	0.05	0.12	0.19	0.23	0.17
Hf	-	0.82	2.10	1.65	2.96	1.05

1. Cumulate gabbro
2. High-level microgabbro
3. Basalt
4. Pillow basalt rim
5. Basalt
6. Tonalite

* Interpolated

K, Rb, Ba, Cs, and Sr contents are very low, and K/Rb, K/Ba, Na_2/K_20 ratios high, typical of mid-ocean ridge basalts (MORB). Rb/Sr ratios are very low (< 0.01), typical of MORB. Although these elements are known to be susceptible to low temperature alteration (e.g. Hart, 1969), consistency in both the abundances and abundance ratios of the PUB basalts as a whole, and between the chilled margin and interior of a single large pillow (Table 2-7; 710a and 710b), suggests that the abundances and abundance ratios of these elements in these particular samples at least have not changed significantly. Comparison of the PUB lavas with MORB is strengthened by the abundances and abundance ratios of elements known to be relatively insensitive to the effects of alteration (e.g. Cann, 1970; Pearce & Cann, 1973; Smith & Smith, 1976). TiO_2/P_2O_5, Ti/Zr and Ti/Y ratios for example, like most MORB, are close to chondritic abundances (Nesbitt & Sun, 1976). Except for sample 712, Zr/Nb ratios are high (30-60) typical of LIL-element depleted or 'normal' MORB (e.g. Erlank & Cable, 1976). Overall however, the abundances of TiO_2, Zr, Nb, Y and REE are comparatively low, and Ni and Cr contents high, for such evolved iron-rich basalts. For example, LREE-depleted MORB with high iron contents (*mg* = 40-50) described from Juan de Fuca Ridge (Kay & others, 1970), and DSDP legs 34 (Mazzullo & Bence, 1976) and 3-15 (Frey & others, 1974) all have markedly higher TiO_2, Zr, Hf, Y and Nb contents. High iron contents coupled with low Ti, Zr, Hf, Y, etc. and high Ni and Cr are a feature however of MgO-poor tholeiitic basalts associated with basalts of the komatiite suite in Archaean terrains. For example, the PUB basalts are very similar in terms of their comparatively low TiO_2, Zr, Y and high Ni and Cr contents (for rocks of such high iron content) with low MgO, iron-rich tholeiitic basalts and metabasalts described from a number of Archaean greenstone belts (e.g. Glikson, 1971, 1979; Hallberg, 1972; Sun & Nesbitt, 1977; Nisbett & others, 1977; Hawkesworth & O'Nions, 1977). Glikson (1971, 1979) and Nesbitt & Sun (1976) have both noted that

transition metals in Archaean.low-MgO tholeiitic basalts are generally some 20% more abundant than in MORB of comparable Mg-value.

REE data for three basalts are presented in Table 2-8, and the chondrite-normalized patterns plotted in Figure 2-6. Two of the basalts,709 and 710a, exhibit strong depletion in LREE, and have La_N/Sm_N ratios of 0.54 and 0.59, typical of LREE-depleted MORB. Both basalts have prominent negative Eu anomalies, suggesting extensive plagioclase fractionation. The similarity in Y, Zr, Nb, Rb and Ba contents among most of the other PUB basalts analysed suggest that REE patterns for these basalts will be similar to those of 709 and 710a. Although similar in terms of La_N/Sm_N ratios, the REE patterns of PUB basalts 709 and 710a differ from most depleted MORB in that both show depletion of middle REE relative to heavy REE (HREE). The PUB basalts have Gd_N/Yb_N ratios of 0.75 and 0.81 whereas most MORB have Gd_N/Yb_N ratios close to 1 (e.g. Sun & Nesbitt, 1978b; Kay & others, 1970; Schilling, 1971; and others). Exceptions are the highly LREE-depleted MORB from DSDP sites 3-14, 18 described by Frey & others (1974), which also show depletion of MREE relative to HREE and are commonly interpreted as being derived from a source previously depleted by extraction of a basaltic melt.

Basalt 712 differs from the other basalts sampled by virtue of its higher TiO_2, P_2O_5, Ba, Rb, Sr, Zr and Nb contents, and markedly lower Zr/Nb ratio. The REE abundances of this basalt are also unlike the others analysed; the chondrite-normalized pattern is flat at about 20 x chondrites, with no Eu anomaly (Fig. 2-6). In terms of its La/Sm ratio this basalt would be categorized as a Group II basalt (Bryan & others, 1976) or simply a 'chondritic' basalt (PART 1 Chapter 5).

The data obtained here when considered in conjunction with the variation in TiO_2 content among the basalts analysed previously (0.7-1.5%, Davies, 1971 and Fig. 2-5) suggest that the PUB lavas display considerable variation in the level of LREE and other incompatible

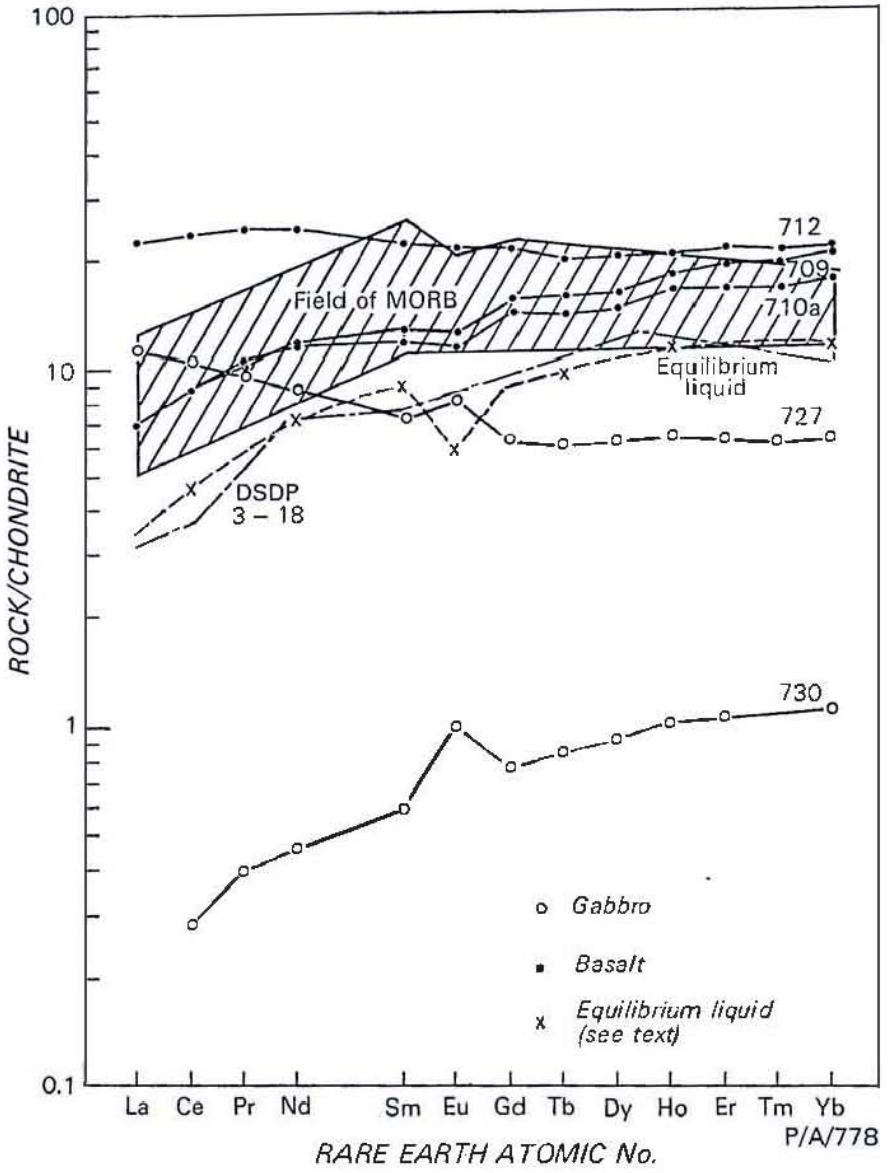

Fig. 2-6. Chondrite-normalized REE patterns for PUB rocks compared to field of MORB and DSDP leg 3-18-7-1 basalt (Frey & others, 1974). Equilibrium liquid refers to calculated liquid in equilibrium with gabbro 730 (see text).

elements. While part of this variation can be attributed to crystal fractionation processes and, possibly, some to element redistribution during low temperature alteration, it is suspected that detailed sampling of the basalt sequence may reveal important systematic variations.

Hornblende granulites

Chemical analysis of a hornblende granulite shows that it has low SiO_2, and is markedly enriched in TiO_2 compared to the PUB gabbros. Similarly, the granulite has appreciably higher levels of Na_2O, K_2O, P_2O_5 and Rb, Zr, Nb and Y than the PUB gabbros. Zr/Nb and K/Rb are markedly lower (6 and 415 respectively) than the PUB gabbros, and are more in line with those of alkalic rocks; alkali contents in the granulite however are markedly lower than those of alkaline rocks. The above chemical characteristics, together with the lack of correlation with the trends displayed by the PUB gabbros (Fig. 2-5), indicate that the hornblende granulites are not hydrated PUB gabbros recrystallized under granulite conditions, and argue that the granulites are genetically unrelated to the PUB gabbros.

3-3. Relationship between the ophiolite layers

Davies (1971) proposed that the gabbro and basalt units of the PUB were genetically related by crystal fractionation processes, and that the layered peridotites and gabbros accumulated from a basaltic magma on the underlying tectonite peridotite. Geochemical studies from other ophiolites suggest that all units exposed in some ophiolites may be related viz. the basal tectonite represents the residue from partial melting processes which generated basaltic magmas which underwent crystal fractionation in a subjacent magma chamber(s) and yielded mafic (peridotitic to gabbroic) cumulates (e.g. Montigny & others, 1973; Allegre & others, 1973; Menzies & Allen, 1973; Kay & Senechal, 1976).

A genetic link between the cumulates and the overlying lavas of

the PUB is suggested by;

i) similar $^{87}Sr/^{86}Sr$ ratios. The values obtained for the cumulate gabbros compare with values of 0.7044 (basalt), 0.7041 (dolerite), and 0.7046 (gabbro) obtained previously (Appendix 1).

ii) similar TiO_2/P_2O_5 and K/Rb ratios of lavas and gabbros (Fig. 2-7),

iii) the similarity in REE patterns between the cumulate gabbro and the LREE-depleted basalts with Eu anomalies. The REE abundance of the magma in equilibrium with cumulate gabbro 730 have been calculated assuming total equilibrium from the REE abundances given in Table 2-8, the modal abundance of the phases in the gabbro (determined by major element mixing program), and published REE partition coefficients (Appendix 1). Errors and assumptions in this approach are outlined in PART 1 Chapter 4.

This approach seems justified for the PUB rocks since the extremely low abundances of LIL elements in the cumulates strongly suggest a close approach to total equilibrium, and that any interstitial material has been expelled. The calculated equilibrium melt is strongly depleted in LREE (Ce_N/Sm_N = 0.5), and has a similar profile (Fig. 2-6) to the gabbro, apart from a marked negative Eu anomaly, but has higher absolute abundances of REE (LREE = 5 x, HREE = 11 x chondrites). The calculated equilibrium melt has a similar REE profile to basalts 709 and 710a (although abundances are higher in the basalts), and closely resembles the highly LREE-depleted DSDP 3-18 basalt (Frey & others, 1974; Fig. 2-6). Since gabbro 730 is strongly differentiated relative to the more magnesian peridotites and gabbros, the level of REE in the parent magma must have been significantly (at least 20%, probably more) lower than that in the melt which equilibrated with the gabbro. The REE pattern of the primary magma(s) can be inferred to have been similar to, or slightly more depleted in LREE than the calculated equilibrium melt since, of the accumulating phases (olivine, orthopyroxene, clinopyroxene, plagioclase), only clinopyroxene will effectively fractionate the REE (plagioclase crystallization will slightly decrease the La/Sm ratio

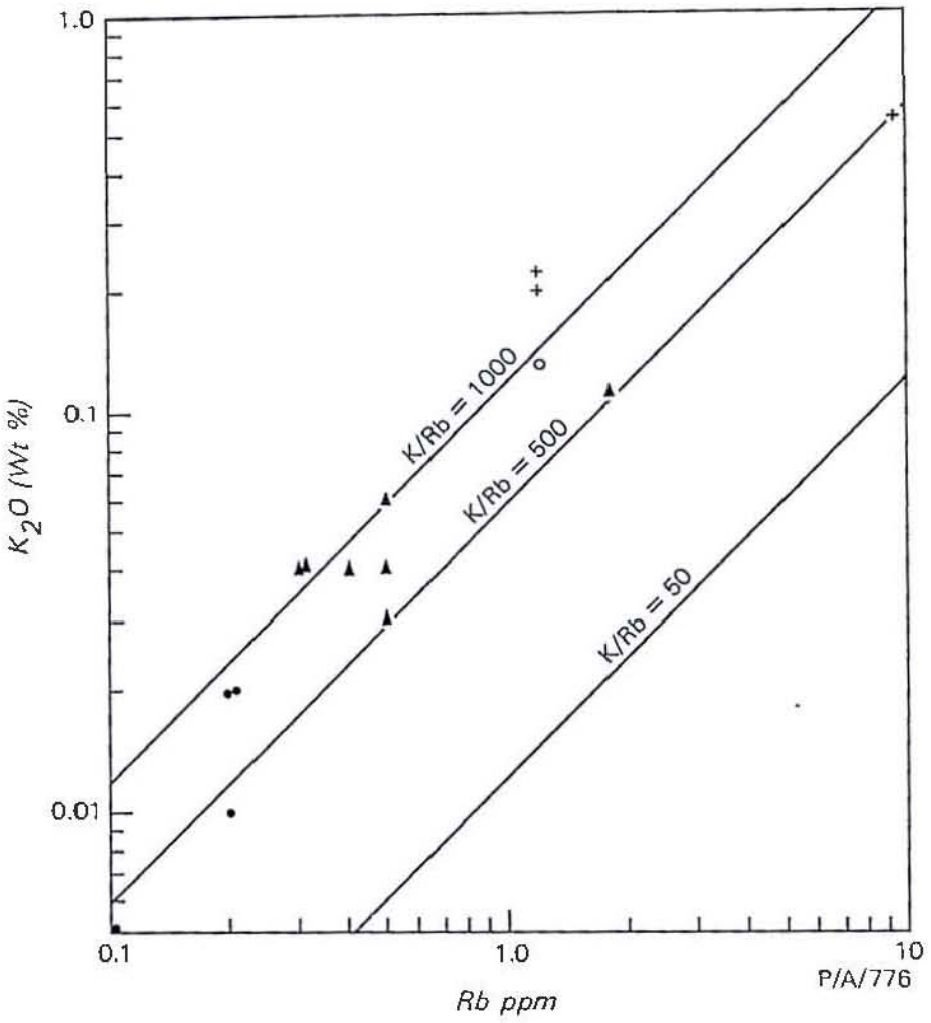

Fig. 2-7. Log K_2O (%) versus Rb (ppm) diagram for PUB cumulate gabbros (closed circles), microgabbro (open circle) and basalts (triangles), crosses = tonalites.

but this effect will be nullified by the greater reverse effect of clinopyroxene). The level of REE in the primary parent magma(s) inferred from the cumulates (HREE ∿ 7-9 x chondrites or less) is therefore compatible with that inferred from the basalts (see 3-4), i.e. less than MORB.

iv) the correlation between Ti and V, as suggested by Montigny & others (1973), since the partition coefficients for Ti and V in olivine, pyroxene and plagioclase crystallizing at high temperature from basaltic magma are less than unity and approximately similar (e.g. Duke, 1976). The good correlation shown in Figure 2-8 between all the members of the PUB ($r = 0.97$) suggests that tectonites may also be genetically related (by partial melting processes) to the gabbros and basalts. Gabbros showing relatively poor correlation have either very large or very small proportions of clinopyroxene. The tonalites show poor correlation.

Plots of log Ni versus log Ti, V also show clear disinction of the tonalites from the members of the PUB. Data for the cumulate gabbros and basalts define a curve which is consistent with a cumulate-liquid relationship. The microgabbro (and to a lesser extent basalt 712) does not fall on this trend but is displaced to higher Ti contents. Data for the harzburgites are inconclusive but not inconsistent with a genetic relationship with the cumulates and basalts.

3-4. Chemical affinities of the PUB

The PUB gabbros and basalts most closely compare with MORB, particularly in regard to their low K, Ba, Rb, Sr and Cs contents. The abundances of TiO_2, Zr, Nb, Hf and HREE are comparatively low for such highly differentiated rocks, and might suggest affinities with island-arc or marginal basin basalts (cf. Gill, 1976), although in terms of Ti-Zr, Ti-Zr-Y etc. (Pearce & Cann, 1973) and K/Rb, K/Ba, etc. (Hart, 1976) discrimination diagrams, the PUB basalts would be classified as MORB (Fig. 2-9). However, in view of the compositional overlap exhibited by basaltic rocks from young island-arcs and marginal basins (e.g. Hawkins, 1976, 1977;

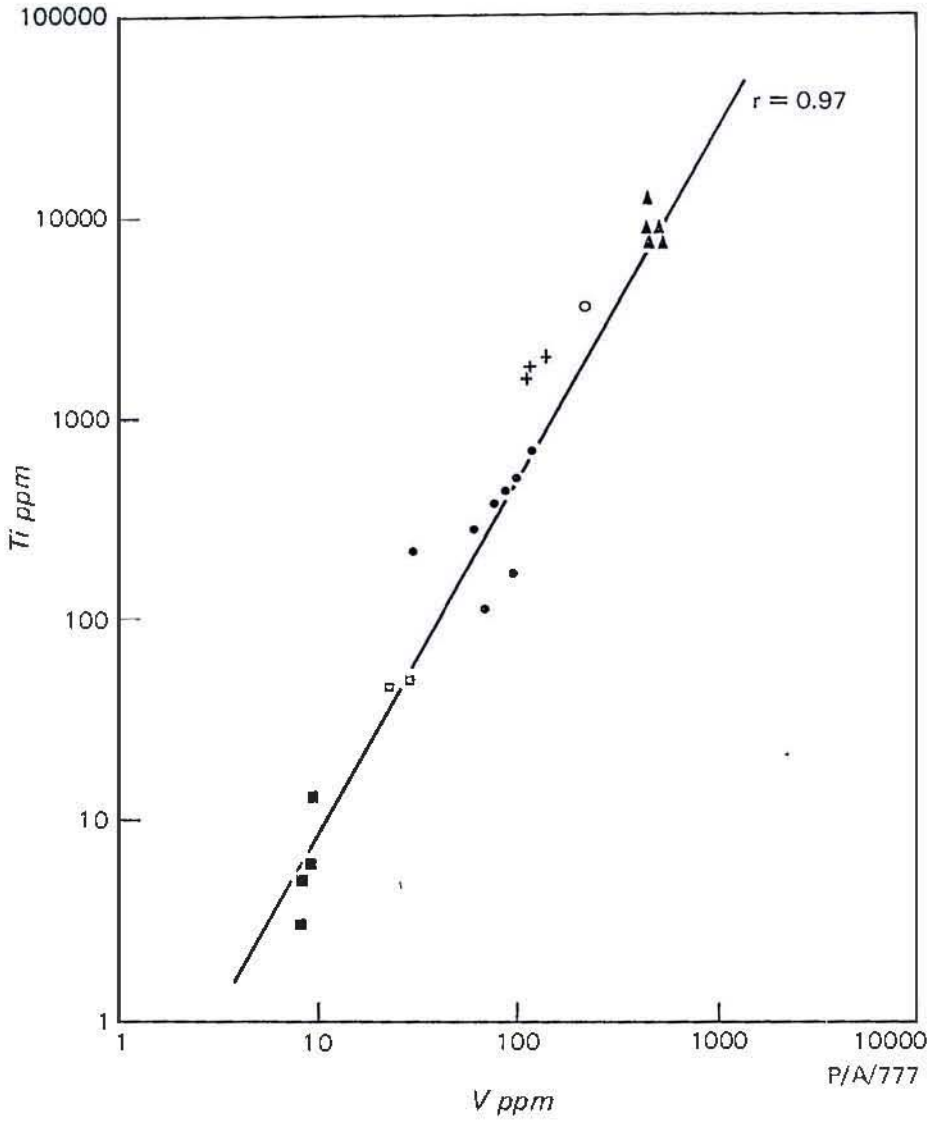

Fig. 2-8. Log Ti-versus log V diagram for PUB rocks. Solid squares = harzburgites, open squares = enstatolite dykes, solid circles = cumulate peridotite and gabbros, open circle = microgabbro, crosses = tonalites, triangles = basalts.

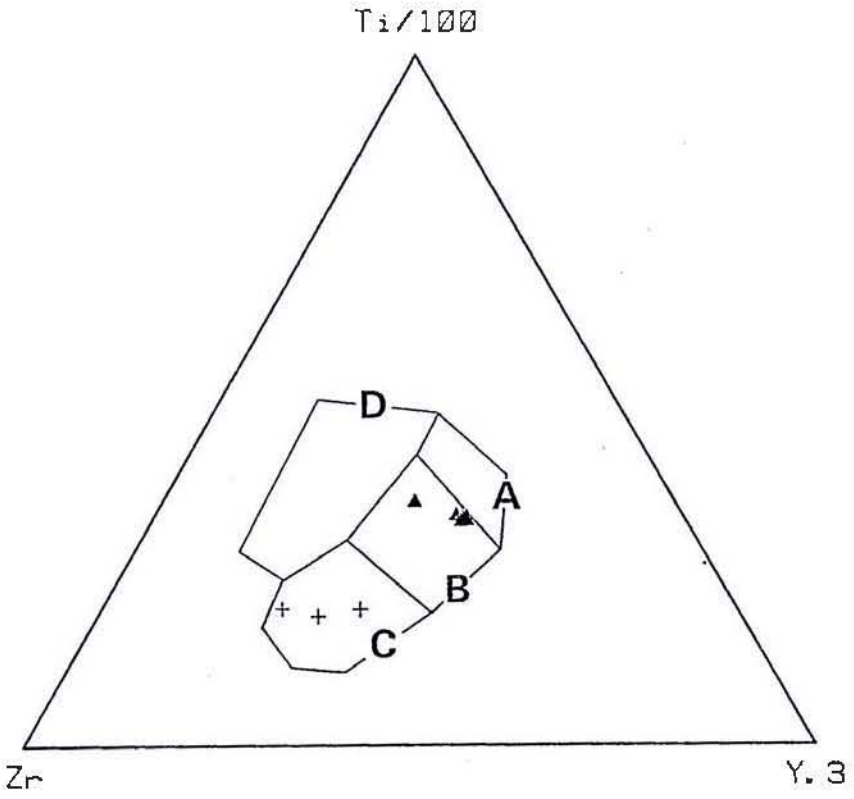

Fig. 2-9. Pearce & Cann (1973) Ti-Zr-Y discriminant diagram showing PUB basalts (triangle) and Eocene tonalites (crosses). Ocean floor basalts plot in field B, island-arc basalts in fields A and B, calc-alkali basalts in B and C, and within-plate basalts in D.

Gill, 1976; Ewart & others, 1977; Tarney & others, 1977), use of rigid classifications based on abundances of elements which primarily reflect mantle heterogeneity may be unreliable.

Magmas parental to the cumulate sequence must have been appreciably more magnesian than represented in the overlying lavas, and, correspondingly, contained appreciably lower levels of incompatible elements. Since the lowermost cumulate rocks contain cumulus olivine $Mg_{90.5}$ with $\sim$ 0.3% NiO (England & Davies, 1973) the parent magma can be inferred to have had a $100Mg/(Mg + Fe^{2+})$ ratio $\sim$ 74 assuming the applicability of the experimentally determined olivine-liquid partition coefficient of Roeder & Emslie (1970), corresponding to about 12-15% MgO. Assuming partition coefficients for Ni between olivine and basaltic melt of this composition at high temperatures (say, 1250-1400^{o}C) of 7.5-10 (Hart & Davis, 1978) or the lower values of 7-5 (Arndt, 1977b), the parent magma contained at least 300, and possibly as much as 500 ppm Ni. Derivation of the ferrobasalts (*mg* $\sim$ 45) containing $\sim$ 75 ppm Ni from such a highly magnesian parent magma by fractional crystallization requires at least 20%, and probably upwards of 40% crystallization. On this basis it seems reasonable to infer that the parent magmas contained $\leq$ 0.8% TiO_2, $\leq$ 50 ppm Zr and $\leq$ 20 ppm Y (i.e. HREE 10 x chondrites). From the REE content of the calculated equilibrium liquid for gabbro 730 it is suggested that the primary parent magma may have had a REE level of 7-9 chondrites. Relatively magnesian basalts with these trace element characteristics are not restricted to any particular tectonic setting, and occur at mid-ocean ridges (e.g. Frey & others,1974; Bryan & others, 1976; Blanchard & others, 1976), marginal basins (e.g. Gill, 1976; Hawkins, 1976; Hawkesworth & others, 1977; Saunders & Tarney, 1979), and island-arcs (e.g. Gill, 1976; Ewart & others, 1977). Low abundances of Ti, REE, Zr, Nb and Hf are particularly characteristic of the island-arc tholeiite suite (Jakeš & Gill, 1970; Gill, 1976; Ewart & others, 1977). However, the comparatively

high Ni and Cr contents of the PUB basalts set them aside from island-arc tholeiites. REE abundances in Archaean basalts are also commonly lower than MORB but are not as depleted in LREE and other LIL elements (e.g. Nesbitt & Sun, 1976; Sun & Nesbitt, 1978b; Jahn & others, 1974; Hawkesworth & O'Nions, 1977). It is concluded therefore that the primary parent magma was highly magnesian, and strongly depleted in LREE and other incompatible elements, similar to the highly depleted basalts at DSDP site 3-14, 18, but the level of REE was appreciably less than MORB sampled to date.

The relatively high $^{87}Sr/^{86}Sr$ ratios of the PUB rocks may be considered evidence against a mid-ocean ridge origin since most fresh MORB have initial ratios $\leq$ 0.7030. Exceptions however are the LIL element-enriched basalts of the Mid-Atlantic Ridge near 35°N, 45°N and the Azores (White & Schilling, 1978) which have higher values. Basalts in these areas and other regions of the ocean floor in the vicinity of oceanic islands have higher abundances of LIL elements, lower abundance ratios of these elements (K/Rb, K/Ba, etc.) and are enriched in LREE compared to typical depleted MORB with lower $^{87}Sr/^{86}Sr$ ratios. The PUB values are more in line with those reported from marginal basins and island-arcs (e.g. Gill, 1976; Meijer, 1976; Tarney & others, 1977; Ewart & others, 1977; Hawkesworth & others, 1977; Weaver & others, 1979). Similar $^{87}Sr/^{86}Sr$ ratios have been reported from the Troodos ophiolite (Peterman & others, 1971; Kay & Senechal, 1976; Spooner & others, 1977), and it is now established that these comparatively high values are a primary feature of gabbros in a number of ophiolites (cf. Allegre & others, in press). Spooner & others (1977) argued that since the Troodos values overlap the higher values of fresh MORB they were consistent with an oceanic crustal origin. Trace element abundances in the Upper Pillow Lavas of the Troodos are significantly different to most MORB (Smewing & others, 1975; Smewing & Potts, 1976; Simonian & Gass, 1978) however, and the origin of the Troodos ophiolite remains a matter of contention (e.g. Kay & Senechal, 1976).

It is therefore not possible, on the basis of the petrologic and geochemical information available at present, to specify a particular tectonic setting for the origin of the PUB. Evidence from the cumulate rocks points to a magnesian olivine-poor tholeiite parent magma bearing similarities with both the mafic basalts of the Upper Pillow Lavas of the Troodos ophiolite and with basaltic komatiites or high-Mg basalts found in Archaean greenstone belts. Trace element data from the overlying basalts compare most closely with highly depleted MORB (such as the DSDP leg 3-18 basalts) but a marginal basin origin cannot be ruled out. The trace element data obtained here and the variation in TiO_2 contents exhibited by the basalts analysed previously (Davies, 1971) indicate that the PUB basalts vary in the levels of incompatible elements,ranging from 'transitional' or 'chondritic' types to highly LREE-depleted basalts. Such variations might reflect progressive depletion of the mantle source with time, as has been suggested for the Troodos lavas (Smewing & Potts, 1976). Detailed sampling of the PUB lavas is needed to establish the range of compositions present, and to identify more magnesian compositions which would allow quantitative testing of fractionation models relating basalt and gabbro layers.

3-5. Tonalites

The tonalites are characterized by high Al_2O_3, and low FeO^t, MgO, TiO_2 and alkali contents; K_2O is conspicuously low for rocks of this silica content. In terms of CaO and $Na_2O + K_2O$ versus silica variation the tonalites are of tholeiitic affinities, and equate with the high-alumina tonalites of Barker & Arth (1976). A feature of the tonalites is their low K_2O, Ba, Rb, Sr, Zr, Nb and Y contents (Table 2-7), and high Na_2O/K_2O, K/Rb etc. ratios, which are in line with those of MORB and island-arc tholeiites. The comparatively high Ni and Cr contents together with the low Rb, Ba and Sr contents rule out an origin by anatexis of sialic crust.

REE abundances determined for sample 703 (Table 2-8) are low, and the chondrite-normalized pattern is fractionated and strongly depleted in HREE at ∿ 3 x chondrites (Fig. 2-10). Low Y values for the other samples indicate similarly low abundances of HREE. The REE pattern and low abundances of Zr, Nb and TiO_2 contrast markedly with felsic rocks found in other ophiolites (Coleman & Peterman, 1975; Kay and Senechal, 1976; Saunders & others, 1979) which are generally accepted as having formed as late-stage differentiates of basaltic magma. Additional evidence against a genetic link between the PUB and the Eocene tonalites is their markedly different TiO_2/P_2O_5 ratios (Fig. 2-11). The more mafic intermediate rocks, basic tonalite and diorite, inferred by Davies (1971) to be differentiates of the PUB, show good correlation with the PUB gabbros and basalts consistent with this interpretation whereas the tonalites (∿ 60% SiO_2) form a separate trend.

Rocks of quartz diorite composition with strongly fractionated REE, and, in particular, near-chondritic HREE abundances similar to the Eocene Papuan tonalites, are commonly interpreted as resulting from either partial melting of a basaltic parent composition leaving residual garnet or hornblende (e.g. Arth & Hanson, 1975; Barker & Arth, 1976), or from fractional crystallization of hornblende (e.g. Arth & others, 1978). An origin for the Papuan tonalites by partial melting of eclogite, or of amphibolite of sub-alkaline basalt or gabbro composition, to leave residual garnet or hornblende is supported by the low total REE, the low abudances of K, Rb, Ba, etc. and MORB-like K/Rb ratios (cf. Arth & Hanson, 1972). Compared to I-type granitoids of tonalitic composition inferred to be the partial melts of mafic crust (e.g. Griffin & others, 1978) the Papuan tonalites are extremely impoverished in LIL-elements, implying a source with very low abundances of these elements.

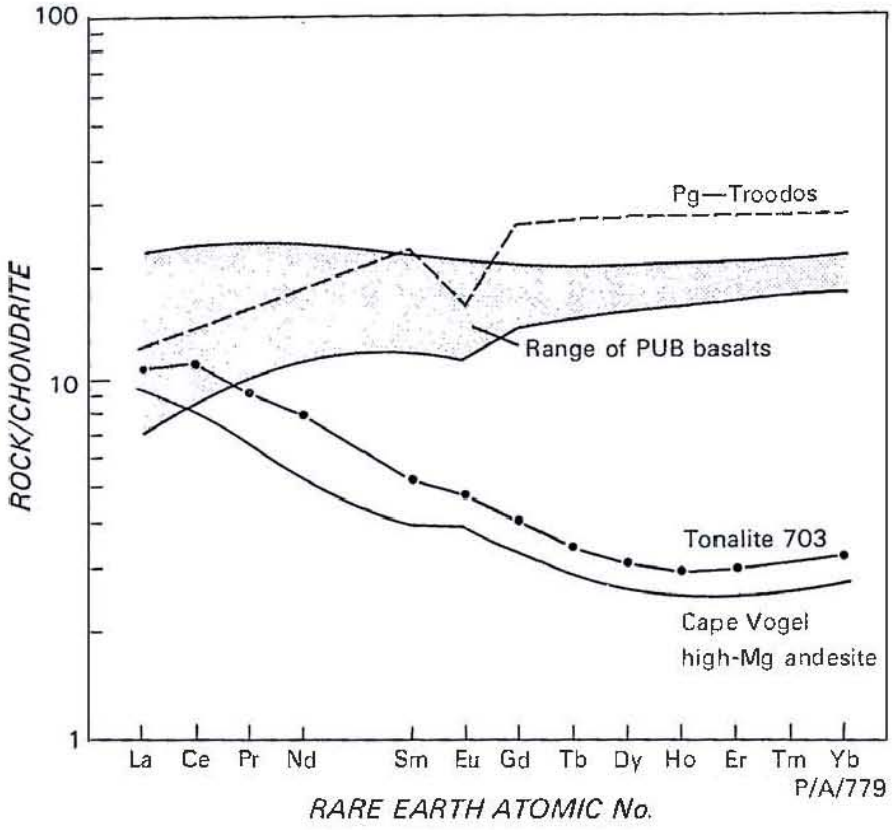

Fig. 2-10. Chondrite-normalized REE pattern for tonalite 703 compared to range shown by analysed PUB basalts, Troodos plagiogranite (Pg, Kay & Senechal, 1976), and Cape Vogel high-Mg andesite (Sun & Nesbitt, 1978). Note similarity in REE pattern of tonalite with the Cape Vogel rock and the marked difference to the PUB basalts.

Although the geochemical data presented here preclude a genetic relationship with the PUB, an origin by crystal fractionation from an alternative mafic parent is possible. Davies (1977) suggested that the tonalites may be co-magmatic with the Eocene andesites and dacites overlying the basalt layer at the northern end of the PUB. The available geochemical data suggest that the tonalites, and possibly the Eocene andesites and dacites, might be related to the pre-Miocene (?Eocene-Oligocene) tholeiitic basalts and andesites of the Cape Vogel region (Dabi Volcanics), many of which also have very low K_2O and TiO_2 abundances (Dallwitz, 1968; Smith & Davies, 1976). The Dabi Volcanics include the highly magnesian clino-enstatite-bearing andesites (Dallwitz & others, 1966) which, on the basis of the limited data of Sun & Nesbitt (1978a), have very low abundances of Ti, Y, Zr, etc. and similar chondrite-normalized REE patterns (but lower absolute levels) to the Papuan tonalites (Fig. 2-10). A genetic relationship between the Cape Vogel high-Mg andesites and the Eocene tonalites is suggested by the similar trends exhibited on the TiO_2-P_2O_5 variation diagram (Fig. 2-11) and the (Mg/(Mg + ΣFe) versus TiO_2 diagram (Fig. 2-12). The data for the clino-enstatite-bearing lavas are scattered due to the accumulative nature of many of the rocks (Dallwitz, 1968), but it would appear that the tonalites might be derived from a parent high-Mg andesite, *mg* ∿ 75 containing ∿ 0.2% TiO_2. Clearly more data, especially trace element data which are completely lacking, are needed for the Dabi Volcanics and the Eocene volcanics at the northern end of the PUB to enable quantitative testing of the fractional crystallization model for the PUB tonalites.

Discussion

Sun & Nesbitt (1978a) suggested that Ti-poor, high-Mg andesites similar to the Cape Vogel lavas are parental to ophiolite sequences characterized by abundant cumulus orthopyroxene, and that such lavas result from hydrous melting of depleted mantle close to a subduction zone.

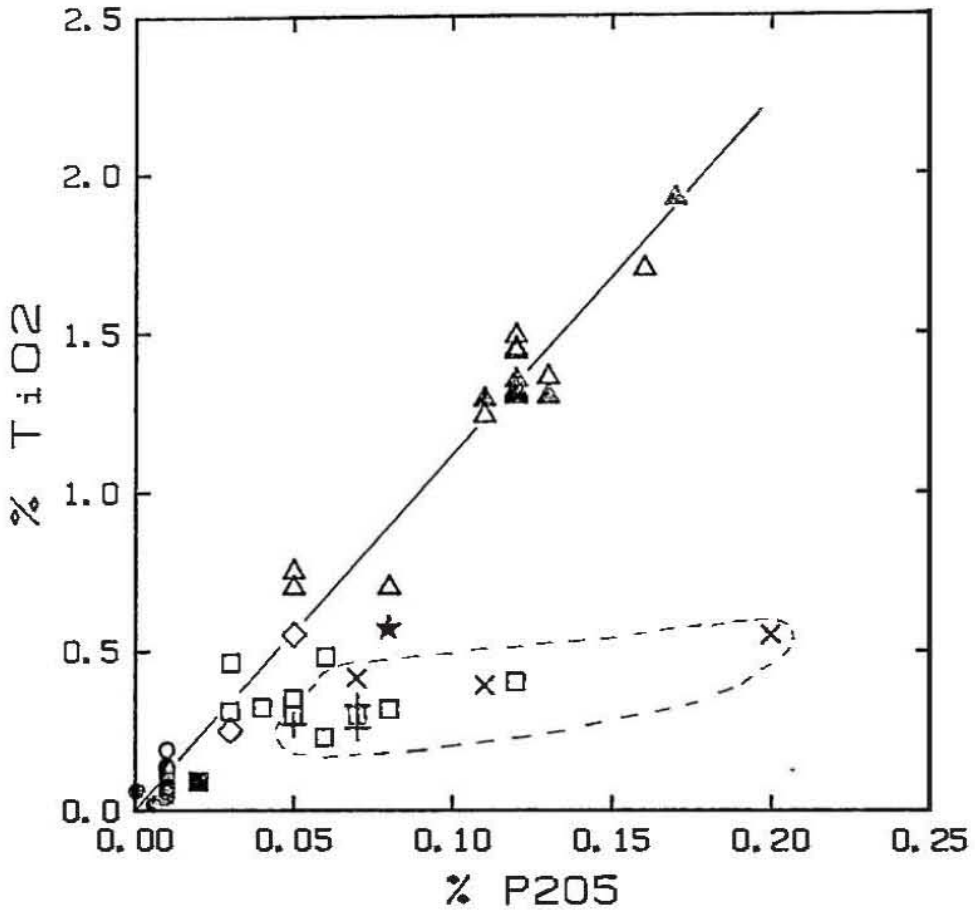

Fig. 2-11. TiO_2 versus P_2O_5 diagram for PUB rocks, Papuan tonalites and Cape Vogel andesites. PUB: Solid circles = gabbros, open circles = gabbros (Davies, 1971), star = microgabbro, solid triangles = basalts, open triangles = basalts (Davies, 1971), diamonds = felsic differentiates (Davies, 1971). Tonalites: + = this study, X = Davies (1971). Cape Vogel magnesian andesites = squares (Dallwitz, 1968). Note correlation among PUB rocks (chondritic ratio) and among tonalites and andesites (lower TiO_2/P_2O_5 ratio).

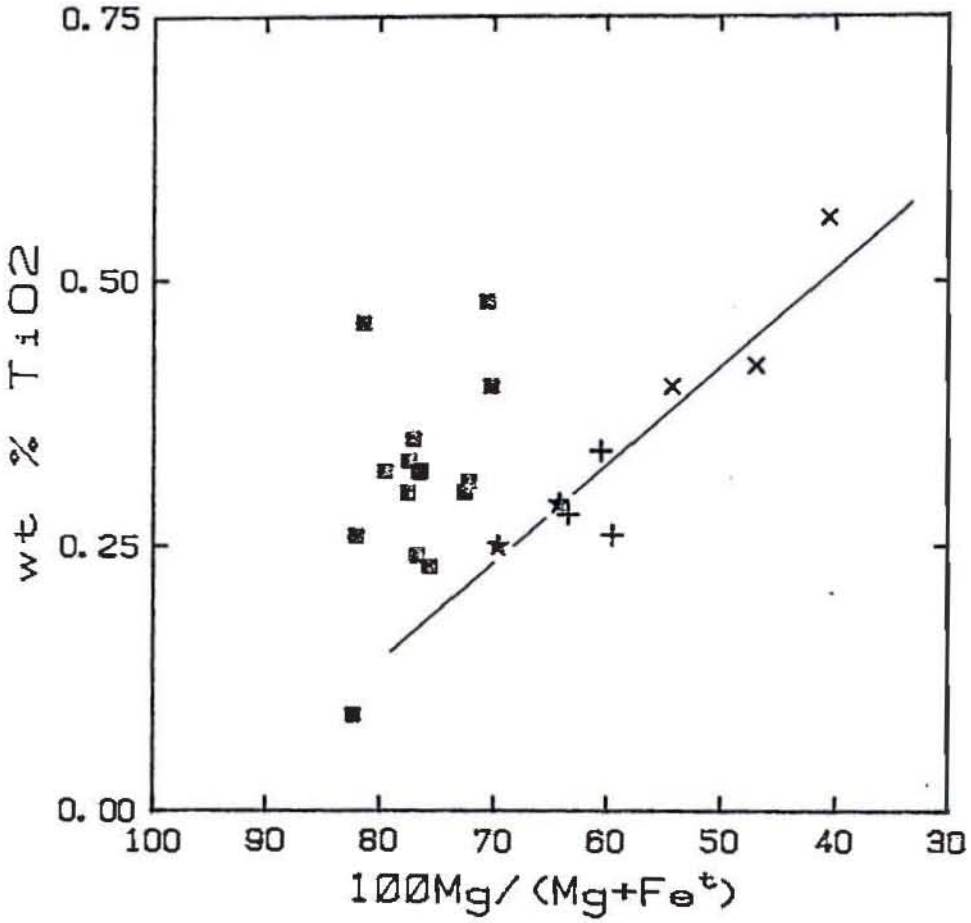

Fig. 2-12. Variation of TiO_2 with 100Mg/(Mg + ΣFe) of Papuan tonalites (crosses) and Cape Vogel high magnesian andesites (squares and stars). + = Table 2-7, X = Davies (1971), squares = Dallwitz (1968), stars = low Ti magnesian Dabi Volcanics (Smith & Davies, 1976).

The geochemical data presented here do not favour a genetic relationship between the PUB and high-Mg andesites similar to those of Cape Vogel. The petrology and geochemistry of the PUB cumulates and basalts argue for a Ti-poor, olivine-poor tholeiite parent magma strongly depleted in LREE and other incompatible elements. The absence of primary hydrous phases in the PUB rocks (except for highly fractionated differentiates) implies a volatile-poor parent magma. This parent magma is considered to result from large degree of partial melting of depleted mantle peridotite at shallow depth under anhydrous conditions (see PART 3). It is proposed that the Ti-poor tholeiitic andesites of the Dabi Volcanics, the andesites and dacites at the northern end of the PUB and the Eocene tonalites are related by crystal fractionation, and represent the early stages of the island-arc magmatism erupted close to a subduction zone (Chapter 4) immediately prior to emplacement of the PUB. The primary high-Mg andesite magmas are considered to result from water-saturated melting of refractory mantle peridotite (Green, 1973, 1976a; Sun & Nesbitt, 1978a) due to dehydration of the underlying downgoing lithospheric slab, and that these hydrous magmas subsequently underwent extensive fractional crystallization of olivine and pyroxene at shallow depths.

CHAPTER 4

ORIGIN OF THE PAPUAN ULTRAMAFIC BELT

The petrology and geochemistry of the PUB do not equivocally define the tectonic environment of formation of the ophiolite (i.e. marginal basin or mid-ocean ridge) and it is necessary to examine the regional geology to establish the tectonic history of southeast Papua.

4-1. Previous models

Davies (1977) and Davies & Smith (1971) proposed that the PUB represents a segment of Jurassic-Cretaceous oceanic crust and mantle of the Pacific plate which was emplaced as a result of attempted subduction of the thick welt of low density Cretaceous sediments at the northeastern margin of the Australian continent in a northeasterly-dipping subduction zone. Davies (1977) gave the date of emplacement of the ophiolite, and deformation and metamorphism of the Cretaceous-Eocene sediments of southeast Papua as early to mid-Eocene, corresponding to the timing of the opening of the Coral Sea. Connelly (1979) argued, on the basis of improved geophysical models resulting from a hypothetical reconstruction of the alignment of the ophiolite, that emplacement occurred even earlier, in the Palaeocene. These interpretations do not accord with the evidence from the regional geology which indicates continuous sedimentation from late Cretaceous to middle Eocene in southeast Papua, and implies that metamorphism and deformation occurred in the late Eocene or Oligocene (Pieters, 1978; Brown, 1977; Brown & others, in press). Further evidence to support a late Eocene or early Oligocene age of emplacement is the distribution of the Eocene tonalitic stocks: the restriction of these bodies* and the Eocene andesite-dacite lavas to the PUB suggests that this magmatic activity

---

* The Eocene intrusives are compositionally and spatially distinct from younger Miocene intrusives (Smith & Davies, 1976).

occurred prior to emplacement of the PUB. This implies emplacement of the PUB not earlier than 50 m.y. b.p.

Karig (1972) proposed a more complex interpretation of the emplacement (and origin) of the Papuan Ultramafic Belt, involving rifting of the Solomon Sea and collision between a reversed arc (represented by the PUB, the Solomon and Woodlark basins, and the islands of the Trobriand group and the Louisiade Archipelago, and continental crust of the south-east Papuan mainland. In this model the PUB would represent frontal-arc basement formed by marginal basin extension associated with an earlier period of subduction and arc magmatism.

Intimately involved in formation of the PUB, its subsequent emplacement and the tectonic evolution of the southeast Papuan region is the origin of the Solomon Sea, since Finlayson & others (1977) have shown that the layers of the PUB are continuous northeastwards with the crust and upper mantle layers of the western Solomon Sea. In the model presented by Davies & Smith (1971) and Davies (1977) the Solomon Sea (and the PUB) represents a segment of trapped Cretaceous ocean floor of the Pacific plate. In Karig's (1972) more complex model the Solomon Sea is relatively young ocean basin, as earlier advocated by Carey (1958), and the PUB is crust and mantle of an older marginal basin.

4-2. Evidence from the Solomon Sea region

Karig (1972) characterized the Solomon Sea as an inactive marginal sea with high heat flow, and suggested that it formed during the mid-Tertiary by back-arc extension as the then-combined Woodlark and Pocklington arc moved south. Recent seismic surveys has shown that the central Solomon Sea is characterized by rough topography (Finlayson & others, 1976), which, together with the high heat flow values (2-3 H.F.U., Macdonald & others, 1973) and the relatively thin crust at the centre of the basin supports a recent origin.

Finlayson & others.(1977) have shown from detailed modelling of seismic, gravity and magnetic data that the crust of the western portion of the Solomon Sea is anomalously thick, ranging from 20-24 km off the Morobe coast and beneath the Trobriand Platform to a maximum of about 27 km at the northeastern edge of the Trobriand platform, from where it decreases gradually to approximately 13 km beneath the central Solomon Sea. Finlayson & others (1977) argued that these thicknesses were excessive for typical oceanic crust, and suggested that a marginal basin origin for the PUB and west Solomon Sea was more likely. They also drew attention to the positive gravity and negative magnetic anomalies associated with the northern side of the Trobriand Platform, and speculated that these features were caused by an ophiolite complex of similar age and extent to the PUB. On the other hand, Davies (1977) argued that the seaward thickening of crust from 'normal oceanic-type' thicknesses exposed in the PUB were the result of volcanism and related plutonism associated with a postulated early Tertiary arc, and subsequent episodes of magmatism during the late Cainozoic. Davies (1977) further argued that the gravity high at the northern edge of the Trobriand Platform could be attributed to bathymetry, and that the corrected free-air anomaly was more diffuse and more closely resembed that found over the basement volcanics of New Britain than that over the PUB.

More fundamental problems not resolved by models which require the Solomon Sea to be a trapped segment of Pacific plate are the 'reversed' polarity (i.e. the arc-trench system faces the continent) of the inferred continent/arc collision zone, and the small time difference between formation and emplacement of the ophiolite. Karig (1974) and Coleman (1975) have claimed that 'reverse' polarity in arcs is not an initial condition but results from reversal of polarity from a 'normal' condition.

The alternative model proposed by Karig (1972) views the PUB-Solomon Sea as a reversed early Tertiary frontal arc system. This implies the existence of a northerly or northeasterly-facing arc-trench system peripheral to the Australian continental margin in the Mesozoic or earliest Tertiary.

4-3. Evidence for a Mesozoic arc-trench system

There is little direct evidence for the existence of Mesozoic arc-trench system in eastern Papua. Johnson & others (1979) have postulated the existence of a southwestward-dipping subduction event beneath eastern Papua in the late Mesozoic to account for the widespread arc-trench type magmatism in the late Cainozoic. As with the volcanism in the Highlands region they interpret the Cainozoic magmatism of SE Papua as resulting, not from contemporaneous subduction, but from diapirism and partial melting of mantle modified during a Cretaceous subduction event. They suggest that the Cainozoic magmatism may have been triggered by uplift.

More substantial evidence for the existence of a Mesozoic arc-trench system in the SE Papuan region is provided by Brown & others (in press) who, from examination of the Cretaceous-Eocene sediments of the central orogenic belt, concluded that a volcanic source lay to north and east, peripheral to the continental margin in the Cretaceous. Brown & others (in press) have proposed that the sediments were deposited in retro-arc basins behind a fringing volcanic arc, and that these evolved, in places, to form remnant arc complexes and back-arc marginal seas which were the sites of formation of the ophiolites throughout the orogenic belt. In this model, broadly that of Karig (1972), emplacement of the PUB results from closure of the marginal basin by subduction in a northeastward-dipping subduction zone associated with an early Tertiary island-arc. The central Solomon Sea might, in this model, represent an early Tertiary marginal sea formed by extension behind the arc-trench system.

While this model is broadly consistent with the known geology the geology of the ophiolite itself places constraints on the nature of the inferred marginal sea. The deep water pelagic and hemipelagic sediments (mostly jaspelitic limestone and marl), and lack of volcanolithic sediments overlying the PUB, clearly indicate that the ophiolite did not form in a shallow inter-arc or retro-arc basin. The depleted MORB-like geochemistry of the PUB basalts is unlike that of basalts erupted in ensialic back-arc basins (cf. Tarney & others, 1979; Weaver & others, 1979), and unlike marginal basin basalts erupted close to an active volcanic arc. Rather, the geochemistry of the PUB basalts indicates a mantle source highly depleted in LIL-elements. Such sources seem to be only tapped by deep rifting (Green, 1971; see PART 1, Chapter 5), thus implying extensive spreading in the basin in which the ophiolite formed.

As with the Marum ophiolite, the most important factor in deciding which model is appropriate for the formation of the PUB is *the age of formation of the ophiolite*. If the PUB is a trapped segment of Pacific plate it should be as old or older than the adjacent segment of Pacific plate, i.e. early Cretaceous or older (Heezen & Fornari, 1975). If the PUB formed in a marginal basin associated with a Cretaceous arc-trench system it should be Cretaceous or younger. As already noted the age of formation of the PUB is not well constrained: the available data point to a general Creaceous age. Resolution of the problem clearly requires more precise dating of the age of formation of the ophiolite. Additional features to be assessed in any plate tectonic model for the region are the opening of the Coral Sea, and the eruption of widespread Cretaceous-Eocene tholeiitic basalts in mainland southeast Papua (Smith & Davies, 1976; Milsom & Smith, 1975).

4-4. Conclusions

Geophysical investigations have shown that the layers of the ophiolite dip north and east and are continuous with the crustal and upper mantle layers of the western Solomon Sea. These surveys also indicate the existence of a low velocity zone in the upper mantle beneath the ophiolite belt (Finlayson & others, 1976). These findings, and the laboratory velocity measurements of Kroenke & others (1974), confirm the geological and petrological conclusions that the PUB represents an overthrust slab of crust and upper mantle of oceanic affinity which dips towards the Solomon Sea, and lend some support to the choked subduction model of emplacement suggested by Davies (1977) and Davies & Smith (1971).

It is not possible on the basis of the petrochemistry of the ophiolite to specify an origin for the PUB, i.e. marginal sea or deep ocean basin. Therefore, although the emplacement of the PUB by overthrusting at a southwestward-facing arc-trench system peripheral to the Australian continental block seems established, it is not clear whether this continent-arc collision resulted from consumption of a marginal sea or of oceanic crust at the leading edge of the Australian plate. The marginal basin model broadly accords with the overall late Cainozoic tectonic history of the region which has been one of arc magmatism and basin extension (e.g. Johnson, 1979 for review) but cannot be entirely reconciled with the regional geology as presently understood. Clearly, any future, more refined model of the tectonic evolution of the Papuan region requires greater knowledge of the late Mesozoic-early Tertiary regional geology and more precise dating of the age of formation of the PUB.

PART 3

ANHYDROUS MELTING OF PERIDOTITE AT 0-15 KB PRESSURE AND THE GENESIS OF THOLEIITIC BASALTS

Contents *page*

SUMMARY 149

CHAPTER 1. INTRODUCTION 151

2. EXPERIMENTAL TECHNIQUE 155

3. MELTING RELATIONS 163

4. COMPOSITIONS OF RESIDUAL PHASES 167

5. EQUILIBRIUM MELT COMPOSITIONS 173

6. PARTIAL MELTING AND THE OCEANIC CRUST - OPHIOLITE MODEL 183

SUMMARY

The anhydrous melting behaviour of two model upper mantle compositions, 'Hawaiian' pyrolite and a spinel lherzolite (Tinaquillo peridotite), has been studied experimentally at temperatures ranging from near, to about 200°C above, the solidus at 0-15 kb pressure. Equilibrium melting results in progressive elimination of phases with increasing temperature. Four main melting fields are recognized; from the solidus these are olivine (ol) + orthopyroxene (opx) + clinopyroxene (cpx) + Al-rich phase (plagioclase at low pressure, spinel at moderate pressure, garnet at high pressure) + liquid (L); ol + opx + cpx + Cr-spinel + L; ol + opx + Cr-spinel + L; ol $\pm$ Cr-spinel + L. Microprobe analyses of the residual phases shows progressive changes to more refractory compositions with increasing proportion of co-existing melt, i.e. increasing Mg/Mg + Fe and Cr/Cr + Al ratios, decreasing Al_2O_3, CaO in pyroxene.

The degree of melting, established by modal analysis, increases rapidly immediately above the solidus (up to 10% melting occurs within 25-30°C of the solidus), and then increases in roughly linear form with increasing temperature.

Equilibrium melt compositions have been calculated by mass balance using the compositions and proportions of residual phases to overcome the problems of iron loss and quench modification of the glass. Compositions from the melting of pyrolite within the spinel peridotite field (i.e. $\sim$ 15 kb) range from alkali olivine basalt (< 15% melting) through olivine tholeiite (20-30% melting) and picrite to komatiite (40-60% melting). Melting in the plagioclase peridotite field produces magnesian quartz tholeiite and olivine-poor tholeiite and, at higher degrees of melting (30-40%), basaltic or pyroxenitic komatiite. Melts from Tinaquillo lherzolite are more silica saturated than those from pyrolite for similar

degrees of partial melting, and range from olivine tholeiite through tholeiitic picrite to komatiite for melting in the spinel peridotite field.

The equilibrium melts are compared with inferred primary magma compositions and integrated with previous melting studies on basalts. The data obtained here and complementary basalt melting studies do not support models of formation of oceanic crust in which the parental magmas of common MORB are attributed to segregation from source peridotite at shallow depths (< 25 km) to leave residual harzburgite. Liquids segregating from peridotite at these depths and with > 20% melting are more silica-rich than common MORB.

CHAPTER 1

INTRODUCTION

1-1. Prelude

It is now generally accepted that basaltic magmas result from partial melting of a peridotitic upper mantle. Previous melting studies on natural basalt and peridotite and simple system analogues (e.g. Green & Ringwood, 1967a; Ito & Kennedy, 1967; Green, 1970, 1971, 1973a, b; Kushiro, 1969; Nicholls, 1974; Eggler, 1974, 1978) have shown that varying degrees of partial melting of peridotite under different conditions (P,T, volatile content) may give rise to a wide spectrum of basaltic compositions, and provide a foundation for our understanding of magma genesis. The results of these studies have been integrated to produce a petrogenetic grid (Green, 1971, 1973b) for the origin of a range of natural basaltic compositions occurring in the ocean basins and on stable continental regions. To date, formulation and experimental testing of the petrogenetic grid have relied largely on basalt crystallisation studies i.e. examination of liquidus and near-liquidus mineralogy of mantle-derived basaltic liquids. However, because of the uncertainties in identifying primary magmas among basalts of tholeiitic composition and, in particular, ocean floor tholeiites, (which, unlike alkali basalts, generally do not carry mantle xenoliths as evidence of their primary nature), direct melting studies of peridotite are necessary to more closely constrain conditions of origin of tholeiitic magmas.

PART 3 represents a study of the anhydrous melting of two different peridotites at 0-15 kb pressure with the aim of examining both the nature of the residual phases and the melt compositions formed upon melting of peridotite at comparatively low pressure. The data obtained show that the equilibrium liquid compositions formed over a relatively wide melting interval are broadly of tholeiitic composition. The experimentally

determined liquid compositions and residual mineralogy are then used to examine models for the genesis of oceanic crust and ophiolites, and various other naturally occurring magnesian tholeiites.

1-2. Composition of the oceanic upper mantle

Evidence supporting the hypothesis of an upper mantle comprised of olivine (Mg_{88-92}), orthopyroxene, clinopyroxene and minor spinel (or garnet) and containing approximately 3-4% CaO and Al_2O_3 has been discussed elsewhere (e.g. Ringwood, 1975 for a review). Previous experimental studies (see Green, 1976b, for review) and, more recently, integration with detailed trace element modelling (Frey & others, 1978) have shown that a calculated peridotite composition - similar to pyrolite $\overline{111}$ (Ringwood, 1966) based on the Hawaiian tholeiites - is capable of yielding a wide range of basalt compositions ranging from olivine melilitite through alkali olivine basalt to olivine tholeiite under varying conditions and degrees of partial melting.* Ringwood's (1966) pyrolite $\overline{111}$ has therefore been chosen as representative of mantle composition in areas of oceanic island volcanism. Although originally proposed as a general, conceptual term '*pyrolite*' is used here for one specific composition (Ringwood, 1966) to enable direct comparison with previous studies on this composition and melting studies on other possible upper mantle compositions. Pyrolite is also a reasonable approximation of upper mantle composition in areas of continental alkali basalt volcanism (Frey & others, 1978). This model composition is LREE-enriched and enriched in incompatible elements relative to the source region for most mid-ocean ridge basalts (Frey & others, 1978; Green & others, 1979). For the latter basalts (MORB), trace element and isotopic studies

---

* The TiO_2 content of Ringwood's (1966) pyrolite $\overline{111}$ composition is now known to be too high for other than the Hawaiian province and 0.3-0.4% TiO_2 is probably a more reasonable estimate for other provinces and other mantle peridotite compositions (Frey & others, 1978).

(e.g. Gast, 1968; Kay & others, 1970; Bryan & others, 1976) indicate a more refractory peridotite source, depleted in incompatible elements. Accordingly, a spinel lherzolite, Tinaquillo peridotite (Green, 1963) has been selected as a specific composition representative of depleted mantle peridotite. In addition to having slightly lower CaO and Al_2O_3 content than the pyrolite composition used, Tinaquillo peridotite is depleted in TiO_2 and incompatible elements, including REE (Philpotts & others, 1972), and is more magnesian than pyrolite. Tinaquillo lherzolite is also of similar composition to the less depleted of the spinel lherzolites examined by Kuno & Aoki (1970), Frey & Green (1974) and Frey & Prinz (1977), and compares with estimates of the upper mantle composition based on averages of spinel lherzolite compositions (e.g. Harris & others, 1967; Maaloe & Aoki, 1977), although CaO and Al_2O_3 contents are higher for Tinaquillo than Maaloe & Aoki's (1977) average oceanic mantle. Tinaquillo lherzolite is also more depleted in incompatible elements than the mantle source composition suggested for DSDP basalt 3-18 by Green & others (1979). Two peridotite compositions have therefore been chosen which, although similar in major elements, represent the two ends of a compositional spectrum in their content of incompatible elements.

In addition to the mantle heterogeneity reflected in basaltic rocks, detailed geochemical studies of peridotite xenoliths in basalts, high temperature peridotites and peridotitic komatiites (e.g. Frey & Green, 1974; Frey & Prinz, 1977; Frey & others, 1978; Sun & Nesbitt, 1977, 1978b) have shown that the mantle chemistry is complex; many source regions have apparently been enriched by addition of a small incompatible element-enriched melt fraction, whereas others have been depleted. Green (1971) and Green & Lieberman (1976) have presented a model of chemical zoning within the mantle, suggesting that the deeper part of the Low Velocity Zone (LVZ) is depleted in incompatible elements and overlain by an enriched layer, due to continuous upward migration of a small melt fraction

(< 2% melt) of olivine melilitite composition. With reference to this model, it is suggested that the peridotite compositions selected may be reasonable *approximations* to the upper and lowermost parts of the LVZ of the mantle, i.e. source regions for magmas of oceanic islands and mid-ocean ridges respectively, but we emphasize that we envisage a *continuum* of mantle compositions from enriched to highly depleted and refractory peridotite.

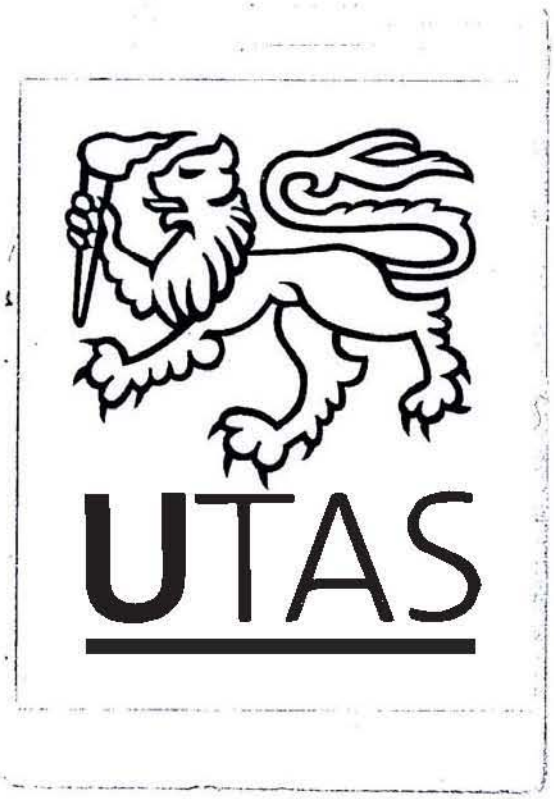

CHAPTER 2

EXPERIMENTAL TECHNIQUE

2-1. Preparation of starting mixes

Starting mixes were prepared from analytical reagent grade chemicals, carefully ground under acetone (< 5 μm) and sintered at 1000°C . The initial mix was then recrushed under acetone and heated to 1000°C in a sealed evacuated silica tube with a quartz - fayalite - magnetite buffer. A split from the mixes was then analysed for FeO and Fe_2O_3 by spectrophotometry. The compositions prepared are presented in Table 3-1. These compositions are of pyrolite and Tinaquillo lherzolite modified by the extraction of 40% olivine to facilitate identification of minor phases. The validity of this approach has been discussed previously (e.g. Green & Ringwood, 1970), and is here re-affirmed by the fact that all runs, including the highest temperature experiments, were oversaturated in olivine. While the use of these modified compositions is relevant to peridotite melting studies in that the correct residual phases are always present, it does introduce a small error in regard to the Mg-value $(\frac{100\ Mg}{Mg + Fe^{++}})$ ratio of the starting mix. Ideally the composition of the olivine removed should be that of the equilibrium residual olivine for each particular P, T and degree of melting. Since this is not feasible, olivine of an average residual composition was removed ($Mg_{91.6}Fe_{8.1}Ni_{0.2}Mn_{0.1}$ for pyrolite and $Mg_{91.9}Fe_{8.0}Ni_{0.0}Mn_{0.1}$ for Tinaquillo lherzolite). For low to moderate degrees of melting the olivine compositions removed are slightly more magnesian than the equilibrium olivine for the original peridotite compositions, and, thus, the mix compositions and phase compositions are slightly too iron-rich for low degrees of melting. The extraction of olivine also produces slightly greater change in Mg-value of residual phases with increasing temperature (percent melting) for the modified peridotite composition than for the unmodified peridotite, due

TABLE 3-1. COMPOSITIONS OF PYROLITE AND TINAQUILLO LHERZOLITE AND MODIFIED EXPERIMENTAL COMPOSITIONS*

	Pyrolite	Pyrolite - 40% ol	Tinaquillo lherzolite	Tinaquillo - 40% ol
SiO_2	45.2	47.9	44.95	47.5
TiO_2	0.71	1.18	0.08	0.13
Al_2O_3	3.54	5.91	3.22	5.35
Fe_2O_3	0.48	0.20**	0.09	0.15
FeO	8.04	8.63	7.58	7.38
MnO	0.14	0.13	0.14	0.18
MgO	37.5	28.8	40.03	32.8
CaO	3.08	5.14	2.99	4.97
Na_2O	0.57	0.95	0.18	0.30
K_2O	0.13	0.22	0.02	0.03
P_2O_5	-	0.06	0.01	0.02
NiO	0.20	0.13	0.26	0.43
Cr_2O_3	0.43	0.72	0.45	0.75
CIPW Norms				
Or	0.8	1.3	0.1	0.2
Ab	5.0	8.0	1.5	2.5
An	6.6	11.2	7.9	13.2
Di	6.8	11.0	5.4	9.0
Hy	15.8	26.5	18.0	30.8
Ol	62.5	38.2	65.9	42.5
Il	1.3	2.2	0.2	0.3
Mt	0.7	0.3	0.1	0.2
Cr	0.6	1.0	0.6	1.1
$100Mg/Mg+Fe^{++}$	89.3	85.6	90.3	88.8
100Mg/Mg+Fe	88.7	85.4	90.4	88.6

* Compositions are of pyrolite (Ringwood, 1966) and pyrolite minus 40% olivine ($Mg_{91.6}Fe_{8.1}Ni_{0.2}Mn_{0.1}$), and Tinaquillo peridotite (Green, 1963) and Tinaquillo minus 40% olivine ($Mg_{91.9}Fe_{8.0}Ni_{0.0}Mn_{0.1}$).

** FeO by spectrophotometry - P. Robinson, analyst.

to the decrease of buffering effect of the larger amounts of olivine. However, these errors are small, and more than compensated for by the improved quenching characteristics due to high proportions of glass to crystals, and the greater accuracy and ease of modal analyses. In addition the higher Fe-content is partly counteracted by the iron loss from the charge (see below).

2-2. Apparatus and methods

Experiments were carried out in solid media (piston-cylinder) high pressure apparatus using a piston-in technique and a pressure correction of minus 10% nominal piston pressure. Pressures have been previously calibrated on the quartz $\rightleftharpoons$ coesite transition at 1100°C, 32 kb, and albite $\rightleftharpoons$ jadeite + quartz at 600°C, 16.2 kb by Brey & Green (1975), and the error in pressure measurement is considered to be $\pm$ 3% at $\sim$ 15 kb but may increase to $\pm$ 20% at < 3 kb. Temperatures ($\pm$5°C) were measured by a Pt - Pt 10% Rh thermocouple. No correction was made for the effect of pressure on the thermocouple emf.

Pyrex glass sleeves with graphite inserts were used in the 0.5 inch diameter furnace assemblies to minimize hydrogen diffusion from dehydration of the outer talc sleeve. Experiments on the stability of buffer assemblages using this furnace assembly indicate prevailing f_{O_2} conditions < NNO (Green, 1976a; D. Gust, pers. comm. 1979). However, the comparatively high Fe^{3+} contents of residual spinels (see below) suggests the f_{O_2} in the runs may have been greater than this, as a consequence of alloying of Fe with the Pt capsule according to the reaction $Pt + 3FeO \rightleftharpoons (Fe, Pt)_{SS} + Fe_2O_3$. Because iron loss is dependent on run duration, the Fe^{3+}/Fe^{2+} ratios of the spinels are not considered a reliable indicator of prevailing f_{O_2}. Samples (15 - 20 mg) were contained in sealed Pt capsules and preheated at 900 - 1000°C for 8-12 hours packed in metallic iron powder in an attempt to presaturate the Pt capsule in iron. All runs were anhydrous,

and the powdered starting mix was dried overnight at 110°C. Several short-duration runs were made using unsealed spec-pure iron capsules. These experiments produced a lower f_{O_2}, did not yield chrome spinel, and in some cases, the charges dissolved iron from the capsule and contained dispersed small spheres of metallic iron.

The 1-atmosphere partial melting experiments were carried out in a 1-atmosphere quenching furnace using 20 mg samples in spec-pure iron capsules sealed in evacuated silica tubes. These samples also resulted in f_{O_2} below the QFM buffer and the charge dissolved additional iron. For these reasons phase relations only, and no compositional data, are presented for the 1-atmosphere experiments.

2-3. Microprobe analyses

The charge was recovered as a coherent cylinder of residual crystals and glass. A small portion of one split was crushed and examined optically in refractive index oil. The other split was mounted, polished, and examined optically in reflected light and by scanning electron microscope. Optimization of the back-scattered and secondary electron images enabled clear resolution and discrimination of all phases (except for fine-grained runs near the solidus), including melt and quench crystals, up to X 2000 magnification. Discrimination of phases was based on form and contrast using the back-scattered electron image in which 'brightness' is dependent on the mean atomic number of the phases in the target. In this way quench phases e.g. quench clinopyroxene rims on primary phases, can be distinguished from primary phases because of the higher Ti, Al and Fe contents in the quench phase compared to the primary equilibrium phase. Scanning electron microscope photographs of some of the experimental charges are given by Jaques & Green (1979) - Appendix 4.

Simultaneous quantitative analysis for 10 elements (Na-Fe) was made using a JEOL JX-50A electron microprobe - scanning electron microscope

fitted with an energy dispersive (EDAX) analytical system based on the method of Reed & Ware (1973, 1975). Operating conditions employed an accelerating voltage of 15 Kv, beam current of 3 nanoamps, a beam diameter of less than 0.5 microns, and 100 seconds counting time. Full details of the method are given by Griffin (1979). Glass analyses and analyses of the bulk charge were made using rapid reduced area scans to minimize alkali volatilization and ensure representative analysis. At least 5 analyses of each phase, including glass and bulk charge, were made for each run: some 2000 analyses were acquired during the study. All iron analyses are reported as weight percent FeO unless otherwise stated.

2-4. Iron Loss

A number of studies (e.g. Green & Ringwood, 1967a; Merrill & Wyllie, 1973; Green, 1973b, 1976a; Stern & Wyllie, 1975) have documented loss of iron from the sample to platinum group metal capsules during experiments, and shown that the extent of iron loss is particularly dependent on temperature and run duration. The problem of iron loss in partial melting experiments was re-examined as part of this study (see Appendix 4), and it was shown that iron is lost preferentially from the charge in the order liquid>olivine>pyroxene, and that this preferential iron loss commonly results in non-equilibrium crystal-liquid and crystal-crystal (e.g. olivine - orthopyroxene) Fe/Mg partitioning, due to the different rates of adjustment of phases to the iron loss. On a local scale this is demonstrated by reverse zoning of larger crystals and by the fact that smaller crystals are generally more magnesian than cores of larger ones. Jaques & Green (1979) stressed that even where iron loss was minimized by presaturation techniques the extent of compositional interchange between sample and container needed to be carefully evaluated. Capsule materials other than Pt (e.g. graphite, molybdenum, spec-pure iron) are difficult to seal and thus f_{O_2} can be only poorly controlled, and

H_2O or CO_2 may gain access to the charge with consequent change to the degree of melting and nature of residual phases.

Pt capsules have been used in the experiments but excessive iron loss from the charge has been circumvented and the consequent effect on the compositions of phases minimized by carrying out repeated runs of varying duration, and monitoring the extent of the iron loss by analysis of the bulk charge after the run. From this, optimum run conditions, in terms of attainment of equilibrium and minimum iron loss, were established. Iron loss in these experiments was also monitored by examining the Fe-Mg partitioning between residual phases using the core composition of large (> 20 μ) orthopyroxene crystals, which re-adjust more slowly to iron loss, as a reference. Since the $K_D^{ol/opx}$ (where $K_D^{A/B} = \frac{(Fe^A)}{(Mg)} \Big/ \frac{(Fe^B)}{(Mg)}$ is known to be insensitive to temperature and pressure and has been determined experimentally as 1.1 ± 0.1 (e.g. Medaris, 1969; Matsui & Nishazawa, 1974; Mori & Green, 1978), this relationship has been used to test the Fe-Mg partitioning between olivine and orthopyroxene for equilibrium. In all except the shortest duration runs, olivine compositions are 1 to 4 mol % more magnesian than the equilibrium value. Data obtained during this and previous partial melting studies (e.g. Green, 1976a; Jaques & Green, 1979) show that the observed olivine - glass Fe-Mg partitioning is variable, being dependent on temperature and run duration (i.e. the extent of iron loss and on quench modification of the glass), and therefore is of little use in determining equilibrium in situations where iron loss has occurred. Similarly, the observed olivine compositions in an experiment cannot be used to constrain the Mg-value* of equilibrium melt unless first corrected for the effect of Fe-loss.

---

* Mg-value = $100Mg/(Mg + Fe^{2+})$

2-5. Determination of liquid compositions and percentage melting

The problem of growth of metastable, non-equilibrium phases, both as discrete crystals and as rims and outgrowths on primary phases, during quenching of the charge, and the consequent modification of melt compositions in partial melting experiments is well known (Green, 1973b, 1976a; Cawthorn & others, 1973; Nicholls, 1974).

The problem of quench modification of the partial melt compositions has been further examined with the aid of the scanning electron microscope coupled to the energy-dispersive microprobe (Appendix 4). It was found that significant quenching problems occur both at comparatively low degrees of melting ($\leq$ 10%) where the solid/liquid proportion is high, and at high degrees of melting (30-40%) where olivine and low Ca-pyroxene readily quench from the low viscosity, magnesian liquid. It was also shown that the combined effects of iron loss and quenching result in glass compositions significantly more silica-rich, and containing less FeO and MgO and generally more Al_2O_3 and CaO, than the equilibrium liquids calculated by either crystal-liquid element partition data or mass balance after allowing for iron loss. For these reasons, equilibrium liquids have been *calculated* by mass balance from a knowledge of the composition and proportions of the residual phases.

The proportions of residual phases were established by point-counting of scanning electron microscope photographs of the polished mount using a transparent 10 x 9 cm grid. A minimum of 1200 points were counted in replicate and averaged. Point counting of phases was not possible for the *high degree melting* runs where olivine or olivine + chrome spinel were residual phases because of strong crystal settling within the charge, even in runs of short duration. For these experiments the equilibrium liquid composition was calculated by mass balance assuming a $K_D^{ol/liquid}$ of 0.3 (Roeder & Emslie, 1970; Green & Ringwood, 1967a) after correcting for iron loss from the charge (cf. Green, 1973b). The use of this fixed K_D may

introduce a small error since it was later found (PART 4) that Fe-Mg partitioning between olivine and liquid is pressure dependent at pressures above 5 kb: K_D increases with pressure resulting in more magnesian equilibrium liquids at higher pressure for olivine of the same composition.

Liquid compositions were calculated by mass balance after conversion of the volume percent modes to weight percent modes using appropriate mineral densities (Tröger, 1956). The liquid density was calculated by the method of Bottinga & Weill (1970) using the least modified, most magnesian glass composition (obtained by reduced-area rapid scans) with adjustment for the effect of pressure on the density (Kushiro & others, 1976). Iteration of the mass balance calculations to overcome the density difference between the equilibrium liquid and the analysed glass made negligible difference to the resultant liquid composition. Compared to the analysed glass compositions (available on request) the calculated liquids are more magnesian, have higher FeO content, lower SiO_2 and, generally, lower Al_2O_3 and CaO contents (Table 3-2) (see also Appendix 4).

An additional uncertainty in the composition of the calculated liquids is Fe_2O_3 of the melt, and, consequently, calculated $\frac{100\ Mg}{Mg + Fe}^{2+}$ ratios, since change in oxidation state may occur during the run. In Tables 3-9 and 3-10 calculated $\frac{100\ Mg}{Mg + Fe}^{2+}$ assume no change in Fe_2O_3 content and $\frac{100\ Mg}{Mg + Fe}$ ratios assume all Fe as Fe^{2+}.

2-6. Errors and limitations

Errors involved in the calculation of the equilibrium liquids are difficult to define precisely. Errors in point counting may be as high as 2 volume % for phases present in excess of 5% due to inhomogeneous distribution, and crystal settling. The effect of a 2% error in the determination of the percentage of melting is shown in Table 3-2 for the melting of pyrolite at 10 kb, 1450°C (residual olivine and chrome spinel)

TABLE 3-2. COMPARISON GLASS AND CALCULATED MELT COMPOSITION, AND ESTIMATED ERRORS

	10 kb 1300°C				10 kb 1450°C			
	Glass	37% melt	39%* melt	41% melt	Glass	71% melt	73% melt	75% melt
SiO_2	51.3	49.3	49.8	49.9	52.4	51.5	51.2	51.0
TiO_2	2.8	3.0	2.7	2.6	1.6	1.7	1.6	1.6
Al_2O_3	12.4	12.8	12.5	12.1	7.9	8.2	8.0	7.8
FeO**	8.9	9.0	9.0	8.5	8.8	9.9	9.5	9.5
MnO	–	0.1	0.1	0.1	–	0.1	0.1	0.1
MgO	10.4	11.5	12.0	13.4	20.7	19.8	21.0	21.7
CaO	11.8	11.2	10.9	10.6	7.1	7.2	7.0	6.8
Na_2O	1.9	2.5	2.4	2.3	1.2	1.3	1.3	1.3
K_2O	0.5	0.6	0.6	0.5	0.3	0.3	0.3	0.3
CIPW NORM								
Or	3.0	3.6	3.6	3.0	1.8	1.8	1.8	1.8
Ab	16.1	21.2	20.3	19.5	10.2	11.0	11.0	11.0
An	23.8	21.9	21.6	21.2	15.3	15.7	15.1	14.6
Di	28.0	27.1	26.2	25.2	15.9	16.1	15.7	15.3
Hy	23.0	3.2	7.2	9.7	44.7	40.0	37.4	36.1
Ol	0.8	17.2	16.0	16.5	9.2	12.2	16.0	18.2
Il	5.3	5.7	5.1	4.9	3.0	3.2	3.0	3.0
100Mg/Mg+ΣFe	67.6	69.5	70.4	73.8	80.7	78.1	79.7	80.3

* Percent melting is of pyrolite minus 40% olivine composition.

** Total iron as FeO

and 10 kb, 1300°C (residual olivine, orthopyroxene and chrome spinel). Uncertaintly of ± 2% in estimation of percentage melting produces small differences in Mg-value and normative compositions which do not however overlap the composition of analysed glass in the runs.

It was not possible to adequately discriminate residual phases in the low degree melting range, i.e. within 25°C of the solidus, due to the fine grainsize of the charge. Long run times to obtain sufficiently large crystals result in excessive iron loss and a non-equilibrium residual assemblage. An additional problem is the nucleation of stable calcic pyroxene: residual clinopyroxenes, particularly at low pressure, showed a range of calcium contents, some being sub-calcic (see later).

CHAPTER 3

MELTING RELATIONS

Data on the experimental runs are presented in Table 3-3. The phase relations of the melting of both pyrolite and Tinaquillo lherzolite at 50°C intervals from the solidus to above the orthopyroxene-out curve are plotted as a function of T and P in Figure 3-1. Also shown are the pyrolite solidus and subsolidus relations previously defined by Green & Ringwood (1967b, 1970). The position of the Tinaquillo lherzolite solidus is shown as approximate only, but appears to lie some 30-40°C above the pyrolite solidus, reflecting its more refractory composition. The subsolidus assemblage at low pressure (0-10 kb) consists of olivine, orthopyroxene, clinopyroxene and plagioclase (plus minor accessory ilmenite, chrome spinel, apatite); at pressures above 10 kb this assemblage is replaced by olivine, aluminous pyroxenes and spinel, and above 25-30 kb by olivine, pyroxenes and garnet (Green & Ringwood, 1967b).

Three main fields have been defined within the melting range studied for anhydrous melting of both peridotites. From near the solidus these are: olivine + orthopyroxene + clinopyroxene + chrome spinel + liquid, olivine + orthopyroxene + chrome spinel + liquid, and olivine $\pm$ chrome spinel + liquid. Incomplete data close to the solidus indicate the presence of a narrow field in which an aluminous phase - plagioclase at low pressure, aluminous spinel at moderate pressure, and garnet at high pressure ($\geq$ 30 kb, Green & Ringwood, 1967b) - co-exists with olivine, 2 pyroxenes and liquid.

The present data, though incomplete, indicate that this phase melts within 25-30°C of the solidus (in the case of aluminous spinel by solid solution change to chrome spinel, Fig. 3-4). The clinopyroxene-bearing field for these peridotites extends some 75-100°C above the solidus and expands at low pressure (< 5 kb), particularly in the case of

TABLE 3-3. EXPERIMENTAL RUN DATA

Run No.	P (kb)	T (°C)	Time (hours)	Capsule	$\frac{100\ Mg}{Mg + Fe}$ Charge	Phases present[a]
			Pyrolite minus 40% olivine			
A555	0	1170	5	Fe	-	Ol + Opx + Cpx + L
A554	0	1200	2.5	Fe	-	Ol + Opx + Cpx + L
A556	0	1225	3	Fe	-	Ol + Opx + L
A553	0	1250	2	Fe	-	Ol + L
958	2.25	1100	2	Pt	85.8	Ol + Opx + Cpx + Pl + Sp + L
T-149	2	1150	3.5	Pt	88.2	Ol + Opx + Cpx + Sp + L
T-111	2	1200	2	Pt	86.0	Ol + Opx + Sp + L
T-107	2	1250	2	Pt	89.5	Ol + Opx + Sp + L
T-185	2	1250	0.5	Pt	86.5	Ol + Opx + Sp + L
T-133	2	1300	1	Pt	87.1	Ol + Sp + L
T-147	5	1200	2.5	Pt	87.2	Ol + Opx + Cpx + Sp + L
T-186	5	1200	0.75	Pt	86.2	Ol + Opx + Cpx + Sp + L
T-104	5	1250	2	Pt	86.9	Ol + Opx + Sp + L
T-167	5	1250	0.75	Pt	86.2	Ol + Opx + Sp + L
T-102	5	1300	2	Pt	87.2	Ol + Opx + Sp + L
T-166	5	1300	0.5	Pt	86.5	Ol + Opx + Sp + L
T-119	5	1350	2	Pt	88.9	Ol + Opx + Sp + L
T-158	5	1350	0.33	Pt	87.0	Ol + Sp + L
956	6.75	1200	2	Pt	85.5	Ol + Opx + Cpx + Sp + L
892	9	1200	2	Pt	86.7	Ol + Opx + Cpx + Sp + L
T-100	10	1250	2	Pt	86.1	Ol + Opx + Cpx + Sp + L
T-140	10	1250	1	Fe	84.6	Ol + Opx + Cpx + L
T-69[b]	10	1300	2	Pt	86.9	Ol + Opx + Sp + L
T-118	10	1350	2	Pt	87.0	Ol + Opx + Sp + L
T-139	10	1350	0.5	Fe	85.1	Ol + Opx + L
T-90	10	1400	2	Pt	88.0	Ol + Opx + Sp + L
T-157	10	1400	0.33	Pt	86.6	Ol + Opx + Sp + L
T-101	10	1450	2	Pt	89.7	Ol + Sp + L
T-138	10	1450	0.25	Fe	83.3	Ol + L
T-148	15	1350	2.5	Pt	87.7	Ol + Opx + Cpx + Sp + L
T-142	15	1400	1	Pt	86.2	Ol + Opx + Sp + L
T-184	15	1450	0.5	Pt	88.4	Ol + Opx + L
T-143	15	1500	0.75	Pt	88.8	Ol + Opx + Sp + L
T-150	15	1550	0.33	Pt	89.2	Ol + L

TABLE 3-3. CONT.

Run No.	P (kb)	T (°C)	Time (hours)	Capsule	100 Mg / Mg + Fe Charge	Phases present[a]
			Tinaquillo lherzolite minus 40% olivine			
T-134	2	1200	2	Pt	90.0	Ol + Opx + Cpx + Sp + L
T-161	2	1200	4	Pt	90.1	Ol + Opx + Cpx + Sp + L
T-123	2	1250	2	Pt	90.0	Ol + Opx + Sp + L
T-121	2	1300	2	Pt	94.8	Ol + Opx + Sp + L
T-199	2	1300	0.5	Pt	89.2	Ol + Opx + Sp + L
T-162	2	1350	0.5	Pt	90.6	Ol + Sp + L
T-163	5	1200	4	Pt	89.4	Ol + Opx + Cpx + Pl + Sp + L
T-132	5	1250	1	Pt	89.0	Ol + Opx + Cpx + Sp + L
T-129	5	1300	2	Pt	90.8	Ol + Opx + Sp + L
T-180	5	1300	0.5	Pt	89.5	Ol + Opx + Sp + L
T-120	5	1350	2	Pt	91.0	Ol + Opx + Sp + L
T-154	5	1400	0.33	Pt	90.0	Ol + Sp + L
T-135	10	1250	2	Pt	89.0	Ol + Opx + Cpx + Sp + L
T-128	10	1300	2	Pt	90.0	Ol + Opx + Cpx + Sp + L
T-136	10	1350	1	Pt	89.2	Ol + Opx + Sp + L
T-137	10	1400	1	Pt	91.3	Ol + Opx + Sp + L
T-141	10	1400	1	Pt	91.4	Ol + Opx + Sp + L
T-155	10	1450	0.5	Pt	90.7	Ol + Sp + L
T-165	10	1500	0.33	Pt	90.8	Ol + Sp + L
T-156	15	1350	3	Pt	91.0	Ol + Opx + Cpx + Sp + L
T-145	15	1400	1	Pt	90.4	Ol + Opx + Sp + L
T-194	15	1400	0.33	Pt	-	Ol + Opx + Sp + L
T-183	15	1450	0.5	Pt	90.6	Ol + Opx + L
T-216	15	1450	0.33	Pt	-	Ol + Opx + L
T-218	15	1500	0.33	Pt	-	Ol + Opx + L
T-164	15	1550	0.5	Pt	91.8	Ol + L

Ol = olivine, Opx = orthopyroxene, Cpx = clinopyroxene, Sp = spinel, Pl = plagioclase, L = liquid (glass)

[a] Primary phases only, excludes quench pyroxene and/or olivine present in most runs.

[b] Additional experiments by Jaques and Green (1979).

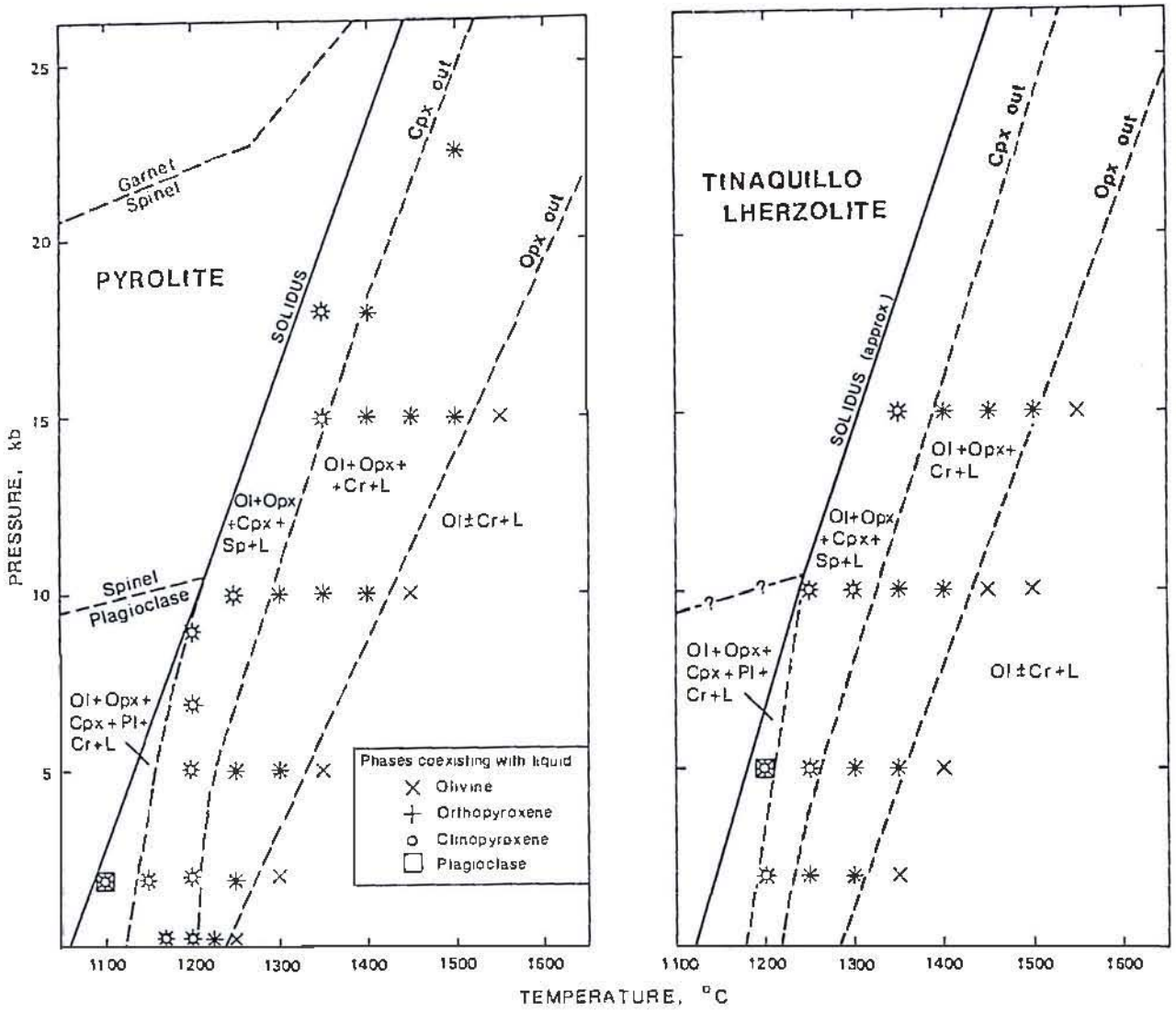

Fig. 3-1. P-T diagram for melting of pyrolite (composition of Ringwood, 1966) and Tinaquillo lherzolite. Ol = olivine, Opx = orthopyroxene, Cpx = clinopyroxene, Sp = spinel, Cr = chrome spinel, Pl = plagioclase, L = liquid. Data for 18 and 22.5 kb pyrolite runs from Green & Ringwood (1967b). Plagioclase-spinel peridotite transition boundaries from Green & Ringwood (1970). The solidus and subsolidus boundaries for Tinaquillo lherzolite are interpolated.

pyrolite. The upper stability limit of orthopyroxene lies approximately 150-200°C above the solidus of both peridotites and the field expands slightly with increasing pressure. The liquidus of either peridotite has not been determined but the pyrolite 1-atmosphere liquidus is approximately 1700-1750°C by comparison with the data for peridotitic komatiite 49J (Green & others, 1975b).

The melting relations defined here (together with the pyrolite melting runs of Green & Ringwood, 1967b) are broadly similar to those established by Ito & Kennedy (1967) and Mysen & Kushiro (1977) for the anhydrous melting of garnet peridotite at 0-40 kb, and 25 and 35 kb respectively. Ito & Kennedy (1967) did not define a field in which clinopyroxene was a residual phase, but noted that garnet and clinopyroxene melted within the temperature interval of approximately 50°C above the solidus at high pressure. The presence of residual orthopyroxene at low pressure (< 5 kb) in our experiments is in agreement with the 1-atmosphere data of Ito & Kennedy (1967), but conflicts with the incongruent melting behaviour of orthopyroxene in the $MgO-SiO_2$ system. This illustrates very well the contrast between the abrupt disappearance of a phase and change in melt proportions characteristic of simple, pure Mg systems (Kushiro, 1969; Presnall & others, 1979), and the gradual reaction and disappearance of a phase over a moderately large temperature interval in complex Fe-Mg systems.

The percentage of melt obtained from the melting of pyrolite and Tinaquillo lherzolite at 15 kb is plotted as a function of temperature in Figure 3-2. Satisfactory determination of the percentage of melting at less than about 10% melting was not achieved because of the experimental difficulties already discussed. From Figure 3-2 it is seen that the amount of melt increases rapidly in the initial stages of melting, and then increases at a steady rate. Comparison of pyrolite and Tinaquillo lherzolite shows that more liquid can be extracted from pyrolite:

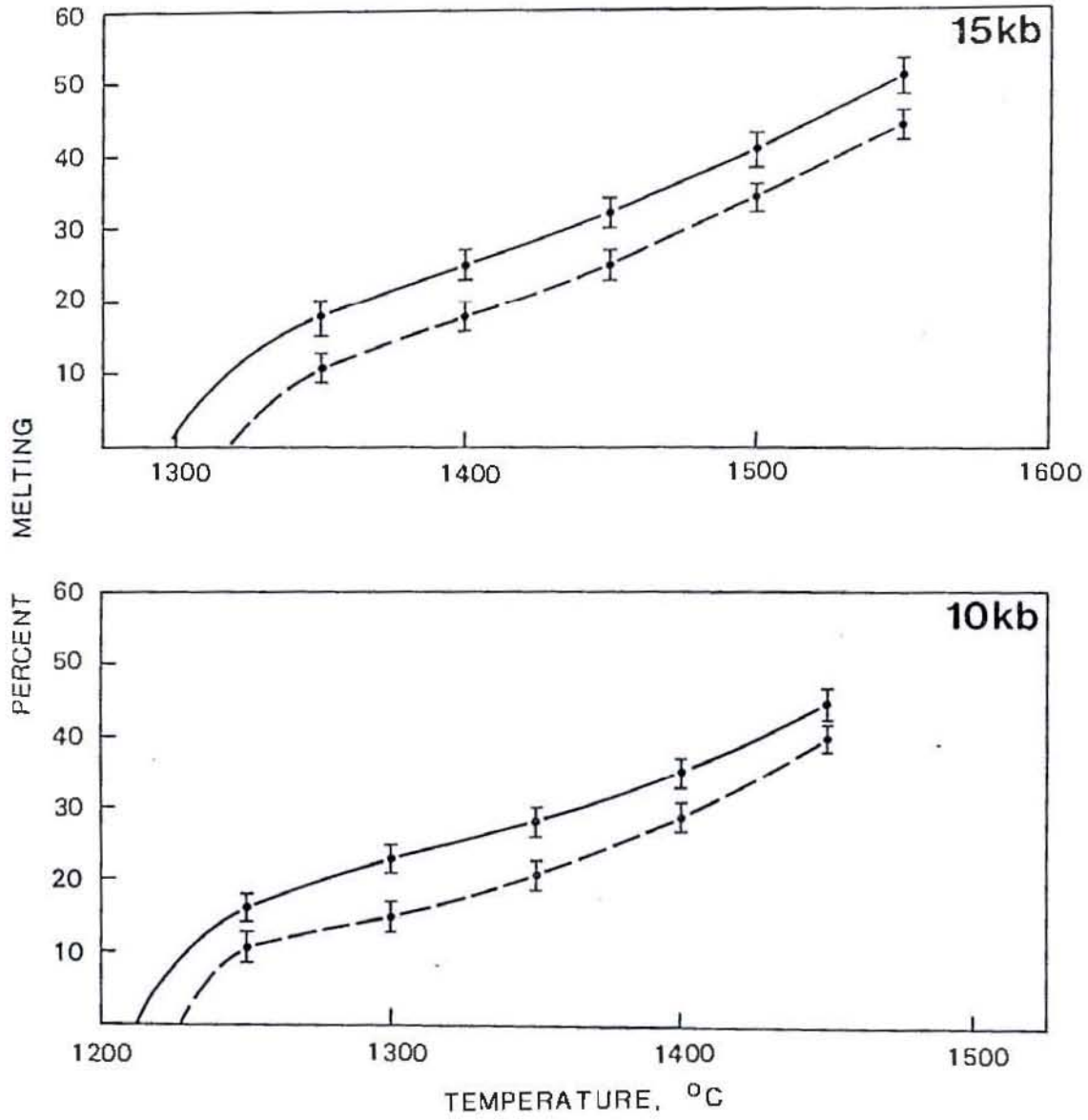

Fig. 3-2. Percent melting versus temperature for melting of pyrolite (solid line) and Tinaquillo lherzolite (dashed line). Note that percent melting is of peridotite compositions, not the experimental (minus 40% olivine) compositions shown in Fig. 3-3. Bars indicate $\pm$ 2% error in determination of liquid.

approximately 20% melt can be derived from pyrolite before clinopyroxene disappears but only about 12-15% melt can be derived from Tinaquillo before clinopyroxene is exhausted. Mysen & Kushiro (1977) claim that the anhydrous melting relations of peridotite resemble those of simple systems, and that melting may approximate an invariant character. This conclusion is not supported by our data (Fig. 3-2). Our data do not permit evaluation of the melting behaviour between the 50°C intervals to determine if minor inflections (cf. Kushiro, 1969), or steps (Wyllie, 1971), occur as phases disappear from the residue. Presnall (1969) has shown graphically that equilibrium melting is a continuous process and we interpret our results as demonstrating the 'smoothing effect' of Fe-Mg, Al-Cr, Al-Si, Na-Ca, solid solutions in the percent melt versus temperature plot. Following the initial stages of melting, where the amount of melt increases rapidly, the percentage of melting increases approximately linearly as a function of temperature. The melting behaviour observed in our experiments bears similarities with that predicted by O'Hara (1968, Fig. 8, stages 3-5), although the observed melting interval is less than that suggested in his model.

Modal variation (volume %) of the residue phases for the modified (-40% olivine) peridotite compositions are shown in Figure 3-3. In each case the melt fraction increases while the proportion of residual phases decreases regularly. Ito & Kennedy (1967) also observed a progressive decrease in the proportion of residual phases and eventual elimination of the phase from the residue. Although the melting of orthopyroxene in the complex composition differs from that in the $CaO-MgO-SiO_2$ system (Kushiro, 1969) and the $CaO-MgO-Al_2O_3-SiO_2$ system (Presnall & others, 1979), comparison of the relative proportions of olivine and orthopyroxene at 2 and 5 kb with the 10 and 15 kb experiments show that the field of orthopyroxene expands with pressure as previously noted (e.g. Green & Ringwood, 1967a). Melts produced by moderate degrees of melting at low pressure are over-

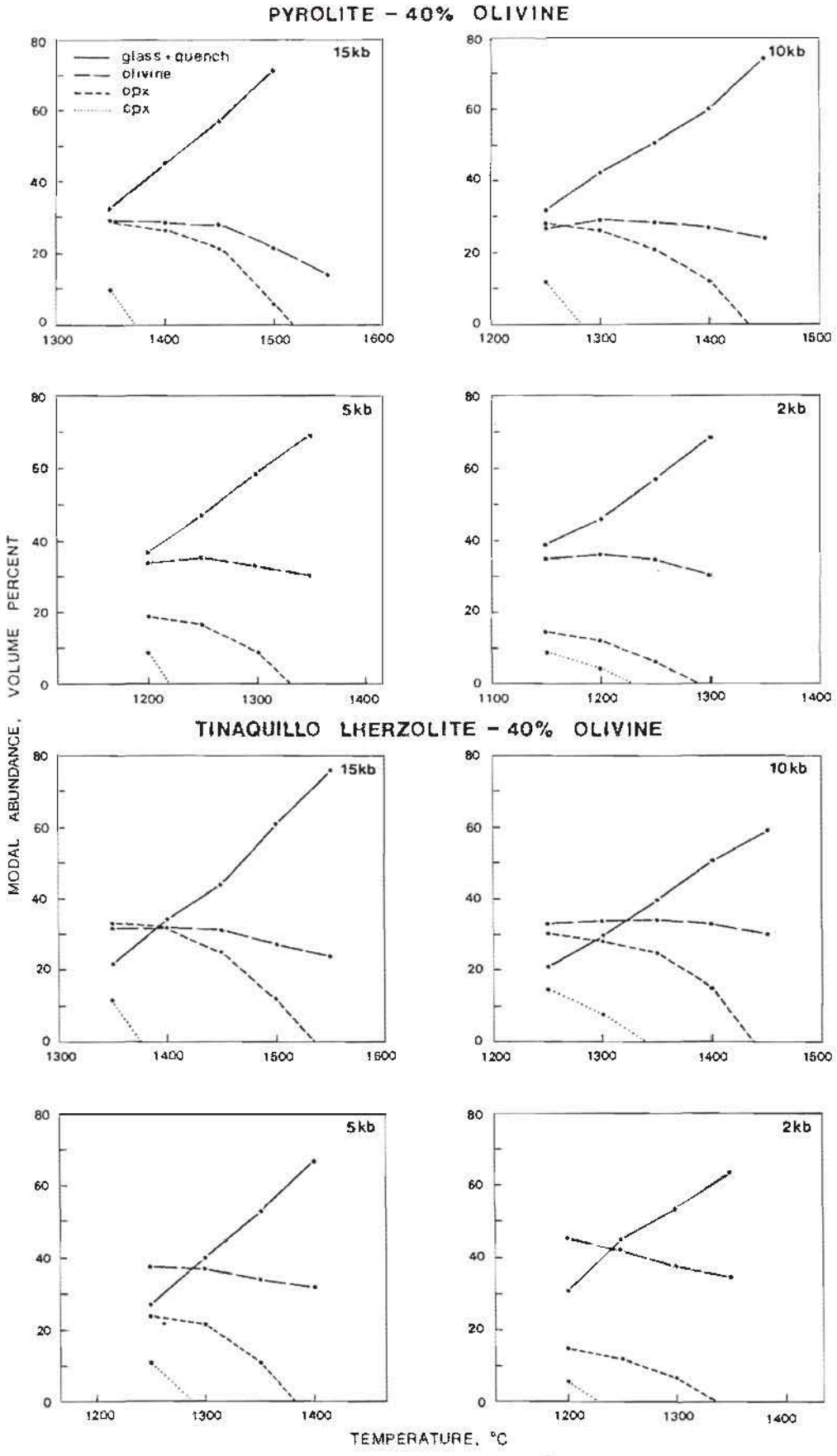

Fig. 3-3. Modal variation (volume %) of run products with temperature. Residual spinel present at 0-1.5% (vol.) is omitted. All quench material counted as melt.

saturated in SiO_2, and become olivine normative at higher pressure (Tables 3-9, 3-10).

Melting experiments have not been carried out in the high degree melting range (> 50% melting) since degrees of partial melting of this order may not be geologically feasible. All our experiments at high degrees of melting ($\geq$ 40%) showed strong crystal settling of olivine in the fluid komatiitic liquid. This observation supports Arndt's (1977a) claim that high degrees (40-80%) of melting of peridotite are unlikely to be attained, because before that degree of melting is reached, a highly fluid picritic-komatiite liquid will segregate from the source peridotite. Green & others (1975b) proposed that peridotitic liquids required unusually rapid rates of diapiric ascent to counter the settling problem, and Arndt (1977a) proposed that peridotitic komatiites result from a process of sequential melting.

CHAPTER 4

COMPOSITIONS OF RESIDUAL PHASES

4-1. Olivine

All runs are oversaturated in olivine. Variation in olivine composition, expressed as changes in $\frac{100Mg}{Mg+Fe}$ with temperature, are shown in Figure 3-4. Olivine adjusts readily to iron loss from the charge and, consequently, where the $K_D^{ol}/_{opx}$ between the analysed olivine and the cores of large orthopyroxene grains show the analysed olivine to be out of equilibrium (i.e. excessively magnesian due to iron loss, as is the case for almost all runs), the equilibrium olivine composition has been calculated using a $K_D^{ol}/_{opx} = 1.1$. Where olivine is the only residual phase, the equilibrium olivine composition has been calculated prior to iron loss, using the analysis of the bulk charge (obtained by rapid reduced area, $\sim$ 250μ, scans) and the original bulk composition.

Olivine $\frac{100Mg}{Mg + Fe}$ ratios progressively increase with temperature (% melting) from less than 88 near the pyrolite solidus to approximately 95 at 15 kb 1550°C ($\sim$ 50% melting) where olivine is the only residual phase. For the Tinaquillo lherzolite composition, residual olivine is more magnesian and $\frac{100Mg}{Mg + Fe}$ ratios range from 90 near the solidus to approximately 95 ($\sim$ 44% melting). Calcium contents for olivine in both peridotites lie in the range 0.2 to 0.4%, and decrease with increasing temperature (% melting).

The rates of adjustment to iron loss from the charge differ for olivine and liquid, or olivine, pyroxene and spinel, and preclude any meaningful examination of Fe-Mg partitioning between phases where iron loss has occurred.

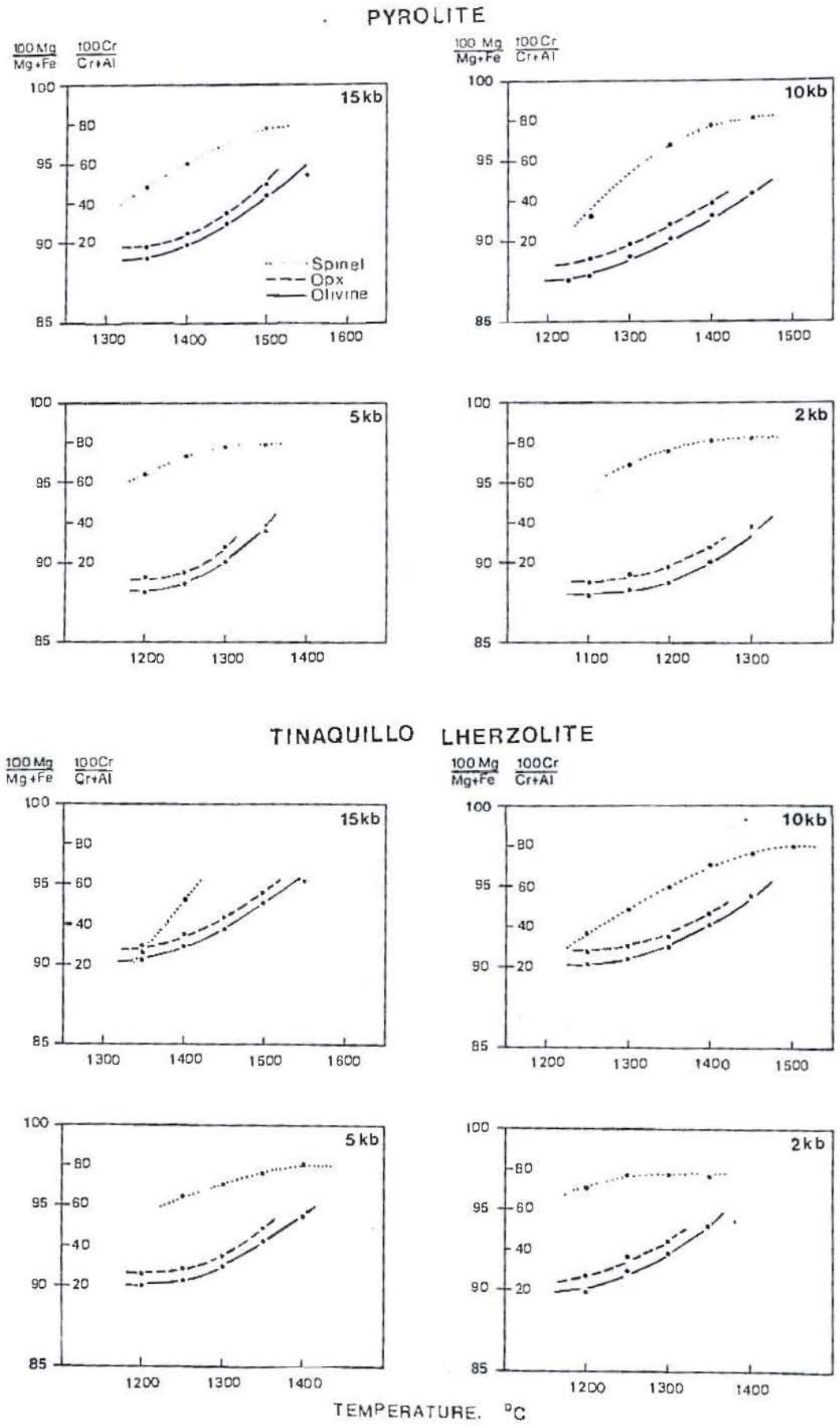

Fig. 3-4. Variation in $\frac{100Mg}{Mg+Fe}$ of olivine and orthopyroxene, and $\frac{100Cr}{Cr+Al}$ of spinel with temperature (see text for derivation of olivine compositions in runs experiencing iron loss).

4-2. Spinel

Spinel analyses are presented in Tables 3-4 and 3-5, and compositional variation, expressed as $\frac{100Cr}{Cr + Al}$ ratios, with temperature shown in Figure 3-4. Variation in spinel composition is dominantly Cr-Al substitution in trivalent cations, and spinels become increasingly chrome-rich with increasing degree of melting until a maximum $\frac{100Cr}{Cr + Al}$ ratio of $\sim$ 80 is reached. Spinels of this composition are highly refractory, containing $\sim$ 55-58 wt % Cr_2O_3, similar to chrome spinels from alpine peridotites and tectonite harzburgite in ophiolites. The $\frac{100Mg}{Mg + Fe}$ ratios increase with increasing temperature, a consequence of increasing degree of melting, and of iron-loss. Compared to chrome spinels from alpine peridotites, ophiolites and stratiform intrusions the experimental spinels are deficient in iron, reflecting both substantial subsolidus re-equilibration of the natural rocks, and, possibly, iron loss from the experimental charge. Calculated Fe^{3+} contents are comparatively high, and may reflect increased f_{O_2} due to the Fe alloying with the Pt capsule.

Chrome spinels near the solidus at low pressure (2-5 kb) are distinctly more chrome-rich than those at higher pressure (10-15 kb). This is consistent with the melting of different subsolidus assemblages of plagioclase + chrome spinel (< 10 kb) and aluminous spinel + aluminous pyroxenes (> 10 kb), and the presence of a plagioclase-field immediately above the solidus at low pressure. The distribution coefficient $K_D = (Al/Cr)_{cpx} / (Al/Cr)_{sp}$ is greater than unity, in accord with experimental data from simple Cr-bearing systems (Dickey & Yoder, 1972) and natural peridotites. The Al_2O_3 content of orthopyroxene shows a direct correlation with the Al_2O_3 of co-existing spinel (Fig. 3-5a), and the $\frac{Cr}{Cr + Al}$ ratios of spinel correlate with the $\frac{Cr}{Cr + Al}$ ratio of co-existing orthopyroxene at constant pressure. Both correlations appear dependent on bulk composition as well as temperature and pressure (Fig. 3-5) as might be

TABLE 3-4. AVERAGE SPINEL ANALYSES PYROLITE

	15 kb			10 kb					5 kb				2 kb			
T°C	1350	1400	1500	1250	1300	1350	1400	1450	1200	1250	1300	1350	1150	1200	1250	1300
TiO_2	1.23	1.18	0.73	1.98	1.13	1.25	1.03	0.65	1.23	1.22	1.03	1.10	2.24	1.10	1.07	1.10
Al_2O_3	25.3	19.3	11.1	22.7	17.4	15.5	10.9	9.04	16.6	12.4	10.2	9.8	14.5	11.5	8.79	8.45
FeO	21.7	18.6	12.0	21.4	19.3	18.5	14.0	12.1	21.2	19.3	18.5	15.4	19.7	17.6	18.0	17.2
MgO	16.3	16.9	17.0	15.4	15.8	16.1	17.2	19.8	15.1	15.2	16.4	16.5	15.0	15.2	16.0	16.5
CaO	0.27	0.50	0.41	0.60	0.56	0.55	0.59	0.15	0.42	0.55	0.63	0.75	0.60	0.41	0.63	0.40
Cr_2O_3	35.2	43.5	58.8	38.5	45.8	48.1	56.3	58.3	45.5	51.3	53.2	56.4	48.0	54.2	55.5	56.4
$\frac{100\ Mg}{Mg + Fe}$	57	62	72	56	59	61	69	75	56	58	61	66	58	61	61	63
$\frac{100\ Cr}{Cr + Al}$	48	60	78	53	64	68	78	81	65	74	78	79	69	76	81	82
$\frac{Cr}{Cr + Al + Fe^{3+}}$	0.42	0.53	0.73	0.47	0.56	0.60	0.70	0.72	0.56	0.65	0.67	0.71	0.61	0.68	0.70	0.72
$\frac{Al}{Cr + Al + Fe^{3+}}$	0.45	0.35	0.21	0.41	0.32	0.28	0.20	0.17	0.31	0.23	0.19	0.18	0.27	0.22	0.17	0.16
$\frac{Fe^{3+}}{Cr + Al + Fe^{3+}}$	0.13	0.12	0.06	0.12	0.12	0.12	0.10	0.11	0.13	0.12	0.14	0.10	0.12	0.10	0.13	0.13
$\frac{100\ Mg}{Mg + Fe}^{2+}$	73	77	80	70	74	75	82	92	91	73	79	79	71	73	77	79

All MnO < 0.15 wt %. Fe^{3+} calculated assuming AB_2O_4 stoichiometry and RO : R_2O_3 = 1 : 1

TABLE 3-5. AVERAGE SPINEL ANALYSES TINAQUILLO LHERZOLITE

	15 kb		10 kb						5 kb				2 kb			
°C	1350	1400	1250	1300	1350	1400	1450	1500	1250	1300	1350	1400	1200	1250	1300	1350
TiO_2	0.25	-	0.25	0.32	0.15	-	-	-	0.18	-	-	-	0.32	0.25		
Al_2O_3	41.3	25.9	37.4	27.0	21.4	14.7	11.9	10.3	18.3	15.4	11.9	10.1	18.4	15.0	12.4	11.0
FeO	13.6	12.5	11.4	14.4	12.8	10.1	9.8	9.60	13.6	11.2	11.7	11.5	13.3	9.66	10.0	10.2
MgO	21.2	19.0	19.6	18.9	18.0	18.3	18.6	19.4	18.6	18.3	18.6	18.4	17.9	18.0	18.5	18.3
CaO	0.36	0.31	0.43	0.53	0.50	0.27	0.27	0.49	0.50	0.60	0.38	0.53	0.55	0.50	0.64	0.58
Cr_2O_3	23.3	42.3	30.9	38.9	47.2	56.6	59.4	60.2	48.8	54.5	57.4	59.5	49.5	56.6	58.4	59.9
$\frac{100\ Mg}{Mg + Fe}$	73	73	75	70	72	76	77	78	71	74	74	74	71	77	77	76
$\frac{100\ Cr}{Cr + Al}$	27	52	36	49	60	72	77	80	64	70	76	80	64	72	76	79
$\frac{Cr}{Cr + Al + Fe^{3+}}$	0.25	0.49	0.34	0.45	0.56	0.68	0.72	0.73	0.58	0.65	0.70	0.73	0.59	0.69	0.71	0.74
$\frac{Al}{Cr + Al + Fe^{3+}}$	0.66	0.44	0.61	0.46	0.38	0.27	0.22	0.19	0.32	0.28	0.22	0.19	0.33	0.27	0.23	0.20
$\frac{Fe^{3+}}{Cr + Al + Fe^{3+}}$	0.09	0.07	0.05	0.09	0.06	0.05	0.06	0.08	0.10	0.07	0.08	0.08	0.08	0.04	0.06	0.06
$\frac{100\ Mg}{Mg + Fe^{2+}}$	87	83	82	83	81	84	86	91	85	85	87	87	82	83	87	86

All MnO < 0.15 wt %. Fe^{3+} calculated assuming AB_2O_4 stoichiometry and RO : R_2O_3 = 1:1.

expected if Cr-Al substitution in spinel is non-ideal (Wood & Nicholls, 1978). As for clinopyroxene, the $K_D^{Al-Cr}_{opx-spinel}$ is greater than unity indicating that Cr is preferentially partitioned into spinel; the K_D's at low pressure are higher than at higher pressure.

4-3. Orthopyroxene

Representative orthopyroxene analyses are presented in Tables 3-6 and 3-7. The $\frac{100Mg}{Mg + Fe}$ ratios of large orthopyroxene grains (Fig. 3-4) increase with temperature (% melting) from about $\frac{100Mg}{Mg + Fe} = 89$ near the pyrolite solidus to 93-94 at the orthopyroxene-out curve. Orthopyroxene from the melting of Tinaquillo lherzolite is slightly more refractory, with $\frac{100Mg}{Mg + Fe}$ ratios of 91-94. Orthopyroxene grains are commonly zoned, with rims which are 1-2 mol % more magnesian, due to iron loss. Al_2O_3 and CaO contents decrease with increasing temperature, and compositions near the orthopyroxene-out curve have very low CaO and Al_2O_3 contents (1-2%). The linear decrease of Al_2O_3 in orthopyroxene with increasing temperature (Fig. 3-5b,c) is further evidence that melting is a continuous process, and that melting is dominated by solid solution behaviour rather than eutectic behaviour. Alumina contents in orthopyroxene are higher at higher (10 to 15 kb) pressure for similar degrees of melting, and co-existing liquids (Tables 3-9, 3-10) are lower in Al_2O_3. The data imply that Al_2O_3 solubility in pyroxene increases with pressure over this pressure range. The solubility of Al_2O_3 in orthopyroxene in spinel peridotite and plagioclase peridotite is at present in dispute (cf. MacGregor, 1974; Obata, 1976; Presnall, 1976). Stroh (1976) has shown that the addition of Fe and Cr to the simple system $MgO - SiO_2 - Al_2O_3$ markedly affects the activities of phases at equilibrium. Because of the complexity of interplay of pressure and temperature, varying % melting, liquid composition and spinel composition, the data is not analysed further in terms of mineral equilibria or P, T dependence of Al_2O_3

TABLE 3-6. SELECTED ORTHOPYROXENE ANALYSES - PYROLITE

P	15 kb				10 kb				5 kb			2 kb			
T°C	1350	1400	1450	1500	1250	1300	1350	1400	1200	1250	1300	1100	1150	1200	1250
SiO_2	54.8	55.4	56.2	56.4	54.5	55.3	55.8	56.8	55.8	56.4	56.9	55.7	56.1	56.6	57.2
TiO_2	0.33	0.37	0.30	0.23	0.58	0.42	0.32	0.22	0.48	0.29	0.20	0.65	0.55	0.37	0.18
Al_2O_3	3.93	2.67	1.76	1.57	3.76	2.72	2.10	0.98	2.25	1.47	0.79	1.89	1.49	0.89	0.65
FeO	6.25	5.97	5.22	4.12	6.81	6.38	5.80	5.06	6.85	6.69	5.84	7.10	6.83	6.64	5.94
MgO	30.8	32.0	33.5	34.9	30.6	31.5	32.9	34.3	31.5	32.5	33.7	31.7	31.9	32.3	33.8
CaO	2.76	2.10	1.46	0.99	2.62	2.42	1.58	1.19	2.35	1.68	1.44	2.46	2.50	2.41	1.43
Cr_2O_3	1.15	1.42	1.58	1.74	1.17	1.30	1.42	1.48	0.65	0.98	1.05	0.45	0.58	0.66	0.82
O = 6															
Si	1.907	1.925	1.941	1.939	1.901	1.924	1.935	1.958	1.944	1.958	1.969	1.942	1.954	1.970	1.977
Al	0.093	0.075	0.059	0.061	0.099	0.076	0.065	0.040	0.056	0.042	0.031	0.058	0.046	0.030	0.023
Al	0.068	0.034	0.013	0.003	0.056	0.036	0.023	-	0.036	0.018	0.001	0.020	0.015	0.007	0.003
Ti	0.009	0.010	0.008	0.006	0.015	0.011	0.008	0.006	0.013	0.008	0.005	0.017	0.014	0.010	0.005
Fe	0.182	0.174	0.151	0.118	0.199	0.186	0.168	0.146	0.200	0.194	0.169	0.207	0.199	0.193	0.172
Mg	1.598	1.657	1.725	1.788	1.591	1.633	1.700	1.762	1.635	1.682	1.738	1.647	1.656	1.675	1.740
Ca	0.103	0.078	0.054	0.037	0.098	0.090	0.059	0.044	0.088	0.062	0.053	0.092	0.093	0.090	0.053
Cr	0.032	0.040	0.043	0.047	0.032	0.036	0.039	0.040	0.018	0.027	0.029	0.012	0.016	0.018	0.022
Total	3.990	3.992	3.993	3.999	3.991	3.991	3.995	3.996	3.989	3.991	3.995	3.996	3.993	3.994	3.995
100 Mg/Mg+Fe	89.8	90.5	92.0	93.8	88.9	89.8	91.0	92.4	89.1	89.6	91.1	88.8	89.3	89.7	91.0
Ca	5.5	4.1	2.8	1.9	5.2	4.7	3.0	2.3	4.5	3.2	2.7	4.7	4.8	4.5	2.7
Mg	84.9	86.8	89.4	92.0	84.3	85.6	88.2	90.2	85.1	86.8	88.7	84.7	85.0	85.6	88.5
Fe	9.7	9.1	7.8	6.1	10.5	9.7	8.8	7.5	10.4	10.0	8.6	10.6	10.2	9.9	8.8

All MnO < 0.15 wt %, Na_2O < 0.2 wt %

TABLE 3-7. SELECTED ORTHOPYROXENE ANALYSES - TINAQUILLO LHERZOLITE

P	15kb				10kb				5kb				2kb		
T^oC	1350	1400	1450	1500	1250	1300	1350	1400	1200	1250	1300	1350	1200	1250	1300
SiO_2	55.0	55.5	56.1	56.9	54.8	55.0	55.8	56.9	55.6	56.3	56.8	57.3	57.1	57.6	57.7
TiO_2	0.10	-	-	-	0.17	0.15	-	-	0.15	0.12	-	-	-	-	-
Al_2O_3	4.29	3.33	2.19	1.68	4.40	3.55	2.78	1.07	2.44	1.49	1.36	0.94	0.91	0.66	0.53
FeO	5.45	5.08	4.66	3.72	5.58	5.40	5.14	4.40	5.86	5.77	5.24	4.35	5.88	5.21	4.70
MgO	31.4	32.4	34.0	35.2	31.4	31.8	32.8	34.9	32.1	32.7	33.1	35.1	32.9	34.0	35.0
CaO	2.71	2.41	1.68	1.12	2.46	2.64	2.01	1.16	2.80	2.67	2.59	1.23	2.55	1.72	1.19
Cr_2O_3	1.11	1.28	1.35	1.39	1.19	1.34	1.45	1.55	0.89	0.94	0.95	1.08	0.64	0.86	0.86
O = 6															
Si	1.904	1.919	1.934	1.949	1.899	1.909	1.929	1.956	1.934	1.953	1.963	1.967	1.977	1.983	1.981
Al	0.096	0.081	0.066	0.051	0.101	0.091	0.071	0.043	0.066	0.047	0.037	0.033	0.023	0.017	0.019
Al	0.079	0.055	0.023	0.017	0.079	0.054	0.032	-	0.034	0.014	0.018	0.005	0.014	0.010	0.002
Ti	0.003	-	-	-	0.004	0.004	-	-	0.004	0.003	-	-	0.003	-	-
Fe	0.158	0.147	0.134	0.107	0.162	0.157	0.149	0.127	0.170	0.167	0.151	0.125	0.170	0.150	0.135
Mg	1.620	1.670	1.747	1.797	1.622	1.645	1.690	1.791	1.664	1.691	1.705	1.795	1.698	1.745	1.791
Ca	0.101	0.089	0.062	0.041	0.092	0.098	0.074	0.043	0.104	0.099	0.096	0.045	0.095	0.063	0.044
Cr	0.030	0.035	0.037	0.038	0.033	0.037	0.040	0.042	0.024	0.026	0.026	0.029	0.018	0.023	0.023
Total	3.991	3.996	4.003	3.999	3.991	3.996	3.995	4.002	4.000	4.000	3.996	4.000	3.995	3.991	3.996
100 Mg/Mg+Fe	91.1	91.9	92.9	94.4	90.9	91.3	91.9	93.4	90.7	91.0	91.9	93.5	90.9	92.1	93.0
Ca	5.4	4.7	3.2	2.1	4.9	5.2	3.9	2.2	5.4	5.1	4.9	2.3	4.8	3.2	2.2
Mg	86.2	87.6	89.9	92.4	86.5	86.5	88.3	91.4	85.8	86.4	87.3	91.3	86.5	89.1	90.9
Fe	8.4	7.7	6.9	5.5	8.6	8.3	7.8	6.4	8.8	8.5	7.8	6.4	8.7	7.7	6.9

All Mn < 0.15 wt %, Na_2O < 0.2 wt %

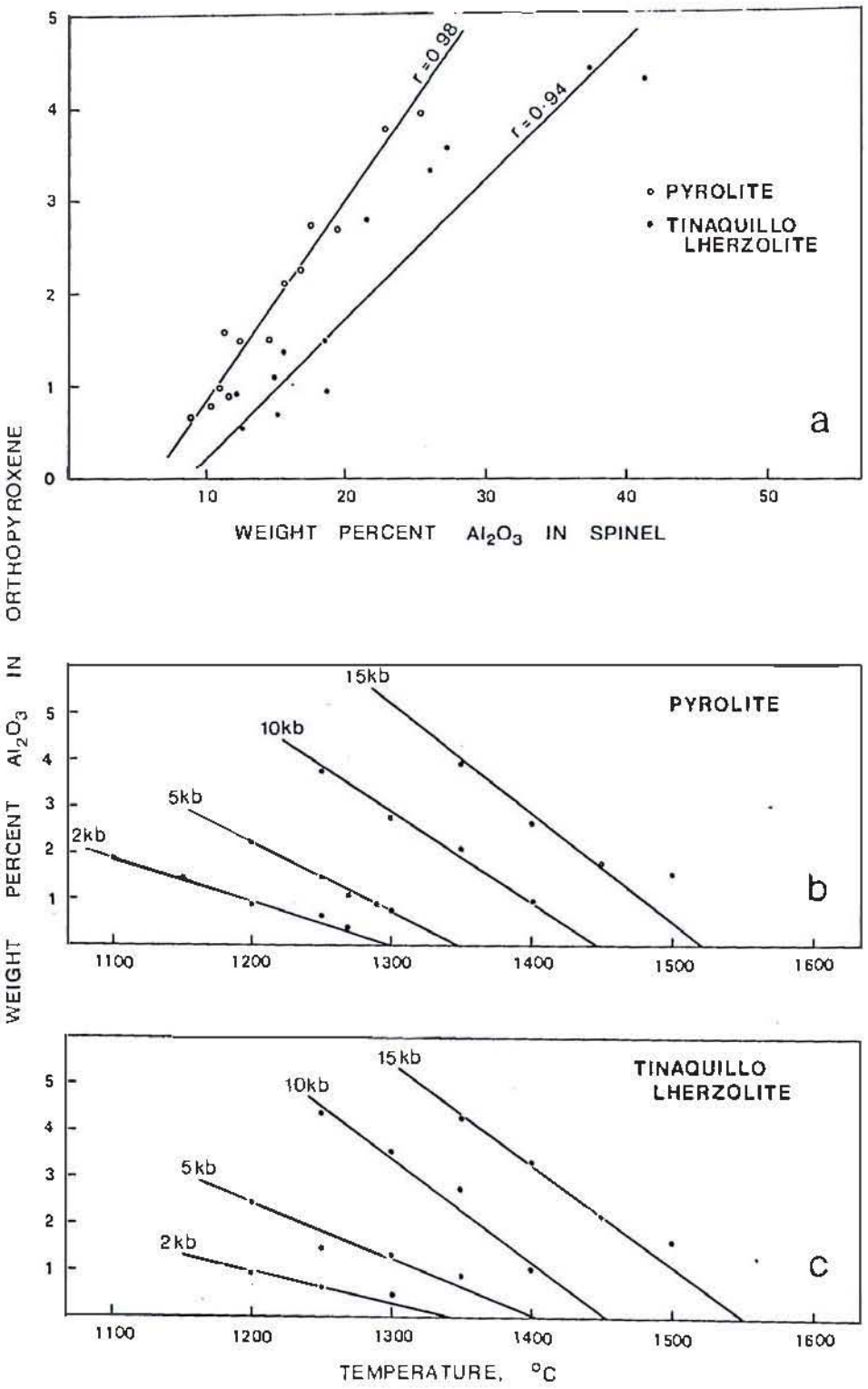

Fig. 3-5a. Variation in Al_2O_3 in spinel with Al_2O_3 in orthopyroxene.

b,c. Variation in Al_2O_3 in orthopyroxene with temperature.

Stars are for melting of pyrolite + 0.3 wt % H_2O

(D.H. Green, unpubl.)

solubility in phases. The data in Tables 3-6 and 3-7 indicate a strong site preference of Al for the tetrahedral position and that this preference increases with temperature. Chromium contents and $\frac{100Cr}{Cr + Al}$ ratios increase with temperature (% melting). Orthopyroxene at 2 and 5 kb has noticeably lower chromium contents than those at 10 and 15 kb, and co-exists with more chromium-rich spinel.

4-4. Clinopyroxene

Selected clinopyroxene compositions are presented in Table 3-8 and plotted in the relevant pyroxene quadrilateral in Figure 3-6. The clinopyroxenes are of diopsidic composition, have low jadeite component, and comparatively low calcium contents. As for orthopyroxene, Al_2O_3 contents are greater at higher pressure for similar degrees of melting and decrease with increasing temperature (decreasing Al_2O_3 content of liquid). Cr_2O_3 contents and $\frac{100Cr}{Cr + Al}$ ratios increase with increasing temperature and, as for orthopyroxene, Cr_2O_3 contents are higher at higher pressure (10-15 kb) for similar degrees of melting reflecting changes in the Cr/Al partitioning between spinel and pyroxene with increasing pressure.

Clinopyroxenes analysed within a single run exhibited a range of CaO contents, especially at low pressure: analyses presented in Table 3-8 are the more calcic examples of the range. The compositions of the residual clinopyroxenes need to be critically examined, particularly in view of the fact that clinopyroxene co-existing with orthopyroxene on anhydrous liquidi are commonly highly subcalcic (e.g. Green & Ringwood, 1967a). More importantly, Green (1976c) has demonstrated the experimental difficulties which exist in the nucleation and growth of subcalcic 'pigeonitic' pyroxenes. Previous studies have shown that the pyroxene miscibility gap narrows, and the field of Ca-poor clinopyroxene contracts towards the En - Di join, with increasing pressure (e.g. Mori, 1978; Hensen, 1973). However, data available at low pressure are mostly

TABLE 3-8. SELECTED CLINOPYROXENE ANALYSES

	Pyrolite						Tinaquillo			
P kb	15	10	5	2	2	2	15	10	10	5
T°c	1350	1250	1200	1100	1150	1200	1350	1250	1300	1250
SiO_2	52.5	52.3	52.5	52.7	54.2	54.2	52.8	52.4	53.4	53.2
TiO_2	0.80	0.90	1.03	1.05	0.72	0.63	0.23	0.27	0.12	0.18
Al_2O_3	4.85	4.40	4.02	3.42	2.14	1.68	4.89	5.11	4.48	4.18
FeO	5.09	4.99	5.13	5.35	5.19	5.10	3.65	4.38	4.29	5.42
MgO	20.5	20.1	20.5	21.2	23.1	24.5	21.5	22.6	24.2	24.6
CaO	14.3	15.9	15.3	15.7	13.9	12.7	15.1	13.4	11.7	11.6
Na_2O	0.55	0.30	0.43	-	-	-	0.40	0.30	0.22	-
Cr_2O_3	1.42	1.15	1.11	0.58	0.75	1.17	1.40	1.52	1.58	0.82
O = 6										
Si	1.885	1.884	1.890	1.898	1.938	1.935	1.887	1.871	1.894	1.893
Al	0.125	0.116	0.110	0.112	0.062	0.065	0.113	0.129	0.106	0.107
Al	0.081	0.071	0.061	0.033	0.028	0.006	0.093	0.086	0.081	0.068
Ti	0.022	0.024	0.028	0.028	0.019	0.017	0.006	0.007	0.003	0.005
Fe	0.153	0.150	0.154	0.161	0.155	0.152	0.109	0.131	0.128	0.161
Mg	1.097	1.079	1.100	1.138	1.231	1.303	1.145	1.203	1.279	1.304
Ca	0.550	0.614	0.590	0.606	0.533	0.486	0.578	0.513	0.445	0.442
Na	0.038	0.021	0.030	-	-	-	0.028	0.021	0.015	-
Cr	0.040	0.033	0.032	0.017	0.021	0.033	0.040	0.043	0.044	0.023
Total	3.991	3.992	3.996	3.993	3.987	3.997	3.998	4.003	3.995	4.003
100 Mg/Mg+Fe	87.8	87.8	87.7	87.6	88.8	89.5	91.3	90.2	90.9	89.0
Ca	30.6	33.3	32.0	31.8	27.8	25.0	31.6	27.8	24.0	23.2
Mg	60.9	58.5	59.6	59.7	64.2	67.1	62.5	65.1	69.1	68.4
Fe	8.5	8.2	8.4	8.5	8.1	7.8	6.0	7.1	6.9	8.5

All MnO < 0.15 wt %

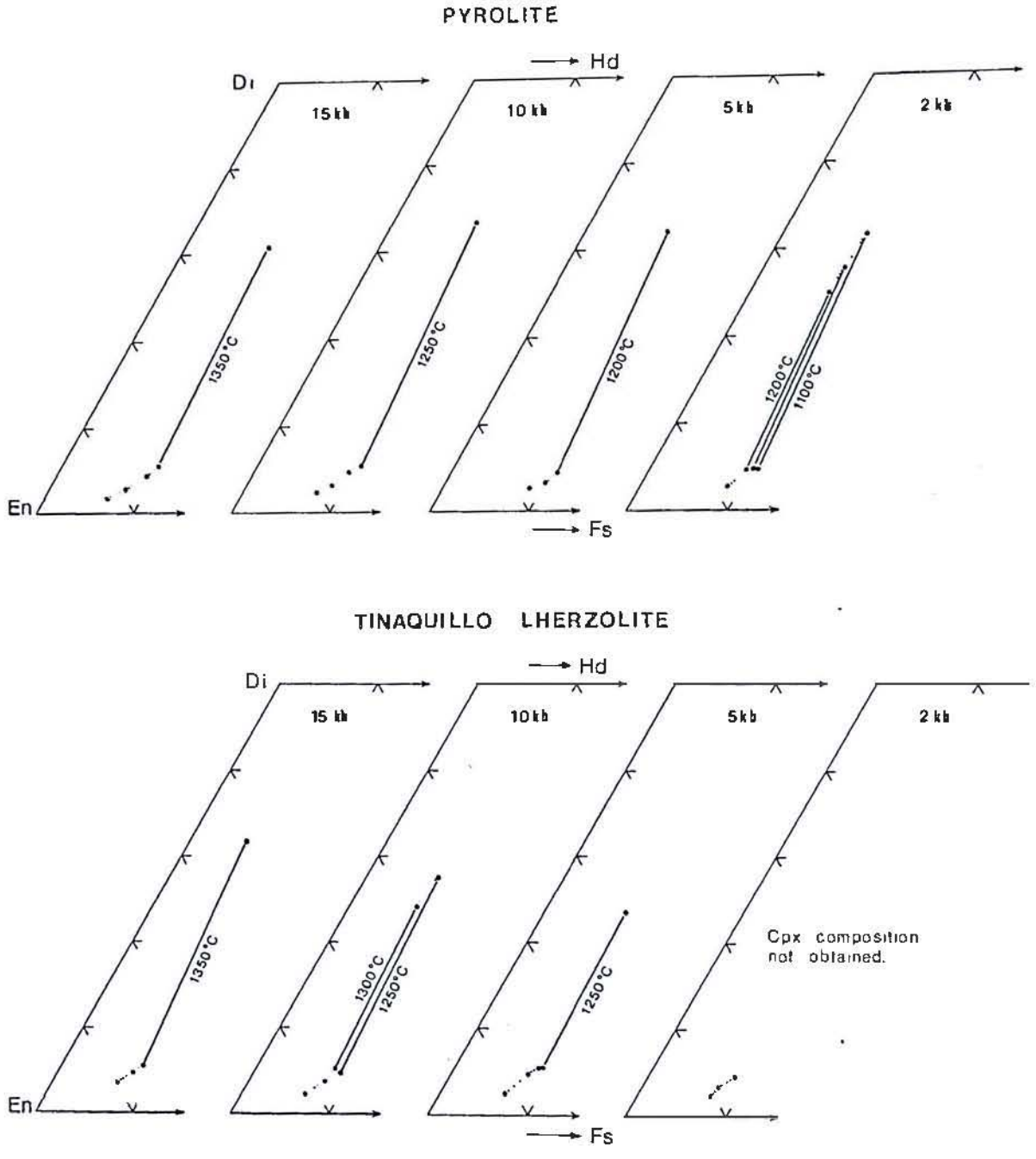

Fig. 3-6. Pyroxene quadrilateral showing compositions of residual pyroxenes.

restricted to the En - Di and Fs - Hd joins (see Mori, 1978 for summary), and only in a few cases have experiments been reversed. Compared to the solvus defined by pyroxenes that have crystallized from basaltic magmas (e.g. Atkins, 1969; Wager & Brown, 1968; Hodges & Papike, 1976), the residual clinopyroxenes examined here are decidedly less calcic. Comparison with experimental data shows that residual clinopyroxenes at 15 kb 1350°C (Table 3-8) lie within the 15 kb 1200°C solvus of Mori (1978) in the Ca-Mg-Fe-SiO_2 system, and both residual pyroxenes are in reasonable agreement (Ca-px slightly less calcic) with the En - Di solvus defined by Lindsley & Dixon (1976). Residual clinopyroxenes at low pressure are less calcic than those defined in En - Di exsolution and dissolution experiments under similar P, T conditions (Warner & Luth, 1974; Mori & Green, 1975; Lindsley & Dixon, 1976).

However, a lack of data in Fe-bearing systems means that the composition of clinopyroxene co-existing with orthopyroxene at high temperature under anhydrous conditions and 0 - 10 kb pressure range is not adequately constrained. Given this uncertainty, we have tentatively accepted the compositions of the most calcic, low alumina clinopyroxenes in our experiments as equilibrium compositions. The possibility that the equilibrium residual clinopyroxene is more calcic does not greatly affect our calculations of the equilibrium liquid compositions if we can assume that the modal abundance of a more calcic pyroxene would be less than that of a less calcic clinopyroxene, i.e. that chemical equilibrium obtains for Ca-Mg-Fe partitioning between the liquid and the total residual pyroxene components regardless of their appearance as orthopyroxene, subcalcic or calcic clinopyroxene. This assumption appears reasonable for Ca-Mg-Fe, but is unlikely to hold for elements such as Al, Ti, Na and Cr, whose partitioning into pyroxene as minor components is likely to be strongly influenced by the nature of the pyroxene.

Clinopyroxene contains more Al than orthopyroxene, in accord with observations on natural co-existing pyroxenes. Mysen & Boettcher (1975) showed that the Cr-Al partitioning between orthopyroxene and clinopyroxene was temperature dependent, and derived an equation for use as a geothermometer. Application of this geothermometer to our data (excluding the 2 kb runs) for co-existing pyroxenes generally gave temperature estimates lower (up to 200°C for the 1350°C runs) than the run conditions, although good agreement was obtained for the 5 and 10 kb pyrolite data. However, our experiments were conducted at considerably higher temperatures than the range considered by Mysen & Boettcher (1975), and it is notable that their data showed departures from their line of best fit at temperatures above 1100°C.

CHAPTER 5

EQUILIBRIUM MELT COMPOSITIONS

The compositions of equilibrium partial melts for each P and T studied have been calculated by mass balance using the data on phase compositions and proportions. These liquid compositions and their CIPW norms are presented in Table 3-9 and 3-10. The basaltic liquids are classified on a normative basis following Green & Ringwood (1967a). Some of the liquids are of komatiitic composition; the terms peridotitic, pyroxenitic and basaltic have been used in a broad sense only since opinion differs as to the classification criteria of magmas of the komatiite suite.

5-1. Pyrolite

At 15 kb liquid compositions range from olivine basalt ($mg \sim 67$ i.e. $\frac{100Mg}{Mg+\Sigma Fe}$) at 18% melting with residual olivine, orthopyroxene, clinopyroxene and spinel to olivine tholeiite ($mg \sim 70$-75) with residual olivine, orthopyroxene and chrome spinel (20 - 30% melting) to tholeiitic picrite to komatiite ($mg \sim 80$) at 40 - 50% melting in equilibrium with residual olivine.

Liquids at 10 kb range from olivine basalt (16% melting) with residual olivine, orthopyroxene, clinopyroxene and spinel through olivine tholeiite (residual olivine, orthopyroxene and chrome spinel) to pyroxene-rich komatiite at 44% melting leaving residual olivine and chrome spinel. Compared to the partial melts at 15 kb, liquids at 10 kb are more aluminous and have a higher *hy/ol* ratio.

Partial melts at low pressure - 5 and 2 kb - are distinctly more silica saturated than those at high pressure, due to expansion of the primary field of olivine into quartz-normative basaltic compositions at the expense of orthopyroxene (as shown by the decrease in modal abundance

TABLE 3-9. CALCULATED EQUILIBRIUM MELT COMPOSITIONS - PYROLITE

P kb	15	15	15	15	15	10	10	10	10	10	5	5	5	5	2	2	2	2
T°c	1350	1400	1450	1500	1550	1250	1300	1350	1400	1450	1200	1250	1300	1350	1150	1200	1250	1300
% melt of Pyrolite	18	25	32	41	51	16	23	28	35	44	20	25	31	38	21	24	31	39
SiO_2	49.0	49.3	50.0	50.5	49.6	49.7	49.8	50.3	50.6	51.2	52.1	52.4	52.6	52.8	52.8	53.0	53.3	52.5
TiO_2	3.2	2.5	2.1	1.7	1.4	3.2	2.7	2.3	1.9	1.6	3.0	2.6	2.3	1.8	2.8	2.6	2.2	1.8
Al_2O_3	12.9	11.7	10.3	8.3	7.0	14.5	12.5	11.3	9.6	8.0	14.9	13.2	11.3	9.1	15.1	13.5	11.0	8.9
Fe_2O_3	0.7	0.5	0.4	0.3	0.2	0.7	0.5	0.4	0.3	0.3	0.6	0.5	0.4	0.3	0.6	0.5	0.4	0.3
FeO	9.5	9.1	9.6	9.7	9.3	8.2	8.5	8.9	9.5	9.2	7.3	7.1	8.4	8.9	7.2	7.3	8.1	9.0
MnO	0.1	0.2	0.2	0.1	0.1	0.2	0.1	0.1	0.1	0.1	0.1	0.1	0.1	0.2	0.1	0.1	0.1	0.1
MgO	11.6	13.2	16.0	20.3	24.9	10.2	12.0	13.9	17.6	21.0	8.9	9.9	12.9	17.2	8.7	10.5	13.3	17.9
CaO	9.1	10.7	9.2	7.4	6.1	9.1	10.9	10.1	8.3	7.0	9.5	11.4	9.7	7.9	9.4	9.7	9.4	7.7
Na_2O	3.1	2.3	1.8	1.4	1.1	3.3	2.4	2.0	1.6	1.3	2.8	2.3	1.9	1.5	2.7	2.3	1.8	1.5
K_2O	0.7	0.5	0.4	0.3	0.3	0.8	0.6	0.5	0.4	0.3	0.6	0.5	0.4	0.3	0.6	0.5	0.4	0.3
CIPW Norm																		
Qt_3	-	-	-	-	-	-	-	-	-	-	0.8	1.1	0.7	-	2.2	2.3	2.0	-
Or	4.1	3.0	2.4	1.8	1.8	4.7	3.6	3.0	2.4	1.8	3.6	3.0	2.4	1.8	3.6	3.0	2.4	1.8
Ab	26.2	19.5	15.2	11.9	9.3	27.9	20.3	16.9	13.5	11.0	23.7	19.5	16.1	12.7	22.9	19.5	15.2	12.7
An	19.2	20.1	18.8	15.5	13.3	22.4	21.6	20.4	17.8	15.1	26.3	24.2	21.1	17.2	27.3	25.0	20.8	16.7
Di	20.9	26.5	21.5	17.0	13.5	18.3	26.1	23.9	18.7	15.7	16.7	25.9	21.7	17.6	15.5	18.5	20.7	17.2
Hy	1.1	7.3	21.8	32.4	31.3	2.5	8.3	19.2	29.0	37.9	22.1	20.6	33.0	44.5	22.3	26.0	34.1	42.7
Ol	21.1	18.1	15.6	17.8	27.8	16.8	14.3	11.7	14.3	15.0	-	-	-	2.2	-	-	-	5.0
Mt	1.1	0.7	0.6	0.4	0.3	1.0	0.7	0.6	0.4	0.4	0.9	0.7	0.6	0.4	0.9	0.7	0.6	0.4
Il	6.1	4.8	4.0	3.2	2.7	6.1	5.1	4.4	3.6	3.0	5.7	4.9	4.4	3.4	5.3	4.9	4.2	3.4
100 $Mg/Mg+Fe^{++}$	68	72	75	79	83	69	72	74	77	80	68	71	73	77	69	72	75	78
100 Mg/Mg+Fe	67	71	74	79	82	67	70	73	76	80	67	70	72	77	67	71	74	78

TABLE 3-10. CALCULATED EQUILIBRIUM MELT COMPOSITIONS - TINAQUILLO LHERZOLITE

P kb	15	15	15	15	15	10	10	10	10	10	5	5	5	5	2	2	2	2
T°c	1350	1400	1450	1500	1550	1250	1300	1350	1400	1450	1250	1300	1350	1400	1200	1250	1300	1350
% melt of Tinaquillo lherzolite	11%	18%	25	34	44	11	15	21	29	40	14	21	29	39	17	24	29	36
SiO_2	47.3	48.0	48.4	49.6	50.4	47.9	49.0	50.2	50.5	51.6	50.3	51.4	51.5	51.8	54.0	53.6	53.3	52.9
TiO_2	0.5	0.4	0.3	0.2	0.2	0.2	0.3	0.3	0.2	0.2	0.3	0.3	0.2	0.20	0.4	0.3	0.3	0.2
Al_2O_3	14.8	12.8	11.8	9.2	7.3	15.7	14.8	12.5	10.5	7.8	18.4	13.9	10.4	8.5	17.2	12.7	10.8	8.7
Fe_2O_3	0.8	0.5	0.4	0.3	0.2	0.8	0.6	0.4	0.3	0.2	0.6	0.4	0.3	0.2	0.6	0.4	0.3	0.2
FeO	9.2	8.4	9.0	9.0	8.3	8.5	7.6	7.6	8.6	8.2	6.1	7.3	8.4	8.3	4.6	6.9	7.7	8.2
MnO	0.3	0.2	0.2	0.2	0.1	0.3	0.2	0.2	0.1	0.2	0.1	0.1	0.1	0.1	0.1	0.1	0.1	0.2
MgO	14.6	15.4	16.1	22.4	26.3	13.3	13.7	15.5	19.2	23.9	10.3	13.5	18.6	22.9	9.0	13.6	16.9	20.8
CaO	11.0	13.2	11.0	8.5	6.7	11.8	12.6	12.3	9.9	7.4	12.5	12.1	9.8	7.5	12.9	11.5	9.9	8.2
Na_2O	1.3	1.0	0.7	0.5	0.4	1.3	1.1	0.9	0.6	0.5	1.3	0.9	0.6	0.5	1.1	0.8	0.6	0.5
K_2O	0.2	0.1	0.07	0.05	0.04	0.2	0.1	0.09	0.06	0.04	0.1	0.09	0.06	0.05	0.1	0.07	0.06	0.05
CIPW Norm																		
Qt_3	-	-	-	-	-	-	-	-	-	-	-	-	-	-	7.7	4.0	1.9	-
Or	1.2	0.6	0.4	0.3	0.2	1.2	0.6	0.5	0.4	0.2	0.6	0.5	0.4	0.3	0.6	0.4	0.4	0.3
Ab	11.0	8.5	5.9	4.2	3.4	11.0	9.3	7.6	5.1	4.2	11.0	7.6	5.1	4.2	9.3	6.8	5.1	4.2
An	34.0	30.1	28.9	22.7	18.0	36.4	35.2	29.8	25.8	18.9	44.1	33.6	25.5	20.8	41.7	30.9	26.6	21.4
Ne	-	-	-	-	-	-	-	-	-	-	-	-	-	-	-	-	-	-
Di	16.6	28.4	20.6	15.5	12.1	17.9	22.0	25.0	18.7	14.2	14.4	21.0	18.5	13.1	17.9	21.0	18.0	15.4
Hy	11.7	9.3	22.1	35.5	42.8	12.4	17.9	25.3	36.6	47.3	26.9	35.1	42.7	49.1	21.2	35.6	46.9	54.7
Ol	23.2	21.5	20.7	20.6	22.6	19.3	13.4	10.4	12.6	14.4	1.4	0.7	6.9	11.8	-	-	-	3.1
Mt	1.2	0.7	0.6	0.4	0.3	1.2	0.9	0.6	0.4	0.3	0.9	0.6	0.4	0.3	0.9	0.6	0.4	0.3
Il	1.0	0.8	0.6	0.4	0.4	0.4	0.6	0.6	0.4	0.4	0.6	0.6	0.4	0.4	0.8	0.6	0.6	0.4
100 Mg/Mg + Fe^{++}	74	77	78	83	85	74	76	78	80	84	75	77	80	83	78	78	80	82
100 Mg/Mg + Fe	73	76	78	82	85	72	75	78	80	84	73	76	79	83	76	77	79	82

of residual orthopyroxene relative to that at higher pressure). Liquids range from quartz tholeiite to pyroxenitic komatiite at higher degrees of partial melting. Quartz tholeiites produced by lower degrees of partial melting have considerably higher abundances of Al_2O_3 and incompatible elements than those produced by large degrees of melting. Melts at low pressure are also distinctly more aluminous for similar degrees of partial melting than those at high pressure where the co-existing residual pyroxenes are aluminous (cf. Green & Ringwood, 1967a).

Variation of oxide percentages with percent melting for each pressure are shown in Fig. 3-7. Silica contents and the degree of silica saturation (at 10 kb and 15 kb) increase with increasing degree of melting to a maximum at, or near, the orthopyroxene-out boundary, then decrease as the liquid becomes more magnesian by melting of residual olivine. MgO contents increase sharply as the residue becomes more refractory at higher degrees of melting. Al_2O_3 contents decrease regularly with increasing degree of melting as do Ti, Na and K, which are readily partitioned into the melt. CaO contents increase as the liquid moves with increasing degree of melting from the olivine - two pyroxene residue field to the olivine-orthopyroxene field, but then decrease, following the elimination of calcic clinopyroxene as a residual phase. The Al_2O_3/CaO ratio, therefore, changes with percent partial melting: at low degrees of partial melting (olivine, orthopyroxene and clinopyroxene in the residue) the Al_2O_3/CaO ratio is higher than that of the source peridotite, whereas at high degrees of melting (olivine or olivine + minor orthopyroxene residual) the Al_2O_3/CaO ratio of the liquid is constant and closely matches that of the source peridotite. Similarly, the Al_2O_3/TiO_2 and CaO/TiO_2 ratios increase with increasing degree of partial melting until the ratio of the source peridotite is reached, as predicted by Sun & Nesbitt (1977). For pyrolite, the Al_2O_3/TiO_2 ratios range from 4 to 5, and CaO/TiO_2 ratios from 3 to 4, and are generally lower than commonly

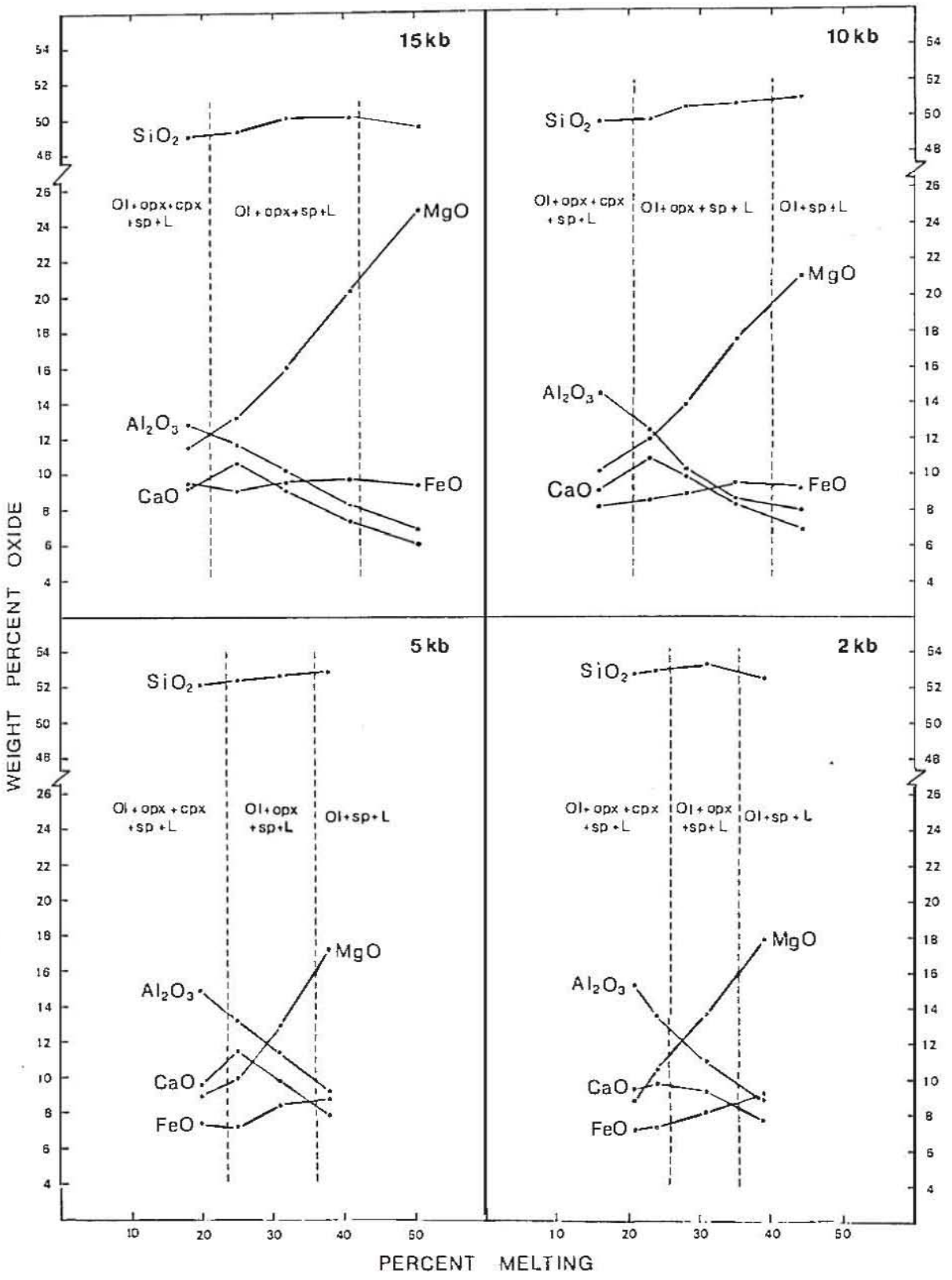

Fig. 3-7. Chemical trends of pyrolite equilibrium liquids with percentage melting. Note 'percent melting' refers to pyrolite, not pyrolite - 40% olivine composition.

observed in 'primitive' magmas from either oceanic island or ocean floor tholeiites, reflecting the high TiO_2 content of the pyrolite composition based on Hawaiian tholeiite.

Partial melting trends are well illustrated on the normative (Jadeite + Tschermak's silicate) - Quartz - Olivine diagram (Green, 1970) which approximates a plane at ∿ 20% diopside parallel to the base of the "Basalt Tetrahedron' (Qz - Fo - Ne - Di). The equilibrium partial melts (data plotted in molecular norms) define curvilinear melting paths (Fig. 3-8a) which show an initial trend towards increasingly hypersthene-normative compositions due to progressive melting of pyroxene from the residue. Liquids formed by high degrees of melting lie on an olivine control line since olivine is the only residual phase. The melting trends clearly demonstrate the increasingly olivine-normative nature of partial melts at high pressure (i.e. 10 kb liquids are more *hy*-normative than those at 15 kb) and show the extension of partial melts at low pressure into the quartz-normative field.

It is clear from the trends that liquids derived by lower degrees of partial melting at high pressure will cross the critical plane of silica undersaturation to alkaline compositions. This accords with previous studies which suggested that alkali olivine basalt could be derived by approximately 10 to 15% melting of pyrolite at pressures greater than 10 kb (Green & Ringwood, 1967a; Green, 1970, 1971). Experimental studies on melting of pyrolite and basaltic compositions have also shown that increasingly undersaturated compositions (olivine basanite to olivine nephelinite and melilitite) result from even lower degrees of melting at high pressures where olivine, orthopyroxene, clino-pyroxene, and garnet (± phlogopite) are residual phases, and demonstrate the importance of H_2O and CO_2 in the genesis of highly undersaturated basalts (Bultitude & Green, 1968; Green, 1970, 1971, 1973a, b; Brey & Green, 1975; Eggler, 1974, 1978).

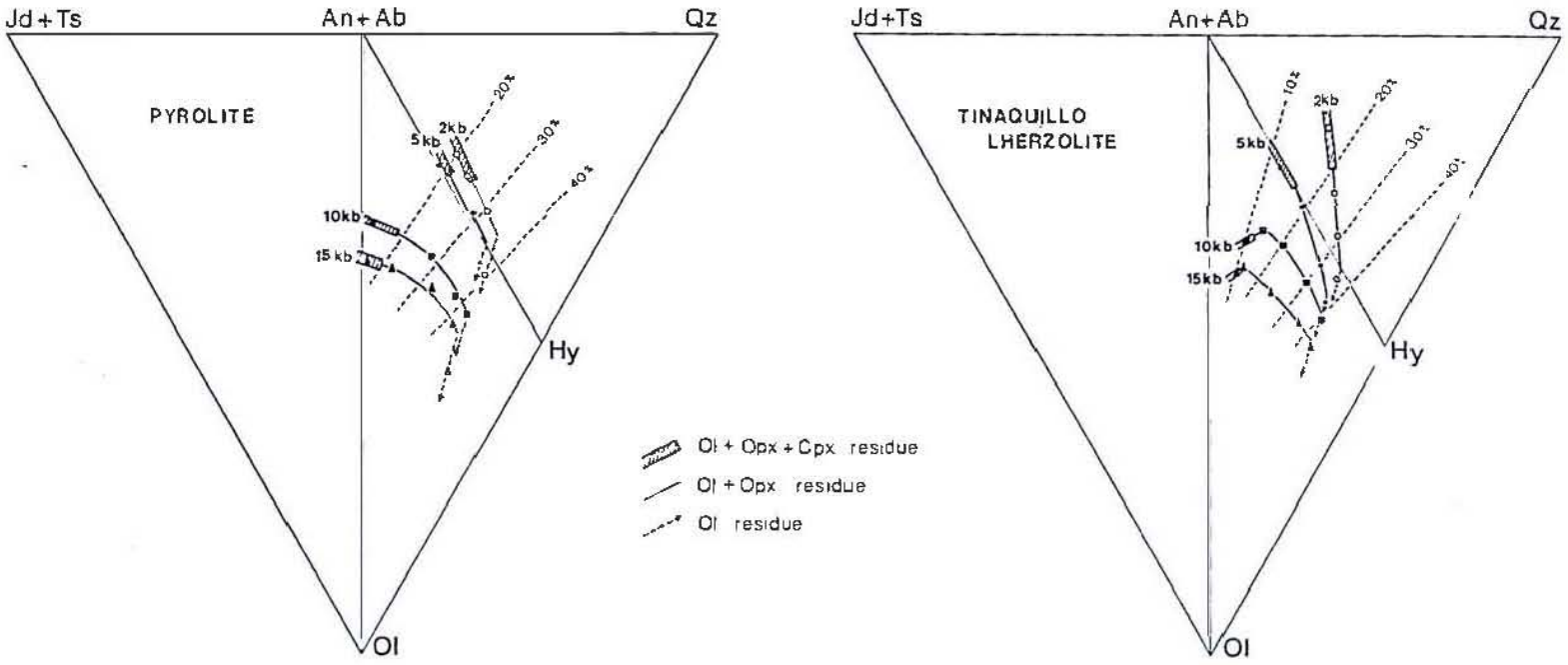

a. b.

Fig. 3-8. Equilibrium melt composition plotted on the surface (Jadeite + Ca-Tschermak's silicate) - Olivine - Quartz. Co-ordinates calculated from the Ne, Ab, An, Hy, Ol, Qz components of the molecular norm as follows:

$Jd + Ts = Ab + An + Ne$ $\quad Qz = Ab + An - Ne + \frac{Hy}{2}$ $\quad Ol = Ol + \frac{Hy}{2}$

Dashed lines indicate percent melting.

Partial melts at low pressure, however, do not trend toward the critical plane of silica undersaturation and low degree (< 10%) partial melts will be saturated to oversaturated in silica, probably aluminous quartz tholeiite, in equilibrium with residual olivine, orthopyroxene, clinopyroxene, plagioclase and chrome spinel. At high degrees of partial melting at low pressure quartz tholeiite liquids cross the plane of silica saturation to olivine-normative compositions.

5-2. Tinaquillo Lherzolite

Partial melts from Tinaquillo lherzolite at 15 kb range from olivine tholeiite ($mg \sim 73$) at approximately 11% melting with residual olivine, orthopyroxene, clinopyroxene and chrome spinel through tholeiitic picrite ($mg \sim 77$) with residual olivine, orthopyroxene and chrome spinel to komatiite ($mg \sim 84$) at about 35-45% melting in equilibrium with residual olivine.

Liquids at 10 kb show a compositional range over the melting interval 11 to 40% melting similar to that at 15 kb except that 10 kb liquids contain more normative hypersthene and lower normative olivine.

Partial melts at low pressure (2 and 5 kb) and low degrees of melting are quartz tholeiite or tholeiite lying practically on the Hy-Plag-Di plane. The quartz tholeiite and tholeiite melts at low degrees of partial melting are highly aluminous, e.g. 17-18% Al_2O_3 with high normative An + Ab content. With higher degrees of melting liquids change to olivine-poor tholeiite composition.

Liquids produced by melting of Tinaquillo lherzolite, although distinctly more magnesian (e.g. Mg_{75-83} compared to Mg_{68-80}), show similar trends to those of pyrolite on the (Jd + Ts) - Qz - Ol diagram (Fig. 3-8b). Melt compositions tend towards hypersthene-normative compositions until orthopyroxene is eliminated, and then lie on an olivine

control line by melting of residual olivine. Melts at higher pressure, 15 kb, are more olivine-normative than those at lower pressure, and melts at low pressure extend into quartz normative compositions. Compared to the partial melts from pyrolite, Tinaquillo liquids are markedly more hypersthene normative at similar degrees of melting and very poor in Ti, Na and K reflecting the refractory nature of Tinaquillo lherzolite. For example, 11% melting of Tinaquillo peridotite (at 15 kb) yields an olivine tholeiite whereas the same amount of melting of pyrolite will produce an alkali basalt. The more *hy*-normative nature of the Tinaquillo liquids is clearly demonstrated on the (Jd + Ts) - Qz - Ol diagram (Fig. 3-8b). Although, like pyrolite melts, the Tinaquillo liquids trend toward the critical plane of silica undersaturation, the 11% melts are well displaced from it. It appears, therefore, that alkaline liquids can only be obtained from refractory peridotites like Tinaquillo at very low degrees of melting (< 5%?) at high pressure ($\geq$ 20 kb). In addition, the very low abundances of incompatible elements (especially LREE) in Tinaquillo lherzolite (Philpotts & others, 1972) argue that alkali basalts cannot be derived from depleted lherzolites similar to Tinaquillo lherzolite.

5-3. Comparison with basalt melting studies

Reversal of the calculated equilibrium melts, i.e. crystallization of each of the liquids at the particular P and T conditions, presents a formidable task. However, previous melting studies on a range of basaltic compositions provide a comparison for the calculated partial melts. The results of the complementary studies are broadly consistent but differ in detail of liquid composition (cf. Fig. 3-8 and Fig. 5, Green, 1970, Fig. 3, Green 1976a).

Green (1970, 1971) inferred from available anhydrous melting studies on olivine tholeiite and high-alumina tholeiite compositions

(Green & Ringwood, 1967a; T.H. Green & others, 1968) that liquids with olivine, orthopyroxene and clinopyroxene as liquidus phases at 9 kb contained ∿ 10-15% normative olivine, 10-15% normative hypersthene and high Al_2O_3 content (15-16%), whereas liquids with olivine and orthopyroxene only as liquidus phases have higher normative hypersthene and olivine, and lower Al_2O_3 content. These studies also suggested that basalts with olivine and orthopyroxene on their liquidi contained approximately 20% normative olivine, 12-14% normative hypersthene and 13-14% Al_2O_3 at 12 kb; ∿ 26% normative olivine, ∿ 12% normative hypersthene and 12-13% Al_2O_3 at 15-16 kb; and ∿ 28% normative olivine, ∿ 12% normative hypersthene at 18 kb (Green, 1970, 1971).

In comparison, data from the partial melting of pyrolite indicate that olivine tholeiite melts at 10 kb are in equilibrium with residual olivine and orthopyroxene and, although they contain 10-15% normative olivine as predicted, they are somewhat richer in normative hypersthene and have lower Al_2O_3 contents than inferred from the basalt crystallization data. This study also indicates that partial melts of pyrolite at 10 kb in equilibrium with residual olivine, orthopyroxene and clinopyroxene are of olivine basalt composition. Similarly, partial melting of pyrolite at 15 kb produces olivine tholeiite liquids with less normative olivine (15-20%) and less Al_2O_3 (10-12.5%) than implied by the basalt crystallization studies. The derivation of alkali olivine basalt at low degrees of partial melting at pressure $\geq$ 15 kb leaving residual olivine, orthopyroxene, clinopyroxene and spinel - also supported by the melting study by Thompson (1975) on a relatively primitive alkali olivine basalt from Skye (Mg = 65, ∿ 3% normative Ne) - is supported by the present study. However, our data do not directly bear on the genesis of more undersaturated rocks since it is now well established that such magmas are generated in presence of H_2O, and, for more undersaturated rocks, CO_2.

The derivation of alkali olivine basalt at low degrees of melting is restricted to pressures > 10 kb, and is obviously favoured by source peridotites with high incompatible element content. At lower pressures (< 10 kb), liquids are enriched in Al_2O_3 and, for low degrees of melting, have high Al_2O_3/CaO ratios - this is consistent with the pattern predicted from the basalt melting studies, and reflects the low Al_2O_3 content of residual pyroxenes at low pressure. However, the effect is most evident in quartz tholeiites and olivine-poor tholeiites, and does not produce liquids resembling ocean-floor tholeiites with ∿ 10% olivine and 15-17% Al_2O_3. Thus, the earlier model for derivation of ocean floor tholeiites (Green & Ringwood, 1967a; Green, 1971), involving segregation of olivine tholeiite magmas at about 30 km depth, has been abandoned in the light of the new data presented here and in recent studies of ocean-floor basalts (Green & others, 1979; PART 4).

The melting studies on both peridotite and basalt are in agreement that melts become more olivine normative at higher pressure. It is suggested that approximately 20-30% melting of pyrolite and lherzolite similar to Tinaquillo lherzolite at 20 kb will produce olivine-rich tholeiite and tholeiitic picrite with approximately 25% normative olivine. Studies by Green & others (1979) and the results presented in PART 4 show that primary picritic magmas of this composition are likely parents to high-alumina olivine tholeiites (MORB) by separation of about 15% olivine, and that these tholeiitic picrite parents segregated at about 60-70 km depth at temperatures of about 1400-1450°C.

5-4. Effect of volatiles in the genesis of tholeiitic basalts

Volatiles, particularly H_2O and CO_2 exert a marked influence on melting of peridotite, affecting the character of the solidus, the stability of residual phases and the melt compositions, particularly at low degrees of melting (e.g. Green, 1973, 1976a; Kushiro, 1969, 1972; Eggler, 1974, 1978; Brey & Green, 1977; Wyllie, 1979). Water is probably the more

significant volatile component in the genesis of most basalts (excluding the highly undersaturated rocks). Melting studies on pyrolite (Green, 1973b), show that for water-undersaturated melting of pyrolite the above-solidus stability field of amphibole is very limited, and, consequently, buffering of any co-existing melt by amphibole will not be significant for most basalts produced at temperatures above the water-undersaturated solidus. For moderate to large degrees of melting, therefore, melts produced under water-saturated conditions will be similar to those produced under anhydrous conditions. Presnall & others (1979) reached the same conclusion and noted that the effects of small amounts of H_2O and CO_2 are opposite and will tend to cancel each other. However, with increased water contents (water-saturated solidus) the primary field of olivine is expanded and liquids become increasingly silica saturated (Kushiro, 1972; Nicholls, 1974; Green, 1973b, 1976a).

The very low H_2O contents (< 0.5%) and low $Fe^{3+}/Fe^{2+} + Fe^{3+}$ of fresh basaltic glasses suggest that water is not important in the genesis of MORB (Moore, 1970; Bryan & Moore, 1977; Langmuir & others, 1977). Moreover, analysis of glass-vapour inclusions in olivine and plagioclase phenocrysts quenched in glassy rims of pillow basalts from mid-ocean ridge spreading centres suggests that the source region may be virtually anhydrous (Delaney & others, 1978). Very low water contents were also found in a similar study of Hawaiian pillow lavas (Muenow & others, 1979) implying that olivine tholeiites in ocean basins in general are derived by water-undersaturated melting of a nearly anhydrous upper mantle. The present experimental study under anhydrous conditions is therefore directly appropriate to the genesis of these basalts.

The results obtained here can be compared with those for water-saturated melting of pyrolite. Since the principal effect of water-saturated melting, at moderate to large degrees of melting, is to expand the field of olivine (Kushiro, 1972), the silica content of the

equilibrium melts under anhydrous conditions may be taken as a *minimum* for similar degrees of melting under hydrous conditions. Comparison of the anhydrous partial melts of pyrolite (Table 3-9) with those from hydrous melting of pyrolite (Green, 1976a; Nicholls, 1974) shows that for similar degrees of partial melting the hydrous melts are distinctly more siliceous, and lower in CaO, MgO and FeO, due to expansion of the field of olivine and of diopside at the expense of orthopyroxene. For example, 28% melting of pyrolite under anhydrous conditions at 10 kb produces an olivine tholeiite (12% normative olivine, 50% SiO_2), whereas 28% of pyrolite under water-saturated conditions produces a magnesian quartz tholeiite containing ∿ 9% normative quartz and ∿ 56% SiO_2 (Green, 1973, 1976a). At lower pressure (5 kb), 25% dry melting produces a quartz tholeiite with ∿ 1% normative quartz (Table 3-9) whereas 25% melting under water-saturated conditions produces a magnesian 'andesite' with ∿ 15% normative quartz (Nicholls, 1974). In both these examples the hydrous melt is distinctly more siliceous, containing about 6% more SiO_2 than an equivalent melt under anhydrous conditions. The anhydrous melting data therefore provide a useful comparison with previous studies of hydrous melting of peridotite.

5-5. Summary

From the results and the foregoing discussion we conclude that:

1) Olivine tholeiites and tholeiitic picrites result from moderate to large degrees of partial melting (10-30% depending on the nature of the source peridotite; 20-30% for pyrolite) at pressures greater than 7-8 kb in equilibrium with olivine + orthopyroxene + chrome spinel ± clinopyroxene.

2) Partial melting at low pressure (5 kb or less) produces quartz tholeiites and tholeiites, and, at high degrees of partial melting, silica-rich olivine-poor tholeiites resembling basaltic and pyroxenitic

komatiite. Melts at low pressure are distinctly more aluminous than those at high pressure, and, at low degrees of melting, are of high-alumina quartz tholeiite composition.

3) Alkali basalts, and more undersaturated rocks, result from less than 15 % melting at pressures greater than 10 kb, and probably greater than 15 kb, to leave a residue of olivine + orthopyroxene $\pm$ clinopyroxene $\pm$ spinel or garnet depending on the pressure.

4) Olivine-rich (peridotitic) komatiites result from high degrees of partial melting (> 40%) at pressures greater than 10 kb to leave residual olivine, or at higher pressures, olivine + orthopyroxene.

These results are integrated in P-T diagrams for both pyrolite and Tinaquillo lherzolite (Fig. 3-9). Our results are thus consistent with evidence from trace elements which suggest that tholeiites are derived by comparatively large degrees of partial melting (20-30%), whereas alkali basalts result from less than 15% of partial melting (e.g. Gast, 1968; Sun & Hanson, 1975; Frey & others, 1978). Trace element abundances in komatiites suggest comparatively large degrees of partial melting, and, in many cases, melting of a mantle source strongly depleted in incompatible elements (e.g. Arndt, 1977a; Arth & others, 1977).

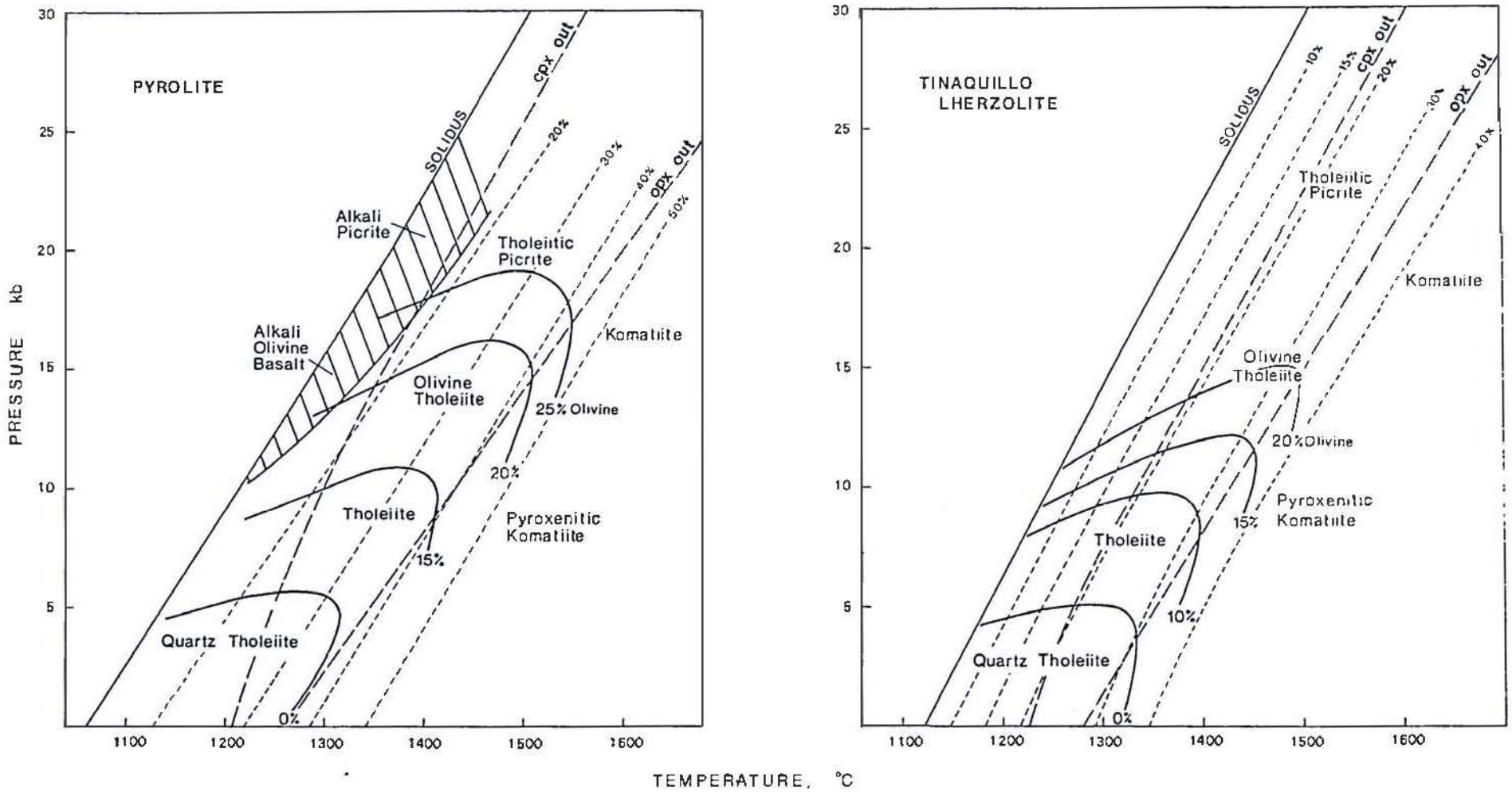

Fig. 3-9. P-T diagram for partial melting of pyrolite and Tinaquillo lherzolite indicating compositions of liquids generated. Long-dashed lines indicate percentage melting, and solid lines indicate percent normative olivine in the melt.

CHAPTER 6

PARTIAL MELTING AND THE OCEANIC CRUST - OPHIOLITE MODEL

6-1. The ophiolite model

Popular models for the formation of ocean crust (e.g. Greenbaum, 1972; Cann, 1974; Christensen & Salisbury, 1975; Dewey & Kidd, 1977) equate ophiolites with oceanic crust generated at present day spreading centres, and regard the various lithologies of both as cogenetic. Thus, the layered cumulate gabbro and peridotite of oceanic layer 3 and ophiolites are generally regarded as accumulation of phases involved in low-pressure crystal fractionation of the overlying basaltic lavas in a magma chamber(s) beneath an axial zone of crustal dilation (as evidenced by dyke swarms). The tectonite harzburgite-dunite basement of ophiolite sequences is generally interpreted as the refractory residue remaining after partial melting which generated the primitive basalts of the pillow lavas. Such models of oceanic crust rely heavily on the ophiolite analogue for information on the lower crustal lithologies, and particularly for internal relationships.

A consequence of ophiolite analogue models for oceanic crust is the implication that partial melting and magma segregation occurred at shallow depth. However, models invoking shallow segregation of MORB (high alumina olivine tholeiites) are at variance with the results of experimental petrology. We have shown that partial melting of peridotite at shallow depths within the plagioclase peridotite field (25 km or less) will produce quartz tholeiite or olivine-poor tholeiite, and *not* MORB-type olivine tholeiite magmas. Crystallization on the more primitive MORB (Green & others, 1979; PART 4) suggest that MORB high-alumina olivine tholeiites are derived from picritic parents segregated at 60-70 km depth. These studies have also shown that high-alumina olivine tholeiites, such as DSDP 3-18 (or their picritic parents) are incapable of yielding

cumulate sequences containing abundant magnesian orthopyroxene (Mg_{87-90}) and highly calcic plagioclase such as occur in the Marum and Papuan ophiolites (PARTS 1 and 2) and a number of other ophiolites (e.g. Church & Riccio, 1977; Coleman, 1977). On these grounds, Green & others (1979) proposed that such cumulate sequences crystallized from magnesian lavas characterized by high SiO_2 contents (> 50% SiO_2, low normative olivine), high CaO and low Na_2O content, and suggested that these magmas might arise by second-stage melting of a refractory peridotite diapir at shallow depth.

Duncan & Green (1979) have suggested that examples of such second-stage melting may be the Ti-poor lavas of the Troodos Complex (Smewing & others, 1975; Simonian & Gass, 1978). Similar Ti-poor, high-silica magnesian basalts have been reported from other ophiolites (e.g. Newfoundland, Church & Coish, 1976; Gale, 1973). Sun & Nesbitt (1978a) inferred that these Ti-poor 'ophiolitic' basalts were not formed at mid-ocean ridges but originated at spreading centres close to a subduction zone by wet melting of mantle severely depleted by one or more previous melting episodes.

The data for the melting of Tinaquillo peridotite, a relatively refractory lherzolite inferred to have been depleted by a previous melting event, show that Ti-poor magnesian quartz tholeiites with high Al_2O_3/TiO_2 ratios can be generated by anhydrous melting of depleted peridotite at low pressure. We believe that the Ti-poor silica-rich basalts of the Upper Pillow Lavas of the Troodos Complex are comparable to the magnesian quartz tholeiite liquids in our anhydrous melting experiments at low pressure, and are distinct from the more silica-rich high-Mg andesites or 'boninites', which probably represent water-saturated melting of refractory peridotite at shallow depth (Green, 1973b, 1976a). The concave upward REE pattern (Sun & Nesbitt, 1978a) and correspondingly higher abundances of K, Rb, Sr and LREE of the high-Mg andesites are best

explained by two-component mixing (i.e. prior depletion and later addition of a LREE-enriched component), as proposed by Green (1976a). We suggest that the added fluid component may have been derived by dehydration of subducting lithosphere at shallow depth, and that high-Mg andesites result from water-saturated melting of peridotite close to the trench in the fore-arc region of an island-arc due to dehydration of the downgoing lithospheric slab. In contrast, magnesian quartz tholeiites such as the Ti-poor, severely LREE-depleted lavas of Troodos (UPL) show no evidence either of excess water, or of addition of an incompatible element-enriched fluid. Duncan & Green (1979) have suggested that they may arise by anhydrous melting of a depleted peridotite diapir at shallow level after yielding olivine tholeiite or tholeiite picrite magmas at greater depth. A similar model has been proposed by Smewing & others (1975) and Smewing & Potts (1976) who invoked a continuous melting process to explain the progressive depletion in incompatible elements (especially REE) of the Troodos Upper Pillow Lavas. It is suggested that second-stage or continuous melting occurs at mid-ocean ridges and in marginal basins but Ti-poor magnesian tholeiites may be more common in back-arc or inter-arc basins where the mantle is refractory having been depleted by previous partial melting episodes (Green, 1973b, 1976a).

6-2. Comparison with mafic tholeiites in other areas

Flood basalts

Continental flood basalts are characterized by an overall chemical uniformity, notably high SiO_2 and Al_2O_3 and low MgO contents; many are more appropriately termed tholeiitic andesites (e.g. Thompson, 1975; Wilkinson & Binns, 1977). A feature of most flood basalts is their enrichment in incompatible elements and high $^{87/86}Sr$ ratios relative to ocean floor tholeiites. Most flood basalts have Mg-values too low to be

considered primary magmas derived from magnesian (pyrolite-like) mantle peridotite, and extensive olivine fractionation is commonly invoked in their petrogenesis (e.g. Cox, 1972; McDougall, 1976). However, mafic olivine-rich lavas have been documented in several areas of flood volcanism, chiefly in Tertiary volcanic province of Baffin Island - West Greenland (Clarke, 1970; Clarke & Pedersen, 1976) and the Nuanetsi Province of Rhodesia (Cox, 1972; Cox & Jamieson, 1974).

Clarke (1970) and Clarke & Pedersen (1976) suggested from the abundance of olivine microphenocrysts and skeletal olivine that the mafic olivine tholeiites of the Baffin Island - West Greenland region represent primary magmas. Clarke (1970) inferred from comparison with the phase relations in model peridotite projections that Baffin Island olivine tholeiites containing approximately 18-20% MgO and 27-30% normative olivine might represent primary magmas derived from partial melting of garnet peridotite at about 30 kb. Associated mafic picrites and more felsic tholeiites were considered to form by olivine accumulation and fractionation respectively (Clarke, 1970). Compared to the partial melts presented here, the Baffin Island - West Greenland olivine tholeiites are lower in SiO_2 and richer in normative olivine, suggesting segregation at greater depth. Similarly, they are more olivine normative than the tholeiitic picrite compositions studied experimentally by Green & others (1979) and in PART 4 which segregated at about 60-70 km suggesting that they may, as inferred by Clarke (1970), represent primary magmas segregated at about 80-100 km depth.

Cox (1972) and Cox & Jamieson (1974) inferred that the Nuanetsi olivine tholeiites containing $\sim$ 15% MgO found at the base of the Karroo might represent primary magmas segregated from residual harzburgite at about 35 km depth since many of the lavas had olivine and orthopyroxene as liquidus and near-liquidus phases at 7-10 kb. While, like the Baffin Island - West Greenland basalts, the Nuanetsi lavas show strong evidence

of olivine control, Cox & Jamieson (1974) invoke polybaric crystal fractionation of both olivine and orthopyroxene. Many of the Nuanetsi lavas containing 12-16% MgO compare with the pyrolite partial melts at 10 kb in equilibrium with olivine and orthopyroxene (although Al_2O_3 and CaO contents are higher in the experimental melts), suggesting that they might be derived at comparatively shallow depths, 25-40 km, by about 20-35% partial melting. The high abundances of incompatible elements, expecially K_2O, in the Nuanetsi lavas indicate that they were derived from a mantle more enriched in incompatible elements (especially K_2O) than pyrolite.

Basaltic komatiites

Pyroxenitic and basaltic komatiites (Arndt & others, 1977), high-Mg basalts (Williams, 1972) or spinifex-textured basalts (Sun & Nesbitt, 1978b), a group of lavas characterized by high SiO_2 contents (50-55% SiO_2; low normative olivine or normative quartz) and high MgO contents (10-20%) are intermediate between peridotitic komatiites and tholeiitic basalts. Opinion is divided as to whether these lavas represent primary magmas formed by lower degrees of melting than peridotitic komatiites, or whether they represent differentiates of more peridotitic primary magmas (e.g. Arth & others, 1977; Sun & Nesbitt, 1978b). Compositionally, many of these magnesian basalts resemble the magnesian olivine-poor tholeiites and quartz tholeiites in our low-pressure melting experiments (except for TiO_2, Na_2O and K_2O), suggesting that they might represent primary magmas formed by about 25-40% melting in the plagioclase peridotite stability field, probably 5-10 kb. This interpretation is supported by melting studies on a spinifex-textured basalt ($\sim$ 55% SiO_2, $\sim$ 12% MgO, Mg = 70) from the Pilbara region (Green & others, in prep.) which shows that olivine and orthopyroxene are co-liquidus phases at about 7 kb, consistent with the partial melting data.

6-3. Conclusions

1) Equilibrium melting under anhydrous conditions results in progressive elimination of phases with increasing T. Four main fields are recognized from the solidus, these are; ol + opx + cpx + aluminous phase (plag, sp or ga) + L; ol + opx + cpx + Cr spinel + L; ol + opx + Cr spinel + L; ol $\pm$ Cr spinel + L. The residual phases progressively change composition to more refractory compositions with increasing proportion of co-existing melt, i.e. increasing 100Mg/Mg + Fe and Cr/Cr + Al ratios, decreasing Al_2O_3 and CaO in pyroxene, etc.

2) The degree of melting increases rapidly immediately above the solidus (up to 10% melting occurs within 25-30^{o}C of the solidus) and then increases in roughly linear form with increasing T.

3) Equilibrium melt compositions from pyrolite within the spinel peridotite field range from alkali olivine basalt (< 15% melting) through olivine tholeiite (20-30%) and picrite to komatiite (40-60% melting). Melting in the plagioclase-peridotite field produces magnesian quartz tholeiite and olivine-poor tholeiite with high alumina contents due to expansion of the primary field of olivine at low pressure. Liquids in equilibrium with olivine, 2 pyroxenes and an aluminous phase (plagioclase, Al-spinel or garnet) result from low degrees of partial melting (< 10%) and are enriched in incompatible elements.

4) Melts from spinel lherzolite are more silica saturated than those from pyrolite for similar degrees of melting. This is primarily a result of the higher alkali content of pyrolite. Melts within the spinel peridotite field range from olivine tholeiite through tholeiitic picrite to komatiite with increasing degree of melting. Although similar (in major elements) olivine tholeiite magmas can be derived from both pyrolite and Tinaquillo lherzolite, the degree of melting for such liquids is lower and the depth of melting is greater for the Tinaquillo lherzolite parent.

5) The results of the peridotite melting study support melting studies on 'primitive' high-alumina olivine tholeiites from the ocean floor which suggest that such magmas result from 10-30% melting (depending on the peridotite source composition) at depths of 60-70 km. The liquidus and near-liquidus phase relations of such basalts are not consistent with oceanic crust models based on the Marum, Papuan, Troodos and Betts Cove ophiolites. The primary magmas which generated these ophiolites are considered to be magnesian quartz tholeiite or olivine-poor tholeiite formed by partial melting of refractory peridotite in the plagioclase-peridotite field (0-25 km).

6) Like most MORB, tholeiitic basalts in other tectonic regions appear to have undergone low pressure crystal-fractionation. Two examples of primary magmas in continental and continental-margin areas may be the olivine-rich lavas of Baffin Island - West Greenland, and of the Nuanetsi province. Our partial melting data are consistent with the derivation of the Baffin Island picritic tholeiites (∿ 30% normative olivine) by partial melting of garnet peridotite (Clarke, 1970) and the Nuanetsi olivine tholeiites (10-15% normative olivine) by 20-35% melting at 25-40 km depth.

7) Basaltic komatiites (12-20% MgO, < 5% normative olivine) may be primary magmas derived by 25-40% melting of plagioclase peridotite.

PART 4

EXPERIMENTAL PETROLOGY AND PETROGENESIS OF A MARGINAL BASIN BASALT

Contents *page*

SUMMARY			191
CHAPTER	1.	INTRODUCTION AND TECHNIQUES	192
	2.	EXPERIMENTAL RESULTS	198
	3.	PETROGENESIS OF THE LAU BASIN BASALT	204

SUMMARY

The liquidus and near liquidus crystallization of a relatively primitive basalt composition from the Lau Basin (basalt 95-1) has been studied experimentally at pressures up to 15 kb. Olivine is the liquidus phase at low pressure (< 12 kb) and is joined by calcic plagioclase and clinopyroxene at lower temperature. Calcic clinopyroxene is the liquidus phase at higher pressure ($\geq$ 12 kb) and there is no near-liquidus field of orthopyroxene. The low pressure experiments show that basalt 95-1 could be a derivative liquid by olivine fractionation from a more olivine-rich parent. Olivine-addition experiments show that a picritic magma (95-1 + 18% olivine Mg_{89}) containing approximately 27% normative olivine is saturated in olivine, orthopyroxene and clinopyroxene at $\sim$ 20 kb and 1450°C.

Examination of olivine-liquid pairs over a range of temperatures (1200-1400°C) and pressures (0-15 kb) indicates that Fe/Mg partitioning is pressure dependent at pressures above 5 kb. Our experiments show variation in K_D from 0.29 - 0.30 at 5 kb, 0.30 - 0.33 at 10 kb to 0.33 - 0.34 at 15 kb.

The experimental study precludes a simple genetic relationship between 95-1 (or its picritic parent) and ophiolite complexes and segments of oceanic lithosphere characterized by cumulus magnesian orthopyroxene and harzburgitic basement. However, basalt 95-1 is characterized by a very high CaO/Na_2O ratio (13.5) and is capable of crystallizing the highly calcic plagioclase (> An_{90}) commonly found as megacrysts in MORB and in cumulate gabbro and peridotite of ophiolites and oceanic crust. As such, basalts like 95-1 may be genetically related to segments of oceanic crust and ophiolites containing olivine, plagioclase and clinopyroxene as the dominant cumulus phases.

CHAPTER 1

INTRODUCTION AND TECHNIQUES

1-1. Introduction

Marginal basins or back-arc basins are a common feature of many arc-trench systems, particularly those in the Western Pacific, and may have been an important feature of convergent plate boundaries in the past. Bathymetric, heat flow, magnetic and seismic property measurements in marginal basins over the past decade point to an origin by crustal dilation and sea-floor spreading partly, if not directly, analogous to that occuring at mid-ocean ridges (e.g. Karig, 1971; Sclater, 1972; Packham & Falvey, 1971). Dredge sampling, particularly in the Lau, Mariana and Scotia basins, has shown that marginal basins are commonly floored by olivine tholeiite basalts similar to mid-ocean ridge basalts (MORB) (Hawkins, 1977; Hart & others, 1972; Tarney & others, 1977; Dietrich & others, 1978) and it is tacitly assumed that they are derived by similar mantle processes. On the other hand the apparent restriction of active back-arc or inter-arc basins to arc-trench systems with well developed arcs and subduction characteristics has prompted models of formation of back-arc spreading related to the down-going lithosphere. Mantle counterflow or convection induced in the over-lying asthenosphere by subducting lithosphere is one of several mechanisms commonly suggested (e.g. Toksöz & Bird, 1977).

Since the original suggestion (Dewey & Bird, 1971) that ophiolites may represent obducted segments of marginal basin crust marginal basins have attracted considerable interest as possible sites for formation of ophiolites and a number of petrologists have attempted to establish a geochemical distinction between oceanic crust formed at mid-ocean ridges and that formed in marginal basins. However, it now seems clear that marginal basin basalts span the entire spectrum of compositions found for MORB, although marginal basin basalts are more radiogenic and commonly enriched in LREE and

other LIL elements over normal MORB (Saunders & Tarney, 1979; Tarney & others, 1977; Gill, 1976; PART 1, Chapter 5). An additional complexity is that many marginal basin basalts appear transitional between MORB and island-arc tholeiites (e.g. Gill, 1976; Hawkesworth & others, 1977; Ewart & others, 1977). It can also be concluded from these studies that the mantle beneath marginal basins is at least as heterogeneous as that beneath mid-ocean ridges.

This part represents an experimental study of one of the more primitive marginal basin olivine tholeiite basalts aimed at defining its melting relations, depth of segregation and residual mineralogy. The low pressure liquidus and near-liquidus phases are then compared with the accumulate sequences observed in ophiolites (particularly the Marum and Papuan ophiolites) and the oceanic crust.

1-2. Sample Selection

Basalt 95-1 from the Lau Basin, a young back-arc or inter-arc basin lying between the Tonga-Kermadec and Lau-Colville ridges at the Australian-Pacific plate boundary (Hawkins, 1976), was selected as a model composition for experimental study. This basalt, one of the most magnesian of the 'least altered' Lau Basin samples described by Hawkins (1976) with $100Mg/(Mg + \Sigma Fe) = 68.5$, is a vitrophyre containing microphenocrysts of magnesian olivine (Mg_{86}) and has a comparatively high Ni content (250 ppm) suggesting that it is relatively unfractionated. The possibility that basalt 95-1 contains resorped phenocrysts is discounted in view of the petrographic evidence to the contrary.

Compositionally basalt 95-1 is an olivine tholeiite similar to the high-alumina olivine tholeiites erupted at mid-ocean ridges, and is particularly similar to the 'MgCa' basalts (terminology of Melsom & others, 1976) reported from DSDP Leg 3 by Frey & others (1974). However, in terms of trace elements basalt 95-1 differs from MORB by virtue of its very low

TiO_2 content and extreme depletion in LREE and other LIL elements (Gill, 1976). The very low TiO_2 content of 95-1 prompted Sun & Nesbitt (1978a) to group it with Ti-poor magnesian tholeiites found in ophiolites and island-arcs which they collectively referred to as 'ophiolitic basalts'.

1-3. Experimental Methods

Sample preparation

A glass of 95-1 composition was prepared by reacting A.R. grade chemicals and fusion in a Pt crucible under Ar atmosphere. Lau Basin basalt 95-1 lies at the iron-rich end of the range of compositions expected in equilibrium with residual mantle peridotite containing olivine Mg_{88-92} e.g. basalt Mg-values 68-78 (Green & others, 1979) and may not be a primary basalt (i.e. derived directly by partial melting of a peridotite mantle source without prior fractional crystallization). Since only olivine occurs as microphenocrysts in the vitrophyre and olivine is the liquidus phase to 12 kb (see below) olivine is considered to be the only phase likely to be involved in pre-eruptional crystal fractionation, and a more magnesian composition (termed 95-2 for convenience) consisting of 95-1 plus 15% olivine was also prepared both as a glass and as sintered oxide mix in a sealed evacuated silica tube. Electron microprobe analyses of the prepared glasses are presented in Table 4-1. The prepared glass 95-1 differs slightly from the natural basalt 95-1 in having slightly less FeO and slightly more Na_2O. These differences arose due to Fe loss to the Pt crucible on fusion, and alkali contamination of the batch of silica used in the preparation of the 95-1 glass. These differences will have little effect on the phase relations other than to slightly raise the liquidus temperature and result in slightly more Mg-rich liquidus olivine and less calcic plagioclase than the natural rock.

All experiments were carried out under anhydrous conditions since we have inferred, by analogy with the very low H_2O contents and Fe^{3+} contents

TABLE 4-1.

COMPOSITIONS USED IN EXPERIMENTAL STUDY

	Lau Basin basalt 95-1	95-1	95-1 + 15% ol 95-2	95-1 + 18% ol 95-3
SiO_2	47.84	47.8	47.0	47.0
TiO_2	0.37	0.4	0.3	0.3
Al_2O_3	15.93	16.2	14.0	13.4
Fe_2O_3	2.20	- 0.39	- 0.52	-
FeO	7.05	8.7* 8.35**	9.4* 8.93**	9.1*
MnO	0.16	0.2	0.10	(0.10)
MgO	11.02	11.2	16.0	16.9
CaO	13.75	13.9	12.1	11.9
Na_2O	1.02	1.4 (1.43)***	0.9	0.9
K_2O	0.03	(0.03)	(0.03)	(0.03)
P_2O_5	0.01	(0.01)	(0.01)	(0.01)
NiO	0.03	(0.03)	(0.05)	(0.05)
Cr_2O_3	0.10	0.12	0.16	0.16
H_2O^+	0.21	-	-	-
H_2O^-	0.29	-	-	-
CIPW NORM				
Or	0.18	0.18	0.18	0.18
Ab	8.63	12.1	7.62	7.62
An	38.80	37.7	34.1	32.4
Di	23.59	25.3	20.9	21.3
Hy	17.61	4.19	10.1	9.88
Ol	6.49	19.4	26.3	27.5
Il	0.70	0.76	0.57	0.57
Mt	3.19	-	-	-
Ap	0.02	0.02	0.02	0.02
$\frac{100Mg}{Mg+\Sigma Fe}$	68.5	69.6	75.2	76.8

* Total iron as FeO

** FeO by spectrophotometry - P. Robinson, analyst.

*** Na_2O by atomic absorption spectroscopy - P. Robinson, analyst

of fresh MORB glasses (e.g. Bryan & Moore, 1977; Delaney & others, 1978; Meunow & others, 1979), that Lau Basin basalt 95-1 was derived under essentially anhydrous conditions. This assumption seems reasonable for MORB-like olivine tholeiites erupted in more evolved marginal basins well removed from a volcanic arc since at that depth the underlying slab will be dehydrated (e.g. Wyllie, 1979) but is unlikely to hold for magmas erupted in the early stages of inter-arc basin formation where magmas are likely to be generated in the presence of water derived from the downgoing lithospheric slab. In any event conclusions drawn from the anhydrous study will also be applicable in general terms to water-undersaturated melting (< 0.4% H_2O in the source).

1-Atmosphere experiments

The sintered oxide mix was used in the 0 kb experiments which were carried out by placing ∿ 20 mg sample in spec-pure iron capsules which were sealed in evacuated silica tubes and suspended in a vertical, Pt-wound, 1-atmosphere quenching furnace. Use of crystalline starting material for low pressure runs is considered preferable since previous studies have shown that vitreous starting material may inhibit nucleation of plagioclase. Microprobe analysis of the bulk change revealed slight gain in Fe from the capsule in some of the 0 kb runs resulting in slightly more Fe-rich liquidus olivine compositions than those obtained in graphite e.g. liquidus olivine $Mg_{89.6}$ at 0 kb compared with $Mg_{90.4}$ at 5 kb.

High pressure experiments

The high pressure experiments were carried out in solid media piston-cylinder apparatus, Boyd & England (1960), with piston-in technique using a pressure correction of minus 10% nominal piston pressure. Temperature ($\pm$ 5°C) was measured using a Pt-90% Pt10%Rh thermocouple with no correction made for the effect of pressure on the thermocouple emf. The prepared glasses were finely crushed under acetone and dried at 110°C overnight. Furnace assemblies were of ½" diameter with pyrex sleeves. Graphite capsules

were used for runs at 10 kb and above since at these pressures previous experiments had shown that this procedure did not cause change in FeO content of the charge. Prevailing f_{O_2} conditions using this furnace assembly are below the Ni-NiO buffer for all temperatures and pressures (Green, 1976a; D. Gust, pers. comm. 1979) and for graphite capsules, below quartz-fayalite-magnetite buffer (Ryabchikov & others, unpubl). Thompson & Kushiro (1972) estimated f_{O_2} conditions using graphite capsules to be in the field of wustite for pressures of 10-20 kb. Sealed Pt capsules, preheated immersed in fine Fe powder at 900-1000°C for 4-6 hours in an attempt to minimize Fe loss, were used for the 2 kb and some 5 kb runs in preference to graphite capsules since at pressures below 5 kb use of graphite capsules results in reducing conditions with $f_{O_2} << QFM$ (Ryabchikov & others, unpubl), which reduce some FeO to metallic Fe in the charges. Near liquidus runs at 5 kb in graphite capsules differed from those in Pt capsules by the presence of chrome spinel in the Pt capsules and its absence in the graphite. Prevailing f_{O_2} conditions using Pt capsules are therefore considered to be greater in the Pt capsules than in the graphite, possibly due to iron loss to the Pt capsule according to the reaction

$$3FeO + Pt \rightleftarrows (Fe,Pt)_{ss} + Fe_2O_3$$

The small amount of iron (up to 10%) lost to the Pt capsule from the charge during the runs resulted in slightly more Mg-rich compositions than those obtained in graphite.

Microprobe analysis

Crushed portions of the run charges were examined optically in refractive index oil. Polished mounts of runs were examined in reflected light and by scanning electron microscope-microprobe. Mineral and glass analyses were obtained using a JEOL JX-50A electron probe microanalyser fitted with an EDAX energy dispersive analytical system and scanning electron microscope at Hobart, and the energy dispersive TPD probe at ANU

(Appendix 1). Optimization of the combined backscattered and secondary electron images enabled resolution and identification of phases at up to 2000 x magnification. Analyses of glass were made using rapid, reduced area scans to minimize alkali volatilization. Between 5 and 20 analyses were carried out on each experimental run and the analyses listed in Tables 4-3 to 4-8 were selected as having totals between 98 and 102% (commonly 98.5 and 100.5%) and acceptable structural formulae.

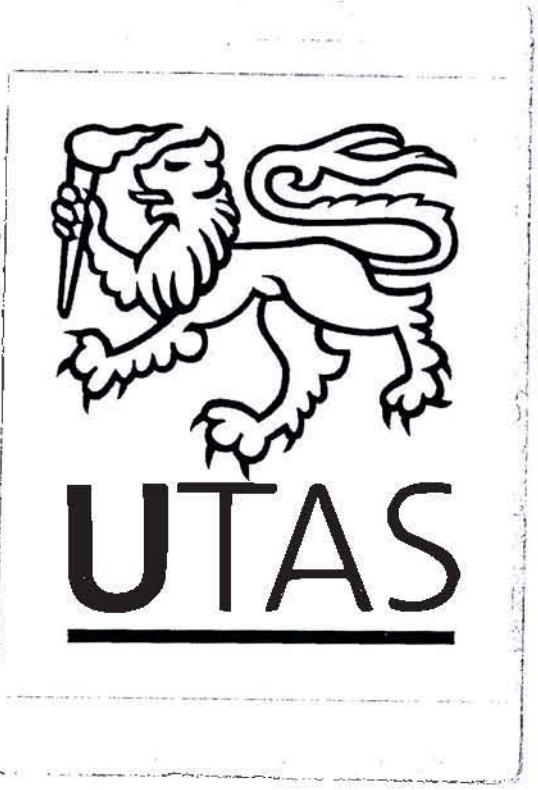

CHAPTER 2

EXPERIMENTAL RESULTS

Experimental run data for the compositions studied are presented in Table 4-2 and phase relations shown as a function of temperature and pressure in Figure 4-1.

2-1. 95-1

Olivine (with minor spinel) is the liquidus phase to 12 kb where it is joined by clinopyroxene. Clinopyroxene is the liquidus phase above 12 kb. Compositions of run products are presented in Table 4-3 and 4-4.

At 5 kb the crystallization sequence is olivine ($Mg_{87.8}$) and chrome spinel ($\frac{100Cr}{Cr + Al}$ = 37, $\frac{100Mg}{Mg + Fe}$ = 70) at 1240°C, followed by plagioclase ($An_{85.6}$) at 1220°C, and clinopyroxene at 1180°C (cf. 95-2). The percentage of crystallization increases markedly at about 1200°C to ∿ 40% crystallization. The liquidus olivine composition is close to, although slightly more magnesian than that of the microphenocrysts in the natural basalt (Mg_{86}) indicating that the microphenocrysts are in equilibrium with the host liquid. The plagioclase composition, $An_{85.6}$, is relatively calcic and similar to the more calcic compositions reported from plagioclase-phyric Lau Basin basalts by Hawkins (1976).

At 10 kb the crystallization sequence is olivine (with minor chrome spinel) at 1290°C followed by clinopyroxene (5% Al_2O_3; $Ca_{32.1}Mg_{59.6}Fe_{8.3}$) at 1260°C, and plagioclase (An_{81}) at 1240°C. Chrome spinel crystallizing at 10 kb is more aluminous, $\frac{100Cr}{Cr + Al}$ = 30.5, than chrome spinel crystallizing at 5 kb.

At 12 kb olivine is joined by aluminous clinopyroxene (Table 4-4) and aluminous clinopyroxene (6% Al_2O_3) alone is the liquidus phase at 15 kb, where the slope of the liquidus changes.

TABLE 4-2

Experimental run data

	Pressure (kbars)	Temp (°C)	Capsule	Material*	Time (minutes)	Run No.	Phase assemblage **
95/1							
	5	1260	C	gl	45	T-44	Gl - above liquidus
	5	1240	C	gl	45	T-39	Ol + gl
	5	1240	Pt	gl	40	T-91	Ol + Sp + gl
	5	1220	C	gl	45	T-42	Ol + plag + gl
	5	1210	C	gl	45	T-43	Ol + plag + gl
	5	1200	C	gl	45	T-40	Ol + plag + gl ***
	10	1300	C	gl	45	T-59	Gl - above liquidus
	10	1290	C	gl	45	T-58	OL + gl - on liquidus
	10	1280	C	gl	45	T-54	Ol + gl
	10	1280	Pt	gl	45	T-92	Ol + Sp + gl
	10	1270	C	gl	45	T-55	Ol + gl
	10	1260	C	gl	45	T-45	Ol + cpx + gl
	10	1240	C	gl	45	T-48	OL + cpx + plag + gl ***
	12	1310	C	gl	45	T-79	Gl - above liquidus
	12	1290	C	gl	45	T-80	Ol + cpx + gl
	15	1360	C	gl	45	T-68	Gl - above liquidus
	15	1340	C	gl	45	T-69	Gl - above liquidus
	15	1320	C	gl	45	T-66	Cpx + gl
	15	1300	C	gl	45	T-62	Cpx + gl ***
95/2							
= 95-1 + 15% ol	0	1360	Fe	cryst	15	AT-17	Gl
	0	1340	Fe	cryst	15	AT-13	Ol + gl
	0	1300	Fe	cryst	60	AT-11	Ol + gl
	0	1230	Fe	cryst	120	AT-15	Ol + plag + gl
	0	1210	Fe	cryst	120	AT-14	Ol + plag + gl
	0	1200	Fe	cryst	60	AT-10	Ol + plag + gl
	0	1190	Fe	cryst	120	AT-12	Ol + plag + cpx + gl
	0	1160	Fe	cryst	60	AT-9	Ol + plag + cpx + gl ***
	0	1130	Fe	cryst	240	AT-16	Ol + plag + cpx - subsolidus
	2	1320	Pt	gl	30	T-188	Ol + gl
	2	1280	Pt	gl	30	T-189	Ol + sp + gl
	2	1240	Pt	gl	40	T-190	Ol + sp + gl
	2	1200	Fe	cryst	120	T-376	Ol + plag + gl
	2	1180	Pt	gl	45	T-200	Ol + plag + cpx + gl ***
	2	1160	Pt	gl	30	T-209	Ol + plag + cpx + gl ***
	5	1360	C	cryst	30	T-369	Gl - above liquidus
	5	1340	C	gl	45	T-179	Ol + gl
	5	1330	Pt	gl	30	T-224	Ol + sp + gl

TABLE 4-2 cont.

	Pressure (kbars)	Temp (°C)	Capsule	Material*	Time (minutes)	Run No.	Phase assemblage **
	5	1300	Pt	gl	30	T-193	Ol + sp + gl
	5	1260	Pt	gl	45	T-195	Ol + sp + gl
	5	1230	Fe	cryst	120	T-375	Ol + gl
	5	1220	Pt	gl	45	T-196	Ol + sp + gl
	5	1210	Pt	gl	45	T-219	Ol + plag + gl
	5	1200	Pt	gl	45	T-197	Ol + plag + cpx + gl ***
	10	1380	C	gl	45	T-181	Gl - above liquidus
	10	1360	C	gl	45	T-176	Ol + gl
	10	1260	C	gl	45	T-205	Ol + cpx + gl
	15	1400	C	gl	45	T-169	Gl - above liquidus
	15	1380	C	gl	45	T-182	Ol + gl
	15	1360	C	gl	45	T-171	Ol + gl
	15	1320	C	gl	45	T-220	Ol + cpx + gl
	18	1400	C	gl	40	T-204	Ol + cpx + gl
	20	1460	C	gl	40	T-221	Gl - above liquidus
	20	1440	C	gl	40	T-213	Cpx + liquid
95/3							
= 95-1 + 18% Ol	18	1420	C	cryst	60	T-352	Ol + gl
	18	1400	C	cryst	60	T-343	Ol + cpx + gl ***
	20	1460	C	cryst	60	T-353	Ol + gl
	20	1450	C	cryst	60	T-364	Ol + cpx + gl
	20	1440	C	cryst	60	T-344	Cpx + gl ***
	22	1480	C	cryst	30	T-414	Glass - above liquidus
	22	1460	C	crypt	60	T-356	Cpx + gl ***
95/3 + 1% Opx	20	1450	C	crypt	60	T-361	Ol + cpx + gl
95/3 + 1% C.En	22	1460	C	cryst	30	T-377	Coarse cpx + gl ***
95/3 + 1% Opx	22	1460	C	crypt	30	T-374	Abundant large quench cpx + gl ***

* Starting material: gl = glass, cryst = crystalline.

** Compositions of run products given in Tables.

*** Run contains quench clinopyroxene; glass composition not reliably that of liquid in equilibrium with primary phases.

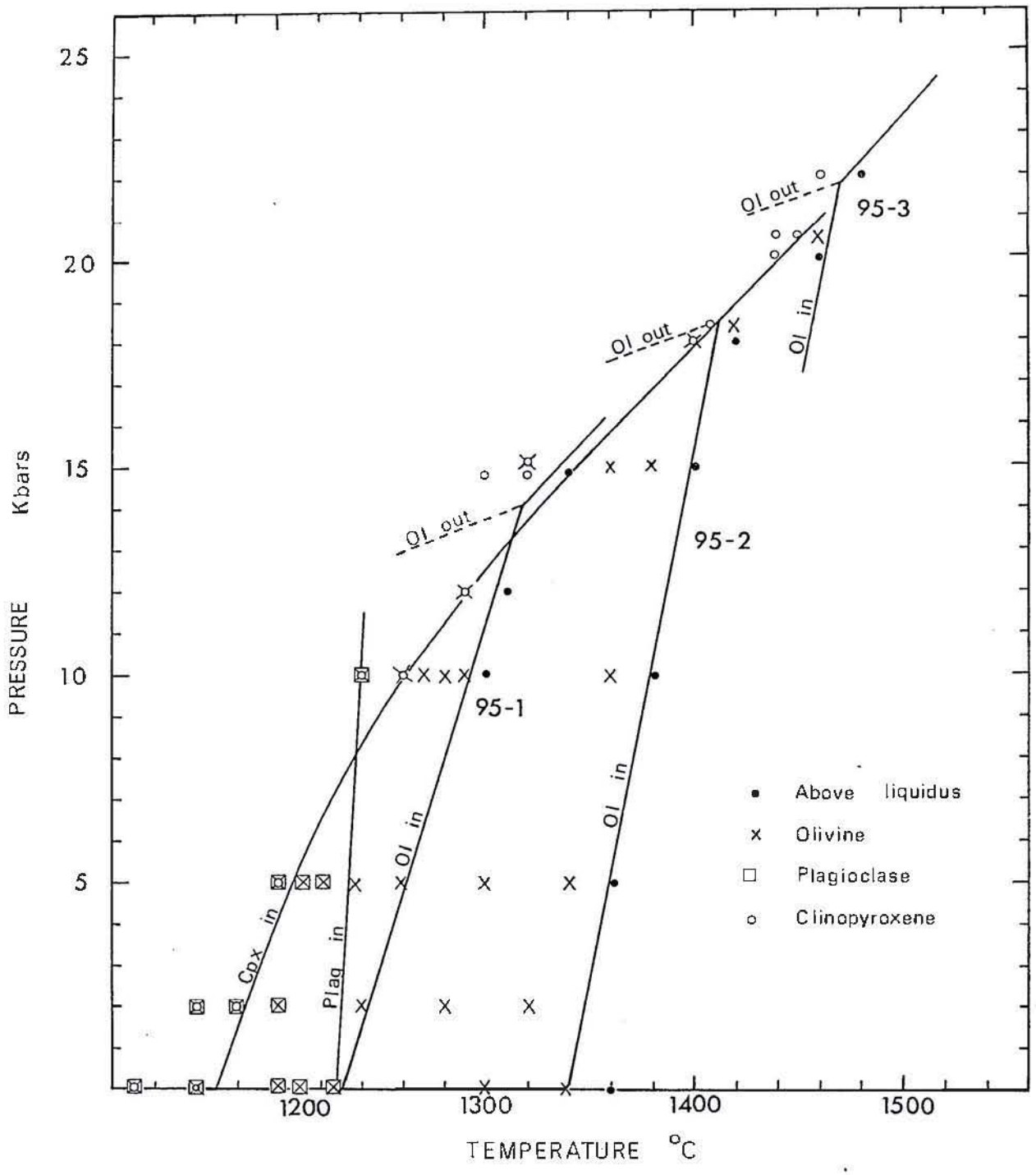

Fig. 4-1. Anhydrous melting relations of 95-1 and olivine-enriched compositions. 95-2 and 95-3.

TABLE 4-3

Glass 95-1 run products at 5 kb

	1a	1b	1c	2a	2b	2c	3a	3b	3c	4a	4b	4c
SiO_2	40.1	-	48.3	40.0	47.5	48.6	40.0	48.1	49.1	39.7	48.1	49.3
TiO_2	-	-	0.40	-	-	0.43	-	-	0.47	-	-	0.42
Al_2O_3	-	35.8	16.4	-	33.6	16.4	-	33.0	15.4	0.66	31.3	15.1
FeO^t	11.7	13.9	8.65	11.8	0.26	8.52	14.0	-	9.34	15.2	0.78	9.91
MnO	0.36	-	0.12	0.36	-	-	0.40	-	-	-	-	-
MgO	47.2	18.5	10.4	47.2	0.28	9.92	44.9	-	8.66	43.6	0.83	8.37
CaO	0.56	0.34	14.2	0.62	16.8	14.6	0.67	17.3	15.5	0.88	17.4	15.3
Na_2O	-	-	1.42	-	1.56	1.49	-	1.59	1.51	-	1.63	1.51
K_2O	-	-	-	-	-	-	-	-	-	-	-	-
Cr_2O_3	0.16	31.5	0.11	-	-	-	-	-	-	-	-	-
O =	4	4		4	8		4	8		4	8	
Si	0.994	-		0.993	2.177		1.002	2.203		0.997	2.216	
Ti	-	-		-	-		-	-		-	-	
Al	-	1.204		-	1.815		-	1.782		0.020	1.700	
Fe^t	0.242	0.332		0.245	0.010		0.293	-		0.319	0.030	
Mn	0.008	-		0.008	-		0.008	-		-	-	
Mg	1.743	0.786		1.746	0.019		1.676	-		1.633	0.057	
Ca	0.015	0.010		0.016	0.826		0.018	0.849		0.024	0.859	
Na	-	-		-	0.139		-	0.141		-	0.146	
K	-	-		-	-		-	-		-	-	
Cr	0.003	0.710		-	-		-	-		-	-	
Total	3.003	3.043		3.006	4.985		2.998	4.976		2.993	5.007	
100 Mg/Mg+Fe	87.8	70.3	68.2	87.7		67.5	85.1		62.3	83.6		60.1
				Ca 85.6			Ca 85.7			Ca 85.5		
				Na 14.4			Na 14.3			Na 14.5		
				K -			K -			K -		

t = Total iron as FeO.

1. 1240°C; a = olivine, b = spinel (run T-91), c = glass
2. 1220°C; a = olivine, b = plagioclase, c = glass
3. 1210°C; a = olivine, b = plagioclase, c = glass
4. 1200°C; a = olivine, b = plagioclase, c = glass

TABLE 4-4

Representative analyses of 95-1 run products at 10, 12 and 15 kb

	1a	1b	2a	2b	2c	3a	3b	4a	4b	4c	5a	5b	5c	6a	6b	6c	7a	7b	8
SiO_2	40.4	48.3	40.2	-	48.3	40.2	48.4	40.0	52.6	48.0	38.6	48.9	52.4	40.1	53.2	48.5	52.0	48.1	48.9
TiO_2	-	0.30	-	-	0.37	-	0.35	-	0.22	0.43	-	-	0.40	-	0.20	0.47	0.27	0.30	0.32
Al_2O_3	-	16.4	-	41.1	16.4	-	16.5	-	4.99	17.5	0.96	32.0	8.26	-	4.18	18.4	6.41	18.1	11.3
FeO^t	11.5	8.54	11.7	12.8	8.56	11.8	8.62	12.2	5.15	8.9	18.9	0.35	6.34	12.0	4.95	9.01	4.85	9.15	5.04
MnO	-	-	-	-	-	-	-	-	-	-	-	-	-	-	-	-	-	-	-
MgO	47.8	10.9	47.7	18.8	10.7	47.6	10.4	47.3	20.8	9.9	40.9	0.53	14.7	47.3	21.3	9.80	20.6	10.0	15.8
CaO	0.41	14.2	0.45	0.36	14.2	0.36	14.3	0.55	15.7	13.8	0.63	16.1	17.5	0.53	15.7	12.3	14.9	12.4	17.7
Na_2O	-	1.43	-	-	1.48	-	1.54	-	-	1.51	-	2.14	-	-	-	1.52	0.58	1.63	0.47
K_2O	-	-	-	-	-	-	-	-	-	-	-	-	-	-	-	-	-	0.10	-
Cr_2O_3	-	-	-	26.9	-	-	-	-	0.58	-	-	-	0.37	0.16	0.58	-	0.39	-	0.37
O =	4		4	4		4		4	6		4	8	6	4	6		6		6
Si	0.996		0.993	-		0.994		0.992	1.888		0.987	2.238	1.889	0.993	1.906		1.864		1.767
Ti	-		-	-		-		-	0.006		-	-	0.011	-	0.005		0.007		0.009
Al	-		-	1.349		-		-	0.211		0.029	1.727	0.351	-	0.177		0.270		0.483
Fe^t	0.236		0.241	0.298		0.244		0.253	0.155		0.404	0.013	0.191	0.249	0.149		0.145		0.152
Mn	-		-	-		-		-	-		-	-	-	-	-		-		-
Mg	1.759		1.758	0.780		1.756		1.748	1.113		1.559	0.036	0.790	1.746	1.136		1.100		0.852
Ca	0.010		0.011	0.011		0.007		0.015	0.604		0.017	0.790	0.676	0.014	0.603		0.571		0.687
Na	-		-	-		-		-	-		-	0.190	-	-	-		0.040		0.033
K	-		-	-		-		-	-		-	-	-	-	-		-		-
Cr	-		-	0.592		-		-	0.016		-	-	0.011	0.003	0.017		0.011		0.010
Total	3.004		3.006	3.030		3.005		3.008	3.992		2.998	4.994	3.919	3.005	3.993		4.008		3.994
$\frac{100\ Mg}{Mg + Fe}$	88.1	69.5	87.9	72.4	69.0	87.8	68.5	87.4	87.8	66.5	79.4		80.5	87.5	88.4	66.0	88.3	66.1	84.8
								Ca 32.3			Ca 80.6	Ca40.8	Ca 31.9		Ca 31.4		Ca 40.6	
								Mg 59.5			Na 19.4	Mg47.7	Mg 60.2		Mg 60.6		Mg 50.4	
								Fe 8.2			K -	Fe11.5	Fe 7.9		Fe 8.0		Fe 9.0	

t = Total iron as FeO. MnO <0.15%

1. 10 kbar 1290°C: a = olivine, b = glass
2. 10 kbar 1280°C: a = olivine, b = spinel (run T-92), c = glass
3. 10 kbar 1270°C: a = olivine, b = glass
4. 10 kbar 1260°C: a = olivine, b = clinopyroxene, c = glass
5. 10 kbar 1240°C: a = olivine, b = plagioclase, c = clinopyroxene
6. 12 kbar 1290°C: a = olivine, b = clinopyroxene, c = glass
7. 15 kbar 1320°C: a = clinopyroxene, b = glass
8. 15 kbar 1300°C: clinopyroxene

2-2. 95-2

Olivine (with minor chrome spinel) is the liquidus phase to 18 kb where it is joined by clinopyroxene. Clinopyroxene is the liquidus phase at 20 kb. Compared to glass 95-1 the olivine-added 95-2 composition expands the field of olivine crystallization raising the liquidus by about 100°C. The pressure at which clinopyroxene occurs on the liquidus is also higher for 95-2. The compositions of run products have been discarded where analyses of the bulk charge show significant iron loss to have occurred in the runs made in Pt capsules.

At 0 kb* olivine (Mg_{90}) is the liquidus phase and crystallizes alone to 1230°C where it is joined by plagioclase. Over this interval the liquid line of descent is dominated by increasing CaO, Al_2O_3 and SiO_2 content, and sharply decreasing MgO (Fig. 4-2). Olivine changes systematically becoming less magnesian with decreasing temperature and increasing degree of crystallization, Mg_{90} at 1340°C, Mg_{85} at 1230°C and Mg_{79} at 1190°C. Plagioclase, An_{91}, crystallizes at 1230°C where the Al_2O_3 content of the liquid is approximately 15-16%, and clinopyroxene $Ca_{40.8}\ Mg_{48.9}\ Fe_{10.3}$ crystallizes at 1190°C where the percentage of crystallization increases markedly, the solidus lying at about 1140-1150°C. The liquid line of descent over the internal 1230-1190°C is dominated by increasing SiO_2 and FeO, and decreasing Al_2O_3 and MgO. Glass compositions in runs below 1200°C are considered to be unreliable because of the presence of quench clinopyroxene rims on primary phases.

At 2 kb and 5 kb olivine (with minor chrome spinel; $\frac{100Cr}{Cr + Al} = 45.9$ at 2 kb; $\frac{100Cr}{Cr + Al} = 44$ at 5 kb) is the liquidus phase and the olivine field extends to about 100°C below the liquidus where it is joined by calcic plagioclase. Plagioclase crystallizing from 95-2 is more calcic than that from 95-1 e.g. An_{91} at 2 kb 1200°C compared to $An_{85.6}$ at 5 kb 1220°C. The point at which plagioclase begins to crystallize differs by only 10°C

---

* The 0 kb and seed experiments were performed by Mr. K.L. Harris.

TABLE 4-5

95 - 2 run products at 0 kbar (Fe capsules)

	1a	1b	2a	2b	3a	3b	3c	4a	4b	4c	5a	5b	5c	6a	6b	6c	6d
SiO_2	40.5	47.4	40.5	48.1	39.6	45.6	48.5	39.9	46.1	49.9	40.1	45.3	51.3	39.0	45.9	53.1	50.4
TiO_2	-	0.32	-	0.27	-	-	0.35	-	-	0.37	-	-	0.55	-	-	-	0.63
Al_2O_3	-	14.0	-	14.8	-	34.0	15.3	-	33.3	14.3	-	34.7	14.0	-	31.8	4.33	13.7
FeO[t]	10.1	10.0	11.3	10.0	14.6	0.35	10.4	15.0	0.51	10.0	14.9	0.84	10.0	19.3	1.41	6.32	11.9
MnO	-	-	-	-	-	-	-	-	-	-	-	-	-	-	-	-	-
MgO	48.9	14.9	47.8	12.5	45.4	0.57	9.88	44.6	0.65	8.9	44.4	1.67	8.03	41.3	1.25	16.8	8.08
CaO	0.41	12.4	0.35	13.5	0.45	18.4	14.6	0.52	18.3	15.3	0.63	16.2	14.8	0.45	71.1	19.5	14.1
Na_2O	-	0.89	-	0.85	-	1.02	1.00	-	1.11	1.17	-	1.19	1.29	-	1.43	-	1.21
K_2O	-	-	-	-	-	-	-	-	-	-	-	-	-	-	-	-	-
Cr_2O_3	-	-	-	-	-	-	-	-	-	-	-	-	-	-	-	-	-
O =	4		4		4	8		4	8		4	8		4	8	6	
Si	0.995		0.999		0.992	2.106		1.000	2.130		1.005	2.087		0.999	2.151	1.930	
Ti	-		-		-	-		-	-		-	-		-	-	-	
Al	-		-		-	1.852		-	1.814		-	1.884		-	1.755	0.185	
Fe[t]	0.208		0.233		0.305	0.014		0.315	0.020		0.313	0.032		0.143	0.055	0.192	
Mn	-		-		-	-		-	-		-	-		-	-	-	
Mg	1.791		1.758		1.698	0.039		1.669	0.045		1.659	0.115		1.576	0.087	0.910	
Ca	0.011		0.009		0.011	0.911		0.013	0.906		0.016	0.800		0.012	0.858	0.759	
Na	-		-		-	0.091		-	0.100		-	0.106		-	0.130	-	
K	-		-		-	-		-	-		-	-		-	-	-	
Cr	-		-		-	-		-	-		-	-		-	-	-	
Total	3.005		3.000		3.008	5.013		2.999	5.013		2.995	5.024		3.001	5.037	3.977	54.8
100 Mg/Mg+Fe	89.6	72.6	88.3	69.2	84.8		62.9	84.1		81.3	84.1		59.0	79.2		82.5	
						Ca 90.9			Ca 90.1			Ca 88.3			Ca 86.8	Ca 40.8	
						Na 9.1			Na 9.9			Na 11.7			Na 13.2	Mg 48.9	
						K -			K -			K -			K -	Fe 10.3	

[t] = Total iron as FeO . MnO <0.15%

1. 1340°C ; a = olivine , b = glass
2. 1300°C ; a = olivine , b = glass
3. 1230°C ; a = olivine , b = plagioclase , c = glass
4. 1210°C ; a = olivine , b = plagioclase , c = glass
5. 1200°C ; a = olivine , b = plagioclase , c = glass
6. 1190°C ; a = olivine , b = plagioclase , c = clinopyroxene , d = glass

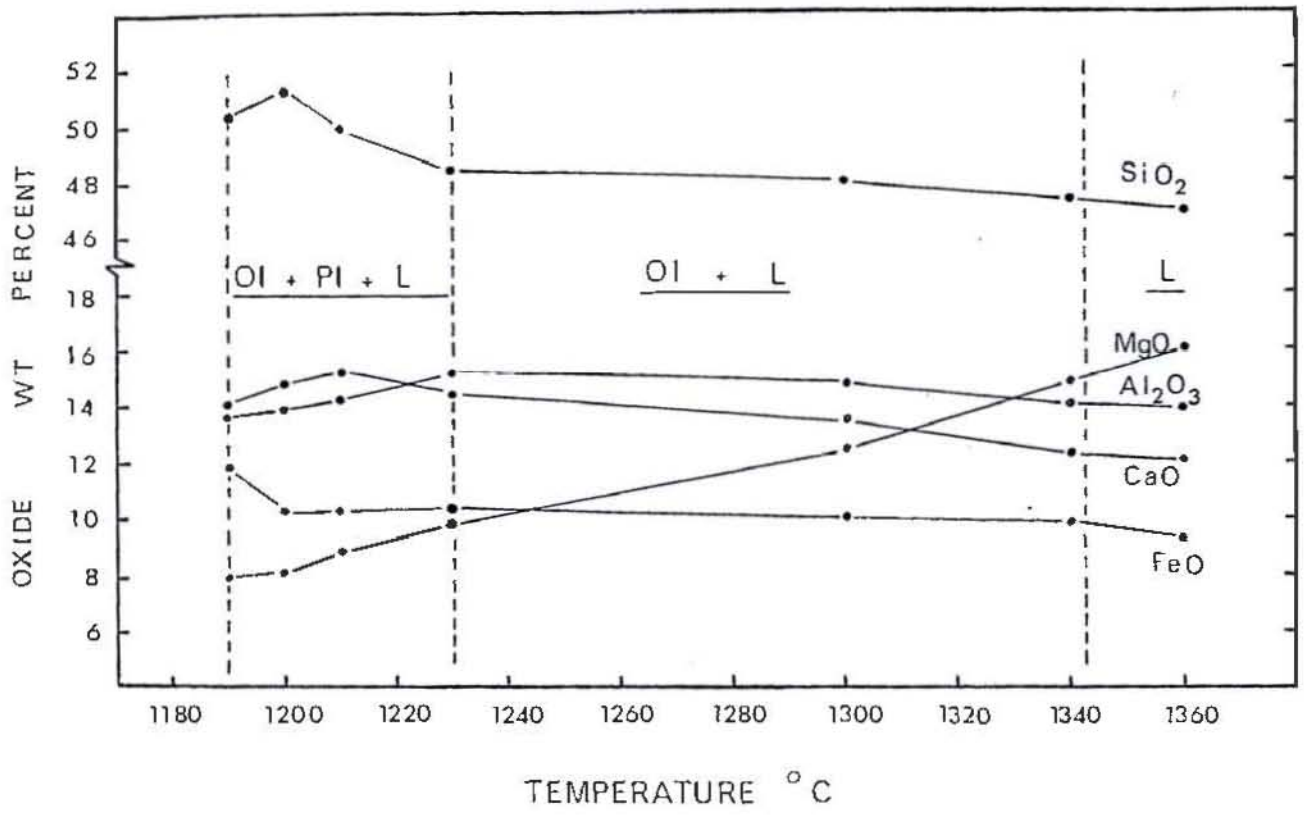

Fig. 4-2. Line of liquid descent for 95-2 at 0 kbar. Clinopyroxene occurs as an additional phase at and below 1190°C.

TABLE 4-6

Selected run products for 95-2 at 2 and 5 kbar (Pt and graphite capsules)

	1	2a	2b	2c	3a	3b	3c	4a	4b	5	6a	6b	6c	7a	7b	8	10a	10b	10c	10d
SiO_2	-	40.7	-	49.2	39.2	47.2	48.0	40.8	47.7	-	40.6	-	49.0	39.7	47.6	47.3	39.6	48.3	52.4	50.9
TiO_2	-	-	-	0.38	-	-	0.47	-	0.37	-	-	-	0.32	-	0.35	-	-	-	-	0.45
Al_2O_3	29.6	-	30.1	15.7	-	32.7	14.1	-	14.0	30.2	-	32.0	15.4	-	15.6	32.7	-	30.9	4.08	14.9
FeO^t	13.3	9.83	13.3	7.60	16.3	0.68	12.0	9.42	9.51	14.5	9.84	15.0	8.63	13.8	10.5	0.63	14.9	0.80	6.59	11.3
MnO	-	-	-	-	-	-	-	-	-	-	-	-	-	-	-	-	-	-	-	-
MgO	19.2	49.2	18.9	12.0	44.1	-	9.4	49.6	15.7	19.4	49.2	18.6	12.0	46.1	11.0	0.89	45.2	0.91	19.2	8.13
CaO	0.48	0.25	0.41	14.2	0.43	18.3	14.8	0.27	12.0	0.49	0.31	0.59	13.7	0.43	14.1	17.2	0.41	17.7	17.4	13.4
Na_2O	-	-	-	0.89	-	1.08	1.23	-	1.02	-	-	-	0.97	-	0.86	1.58	-	1.37	-	0.93
K_2O	-	-	-	-	-	-	-	-	-	-	-	-	-	-	-	-	-	-	-	-
Cr_2O_3	37.4	-	37.3	-	-	-	-	-	-	35.4	-	33.8	-	-	-	-	-	-	9.35	-
O =	4	4	4		4	8		4		4	4	4		4		8	4	8	6	
Si	-	0.996	-		0.991	2.177		0.996		-	0.996	-		0.992		2.171	0.992	2.226	1.903	
Ti	-	-	-		-	-		-		-	-	-		-		-	-	-	-	
Al	1.019	-	1.035		-	1.779		-		1.039	-	1.097		-		1.770	-	1.679	0.174	
Fe^t	0.325	0.201	0.324		0.345	0.026		0.192		0.353	0.202	0.365		0.288		0.024	0.311	0.031	0.200	
Mn	-	-	-		-	-		-		-	-	-		-		-	-	-	-	
Mg	0.836	1.798	0.821		1.662	-		1.806		0.845	1.798	0.806		1.716		0.061	1.691	0.063	1.039	
Ca	0.015	0.006	0.013		0.012	0.904		0.006		0.015	0.008	0.018		0.012		0.846	0.010	0.874	0.676	
Na	-	-	-		-	0.097		-		-	-	-		-		0.141	-	0.123	-	
K	-	-	-		-	-		-		-	-	-		-		-	-	-	-	
Cr	0.864	-	0.860		-	-		-		0.818	-	0.777		-		-	-	-	0.010	
Total	3.059	3.003	3.053		3.009			3.003		3.071	3.004	3.063	71.2	3.008		5.014	3.007	4.995	4.004	
100 Mg/Mg + Fe	72.0	89.9	71.7	73.9	82.8		58.3	90.4	74.6	70.5	89.9	68.8		85.6	65.2		84.4		83.9	56.3
						Ca 90.4									Ca 85.7		Ca 87.7	Ca 35.3		
						Na 9.6									Na 14.3		Na 12.3	Mg 54.3		
						K -									K -		K -	Fe 10.4		

t = total iron as FeO. MnO < 0.15%

1. 2 kbar 1280°C; spinel
2. 2 kbar 1240°C; a = olivine, b = spinel, c = glass
3. 2 kbar 1200°C; a = olivine, b = plagioclase, c = glass
4. 5 kbar 1340°C; a = olivine, b = glass
5. 5 kbar 1300°C; spinel
6. 5 kbar 1260°C; a = olivine, b = spinel, c = glass
7. 5 kbar 1230°C; a = olivine, b = glass
8. 5 kbar 1210°C; plagioclase
9. 5 kbar 1200°C; a = olivine, b = plagioclase, c = clinopyroxene, d = glass

(i.e. within experimental error, $\pm$ 5°C) between the two compositions. Clinopyroxene $Ca_{35.3}$ $Mg_{54.2}$ $Fe_{10.4}$ crystallizes at 1180°C (2 kb) and 1200°C (5 kb) and is relatively aluminous containing 4-6% Al_2O_3. The percentage of crystallization increases markedly at the point where clinopyroxene begins to crystallize and this is evidenced by the sharp decrease in 100Mg/(Mg + Fe) ratio of the co-existing olivine.

Olivine is the liquidus phase at 10 and 15 kb. Aluminous clinopyroxene with moderate CaO content (Table 4-7) crystallizes with olivine at 18 kb 1400°C. Clinopyroxene $Ca_{23.7}$ $Mg_{67.7}$ $Fe_{8.5}$ alone crystallizes at 20 kb where the liquidus changes slope. Compared to the liquidus clinopyroxene in 95-1 this pyroxene is more magnesian and considerably less calcic (Table 4-7), being of subcalcic composition. As for 95-1 composition there is no liquidus or near-liquidus field of orthopyroxene.

2-3. Depth of magma segregation

Lack of a liquidus or near-liquidus field of orthopyroxene for both 95-1 and 95-2 is at variance with evidence which strongly support the view that orthopyroxene is an expected residual phase from partial melting of mantle peridotite to yield olivine tholeiites (or their tholeiitic picrite parents). Firstly non-cumulus magnesian harzburgite and lherzolite are far more common in nature than non-cumulus dunite; non-cumulus magnesian wehrlite is rare. Secondly anhydrous melting studies on five model mantle peridotite compositions (Ito & Kennedy, 1967; Mysen & Kushiro, 1977; PART 3) from 0 to 40 kb pressure show that orthopyroxene is a residual phase for all except high degrees of melting where olivine ($\pm$ chrome spinel) is the residual phase. No field of olivine-clinopyroxene (wehrlite) or plagioclase wehrlite was found in any of the studies.

Comparison of the liquidi of 95-1 and 95-2 with the melting relations of the two peridotite compositions (pyrolite and Tinaquillo peridotite) studied in PART 3 shows that olivine and orthopyroxene are

TABLE 4-7

Representative analyses of 95-2 run products at 10, 15, 18 and 20 kbar

	1a	1b	2a	2b	2c	3a	3b	4a	4b	5a	5b	5c	6a	6b
SiO_2	40.8	47.6	40.0	51.6	48.8	40.6	47.9	40.4	48.6	40.1	53.1	47.0	51.9	46.3
TiO_2	-	0.32	-	-	0.32	-	0.33	-	0.38	-	-	0.32	-	0.30
Al_2O_3	-	14.2	-	7.03	15.8	-	14.2	-	14.8	-	7.10	14.9	7.51	15.2
FeO[t]	9.96	9.48	12.7	4.50	9.37	10.7	9.55	11.1	9.21	11.5	5.48	10.3	5.18	9.95
MnO	-	-	-	-	-	-	-	0.12	-	-	0.12	-	-	-
MgO	49.2	15.4	46.9	18.6	10.5	48.6	14.8	47.9	13.3	48.2	23.3	14.5	23.1	15.00
CaO	-	12.1	0.36	17.8	14.3	0.17	12.4	0.48	12.7	0.29	12.2	12.1	11.3	12.3
Na_2O	-	0.89	-	-	0.90	-	0.81	-	0.90	-	-	0.85	-	0.87
K_2O	-	-	-	-	-	-	-	-	-	-	-	-	-	-
Cr_2O_3	-	-	-	0.63	-	-	-	-	-	-	0.46	-	0.31	-
O =	4		4	6		4		4		4	6		6	
Si	1.000		0.994	1.855		0.997		0.997		0.990	1.854		1.849	
Ti	-		-	-		-		-		-	-		-	
Al	-		-	0.298		-		-		-	0.292		0.316	
Fe[t]	0.204		0.264	0.135		0.219		0.229		0.236	0.160		0.155	
Mn	-		-	-		-		0.003		-	0.004		-	
Mg	1.797		1.738	0.998		1.782		1.762		1.773	1.215		1.229	
Ca	-		0.010	0.681		0.004		0.013		0.007	0.457		0.431	
Na	-	-	—			-		-		-	-		-	
K	-		-	-		-		-		-	-		-	
Cr	-		-	0.017		-		-		-	0.013		0.009	
Total	3.000		3.006	3.987		3.003		3.003		3.009	3.994		3.988	
100 Mg / Mg + Fe	89.8	74.3	86.8	88.1	66.6	89.0	73.4	88.5	72.0	88.2	88.4	71.5	88.8	72.9
			Ca 37.5							Ca 24.9		Ca 23.7		
			Mg 55.0							Mg 66.3		Mg 67.7		
			Fe 13.5							Fe 8.7		Fe 8.5		

[t] = total iron as FeO

1. 10 kbar 1360°C; a = olivine, b = glass
2. 10 kbar 1260°C; a = olivine, b = clinopyroxene, c = glass
3. 15 kbar 1380°C; a = olivine, b = glass
4. 15 kbar 1360°C; a = olivine, b = glass
5. 18 kbar 1400°C; a = olivine, b = clinopyroxene, c = glass
6. 20 kbar 1440°C; a = clinopyroxene, b = glass

residual phases for the entire P-T range defined by the 95-1 liquidus and the bulk of the P-T range of 95-2, except at low pressure (Fig. 4-3). Derivation of 95-2 and similar tholeiitic picrites from melting of peridotite at low pressure (0-5 kb) can be ruled out because liquids formed by partial melting of peridotite in that pressure range and at appropriate temperature are not of olivine tholeiite or tholeiitic picrite composition but magnesian quartz tholeiite (PART 3).

Since neither of the compositions studied has orthopyroxene as a near-liquidus phase and because Green & others (1979) demonstrated that addition of ∿ 17% olivine to DSDP basalt 3-18 resulted in a shift of the olivine-pyroxene cotectic to higher pressures where the increased activity of pyroxene at the expense of olivine resulted in orthopyroxene as a co-liquidus phase we have added a further 3% olivine to 95-2 in an attempt to define the P-T conditions where olivine co-exists with orthopyroxene (+ clinopyroxene). This new composition, termed 95-3 ($100Mg/(Mg+\Sigma Fe) = 76.8$ Table 4-1) has olivine ($Mg_{91.4}$), as a liquidus phase to 20 kb and the olivine-clinopyroxene cotectic moves to higher pressure. Clinopyroxene co-existing with olivine at 18 kb 1400°C and clinopyroxene crystallizing alone at 20 kb 1400°C and 22 kb 1460°C is distinctly subcalcic and strongly zoned from low Al_2O_3, low CaO cores to more calcic and aluminous rims (Table 4-8). No near-liquidus field of orthopyroxene was observed.

Previous studies on various basalts have found that orthopyroxene occurred as a liquidus phase between the P-dependent fields of olivine at lower pressure and clinopyroxene at higher pressure and have shown that clinopyroxenes co-existing with orthopyroxene on anhydrous liquidi are extremely subcalcic (e.g. Green & Ringwood, 1976a; Green & Hibberson, 1970; Green & others, 1975a). Moreover study of liquidus pyroxenes in lunar basalts has shown that experimental difficulties exist in crystallization of orthopyroxene and that metastable nucleation and growth of subcalcic ('pigeonitic') clinopyroxenes in place of the stable co-existing

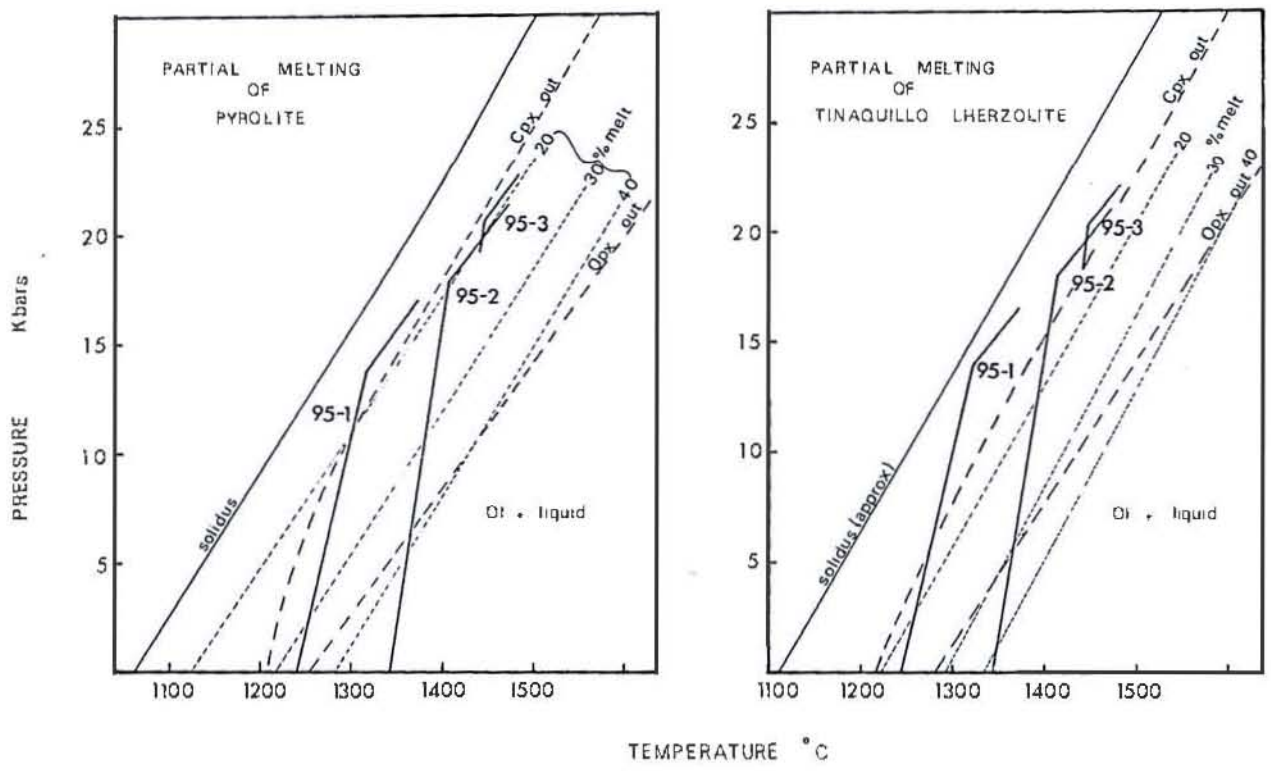

Fig. 4-3. Summary of partial melting data for pyrolite and Tinaquillo lherzolite (PART 3) compared with experimental liquids of basalt 95-1 and olivine-enriched compositions.

orthopyroxene-clinopyroxene pair commonly occurs (Green, 1976c). Because of this and the subcalcic nature of the near-liquidus clinopyroxenes crystallized from 95-3 composition we have added enstatite seeds to test for orthopyroxene saturation.

Two seed compositions were used: 1) Tem-Pres synthetic clinoenstatite, 2) bronzite 2539, $Ca_1Mg_{85}Fe_{14}$, 0.9% Al_2O_3. The seeds were crushed to 5-10μ grainsize and 1% wt added to 95-3 composition. Experiments were run at 20 kb 1450°C (ol+cpx+gl) and at 22 kb 1460°C (cpx+gl). No relic seeds were observed in any of the runs and none crystallized primary orthopyroxene. Subcalcic clinopyroxene co-existing with olivine at 20 kb 1450°C has extremely subcalcic cores (∿ 6% CaO) with low alumina contents (Table 4-8). Clinopyroxene at 22 kb 1460°C is of subcalcic composition. The seed experiments reaffirm previous difficulties experienced in nucleating co-existing orthopyroxene and calcic clinopyroxene rather than metastable low-calcium pyroxene. The experiments have not demonstrated crystallization of orthopyroxene but we infer from the extremely subcalcic nature of the clinopyroxene that 95-3 composition, i.e. 95-1 + 18% olivine is close to saturation in orthopyroxene as well as calcic clinopyroxene and lies on or very close to the two pyroxene boundary.

We interpret these data to indicate that a picritic magma containing approximately 27% normative olivine and parental to 95-1 by the separation of about 15 to 18% olivine (mean composition Mg_{89}) segregated from residual lherzolite (olivine, orthopyroxene and clinopyroxene in residue) at about 70 km (∿ 20 kb) at a temperature of about 1450°C. This depth of magma segregation is very similar to that invoked for DSDP basalt 3-18 (Green & others, 1979) except that a harzburgite rather than a lherzolite residue was inferred for DSDP 3-18.

2-4. Olivine-melt equilibria

Previous experimental studies on both terrestrial (Roeder & Emslie, 1970; Roeder, 1974) and lunar basalts (Longhi & others, 1978) have shown

TABLE 4-8
95-3 run products

	1a	1b	1c	1d	1e	2a	2b	3a	3b	3c	3d	4a	4b	4c
SiO_2	40.3	54.9	52.4	51.7	46.9	53.6	52.2	55.1	54.3	52.4	46.8	40.6	55.4	54.1
TiO_2	-	-	-	-	0.35	-	-	-	-	-	0.30	-	-	-
Al_2O_3	-	3.42	7.20	7.77	15.4	6.14	7.78	4.29	5.01	8.22	14.3	-	3.34	5.59
FeO^t	11.2	5.66	4.85	4.94	10.1	5.35	4.80	5.84	5.61	4.94	10.1	9.83	5.97	5.39
MnO	-	-	-	-	-	-	-	-	-	-	-	-	-	-
MgO	48.1	26.0	21.5	20.8	13.8	24.3	21.8	28.3	26.7	22.8	15.5	49.6	29.4	26.4
CaO	0.32	10.0	14.0	14.4	12.4	10.6	13.4	6.44	8.40	11.7	11.9	-	5.95	8.58
Na_2O	-	-	-	-	1.05	-	-	-	-	-	1.09	-	-	-
K_2O	-	-	-	-	-	-	-	-	-	-	-	-	-	-
Cr_2O_3	-	-	-	0.45	-	-	-	-	-	-	-	-	-	-
O =	4	6	6	6		6	6	6	6	6		4	6	6
Si	0.994	1.937	1.864	1.844		1.891	1.853	1.925	1.906	1.850		0.993	1.934	1.896
Ti	-	-	-	-		-	-	-	-	-		-	-	-
Al	-	0.142	0.302	0.327		0.255	0.326	0.177	0.207	0.342		-	0.137	0.231
Fe^t	0.231	0.167	0.144	0.147		0.158	0.143	0.171	0.165	0.146		0.201	0.174	0.158
Mn	-	-	-	-		-	-	-	-	-		-	-	-
Mg	1.770	1.367	1.140	1.106		1.277	1.153	1.473	1.397	1.199		1.811	1.527	1.380
Ca	0.008	0.378	0.534	0.550		0.401	0.510	0.241	0.316	0.443		-	0.222	0.322
Na	-	-	-	-		-	-	-	-	-		-	-	-
K	-	-	-	-		-	-	-	-	-		-	-	-
Cr	-	-	-	0.013		-	-	-	-	-		-	-	-
Total	3.003	3.992	3.985	3.986		3.982	3.984	3.987	3.990	3.979		3.007	3.997	3.989
100 Mg/Mg+Fe	88.4	89.1	88.8	88.2	70.9	89.0	89.0	89.6	89.5	89.2	73.1	90.0	89.8	89.7
Ca		19.8	29.4	30.5		21.8	28.2	12.8	16.8	24.8			11.5	17.3
Mg		71.5	62.7	61.3		69.6	63.9	78.2	74.4	67.1			79.4	74.2
Fe		8.7	7.9	8.2		8.6	7.9	9.1	8.8	8.2			9.1	8.5

t = Total iron as FeO. MnO< 0.15%, limit of detection for Na_2O = 0.2%

1. 18 kbar 1400°C; a = olivine, b = clinopyroxene core, c = clinopyroxene midway, d = clinopyroxene rim, e = glass
2. 20 kbar 1440°C; a = clinopyroxene core, b = clinopyroxene
3. 22 kbar 1460°C; a = clinopyroxene core, b = clinopyroxene midway, c = clinopyroxene rim, d = glass
4. 95-3 + 1% Enstatite; a = olivine, b = clinopyroxene core, c = clinopyroxene rim.

that Fe-Mg partitioning between olivine and liquid $\frac{x^{ol}_{FeO} \cdot x^{L}_{MgO}}{x^{ol}_{MgO} \cdot x^{L}_{FeO}}$ is nearly constant (0.3 ± 0.03) over a range of temperature and compositions. Data for olivine-liquid pairs from the 0 kb experiments have been plotted in Fig. 4-4a and for the high pressures in Fig. 4-4b. Experiments performed in platinum capsules have been excluded due to uncertainties introduced by iron loss. All iron is assumed to be FeO since the Fe_2O_3 content of the starting mix was low ($Fe_2O_3/FeO \sim 0.05$) and the furnace assembly used results in reducing conditions with f_{O_2} sufficiently low to inhibit crystallization of spinel. Data are plotted as mole percent oxide and equations calculated following Roeder & Emslie (1970). Also included are unpublished data for two runs on a basalt similar in composition to 95-2. Data for 95-1 at 5 kb 1200°C are not included because of the presence of quench clinopyroxene.

Although limited, the data in Fig. 4-4 show that the regression lines for log K^{Fe} and log K^{Mg} are mutually parallel in both the 0 kb and high pressure experiments indicating that K_D is practically independent of temperature (Roeder & Emslie, 1970). Equations obtained by regression lines through the 0, 5 and 10 kb data points are listed in Table 4-9. The 0 kb and 5 kb data for log K^{Fe} and log K^{Mg} (Fig. 4-4) are in agreement (within experimental error) whereas the 10 kb data points are displaced to higher log K values. This displacement results in a systematic increase in K_D with pressure, e.g. 0.29-0.30 at 5 kb, 0.30-0.33 at 10 kb and 0.33-0.34 at 15 kb. The increase of K_D with pressure is such that olivine co-existing with a given liquid at high pressure is more iron-rich than olivine co-existing with the same liquid at low pressure (cf. Tables 4-3 to 4-7). Our data therefore supports previous suggestions (Longhi & others, 1978; Bender & others, 1978) that pressure does effect Fe-Mg partitioning between olivine and liquid above 5 kb.

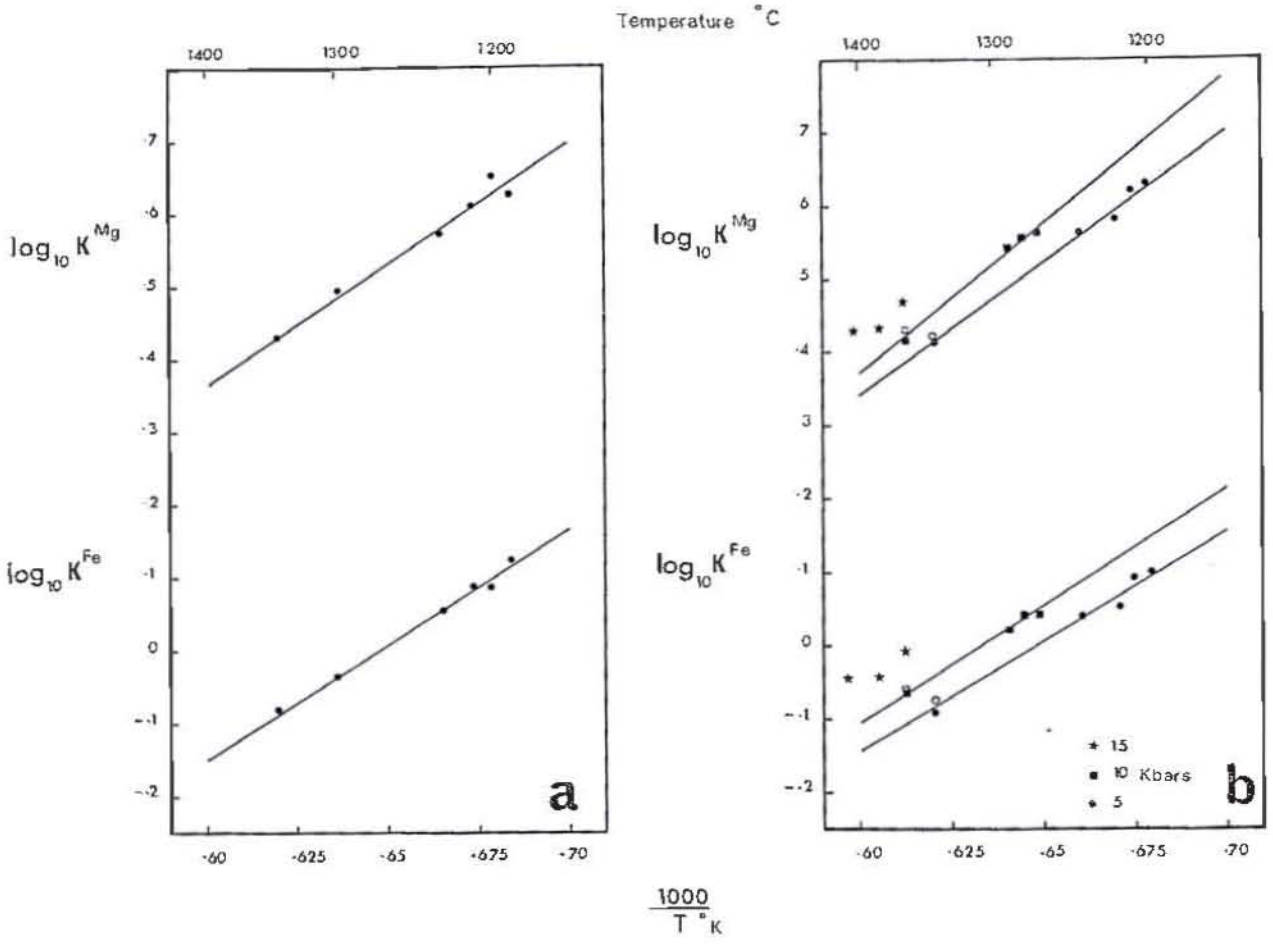

Fig. 4-4. Logarithmic plot of distribution coefficients K^{Fe}_{Ol-L} and K^{Mg}_{Ol-L} as functions of inverse temperature.

a) data for 0 kbar experiments, b) high pressure experiments (excluding those made in Pt capsules). Open circles and squares are for basaltic composition similar to 95-2.

TABLE 4-9.

Temperature dependence of Fe-Mg partitioning for olivine - liquid pairs according to the reaction

$$\log_{10} K = \frac{B}{T^{\circ}K} + A$$

P	log (K)	B	A	r
0 Kb	K^{Fe}	3.129	-2.022	0.994
	K^{Mg}	3.240	-1.571	0.985
5 Kb	K^{Fe}	3.028	-1.833	0.987
	K^{Mg}	3.632	-1.960	0.995
10 Kb	K^{Fe}	3.177	-2.008	0.996
	K^{Mg}	4.039	-2.048	0.995

CHAPTER 3

PETROGENESIS OF THE LAU BASIN BASALT

3-1. Crystal fractionation

Hawkins (1976) suggested that the Lau Basin basalts had undergone low pressure crystal fractionation involving olivine Mg_{88}, and possibly plagioclase since microphenocrysts of these phases occur in the more primitive of the Lau Basin basalts. Our experimental results show that the crystallization interval between olivine and plagioclase is small (Fig. 4-1). As shown in Figure 4-2, fractionation of olivine and plagioclase will result in an increase in Fe/Mg and Na/Ca ratios, and an increase in SiO_2 and decrease in Al_2O_3 content. Clinopyroxene fractionation, additional to olivine and plagioclase, seems likely for the most evolved Lau Basin basalts; fractionation of all three phases will result in increased Fe/Mg and Na/Ca ratios and increased abundances of incompatible elements (including TiO_2) but little change in SiO_2 content. While fractional crystallization of olivine, olivine + plagioclase and olivine + plagioclase + clinopyroxene can account for much of the variation in major element geochemistry exhibited by the Lau Basin basalts, variations in trace element abundances cannot be satisfactorily explained by crystal fractionation (Gill, 1976). In particular, the very low abundances of LIL elements of basalt 95-1 mean that it cannot be parental to more evolved Lau Basin basalts many of which have considerably higher abundances of LIL elements.

Numerous petrologic studies have stressed the importance of crystal fractionation in mid-ocean ridge basalts and it is now clear that most MORB have undergone variable degrees of fractionation of olivine (+ spinel), olivine + plagioclase, or olivine + plagioclase + pyroxene (e.g. Miyashiro & others, 1969; Kay & others, 1970; Bryan & others, 1976; Hekinian & others, 1976; Blanchard & others, 1976; Flower & others, 1977; Rhodes & others, 1979). The similarity in liquidus phases and magma compositions of the Lau Basin

basalts, and olivine tholeiites from other marginal basins, suggests that crystal fractionation of olivine, plagioclase and pyroxene is equally important in modifying compositions of basalts erupted in marginal basins.

3-2. Plagioclase compositions

The calcic plagioclase compositions obtained in this study are similar to the bytownite compositions observed in the more primitive MORB. Hekinian & others (1976) recognized a correlation with crystal size and morphology and noted that phenocrysts are more calcic (An_{75-85}) than microphenocrysts (An_{70-80}) and microlites (An_{60-75}). Xenocrysts and megacrysts are generally highly calcic, An_{89-95} (Bryan & others, 1976; Hekinian & others, 1976; Flower & others, 1977; Donaldson & Brown, 1977) although exceptions have been reported (Bryan & Moore, 1977). Donaldson & Brown (1977) have pointed out that the calcic megacrysts are too calcic to be in equilibrium with their host compositions. The data obtained in this study are particularly relevant to this problem since Lau Basin basalt 95-1 has a higher CaO/Na_2O ratio than any other basalt from the ocean basins. The liquidus plagioclase for 95-2 (CaO/Na_2O = 13.5) is $An_{90.9}$, and for 95-1 glass (CaO/Na_2O = 9.7) is $An_{85.6}$, and in reasonable agreement with the compositions predicted from crystal-liquid equilibria (Drake, 1976). This crystal-liquid partitioning is thought to be independent of pressure (Drake, 1976) although Green & others (1979) noted that plagioclase crystallized from DSDP 3-18, in the absence of other calcium-bearing phases, became slightly less calcic at higher pressure. Bender & others (1978) in the experimental study of FAMOUS basalt 527-1-1, also noted that the first formed plagioclase became more sodic with increasing pressure. Our data for 95-1 show that the plagioclase crystallized at 10 kb is more sodic than that at 5 kb, i.e. $An_{85.6}$ at 5 kb, An_{81} at 10 kb. However, the presence of co-existing clinopyroxene in the 10 kb run means that this change may be due to changed (Ca/Na) ratio in the liquid rather

CHAPPELL, B.W., COMPSTON, W., ARRIENS, P.A., & VERNON, M.J., 1969 - Rubidium and strontium determinations by X-ray fluorescence spectrometry and isotope dilution below the part per million level. *Geochimica et Cosmochimica Acta, 33, 1002-6.*

CHRISTENSEN, N.I., & SALISBURY, M.H., 1975 - Structure and constitution of the lower oceanic crust. *Reviews of Geophysics and Space Physics, 13, 57-86.*

CHURCH, W.R., & COISH, R.A., 1976 - Oceanic versus island-arc origin of ophiolites. *Earth and Planetary Science Letters, 31, 8-14.*

CHURCH, W.R., & RICCIO, L., 1977 - Fractionation trends in the Bay of Islands ophiolite of Newfoundland: polycyclic cumulate sequences in ophiolites and their classification. *Canadian Journal of Earth Science, 14, 1156-65.*

CLAGUE, D.A., & BUNCH, T.E., 1976 - Formation of ferrobasalt at East Pacifc midocean spreading centres. *Journal of Geophysical Research, 81, 4247-56.*

CLARKE, D.B., 1970 - Tertiary basalts of Baffin Bay: possible primary magma from the mantle. *Contributions to Mineralogy and Petrology, 25, 203-24.*

CLARKE, D.B., & PEDERSEN, A.K., 1976 - Tertiary volcanic province of West Greenland. *In* ESCHER, A., & WATTS, W.S. (Editors) GEOLOGY OF GREENLAND, 365-85. *Geological Survey of Greenland.*

COLEMAN, P.J., 1975 - On island arcs. *Earth Science Reviews, 11, 47-80.*

COLEMAN, R.G., 1977 - OPHIOLITES. *Springer-Verlag, Berlin.*

COLEMAN, R.G. & PETERMAN, Z.E., 1975 - Oceanic plagiogranite. *Journal of Geophysical Research, 80, 1099-108.*

CONNELLY, J.B., 1979 - Mode of emplacement of the Papuan Ultramafic Belt. *BMR Journal of Australian Geology and Geophysics, 4, 57-65.*

Melsom & Thompson, 1970; Bonatti & others, 1971; Hodges & Papike, 1976).

The presence of magnesian orthopyroxene in cumulate peridotite and gabbro from the ocean floor conflicts with the melting relations of relatively primitive MORB studied previously (Green & others, 1979; Bender & others, 1978) and of 95-1 studied here: these studies show that orthopyroxene is not a near-liquidus phase at low pressure. Bender & others (1978) claimed that FAMOUS basalt 527-1-1 ($100Mg/(Mg + \Sigma Fe) = 68$, 18% normative olivine) was multiply saturated (olivine, orthopyroxene, and clinopyroxene) at 10.5 kb. However, orthopyroxene was in fact only crystallized in one run at 15 kb where it occurred alone 40°C below clinopyroxene liquidus, and the assemblage claimed to have equilibrated at 10.5 kb shows non-equilibrium Fe-Mg partitioning. Orthopyroxene is however a near-liquidus phase at low pressure for the more fractionated MORB studied by Kushiro & Thompson (1972), and Fujii & Kushiro (1977). For these compositions, Mg-values of 66 and 60 respectively, orthopyroxene co-exists with olivine, plagioclase and clinopyroxene at or near the liquidus at 5-8 kb. This orthopyroxene would not be more magnesian than Mg_{87}. If these magmas are primary and their depth of segregation is $\sim$ 20-30 km then we must envisage a mantle source peridotite with olivine $\leq Mg_{86}$, thus differing considerably from previous estimates of the composition of the oceanic upper mantle (PART 3), and from the source peridotite (olivine $\sim Mg_{90}$) for ocean floor basalt DSDP 3-18 (Green & others, 1979). Inhomogeneity of this extent in such a key parameter as the Mg/(Mg + Fe) of the upper mantle has been argued previously for continental areas (Wilkinson & Binns, 1977), and might possibly be a feature of the 'primitive' upper mantle source regions in the oceanic regime, although evidence from lherzolite nodules in oceanic regimes appears to favour a more refractory oceanic mantle. If we accept as a reasonable constraint that oceanic upper mantle source regions should have olivine of $Mg_{90 \pm 2}$, then addition of olivine ($\pm$ other phases) to basalts

such as those studied by Kushiro & Thompson (1972) and Fujii & Kushiro (1977) is necessary to deduce their parental compositions. Multiple saturation of these basalts at 5-8 kb means that there is no clear compositional trend to be reversed to lead back to parental compositions. Additional evidence against a primary origin for these basalts are their low Ni contents which are appreciably lower than commonly inferred for primitive magmas (e.g. Allegre & others, 1977; Sato, 1977). We thus conclude that these magmas are themselves not of appropriate composition to precipitate the accumulative phases of Mg-orthopyroxene-bearing ophiolite complexes, nor are they appropriate as partial melts in equilibrium with the refractory harzburgite of ophiolite complexes.

Magnesian orthopyroxene may be expected to crystallize at low pressure from more silica-rich strongly hypersthene-normative liquids such as the magnesian olivine-poor and quartz tholeiites (50-54% SiO_2) found in a number of ophiolites (see PART 3, Chapter 6; and compilations by Duncan & Green 1979; Sun & Nesbitt, 1978a). Preliminary experimental results (R.A. Duncan, pers. comm. 1979) on a magnesian olivine-poor tholeiite composition inferred to be parental to the Upper Pillow Lavas supports this view. Sun & Nesbitt (1978a), following Church & Riccio's (1977) observation of the association of olivine-orthopyroxene cumulate sequences in ophiolites with Ti-poor high silica magnesian lavas, referred to these magmas as 'ophiolitic basalts'. Duncan & Green (1979) have distinguished quartz tholeiites and olivine-poor tholeiites developed at spreading centres from high-magnesian 'andesites', apparently generated in island-arc situations. These authors used compositions from Troodos ophiolite complex and Cape Vogel, Papua New Guinea respectively to typify the two magma types.

Magnesian quartz tholeiites or magnesian tholeiites with low normative olivine similar to either the 'Troodos type' or 'Cape Vogel type', have not been recovered from marginal basins to date but low-TiO_2 silica

saturated basalts and basaltic andesites are common in the Tonga and Kermadec Islands immediately east of the Lau Basin (Ewart & others, 1977). These lavas have low abundances of REE and other incompatible elements. Olivine-normative basalts also occur in the Tong-Kermadec chain and their compositions overlap the olivine tholeiites of the Lau Basin (Ewart & others, 1977).

We conclude that although olivine tholeiites like the Lau Basin basalt studied here are an important magma type occurring in back-arc basins, differing in some chemical characteristics from both 'primitive' MORB and from highly magnesian andesites and basaltic andesites in island-arcs, these basalts - high alumina MgCa olivine tholeiites - are not related to ophiolite sequences characterized by highly magnesian cumulate orthopyroxene and residual harzburgite.

3-4. Composition of the mantle beneath Lau Basin

From our experimental study we concluded that the picritic tholeiite parental to olivine tholeiite 95-1 segregated at about 70 km to leave residual olivine, orthopyroxene and clinopyroxene (+ chrome spinel). These results and the composition of the picritic parent are now used to infer the composition of the source peridotite. From the very low abundances of TiO_2, Na_2O, K_2O, P_2O_5 and LIL elements of 95-1 it can be reasonably inferred that it (and its picritic parent) were derived from a peridotite more refractory than 'Hawaiian' pyrolite. This is confirmed by examination of the melting relations of pyrolite (Fig. 4-3 and PART 3) which show that clinopyroxene is not a residual phase in melting at 20 kb 1450°C. Clinopyroxene is a residual phase (together with olivine and orthopyroxene) at 20 kb 1450°C for the more refractory Tinaquillo peridotite however (PART 3). The data presented in PART 3 suggest that tholeiitic picrite Mg $\sim_{75}$ may be formed by about 18% melting of a peridotite similar to Tinaquillo peridotite at about 20 kb 1450°C.

This melt will be in equilibrium with olivine ($Mg_{91 \pm 0.5}$), orthopyroxene, clinopyroxene and chrome spinel. The 15 kb data (PART 3) suggest that for $\sim$ 15-20% melting of Tinaquillo the modal proportions of the residual phases will be approximately olivine 65, orthopyroxene 29, clinopyroxene 5 and chrome spinel 1. We have calculated a peridotite source composition using these relative proportions, the compositions of residual pyroxenes and spinel from melting of Tinaquillo peridotite at 15 kb 1400°C (PART 3) and olivine Mg_{90}. Our estimate compares favourably with previous estimates of the oceanic upper mantle (Table 4-10) and is very similar to Tinaquillo lherzolite, although less magnesian and richer in Al_2O_3 and CaO. Estimates made using the composition of liquidus olivine and near-liquidus low-calcium pyroxene for 95-3 at 20 kb gave very similar results apart from a slightly higher CaO content.

We have also calculated the REE abundances in the model source peridotite using the REE data for 95-1 (Gill, 1976), diluted by addition of 18% olivine, and the partition coefficients of Frey & others (1978) (Appendix 1). The calculated REE abundances in the source are very low and strongly depleted in LREE with $La_N/Sm_N \sim 0.5$, $La_N/Yb_N = 0.17$ and LREE $\sim$ 0.2 x chondrites and HREE $\sim$ 1 x chondrites. These estimates are less than previous estimates of the REE content of the oceanic upper mantle which imply HREE abundance equal to 2-3 chondrites (e.g. Frey & others, 1978; Green & others, 1979). The REE abundances in the mantle source for 95-1 parent are similar to strongly LREE-depleted Tinaquillo and Lizard peridotites and generally lower than spinel lherzolite nodules and alpine peridotites (e.g. Frey & others, 1971; Frey & Green, 1974; Loubet & others, 1975). We interpret this extreme depletion in LREE and overall low abundance of REE to indicate the mantle source for 95-1 is residual after previous extraction of a basaltic melt.

Sun & Nesbitt (1978a) have shown that a number of Ti-poor basalts from island-arcs and ophiolites have CaO/TiO_2 and Al_2O_3/TiO_2 ratios

TABLE 4-10.

ESTIMATED MANTLE COMPOSITION

	A	B	C	D	E	F	G
% Melt	15-20	24					
% Olivine	(65	57.5					
% Orthopyroxene	(29	18					
% Clinopyroxene	(5	-					
% Spinel	(1	0.5					
SiO_2	45-45.2	45.0	45.0	45.2	46.1	44.2	44.5
TiO_2	0.08-0.09	0.17	0.08	0.71	0.2	0.13	0.25
Al_2O_3	3.6-4.2	4.4	3.22	3.5	4.3	2.05	4.5
FeO	8.4-8.5	7.6	7.66	8.6	8.2	8.29	8.5
MnO	0.1	0.11	0.14	0.14	-	0.13	0.14
MgO	38.7-37.4	38.8	40.0	37.5	37.6	42.2	38.0
CaO	3.1-3.6	3.4	2.99	3.1	3.1	1.92	3.2
Na_2O	0.15-0.20	0.40	0.18	0.57	0.4	0.27	0.50
K_2O	0.005-0.006	0.003	0.02	0.13	0.03	0.06	0.02
Cr_2O_3	0.55-0.53	0.45	0.45	0.43	-	0.44	0.40
NiO	0.26-0.24	0.26	0.26	0.20	-	0.23	-
$\frac{100\ Mg}{(Mg + \Sigma Fe)}$	89.1-88.7	90.1	90.3	88.6	89.1	90.0	88.3

A. Estimated source composition for 95-1 parent

B. Estimated source composition for DSDP 3-18 parent (Green & others, 1979)

C. Tinaquillo peridotite (Green, 1963)

D. Pyrolite (Ringwood, 1966)

E. Pyrolite (Ringwood, 1975)

F. Average of 384 spinel lherzolites (Maaloe & Aoki, 1977)

G. Estimated source composition (Bender & others, 1978)

significantly higher than MORB, and suggested that these features are due to depletion of the mantle beneath island-arcs by prior ocean-ridge type magmatism. A similar conclusion had previously been reached by Green (1973a, 1976a) who noted that TiO_2, Na_2O, REE and other incompatible elements are commonly lower in island-arc tholeiites and basaltic andesites than in mid-ocean ridge tholeiites.

The minor and trace element geochemistry of Lau Basin basalt 95-1 is therefore consistent with partial melting of a mantle source depleted by prior magmatic activity, possibly at a mid-ocean ridge. The low abundances of HREE in *other* Lau Basin basalts (Gill, 1976) is also consistent with derivation from a source more depleted in these elements than the source for most MORB, however the enrichment in Ba, LREE, K, Rb and Sr of some of the Lau Basin rocks probably indicates *addition* of a low-temperature melt or fluid phase enriched in these elements, possibly from subducted lithosphere.

CONCLUSIONS

The Marum and Papuan ophiolites dip from the continental margin towards accreted Paleogene island-arcs, and appear to represent frontal-arc basement emplaced as a result of mid-Tertiary continent/arc collision. Both ophiolites comprise thick (∿ 3-4 km) sequences of layered ultramafic and mafic cumulates overlying refractory tectonite peridotite. Basaltic pillow lavas are associated with both ophiolites: in the Papuan ophiolite the basalts overlie the cumulates and are an integral part of the ophiolite succession whereas in the Marum the basalts are in tectonic contact with the plutonic rocks and chemically distinct.

The cumulate sequences are layered on a gross scale (peridotite to gabbro) and exhibit igneous layering and primary cumulus textures indicative of magmatic crystallization in large magma chambers from liquids of gradually evolving composition. Superimposed on the gross layering are a number of cyclic units of variable thickness which, together with the limited differentiation (compared to stratiform intrusions such as Skaergaard) and irregular cryptic variation exhibited by the cumulus minerals, points to an open magma chamber(s) with periodic influxes of fresh magma which then mixed with the fractionated liquids of the previous pulse sufficient to retard differentiation. In both ophiolites the major cumulus phases are olivine, clinopyroxene, orthopyroxene and plagioclase. Various geothermometers and geobarometers, together with thermodynamic calculations involving silica buffers, suggest that the Marum cumulates crystallized at high temperatures, 1200-1300^{o}C, and low pressures, 1 - 2 kb, under low f_{O_2}. The early crystallization of magnesian orthopyroxene (∿ Mg_{90}) and the overall prominance of orthopyroxene as a crystallizing phase in both ophiolite sequences conflicts with the low pressure crystallization behaviour of MORB-type high-alumina olivine tholeiites. The parent magma(s) for the Marum and Papuan cumulate sequences is considered to have been of magnesian

olivine-poor or quartz tholeiite composition, similar to that represented among the Upper Pillow Lavas of the Troodos ophiolite. This interpretation is supported by the trace element geochemistry of the cumulates which indicate that the parent magmas were more depleted in LREE and high valence cations (Ti, Zr, Y) than presently sampled MORB. It is also clear from the highly magnesian nature of the early cumulus olivine that the parental magmas were appreciably more magnesian than represented among the basalts of the Papuan ophiolite which have undergone extensive fractionation of olivine, spinel, pyroxene and plagioclase.

The importance of low pressure crystal fractionation in the formation of the Papua New Guinea ophiolites is also reiterated by the fact that in neither ophiolite do basaltic or doleritic dykes cut the lower mafic cumulates or the underlying peridotites; in the Papuan Ultramafic Belt dolerite dykes, apparently feeders to the overlying basalts, are rootless. This implies that the basalts were fed from the magma chamber and that all the lavas are derivative liquids, buffered by prior fractionation of olivine, spinel, pyroxene and plagioclase. An additional observation concerning cumulate-magma relationships is the close approach of the cumulates to total equilibrium crystal-liquid partitioning: intercumulus melt has been expelled and incompatible elements are entirely partitioned into the liquid. This fact will be of importance in attempts to relate apparently comagmatic liquids by least squares mixing models since incompatible elements will increase logarithmically rather than linearly. Admixing of magmas at different stages of differentiation in subjacent magma chambers will lead to further complexities in both major and trace element geochemistry.

In both the Marum and Papuan ophiolites there is evidence to suggest the existence of parent magmas of differing composition. This is most apparent in the Papuan Ultramafic Belt where the cumulate stratigraphy in the Bowutu Mountains differs from that in the remainder of the ophiolite

(Davies, 1971); in the Marum ophiolite this is indicated by differences in the order of crystallization of some cyclic units. Differences in magma compositions as revealed by different accumulate sequences are important to define the range of primary magma compositions (particularly if the extrusives are buffered, residual liquids), and the extent to which each magma pulse crystallizes independently or mixes with previous pulses. However, detailed studies in this direction would be more profitably conducted in ophiolites with better exposure than the PNG examples such as the Semail Ophiolite in Oman (cf. Coleman, 1977).

This study has also shown that harzburgite underlying the cumulate sequences is petrologically and chemically consistent with an origin as the refractory residue of large degrees of partial melting of mantle peridotite at shallow depth. The lack of basaltic or gabbroic dykes intruding the harzburgite, the fact that the cumulates rest directly on the harzburgite, and the apparently transitional contact between harzburgite and overlying dunite shown by interfingering of dunite lenses and similarity in deformation history in the Marum ophiolite make it unlikely that the harzburgite represents an older, pre-existing segment of oceanic mantle. A genetic relationship between the tectonites and overlying cumulates is also suggested by trace element correlations. The extreme depletion of lithophile elements in the harzburgites indicates that the process of melt extraction was highly efficient, and that the source peridotite had been depleted in incompatible elements by an earlier period of magma extraction. The data obtained in the partial melting study (PART 3) show that partial melts co-existing with harzburgite of this composition are of magnesian olivine-poor tholeiite or quartz tholeiite composition, which is consistent with the inferences made from the petrology of the cumulate sequences.

Probably the most important conclusion from this study is that ophiolites with cumulate sequences similar to the Marum and Papuan Ultra-

mafic Belt are not directly related to MORB-type high-alumina olivine tholeiites. The data obtained in the partial melting study and the marginal basin basalt crystallization study (PART 4) support the conclusions reached by Green & others (1979) that MORB are derived by fractionation of olivine from tholeiitic picrite parent magmas which segregated from residual harzburgite or lherzolite at ∿ 60-70 km depth. Models of oceanic crust based entirely on ophiolites similar to those of Papua New Guinea, e.g. Troodos, where silica saturated to oversaturated magnesian lavas are derived by partial melting of depleted peridotite at shallow depth to leave refractory harzburgite do not adequately describe magmatic processes occurring at present day mid-ocean ridges where direct knowledge of the deeper oceanic crust and mantle is based on dredge hauls and a small number of limited DSDP intersections. However, Green & others (1979) and Duncan & Green (1979) have argued that the forsteritic olivine (Mg_{91}), anorthitic plagioclase and rare magnesian chrome diopside xenocrysts found in some MORB cannot have crystallized from their host basalts but crystallized from more silica saturated liquids of magnesian olivine-poor tholeiite or quartz tholeiite composition. This implies a close spatial and temporal relationship between MORB and the more silica-saturated melts. Duncan & Green (1979) suggest that such magmas are derived by second stage melting of peridotite which had earlier given rise to MORB at greater depth, and that these second stage melts might constitute 10-20% of the oceanic crust. This being the case, models of present day oceanic crust need to include provision for generation of magmas of different composition at varying depths. An additional point arising from the experimental studies of MORB is that the Al_2O_3 and CaO contents of the residual pyroxenes at the depth of magma segregation (60-70 km) are such that the harzburgite assemblage will recrystallize at lower pressure to lherzolite with less aluminous pyroxenes and less calcic orthopyroxene. Consequently, unless second stage or multistage melting is

common lherzolite rather than harzburgite as implied by the ophiolite analogue may be the more dominant mantle rock type beneath mid-ocean ridges.

The experimental study of the Lau Basin basalt 95-1 (PART 4) has shown similar melting and low pressure crystallization behaviour to MORB studied previously, and rules out a genetic relationship between marginal basin high-alumina olivine tholeiites and ophiolites similar to those of Papua New Guinea. Lau Basin basalt 95-1 forms one end of a compositional spectrum of marginal basin basalts and there is a need for experimental studies on other compositions. Of particular interest is the petrology and petrogenesis of the high magnesian andesite or boninite suite and their relationship to ophiolites, particularly ophiolites with cumulate harzburgite and orthopyroxenite (cf. Varne & Brown, 1979). The apparent occurrence of this suite in the fore-arc region of island-arcs might mean that new crust is formed *in front of* as well as behind island-arcs. In the case of the Papuan Ultramafic Belt however the high magnesian andesite clearly post-dated ophiolite formation.

REFERENCES

ALLEGRE, C.J., MONTIGNY, R., & BOTTINGA, Y., 1973 - Cortége ophiolitique et cortége oceanique, geochimie comparée et mode degénese. *Société Géologiqué de France - Bulletin, 15, 461-77.*

ALLEGRE, C.J., TREUIL, M., MINSTER, J., MINSTER, B., & ALBAREDE, F., 1977 - Systematic use of trace elements in igneous process. Part 1: Fractional crystallization processes in volcanic suites. *Contributions to Mineralogy and Petrology, 60, 57-65.*

ALLEGRE, C.J., DUPRE, B., HAMELIN, B., MONTIGNY, R., RICHARD, P., & ROUSSEAU, D., in press - Systematics in radiogenic isotopic ratio in ophiolites complex. *Proceedings volume for conference 'Mafic-Ultramafic association in orogenic belts', Grenoble, 1977.*

ANONYMOUS, 1972 - Penrose field conference on ophiolites. *Geotimes, 17, 24-5.*

ARCULUS, R.J., 1979 - Silica activity and the classification of alkalic and tholeiitic basalts. *American Mineralogist, 65, 436-9.*

ARCULUS, R.J., & WILLS, K.J.A., in press - The petrology of cumulate blocks and inclusions from the Lesser Antilles island-arc. *Journal of Petrology.*

ARNDT, N.T., 1977a - Ultrabasic magmas and high degree melting of the mantle. *Contributions to Mineralogy and Petrology, 61, 205-21.*

ARNDT, N.T., 1977b - Partitioning of Nickel between olivine and ultrabasic and basic komatiite liquids. *Carnegie Institution of Washington - Yearbook 76, 553-7.*

ARNDT, N.T., NALDRETT, A.J., & PYKE, D.R., 1977 - Komatiitic and iron-rich tholeiitic lavas of Munro Township, northeast Ontario. *Journal of Petrology, 18, 319-69.*

ARTH, J.G., ARNDT, N.T., & NALDRETT, A.J., 1977 - Genesis of Archaean komatiites from Munro Township, Ontario: Trace element evidence. *Geology, 5, 590-4.*

ARTH, J.G., BARKER, F., PETERMAN, Z.E., & FRIEDMAN, I., 1978 - Geochemistry of the gabbro-diorite-tonalite-trondhjemite suite of southwest Finland and its implications for the origin of tonalitic and trondhjemitic magmas. *Journal of Petrology, 19, 289-316.*

ARTH, J.G., & HANSON, G.N., 1972 - Quartz diorites derived by partial melting of eclogite or amphibolite at mantle depths. *Contributions to Mineralogy and Petrology, 37, 161-74.*

ARTH, J.G., & HANSON, G.N., 1975 - Geochemistry and origin of the early Precambrian crust of northeastern Minnesota. *Geochimica et Cosmochimica Acta, 39, 325-62.*

ATKINS, F.B., 1969 - Pyroxenes of the Bushveld Intrusion, South Africa. *Journal of Petrology, 10, 222-49.*

AUMENTO, F., MITCHELL, W.S., & FRATTA, M., 1976 - Interaction between sea water and oceanic layer two as a function of time and depth. *Canadian Mineralogist, 14, 269-90.*

AYUSO, R.A., BENCE, A.E., & TAYLOR, S.R., 1976 - Upper Jurassic tholeiitic basalts from DSDP Leg 11. *Journal of Geophysical Research, 81, 4305-25.*

BAILEY, J.C., & NOE-NYGAARD, A., 1976 - Chemistry of Miocene plume tholeiites from northwest Iceland. *Lithos, 9, 185-201.*

BARKER, F., & ARTH, J.G., 1976 - Generation of trondhjemitic-tonalitic liquids and Archaean bimodal trondhjemite-basalt suites. *Geology,4, 596-600.*

BECCALUVA, L., OHNENSTETTER, D., OHNENSTETTER, M., & VENTURELLI, G., 1977 - The trace element geochemistry of the Corsican Ophiolites. *Contributions to Mineralogy and Petrology, 64, 11-31.*

BENCE, A.E., & TAYLOR, S.R., 1976 - Petrogenesis of Mid-Atlantic Ridge basalts at DSDP Leg 37 holes 332A and 332B from major and trace element geochemistry. *In* AUMENTO, F., MELSOM, W.G., & OTHERS (Editors), INITIAL REPORTS OF THE DEEP SEA DRILLING PROJECT, 37. *US Government Printing Office, Washington, D.C.*

BENDER, J.F., HODGES, F.N., & BENCE, A.E., 1978 - Petrogenesis of basalts from the Project FAMOUS area: experimental study from 0-15 kb. *Earth and Planetary Science Letters, 41, 277-302.*

BLANCHARD, D.P., RHODES, J.M., DUNGAN, M.A., RODGERS, K.V., DONALDSON, C.H., BRANNON, J.C., JACOBS, J.W., & GIBSON, E.K., 1976 - The chemistry and petrology of basalts from Leg 37 of the Deep Sea Drilling Project. *Journal of Geophysical Research, 81, 4231-46.*

BOLAND, J.N., 1974 - Lamellar structures in low-calcium orthopyroxenes. *Contributions to Mineralogy and Petrology, 47, 215-22.*

BONATTI, I., HONNOREZ, J., & FERRARA, G., 1970 - Peridotite-gabbro-basalt complex from the equatorial Mid-Atlantic ridge. *Philosophical Transactions of the Royal Society of London, 268A, 385-402.*

BOTTINGA, Y., & WEILL, F.F., 1970 - Densities of liquid silicate systems calculated from partial molar volumes of oxide components. *American Journal of Science, 269, 169-92.*

BOYD, F.R., & ENGLAND, J.L., 1960 - Apparatus for phase equilibrium measurements at pressures up to 50 kb and temperatures up to 1750°C. *Journal of Geophysical Research, 65, 741-8.*

BREY, G., & GREEN, D.H., 1975 - The role of CO_2 in the genesis of olivine melilitite. *Contributions to Mineralogy and Petrology, 49, 93-103.*

BREY, G., & GREEN, D.H., 1977 - Petrogenesis of olivine melilitite and kimberlite and melting of peridotite C-O-H. *Extended abstracts of the Second International Kimberlite Conference, Santa Fe, 1977.*

BROWN, C.M., 1977 - Yule, Papua New Guinea, 1:250 000 Geological Series. *Bureau of Mineral Resources, Australia-Explanatory Notes SC/55-2.*

BROWN, C.M., PIGRAM, C.J., & SKWARKO, S., in press - Mesozoic stratigraphy and geological history of Papua New Guinea. *Paleogeography, Paleoclimatology and Paleoecology.*

BROWN, G.M., 1967 - Mineralogy of basaltic rocks. *In* HESS, H.H., & POLDERVAART, A., (Editors), BASALTS, volume 1, 103-63. *Interscience, New York.*

BRYAN, W.B., & MOORE, J.G., 1977 - Compositional variations of young basalts in the Mid-Atlantic Ridge rift valley near lat. 36°49'N. *Geological Society of America-Bulletin 88, 556-70.*

BRYAN, W.B., & THOMPSON, G., 1977 - Basalts from DSDP Leg 37 and the FAMOUS area: compositional and petrogenetic comparisons. *Canadian Journal of Earth Science, 14, 875-85.*

BRYAN, W.B., THOMPSON, G., FREY, F.A., & DICKEY, J.S., 1976 - Inferred geological settings and differentiation in basalts from the Deep Sea Drilling Project. *Journal of Geophysical Research, 81, 4285-304.*

BUDDINGTON, A.F. & LINDSLEY, D.H., 1964 - Iron-titanium oxide minerals and synthetic equivalments. *Journal of Petrology, 5, 310-57.*

BULTITUDE, R.J., & GREEN, D.H., 1968 - Experimental study at high pressures on the origin of olivine melilitite and olivine melilitite nephelinite magmas. *Earth and Planetary Science Letters, 3, 325-37.*

BURNS, R.G., 1970 - MINERALOGICAL APPLICATIONS OF CRYSTAL FIELD THEORY. *Cambridge University Press.*

BYERLY, G.R., MELSON, W.G., & VOGT, P.R., 1976 - Rhyodacites, andesites, ferro-basalts, and ocean tholeiites from the Galapagos spreading centre. *Earth and Planetary Science Letters, 30, 215-21.*

CAMERON, E.N., 1969 - Postcumulus changes in the eastern Bushveld Complex. *American Mineralogist, 54, 754-79.*

CAMERON, E.N., 1978 - The Lower Zone of the Eastern Bushveld Complex in the Olifants River trough. *Journal of Petrology, 19, 437-62.*

CAMERON, W.E., NISBET, E.G., & DIETRICH, V.J., 1979 - Boninites, komatiites and ophiolitic basalts. *Nature, 280, 550-3.*

CAMPBELL, I.H., 1977 - A study of cumulate processes and macrorhythmic layering in the Jimberlana Intrusion of Western Australia. Part 1: The upper layered series. *Journal of Petrology, 18, 183-215.*

CAMPBELL, I.H., 1978 - Some problems with cumulus theory. *Lithos, 11, 311-23.*

CAMPBELL, I.H., & BORLEY, G.D., 1974 - The geochemistry of pyroxenes from the lower layered series of the Jimberlana Intrusion, Western Australia. *Contributions to Mineralogy and Petrology, 47, 281-97.*

CANN, J.R., 1969 - Spilites from the Carlsberg Ridge, Indian Ocean. *Journal of Petrology, 10, 1-19.*

CANN, J.R., 1970 - Rb, Sr, Y, Zr and Nb in some ocean floor basaltic rocks. *Earth and Planetary Science Letters, 10, 7-11.*

CANN, J.R., 1971 - Major element variations in ocean floor basalts. *Philosophical Transactions of the Royal Society of London, 268A, 495-505.*

CANN, J.R., 1974 - A model for oceanic crustal structure developed. *Geophysical Journal of the Royal Astronomical Society, 39, 169-74.*

CAREY, S.W., 1958 - The tectonic approach to continental drift. *In* CAREY, S.W. (Convenor), CONTINENTAL DRIFT. A SYMPOSIUM, 177-355. *University of Tasmania, Hobart.*

CARMICHAEL, I.S.E., 1967 - The iron-titanium oxides of salic volcanic rocks and their associated ferromagnesian silicates. *Contributions to Mineralogy and Petrology, 14, 36-64.*

CARMICHAEL, I.S.E., TURNER, F.J., & VERHOOGEN, J., 1974 - IGNEOUS PETROLOGY. *McGraw-Hill, New York.*

CAWTHORN, R.G., FORD, C.E., BIGGAR, G.M., BRAVO, M.S., & CLARKE, D.B., 1973 - Determination of the liquid composition in experimental samples: discrepancies between microprobe analyses and other methods. *Earth and Planetary Science Letters, 21, 1-5.*

CHALLIS, G.A., 1965 - The origin of New Zealand ultramafic intrusions. *Journal of Petrology, 6, 322-64.*

COOMBS, D.S., 1963 - Trends and affinities of basaltic magmas and pyroxenes as illustrated on the diopside-olivine-silica diagram. *Mineralogical Society of America Special Paper 1, 227-50.*

COX, K.G., 1972 - The Karroo volcanic cycle. *Journal of the Geological Society of London, 128, 311-36.*

COX, K.G., & JAMIESON, B.G., 1974 - The olivine-rich lavas of Nuanetsi: a study of polybaric magmatic evolution. *Journal of Petrology, 14, 269-301.*

DALLWITZ, W.B., 1968 - Chemical composition and genesis of clinoenstatite-bearing volcanic rocks from Cape Vogel, Papua: A discussion. *In* PROCEEDINGS OF THE 23RD INTERNATIONAL GEOLOGICAL CONGRESS, 2, 229-42.

DALLWITZ, W.B., GREEN, D.H., & THOMPSON, J.B., 1966 - Clinoenstatite in a volcanic rock from Cape Vogel, Papua. *Journal of Petrology, 7, 375-403.*

DAVIES, H.L., 1971 - Peridotite-gabbro-basalt complex in eastern Papua: an overthrust plate of oceanic mantle and crust. *Bureau of Mineral Resources, Australia - Bulletin 128.*

DAVIES, H.L., 1977 - Crustal structure and emplacement of ophiolite in southeast Papua New Guinea. *Geological Survey of Papua New Guinea Report 77/15.*

DAVIES, H.L., & SMITH, I.E., 1971 - Geology of eastern Papua. *Geological Society of America-Bulletin 82, 3299-312.*

DELANEY, J.R., MUENOW, D.W., & GRAHAM, D.G., 1978 - Abundance and distribution of water, carbon and sulfur in the glassy rims of submarine pillow basalts. *Geochimica et Cosmochimica Acta, 42, 581-94.*

DEWEY, J.F., & BIRD, J.M., 1971 - Origin and emplacement of the ophiolite suite: Appalachian ophiolites in Newfoundland. *Journal of Geophysical Research, 76, 3179-206.*

DEWEY, J.F., & KIDD, W.S.F., 1977 - Geometry of plate accretion. *Geological Society of America-Bulletin 88, 960-8.*

DICK, H.J.B., 1977 - Partial melting in the Josephine Peridotite 1, the effect on mineral composition and its consequence for geobarometry and geothermometry. *American Journal of Science, 277, 801-32.*

DICK, H.J.B., 1979 - The geochemistry of chrome spinel in FAMOUS basalts and a model for magma genesis at an ocean ridge. *Contributions to Mineralogy and Petrology,* in press.

DICK, H.J.B., & BRYAN, W.B., 1979 - Variation in basalt phenocryst mineralogy and rock composition in DSDP hole 396B. *In* DMITRIEV, L., HEIRTZLER, J., & OTHERS (Editors), INITIAL REPORTS OF THE DEEP SEA DRILLING PROJECT, LEG 46, 215-25. *US Government Printing Office, Washington, D.C.*

DICKEY, J.S., Jr., 1970 - Partial fusion products in alpine-type peridotites: Serrannia de Ronda and other examples. *Mineralogical Society of America Special Publication 3, 33-49.*

DICKEY, J.S., Jr., & YODER, H.S. Jr., 1972 - Partitioning of chromium and aluminium between clinopyroxene and spinel. *Carnegie Institution of Washington - Yearbook 71, 384-92.*

DIETRICH, V., EMMERMAN, R., OBERHANSLI, R., & PUCHELT, H., 1978 - Geochemistry of basaltic and gabbroic rocks from the West Mariana Basin and the Mariana Trench. *Earth and Planetary Science Letters, 39, 127-48.*

DONALDSON, C.H., & BROWN, R.W., 1977 - Refractory megacrysts and magnesian-rich inclusions within spinel in oceanic tholeiites: Indicators of magma mixing and parental compositions. *Earth and Planetary Science Letters, 37, 81-9.*

DOSTAL, J., & MUECKE, G.K., 1978 - Trace element geochemistry of the peridotite-gabbro-basalt suite from DSDP Leg 37. *Earth and Planetary Science Letters, 40, 415-22.*

DOW, D.B., SMIT, J.A.J., BAIN, J.H.C., & RYBURN, R.J., 1972 - Geology of the South Sepik region, New Guinea. *Bureau of Mineral Resources, Australia - Bulletin 133.*

DRAKE, M.J., 1976 - Plagioclase-melt equilibria. *Geochimica et Cosmochimica Acta, 40, 457-65.*

DUKE, J.M., 1976 - Distribution of the period four transition elements among olivine, calcic clinopyroxene and mafic silicate liquid: Experimental results. *Journal of Petrology, 4, 499-521.*

DUNCAN, R.A., & GREEN, D.H., 1979 - The role of multi-stage melting in the formation of oceanic crust. *Geology,* in press.

DUNGAN, M.A., & RHODES, J.M., 1978 - Residual glasses and melt inclusions in basalts from DSDP Legs 45 and 46: Evidence for magma mixing. *Contributions to Mineralogy and Petrology, 67, 417-31.*

EGGLER, D.H., 1974 - Effect of CO_2 on the melting of peridotite. *Carnegie Institution of Washington - Yearbook 74, 468-74.*

EGGLER, D.H., 1978 - The effect of CO_2 upon partial melting of peridotite in the system Na_2O-CaO-Al_2O_3-MgO-SiO_2-CO_2 to 35 kb, with an analysis of melting in a peridotite-H_2O-CO_2 system. *American Journal of Science, 278, 305-43.*

ELLIS, D.J., 1979 - Granulites from Enderby Land, Antarctica. *Unpublished Ph.D. thesis, University of Tasmania.*

ENGLAND, R.N., & DAVIES, H.L., 1973 - Mineralogy of ultramafic cumulates and tectonites from eastern Papua. *Earth and Planetary Science Letters, 17, 416-25.*

ERLANK, A.J., & KABLE, E.J.D., 1976 - The significance of incompatible elements in mid-Atlantic ridge basalts from 45°N with particular reference to Zr/Nb. *Contributions to Mineralogy and Petrology, 54, 281-91.*

EVANS, B.W., & FROST, B.R., 1975 - Chrome-spinel in progressive metamorphsim - a preliminary analysis. *Geochimica et Cosmochimica Acta, 39, 959-72.*

EVANS, B.W., & WRIGHT, T.L., 1972 - Composition of liquidus chromite from the 1959 (Kilauea Iki) and 1965 (Makaopuhii) eruptions of Kilauea volcano. *American Mineralogist, 57, 217-30.*

EWART, A., & BRYAN, W.B., 1972 - The petrology and geochemistry of the igneous rocks of Eua, Tongan Islands. *Geological Society of America-Bulletin 83, 3281-98.*

EWART, A., BROTHERS, R.N., & MATEEN, A., 1977 - An outline of the geology and geochemistry, and the possible petrogenetic evolution of the volcanic rocks of the Tonga-Kermadec-New Zealand island arc. *Journal of Volcanology and Geothermal Research, 2, 205-50.*

FINLAYSON, D.M., DRUMMOND, B.J., COLLINS, C.D.M., & CONNELLY, J.B., 1977 - Crustal structures in the region of the Papuan Ultramafic Belt. *Physics of the Earth and Planetary Interiors, 14, 13-29.*

FINLAYSON, D.M., MUIRHEAD, K.J., WEBB, J.P., GIBSON, G., FURUMOTO, A.S., COOKE, R.J.S., & RUSSELL, A.J., 1976 - Seismic investigation of the Papuan Ultramafic Belt. *Geophysical Journal of the Royal Astronomical Society, 44, 45-60.*

FLOWER, M.F.J., ROBINSON, P.T., SCHMINKE, H.U., & OHNMACHT, W., 1977 - Magma fractionation systems beneath the Mid-Atlantic Ridge at 36-37°N. *Contributions to Mineralogy and Petrology, 64, 167-95.*

FREY, F.A., BRYAN, W.B., & THOMPSON, G., 1974 - Atlantic Ocean floor: geochemistry and petrology of basalts from Legs 2 and 3 of the Deep Sea Drilling Project. *Journal of Geophysical Research, 79, 5507-27.*

FREY, F.A., & GREEN, D.H., 1974 - The mineralogy, geochemistry and origin of lherzolite inclusions in Victorian basanites. *Geochimica et Cosmochimica Acta, 38, 1023-59.*

FREY, F.A., GREEN, D.H., & ROY, S.D., 1978 - Integrated models of basalt petrogenesis: a study of quartz tholeiites to olivine melilitites from S.E. Australia utilizing geochemical and experimental data. *Journal of Petrology, 19, 463-513.*

FREY, F.A., HASKIN, L.A., & HASKIN, M.A., 1971 - Rare-earth abundances in some ultramafic rocks. *Journal of Geophysical Research, 76, 2057-70.*

FREY, F.A., & PRINZ, M., 1977 - Ultramafic inclusions from San Carlos, Arizona: Petrologic and geochemical data bearing on their petrogenesis. *Earth and Planetary Science Letters, 38, 129-76.*

FUJII, T., & KUSHIRO, I., 1977 - Melting relations and viscosity of an abyssal tholeiite. *Carnegie Institution of Washington - Yearbook 76, 461-5.*

GALE, G.H., 1973 - Paleozoic basaltic komatiite and ocean-floor type basalts from northeastern Newfoundland. *Earth and Planetary Science Letters, 18, 22-8.*

GAST, P.W., 1968 - Trace element fractionation and the origin of tholeiitic and alkaline magma types. *Geochimica et Cosmochimica Acta, 32, 1057-86.*

GILL, J.B., 1976 - Composition and age of Lau Ridge and Basin volcanic rocks: implications for evolution of inter-arc basins. *Geological Society of America-Bulletin 87, 1384-95.*

GLIKSON, A.Y., 1971 - Primitive Archaean element distribution patterns: chemical evidence and geotectonic significance. *Earth and Planetary Science Letters, 12, 309-20.*

GLIKSON, A.Y., 1979 - Siderophile and lithophile trace-element evolutions of the Archaean mantle. *BMR Journal of Australian Geology and Geophysics, 4, 253-79.*

GOODE, A.D.T., 1974 - Oxidation of natural olivines. *Nature, 248, 500-1.*

GOODE, A.D.T., 1976 - Small scale primary cumulus igneous layering in the Kalka layered intrusion, Giles Complex, Central Australia. *Journal of Petrology, 17, 379-97.*

GREEN, D.H., 1963 - Alumina content of enstatite in a Venezuelan high temperature peridotite. *Geological Society of America-Bulletin 74, 1397-402.*

GREEN, D.H., 1970 - The origin of basaltic and nephelinitic magmas. *Transactions of the Leicester Literary and Philosophical Society, 64, 26-54.*

GREEN, D.H., 1971 - Compositions of basaltic magmas as indicators of origin: application to oceanic volcanism. *Philosophical Transactions of the Royal Society of London, 268A, 707-25.*

GREEN, D.H., 1973a - Contrasted melting relations in a pyrolite upper mantle under mid-oceanic ridge, stable crust and island arc environments. *Tectonophysics, 17, 285-97.*

GREEN, D.H., 1973b - Experimental studies on a model upper mantle composition at high pressure under water-saturated and water-undersaturated conditions. *Earth and Planetary Science Letters, 19, 37-53.*

GREEN, D.H., 1976a - Experimental testing of 'equilibrium' partial melting of peridotite under water-saturated, high pressure conditions. *Canadian Mineralogist, 14, 255-68.*

GREEN, D.H., 1976b - Experimental petrology in Australia - A review. *Earth Science Reviews, 12, 99-138.*

GREEN, D.H., 1976c - Orthopyroxene in the lunar interior and constraints on early lunar differentiation. *Lunar Science, VII, 336-8.*

GREEN, D.H., HIBBERSON, W.O., 1970 - The instability of plagioclase in peridotite at high pressure. *Lithos, 3, 209-21.*

GREEN, D.H., HIBBERSON, W.O., & JAQUES, A.L., 1979 - Petrogenesis of mid-ocean ridge basalts. *In* McELHINNY, M.W. (Editor), THE EARTH: ITS ORIGIN, STRUCTURE AND EVOLUTION, 265-95. *Academic Press, London.*

GREEN, D.H., & LIEBERMAN, R.C., 1976 - Phase equilibria and elastic properties of a pyrolite model for the oceanic upper mantle. *Tectonophysics, 32, 61-92.*

GREEN, D.H., NICHOLLS, I.A., VILJOEN, M., & VILJOEN, R., 1975b - Experimental demonstration of the existence of peridotite liquids in earliest Archaean magmatism. *Geology, 3, 11-4.*

GREEN, D.H., & RINGWOOD, A.E., 1967a - The genesis of basaltic magmas. *Contributions to Mineralogy and Petrology, 15, 103-90.*

GREEN, D.H., & RINGWOOD, A.E., 1967b - The stability fields of aluminous pyroxene peridotite and garnet peridotite and their relevance to upper mantle structure. *Earth and Planetary Science Letters, 3, 151-60.*

GREEN, D.H., & RINGWOOD, A.E., 1970 - Mineralogy of peridotite compositions under upper mantle conditions. *Physics of the Earth and Planetary Interiors, 3, 359-71.*

GREEN, D.H., RINGWOOD, A.E., HIBBERSON, W.O., & WARE, N.G., 1975a - Experimental petrology of Apollo 17 mare basalts. *Proceedings of the 6th Lunar Science Conference, 871-93.*

GREEN, D.H., RINGWOOD, A.E., WARE, N.G., & HIBBERSON, W.O., 1972 - Experimental petrology and petrogenesis of Apollo 14 basalts. *Proceedings of the 3rd Lunar Science Conference, 1, 197-206.*

GREEN, D.H., NESBITT, R.W., & SUN, S-S., in prep. - Experimental evidence for primary liquids, extrusion temperature and conditions of origin of Archaean ultramafic liquids.

GREEN, T.H., GREEN, D.H., & RINGWOOD, A.E., 1967 - The origin of high alumina basalts and their relationships to quartz tholeiites and alkali basalts. *Earth and Planetary Science Letters, 2, 41-51.*

GREENBAUM, D., 1972 - Magmatic processes at ocean ridges: evidence from the Troodos Massif, Cyprus. *Nature, 238, 18-21.*

GRIFFIN, B.J., 1979 - Energy dispersive analysis system calibration and operation with TAS-SUEDS, and advanced interactive data-reduction package. *University of Tasmania, Department of Geology Publication, 343.*

GRIFFIN, T.J., WHITE, A.J.R., & CHAPPELL, B.W., 1978 - The Moruya Batholith and geochemical contrasts between Moryua and Jindabyne suites. *Geological Society of Australia - Journal, 25, 235-47.*

HALLBERG, J.A., 1972 - Geochemistry of Archaean volcanic belts in the Eastern Goldfields region of Western Australia. *Journal of Petrology, 13, 45-56.*

HALLBERG, J.A., & WILLIAMS, D.A.C., 1972 - Archaean mafic and ultramafic rock associations in the Eastern Goldfields region, Western Australia. *Earth and Planetary Science Letters, 15, 191-200.*

HAMILTON, D.L., & ANDERSON, G.M., 1967 - Effects of water and oxygen pressures on the crystallization of basaltic magmas. *In* HESS, H.H., & POLDERVAART, A. (Editors), BASALTS, volume 1, 445-82.

HARRIS, P.G., REAY, A., & WHITE, I.G., 1967 - Chemical composition of the upper mantle. *Journal of Geophysical Research, 72, 6359-69.*

HART, R.A., 1970 - Chemical exchange between seawater and deep ocean basalts. *Earth and Planetary Science Letters, 9, 269-79.*

HART, S.R., 1969 - K, Rb, Cs contents and K/Rb, K/Cs ratios of fresh and altered submarine basalts. *Earth and Planetary Science Letters, 6, 295-303.*

HART, S.R., 1976 - LIL element geochemistry, Leg 34 basalts. *In* YEATES, R.S., & HART, S.R. (Editors), INITIAL REPORTS OF THE DEEP SEA DRILLING PROJECT, 34, 283-8. *US Government Printing Office, Washington, D.C.*

HART, S.R., & DAVIS, K., 1978 - Nickel partitioning between olivine and silicate melt. *Earth and Planetary Science Letters, 40, 203-19.*

HART, S.R., GLASSEY, W.E., & KARIG, D.E., 1972 - Basalts and seafloor spreading behind the Mariana island arc. *Earth and Planetary Science Letters, 15, 12-8.*

HASKIN, L.A., & HASKIN, M.A., 1968 - Rare-earth elements in the Skaergaard intrusion. *Geochimica et Cosmochimica Acta, 32, 433-47.*

HASKIN, L.A., & KOROTEV, R.L., 1977 - Test of a model for trace element partition during closed-system solidification of a silicate liquid. *Geochimica et Cosmochimica Acta, 41, 921-39.*

HAWKESWORTH, C.J., O'NIONS, R.K., PANKHURST, R.J., HAMILTON, P.J., & EVENSEN, N.M., 1977 - A geochemical study of island-arc and back-arc tholeiites from the Scotia Sea. *Earth and Planetary Science Letters, 36, 253-62.*

HAWKESWORTH, C.J., & O'NIONS, R.K., 1977 - The petrogenesis of some Archaean volcanic rocks from Southern Africa. *Journal of Petrology, 18, 487-519.*

HAWKINS, J.W., 1976 - Petrology and geochemistry of basaltic rocks of the Lau Basin. *Earth and Planetary Science Letters, 28, 283-97.*

HAWKINS, J.W., 1977 - Petrologic and geochemical characteristics of marginal basin basalts. *In* TALWANI, M., & PITMAN, W.C., 111 (Editors), ISLAND ARCS, DEEP SEA TRENCHES AND BACK-ARC BASINS, 355-65. *American Geophysical Union, Washington.*

HEEZEN, B.C., & FORNARI, D.J., 1975 - Geological map of the Pacific Ocean, 1:35 000 000. *In* ANDREWS, J.E., PACKHAM, G., & OTHERS (Editors), INITIAL REPORTS OF THE DEEP SEA DRILLING PROJECT, 30, map supplement. *US Government Printing Office, Washington*, D.C.

HEKINIAN, R., 1973 - Petrology of the Ninetyeast Ridge (Indian Ocean) compared to other aseismic ridges. *Contributions to Mineralogy and Petrology, 43, 125-47.*

HEKINIAN, R., MOORE, J.G., & BRYAN, W.B., 1976 - Volcanic rocks and processes of the mid-Atlantic ridge rift valley near $36^{o}49'$N. *Contributions to Mineralogy and Petrology, 57, 145-62.*

HELLMAN, P.L., & HENDERSON, P., 1977 - Are rare earths mobile during spilitization? *Nature, 267, 32-40.*

HELLMAN, P.L., SMITH, R.E., & HENDERSON, P., 1977 - Rare earth element investigation of the Cliefden Outcrop, N.S.W., Australia. *Contributions to Mineralogy and Petrology, 65, 155-64.*

HENSEN, B.J., 1973 - Pyroxenes and garnets as geothermometers and geobarometers. *Carnegie Institution of Washington - Yearbook 72, 527-34.*

HERZBERG, C.T., 1978 - Pyroxene geothermometry and geobarometry: experimental and thermodynamic evaluation of some subsolidus phase relations involving pyroxenes in the system $CaO-MgO-Al_2O_3-SiO_2$. *Geochimica et Cosmochimica Acta, 42, 945-57.*

HERZBERG, C.T., & CHAPMAN, N.A., 1976 - Clinopyroxene geothermometry of spinel lherzolites. *American Mineralogist, 61, 626-37.*

HESS, H.H., 1960 - Stillwater Igneous Complex, Montana. *Geological Society of America - Memoir 80.*

HILL, R.T., & ROEDER, P.L., 1974 - The crystallization of spinel from basaltic liquid as a function of oxygen fugacity. *Journal of Geology, 82, 709-29.*

HIMMELBERG, G.R., & FORD, A.B., 1977 - Iron-titanium oxides of the Dufek intrusion, Antarctica. *American Mineralogist, 62, 623-33.*

HIMMELBERG, G.R., & LONEY, R.A., 1973 - Petrology of the Vulcan Peak alpine-type peridotite, southwest Oregon. *Geological Society of America-Bulletin 84, 1585-1600.*

HODGES, F.N., & PAPIKE, J.J., 1976 - DSDP Site 334: magmatic cumulates from oceanic layer 3. *Journal of Geophysical Research, 81, 4135-51.*

HODGES, F.N., PAPIKE, J.J., & BENCE, A.E., 1976 - Mineral chemistry of deep sea basalts. *Transactions of the American Geophysical Union (EOS), 57, 406.*

HUTCHISON, D.S., 1975 - Basement geology of the North Sepik region, Papua New Guinea. *Bureau of Mineral Resources, Australia, File 75/162 (unpublished).*

HOLMES, K.D., & HALL, R.J., 1975 - Marum nickeliferous laterite, Madang District, PNG. *In* KNIGHT, C.L., (Editor), ECONOMIC GEOLOGY OF AUSTRALIA AND PAPUA NEW GUINEA, 1011-17. *Australasian Institute of Mining and Metallurgy, 1, Metals.*

IRVINE, T.N., 1965 - Chromian spinel as a petrogenetic indicator. Part 1. Theory. *Canadian Journal of Earth Science, 2, 648-72.*

IRVINE, T.N., 1967 - Chromium spinel as a petrogenetic indicator. Part 11. Petrologic application. *Canadian Journal of Earth Science, 4, 71-103.*

TABLE 1b. COMPARISON OF TRACE ELEMENT DATA

	1	2	3	4	5	6	7	8	9	10	11	12
Ba	691	690	<10	~1	<10	1	<10	26	10	28	10	32
Rb		47	<0.1	0.06	<0.1(0.03)	0.06	0.3	0.5	0.5	0.45	0.8	0.7
Sr		334		0.4	59(52)	53	53	48	229	216	108	105
Zr		185			2(3)	1.8	293	253	97	97	119	119
Nb		13			1	0.4	16	16	5	6.6	5	6.6
Y		40			5(4)	5.1	77	83	20	26	38	-
La	26	24	<2				18	21	5	7.3	5	6.3
Ce	58	54	<3				52	50	20	20	21	18.7
Nd	24	29	<2				32	34	10	14.3	12	12.2
Sc		31		9								
V	369	380	28	30								
Cr	13	13	2280	2730								
Ni	9	11	2350	2339								
Cu	16	16	8	9								
Zn	129	125	45	43								

1. XRF values for BCR-1
2. Preferred values for BCR-1; compilation by M. Kaye, Dept Geology, ANU
3. XRF values for PCC-1
4. Preferred values for PCC-1; M. Kaye; Flanagan (1973)
5. XRF values for gabbro 1020. Numbers in parentheses obtained by RSES XRF
6. Spark source mass spectrometer values for gabbro 1020
7. XRF values for basalt 565
8. MS7 data for basalt 565
9. XRF values for basalt 524
10. MS7 data for basalt 524
11. XRF values for basalt 508
12. MS7 data for basalt 508

JACKSON, E.D., & THAYER, T.P., 1972 - Some criteria for distinguishing between stratiform, concentric and alpine peridotite-gabbro complexes. *24th International Geological Congress, Section 2, 289-96.*

JAHN, B.M., SHIH, C.Y., & MURTHY, V.R., 1974 - Trace element geochemistry of Archaean volcanic rocks. *Geochimica et Cosmochimica Acta, 38, 611-27.*

JAKEŠ, P., & GILL, J., 1970 - Rare earth elements and the island-arc tholeiitic series. *Earth and Planetary Science Letters, 9, 17-28.*

JAQUES, A.L., 1978 - Marum ophiolite 1:100 000 preliminary map. *Bureau of Mineral Resources, Australia (unpublished).*

JAQUES, A.L., CHAPPELL, B.W., & TAYLOR, S.R., 1978 - Geochemistry of LIL-element enriched tholeiites from the Marum ophiolite complex, northern Papua New Guinea. *BMR Journal of Australian Geology and Geophysics, 3, 297-310.*

JAQUES, A.L., & GREEN, D.H., 1979 - Determination of liquid compositions in high-pressure melting of peridotite. *American Mineralogist, 64, 1312-21.*

JAQUES, A.L., & ROBINSON, G.P., 1977 - The continent/island-arc collision in northern Papua New Guinea. *BMR Journal of Geology and Geophysics, 2, 289-303.*

JOHANNES, W., 1978 - Melting of plagioclase in the system Ab-An-H_2O and Qz-Ab-An-H_2O at P_{H_2O} = 5 kbars, an experimental problem. *Contributions to Mineralogy and Petrology, 66, 195-303.*

JOHNSON, R.W., 1979 - Geotectonics and volcanism in Papua New Guinea: a review of the late Cainozoic. *BMR Journal of Australian Geology and Geophysics, 4, 181-207.*

JOHNSON, R.W., MACKENZIE, D.E., & SMITH, I.E.M., 1978 - Delayed partial melting of subduction-modified mantle in Papua New Guinea. *Tectonophysics, 46, 197-216.*

KARIG, D.E., 1971 - Origin and development of marginal basins in the western Pacific. *Journal of Geophysical Research, 76, 2542-61.*

KARIG, D.E., 1972 - Remnant arcs. *Geological Society of America-Bulletin 83, 1057-68.*

KARIG, D.E., 1974 - Evolution of arc systems in the western Pacific. *Annual Reviews of Earth and Planetary Sciences, 2, 51-75.*

KAY, R.W., & GAST, P.W., 1973 - The rare earth content and origin of alkali-rich basalts. *Journal of Geology, 81, 653-82.*

KAY, R.W., HUBBARD, N.J., & GAST, P.W., 1970 - Chemical characteristics of oceanic ridge volcanic rocks. *Journal of Geophysical Research, 75, 239-54.*

KAY, R.W., & SENECHAL, R.G., 1976 - The rare earth chemistry of the Troodos ophiolite complex. *Journal of Geophysical Research, 81, 964-70.*

KRETZ, R., 1963 - Distribution of magnesium and iron between orthopyroxene and calcic clinopyroxene in natural mineral assemblages. *Journal of Geology, 71, 773-85.*

KROENKE, L.W., MANGHNANI, M.H., RAI, C.S., RAMANANANTOANDRO, R., & FRYER, P., 1976 - Elastic properties of ultramafic rocks from Papua New Guinea: composition and structure of the upper mantle. *In* SUTTON, G.H., MANGHNANI, M.H., & MOBERLY, R., (Editors) THE GEOPHYSICS OF THE PACIFIC OCEAN BASIN AND ITS MARGIN. *American Geophysical Union Geophysical Monograph 13, 407-21.*

KUNO, H., & AOKI, K., 1970 - Chemistry of ultramafic nodules and their bearing on the origin of basaltic magmas. *Physics of the Earth and Planetary Interiors, 3, 273-301.*

KURODA, N., & SHIRAKI, K., 1975 - Boninite and related rocks of Chichijima, Bonin Islands, Japan. *Reports of the Faculty of Science, Shizuoka University, 10, 145-55.*

KUSHIRO, I., 1969 - The system forsterite-diopside-silica with and without water at high pressures. *American Journal of Science, 267A, 269-94.*

KUSHIRO, I., 1972 - Effect of water on the composition of magmas formed at high pressures. *Journal of Petrology, 13, 311-34.*

KUSHIRO, I., & THOMPSON, R.N., 1972 - Origin of some abyssal tholeiites from the Mid-Atlantic Ridge. *Carnegie Institution of Washington - Yearbook 71, 403-6.*

KUSHIRO, I., YODER, H.S. Jnr, & MYSEN, B.O., 1976 - Viscosities of basalt and andesite melts at high pressure. *Journal of Geophysical Research, 81, 6351-6.*

LANGMUIR, C.H., BENDER, J.B., BENCE, A.E., HANSON, G.N., & TAYLOR, S.R., 1977 - Petrogenesis of basalts from the FAMOUS area: Mid-Atlantic Ridge. *Earth and Planetary Science Letters, 36, 133-56.*

LEAKE, B.E., 1965 - The relationship between composition of calciferous amphibole and grade of metamorphism. *In* PICHER, W.S., & FLINN, G.W. (Editors), CONTROLS OF METAMORPHISM, 299-318. *Oliver & Boyd, London.*

LEAKE, B.E., 1978 - Nomenclature of amphiboles. *Canadian MIneralogist, 16, 501-20.*

LINDSLEY, D.H., & DIXON, S.A., 1976 - Diopside-enstatite equilibria at 850° to 1400°C, 5 to 35 kb. *American Journal of Science, 276, 1285-301.*

LINDSLEY, D.H., KING, H.E. Jnr, & TURNOCK, A.C., 1974 - Composition of synthetic augite and hypersthene co-existing at 810°C. *Geophysical Research Letters, 1, 134-6.*

LONEY, R.A., & HIMMELBERG, G.R., 1976 - Structure of the Vulcan Peak alpine-type peridotite, southwest Oregon. *Geological Society of America-Bulletin 87, 259-74.*

LONEY, R.A., HIMMELBERG, G.R., & COLEMAN, R.G., 1971 - Structure and petrology of the alpine-type peridotite at Burro Mountain, California. *Journal of Petrology, 12, 245-309.*

LONGHI, J., WALKER, D., & HAYS, J.F., 1978 - The distribution of Fe and Mg between olivine and lunar basaltic liquids. *Geochimica et Cosmochimica Acta, 42, 1545-58.*

LOUBET, M., SHIMIZU, N., & ALLEGRE, C.J., 1975 - Rare earth elements in alpine peridotites. *Contributions to Mineralogy and Petrology, 53, 1-12.*

MAALOE, S., 1978 - The origin of rhythmic layering. *Mineralogical Magazine, 42, 337-45.*

MAALOE, S., & AOKI, K., 1977 - The major element composition of the upper mantle estimated from the composition of lherzolites. *Contributions to Mineralogy and Petrology, 64, 161-73.*

MACDONALD, G.A., & KATSURA, T., 1964 - Chemical composition of Hawaiian lavas. *Journal of Petrology, 5, 82-133.*

MACDONALD, K.C., LUYDENCK, B.P., & VON HERZEN, R.P., 1973 - Heat flow and plate boundaries in Melanesia. *Journal of Geophysical Research, 78, 2537-46.*

MACGREGOR, I.D., 1974 - The system $MgO-Al_2O_3-SiO_2$: Solubility of Al_2O_3 in enstatite for spinel and garnet peridotite compositions. *American Mineralogist, 50, 110-9.*

MALPAS, J., 1978 - Magma generation in the upper mantle, field evidence from ophiolite suites, and application to the generation of oceanic lithosphere. *Philosophical Transactions of the Royal Society of London, 288A, 527-46.*

MALPAS, J., & STRONG, D.F., 1975 - A comparison of chrome-spinels in ophiolites and mantle diapirs of Newfoundland. *Geochimica et Cosmochimica Acta, 39, 1045-60.*

MASUDA, A., & JIBIKI, H., 1973 - Rare-earth patterns of Mid-Atlantic Ridge gabbros: continental nature? *Geochemical Journal, 7, 55-65.*

MATHIESON, C.I., 1975 - Magnetites and ilmenites in the Somerset Dam layered basic intrusion, southeastern Queensland. *Lithos, 8, 93-111.*

MATSUI, Y., & NISHAZAWA, O., 1974 - Iron (11)-magnesium exchange equilibrium between olivine and calcium-free pyroxene at a temperature range 800° to 1300°C. *Société Mineralogié et Crystallographié de France - Bulletin 97, 122-30.*

MAZULLO, L.J., & BENCE, A.E., 1976 - Abyssal tholeiites from DSDP Leg 34: Nazca Plate. *Journal of Geophysical Research, 81, 4327-51.*

McBIRNEY, A.R., & NOYES, R.M., in press - Crystallization and layering of the Skaergaard Intrusion. *Journal of Petrology.*

McBIRNEY, A.R., & WILLIAMS, H., 1969 - Geology and petrology of the Galapagos Islands. *Geological Society of America - Memoir 118.*

McDOUGALL, I., 1976 - Geochemistry and origin of basalt of the Columbia River Group, Oregon and Washington. *Geological Society of America-Bulletin 87, 777-92.*

MEDARIS, L.G. Jnr, 1969 - Partitioning of Fe^{++} and Mg^{++} between co-existing synthetic olivine and orthopyroxene. *American Journal of Science, 267, 945-68.*

MEDARIS, L.G. Jnr, 1972 - High pressure peridotites in southwest Oregon. *Geological Society of America-Bulletin 83, 41-58.*

MEDARIS, L.G. Jnr, 1975 - Co-existing spinel and silicates in alpine peridotites of the granulite facies. *Geochimica et Cosmochimica Acta, 39, 947-58.*

MEHNERT, K.R., BUSCH, W., & SCHNEIDER, G., 1973 - Initial melting at grain boundaries of quartz and feldspar in gneisses and granulites. *Neues Jahrbook Mineralogie, Monatschefte, 165-83.*

MEIJER, A., 1976 - Pb and Sr isotopic data bearing on the origin of volcanic rocks from the Mariana island-arc system. *Geological Society of America-Bulletin 87, 1358-69.*

MELSOM, W.G., HART, S.R., & THOMPSON, G., 1972 - St. Paul's Rocks, equatorial Atlantic: petrogenesis, radiometric ages, and implications on sea-floor spreading. *Geological Society of America-Memoir 132, 241-72.*

MELSOM, W.G., & THOMPSON, G., 1970 - Layered basic complex in oceanic crust, Romanche Fracture, equatorial Atlantic Ocean. *Science, 168, 817-20.*

MELSOM, W.G., VALLIER, T.L., WRIGHT, T.L., BYERLY, G., & NELEN, J., 1976 - Chemical diversity of abyssal volcanic glass erupted along Pacific, Atlantic, and Indian ocean sea-floor spreading centres. *In* SUTTON, G.H., MANGHNANI, M.H., & MOBERLY, R. (Editors), THE GEOPHYSICS OF THE PACIFIC OCEAN BASIN AND ITS MARGIN. *American Geophysical Union Geophysical Monograph, 13, 351-67.*

MENZIES, M., 1973 - Mineralogy and partial melt textures within an ultramafic-mafic body. *Contributions to Mineralogy and Petrology, 42, 273-85.*

MENZIES, M., 1975 - Spinel compositional variation in the crustal and mantle lithologies of the Othris ophiolite. *Contributions to Mineralogy and Petrology, 51, 303-9.*

MENZIES, M., & ALLEN, C., 1974 - Plagioclase lherzolite-residual mantle relationships within two eastern Mediterranean ophiolites. *Contributions to Mineralogy and Petrology, 45, 197-213.*

MENZIES, M., & BLANCHARD, D., 1977 - The Smartville arc-ophiolite, Sierra Nevada, California: geochemical evidence. *Transactions of the American Geophysical Union (EOS), 12, 1245.*

MENZIES, M., BLANCHARD, D., BRANNON, J., & KOROTEV, R., 1977 - Rare earth and trace element geochemistry of a fragment of Jurassic seafloor, Point Sal, California. *Geochimica et Cosmochimica Acta, 41, 1419-30.*

MERCIER, J-C.C., & NICOLAS, A., 1975 - Textures and fabrics of upper-mantle peridotites as illustrated by xenoliths from basalts. *Journal of Petrology, 16, 454-87.*

MERRILL, R.B., & WYLLIE, P.J., 1973 - Absorption of iron by platinum capsules in high pressure rock melting experiments. *American Mineralogist, 58, 16-20.*

MILSOM, J.S., 1973- Papuan ultramafic belt: gravity anomalies and the emplacement of ophiolites. *Geological Society of America-Bulletin 84, 2243-58.*

MILSOM, J.S., 1975 - Madang district helicopter gravity survey, 1974. *Geological Survey of Papua New Guinea Report 75/15.*

MILSOM, J.S., & SMITH, I.E.M., 1975 - Southeastern Papua: Generation of thick crust in a tensional environment? *Geology, 3, 117-20.*

MIYASHIRO, A., SHIDO, F., & EWING, M., 1969 - Diversity and origin of abyssal tholeiite from the Mid-Atlantic ridge near 24°and 30°N latitude. *Contributions to Mineralogy and Petrology, 23, 38-52.*

MIYASHIRO, A., SHIDO, F., & EWING, M., 1970 - Crystallization and differentiation in abyssal tholeiites and gabbros from mid-ocean ridges. *Earth and Planetary Science Letters, 7, 361-5.*

MONTIGNY, R., BOUGAULT, H., BOTTINGA, Y., & ALLEGRE, C.J., 1973 - Trace element geochemistry and genesis of the Pindos ophiolite suite. *Geochimica et Cosmochimica Acta, 37, 2135-47.*

MOORE, J.G., 1970 - Water content of basalt erupted on the ocean floor. *Contributions to Mineralogy and Petrology, 28, 272-9.*

MOORE, J.G., & EVANS, B.W., 1967 - The role of olivine in crystallization of the prehistoric Makaopuhi tholeiitic lava lake, Hawaii. *Contributions to Mineralogy and Petrology, 15, 202-23.*

MORI, T., 1978 - Experimental study of pyroxene equilibria in the system $CaO-MgO-FeO-SiO_2$. *Journal of Petrology, 19, 45-65.*

MORI, T., & GREEN, D.H., 1975 - Pyroxenes in the system $Mg_2Si_2O_6$ - $CaMgSi_2O_6$ at high pressure. *Earth and Planetary Science Letters, 26, 277-86.*

MORI, T., & GREEN, D.H., 1978 - Laboratory duplication of phase equilibria observed in natural garnet lherzolites. *Journal of Geology, 86, 83-97.*

MUENOW, D.W., GRAHAM, D.G., LIU, N.W.K., & DELANEY, J.R., 1979 - Water poor glass-vapour inclusions in phenocrysts from Hawaiian pillow basalts. *Earth and Planetary Science Letters, 42, 71-6.*

MURALI, A.V., LEEMAN, W.P., M.A., M.S., & SCHMITT, R.A., in press - Evaluation of fractionation hybridization models for Kilauea eruptions and probable mantle source of Kilauea and Mauna Loa tholeiite basalts, Hawaii. *Journal of Petrology.*

MYSEN, B.O., & BOETTCHER, A.L., 1975 - Melting of a hydrous mantle: 11. Geochemistry of crystals and liquids formed by anatexis of mantle peridotite at high pressures and high temperatures as a function of controlled activities of water, hydrogen, and carbon dioxide. *Journal of Petrology, 16, 549-93.*

MYSEN, B.O., & KUSHIRO, I., 1977 - Compositional variations of co-existing phases with degree of melting of peridotite in the upper mantle. *American Mineralogist, 62, 843-65.*

NESBITT, R.W., & SUN, S-S., 1976 - Geochemistry of Archaean spinifex-textured peridotites and magnesian and low magnesian tholeiites. *Earth and Planetary Science Letters, 31, 433-53.*

NEUMANN, E.R., 1974 - The distribution of Mn^{2+} and Fe^{2+} between ilmenites and magnetites in igneous rocks. *American Journal of Science, 274, 1074-88.*

NICHOLLS, I.A., 1974 - Liquids in equilibrium with peridotitic mineral assemblages at high water pressures. *Contributions to Mineralogy and Petrology, 45, 289-316.*

NICOLAS, A., BOUCHEZ, J.L., BOUDIER, F., & MERCIER, J-C., 1971 - Textures, structures and fabrics due to solid state flow in some European lherzolites. *Tectonophysics, 12, 55-86.*

NICOLAS, Á., & JACKSON, E.D., 1972 - Repartition en deux provinces des péridotites des chaines alpines longeant la Méditerranee: implications géotectoniques. *Bulletin Suis de Minéralogie et Pétrographie, 52, 479-95.*

NISBETT, E.G., BICKLE, M.J., & MARTIN, A., 1977 - The mafic and ultramafic lavas of the Belingwe greenstone belt, Rhodesia. *Journal of Petrology, 18, 521-66.*

NORRISH, K., & CHAPPELL, B.W., 1977 - X-ray fluorescence spectrometry. *In* ZUSSMAN, J. (Editor), PHYSICAL METHODS IN DETERMINATIVE MINERALOGY, 201-72. *Academic Press, London, second edition.*

NORRISH, K., & HUTTON, J.Y., 1969 - An accurate X-ray spectrographic method for the analysis of a wide range of geological samples. *Geochimica et Cosmochimica Acta, 33, 431-54.*

NWE, Y.Y., 1976 - Electron-probe studies of the earlier pyroxenes and olivines from the Skaergaard Intrusion, East Greenland. *Contributions to Mineralogy and Petrology, 55, 105-26.*

OBATA, M., 1976 - The solubility of Al_2O_3 in orthopyroxenes in spinel and plagioclase peridotites and spinel pyroxenite. *American Mineralogist, 61, 804-16.*

O'HARA, M.J., 1967 - Mineral paragenesis in ultrabasic rocks. *In* WYLLIE, P.J. (Editor), ULTRAMAFIC AND RELATED ROCKS, 393-401. *John Wiley & Sons, New York.*

O'HARA, M.J., 1968 - The bearing of phase equilibria studies in synthetic and natural systems on the origin and evolution of basic and ultrabasic rocks. *Earth-Science Reviews, 4, 69-133.*

OSBORN, E.F., & TAIT, D.B., 1952 - The system diopside-forsterite- anorthite. *American Journal of Science, Bowen Volume, 413-33.*

PACKHAM, G.H., & FALVEY, D.A., 1971 - An hypothesis for the formation of marginal seas in the western Pacific. *Tectonophysics, 11, 79-109.*

PAGE, R.W., 1976 - Geochronology of igneous and metamorphic rocks in the New Guinea Highlands. *Bureau of Mineral Resources - Bulletin 162.*

PAGE, R.W., & JOHNSON, R.W., 1974 - Strontium isotope ratios of Quaternary volcanic rocks from Papua New Guinea. *Lithos, 7, 91-100.*

PARROT, J.F., 1977 - Assemblage ophiolitique du Baër-Bassit et termes effusifs du volcano-sédimentaire. *Travaux et Documents de l'O.R.S.T.O.M., 72.*

PASTER, T.P., SCHAUWECKER, D.S., & HASKIN, L.A., 1974 - The behaviour of some trace elements during solidification of the Skaergaard layered series. *Geochimica et Cosmochimica Acta, 38, 1549-77.*

PEARCE, J.A., & CANN, J.R., 1971 - Ophiolite origin investiaged by discriminant analysis using Ti, Zr, and Y. *Earth and Planetary Science Letters, 12, 339-49.*

PEARCE, J.A., & CANN, J.R., 1973 - Tectonic setting of basic volcanic rocks determined using trace element analysis. *Earth and Planetary Science Letters, 19, 290-300.*

PETERMAN, Z.E., COLEMAN, R.G., & HILDRETH, R.A., 1971 - Sr^{87}/Sr^{86} in mafic rocks of the Troodos Massif, Cyprus. *United States Geological Survey - Professional Paper 750-D, D157-61.*

PIETERS, P.E., 1978 - Port Moresby-Kalo-Aroa, Papua New Guinea, 1:250 000 Geological Series. *Bureau of Mineral Resources Australia - Explanatory Notes SC 55-6, 7, 11.*

PHILLPOTTS, J.A., SCHNETZLER, C.C., & THOMAS, H.H., 1972 - Petrogenetic implications of some new geochemical data on eclogitic and ultrabasic inclusions. *Geochimica et Cosmochimica Acta, 36, 1131-66.*

PRESNALL, D.C., 1969 - The geometrical analysis of partial fusion. *American Journal of Science, 267, 1178-94.*

PRESNALL, D.C., 1976 - Alumina content of enstatite as a geobarometer for plagioclase and spinel lherzolites. *American Mineralogist, 61, 582-8.*

PRESNALL, D.C., DIXON, J.R., O'DONNELL, T.H., & DIXON, S.A., 1979 - Generation of mid-ocean ridge basalts. *Journal of Petrology, 20, 3-35.*

PRINZ, M., KEIL, K., GREEN, J.A., REID, A.M., BONATTI, E., & HONNOREZ, J., 1976 - Ultramafic and mafic dredge samples from the equatorial Mid-Atlantic Ridge and fracture zones. *Journal of Geophysical Research, 81, 4087-103.*

REED, S.J.B., & WARE, N.G., 1973 - Quantitative electron microprobe analysis using a lithium-drifted silicon detector. *X-ray Spectrometry, 2, 69-74.*

REED, S.J.B., & WARE, N.G., 1975 - Quantitative electron microprobe analysis of silicates using energy-dispersive X-ray spectrometry. *Journal of Petrology, 16, 499-515.*

RHODES, J.M., DUNGAN, M.A., BLANCHARD, D.P., & LONG, P.E., 1979 - Magma mixing at mid-ocean ridges: evidence from basalts drilled near 22°N on the Mid-Atlantic Ridge. *Tectonophysics, 55, 35-61.*

RINGWOOD, A.E., 1966 - The chemical composition and origin of the earth. *In* HURLEY, P.M. (Editor), ADVANCES IN EARTH SCIENCE, 287-356. *MIT Press, Cambridge.*

RINGWOOD, A.E., 1975 - COMPOSITION AND PETROLOGY OF THE EARTH'S MANTLE. *McGraw-Hill, New York.*

RINGWOOD, A.E., 1979 - Composition and origin of the earth. *In* McELHINNY, M.W. (Editor), THE EARTH: ITS ORIGIN, STRUCTURE AND EVOLUTION, 1-58. *Academic Press, London.*

ROBERTSON, A.H.F., & HUDSON, J.D., 1973 - Cyprus umbers: chemical precipitates on a Tethyan ocean ridge. *Earth and Planetary Science Letters, 18, 93-101.*

ROBINSON, G.P., 1973 - Stratigraphy and structure of the Huon Peninsula, New Guinea within the framework of the Outer Melanesian Arc. *In* FRASER, R., (Editor), OCEANOGRAPHY OF THE SOUTH PACIFIC 1972. *New Zealand National Commission for UNESCO, Wellington.*

ROBIE, R.A., HEMINGWAY, B.S., & FISHER, J.R., 1978 - Thermodynamic properties of minerals and related substances at 298.15°K and 1 bar (10^5 pascals) pressure and at higher pressure. *United States Geological Survey - Bulletin 1452.*

ROBIE, R.A., & WALDBAUM, D.R., 1968 - Thermodynamic properties of minerals and related substances at 298.15°K (25.0°C) and one atmosphere (1.013 bars) pressure and at higher pressure. *United States Geological Survey - Bulletin 1259.*

RODGERS, K.A., 1973 - Chrome-spinels from the Massif Du Sud, southern New Caledonia. *Mineralogical Magazine, 39, 326-39.*

ROEDER, P.L., 1974 - Activity of iron and olivine solubility in basaltic liquids. *Earth and Planetary Science Letters, 23, 397-410.*

ROEDER, P.L., CAMPBELL, I.A., & JAMIESON, H.E., 1979 - A re-evaluation of the olivine-spinel geothermometer. *Contributions to Mineralogy and Petrology, 68, 325-34.*

ROEDER, P.L., & EMSLIE, R.F., 1970 - Olivine-liquid equilibrium. *Contributions to Mineralogy and Petrology, 29, 275-89.*

ROSS, M., & HUEBNER, J.S., 1975 - A pyroxene geothermometer based on composition - temperature relationships of naturally occurring orthopyroxene, pigeonite and augite. *Extended abstracts of the International Conference on Geothermometry and Geobarometry, Pennsylvania State University, 1975.*

RYABCHIKOV, I.D., GREEN, D.H., & BREY, G., unpublished - The oxidation state of carbon in the environment of the Low Velocity Zone. *Unpublished manuscript.*

SATO, H., 1977 - Nickel content of basaltic magmas: identification of primary magmas and a measure of the degree of olivine fractionation. *Lithos, 10, 113-20.*

SAUNDERS, A.D., & TARNEY, J., 1979 - The geochemistry of basalts from a back-arc spreading centre in the East Scotia Sea. *Geochimica et Cosmochimica Acta, 43, 555-72.*

SAUNDERS, A.D., TARNEY, J., STERN, C., & DALZIEL, I.W.D., 1979 - Geochemistry of Mesozoic marginal basin floor igneous rocks from southern Chile. *Geological Society of America-Bulletin 90, 237-58.*

SCHILLING, J-G., 1971 - Sea-floor evolution - Rare earth evidence. *Philosophical Transactions of the Royal Society of London, 268A, 663-706.*

SCHILLING, J-G., 1973 - Iceland mantle plume: Geochemical study of Reykjanes ridge. *Nature, 242, 565-71.*

SCHILLING, J-G., 1975 - Rare-earth variations across 'normal segments' of the Reykjanes Ridge, 60-53°N, Mid-Atlantic Ridge, 29°S, and East Pacific Rise, 2-19°S, and evidence on the composition of the underlying low velocity layer. *Journal of Geophysical Research, 80, 1459-70.*

SCLATER, J., HAWKINS, J., MAMMERICKX, J., & CHASE, C., 1972 - Crustal extension between the Tonga and Lau ridges: petrologic and geophysical evidence. *Geological Society of America-Bulletin 83, 505-18.*

SHAW, D.M., 1970 - Trace element fractionation during anatexis. *Geochimica et Cosmochimica Acta, 34, 331-40.*

SIGURDSSON, H., 1976 - Spinels in Leg 37 basalts and peridotites: phase chemistry and zoning. *In* AUMENTO, F., MELSOM, W.G., & OTHERS, (Editors) INITIAL REPORTS OF THE DEEP SEA DRILLING PROJECT, 37, 775-94. *US Government Printing Office, Washington, D.C.*

SIGURDSSON, H., & SCHILLING, J-G., 1976 - Spinels in Mid-Atlantic Ridge basalts: chemistry and occurrence. *Earth and Planetary Science Letters, 29, 7-20.*

SIGVALDSON, G.E., 1974 - Basalts from the centre of the assumed Icelandic mantle plume. *Journal of Petrology, 15, 497-524.*

SIMONIAN, K.O., GASS, I.G., 1978 - Arakapas fault belt, Cyprus: A fossil transform fault. *Geological Society of America-Bulletin 89, 1220-30.*

SINTON, J.M., 1977 - Equilibration history of the basal alpine-type peridotite, Red Mountain, New Zealand. *Journal of Petrology, 18, 216-46.*

SINTON, J.M., 1979 - Petrology of (alpine-type) peridotites from Site 395, DSDP Leg 45. *In* MELSOM, W.G., RABINOWITZ, P.D., & OTHERS (Editors) INITIAL REPORTS OF THE DEEP SEA DRILLING PROJECT, 45, 595-601. *US Government Printing Office, Washington, D.C.*

SMEWING, J.D., & POTTS, P.J., 1976 - Rare earth abundances in basalts and metabasalts from the Troodos massif, Cyprus. *Contributions to Mineralogy and Petrology, 57, 245-58.*

SMEWING, J.D., SIMONIAN, K.O., & GASS, I.G., 1975 - Metabasalts from the Troodos massif, Cyprus: Genetic implications deduced from petrography and trace element geochemistry. *Contributions to Mineralogy and Petrology, 51, 49-64.*

SMITH, D., & LINDSLEY, D.H., 1971 - Stable and metastable augite crystallization trends in a single basalt flow. *American Mineralogist, 56, 225-33.*

SMITH, I.E., & DAVIES, H.L., 1976 - Geology of the southeast Papuan mainland. *Bureau of Mineral Resources, Australia - Bulletin 165.*

SMITH, R.E., 1968 - Redistribution of major elements in alteration of some basic lavas during regional metamorphism. *Journal of Petrology, 9, 191-219.*

SMITH, R.E., & SMITH, S.E., 1976 - Comments on the use of Ti, Zr, Y, Sr, K, P and Nb in classification of basaltic magmas. *Earth and Planetary Science Letters, 32, 114-20.*

SPOONER, E.T.C., CHAPMAN, H.J., & SMEWING, J.D., 1977 - Strontium isotopic contamination and oxidation during ocean floor hydrothermal metamorphism of the ophiolitic rocks of the Troodos Massif, Cyprus. *Geochimica et Cosmochimica Acta, 41, 873-90.*

SPRY, A., 1969 - METAMORPHIC TEXTURES. *Pergamon Press, Oxford.*

STERN, C.R., & WYLLIE, P.J., 1975 - Effect of iron absorption by noble-metal capsules on phase boundaries in rock melting experiments at 30 kb. *American Mineralogist, 60, 681-9.*

ST JOHN, V.P., 1970 - The gravity field and structure of Papua New Guinea. *Journal of the Australian Petroleum Exploration Association, 10, 41-55.*

STROH, J.M., 1976 - Solubility of alumina in orthopyroxene plus spinel as a geobarometer in complex systems. Application to spinel-bearing alpine-type peridotite. *Contributions to Mineralogy and Petrology, 54, 173-88.*

SUEN, C.J., FREY, F.A., & MALPAS, J., in press - Bay of Islands ophiolite suite, Newfoundland: Petrologic and geochemical characteristics with emphasis on rare-earth element geochemistry. *Earth and Planetary Science Letters.*

SUN, S-S., & HANSON, G.N., 1975 - Origin of the Ross Island basanitoids and limitations on the heterogeneity of mantle sources for alkali basalts and nephelinites. *Contributions to Mineralogy and Petrology, 52, 77-106.*

SUN, S-S., & NESBITT, R.W., 1977 - Chemical heterogeneity of the Archaean mantle, composition of the earth and mantle evolution. *Earth and Planetary Science Letters, 35, 429-48.*

SUN, S-S., & NESBITT, R.W., 1978a - Chemical regularities and genetic significance of ophiolitic basalts. *Geology, 6, 689-93.*

SUN, S-S., & NESBITT, R.W., 1978b - Petrogenesis of Archaean ultrabasic and basic volcanics: Evidence from rare earth elements. *Contributions to Mineralogy and Petrology, 65, 301-25.*

TARNEY, J., SAUNDERS, A.D., & WEAVER, S.D., 1977 - Geochemistry of volcanic rocks from the island arcs and marginal basins of the Scotia Arc region. *In* TALWANI, M., & PITMAN, W.C. (Editors), ISLAND ARCS, DEEP SEA TRENCHES, AND BACK-ARC BASINS, 367-77. *American Geophysical Union, Washington, D.C.*

TAYLOR, S.R., & GORTON, M.P., 1977 - Geochemical application of spark source mass spectrography - 3. Element sensitivity, precision and accuracy. *Geochimica et Cosmochimica Acta, 41, 1375-80.*

THAYER, T.P., 1963 - Flow-layering in alpine peridotite-gabbro complexes. *Mineralogical Society of America Special Paper 1, 55-61.*

THAYER, T.P., 1967 - Chemical and structural relations of ultramafic and feldspathic rocks in alpine intrusive complexes. *In* WYLLIE, P.J. (Editor), ULTRAMAFIC AND RELATED ROCKS, 222-38. *John Wiley & Sons, New York.*

THAYER, T.P., 1969 - Gravity differentiation and magmatic re-emplacement of podiform chromite deposits. *In* WILSON, H.D.B. (Editor), MAGMATIC ORE DEPOSITS. *Economic Geology Monograph 4, 132-46.*

THOMPSON, G., BRYAN, W.B., FREY, F.A., & SUNG, C.M., 1975 - Petrology and geochemistry of basalts and related rocks from sites 214, 215, 216, DSDP Leg 22, Indian Ocean. *In* VON DER BORCH, C.C., SCLATER, J.G., & OTHERS (Editors), INITIAL REPORTS OF THE DEEP SEA DRILLING PROJECT, 22, 459-68. *US Government Printing Office, Washington, D.C.*

THOMPSON, R.N., 1975 - Primary basalts and magma genesis 11. Snake River plain, Idaho, U.S.A. *Contributions to Mineralogy and Petrology, 52, 157-64.*

THOMPSON, R.N., & KUSHIRO, I., 1972 - The oxygen fugacity within graphite capsules in piston-cylinder apparatus at high pressures. *Carnegie Institution of Washington - Yearbook 71, 615-6.*

TOKSOZ, M.N., & BIRD, P., 1977 - Formation and evolution of marginal basins and continental plateaux. *In* TALWANI, M., & PITMAN, W.C. (Editors), ISLAND ARCS, DEEP SEA TRENCHES AND BACK-ARC BASINS, 379-93. *American Geophysical Union, Washington, D.C.*

TROGER, W.E., 1956 - OPTISCHE BESTIMMUNG DER GESTEINBILDENDEN MINERALE TEIL 1. *Schweizerbart'sche Verlagsbuchhandling, Stuttgart.*

TUREKIAN, K.K., & WEDEPOHL, K.H., 1961 - Distribution of the elements in some major units of the Earth's crust. *Geological Society of America-Bulletin 72, 175-92.*

VALLANCE, T.G., 1974 - Spilitic degradation of a tholeiitic basalt. *Journal of Petrology, 15, 79-96.*

VARNE, R., & BROWN, A.V., 1978 - The geology and petrology of the Adamsfield Ultramafic Complex, Tasmania. *Contributions to Mineralogy and Petrology, 67, 195-207.*

VERNON, R.H., 1970 - Comparative grain-boundary studies of some basic and ultrabasic granulites, nodules and cumulates. *Scottish Journal of Geology, 6, 337-51.*

VILJOEN, M.J., & VILJOEN, R.P., 1969 - The geology and geochemistry of the lower ultramafic unit of the Onverwacht Group and a proposed new class of igneous rocks. *Geological Society of South Africa - Special Publication 2, 55-86.*

VOGT, P.R., & BYERLY, G.R., 1976 - Magnetic anomalies and basalt composition in the Juan de Fuca-Gorda Ridge area. *Earth and Planetary Science Letters, 33, 185-207.*

VOLL, G., 1960 - New work on petrofabrics. *Liverpool Manchester Geological Journal, 2, 503-67.*

WAGER, L.W., & BROWN, G.M. 1968 - LAYERED IGNEOUS ROCKS. *Oliver and Boyd, Edinburgh.*

WARNER, R.D., & LUTH, W.C., 1974 - The diopside-orthoenstatite two-phase region in the system $CaMgSi_2O_6$-$Mg_2Si_2O_6$. *American Mineralogist, 59, 98-109.*

WEAVER, S.D., SAUNDERS, A.D., PANKHURST, R.J., & TARNEY, J., 1979 - A geochemical study of magmatism associated with the initial stages of back-arc spreading. *Contributions to Mineralogy and Petrology, 68, 151-69.*

WEEDON, D.S., 1965 - The layered ultrabasic rocks of Sgurr Dubh, Isle of Skye. *Scottish Journal of Geology, 1, 42-68.*

WELLS, P.R.A., 1977 - Pyroxene thermometry in simple and complex systems. *Contributions to Mineralogy and Petrology, 62, 129-39.*

WHITE, W.M., & BRYAN, W.B., 1977 - Sr-isotope, K, Rb, Cs, Sr, Ba and rare-earth geochemistry of basalts from the FAMOUS area. *Geological Society of America-Bulletin 88, 571-6.*

WHITE, W.M., & SCHILLING, J-G., 1978 - The nature and origin of geochemical variation in Mid-Atlantic Ridge basalts from the Central North Atlantic. *Geochimica et Cosmochimica Acta, 42, 1501-16.*

WILKINSON, J.F.G., & BINNS, R.A., 1977 - Relatively iron-rich lherzolite xenoliths of the Cr-diopside suite: A guide to the primary nature of anorogenic tholeiitic andesite magmas. *Contributions to Mineralogy and Petrology, 65, 199-212.*

WILLIAMS, D.A.C., 1972 - Archaean ultramafic, mafic and associated rocks, Mt. Monger, Western Australia. *Geological Society of Australia - Journal, 19, 163-88.*

WILLIAMS, D.A.C., & HALLBERG, J.A., 1973 - Archaean layered intrusions of the Eastern Goldfields region, Western Australia. *Contributions to Mineralogy and Petrology, 38, 45-70.*

WOOD, B.J., & BANNO, S., 1973 - Garnet-orthopyroxene and orthopyroxene-clinopyroxene relationships in simple and complex systems. *Contributions to Mineralogy and Petrology, 42, 109-24.*

WOOD, B.J., & NICHOLS, J., 1978 - The thermodynamic properties of reciprocal solid solutions. *Contributions to Mineralogy and Petrology, 66, 389-400.*

WOOD, D.A., 1976 - Spatial and temporal variation in the trace element geochemistry of the eastern Iceland flood basalt succession. *Journal of Geophysical Research, 81, 4353-60.*

WOOD, D.A., GIBSON, I.L., & THOMPSON, R.N., 1976 - Element mobility during zeolite facies metamorphism of the Tertiary basalts of eastern Iceland. *Contributions to Mineralogy and Petrology, 55, 241-54.*

WYLLIE, P.J., 1971 - THE DYNAMIC EARTH: TEXTBOOK IN GEOSCIENCES. *John Wiley & Sons, New York.*

WYLLIE, P.J., 1979 - Magmas and volatile components. *American Mineralogist, 64, 469-500.*

ZONENESHAIN, L.P., & KUZMIN, M.I., 1978 - The Khan-Taishir ophiolite complex of Western Mongolia, its petrology, origin and comparison with other ophiolitic complexes. *Contributions to Mineralogy and Petrology, 65, 95-109.*

APPENDIX 1

ANALYTICAL TECHNIQUES

Microprobe analysis

Quantative analyses (Na-Fe) of the mineral phases in the Marum and Papuan ophiolites and the major element compositions of the Tumu River basalts were determined by TPD electron microprobe at RSES, ANU using an Ortec Li-drifted silicon detector following the energy dispersive method of Reed & Ware (1973, 1975). The emitted X-ray spectrum was accumulated over 100 seconds in a Northern Scientific (NS710) multichannel pulse height analyser at a count rate of about 5000 counts per second (cps). Peak intensities were measured by summing counts in groups of channels corresponding to the full width at half maximum (FWHM) of each peak. Resolution of the energy spectrum at FWHM for the Mn K_α peak is about 170 eV and results in satisfactory resolution of the Na, Mg, Al and Si K_α peaks. The analytical conditions employed an electron beam accelerating voltage of 15 kV, a beam diameter of about 1 micron and a beam current of 3 nannoamps. Precision is generally better than 1.5% relative, and accuracy is better than 2% relative. Limits of detection are Na ($\sim$ 0.2%), Mg-Al (0.1%), Mn (0.09%), Cr (0.08%), Ti, Ca and K (0.07%). The accuracy of the microprobe data can be assessed from the comparison of the data obtained for standard rocks BCR-1 and JB-1 (Table 1a) which were melted on an iridium strip heater and analysed by microprobe with the recommended values of Flanagan (1973) and Ando & others (1974) recalculated volatile-free to 100%. Most of the standard deviation is due to heterogeneity in the glasses, especially for BCR-1 which proved difficult to homogenize on the iridium strip (due probably to the high iron content). Analyses of rocks performed by microprobe after fusion on an iridium strip heater are also compared with analyses made by XRF (in triplicate) following the method of Norrish & Hutton (1969).

TABLE 1a. COMPARISON OF MAJOR ELEMENT ANALYSES BY PROBE AND XRF

	1	2	3	4	5	6	7	8	9	10
SiO_2	55.40(37)	55.65	53.70(35)	53.53	50.73	50.69	48.15	48.12	49.04	49.44
TiO_2	2.25(7)	2.24	1.32(7)	1.38	0.08	0.15	<0.07	0.04	3.63	3.70
Al_2O_3	13.72(15)	13.89	14.79(25)	14.87	12.87	12.81	18.18	18.02	12.43	12.48
FeO$^{\Sigma}$	12.59(23)	12.36	8.38(15)	8.31	7.17	6.99	3.05	3.03	16.91	16.72
MnO	0.12(7)	0.18	<0.09	0.15	<0.09	0.17	<0.09	0.08	0.24	0.28
MgO	3.70(19)	3.53	8.02(9)	7.91	13.83	13.76	11.99	11.88	4.80	4.61
CaO	7.11(8)	7.06	9.53(9)	9.50	14.76	14.86	18.19	18.40	7.97	7.98
Na_2O	3.36(8)	3.34	2.79(7)	2.87	0.56	0.57	0.44	0.43	4.90	4.73
K_2O	1.75(5)	1.74	1.47(4)	1.47	<0.07	0.002	<0.07	0.002	0.08	0.06
Na_2O*	3.25	3.27	2.72	2.80	0.57		0.43		4.58	
K_2O	-	1.70	1.42	1.43	0.002		0.001		0.05	
P_2O_5	0.38	0.36	0.29	0.26	0.009	0.01	0.010	0.01	0.49	0.53
MnO	0.19	0.18	-	0.15						

1. Microprobe determination (10 analyses) of BCR-1. Numbers in parentheses are errors and refer to the last decimal place (S)
2. Recommended values for BCR-1 (Flanagan, 1973)
3. Microprobe determination of JB-1 (15 analyses)
4. Recommended values for JB-1 (Ando and others, 1974)
5. Microprobe - gabbro 1020
6. XRF - gabbro 1020
7. Microprobe - gabbro 191
8. XRF - gabbro 191
9. Microprobe - basalt 565
10. XRF - basalt 565

All major element analyses normalized to 100%.

*Na_2O and K_2O by atomic absorption spectroscopy.
P_2O_5 and MnO by XRF on pressed powder pellets.

Simultaneous quantitative analyses for 10 elements (Na-Fe) of the experimental run products was made largely using a JEOL JX 50A electron microprobe - scanning electron microscope fitted with an EDAX energy dispersive analytical system at the Central Science Laboratory, Hobart. The analytical method follows that of Reed & Ware (1973, 1975) and is described in detail by Griffin (1979). Operating conditions employed an accelerating voltage of 15 kV, beam current of 3 nannoamps, a beam diameter of less than 0.5 microns, and 100 seconds counting time. Comparative studies and additional data were obtained by TPD probe. Glass analyses and analyses of the bulk charges were made by rapid reduced area scans ($\sim$250μ) to avoid alkali volatilisation and ensure representative analysis. SEM photographs of the run products were obtained using a Polaroid camera with high speed (107) film.

Sample preparation

Between 0.5 and 2 kg (depending on grainsize and available sample size) of rock, free from veins or weathered surfaces were reduced to approximately 1 cm^3 in a jaw crusher, and crushed to coarse sand size in a tungsten carbide mill. The jaw crusher and mill were cleaned between samples by wire bush, acetone and dry ice. A 50-70 gm split was then crushed to -200 mesh in a tungsten carbide Sieb mill. The PUB samples were crushed in an agate mill. Between samples the mill was cleaned with washed quartz sand, acetone and an initial sample crush which was subsequently disgarded. The use of the tungsten carbide mill precluded the determination of Co and W. However, examination of the spark source photoplates for a harzburgite sample showed that W contamination was minimal and that no other contamination (e.g. Pb) was introduced during crushing.

X-ray fluorescence spectroscopy

Major abundances in the Marum peridotites and gabbros and all PUB samples, and all trace element abundances were determined at the

standard. The method is similar to that described by Cooper (1963) for potassium determination. All analyses were performed in duplicate.

FeO in the Marum samples was determined by potentiometric titration against $K_2Cr_2O_4$ using a $Pt\text{-}Pt_{80}Rh_{20}$ bimetallic electrode (Kiss, 1977) following solution in acid under N_2 atmosphere. FeO in the PUB samples was determined by Mr. J. Wasik by dissolution in HF followed by titration against potassium dichromate.

H_2O^+ in the Marum samples was determined as loss-on-ignition after heating to 1050°C for 20 minutes, with allowance for the oxidation of FeO. Volatiles in the PUB samples were determined by Mr. J. Wasik at the Department of Geology. For these analyses H_2O^- is the percentage of weight loss after heating the sample to 110°C for 90 minutes. H_2O^+ and CO_2 were measured by heating a sample for 30 minutes in a tube furnace at 1000-1050°C in a stream of dry, CO_2-free nitrogen. H_2O and CO_2 given off were collected and weighed in microabsorption tubes.

Major elements (except MnO and P_2O_5) for the Tumu River basalts were determined by TPD electron microprobe using a 40μ beam after fusion on an iridium strip (Nicholls, 1974). Glasses were prepared in duplicate and at least five analyses made of each. Glasses were homogeneous and precision is estimated to be better than 5%, mostly 2%. Good agreement was obtained in analyses of standard rocks JB-1 and BCR-1 and for XRF analysis of selected samples (Table 1a). MnO and P_2O_5 contents were determined by XRF on pressed powder pellets by linear calibration with USGS standard rocks with a precision of 5-7%. Na_2O and K_2O were determined for selected samples by atomic absorption spectroscopy; agreement obtained with probe data indicates no loss of alkalis on fusion.

Trace elements

Trace elements Sc, V, Cr, Ni, Cu, Zn, Ba, Rb, Sr, Y, Zr, Nb, La, Ce and Nb were determined by XRF on pressed powder pellets following the method of Norrish & Chappell (1977). X-ray counts were automatically

corrected for detector dead time, and instrument drift was monitored against an internal standard. The analytical line determined and operating conditions employed, selected to maximize the count rate and minimize inter-element interferences, are described by Norrish & Chappell (1977). Background peaks were measured on either side of the peak position and the background profile corrected for non-linearity using one or more of the following; spec pure Al_2O_3, spec pure SiO_2 and "Herasil" silica glass. Further empirical corrections to the measured intensities were applied to overcome inter-element interferences (Norrish & Chappell, 1977).

The concentration (p) of a trace element is related to the intensity of emitted characteristic radiation (c) by the formula

$$p = \frac{A \times c}{K}$$

where A is the mass absorption coefficient of the sample for the radiation being analysed and K is a constant for particular analytical conditions which is calculated from analysis of standards of known A and p under the same analytical conditions.

Mass absorption coefficients for samples were measured for the heavier elements (Sr_{K_α} and Rb_{K_α}) on rock powder pressed into a perspex holder of known diameter. The attenuation (I_o/I) of the measured wavelength was measured and the mass absorption calculated from the relationship

$$A = \frac{I}{px} \ln(I_o/I) \text{ where } px = \text{mass cm}^{-2}.$$

Mass absorpitons for elements of shorter wavelength were calculated from the major element composition. Additional analyses of a number of trace elements were made using a corrected peak-to-corrected background approach for estimation of mass absorption coefficients and calibration against synthetic and natural rock standards.

Determination of Rb and Sr abundances at low levels was made following the method of Chappell & others (1969). Similarly long counting

times (200 seconds peak, 100 seconds background) were used in the determination of certain other trace elements at very low levels in the peridotites and gabbros.

Spark Source Mass Spectrometry

The abundances of REE (La - Yb), Th, U, Pb, Hf, Cs, Sn, Zr, and Nb and in some cases Rb and Sr, were determined by spark source mass spectrometry (Taylor, 1965, 1971) using the improved data reduction method of Taylor & Gorton (1977) on an AEI MS7 spark source mass spectrometer at RSES, ANU. Because the method uses Lu as an internal standard the abundance of Lu cannot be directly determined. The abundance of Tm was only determined in favourable circumstances where the resolution of the spectrograph was such as to resolve the Tm line from a carbon multiple.

Sample preparation involved mixing of 100 mg of powdered sample with an identical amount of powdered graphite mix containing a known amount of Lu as Lu_2O_3. Mix F (containing 50 ppm Lu) was used for most samples but for the peridotites and gabbros with low abundances of REE mixes E and E/2 were used. Electrodes pressed from this mixture were then subjected to a pulsed high voltage RF spark under vacuum in the source of the mass spectrometer and the ion beam produced focussed and collected on an Ilford Q-2 photographic plate. The densities of the mass lines were determined by microphotometer-densitometer, and the density - intensity relationship of the photoplates calibrated by plotting the densities of lines for isotope pairs (e.g. $^{134}Ba/^{135}Ba/^{137}Ba$) against their known abundance ratios. The slope of the line drawn through these points is a measure of the plate response to incident ion beam intensity, and is used to obtain relative intensity values from the densitometer readings obtained on individual exposures. These intensity values are then ratioed to the intensity of the internal standard line on the same exposure to obtain the abundance of the nuclide. The ratio measurements

are then converted to elemental abundance data by calibration with known geological standards. The cumputer program also applied corrections for natural Lu, interferences on ^{176}Lu by ^{176}Hf and ^{176}Yb, and for LREE and Ba oxide and carbide on the heavy REE. These interferences, discussed in detail by Taylor & Gorton (1977), which may be severe in strongly fractionated LREE-enriched patterns were not significant for most of the samples analysed here. ^{139}La in plagioclase-rich gabbros suffered obvious interference from the CaAl carbide. Additional interference at low concentrations were observed on ^{163}Dy, and on ^{140}Ce in the pyroxenite.

Accuracy and precision of the method are dependent on precise determination of the photoplate intensity-density relationship, and on the number of graded exposures used to determine the abundance of each element. Generally two (in some cases three) photoplates were exposed for each sample, and each contained up to 15 graded exposures with determinations for a number of elements based on more than one isotope. Generally the measured abundance of each element was based on between 8-24 determinations but in the peridotites determinations of some of the heavier elements were based on less than this (5-7). Precision and accuracy of the technique are discussed in detail by Taylor & Gorton (1977). The precision of the analyses presented here, expressed as relative deviation of standardized intensities was mostly better than 5%, and commonly 3% or less. Overall precision and accuracy of the method are believed to be REE, Th, U, Hf, Ba (+ 5%), and Zr, Nb, Y and others (10-15%). Trace element data obtained by spark source mass spectrometry are compared with data obtained by XRF (Table 1b) together with recent MS7 data for USGS standard rock BCR-1 (Taylor & Gorton, 1977). Overall agreement between XRF and MS7 data was generally better than 15% and commonly better than 10%, except for Ba for which good agreement was only obtained at high levels, and for REE, Nb, Y, Zr at low levels ($<$ 10 ppm). All data reported or presented have been normalized to the chondrite-normalizing values of Taylor & Gorton (1977).

TABLE 1c. COMPARISON OF REE DATA

	1	2	3
La	0.315	24.2	24.6
Ce	0.813	53.7	53.6
Pr	0.116	6.50	6.60
Nd	0.597	28.5	29.3
Sm	0.192	6.7	6.44
Eu	0.0722	1.95	2.01
Gd	0.259	6.55	6.25
Tb	0.049	1.08	1.07
Dy	0.325	6.39	6.44
Ho	0.073	1.33	1.32
Er	0.213	3.70	3.73
Tm	0.030	0.51	0.61
Yb	0.208	3.48	3.69
Lu	0.0323	0.55	0.59

1. REE chondrite normalizing values.
2. BCR-1 'best estimate'.
3. Average 7 determinations by MS7 RSES.

All data from Taylor & Gorton (1977).

Overall agreement between XRF and MS7 data was generally better than 15% and commonly better than 10%, except for Ba for which good agreement was only obtained at high levels, and for REE, Nb, Y, Zr at low levels ($<$ 10 ppm). All data reported or presented have been normalized to the chondrite-normalizing values of Taylor & Gorton (1977) which are given in Table 1c.

Strontium isotope ratios

Initial $^{87}Sr/^{86}Sr$ ratios have been determined for 4 gabbros from the Marum ophiolite and 2 gabbros from the PUB by Dr. R.W. Page at the RSES, ANU. These values together with 4 unpublished determinations made previously by Dr. P.A. Arriens, and provided by kind permission, are presented in Table 1d. The new analyses were run on a Nuclide mass spectrometer following the analytical method described by Page & Johnson (1974). The measured value for NBS standard 987 was 0.71027 $\pm$ 0.00007.

Partition coefficients

Partition coefficients for various phases selected from the literature are presented in Table 1e. The values for olivine, orthopyroxene and clinopyroxene lie at the low end of the range of partition coefficient values found for these elements.

Activity - Composition relationships

The following activity - composition relationships have been used in the thermodynamic calculations.

$a^{ol}_{Mg_2SiO_4} = (X^{ol}_{Mg})^2$ - Irvine (1965)

$a^{opx}_{Mg_2Si_2O_6} = (X^{M1}_{Mg})\ (X^{M2}_{Mg})$ - Wood & Banno (1973)

$a^{opx}_{MgAl_2SiO_6} = (X^{M1}_{Al})\ (X^{M2}_{Mg})$ - Wood & Banno (1973)

$a^{cpx}_{Mg_2Si_2O_6} = (X^{M1}_{Mg})\ (X^{M2}_{Mg})$ - Wood & Banno (1973)

$a^{cpx}_{CaAl_2SiO_6} = (X^{M2}_{Ca})\ (X^{M1}_{Al})$ - Herzberg (1978)

$a^{sp}_{MgAl_2O_4} = (X^{sp}_{Mg})\ (Y^{sp}_{Al})^2$ - Irvine (1965)

$a^{plag}_{CaAl_2Si_2O_8} = X^{plag}_{Ca}$ - Obata (1976)

TABLE 1d. STRONTIUM ISOTOPE RATIOS

Sample No.	Rock	Rb	Sr	Rb/Sr	$^{87}Sr/^{86}Sr$
Marum					
1. 123A	anorthosite	0.60	259	0.00232	0.7037
2. 131	gabbro	0.19	133	0.00143	0.7038
3. 225	gabbro	<0.1	64	<0.0015	0.7031
4. 1020	gabbro	0.06	59	0.00102	0.7033
Papuan Ultramafic Belt					
5. 728	gabbro	<0.1	90	<0.001	0.7036
6. 730	gabbro	0.04	92	0.00043	0.7035
		(Coordinates)			
7. 972	basalt	(080114734)			0.7044
8. 1015	dolerite	(08514750)			0.7041
9. 532	gabbro	(073714713)			0.7046
Tonalites (Eocene)					
10. 976		(074514730)			0.6964
					0.7044
11. 1235		(074714723)			0.7039
					0.7046
12. 1228		(074914724)			0.6950

Analyses 1 - 6 by Dr R.W. Page

Analyses 7 - 12 by Dr P.A. Arriens (1970, unpub. report)

Coordinates are in degrees of latitude and longitude

TABLE 1e. PARTITION COEFFICIENTS

	ol	opx	cpx	plag
La	0.0005[1]	0.0005[1]	0.02[1]	
Ce	0.0008	0.0009	0.04	0.12[2]
Nd	0.0013	0.0019	0.09	0.081
Sm	0.0019	0.0028	0.14	0.067
Eu	0.0019	0.0036	0.16	0.34
Gd				0.063
Tb	0.0019	0.0059	0.19	
Dy				0.055
Ho	0.0020	0.0089	0.195	
Er				0.063
Yb	0.0040	0.0286	0.20	0.067
Ti	0.02-0.07[3]	0.06-0.11[3]	0.23-0.50(0.34)[4]	<0.01
Zr	0.01	0.01	0.05-0.22[5]	<0.01[5]

1. REE p.c. from Frey & others (1978).
2. REE p.c. from Arth (1976; average).
3. Compilation by Irving (1978).
4. Duke (1976).
5. McCallum & Charette (1978).

REFERENCES

ANDO, A., KURASAWA, H., OHMORI, T., & TAKEDA, E., 1974 - 1974 compilation of data on the GSJ geochemical reference samples JG-1 granodiorite and JB-1 basalt. *Geochemical Journal, 8, 175-92.*

ARTH, J.G., 1976 - Behaviour of trace elements during magmatic processes - a summary of theoretical models and their applications. *Research Journal of the US Geological Survey, 4, 41-7.*

CHAPPELL, B.W., COMPSTON, W., ARRIENS, P.A., & VERNON, M.J., 1969 - Rubidium & strontium determinations by X-ray fluorescence spectrometry and isotope dilution below the part per million level. *Geochimica et Cosmochimica Acta, 33, 1002-6.*

COOPER, J.A., 1963 - The flame photometric determination of potassium in geological materials used for potassium-argon dating. *Geochimica et Cosmochimica Acta, 27, 525-46.*

DUKE, J.M., 1976 - Distribution of the period four transition elements among olivine, calcic clinopyroxene and mafic silicate liquid: Experimental results. *Journal of Petrology, 4, 499-521.*

FLANAGAN, F.J., 1973 - 1972 values for international geochemical reference samples. *Geochimica et Cosmochimica Acta, 37, 1189-200.*

FREY, F.A., GREEN, D.H., & ROY, S.D., 1978 - Integrated models of basalt petrogenesis: a study of quartz tholeiites to olivine melilitites from S.E. Australia utilizing geochemical and experimental petrological data. *Journal of Petrology, 19, 463-513.*

GRIFFIN, B.J., 1979 - Energy dispersive analysis system calibration and operation with TAS-SUEDS, an advanced interactive data-reduction package. *University of Tasmania, Department of Geology Publication 343.*

HERZBERG, C.T., 1978 - Pyroxene geothermometry and geobarometry: experimental and thermodynamic evaluation of some subsolidus phase relations involving pyroxenes in the system $CaO-MgO-Al_2O_3-SiO_2$. *Geochimica et Cosmochimica Acta, 42, 945-57.*

IRVINE, T.N., 1965 - Chromian spinel as a petrogenetic indicator. Part 1. Theory. *Canadian Journal of Earth Science, 2, 648-72.*

IRVING, A.J., 1978 - A review of experimental studies of crystal/liquid trace element partitioning. *Geochimica et Cosmochimica Acta, 42, 743-70.*

KISS, E., 1977 - Rapid potentiometric determination of the iron oxidation state in silicates. *Analytica Chimica Acta, 89, 303-14.*

McCALLUM, I.S., & CHARETTE, M.P., 1978 - Zr and Nb partition coefficients: Implications for the genesis of mare basalts, KREEP and sea floor basalts. *Geochimica et Cosmochimica Acta, 42, 859-69.*

NICHOLLS, I.A., 1974 - A direct fusion method of preparing silicate glasses for energy dispersive electron microprobe analysis. *Chemical Geology, 14, 141-57.*

NORRISH, K., & CHAPPELL, B.W., 1977 - X-ray fluorescence spectrometry. *In* ZUSSMAN, J., (Editor), PHYSICAL METHODS IN DETERMINATIVE MINERALOGY, 201-72. *Academic Press, London, second edition.*

NORRISH, K., & HUTTON, J.Y., 1969 - An accurate X-ray spectrographic method for the analysis of a wide range of geological samples. *Geochimica et Cosmochimica Acta, 33, 431-54.*

OBATA, M., 1976 - The solubility of Al_2O_3 in orthopyroxene in spinel and plagioclase peridotites and spinel pyroxenite. *American Mineralogist, 61, 804-16.*

PAGE, R.W., & JOHNSON, R.W., 1974 - Strontium isotope ratios of Quaternary volcanic rocks from Papua New Guinea. *Lithos, 7, 91-100.*

REED, S.J.B., & WARE, N.G., 1973 - Quantitative electron microprobe analysis using a lithium-drifted silicon detector. *X-ray Spectrometry, 2, 69-74.*

REED, S.J.B., & WARE, N.G., 1975 - Quantitative electron microprobe analysis of silicates using energy-dispersive X-ray spectrometry. *Journal of Petrology, 16, 499-515.*

TAYLOR, S.R., 1965 - Geochemical analysis by spark source mass spectrography. *Geochimica et Cosmochimica Acta, 29, 1243-62.*

TAYLOR, S.R., 1971 - Geochemical applications of spark source mass spectrography-11. Photoplate data processing. *Geochimica et Cosmochimica Acta, 35, 1187-96.*

TAYLOR, S.R., & GORTON, M.P., 1977 - Geochemical application of spark source mass spectrography-111. Element sensitivity, precision and accuracy. *Geochimica et Cosmochimica Acta, 41, 1375-80.*

WOOD, B.J., & BANNO, S., 1973 - Garnet-orthopyroxene and orthopyroxene-clinopyroxene relationships in simple and complex systems. *Contributions to Mineralogy and Petrology, 42, 109-24.*

APPENDIX 2

LOCALITIES AND BRIEF DESCRIPTIONS OF ANALYSED SAMPLES

The samples tabulated here are selected from some 600 rocks collected and examined. Sample numbers used throughout the thesis refer to the BMR-GSPNG field numbers. The Marum samples have the prefix 7454 (001-288), 7554 (400-497) and 7654 (500-578), and were collected by me. Additional samples 74541007, -1020, - 1030, -1040, -1046, -1053, -1057, and -1104 were collected by C.J. Pigram. Carpentaria Exploration Co., through the agency of Mr. K. Holmes, kindly made the drill core material available for study. The Papuan Ultramafic Belt samples have the prefix 75522 and were collected in collaboration with Dr. H.L. Davies. The sample numbers given in parenthesis refer to registered numbers of material housed in the Department of Geology, University of Tasmania. Additional material is held at the GSPNG, Port Moresby.

Place names and locality data for the Marum samples are taken from the 1:100 000 scale geological map of the Marum ophiolite complex. Information for the Papuan Ultramafic Belt samples was taken from respective 1:100 000 scale topographic maps.

The following abbreviations are used: ol = olivine, chr = chrome spinel, opx = orthopyroxene, cpx = clinopyroxene, plag = plagioclase, qtz = quartz, hbl = hornblende, mag = magnetite, ilm = ilmenite, chlor = chlorite, sauss = saussurite, cum = cumulus, postcum = postcumulus, intercum = intercumulus, poik = poikilitic, phenos = phenocrysts, microphenos = microphenocrysts, o/c = outcrop.

Modal percentages are based on visual estimates except where given to a decimal place (petmix modelling and/or point counting).

BMR-GSPNG TASUNI

MARUM OPHIOLITE - Tectonite peridotites

046	48722	Harzburgite; faulted o/c, Marum R, 5°34'S 145°09'E. Xenoblastic; ol (74%), opx (25%), chr (1%); 20% serpentinization.
087	48723	Harzburgite-dunite; drill core DDH 67 29m. Xenomorphic; ol (95%), opx (4%), chr (1-2%). Extensively recrystallized.
088	48724	Harzburgite-dunite; drill core DDH 67 40m. Xenoblastic; ol (95%), opx (4%), chr (1-2%, commonly embayed).
089	48725	Harzburgite; drill core DDH 70 30m. Xenomorphic to xenomorphic granular; ol (75%), opx (24%), chr (1%). Extensively recrystallized.
090	48726	Harzburgite; drill core DDH 70 32m, intercalated dunite. Xenoblastic; ol (80%), opx (19%), chr (1%).
257	48727	Enstatolite; residual boulder near fault zone, Marum R, 5°34'S 145°07'E. Xenomorphic granular, strongly deformed; opx, cpx (extensively altered to tremolite), chr.
410	48728	Dunite; lens in harzburgite, 5°33'S 145°13'E. Xenoblastic; ol (97%), chr (3%, small disseminated subhedra).
411	48729	Dunite; lens in harzburgite, 5°33'S 145°12'E. Xenoblastic; ol (97%), chr (3%).
413	48730	Enstatolite; layer in banded peridotite, river boulder 5°33'S 145°12'E. Xenoblastic granular; opx, cpx, ol, disseminated chr.
414	48731	Dunite; lens in harzburgite, 5°34'S 145°12'E. Xenoblastic; ol (98%), chr (2%, disseminated).
418	48732	Harzburgite; massive, 5°35'S 145°12'E. Xenoblastic; ol (strongly serpentinized), opx (30%), chr (euhedral 1%).
423	48733	Harzburgite; float, 5°33'S 145°13'E. Xenoblastic; ol (80%), opx (19%), chr (1%). Protogranular.

425	48734	Harzburgite; as for 423. Xenoblastic; ol (74%, 2-3mm), opx (20%, 1-3mm), cpx (4%), chr (1%).
426	48735	Harzburgite; as for 423. Xenoblastic; ol (79%), opx (20%), chr (1%, commonly embayed).
473	48736	Harzburgite; drill core DDH 70 32m. Xenoblastic, little deformation; ol (79%), opx (20%), chr (1%).
474	48737	Harzburgite; drill core DDH 70 32.5m. Xenoblastic; ol (85%), opx (15%), chr (1%).
477	48738	Dunite; intercalated with harzburgite, drill core DDH 67. Xenoblastic; ol, chr (2%, disseminated, sub-euhedral to rounded).
479	48739	Harzburgite; drill core DDH 67 40m. Xenoblastic; ol (85%), opx (14%), chr (1%).
488	48740	Harzburgite; foliated, Baia R, 5°37'S 145°16'E. Xenoblastic; ol (70%, 2.5-5mm), opx (29%, 1-3mm), cpx (exsolved, trace), chr (1%).
489	48741	Harzburgite; foliated, Baia R, 5°37'S 145°15'E. Xenoblastic; ol (76.7%, <3mm), opx (22.7%), chr (0.6%).
490	48742	Harzburgite; foliated, Baia R, 5°37'S 145°14'E. Xenoblastic; ol (87.9%, up to 7mm, mostly 3-5mm) opx (11.5%, mostly 2-4mm), chr (0.6%).
491	48743	Enstatite-rich pyroxenite; dyke in harzburgite, Baia R, 5°37'S 145°14'E. Xenoblastic granular; opx (up to 5mm), cpx (small polygonal grains), ol (small), chr.
492	48744	Harzburgite; foliated, Baia R, 5°37'S 145°14'E. Xenoblastic; ol (80%, 2.5-5mm), opx (18%), cpx (small anhedra, 1%), chr (1%).

Cumulates

001	48745	Norite-gabbro; massive, Yomi R, 5°37'S 145°03'E. Allotriomorphic granular; plag (60%), opx (17%), cpx (15%), Fe-Ti oxide (8%); secondary amphibole.
005	48746	Leuconorite-gabbro; rhythmic and flow layering, Yomi R, 5°35'S 145°04'E. Deformed granular to mortar texture; plag (55%), opx (20%), opx (20%), Fe-Ti oxide (5%), abundant secondary amphibole.

008	48747	Norite-gabbro; rhythmic layering in o/c, Yomi R, $5^{o}33'S$ $145^{o}02'E$. Allotriomorphic granular, plag (55%), opx (30%), cpx (15%), Fe-Ti oxide, trace FeS. Secondary uralite.
010	48748	Norite-gabbro; rhythmic layering, tributary to Yomi R, $5^{o}32'S$ $145^{o}01'E$.
045	84749	Ol-bearing pyroxenite-rich norite-gabbro; isolated o/c with rhythmic layering, Marum R, $5^{o}33'S$ $145^{o}08'E$. Allotriomorphic granular; ol (5%), plag (35%), cpx (35%), opx (20%).
051	48750	Ol-bearing websterite; interlayered with dunite, Gagiowa R, $5^{o}33'S$ $145^{o}09'E$. Allotriomorphic granular; ol (4%), opx (33.5%), cpx (62.4%).
059	48751	Cpx-bearing dunite; massive, Imbrum R, $5^{o}44'S$ $145^{o}17'E$. Ol(xenomorphic), cpx (intercum, granular in px-rich layers; poik in px-poor layers), chr (stringers flattened in plane of foliation). Strongly serpentinized.
061	48752	Ol norite-gabbro, layered boulder, Imbrum R, $5^{o}44'S$ $145^{o}18'E$. Hypidiomorphic granular; ol (15%), opx (20%), cpx (20%), plag (45%).
071	48753	Ol-bearing norite-gabbro; layered o/c in E tributary to Simbai R, $5^{o}20'S$ $144^{o}52'E$. Allotriomorphic granular; ol (5%, serpentinized), plag (60%), opx (20%), cpx (15%).
073	48754	Ol norite-gabbro; layered o/c in E tributary to Simbai R, $5^{o}21'S$ $144^{o}53'E$. Hypidiomorphic granular; ol (10%), cpx (15%), opx (20%), plag (55%).
092	48755	Dunite; drill core DDH 71 19m. Xenomorphic granular, deformed adcumulate? ol (deformed, 2-5mm), chr (1-2% sub-euhedral, 200μ), 15-20% serpentine.
107	48756	Bronzitite; interlayered with ol pyroxenite, upper Gagiowa R, $5^{o}37'S$ $145^{o}10'E$. Allotriomorphic granular; opx, cpx (relics at grain boundaries), chr (tiny <50μ). Secondary tremolite, talc.
120	48757	Ol-bearing norite-gabbro; parallel fold, river boulder, Wendink R, $5^{o}26'S$ $144^{o}52'E$. Hypidiomorphic granular; ol (6%), plag (66%), cpx (20%), opx (10%). Extensive alteration.

123	48758	Anorthosite; rhythmic layering of anorthosite and norite-gabbro, tributary to Mambu R, 5°29'S 144°59'E. Allotriomorphic granular; plag, cpx, opx, mag, ilm, apatite (trace). Uralite alteration common.
128	48759	Flaser gabbro; parallel fold in flow layered norite-gabbro, tributary to Nep R, 5°29'S 144°09'E. Xenoblastic mortar texture common; plag + qtz xenoblasts with sutured margins (60%), matrix of opx, cpx, qtz, mag, ilm, apatite (trace).
129	48760	Mylonitic gabbro; flow layering, tributary to Nep R, 50m upstream from 128. Blastomylonitic, mortar texture; plag, cpx, opx, mag, ilm, qtz.
131	48761	Norite-gabbro; rhythmic layering, tributary to Nep R, 5°28'S 144°56'E. Allotriomorphic granular; plag (65%), cpx (15%), opx (19%), Fe-Ti oxide (1%). Alteration of px to uralite.
148	48762	Ferronorite-gabbro; mineral-graded layering, N tributary to Nep R, 5°33'S 144°54'E. Allotriomorphic granular; plag (55%), opx (15%), cpx (15%), mag, ilm (15%).
150	48763	Gabbro pegmatoid, intrudes layered norite-gabbro, N tributary to Nep R 150m upstream from 148. Hypidiomorphic granular to eutectic-like intergrowths; plag (70%), opx (10%), cpx (15%), mag, ilm (5%). Extensive alteration of px to hbl.
162	48764	Ol-bearing norite-gabbro; rhythmic layering, Mambu R, 5°31'S 145°02'E. Allotriomorphic granular to poikilitic (opx); ol (8%), plag (45%), cpx (22%), opx (25%). Symplectitic ol-opx-mag.
163	48765	Ferronorite-gabbro; rhythmic and mineral-graded layering, Mambu R, 5°32'S 145°01'E. Allotriomorphic granular; plag, cpx, opx, mag, ilm (up to 15% in oxide-rich layers).
166	48766	Lherzolite; interlayered with ol pyrox, plag lherzolite, S tributary to Wendink R, 5°25'S 144°51'E. Cum. ol, opx; poik cpx & opx, tiny disseminated chr.

167	48767	Plag lherzolite; interlayered with plag lherzolite, plag websterite, S tributary to Wendink R, 5°25'S 144°51'E. Cum ol, opx, cpx; postcum opx (poik) plag; tiny disseminated chr.
168	48768	Plag lherzolite; massive, S tributary to Wendink R, 5°26'S 144°50'E. Cum ol, chr; postcum (poik) opx, plag, cpx.
169	48769	Qtz dolerite; dyke intruding layered gabbro, tributary to Wendink R, 5°25'S 144°51'E. Fg subophitic; plag, cpx, hbl, Fe-Ti oxide; extensive alteration.
174	48770	Ol-bearing norite-gabbro; rhythmic layering, Wendink R, 5°25'S 144°51'E. Allotriomorphic granular; ol (<5%), cpx (20%), opx (15%), plag (60%).
180	48771	Wehrlite; interlayered with dunite, Wendink R, 5°24'S 144°50'E. Hypidiomorphic granular; ol (15%, embayed), cpx (65%), opx (20%).
186	48772	Plag lherzolite; massive, N tributary to Wendink R, 5°26'S 144°52'E. Cum ol, opx, chr; postcum opx, cpx, plag, commonly poik.
189	48773	Lherzolite; massive o/c with prominant oikocrysts (cpx, opx, plag), N tributary to Wendink R, 5°26'S 144°53'E. Cum ol, chr; postcum cpx, opx, plag.
191	48774	Ol norite-gabbro; rhythmic layering of ol and plag, phase contact (plag in) N tributary to Wendink R, 5°26'S 144°53'E. Allotriomorphic granular ol, opx, cpx, plag. Slight serpentinization of ol and some sauss after plag.
198	48775	Ol-bearing norite-gabbro; rhythmic isomodal layering, N tributary to Imbrum R, 5°43'S 145°16'E. Allotriomorphic to hypidiomorphic granular; ol (< 5%), plag (65%), opx (10%), cpx (20%).
203	48776	Plag lherzolite; interlayered with dunite and lherzolite, Kandandau R, 5°22'S 144°53'E. Cum ol, chr; postcum cpx, opx, plag.
207	48777	Wehrlite; interlayered with dunite, Kandandau R, 5°23'S 144°53'E. Cum ol, chr; poik cpx. Extensively altered.

208	48778	Wehrlite; interlayered with dunite and lherzolite, E tributary to Baia R, 5°38'S 145°16'E. Cum ol, chr; postcum cpx. Extensive serpentinization.
209	48779	Wehrlite; 50m upstream from 208, 5°38'S 145°16'E. Cum ol, cpx, cr; postcum cpx.
210	48780	Lherzolite; massive, E tributary to Baia R, 5°39'S 145°16'E. Cum ol, cpx; postcum cpx. Extensively serpentinized.
219	48781	Ol websterite; interlayered with troctolitic norite-gabbro, E tributary to Baia R, 5°40'S 145°15'E.
220	48782	Dunite; interlayered with chromitite, E tributary to Baia R, 5°38'S 145°16'E. As for 221.
221	48783	Chromitite-dunite, fine scale rhythmic layering, as for 220. Xenoblastic, ol (strained anhedra), chr (subhedral interlocking, interstitial of serp and/or kammererite).
225	48784	Ol-bearing norite-gabbro; rhythmic layering, E tributary to Baia R, 5°38'S 145°16'E. Allotriomorphic to hypidiomorphic granular; ol (3.4%), opx (9.6%), cpx (45.8%), plag (41.1%).
227	48785	Ol websterite; interlayered with wehrlite, E tributary to Baia R, 5°39'S 145°16'E. Hypidiomorphic granular; ol (10%), opx (10%), cpx (80%).
238	48786	Lherzolite; interlayered with wehrlite and ol pyroxenite, Okura R, 5°26'S 145°0'E. Cum ol, opx, cpx, chr; postcum opx, cpx.
243	48787	Plag lherzolite; interlayered with dunite and wehrlite, Okura R, 5°27'S 145°0'E. Cum ol, chr, opx, postcum cpx, plag, opx.
249	48788	Websterite; Marum R, 5°34'S 145°07'E. Allotriomorphic granular, cpx (60%), opx (40%), some uralitic alteration.
264	48789	Plag websterite; interlayered with websterite and norite-gabbro, lower Marum R, 5°32'S 145°10'E. Allotriomorphic granular, cpx (45%), opx (40%), plag (15%).

267	48790	Lherzolite; interlayered with wehrlite and pyroxenite, lower Marum R, 5°32'S 145°10'E. Cum ol (35%), opx (25%), cpx(40%), chr (small rounded); postcum cpx.
271	48791	Pl lherzolite; interlayered with pyroxenite, Wendink R, 5°26'S 144°54'E. Cum ol, chr; postcum opx, cpx (poik), plag.
415	48792	Lherzolite; layered river boulder, 5°34'S 145°12'E. Xenoblastic granular; cum ol (70), cpx(10%), opx(20%), chr(subhedral <2%); postcum cpx.
421	48793	Dunite; river boulder, 5°33'S 145°13'E. Xenomorphic granular; ol(2-6mm, deformed), chr (sub to euhedral).
428	48794	Dunite; massive, tributary to Gagiowa R, 5°34'S 145°10'E. Xenomorphic, adcumulate; ol(up to 4mm, deformed), chr(1-2%, disseminated with mineral-graded layering).
431	48795	Gabbro pegmatoid; river boulder, Gagiowa R, 5°34'S 145°11'E. Hypidiomorphic granular; opx, cpx(altered to hbl), plag(extensively altered to sauss), Fe-Ti oxide, qtz. Secondary epidote, actinolite, albite.
441	48796	Pl lherzolite; interlayered with ol norite-gabbro and troctolite, 5°41'S 145°17'E. Xenoblastic, ol (kink bands, deformed, 0.5-5mm), chr (1-2% subhedra, disseminated).
497	48797	Layered chromitite-dunite; small river boulder, Gagiowa R. Rounded, coalesced chr with interstitial ol.
502	48798	Lherzolite; E tributary to Baia R, 5°38'S 145°15'E. Cum ol (extensively altered to serp), cpx, opx; extensive alteration to secondary amphibole.
503	48799	Lherzolite; interlayered with pyroxenite and wehrlite, 5°38'S 145°15'E. Cum ol, opx, cpx, postcum cpx, opx.
504	48800	Cpx-bearing dunite; passes downstream into dunite and upstream into wehrlite, 5°37'S 145°15'E. Cum ol, chr; interstitial postcum cpx.

541	48801	Gabbro pegmatoid; intrudes serpentinite, junction of Gagiowa and Tukange R, 5°37'S 145°10'E. Hypidiomorphic granular; plag (extensively altered to sauss), opx, cpx (extensively altered to hbl, Fe-Ti oxide.
543	48802	Gabbro pegmatoid; river boulder, Gagiowa R, 5°37'S 145°10'E. As for 543 but less altered.
545	48803	Uralitized dolerite; river boulder, upper Gagiowa R, 5°37'S 145°10'E. Granopyric texture; saussuritized plag, uralitized cpx (augite), mag with ilm(111) lamellae.
567	48804	Dunite; river boulder, Gagiowa R. Xenomorphic granular; ol, chr, recrystallized.
571	48805	Dunite; river boulder, Gagiowa R.
576	48806	Microgabbro; river boulder, headwaters of tributary to Mambu R, 5°29'S 144°59'E. Granular to subophitic; plag altered to sauss, cpx, hbl, Fe-Ti oxide, qtz.
578	48807	Granophyric diorite; intrudes norite-gabbro, headwaters of tributary to Mambu R, 5°29'S 144°59'E. Hypidiomorphic granular; plag (zoned), green hbl (poik), opx, qtz.
1020	48808	Norite-gabbro; layered gabbro, Singari R, 5°32'S 145°05'E. Allotriomorphic granular; plag(34.1%), cpx(37.2%), opx(28.8%), rare interstitial CuFeS.
1040	48809	Websterite; interlayered with norite-gabbro, Undago R. 5°30'S 145°03'E. Allotriomorphic granular, opx, cpx, minor plag.
1046	48810	Dunite; chromitite layering, Gagiowa R, 5°35'S 145°12'E. Chr rich layers in dunite.
1104	48811	Plag websterite, interlayered with norite-gabbro, 5°17'S 144°51'E. Allotriomorphic granular; opx, cpx, plag.

Tumu River Basalts

034	48812	Spilite; lava breccia, Tumu R, 5°38'S 144°11'E. Porphyritic to glomerophyric; plag phenos (euhedral, 1-2mm), microphenos of plag and cpx in turbid glassy groundmass.
035	48813	Spilite; pillow lava, Tumu R, 5°39'S 144°11'E. Microphenos of albitized plag and cpx in turbid hemicrystalline groundmass with cpx-plag variolites. Secondary calcite, chlor, hematite.
036	48814	Spilitic pillow basalt; Tumu R, 5°39'S 144°11'E. Plag microphenos (10%) seriate to intergranular groundmass with skeletal Fe-Ti oxide, secondary chlor, calcite.
080	48815	Spilite; clast from lava breccia, Marum R, 5°36'S 145°05'E. Microphenos of plag (albitized) and cpx seriate to groundmass microlites.
081	48816	Spilitic lava breccia; Marum R, 5°36'S 145°05'E. Plag microphenos seriate to intergranular groundmass. Some chlorite, calcite and albite veins.
083	48817	Spilite; clast from lava breccia, Marum R, 5°37'S 145°05'E. Microlites of plag and cpx in altered glassy groundmass. Secondary zeolite, qtz and calcite.
143	48818	Metabasalt; lava flow, Tan R. 5°28'S 144°53'E. Abundant ol phenos (now chlor) in chloritized glass with quench cpx.
434	48819	Spilitic dolerite; tributary to Tumu R, 5°37'S 145°13'E. Subophitic to intergranular textured dolerite, abundant chlor, smectite.
435	48820	Spilitized dolerite; tributary to Tumu R, 5°37'S 145°13'E. Subophitic dolerite.
438	48821	Spilite; tributary to Tumu R, 5°37'S 145°13'E. Intergranular ferrobasalt, abundant smectite.
465	48822	Spilitic high-Al basalt; pillow lava, upper Anagre R, 5°35'S 145°15'E. Glomeroporphyritic; plag phenos (albitized up to 3mm) in altered groundmass of variolitic (quench) plag and cpx.

468	48823	Spilite; river boulder, upper Anagre R, 5°36'S 145°16'E. Intergranular textured ferrobasalt, abundant Fe-Ti oxide.
508	48824	Spilite; lava flow, 5°31'S 144°57'E. Intergranular basalt, with secondary smectite, calcite and pyrite.
521	48825	Metabasite; sheared basalt, Tang R, 5°27'S 144°53'E. Schistose, abundant chlor, epidote, tremolite, albite, accessory sphene, Fe-Ti oxide.
522	48826	Metabasite; as for 521
524	48827	Metabasite; as for 521
539	48828	Spilite; float, Tukange R, 5°37'S 145°11'E. Subophitic, abundant skeletal Fe-Ti oxide, secondary smectite.
540	48829	Spilite; float, Tukange R, 5°37'S 145°11'E. Plag phenos (2mm) seriate to intergranular groundmass with areas of quench crystallization.
549	48830	Metadolerite; Tityilba R, 5°37'S 145°11'E. Fg subophitic dolerite with abundant secondary albite, epidote, chlor, Fe-Mn oxide.
550	48831	Spilite; float, Tityilba R, 5°37'S 145°11'E. Intergranular textured ferrobasalt, Fe-Ti oxide (15%), abundant secondary smectite, albite, epidote.
553	48832	Spilitized dolerite; dyke in Tityilba R, 5°39'S 145°11'E. Subophitic to intergranular texture with abundant granular Fe-Ti oxide, abundant secondary zeolite, smectite, epidote, prehnite, albite.
558	48833	Spilite; Tumu R, 5°40'S 145°13'E. Microphenos of plag, cpx and Fe-Ti oxide seriate to aphanitic intergranular groundmass.
560	48834	Spilite; float Tumu R, 5°39'S 145°12'E. Aphanitic intergranular texture, secondary chlorite and pyrite.
561	48835	Spilitic basalt; Tumu R, 5°39'S 145°12'E. Intergranular textured ferrobasalt, abundant smectite.
562	48836	Spilite; river boulder, Tumu R, 5°39'S 145°12'E. Plag and cpx microphenos, abundant Fe-Ti oxide.

563	48837	Spilitic basalt; float Tumu R, 5°39'S 145°12'E. Microphenos of plag (albitized) seriate to intergranular groundmass.
565	48838	Spilite; float, Tumu R, 5°36'S 145°13'E. Plag and cpx microphenos, abundant Fe-Ti oxide.
566	48839	Spilite; float Tumu R, 5°39'S 145°12'E. Intergranular basalt, secondary smectite, sphene and pyrite.
1007	48840	Metadolerite; dyke in pillow lava, Maula R, 5°17'S 144°50'E. Subophitic to ophitic, albitized plag, secondary chlor and sphene.
1030	48841	Spilitized pillow lava; Mamp R, 5°32'S 144°56'E. Intergranular basalt, variolites of plag and cpx. Secondary chlor, prehnite and calcite.
1053	48842	Qtz dolerite; dyke in lava sequence, Simbai R, 5°23'S 144°47'E.
1057	48843	Metabasalt; massive lava flow, 5°30'S 144°55'E. Variolitic plag (albitized) and cpx in turbid Fe-Ti oxide-charged glass with secondary calcite and zeolite.
		Sediments
512	48844	Argillite; argillite and red cherty micrite intercalated with fragmented lava, Likli R, 5°31'S 144°55'E.
544	48845	Argillite; interbedded argillite and breccia, Gagiowa R, 5°37'S 145°12'E.
526	48846	Picrite; lava flow associated with greywacke, argillite and basalt, 5°27'S 144°50'E. Picrite;xenocrystal olivine, phenos of ol, cpx.
PAPUAN ULTRAMAFIC BELT		
703	46819	Tonalite; o/c Waria R, 8°00'S 147°23'E. Plag and hbl phenos seriate to hypidiomorphic matrix of hbl, plag, qtz, biotite, mag, apatite. Secondary actinolite, biotite, sauss, epidote, chlorite, sphene.
704	46820	Tonalite with mafic clots; river boulder Waria R, 8°00'S 147°23'E. As for 703 but more hbl and more altered; hbl clots altered to actinolite.

705	46821	Tonalite with mafic xenoliths; as for 704. As for 703, strong zoning in plag phenos, relic opx in mafic clot.
706	46822	Basalt; o/c pillow lava; Waria R, 8°01'S 147°29'E. Fg intergranular; plag and cpx microlites, abundant Fe-Ti oxide interstitial qtz mesostasis, secondary qtz, uralite, epidote, chlorite.
707	46823	Basalt; as for 706, but with rare cpx microphenos, qtz-chlorite vesicles and veins.
708	46824	Basalt; as for 706. Vfg as for 706, strongly chloritized, secondary chlorite, qtz.
709	46825	Basalt; river boulder, Waria R, 8°01'S 147°29'E. Fg intergranular to pilotaxitic, with plag laths and sparse cpx microphenos. Fe-oxide abundant, chlorite, uralite, epidote.
710	46826	Basalt; single pillow with chilled margin, river boulder, as for 709. As for 709, but with more extensively chloritized veins of epidote.
711	46827	Basalt; as for 709. Intergranular basalt, cpx microphenos.
712	46828	Basalt; as for 709. Fg intergranular, plag phenos, abundant Fe-oxide, common anhedral chlorite in groundmass.
713	46829	Basalt; as for 709. As for 711.
714	46830	Harzburgite; o/c Chirima R, 8°35'S 147°34'E. Xenoblastic porphyroclastic; augen of opx (17%), matrix of recrystallized ol (70%), and chr (0.8%), 12% serpentine.
715	46831	Harzburgite; boulder Chirima R, 8°35'S 147°34'E. Similar to 714.
716	46832	Harzburgite; as for 715. Xenoblastic, porphyroclastic; augen of opx (13.2%), in matrix of ol (76.6%) and chr (0.6%) with 9.6% serpentine.
717	46833	Enstatolite; as for 715. Similar to 716.

718	46834	Enstatolite; as for 715. Xenoblastic; deformed opx with disseminated chr euhedra and minor ol (5%).
719	46835	Ol pyroxenite; as for 715. Xenoblastic to hypidiomorphic granular cpx and ol, minor chr.
720	46836	Harzburgite; as for 715. Similar to 716.
721	46837	Pyroxenite; as for 715. Hypidiomorphic granular, mainly opx extensively altered to tremolite and talc.
722	46838	Enstatolite; as for 715. Similar to 718 but less deformed, secondary tremolitic amphibole.
723	46839	Hbl granulite; faulted o/c in tributary to Mambare R, 8°04'S 147°39'E. Allotriomorphic granular; ol, opx, cpx, hbl (brown), plag, mag, ilm. Some uralite, sauss.
724	46840	Hbl granulite; as for 723. Similar to 723 but more altered with veins of uralite, sauss and serpentine.
725	46841	Harzburgite; river boulder, tributary to Mambare R, 8°04'S 147°39'E. Similar to 716.
726	46842	Harzburgite; as for 725. Similar to 716.
727	46843	Granular microgabbro; river boulder Opi R, 8°38'S 147°54'E. Fg allotriomorphic granular; plag, cpx (altered in part to hbl).
728	46844	Norite-gabbro; o/c Opi R, 8°38'S 147°54'E. Allotriomorphic granular, weak lineation of plag; plag (45%), opx (20%), cpx (25%).
729	46845	Ol-norite-gabbro; as for 727. Hypidiomorphic; ol anhedra, embayed (10-15%), plag (40%), opx, cpx (extensively altered to uralite).
730	46846	Norite-gabbro; as for 727. Allotriomorphic granular; plag (41.0%), opx (29.7%), cpx (30.3%).
731	46847	Norite-gabbro; as for 727. Similar to 730 but some alteration of px to uralite.
732	46848	Troctolite; as for 727. Hypidiomorphic, ol (embayed, serpentinized 30%), plag (50%), poik cpx, opx (altered to uralite in part).

733	46849	Plag lherzolite; as for 727. Hypidiomorphic; ol (embayed, serpentinized) and plag enclosed in poik opx, cpx, rare chr.
734	46850	Troctolitic-norite-gabbro; as for 727. Similar to 732.
736	46851	Lherzolite; as for 727. Embayed ol; opx, minor cpx, chr. Talc - serpentine alteration.
735	46852	Lherzolite; as for 715. As for 736.

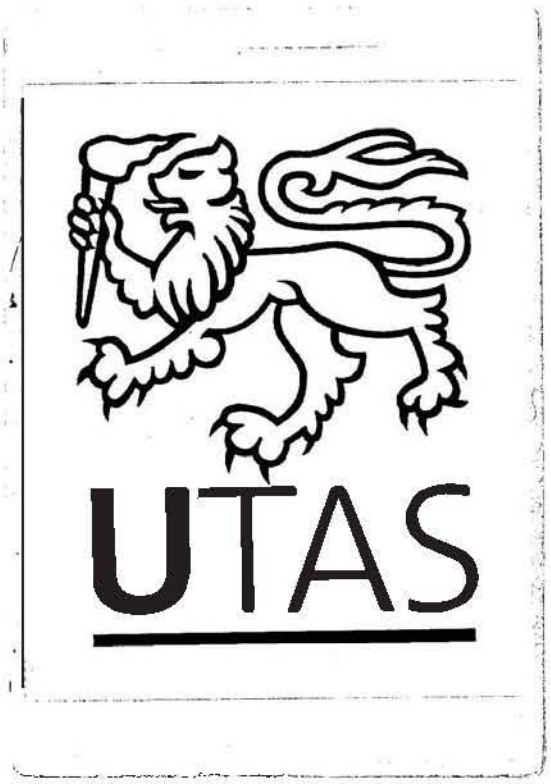

BMR Journal of Australian Geology & Geophysics, 2 (1977) 289-303

The continent/island-arc collision in northern Papua New Guinea

A. L. Jaques and G. P. Robinson*

Recent geological mapping in the north coast ranges of Papua New Guinea has recognised a Paleogene island arc. This arc is believed to have faced southward, and formed at the northeastern boundary of the Indo-Australian plate. The arc collided with continental crust of the Indo-Australian plate to the south; collision is thought to have occurred first in the west in the Early Miocene and to have progressed eastwards. Crustal shortening on collision resulted in foreland-type folding and thrusting at the continental margin, emplacement of ophiolite allochthons from the arc-trench gap at the collision zone, and uplift and fracturing of the accreted arc. Post-collision plate adjustments are thought to include extensive transcurrent faulting about the former plate boundary, southward thrusting of part of the arc (Finisterre-Hnon block), and extensive faulting in a complex linear zone extending from south of Manus Island through New Ireland and the Solomon Islands. Present-day interaction between the Indo-Australian and Pacific plates is spread over a wide zone in which at least two minor plates are involved.

Despite previous claims, plots of the most accurately located earthquake foci define a northward-dipping seismic zone beneath the Late Cainozoic volcanoes at the southern margin of the Bismarck Sea. We find no evidence to substantiate a reversal of arc polarity at any time after the Mid-Tertiary collision. Mid to Late Cainozoic magmatism in central Papua New Guinea appears to have been triggered by uplift inducing partial melting of mantle modified by Cretaceous subduction. The present-day northward-dipping seismic zone is believed to be a vestige of the Early Tertiary subduction zone; the banging slab is now slowly sinking and equilibrating with the mantle. If northern New Guinea can be considered to be the type example of a continent/island-arc collision then reversal of arc polarity may not be a necessary consequence of such collisions.

Introduction

In a recent review of island arcs Coleman (1975a) lists three mechanisms for continent/island-arc collisions: retracking following polarity reversal of a marginal arc complex; rafting of a continent over a subduction zone which dips below an oceanic arc; and encroachment against a fringing arc by a continent over a subduction zone dipping below the continent. According to widely accepted plate tectonic theory a reversal of arc polarity should occur in the first two instances. To date there are few well documented examples of continent/island-arc collisions, probably because it is difficult to recognise facing criteria in former arc-trench systems.

Northern Papua New Guinea is widely cited as a probable example of a continent/island-arc collision. Several previous interpretations of the tectonic evolution of the New Guinea region suggest that a southward-facing Tertiary island-arc collided with the continent to the south in the Mid-Tertiary, and that after collision the direction of subduction reversed to dip southwards beneath the continent and the accreted arc (e.g. Dewey & Bird, 1970; Johnson & Molnar, 1972; Karig, 1972; Hamilton, 1973; Dickinson, 1973). Until recently the geology of the north coast ranges of Papua New Guinea was known only from early reconnaissances. Systematic 1:250 000 scale regional mapping since 1970 of the Adelbert and Finisterre Ranges and the Huon Peninsula region by the Geological Survey of Papua New Guinea (Robinson and others, 1974; Jaques & Robinson, 1975; Robinson, 1976), and of the Bewani and Torricelli Mountains to the west, by BMR (Hutchison, 1975) coupled with isotopic and palaeontologic dating, and regional geophysical surveys (gravity, aeromagnetic, and seismic), now permit a re-examination of earlier interpretations. This paper presents a synthesis of the geology of the Adelbert-Finisterre-Huon region and adjacent northern Bismarck and Schrader Ranges in northeastern mainland Papua New Guinea, and outlines a plate tectonic model for the origin of the region invoking a Mid-Tertiary continent/island-arc collision. Present-day volcanism off the north coast of mainland Papua New Guinea is associated with a steeply northward-dipping (almost vertical) Benioff Zone, and the evidence suggests that, contrary to theoretical predictions and previous interpretations, a reversal of arc polarity has not occurred since collision. The significance of this for continent/island-arc collisions in general is discussed, and an alternative model to explain the Middle to Late Cainozoic magmatism in the Papua New Guinea Highlands and the Late Cainozoic volcanism at the southern margin of the Bismarck Sea is examined.

Regional framework

Essential elements of the regional geology of the newly independent country of Papua New Guinea have been outlined by Thompson & Fisher (1965), Bain (1973), and Dow (1976), and geologic maps at scales of 1:1 000 000 (BMR, 1972) and 1:2 500 000 (D'Addario and others, 1975) have been compiled from standard 1:250 000 scale geologic maps. For simplicity, this paper recognises only three major geotectonic provinces in Papua New Guinea (Fig. 1).

Southwest Papuan Platform

The Southwest Papuan Platform (Brown and others, 1975) consists of sialic crust—Palaeozoic metamorphic and granitic rocks—overlain by Mesozoic and Cainozoic shelf sediments (APC, 1961), and forms a stable basement extension of continental Australia. A northeastern extension of the basement platform underlies Mesozoic miogeosynclinal shale and Tertiary limestone of the Papuan Fold Belt (Bain, 1973)—a zone of detachment tectonics (Jenkins, 1974)—and forms the core of a basement high in the Papua New Guinea Highlands—the Kubor Anticline (Bain and others, 1975). In places the fold belt is blanketed by volcanic rocks from several large Quaternary stratovolcanoes. The

* present address—Department of Geology, University of Tasmania, P.O. Box 252C, Hobart, Tasmania.

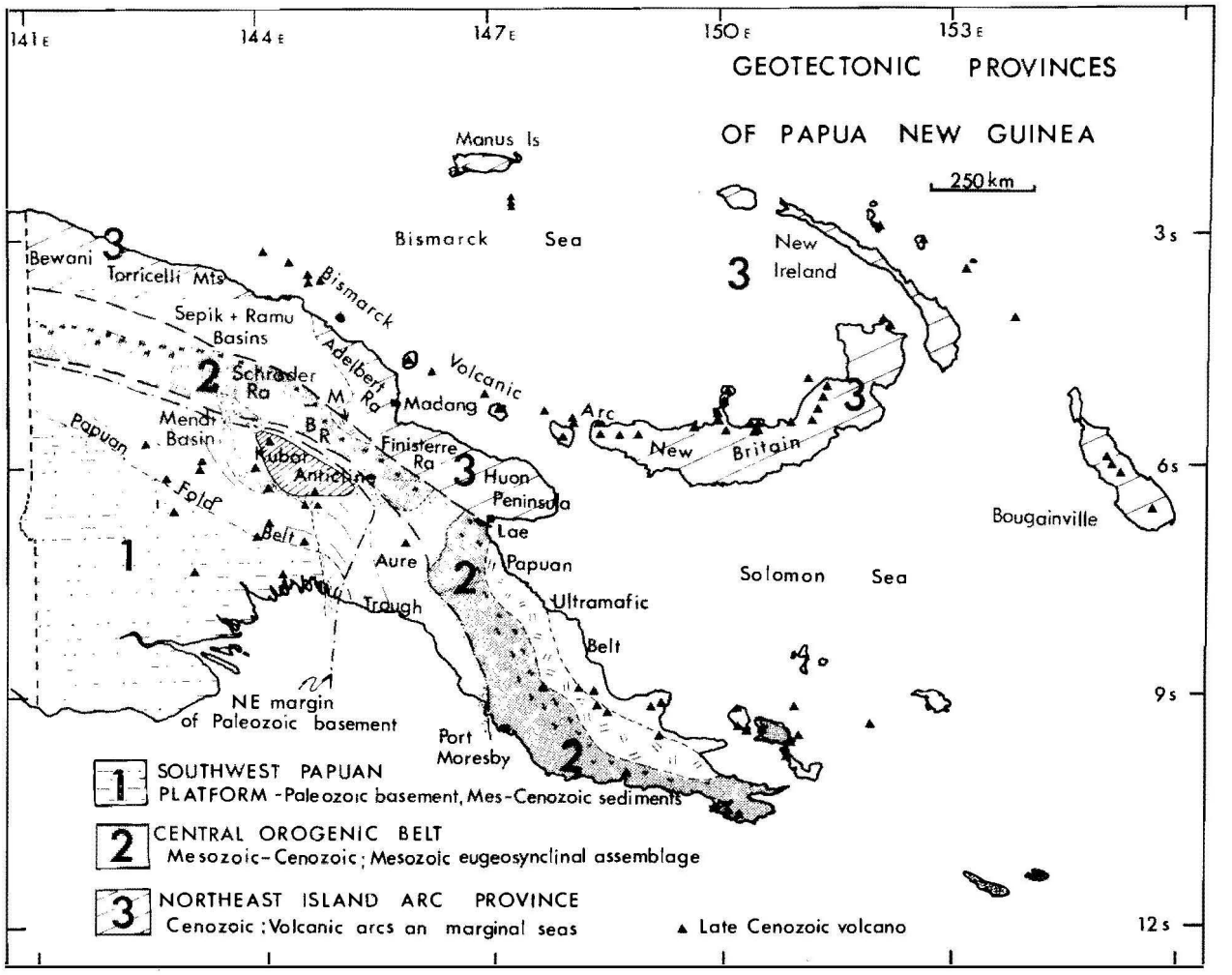

Figure 1. Major geotectonic provinces of Papua New Guinea; adapted after Bain (1973). Marum ophiolite complex; BR = Bismarck Range.

platform is isostatically stable, and has a crustal thickness of 30-35 km (St John, 1970; Jenkins, 1974).

Central Orogenic Belt

The central orogenic belt, or New Guinea Mobile Belt Dow and others, 1972; (Bain, 1973; Bain and others, 1975; Dow, 1976), lies to the north and east of the Southwest Papuan Platform, and extends from the Owen Stanley Ranges of the Papuan Peninsula through the Papua New Guinea Highlands (Fig. 1). This province, of Mesozoic-Cainozoic age, consists mainly of a thick sequence of Mesozoic to early Tertiary geosynclinal sediments and volcanics which have been strongly folded, faulted, and metamorphosed on the outer northern and eastern margin. Ophiolite allochthons form a discontinuous belt along the outer margin, the largest of which, the Papuan Ultramafic Belt, is believed to be a 10-16 km-thick thrust sheet of oceanic crust and mantle emplaced in Eocene-Oligocene times (Davies, 1971). A smaller ophiolite body, the Marum ophiolite complex, some 90 km long, lies on the northern side of the Bismarck Range centred at about 145°E, and is thrust over low-grade metasedimentary rocks of Cretaceous to Eocene age, which form part of a large structural belt affected by foreland-type folding and thrusting with superimposed intense strike-slip faulting. Farther south, approaching the Kubor Anticline, the Late Mesozoic sedimentary succession is continuous (Bain and others, 1975); to the southwest the succession passes into the Mesozoic shelf strata of the South West Papuan Platform.

A number of major Mid to Late Cainozoic, mostly mid-Miocene (Page, 1976), intermediate plutons intrude over the entire length of the central orogenic belt, and some of these have associated gold and copper mineralisation. The Aure Trough and the Mendi Basin are Tertiary geosynclinal basins, which lap over the deformed Mesozoic-Early Tertiary strata from the Southwest Papuan Platform. Late Cainozoic volcanism both in the Highlands and in southeast Papua has constructed large stratocones; some of these have recently been active (Johnson and others, 1973). Crustal thickness beneath the central orogenic belt are comparable to those of the Platform—i.e., 30-35 km (St John, 1970).

Northern Island Arc Province

This province includes the islands of the Bismarck Archipelago, the Bismarck and Solomon Seas, and the north coast ranges. The region is defined by a high level of seismicity and is characterised by active tectonism and volcanism in the Bismarck volcanic arc (Johnson and others, 1971, 1973) at the southern margin of the Bismarck Sea, and in the Bougainville-Solomon Islands chain. The province is made up almost entirely of Cainozoic rocks. The larger islands of the Bismarck Archipelago (i.e., New Britain, New Ireland) and the north coast ranges, consist predominantly of Tertiary volcanic and sedimentary rocks, and are believed to have originated as Tertiary island arcs (Thompson & Fisher, 1965; Bain, 1973; Dow, 1976; D'Addario and others, 1976). The Bewani and Torricelli

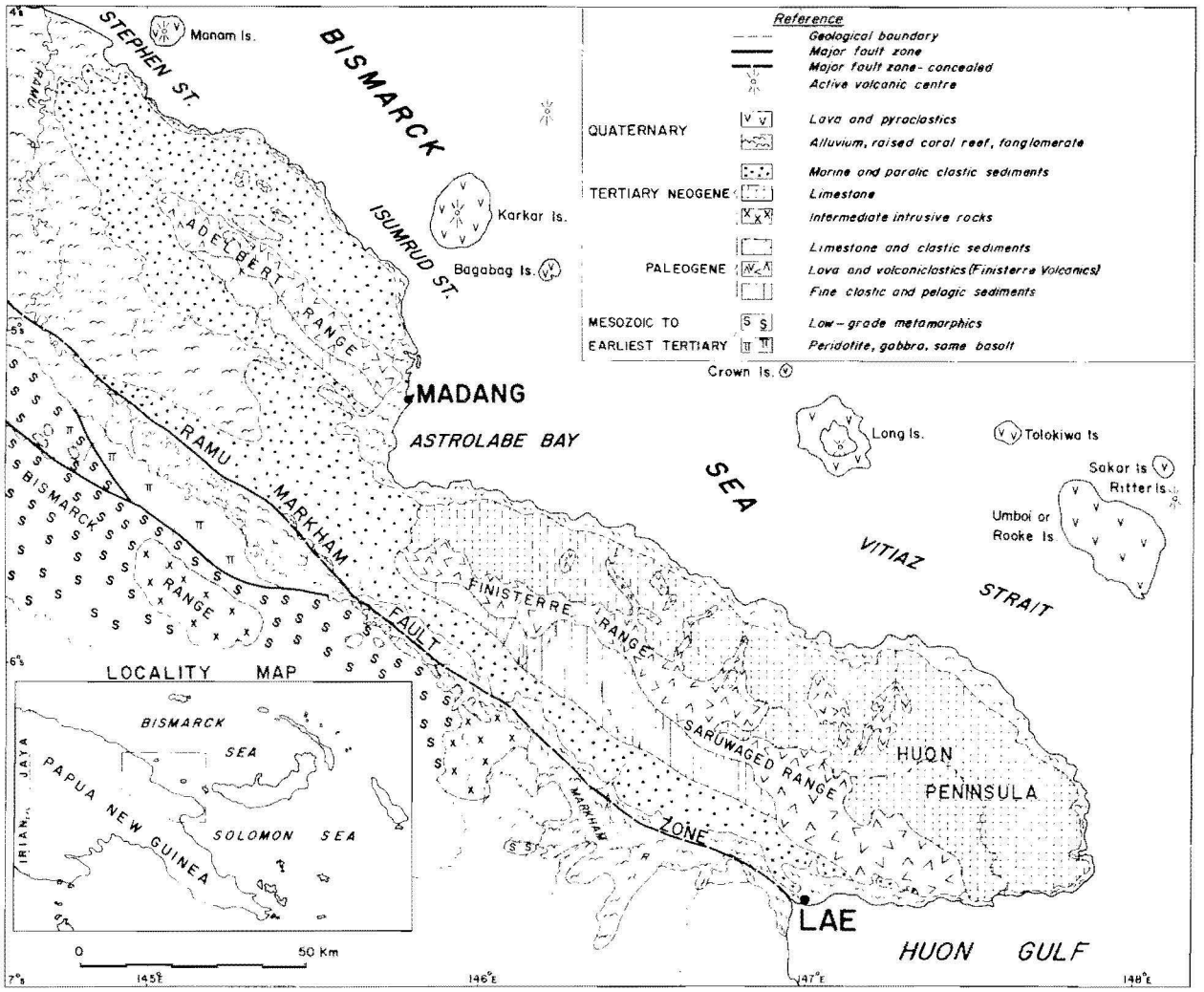

Figure 2. Simplified geology of the Adelbert-Finisterre Range-Huon Peninsnla region, northern Papua New Guinea. Geology adapted after BMR (1972), Robinson and others (1974), and Jaques & Robinson (1975), Robinson (1976).

Mountains to the west also include Cretaceous volcanic rocks; strike-slip faulting is intense (Hutchison, 1975). The Bismarck Sea is considered to be an active Tertiary marginal basin, with sea floor spreading taking place in the east-west seismic zone that crosses the basin (Connelly 1974, 1976). The crust thins rapidly northward from continental-type thicknesses (30-35 km) beneath the north coast ranges (Brooks, 1969; St John, 1970) and New Britain (Finlayson & Cull, 1973) to about 18-20 km under the Bismarck Sea (Connelly, 1976).

Geology of collision area

The region discussed (Fig. 2) involves the north coast ranges (Adelbert, Finisterre Ranges, Huon Peninsula) of the northeast island arc province, and the Bismarck and Schrader Ranges of the central orogenic belt to the south. The simplified geology is shown in Figure 2, and Table 1.

The two provinces are separated by the elongate, alluviated, graben-like Ramu-Markham Valley (Figs. 2, 3) which coincides with a major fault system, the Ramu-Markham Fault Zone. This fault zone is believed to extend some 300 km in a northwest-southeasterly direction. The nature of faulting along the zone has not been determined precisely, but considerable horizontal as well as vertical movements seem likely. Faulting, in particular strike-slip faulting, is not confined to the Ramu-Markham Fault Zone,

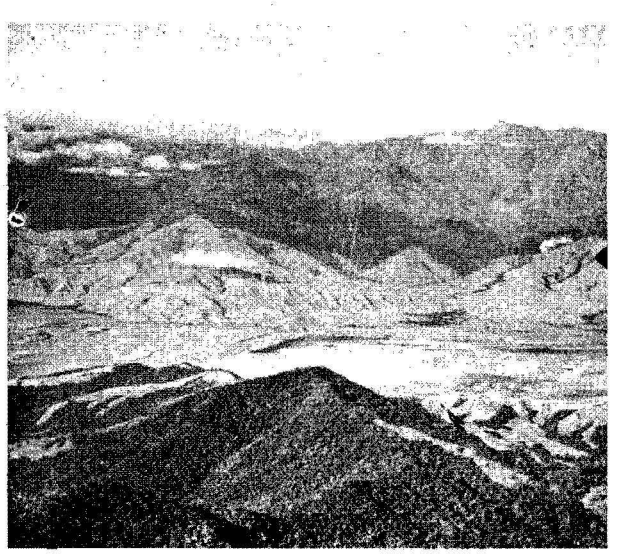

Figure 3. Photograph taken looking south toward the alluviated Ramu-Markham valley. The valley extends some 350 km, and is from about 5-25 km wide. The valley floor is of less than 500 m elevation, and contrasts with the mountains both north and south. The valley coincides with the Ramu-Markham Fault Zone, which is believed to be a major fault with considerable transcurrent displacement.

but is common both in the north coast ranges and in the Bismarck and Schrader Ranges. The predominant trend in all cases is northwest.

Adelbert-Finisterre-Huon region

The extremely rugged, mountainous (up to 4100 m) Adelbert and Finisterre Ranges trend northwestward, and comprise Cainozoic sedimentary and volcanic rocks exposed in a series of northwest-trending fault blocks which dip northeastward. Faults bounding the tilted blocks are predominantly high-angle normal faults downthrown to the south (Figs. 4, 5). The fault blocks are cut by numerous strike-slip faults, and, on the northern slopes of the Finisterre Range-Huon Peninsula, by normal faults (Fig. 5); all faults trend northwestward. Superimposed on these is a series of composite fractures, whose areal distribution suggests that most may have formed initially as shears but took on a tensional character during uplift. Aeromagnetic surveys (Continental Oil Co. Aust., 1969) have defined a number of northeasterly trending basement faults normal to the dominant structural trend. The Adelbert and Finisterre Ranges are offset along such a trend, suggesting dextral transcurrent faulting along a line trending southwest from Madang. A pronounced northeast-southwest submarine excarpment lying off Madang in Astrolabe Bay may be the offshore extension of this inferred fault. The age of the offset is not known, but probably pre-dates the late Neogene as there is no evidence of meridional faulting in the latest Neogene strata south of Madang; nor are the volcanoes of the Bismarck volcanic arc offset.

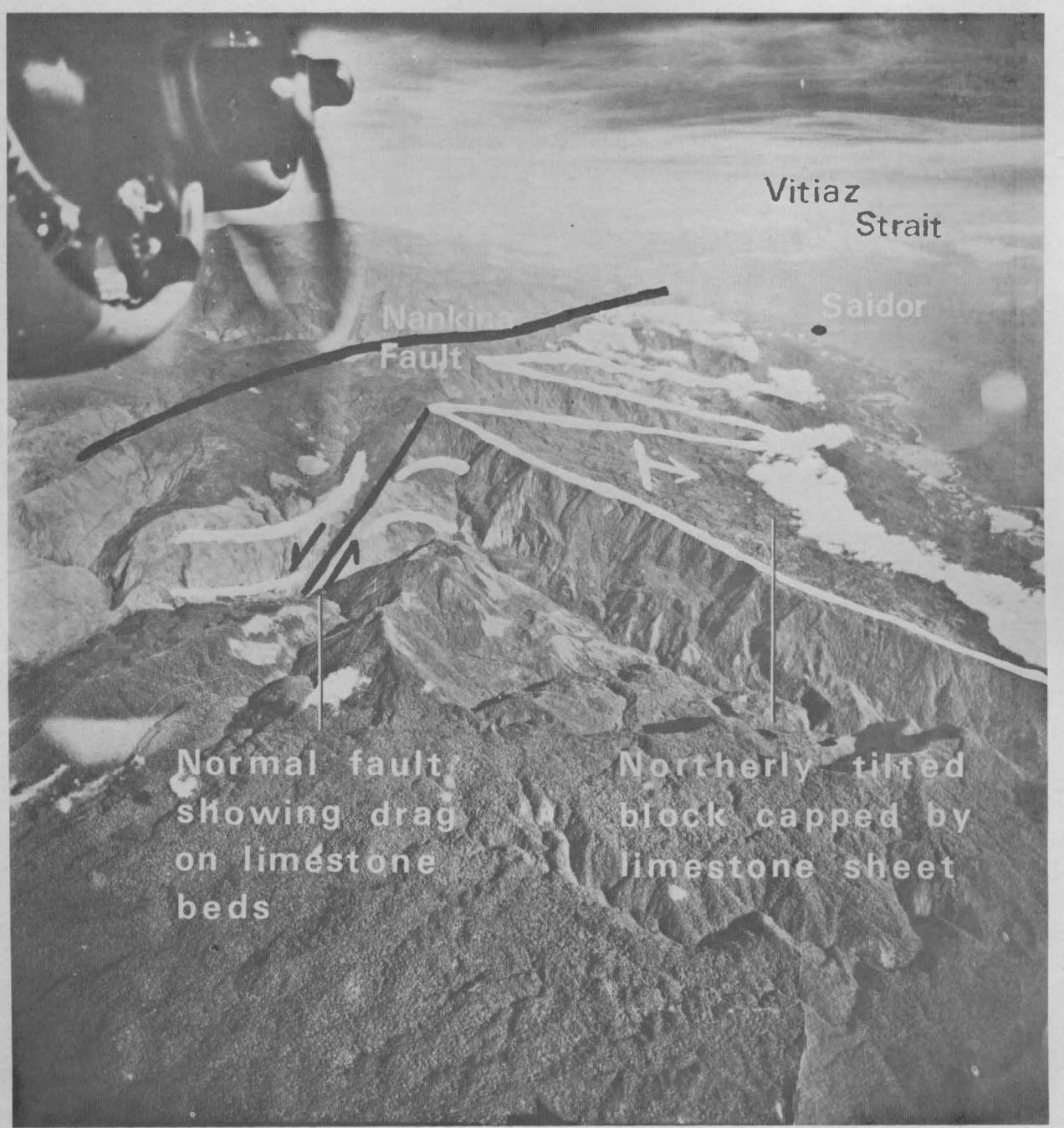

Figure 4. Oblique aerial photograph showing northeastward-tilted block of Miocene limestone. Note downthrown block to south with drag folding of limestone. Photograph taken looking west along the central Finisterre Range (about 145° 40′ E) from 8000 m. Limestone sheet is about 1 km thick.

The oldest rocks exposed in the Adelbert-Finisterre-Huon region, with the possible exception of some bodies of tectonised peridotite (see later), are highly sheared Eocene hemipelagic and pelagic sediments, dominantly cherty argillite, which are exposed on the southern flanks of the Adelbert and Finisterre Ranges. The argillite is overlain by dominantly Oligocene (late Eocene to early Miocene) basalt, and low silica-andesite lava and volcaniclastic rocks (Finisterre Volcanics), which form the central peaks of the ranges. The Finisterre Volcanics are unconformably overlain by thick sequences of Neogene (Miocene-Pliocene) limestone and clastic sediments. The limestone forms a prominent northward-dipping sheet on the northern slopes of the Finisterre Range and Huon Peninsula (Figs. 4, 5); only discontinuous remnants occur in the Adelbert Range. Raised Quaternary coral reefs fringe much of the north coast, particularly the Huon Peninsula where a spectacular flight of reef occurs (Chappell, 1974; Robinson, 1976). The Neogene clastic sediments form thick wedges flanking the Eocene argillite and Oligocene volcanics from which they are derived (with extensive reworking) in the Adelbert and western and southern Finisterre Range (Fig. 2). Greatest thicknesses occur in an elongate, northwest-trending structural basin (Ramu Basin) south and southwest of the Adelbert Range, where they are mostly covered by Pleistocene sediments and Quaternary alluvium. At the

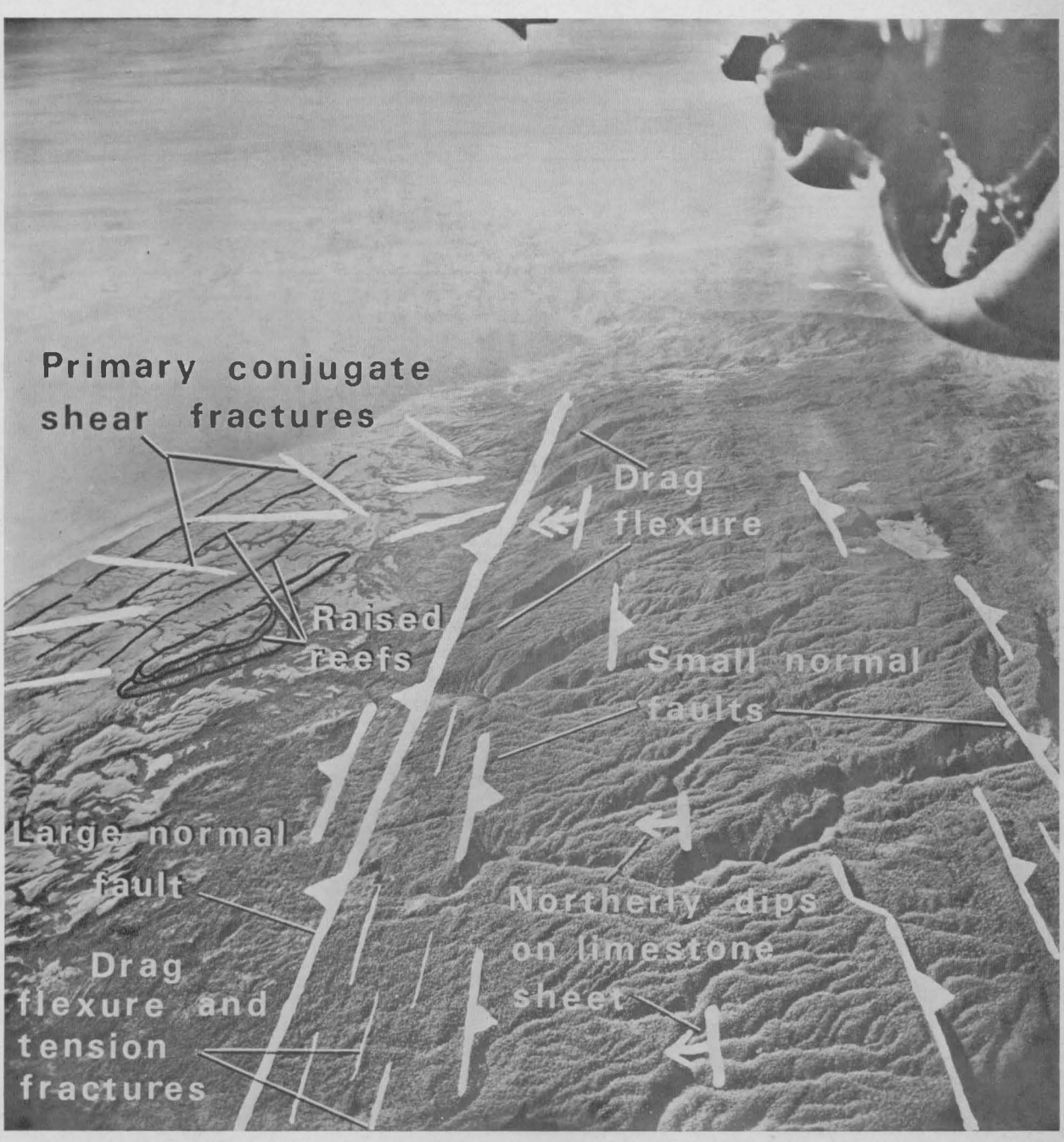

Figure 5. **Oblique aerial photograph of northeastward-dipping Miocene-Pliocene limestone sheet in the Huon Peninsula, showing northward-tilted fault blocks downthrown to the south. Note the drag flexure with tension fractures of the limestone by the large normal fault at the front (north) of the sheet. Raised Quaternary coral terraces, up to 600 m high, north of the fault have been described by Chapell (1974); elements of a Holocene fracture set are evident. Note also the large bottlenecked valleys at the front of the limestone sheet cut by consequent rivers and streams. Photograph taken looking east along Huon Peninsula at about 147° 30′ E, from 8000 m.**

northern margin of the Ramu Basin the clastic sequence rests unconformably on Eocene argillite. Further south aeromagnetic and gravity patterns (St John, 1970) suggest a floor of dense, basic rocks. Results of a more recent gravity survey (Milsom, 1975), and the occurrence of Jurassic gabbro-peridotite basement unconformably overlain by Neogene (early-middle Miocene and younger) sediments at a depth of 2000 m in Keram No. 1 wildcat well (Harrison, 1974) drilled in the Ramu Basin southwest of the Adelbert Range (at 4° 26′ S, 144° 09′ E), have been interpreted as indicating a floor of oceanic crust in the southern part of the basin (Jaques & Robinson, 1975).

Ophiolite belt

The Marum ophiolite complex lies immediately south of the alluvium-covered Ramu Basin, and is bounded by major faults to the north and south. The complex consists of two major thrust sheets: a radiolarite-pillow basalt-spilite (with some diabase) allochthon lies to the south of and beneath a larger sheet of peridotite, pyroxenite, and layered norite-gabbro. At the base of the larger sheet harzburgite, with some dunite, is overlain by a thick sequence of cumulus peridotite, pyroxenite and layered norite, gabbro and anorthositic gabbro.

Pelagic sediments, including radiolarites of probable Eocene age, overlie and are intercalated with pillow basalts of the other major thrust sheet, and pass upwards into a sequence of argillite, radiolarite, tuffaceous argillite and graywacke, and tuff. The upper part of this sequence is intruded by pyroxene and hornblende-phyric basalt and basaltic andesite of island-arc affinities.

Windows exposed in several river sections show an imbricate zone of low-grade metamorphic rocks at the base of the harzburgite, with thrust surfaces dipping northeastward at a shallow angle. The dip of the thrusts and the northeastward-dip of igneous layering in many of the cumulate rocks suggests emplacement from the northeast as a series of shallow-dipping thrusts. In addition, the northeasterly displacement of the regional gravity high associated with the ophiolite complex toward the Ramu valley suggests thickening of dense basic rocks beneath the Ramu valley (Milsom, 1975), consistent with this interpretation.

Emplacement of the ophiolite complex clearly postdates the (?)Early Eocene as it is thrust over low-grade metamorphosed sediments of Late Cretaceous to Eocene age. An upper limit of middle Miocene is suggested by the unconformable relationship between the gabbro-peridotite basement (interpreted as oceanic crust) and Neogene strata in the Keram well. Farther west in the south Sepik region there is stratigraphic evidence that ophiolite bodies occupying a similar tectonic and stratigraphic setting were emplaced in post-Eocene and pre-middle Miocene times (Dow and others, 1972).

Small faulted bodies of peridotite (commonly serpentinite), pyroxenite, and gabbro (dismembered ophiolites) occur as klippen on, and thrust slices in, low-grade metamorphic rocks farther west (144° E) in the Schrader Range. Small bodies of harzburgite, dunite, and serpentinite of unknown age have also been recorded from the Huon Peninsula (Robinson, 1976) where they crop out amongst the Finisterre Volcanics; relationships are uncertain.

Metamorphic belt

The metamorphic rocks of the northern Bismarck Ranges, and Schrader Range immediately west, are mostly low-grade metamorphosed pelites. Quartz-veined slate, phyllite, and graphite and mica schist crop out east of the ophiolite belt, and grade laterally into, and in many cases are faulted against, fossiliferous flysch, mostly dark coloured shale and siltstone, but with some sandstone, conglomerate and limestone of late Cretaceous to Eocene age (Bain, 1967; Dow & Dekker, 1964; Jaques & Robinson, 1975; Dow and others, 1972; A. L. Jaques and C. J. Pigram, unpublished data). The metapelites contain abundant quartzo-feldspathic and metamorphic detritus (e.g., quartzite, quartz-mica schist) derived from pre-Mesozoic granitic and metamorphic rocks (i.e., the continental basement) and reworked basement-derived sediments. In addition many contain abundant volcanic detritus, some of which is tuffaceous, indicating contemporaneous volcanism (Thompson, 1967; Harrison, 1969; Dow, 1976). The flysch sequence is interpreted as continental slope and continental rise deposits formed at the margin of the continental mass (platform) to the south.

The degree of deformation and grade of metamorphism, mostly lower greenschist, decrease to the south toward the platform. At least two, and in places three (C. J. Pigram, pers. comm., 1976), phases of deformation are apparent (McMillan & Malone, 1960; Robinson and others, 1974). Early formed folds are commonly overturned to the southwest and asymmetric (many are isoclinal), and cleavage is commonly parallel to bedding; fold axes trend northwest. Second-generation folds are of a smaller scale and more open.

Thrusting occurs over a wide zone at the northern margin of the orogenic belt. Allochthonous strata, bounded in places by curvilinear thrusts dipping northeastward, pass southwestwards towards the Kubor area into thick successions of autochthonous coherent strata of uniform age and lithology. Farther south the autochthonous strata pass into a thick continuous Mesozoic succession at the margin of the platform.

Stratigraphic and structural relations indicate a post-mid Eocene and pre-mid Miocene metamorphic event; this age is consistent with that obtained from stratigraphic relations and isotopic dating for metamorphism of similar rocks farther west in the south Sepik area (see later). There is also some stratigraphic evidence in the Bismarck Range to suggest an earlier (Cretaceous?) metamorphic event McMillan & Malone, 1960; (Robinson and others, 1974; C. J. Pigram, pers. comm., 1976).

Interpretation

The close stratigraphic and structural similarities between the Adelbert-Finisterre-Huon region, and New Britain and the other islands of the Outer Melanesian Arc provide compelling evidence that the north coast ranges originated as a Tertiary island arc, and have since become attached to the continental mass to the south (Thompson & Fisher, 1965; Robinson, 1973; Bain, 1973; Dow, 1976). South of the island arc (Adelbert-Finisterre-Huon arc) the ophiolite belt and outer margin of the central orogenic belt, with the zone of metamorphism and foreland-type thrusting, mark the zone of collision. Figure 6 shows the morphologic and structural relations of these tectonic elements.

Adelbert-Finisterre-Huon Arc

The Adelbert-Finisterre-Huon arc comprises pre-volcanic, volcanic, and post-volcanic assemblages.

Pre-volcanic argillite. The Eocene argillite is believed to have been deposited on the sea floor, and to grade laterally southwards into the Late Cretaceous-Eocene metapelites (Robinson and others, 1974); similar pelagic-hemipelagic sediments overlie the metabasalts of the

Marum ophiolite complex. Sediments low in the argillite sequence are derived from continental basement and predate volcanism in the arc. Argillites higher in the sequence are tuffaceous, and grade into the volcanic and volcaniclastic rocks of the Finisterre Volcanics; the upper part of the argillite is synvolcanic.

Volcanic arc. The abundant, diverse volcaniclastic rocks of the Finisterre Volcanics are lithologically similar to coeval volcanic sequences on New Britain and the other Tertiary island arcs of outer Melanesia. The absence of continent-derived material from the thick volcaniclastic-volcanic pile, and occurrence of pillow lava and radiolarian chert and argillite at the base of the formation, imply that the volcanic arc was oceanic. Lateral transitions from lava to lava breccia to volcanic paraconglomerate to conglomerate to turbidite have been observed in places, and this, together with the abundance of epiclastic rocks, indicates development of extensive clastic aprons about a chain of emergent and near-emergent volcanic centres.

Volcanism in the arc ceased in the Early Miocene, although inter-tonguing relationships between basalt flows and Miocene limestone in the Huon Peninsula (Robinson, 1976) suggest that volcanism may have continued slightly longer in that area. The early Miocene cessation of volcanism coincides with the timing of metamorphism in the outer portion of the orogenic belt, the emplacement of ophiolites and correspondingly the continent/island arc collision (see later).

Post-volcanic-arc assemblages. The contrasting post-volcanic depositional regimes of the western and eastern part of the arc indicate that tectonic events were not synchronous along the arc. In the west the volcanics and argillite were uplifted immediately after cessation of volcanism, and yielded the thick clastic wedge. This uplift coincided with the timing of the orogenesis south of the arc, and we interpret uplift of the western part of the arc to be the direct result of collision of that segment of the arc with the continental mass. Uplift, we suggest, may be the isostatic reaction to underthrusting, or attempted underthrusting of sialic material.

Limestone was deposited in the eastern part of the arc in the northern Finisterre Range-Huon Peninsula region, which was not uplifted until the Pliocene. Uplift since then has been rapid: some 3000 m of uplift has occurred since the late Pliocene. The raised Quaternary coral-reef terraces of northeast Huon Peninsula indicate rapid present-day uplift (Chappell, 1974). We interpret the younger uplift of the eastern part of the Adelbert-Finisterre-Huon arc as indicating a slightly younger collision of that segment of the arc.

Collision zone

Blueschist terrains and ophiolite belts are widely held to mark former convergent plate boundaries. Although ophiolites are conspicuous, melanges containing high-pressure mineral assemblages have not been reported from the Bismarck Range (rare pumpellyite has been found in some metabasites). The outer margin of the central orogenic belt is generally regarded as the zone of interaction between opposing crustal plates (e.g., Thompson & Fisher, 1965; Bain, 1973; Dow, 1976). The foreland-type of folding and thrusting, the nature of the metasediments—i.e., continental slope and rise type, and the lateral transition from deformed allochthonous to undeformed autochthonous successions toward the continental platform in the southwest, provide compelling evidence that the outer margin of the central orogenic belt marks the site of a collision

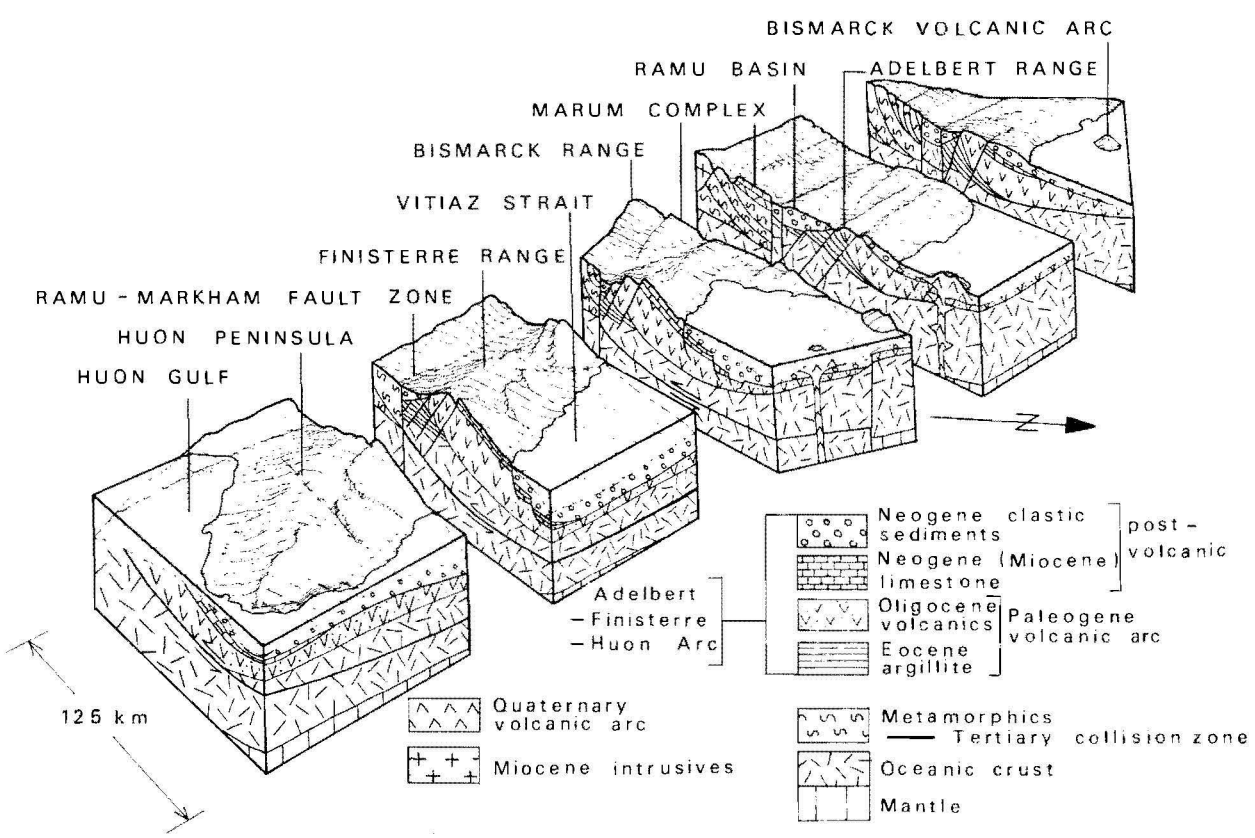

Figure 6. Block diagram showing structure and petrotectonic assemblages of the Adelbert-Finisterre-Huon arc to the north, and the collision zone to the south. Vertical exaggeration is about 2.5 times.

between the continent and its welt of marginal sediments to the south, and the island arc to the north.

High-pressure metamorphic rocks associated with ophiolites have been mapped farther west in the south Sepik region (142-144° E), where lawsonite and glaucophane-bearing rocks, amphibolite, and, locally, eclogite, form a melange within low-grade metamorphic rocks similar to those of the Bismarck and Schrader Ranges (Ryburn, 1976; Dow and others, 1972). Isotopic dating (Page, 1976), and structural relations (Dow, 1972), indicate a late Oligocene-early Miocene age of metamorphism. Immediately north of the blueschist belt lies another metamorphic belt of similar age characterised by low to moderate pressure, and higher temperature mineral assemblages. Ryburn (1976) has interpreted the two belts as constituting a paired metamorphic belt associated with a northward-dipping Early Tertiary subduction zone.

The similar tectonic setting and close stratigraphic similarities between the south Sepik region and the Bismarck and Schrader Ranges lead us to infer that the former subduction zone associated with the Palaeogene Adelbert-Finisterre-Huon arc was choked by the wedge of sediments at the continental margin, resulting in collision between the continent and the island arc. Rocks of the trench melange, including metamorphic rocks with high-pressure mineral assemblages, may lie beneath the northern edge of the Bismarck and Schrader Ranges, the Ramu-Markham valley, and possibly beneath the ophiolite slabs forming the floor of the southern part of the Ramu Basin. The Marum ophiolite complex represents a segment of oceanic crust and mantle from the arc-trench gap region of the upper plate thrust over the choked subduction zone as a consequence of the collision.

Plate tectonic reconstruction

Late Mesozoic—Early Tertiary

Late Mesozoic-Early Tertiary plate configurations and tectonic events are not well understood at this stage, but several important events seem clear. Cretaceous (early Cretaceous?) andesites in the northern central orogenic belt probably formed in a volcanic arc at the northern margin of the continental crustal platform, most likely as a result of southwestward subduction beneath the continent, as suggested by Johnson and others (1977). Formation of oceanic crust of the ophiolite belt appears to be caused by a period of Late Mesozoic-Early Tertiary sea-floor spreading or marginal basin formation peripheral to the volcanic arc and the continent. Extensive deposition of fine clastic sediments (dominantly marine shale) occurred on an extensive continental shelf, slope and rise in the Late Cretaceous to Eocene. These continental margin sediments are thought to have graded into the deeper water, more distal Eocene argillites and cherty micrites. This sequence of events implies that the northern (northeastern) edge of the continent changed from a convergent type in the Early Cretaceous to a divergent or Atlantic-type in the Late Cretaceous-Eocene.

Separation of Australia and Antarctica about 50-55 m.y. ago (Weissel & Hayes, 1971) is thought to have initiated northward movement of the Australian continent, and resulted in rifting and opening of the Coral Sea (Mutter, 1975), eruption of voluminous Eocene tholeiitic submarine basalts in southeast Papua (Davies & Smith, 1971; Milsom & Smith, 1975), and emplacement of the Papuan Ultramafic Belt (Davies, 1971). Tectonic syntheses of these events are provided by Davies & Smith (1971), and Pieters (1974).

Oligocene (Fig. 7)

Farther north and east, removed from the continental margin, plate convergence resulted in the formation of an extended arc-trench system with a northward to northeastward-dipping subduction zone in which oceanic crust at the leading edge of the continent was consumed—i.e., a southward-facing island-arc. Subduction-related volcanism commencing in the late Eocene, and continuing throughout the Oligocene and early Miocene, produced a chain of volcanic centres with extensive clastic aprons. As volcanism waned, fringing reef developed about near-emergent centres in the early Miocene. Early formed trends in the western part of the Bismarck Sea marginal basin parallel the north coast ranges (Connelly, 1976), and are probably of Tertiary, possibly Oligocene (Tilbury, 1975) age. We speculate that basin formation began in the Early Tertiary by a form of back-arc spreading related to mantle upwelling above the northward-dipping Paleogene subduction zone.

Miocene

Continued plate convergence in the early Miocene brought the continent (with its wedge of sediments at the margin) to the subduction zone where the buoyancy of the continental crust arrested subduction, resulting in the collision of the western segment of the Adelbert-Finisterre-Huon arc with the continental margin; volcanism in the arc ceased. The stresses of continued plate convergence were taken up by crustal shortening, in particular by 1) deformation and thrusting at the continental margin; 2) thrusting of oceanic crust from the arc-trench gap over the subduction zone and continental margin; and 3) arching, fracturing, and uplift of the western part of the arc. Examination of fractures in the Huon Peninsula has defined a major set of early fractures which are interpreted as forming a first order conjugate shear system, whose northerly trending acute bisectrix may be interpreted as being the direction of primary stress resulting from the collision (Robinson, 1973). An additional response to continued plate interaction was the formation of numerous northwesterly trending transcurrent faults at and near the former plate boundary. The Ramu-Markham Fault Zone, for example, is believed to be a post-collision transcurrent fault approximating the former plate boundary. Adjustments elsewhere along the plate boundary may also have accommodated plate convergence.

Thick limestone sheets were deposited as broad tabular platform reefs on submarine stepped blocks in the eastern part of the arc, suggesting that collision had not yet occurred in that segment of the arc. This implies that collision involved rotational closure by subduction of sea-floor between the continent and arc, and that after collision in the west a section of sea-floor existed between the eastern end of the arc and the continent. The inferred configuration (Fig. 7) may have been similar to the present-day distribution of the Solomon Sea between New Britain and mainland Papua New Guinea. Southward thrusting of the Finisterre-Huon block, probably along shallow-dipping thrusts as proposed by St John (1970), and Milsom (1975), on the basis of the regional gravity pattern, took place in the Late Miocene or Pliocene.

The collision, and cessation of volcanism in the arc in the Early Miocene, coincides with a short-lived but widespread period of calc-alkalic to alkalic plutonism and volcanism along the axis of New Guinea in the Middle Miocene (Page & McDougall, 1970; Page, 1976). Many of these rocks are a similar composition to island-arc rocks, suggesting that underthrust hydrated lithosphere was important in their

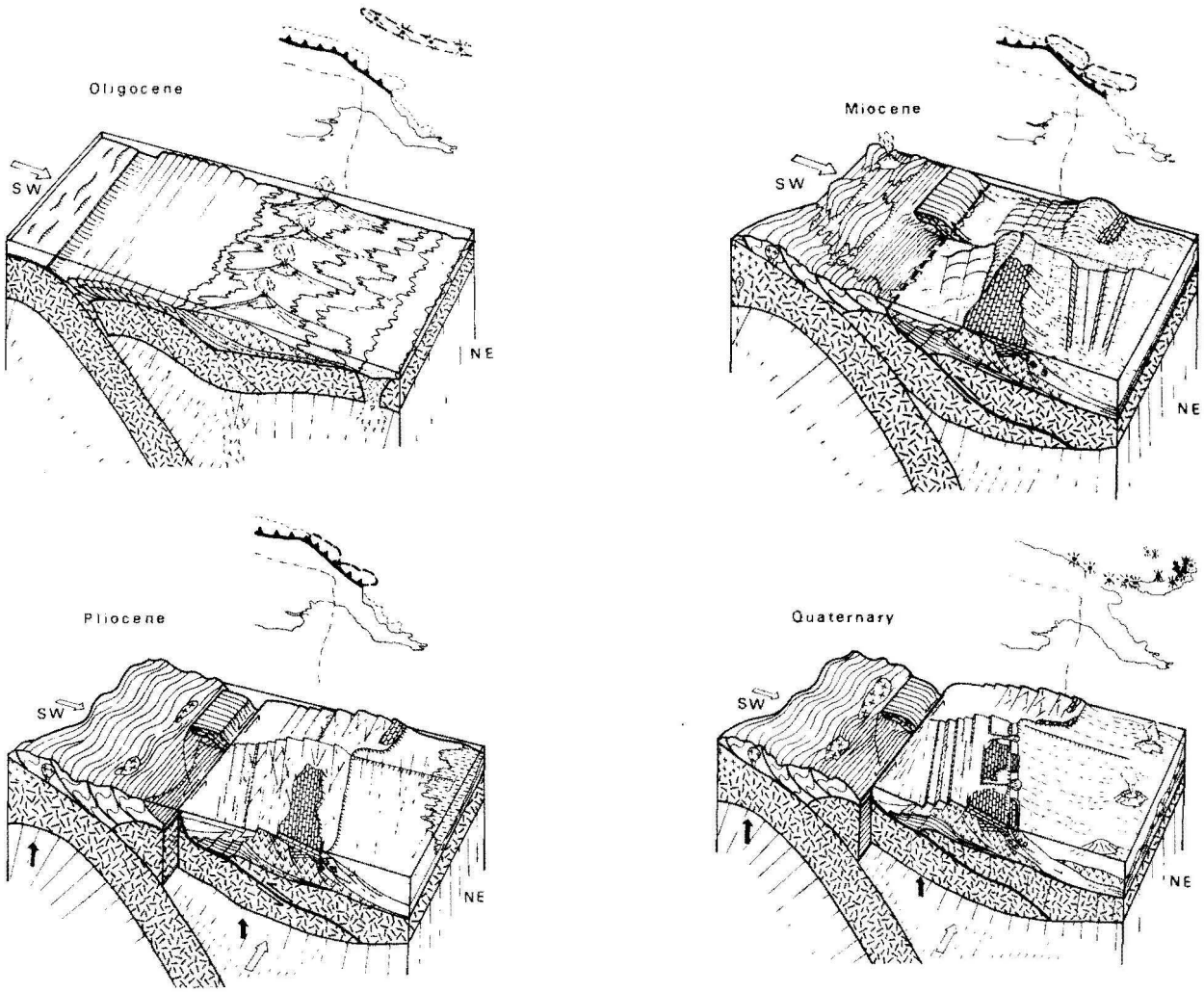

Figure 7. **Block diagrams illustrating conceptual Tertiary evolution of the Adelbert-Finisterre-Huon region as an island arc, followed by collision with the continental margin in the early Miocene. Vertical exaggeration is about 2.5 times. Crustal thickness (see text) is based largely on estimates by St John (1970), and is about 35 km beneath the central orogenic belt and the north coast ranges, and 18-20 km beneath the Bismarck Sea.**

TABLE 1. SUMMARY OF STRATIGRAPHY OF ADELBERT-FINISTERRE-HUON REGION

Unit	*Lithology*	*Remarks*
Neogene clastic sediments	Calcareous, lithic sandstone, siltstone, mudstone; some limestone and conglomerate. Lignite common.	Uncomformable on Eocene argillite, Finisterre Volcanics. Dated by planktonic foraminifera as Mid-Miocene to Latest Pliocene-Pleistocene. Extensive in Adelbert Range. Greatest thickness in Ramu Basin where 4-5000m deposited in elongate troughs between tectonically active basement ridges. Regressive and transgressive sequences, onlapping and foresetting of beds, diachronous beds, deltaic deposits. Marine and paralic sediments.
Neogene limestone	Massive algal-foraminiferal biomicrite and biocalcirudite; well-bedded calcarenite, calcilutite and calcareous mudstone.	Unconformable on argillite and Finisterre Volcanics. Dated as Early-Middle Miocene to Late Pliocene. Form northerly-dipping 1000m-thick resistant sheets in northern flank of Finisterre Range-Huon Peninsula. Only discontinuous sheet remnants in Adelbert Range. Miocene algal-foraminiferal biomicrite represents reef complexes formed as broad tabular platforms on submarine faulted step blocks (Robinson, 1973, 1976). Coarse biocalcirudites (reef talus deposits) surround platform reef complexes, pass into bedded biomicrite, calcarenite and calcilutite.
Oligocene(late Eocene-early Miocene) volcanics (Finisterre Volcanics)	Basalt and basaltic andesite lava breccia, lava, and volcaniclastic rocks, including tuffaceous lithic greywacke, tuff, peperite and peperitic breccia, palagonitic breccia, pillow lava, agglomerate, volcanic conglomerate. Argillite at base, limestone lenses at top.	Gradational contact with underlying Eocene argillite. About 4500m thick. K-Ar dates 34-22 m.y. (Jaques, 1976). Limestone lenses at top of Early Miocene age. Mostly dip steeply north. Strongly indurated; minor zeolite facies metamorphism. Pillow lava at base. Lava subordinate to variety of volcaniclastic rocks—autoclastic, pyroclastic and epiclastic rocks. Lavas of high-K calc-alkalic and shoshonitic affinities.
Eocene argillite	Indurated, strongly jointed, veined cherty argillite, chert, siltstone, tuffaceous lithic greywacke, cherty micrite.	Base not exposed. Dated as Mid to Late Eocene in part. Gradational contact with overlying Finisterre Volcanics. Strongly indurated, veined, sheared. Mostly dips northwards. Unknown thickness. Extensive zeolite facies metamorphism. Sediments lower in sequence derived from continent crust—quartzo-feldspathic detritus common. Upper part of sequence contains abundant volcanic detritus.

derivation from the upper mantle. Although some underthrusting may have taken place at the northern edge of the continent at or immediately after collision in the early Miocene, there is no geological evidence to indicate that an extensive southwestward-dipping subduction zone existed at that time, either north or south of the Adelbert-Finisterre-Huon arc. The present-day northward-dipping seismic zone beneath Vitiaz Strait defined by earthquake foci (see later; Figs. 8, 9) is believed to be a vestige of the northward-dipping Palaeogene arc-trench system (Johnson, 1976, 1977; Johnson & Jaques, 1977). In the absence of geological evidence to support a southwestward-dipping subduction zone in the Mid-Miocene, Johnson and others, (1977) invoke prior (Cretaceous) enrichment and modification of the base of the lithosphere, and generation of island-arc type primary magmas by partial melting on uplift.

Pliocene

Clastic sedimentation on the southern flanks of the arc extended progressively eastwards during the Miocene-Pliocene; limestone deposition continued in the north and east. Uplift of the Huon Peninsula in the Pliocene coincides with the eruption of valley-fill basalts in that area, and the emplacement of scattered diabase dikes and gabbro-diorite stocks and porphyries along the length of the arc. Subduction-related volcanism in the Bismarck volcanic arc to the north also probably commenced about this time. We suggest that the resurgence of volcanism may be the result of subduction of the remaining intervening lithosphere between the Huon Peninsula and the central orogenic belt in the Markham valley region; this completed the final stages of the continent/island-arc collision. Uplift resulted in crestal arching and fracturing, and formation of a complex fracture system with many early-formed shears changing to tensional fractures. Isostatic reaction to underthrusting of sialic material, and probably southward thrusting of the Finisterre-Huon block in the Miocene-Pliocene, may have been the cause of uplift. This thrusting might explain the presence of the small peridotite bodies of the Huon Peninsula, and perhaps, the regional gravity high over that region (St John, 1970). West-northwestward-trending sinistral shears found throughout the north coast ranges are interpreted as indicating widespread transcurrent motion throughout the collision zone caused by northwestward movement of the Pacific plate (and subplates) relative to the continent.

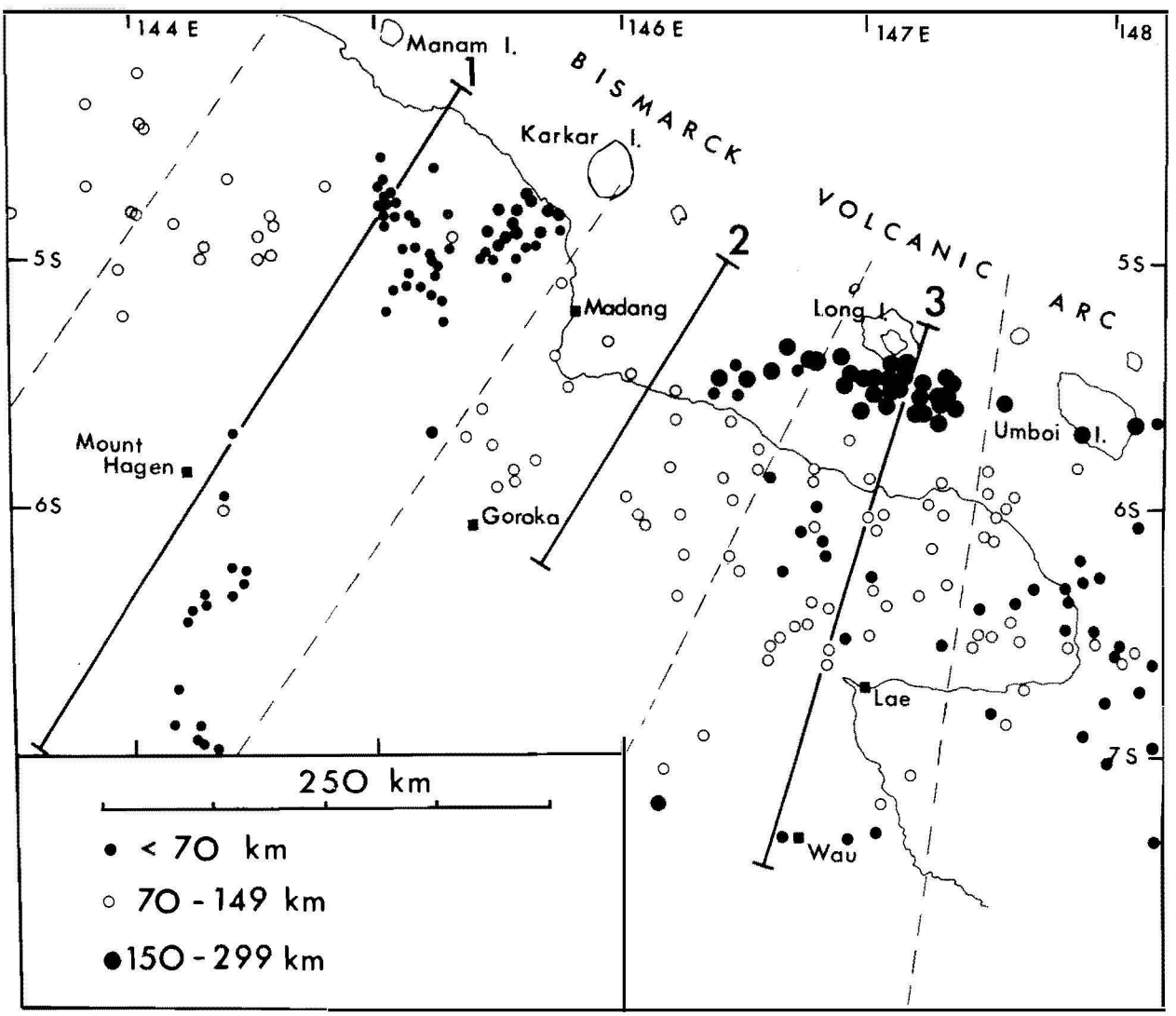

Figure 8. Plot of 1969-1974 earthquake epicentres and cross-sections showing foci in the northern Papua New Guinea region. Sources and selection criteria for the earthquakes (V. F. Dent, pers. comm., 1976): 1969-1970 events; Regional Catalogue of Earthquakes, vols. 6-7 (The International Seismological Centre, Scotland) showing only events recorded by at least 10 stations, and with coordinates given to two decimal places. Events between January 1971 and June 1974: Earthquake Data File of BMR, Canberra; only events recorded by at least 10 stations were used.

Quaternary

Uplift continued in the north coast ranges; extensive deposition of alluvium occurred in the Ramu and Markham valleys, and sedimentation in the Ramu Basin became terrestial after the Pleistocene. Holocene uplift exposed the flight of coral terraces on the northeastern Huon Peninsula.

Extensive Quaternary (partly Late Pliocene) volcanism occurred in the central highlands of Papua New Guinea. Although the volcanic rocks are chemically comparable to subduction-related island-arc and continental margin-type lavas the volcanoes are, with one exception, underlain by continental crust some 30-35 km thick (Mackenzie, 1976). Seismicity plots (Johnson and others, 1971; Figs. 8, 9) show that except for one volcano there are no underlying intermediate-to-deep focus earthquakes which can be attributed to a currently active Benioff zone. Johnson and others (1977) suggest that the volcanism is the result, not of contemporaneous subduction, but of partial melting of a source at the base of the lithosphere which had been modified by the introduction of fluids from a slab dipping beneath the continental margin in the Late Mesozoic. Diapirism and partial melting may have been initiated by periods of uplift following the mid-Tertiary collision. Evidence for the Cretaceous mantle modification are the Cretaceous andesites, and the recent recognition (D. E. Mackenzie, pers. comm., 1977) of a Cretaceous "psuedoisochron" (Brooks and others, 1976) in relatively unfractionated rocks from several Highlands volcanoes.

Present-day regime

The present-day plate boundary configuration in the region is complex. The distribution of earthquake epicentres suggests that at least two minor plates lie trapped between the larger Pacific and Indo-Australian plates (Johnson & Molnar, 1972; Curtis, 1973a, b; Krause, 1973). The chain of late Cainozoic volcanoes at the southern margin of the Bismarck Sea—the Bismarck volcanic arc (Johnson and others, 1971, 1973)—includes a number of active centres; eruptions on Manam, Karkar, and Long Islands occurred in 1973-75 (Cooke and others, 1976). Volcanism at the eastern end of the arc (north of New Britain) can be related to the northward subduction of the Solomon Sea beneath New Britain (Johnson, 1976).

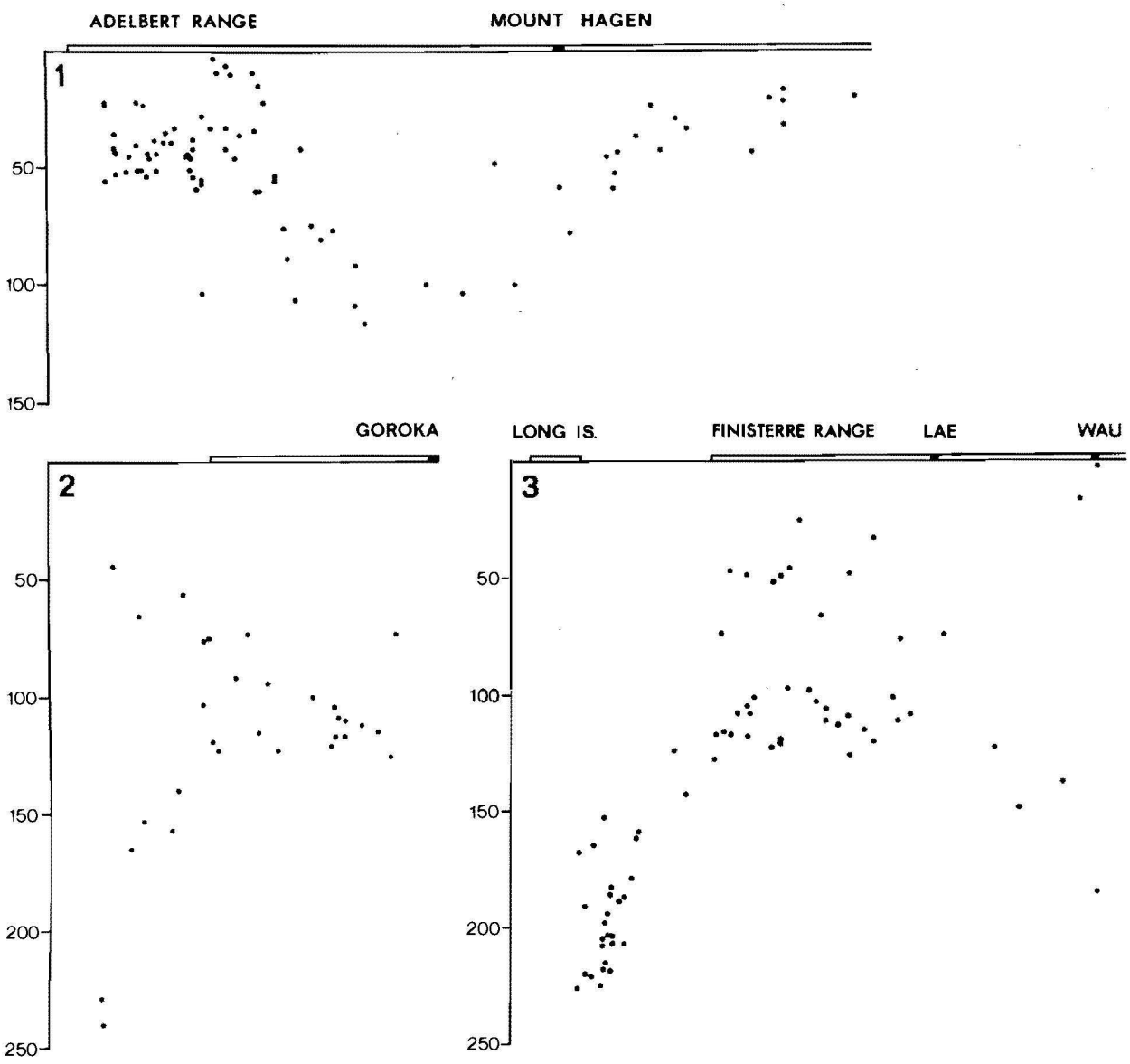

Figure 9. Cross-sections of earthquakes plotted against depth (km). Data from Johnson 1977.

Tectonic events in the western part of the arc are more complex; a submarine trench is lacking, and plots of earthquake foci show an absence of intermediate focus earthquakes west of Karkar Island (Fig. 8). East of Karkar Island, however, a well-defined seismic zone dips steeply northwards beneath Long Island to almost 250 km. Steep dip-slip underthrust mechanisms have been obtained for some of these events (Ripper, 1975). Other apparent inclined seismic zones are also evident in Figure 8. Both northward and southward-dipping 'zones' are apparent in Section 1, and in Section 2 a shallow southward-dipping 'zone' intersects the deeper northward-dipping one. The events defining these 'zones' are all less than 125 km deep (most are less than 100 km), and as the thickness of lithosphere beneath the southern part of the platform (Fig. 3) has been determined as about 125 km (Brooks, 1969), we believe that the earthquakes cannot be assumed to represent penetration of subducted lithosphere into the underlying asthenosphere. Some of the shallow events beneath the north coast ranges are associated with strike-slip faulting (Robinson and others, 1974; Everingham, 1976). Other earthquakes, particularly those south of the collision zone, may indicate overthrusting, possibly within lithosphere that may be thicker than normal. Focal mechanism solutions do not appear to clarify interpretations of the tectonic setting, as strike-slip, dip-slip overthrust, dip-slip and normal solutions have all been obtained (Ripper, 1975).

A few intermediate-depth earthquakes localised in the Highlands-Wau area give the impression of a south-southwest-dipping structure in Section 3. However, Dent (1976) examined the distribution of these events in detail by plotting them on several planes with different azimuths, and concluded that a localised seismic zone dips at about 30° towards 230-240°. Dent (1976) postulated that the earthquakes were related to rare intermediate-depth events that form a diffuse band extending south-southeastwards beneath the Papuan Ultramafic Belt into the western Solomon Sea area. Although the significance of these earthquakes remains obscure, Dent's interpretation is consistent with those of Curtis (1973), and Ripper (1975b), who considered that the events are part of a generally vague seismic zone dipping away from the Solomon Sea area. While it seems likely that the events are associated with underthrust lithosphere, there is no justification in assuming that these earthquakes beneath the orogenic belt are evidence for an extensive seismically active slab extending westwards beneath the stable platform and the Highlands volcanic province.

Lateral changes in chemistry and an increase in volcanic volumes along the western portion of the arc have been recognised by Johnson (1976, 1977), who relates the variation to an increase in the rate of plate convergence along a northward-dipping subduction zone away from a pole of rotation centred in northwest mainland Papua New Guinea. The Quaternary volcanism is believed to be related to reactivated subduction of the same, but now steepened, subduction slab responsible for the Palaeogene volcanism (Johnson, 1976, 1977; Johnson and others, 1977). It is suggested that reactivation of the slab occurred in the Late Pliocene—possibly by rotational closing of sea floor between the eastern portion of the Adelbert-Finisterre-Huon arc and the continental margin. The absence of deep-focus earthquakes beneath the Bismarck volcanic arc, and of intermediate focus events in the far western part of the arc, is attributed to thermal equilibration of subduction slab and surrounding mantle under slow rates of subduction (Johnson, 1976).

Additional responses to present-day plate convergence at this boundary are found in the Adelbert-Finisterre Range-Huon Peninsula. Focal mechanism solutions (Everingham, 1975), and the spatial distribution of epicentres associated with two clusters of shallow-focus earthquakes in the eastern Adelbert Range (Fig. 8), strongly suggest that the two clusters form a conjugate shear system related to north-northeast-south-southwest primary stress (Cooke and others, 1976). This supports earlier interpretations based on mapping sets of Quaternary fractures (Fig. 5), recognised as conjugate shear systems with a northeasterly trending acute bisectrix (Robinson, 1973, 1976), that the north coast ranges form a zone of compression imposed by interaction between the Indo-Australian and Pacific plates (and subplates). Strike-slip faulting is common both north and south of the Ramu-Markham Fault Zone, suggesting that part of the present-day convergence is achieved by transcurrent motion. The Ramu-Markham Fault Zone is believed to be a sinistral transcurrent fault, but unequivocal evidence of both past displacements and present-day movement is lacking. As pointed out by Coleman & Packham (1976), the geological data appear to be in conflict with the high rate of convergence of the Indo-Australian and Pacific plates, of the order of 14.5 cm per year along an azimuth of 78° (Le Pichon and others, 1973), estimated for the New Guinea region from sea-floor spreading data. Rather the broad belt of earthquake epicentres coinciding with zones of strong transcurrent faulting suggest that present-day plate interaction in the region is spread over a broad zone and that no single, finite plate boundary can be identified (Johnson, 1976).

Discussion and conclusions

Recent geological information from northeastern Papua New Guinea has enabled reconstruction of Tertiary tectonic events associated with the Mid-Tertiary collision between a southward-facing island arc to the north and the continental mass to the south. Our model is similar to that proposed by Dewey & Bird (1970), and more recently by Dewey (1976), for collision at Atlantic-type continental margins (Dewey, 1976, Fig. 4 D, E, F). However, unlike a number of previous interpretations and theoretical predictions we find no evidence to substantiate a reversal of the direction of subduction following the collision. Models invoking short-lived southward-dipping subduction in the Mid to Late Cainozoic to explain the magmatism in central Papua New Guinea find little support from the geology, although the possibility of some underthrusting at the northern continental margin is not discounted. Late Cainozoic volcanism in the Bismarck volcanic arc at the southern margin of the Bismarck Sea is related to a steeply inclined seismic zone which dips northwards beneath Vitiaz Strait (Johnson, 1976). This seismic zone is believed to be a vestige of the Early Tertiary northward-dipping subduction zone: the hanging slab is slowly sinking and equilibrating with the mantle under slow rates of subduction.

Johnson & Jaques (1977) point out that this interpretation has implications for continent/island-arc collisions in general, as northern New Guinea is widely accepted as a classic example of a region in which a reversal of arc polarity took place after collision. Johnson & Jaques (1977) argue that, not only is there no compelling evidence for a present-day southward-dipping subduction zone beneath mainland Papua New Guinea, but that such a zone is unlikely to form in the presence of an active marginal basin at the rear of an arc where heat flow is generally high. The limited data available for the Bismarck Sea (Halunen & Von Herzen, 1973; see also Karig, 1973, p. 360) suggest that heat flow may be high and typical of active marginal basins. High heat flow and thin lithosphere are the antithesis of conditions

normally considered to be prerequisites for the initiation of subduction (Ringwood, 1975).

We believe the stresses of convergence of the Indo-Australian and Pacific plates after collision were taken up by 1) transcurrent movements at and about the former plate boundary; 2) crustal telescoping and shortening at the collision zone; 3) fracturing, faulting, and uplift of the accreted arc; and 4) large sinistral transcurrent movements along a complex linear zone through the Solomon Islands, New Ireland, and south of Manus Island. These responses may have generated the present-day tectonic regime in which a number of minor plates form a broad zone of interaction.

The striking structural and stratigraphic similarities between north coastal Papua New Guinea and the islands of the Outer Melanesian Arc have been pointed out previously (Robinson, 1973; see also Coleman, 1970; Coleman & Packham, 1976).

The majority of plate-tectonic reconstructions made to date regard the islands of the Outer Melanesian Arc as having formed as an extended, fractured island-arc system in response to Early Tertiary interaction between the Indo-Australian and Pacific plates. However, interpretations of the polarity of that arc differ: a southwestward-facing arc system has been inferred by some authors (Robinson, 1969, 1973; Curtis, 1973b; Mallick, 1973), whereas a Late Tertiary reversal of polarity from a previously northeasterly facing arc-trench system has been argued on geochemical (Mitchell & Warden, 1971; Gill & Gorton, 1973; Colley & Warden, 1974), and structural and stratigraphic grounds (Karig & Mammerickx, 1972; Falvey, 1975). However, much of the evidence (at least for the Solomon Islands) is not compelling, and the case for viewing the Outer Melanesian Arc as a northeastward-facing arc in the Palaegoene cannot be regarded as proven (Coleman, 1975b). The relationship of the Adelbert-Finisterre-Huon arc to the islands of the Outer Melanesian Arc therefore remains unresolved; the marked similarities suggest a contiguous Palaeogene arc system prior to the continent/island-arc collision in the Miocene. Breakup of the arc by transcurrent faulting associated with the collision, and interaction with thickened oceanic crust of the Ontong Java Plateau (Kroenke, 1972), may be responsible for many of the present apparently anomalous features in the region.

Acknowledgements

We thank our colleagues at the Geological Survey of Papua New Guinea and the Bureau of Mineral Resources for assistance during field work and for stimulating discussions. Thanks are due to D. J. Belford (BMR) for numerous micropalaentological determinations, and to V. F. Dent (GSPNG) for providing the earthquake epicentre plot. Helpful discussions with, and comments and criticisms of an earlier draft manuscript particularly by, R. W. Johnson, and also by P. J. Coleman, W. B. Dallwitz, D. H. Green, D. S. Hutchison, D. E. Mackenzie, J. S. Milsom, C. J. Pigram, R. J. Ryburn and C. F. Burrett are greatly appreciated. The paper was reviewed by M. J. Rickard and J. C. Mutter

References

AUSTRALASIAN PETROLEUM CO. (APC) 1961—Geological results of petroleum exploration in Western Papua, 1937-1961, by the Australasian Petroleum Co. Pty. Ltd: *Journal of the Geological Society of Australia*, **8**, 1-133.

BAIN, J. H. C., 1967—Schrader Range, New Guinea—reconnaissance geology, *Bureau of Mineral Resources, Australia*. File 67/94 (unpublished).

BAIN, J. H. C., 1973—A summary of the main structural elements of Papua New Guinea, *in* COLEMAN, P. J. (Editor) THE WESTERN PACIFIC: ISLAND ARCS, MARGINAL SEAS, GEOCHEMISTRY. *University of Western Australia Press, Perth*.

BAIN J. H. C., MACKENZIE, D. E., & RYBURN, R. J., 1975—Geology of the Kubor Anticline, central highlands of Papua New Guinea: *Bureau of Mineral Resources, Australia, Bulletin* **155**.

BMR, 1972—Geology of Papua New Guinea: 1:1 000 000 map. *Bureau of Mineral Resources, Australia, Canberra*.

BROOKS, C., JAMES, D. E., HART, S. R., & HOFFMAN, A. W., 1976—Rb-Sr mantle isochrons. *Annual Report of the Department of Terrestrial Magnetism, Carnegie Institute, Washington*, **75**, 176-207.

BROOKS, J. A., 1969—Rayleigh wave dispersion studies of crustal and upper mantle structure in New Guinea. Ph.D. Thesis, *University of Tasmania, Hobart*, (unpublished).

BROWN, C. M., PIETERS, P. E., & ROBINSON, G. P., 1975—Stratigraphic and structural development of the Aure Trough and adjacent shelf and slope areas. *Journal of the Australian Petroleum Exploration Association*, **15**, 61-71.

CHAPELL J., 1974—Geology of coral terraces on Huon Peninsula, New Guinea: A study of Quaternary tectonic movements and sea level changes. *Bulletin of the Geological Society of America*, **85**, 553-70.

COLEMAN, P. J., 1970—Geology of the Solomon and New Hebrides Islands as parts of the Melanesian Re-entrant, Southwest Pacific. *Pacific Science*, **24**, 284-314.

COLEMAN, P. J., 1975a—On island arcs. *Earth Science Review*, **11**, 47-80.

COLEMAN, P. J., 1975b—The Solomons as a non-arc. *Bulletin of the Australian Society of Exploration Geophysicists*, **6**, 60-1.

COLEMAN, P. J., & PACKHAM, G. H., 1976—The Melanesian borderlands and India-Pacific plates boundary. *Earth Science Review*, **12**, 197-233.

COLLEY, H., & WARDEN, A. J., 1974—Petrology of the New Hebrides. *Bulletin of the Geological Society of America*, **85**, 1635-46.

CONNELLY, J. B., 1974—A structural interpretation of magnetic and seismic profile records in the Bismarck Sea, Melanesian Archipelago. *Journal of the Geological Society of Australia*, **21**, 459-69.

CONNELLY, J. B., 1976—Tectonic development of the Bismarck Sea based on gravity and magnetic modelling. *Geophysical Journal*, **45**, 23-40.

CONTINENTAL OIL COMPANY OF AUSTRALIA PTY LTD, 1969—Final Madang aeromagnetic survey, Ramu River basin, Madang block, New Guinea. *Geological Survey of Papua New Guinea*, File 19 AR (unpublished).

CONTINENTAL OIL COMPANY OF AUSTRALIA PTY LTD, 1970—Final report, Madang seismic survey, Ramu River basin, Madang block, New Guinea. *Geological Survey of Papua New Guinea*, File 19 AQ (unpublished).

COOKE, R. J. S., MCKEE, C. O., DENT, V. F., & WALLACE, D. A., 1976—A striking sequence of volcanic eruptions in the Bismarck Volcanic Arc, Papua New Guinea. *In* JOHNSON, R. W. (Editor), VOLCANISM IN AUSTRALASIA. Elsevier Publishing Co., Amsterdam, 149-72.

CURTIS, J. W., 1973a—The spatial seismicity of Papua New Guinea and the Solomon Islands. *Journal of the Geological Society of Australia*, **20**, 1-19.

CURTIS, J. W., 1973b—Plate tectonics of the Papua New Guinea-Solomon Islands region. *Journal of the Geological Society of Australia*, **20**, 21-36.

D'ADDARIO, G. W., DOW, D. B., & SWOBODA, R., 1975—Geology of Papua New Guinea, 1:2 500 000. *Bureau of Mineral Resources, Australia, Canberra*.

DAVIES, H. L., 1971—Peridotite-gabbro-basalt complex in eastern Papua: an overthrust of oceanic mantle and crust. *Bureau of Mineral Resources Australia, Bulletin* **128**.

DAVIES, H. L., & SMITH, I. E., 1971—Geology of eastern Papua. *Bulletin of the Geological Society of America*, **82**, 3299-312.

DENHAM, D., 1969—Distribution of earthquakes in the New Guinea-Solomon Islands region. *Journal of Geophysical Research*, **74**, 4290-9.

DENHAM, D., 1973—Seismicity, focal mechanisms and the boundaries of the Indo-Australian plate. *In* COLEMAN, P. J. (Editor), THE WESTERN PACIFIC: ISLAND ARCS, MARGINAL SEAS, GEOCHEMISTRY. *University of Western Australia Press, Perth*.

DENHAM, D., 1975—Distribution of underthrust lithospheric slabs and focal mechanisms—Papua New Guinea-Solomon Islands region. *Bulletin of the Australian Society of Exploration Geophysicists*, **6**, 35-7.

DENT, V. F., 1976—The seismicity pattern near Mount Yelia, Papua New Guinea. *Geological Survey of Papua New Guinea*, File 1976/22 (unpublished).

DEWEY, J. F., 1976—Ophiolite obduction. *Tectonophysics*, **31**, 93-120.

DEWEY, J. F., & BIRD, J. M., 1970—Mountain belts and the new global tectonics. *Journal of Geophysical Research*, **75**, 2625-47.

DICKINSON, W. R., 1973—Reconstruction of past arc-trench systems from petrotectonic assemblages in the island arcs of the western Pacific. *In* COLEMAN, P. J., (Editor), THE WESTERN PACIFIC: ISLAND ARCS, MARGINAL SEAS, GEOCHEMISTRY. *University of Western Australia Press, Perth.*

DOW, D. B., 1976—Geology of Papua New Guinea. *In* KNIGHT, C. L. (Editor), THE ECONOMIC GEOLOGY OF AUSTRALIA AND PAPUA NEW GUINEA. *Australasian Institute of Mining and Metallurgy, Melbourne*, 823-36.

DOW, D. B., & DEKKER, F. E., 1964—The geology of the Bismarck Mountains, New Guinea. *Bureau of Mineral Resources Australia, Report* **76.**

DOW, D. B., SMITH, J. A. J., BAIN, J. H. C., & RYBURN, R. J., 1972—Geology of the South Sepik region, New Guinea. *Bureau of Mineral Resources, Australia, Bulletin* **133.**

EVERINGHAM, I. B., 1975—Seismological report on the Madang earthquake of 31 October 1970 and aftershocks. *Bureau of Mineral Resources, Australia, Report*, **176.**

FALVEY, D., 1975—Arc reversals, and a tectonic model for the North Fiji Basin. *Bulletin of the Australian Society of Exploration Geophysicists*, **6**, 47-9.

FINLAYSON, D. M., & CULL, J. P., 1973—Structural profiles in the New Britain-New Ireland island arc structures. *Journal of the Geological Society of Australia*, **20**, 37-48.

GILL, J. B., & GORTON, M., 1973—A proposed geological and geochemical history of Eastern Melanesia. *In* COLEMAN, P. J., (Editor), THE WESTERN PACIFIC: ISLAND ARCS, MARGINAL SEAS, GEOCHEMISTRY. *University of Western Australia Press, Perth.*

HALUNEN, A. J., & VON HERZEN, R. P., 1973—Heat flow in the western equatorial Pacific Ocean. *Journal of Geophysical Research*, **78**, 5195-208.

HAMILTON, W., 1973—Tectonics of the Indonesian region. *Bulletin of the Geological Society of Malaysia*, **6**, 3-10.

HARRISON, J., 1969—A review of the sedimentary history of the island of New Guinea. *Journal of the Australian Petroleum Exploration Association*, **9**, 41-8.

HARRISON, J., 1974—Keram No. 1 well completion report. *General Crude Oil Company International Ltd.*, Report (unpublished).

HUTCHISON, D. S., 1975—Basement geology of the North Sepik region, Papua New Guinea. *Bureau of Mineral Resources Australia*, File 75/162 (unpublished).

JAKES, P., & WHITE, A. J. R., 1969—Structures of the Melanesian arcs and correlation with distribution of magma types. *Tectonophysics*, **8**, 223-36.

JAQUES, A. L., 1976—High K_2O-island arc volcanics from the Finisterre and Adelbert Ranges, northern Papua New Guinea. *Bulletin of the Geological Society of America*, **87**, 861-7.

JAQUES, A. L., & ROBINSON, G. P., 1975—Explanatory notes on the Bogia geological map. Papua New Guinea Geological Survey, File 74/18 (unpublished).

JENKINS, D. A. L., 1974—Detatchment tectonics in Western Papua New Guinea. Bulletin of the Geological Society of America, **85**, 533-48.

JOHNSON, R. W., 1976—Late Cenozoic volcanism and plate tectonics at the southern margin of the Bismarck Sea, Papua New Guinea. *In* JOHNSON, R. W., (Editor)—VOLCANISM IN AUSTRALASIA. *Elsevier Publishing Co., Amsterdam.*

JOHNSON, R. W., 1977—Distribution and major-element chemistry of late Cainozoic volcanoes at the southern margin of the Bismarck Sea, Papua New Guinea. *Bureau of Mineral Resources, Australia, Report* **188.**

JOHNSON, R. W., & JAQUES, A. L., in press—Continental-arc collision and reversals of arc polarity. New interpretations from a critical area, Tectonophysics.

JOHNSON, R. W., MACKENZIE, D. E., & SMITH, I. E., 1971—Seismicity and Late Cenozoic volcanism in parts of Papua New Guinea. *Tectonophysics*, **12**, 15-22.

JOHNSON, R. W., MACKENZIE, D. E., & SMITH, I. E. M., in press—Delayed partial melting of subduction-modified mantle in Papua New Guinea, Tectonophysics.

JOHNSON, R. W., MACKENZIE, D. E., SMITH, I. E., & TAYLOR, G. A. M., 1973—Distribution and petrology of Late Cenozoic volcanoes in Papua New Guinea. *In* COLEMAN, P. J. (Editor), THE WESTERN PACIFIC: ISLAND ARCS, MARGINAL SEAS, GEOCHEMISTRY: *University of Western Australia Press, Perth.*

JOHNSON, T., & MOLNAR, P., 1972—Focal mechanisms and plate tectonics of the southwest Pacific. *Journal of Geophysical Research*, **77**, 5000-32.

KARIG, D. E., 1972—Remnant arcs. *Bulletin of the Geological Society of America*, **83**, 1057-68.

KARIG, D. E., 1973—Comparison of island arc-marginal basin complexes in the Northwest and Southwest Pacific. *In* COLEMAN, P. J., (Editor), THE WESTERN PACIFIC: ISLAND ARCS, MARGINAL SEAS, GEOCHEMISTRY. *University of Western Australia Press, Perth.*

KARIG, D. E., 1974—Evolution of arc systems in the western Pacific. *Annual Review of Earth and Planetary Sciences*, **2**, 51-76.

KARIG, D. E., & MAMMERICKX, J., 1972—Tectonic framework of New Hebrides island arc system. *Marine Geology*, **12**, 187-205.

KARIG, D. E., & SHARMAN, G. F., 1975—Subduction and accretion in trenches. *Bulletin of the Geological Society of America*, **86**, 377-89.

KRAUSE, D. C., 1973—Crustal plates of the Bismarck and Solomon Seas. *In* FRASER, R. (Editor), Oceanography of the South Pacific 1972. *New Zealand National Commission for UNESCO*, 217-280.

KROENKE, L. W., 1972—Geology of the Ontong Java Plateau. *Hawaii Institute of Geophysics* Publication **HIG 72-75.**

LE PICHON, X., FRANCHETEAU, J., & BONNIN, J., 1973—PLATE TECTONICS. *Elsevier Publishing Co., Amsterdam.*

MACKENZIE, D. E., 1976—Nature and origin of late Cenozoic volcanism in Western Papua New Guinea. *In* JOHNSON, R. W. (Editor), VOLCANISM IN AUSTRALASIA. *Elsevier Publishing Co., Amsterdam.*

MALLICK, D. I. J., 1973—Some petrological and structural variations in the New Hebridies. *In* COLEMAN, P. J., (Editor)—THE WESTERN PACIFIC: ISLAND ARCS, MARGINAL SEAS, GEOCHEMISTRY. *University of Western Australia Press, Perth.*

MCMILLAN, N. J., & MALONE, E. J., 1960—The geology of the eastern central highlands of New Guinea. *Bureau of Mineral Resources, Australia, Report* **48.**

MILSOM, J. S., 1975—Madang district helicopter gravity survey, 1974. *Papua New Guinea Geological Survey* File 75/15 (unpublished).

MILSOM, J. S., & SMITH, I. E., 1975—Southeastern Papua: Generation of thick crust in a tensional environment. *Geology*, **3**, 117-20.

MITCHELL, A. H. G., & WARDEN, A. J., 1971—Geological evolution of the New Hebrides island arc. *Journal of the Geological Society of London*, **127**, 501-29.

MUTTER, J. C., 1975—Basin evolution and marginal plateau subsidence in the Coral Sea. *Bulletin of the Australian Society of Exploration Geophysicists*, **6**, 35-7.

PAGE, R. W., 1976—Geochronology of igneous and metamorphic rocks in the New Guinea highlands. *Bureau of Mineral Resources, Australia, Bulletin* **162.**

PAGE, R. W., & MCDOUGALL, I., 1970—Potassium-argon dating of the Tertiary fl-2 stage in New Guinea and its bearing on the geological time scale. *American Journal of Science*, **269**, 321-42.

PAGE, R. W., 1972—Ages of mineralisation of gold and porphyry copper deposits in the New Guinea Highlands. *Economic Geology*, **67**, 1034-48.

PIETERS, P. E., 1974—Explanatory notes on the Port Moresby, Kalo, Aroa geological map. *Papua New Guinea Geological Survey*, File 74/28 (unpublished).

RINGWOOD, A. E., 1975—COMPOSITION AND PETROLOGY OF THE EARTH'S MANTLE. *McGraw Hill, New York.*

RIPPER, I. D., 1975—Seismicity and earthquake focal mechanisms in the New Guinea/Solomon Islands region. *Bulletin of the Australian Society of Exploration Geophysicists*, **6**, 80-1.

ROBINSON, G. P., 1969—The geology of north Santo: *New Hebrides Geological Survey Regional Report.*

ROBINSON, G. P., 1973—Stratigraphy and structure of the Huon Peninsula, New Guinea within the framework of the Outer Melanesian Arc. *In* FRASER, R., (Editor), Oceanography of the South Pacific 1972. *New Zealand National Commission for UNESCO, Wellington.*

ROBINSON, G. P., 1976—Geology of the Huon Peninsula. *Papua New Guinea Geological Survey, Memoir* **2.**

ROBINSON, G. P., JAQUES, A. L., & BROWN, C. M., 1974—Explanatory notes on the Madang geological map. *Papua New Guinea Geological Survey*, File 74/13 (unpublished).

RYBURN, R. J., 1976—Median tectonic line in Papua New Guinea: a continent-island arc collision suture. *Bureau of Mineral Resources*, File 76/35 (unpublished).

ST JOHN, V. P., 1970—The gravity field and structure of Papua New Guinea. *Journal of the Australian Petroleum Exploration Association*, **10,** 41-55.

THOMPSON, J. E., 1967—A geological history of eastern New Guinea. *Journal of the Australian Petroleum Exploration Association*, **7,** 83-93.

THOMPSON, J. E. & FISHER, N. H., 1965—Mineral deposits of Papua New Guinea and their tectonic setting. *Proceedings of the 8th Mining and Metallurgical Congress, Australia-New Zealand*, **6,** 115-48.

TILBURY, L. A., 1975—Lineations in the Bismarck Sea. *Bulletin of the Australian Society of Exploration Geophysicists*, **6,** 72-3.

WATTS, M. D., 1969—Sepik river helicopter gravity survey, TPNG, 1968. *Bureau of Mineral Resources, Australia*, File 69/124 (unpublished).

APPENDIX 4

American Mineralogist, Volume 64, pages 1312–1321, 1979

Determination of liquid compositions in high-pressure melting of peridotite

A. L. JAQUES[1] AND D. H. GREEN

Department of Geology, University of Tasmania
Hobart, Tasmania 7001

Abstract

Experimental problems in the determination of liquid compositions from the partial melting of peridotite are examined in the light of data obtained in an experimental study of the anhydrous melting of peridotite. A scanning electron microscope coupled with an energy-dispersive microprobe has been employed to examine the nature of quench phases and their effect on the melt composition, and to examine the effect of iron loss on crystal–melt equilibria. In most cases the problems of iron loss, non-equilibrium, and quench modification of the melt composition preclude direct determination of the composition of partial melts, even under anhydrous conditions. Provided the modal proportions and compositions of residual phases are known, and due allowance made for preferential adjustment of residual phases to iron loss, the compositions of equilibrium partial melts may be obtained by mass-balance calculations.

Introduction

It is now generally recognized that basaltic magmas arise by partial melting of upper mantle peridotite, dominated by magnesian olivine and orthopyroxene. Accurate determination of the liquid compositions formed by partial melting of peridotite under known conditions (melt proportion, temperature, pressure, residual phase compositions and proportions, and volatile content) is therefore an important goal in experimental petrology. A number of studies towards this end have been attempted on a variety of natural peridotite compositions under differing P–T conditions and volatile contents.

In the earliest studies, phase relations only were determined and liquid compositions broadly inferred (*e.g.* Ito and Kennedy, 1967). In later experiments the compositions of the residual crystals and the quenched glass were determined by electron microprobe and the percentage of melt estimated visually (*e.g.* Kushiro *et al.*, 1972; Mysen and Boettcher, 1975; Nehru and Wyllie, 1975). More recently Mysen and Kushiro (1977) have used beta-track counting of charges spiked with radioactive tracers to more accurately determine the percentage of melting and have relied on microprobe analysis of quenched glasses to yield compositions of the melt phase.

Implicit in this experimental approach is the assumption that the directly determined quenched glass composition is that of the equilibrium melt for those particular conditions. This assumption can be criticized on two grounds. Firstly, iron loss from the sample to the noble-metal capsules used in partial melting experiments is well documented (*e.g.*, Nehru and Wyllie, 1975; Green, 1976; and others). The extent of iron loss is dependent on temperature and run duration, and since iron is not lost uniformly from the charge, Fe/Mg partitioning between crystal and liquid varies as a function of run duration (Stern and Wyllie, 1975; see below). Apart from changing the MgO/FeO ratio of the silicate charge, iron loss also increases the silica saturation of the bulk composition and probably of any melt component (O'Hara and Humphreys, 1977). Secondly, the growth of metastable quench crystals during the quenching of the glass can significantly modify the composition of the glass from that of the equilibrium melt (Green, 1973, 1976; Cawthorn *et al.*, 1973; Nicholls, 1974). These problems in the direct determination of the equilibrium partial melt composition have been the focus of debate in the past concerning the hydrous melting of peridotite (*e.g.* Mysen *et al.*, 1974; Green, 1973, 1976). Green showed that these problems could be

[1] Present address: Bureau of Mineral Resources, Canberra City, A.C.T. 2601, Australia.

0003-004X/79/1112-1312$02.00

overcome and a reliable estimate of the equilibrium melt could be calculated from a knowledge of the composition of the residual phases and the bulk charge using crystal/liquid partition data.

Mysen and Kushiro (1977) considered that these problems did not greatly effect the results of their study on the anhydrous melting of peridotite, and presented a suite of glass compositions ranging from 'alkali picrite' to 'olivine tholeiite' to 'peridotitic komatiite' as the equilibrium melts from peridotite. While the compositional range of liquids is consistent with earlier interpretations of melting at this pressure (Green and Ringwood, 1967) and is broadly that anticipated over such a melting interval, discrepancies among the data cast doubt on the validity of these directly determined glass compositions as the true unmodified equilibrium melts for the stated percentage of melting. As part of a similar melting study we have evaluated the problems involved in conducting such experiments, and find that the problems can be severe enough in many cases to preclude direct determination of equilibrium melt compositions. Here we present an alternative approach for calculation of equilibrium liquid compositions.

Table 1. Compositions of starting material

	Pyrolite - 40% olivine	Tinaquillo peridotite - 40% olivine
SiO_2	47.9	47.5
TiO_2	1.18	0.13
Al_2O_3	5.91	5.35
Fe_2O_3	0.20	0.15
FeO	8.63	7.38
MnO	0.13	0.18
MgO	28.8	32.8
CaO	5.14	4.99
Na_2O	0.95	0.30
K_2O	0.22	0.03
P_2O_5	-	0.02
Cr_2O_3	0.72	0.75
NiO	0.18	0.43
$100Mg/Mg+Fe^{++}$	85.6	88.8
$100Mg/Mg+Fe$	85.3	88.6

Experimental methods

Technique

Two peridotite compositions derived from pyrolite (Ringwood, 1966; Green, 1973, 1976) and Tinaquillo peridotite (Green, 1963) have been studied. In each case the composition used in the experiments is that of the peridotite minus 40 percent olivine to facilitate identification of minor phases and increase the relative proportion of melt and minor phases without eliminating olivine. Compositions (Table 1) were prepared from AR grade chemicals and sintered at 1000°C.

Experiments were carried out in a solid-media (piston cylinder) high-pressure apparatus, using piston-in technique and a pressure correction of minus 10 percent nominal piston pressure. Temperatures were measured by a Pt–Pt90Rh10 thermocouple with no correction for the effect of pressure on the thermocouple emf. Pyrex-glass sleeves with graphite inserts were used in 0.5-inch diameter furnace assemblies to minimize hydrogen diffusion from the dehydrating outer talc sleeve. Samples (15–20 mg) were sealed in Pt capsules and preheated at 900°–1000°C for 8–12 hours, packed in metallic iron powder in an attempt to presaturate the capsule in iron. All runs were anhydrous and the powdered starting mix was dried overnight at 110°C. Spec-pure iron capsules were used in some short-duration runs. These experiments produced an fO_2 lower than that in the Pt capsules, resulting in elimination of chrome spinel, and in some cases the charge dissolved iron from the capsule.

Microprobe analysis

The charge was recovered as a coherent cylinder of crystals and glass. A portion of one split was examined in refractive-index oils. The polished mount containing the other split was examined optically in reflected light and by scanning electron microscope using a JEOL JX 50A electron microprobe–scanning electron microscope (SEM) fitted with an energy-dispersive (EDAX) analytical system. Simultaneous quantitative analysis for 10 elements (Na to Fe) of residual phases, quench phases, glass, and bulk charge was obtained by the method of Reed and Ware (1973, 1975). Optimization of the backscattered and secondary electron images enabled clear resolution and discrimination of all phases including melt and quench crystals at up to 2000 times magnification (Fig. 1). Discrimination of phases was based on both form and contrast from the back-scattered electron image, which is dependent on the mean atomic number of the target. In this way Fe-rich rims on primary phases and quench phases, *e.g.* quench clinopyroxene, can be distinguished by the higher Fe, Al, and Ti contents compared to the primary equilibrium phases. Glass analyses and analyses of the bulk charge were made with rapid reduced-area scans to

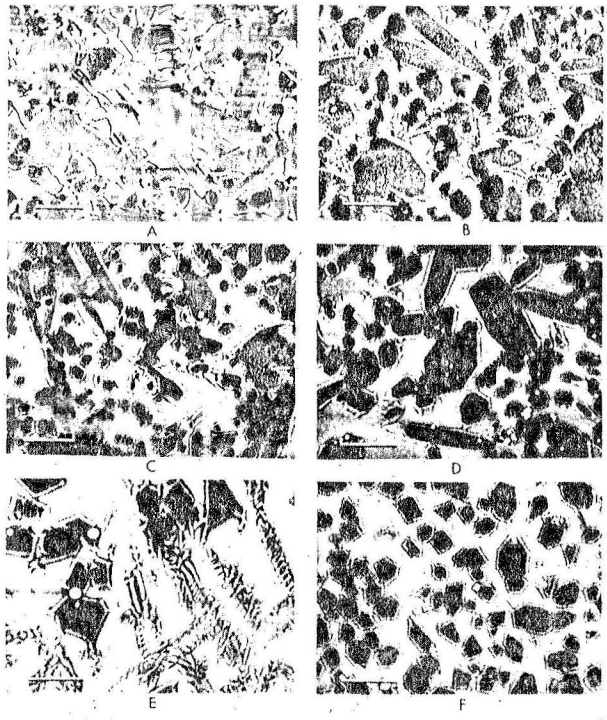

Fig. 1. Scanning electron microscope photographs of partial melting runs of pyrolite – 40 percent olivine and spinel lherzolite – 40 percent olivine, showing metastable quench phases. Scale bar is 20μ long. Quench outgrowths of clinopyroxene appear bright, as do thin quench rims of more Fe-rich olivine on primary olivine (note Figs. 1E, F particularly). (A) Pyrolite, 15 kbar, 1350°C. A low percentage melting run. Residual phases are olivine (small dark euhedra), orthopyroxene (large tabular crystals), clinopyroxene (small lighter euhedra), and chrome spinel (tiny bright euhedra). Melt is light interstitial material. Quench clinopyroxene forms light-colored rims on residual phases. Note the drastic reduction of the liquid volume by the quench phases. Compositions of phases are given in Table 4. (B) Pyrolite, 15 kbar, 1400°C. Quench clinopyroxene forms rims on residual olivine and orthopyroxene. Note the presence of some discrete quench clinopyroxene in the glass (crosses, lower right) and the larger percentage of melt. (C) Pyrolite, 10 kbar, 1300°C. Quench clinopyroxene rims residual olivine and orthopyroxene, and forms discrete crystals in the glass (small crosses, lower center). Compositions given in Table 3. (D) Pyrolite, 10 kbar, 1350°C. Like C but note the higher percentage of melt. Quench clinopyroxene is less abundant and modification of the glass composition is less severe than for A, B, and C. (E) Pyrolite, 10 kbar, 1450°C. Skeletal and dendritic quench low-calcium pyroxene forming conical spirals in glass, and dendritic rims on residual olivine. Note the similarity in the quench forms to those found in some komatiites. (F) Spinel lherzolite, 10 kbar, 1450°C. Quench low-calcium pyroxene and olivine on residual olivine. Compositions given in Table 5.

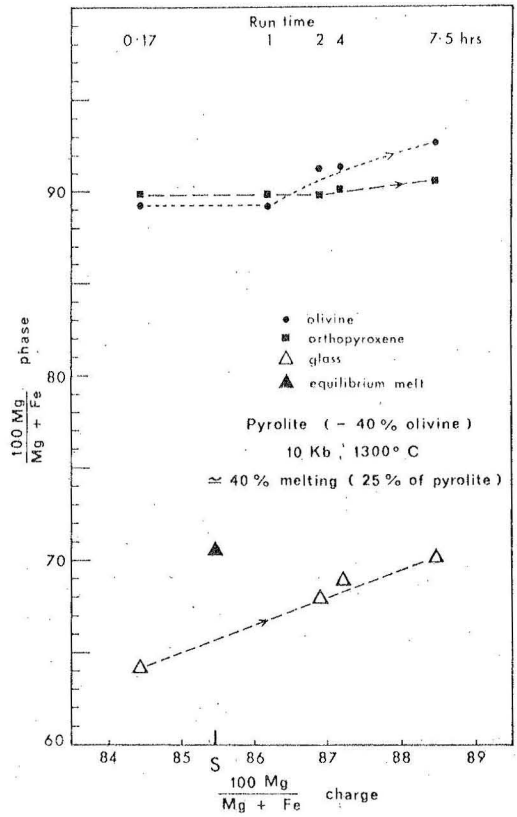

Fig. 2. 100Mg/(Mg+Fe) ratios of the residual phase (excluding Cr spinel) and glass with varying run times. S = starting composition. Olivine and glass compositions become increasingly Mg-rich as iron is lost from the charge with increasing run time. The capsules used in the 2-, 4-, and 7½-hour runs were packed in metallic iron powder for 8–12 hours at 900–1000°C in an attempt to presaturate the capsule in iron. Compositional data from Table 3.

minimize alkali volatilization and ensure representative analysis. The ability of scanning electron microscopy to discriminate phases such as olivine and orthopyroxene, clinopyroxene and glass, and to reveal compositional differences (quench rims) within phases is demonstrated in Figure 1 and confirmed by quantitative analyses of the visually discriminated areas. This technique thus permits modal analysis of these fine-grained experimental charges.

Modal analysis

Modal analysis, including the percentage of melt, was made by point counting of the SEM photographs using a 10 cm × 9 cm transparent grid; all quench phases were counted as glass. A minimum of 1200 points were counted in replicate and averaged.

Calculation of equilibrium liquid compositions

The compositions of the equilibrium liquids were calculated by mass balance after conversion of the volume percent modes to weight percent modes from appropriate mineral densities. The liquid density was calculated by the method of Bottinga and Weill

Table 2. Experimental run data

Run No.	P (kbars)	T °C	Time (hours)	Capsule	Phases present	100 Mg/Mg + Fe charge	.ol	opx
					Pyrolite - 40% olivine			
T-168	10	1300	0.17	Fe	ol + opx + quench cpx + gl	84.5	89.1	89.8
1012	10	1300	1	Pt	ol + opx + quench cpx + gl	86.2	89.1	89.9
T-89	10	1300	2	Pt	ol + opx + Cr + quench cpx + gl	86.9	91.0	89.8
T-144	10	1300	4	Pt	"	87.2	91.3	90.4
T-178	10	1300	7.5	Pt	ol + opx + cpx + Cr + quench cpx + gl	88.4	93.0	90.5
T-118	10	1350	2	Pt	ol + opx + Cr + quench cpx + gl	87.0	92.8	91.3
T-139	10	1350	0.5	Fe	ol + opx + quench cpx + gl	85.1	90.1	91.0
T-101	10	1450	?	Pt	ol + Cr + quench px + gl	89.7	95.8	-
T-138	10	1450	0.25	Fe	ol + quench px + gl	83.3	91.6	-
T-148	15	1350	2.5	Pt	ol + opx + cpx + Cr + quench cpx + gl	87.7	92.2	89.8
T-142	15	1400	1	Pt	ol + opx + Cr + quench cpx + gl	86.2	92.0	90.5
					Tinaquillo lherzolite - 40% olivine			
T-155	10	1450	0.5	Pt	ol + Cr + quench px + gl	90.7	95.6	-

ol = olivine; opx = orthopyroxene; cpx = clinopyroxene; Cr = chrome spinel; gl = glass

(1970) using the least modified, most magnesian glass composition (obtained by reduced area rapid scans) with adjustment for the effect of pressure on the density (Kushiro *et al.*, 1976). Iteration of the mass-balance calculations to overcome the density difference between the equilibrium liquid and the analyzed glass made negligible difference to the resultant liquid composition. Two examples of liquids determined in this way are shown in Table 3, Figures 2 and 3, and Table 4, Figure 4. The SEM photographs of these runs are illustrated in Figure 1.

Point counting of phases was not possible for the high-degree melting runs where olivine alone or olivine and chrome spinel were residual phases, because of strong crystal settling within the charge even in runs of short duration. For these experiments (*e.g.* Fig. 5, Table 5) the liquid composition was calculated assuming a $K_D$ol/liquid of 0.3 (Roeder and Emslie, 1970; Green and Ringwood, 1967) after allowance for iron loss from the charge (Green, 1973).

Experimental results

In the three examples presented in detail in Figures 1–5 and Tables 1–5, the calculated equilibrium

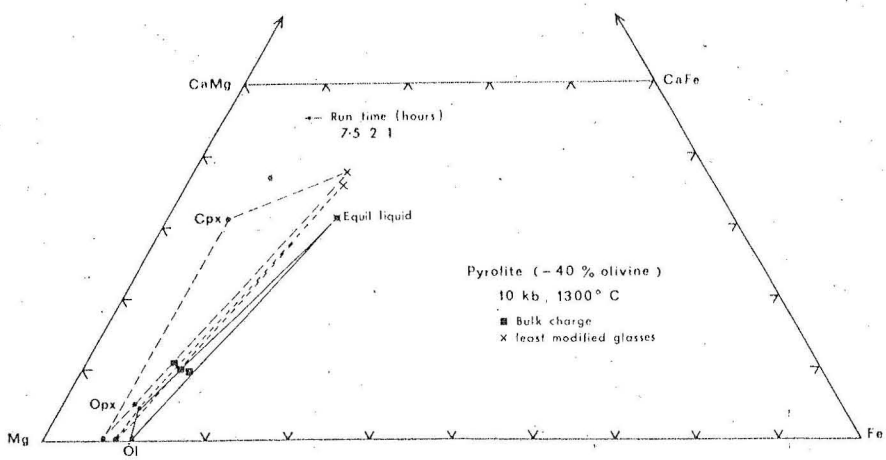

Fig. 3. Data from Fig. 2 for 1-, 2-, and 7½-hour runs at 10 kbar, 1300°C, illustrating effect of Fe loss. Squares indicate the bulk charge composition after the run. Tie lines join coexisting residual phases with least modified glass compositions. Note that the iron loss from the charge for the 7½-hour run has been sufficient to stabilize clinopyroxene in the residue.

Table 3. Compositions of phase for melting of pyrolite – 40 percent olivine at 10 kbar, 1300°C

	0.17 hours			1 hour					
	ol	opx	gl	large olivine[1] core	large olivine[1] rim[3]	small ol[2]	large opx core	large opx rim	melt[4]
SiO_2	40.5	54.8	52.0	40.6	40.5	41.0	55.1	54.0	49.8
TiO_2	–	0.47	2.87	–	–	–	0.43	0.85	2.7
Al_2O_3	–	2.93	13.2	–	–	–	2.52	3.63	12.5
FeO^t	10.5	6.39	8.99	10.5	10.3	10.2	6.42	6.24	9.0
MnO	–	–	–	0.20	0.34	0.40	–	–	0.1
MgO	48.3	31.7	9.11	98.1	48.5	48.0	31.7	31.1	12.0
CaO	0.31	2.35	11.0	0.39	0.36	0.38	2.42	2.58	10.9
Na_2O	–	–	1.97	–	–	–	–	–	2.4
K_2O	–	–	0.47	–	–	–	–	–	0.55
Cr_2O_3	0.38	1.30	0.35	–	–	–	1.35	1.60	–
Si	0.997	1.909		1.001	.996	1.007	1.921	1.885	
Ti	–	0.012		–	–	–	0.011	0.022	
Al	–	0.120		–	–	–	0.104	0.149	
Fe	0.216	0.186		0.216	0.211	0.209	0.187	0.182	
Mn	–	–		0.004	0.008	0.008	–	–	
Mg	1.771	1.649		1.767	1.780	1.758	1.647	1.618	
Ca	0.008	0.088		0.010	0.010	0.010	0.090	0.096	
Na	–	–		–	–	–	–	–	
Cr	0.007	0.036		–	–	–	0.037	0.044	
Total	3.000	4.000		2.999	3.005	2.993	3.997	3.996	
$\frac{100\ Mg}{Mg+Fe}$	89.1	89.8	64.3	89.1	89.4	89.4	89.8	89.9	70.4
Ca		4.6	33.1				4.7	5.1	
Mg		85.8	45.9				85.6	85.3	
Fe		9.7	21.0				9.7	9.6	

t = total iron as FeO

1. large olivine = $\geq 10\mu$

2. small olivine = $\leq 5\mu$

3. = rim compositions were obtained avoiding quench rims of pyroxene and olivine.

4. = calculated equilibrium melt composition, using modal analysis, analysed crystalline phase from 1-hr run and original bulk composition

liquid composition differs from the analyzed glass compositions. The nature of the calculated equilibrium melt at 10 kbar, 1300°C, produced by approximately 25 percent melting of pyrolite, is olivine tholeiite with 16 percent normative olivine; all analyzed glasses are higher in SiO_2 and lower in normative olivine than the calculated melts, with both the 0.17-hour and 7.5-hour runs containing normative quartz. At 15 kbar, 1350°C the degree of melting of pyrolite is about 18 percent and the equilibrium melt is alkali olivine basalt. All glass analyses are hypersthene normative and have considerably less MgO and more SiO_2, Al_2O_3, and CaO than the calculated melt. At 10 kbar, 1450°C the Tinaquillo lherzolite composition is about 40 percent molten, and the composition of the calculated melt, with very high MgO and SiO_2, is strongly hypersthene- and olivine-normative, resembling pyroxene-rich komatiitic liquids. In the follow-

Table 3. (continued)

2 hours						7.5 hours						
large olivine core	rim	small ol	large opx core	rim	gl	large ol core	rim	small ol	large opx core	rim	cpx	gl
40.7	41.0	40.8	54.8	55.0	51.3	41.2	41.0	41.0	55.0	55.3	53.1	51.2
–	–	–	0.42	0.42	2.85	–	–	–	0.52	0.50	0.70	3.12
–	–	–	2.72	2.40	12.4	–	–	–	2.70	2.66	3.33	13.2
8.70	8.30	8.21	6.42	6.23	8.93	7.57	6.96	6.90	5.97	5.72	4.59	7.64
0.35	0.35	0.36	–	–	–	0.21	–	–	–	–	–	–
49.8	49.80	50.2	31.7	32.4	10.4	50.7	51.7	51.8	31.9	31.5	21.7	10.2
0.41	0.60	0.39	2.45	2.50	11.8	0.36	0.32	0.40	2.70	3.22	15.0	12.1
–	–	–	–	–	1.86	–	–	–	–	–	–	1.90
–	–	–	–	–	0.50	–	–	–	–	–	–	0.58
–	–	–	1.46	1.05	–	–	–	–	1.20	1.08	1.53	–
0.995	0.999	0.995	1.912	1.915		1.000	0.993	0.992	1.913	1.923	1.906	
–	–	–	0.011	0.011		–	–	–	0.014	0.013	0.019	
–	–	–	0.112	0.099		–	–	–	0.111	0.109	0.141	
0.178	0.170	0.167	0.187	0.181		0.154	0.141	0.140	0.174	0.167	0.138	
0.007	0.007	0.008	–	–		0.004	–	–	–	–	–	
1.814	1.810	1.825	1.648	1.682		1.833	1.865	1.867	1.657	1.633	1.161	
0.011	0.016	0.010	0.092	0.093		0.009	0.008	0.010	0.101	0.120	0.576	
–	–	–	–	–		–	–	–	–	–	–	
–	–	–	0.040	0.029		–	–	–	0.033	0.030	0.044	
3.005	3.001	3.005	4.001	4.010		3.000	3.007	3.008	4.001	3.995	3.983	
91.1	91.4	91.6	89.8	90.3	67.5	92.3	93.0	93.0	90.5	90.8	89.4	70.3
			4.8	4.8	35.5				5.2	6.3	30.7	37.6
			85.5	86.0	43.5				85.8	85.1	61.9	43.9
			9.7	9.3	21.0				9.0	8.7	7.4	18.5

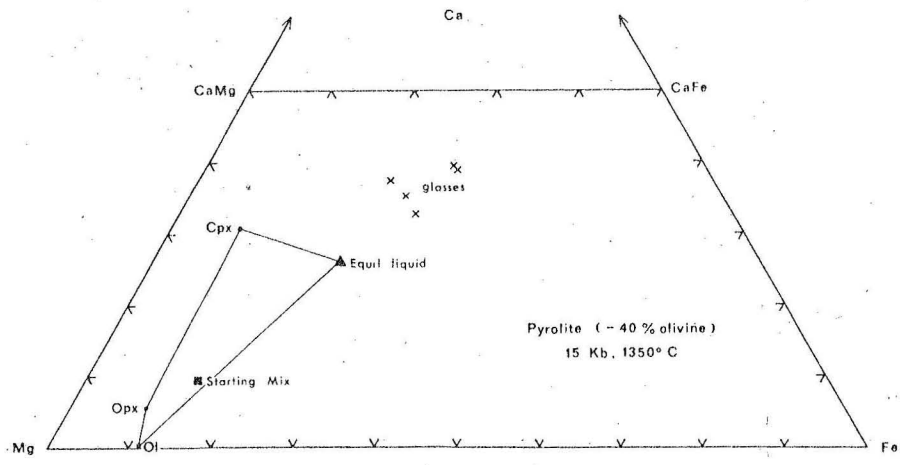

Fig. 4. Ca–Mg–Fe diagram illustrating the effect of quench growth of Ca pyroxene on the determined liquid compositions. The equilibrium liquid is calculated (see text). Compositions given in Table 4.

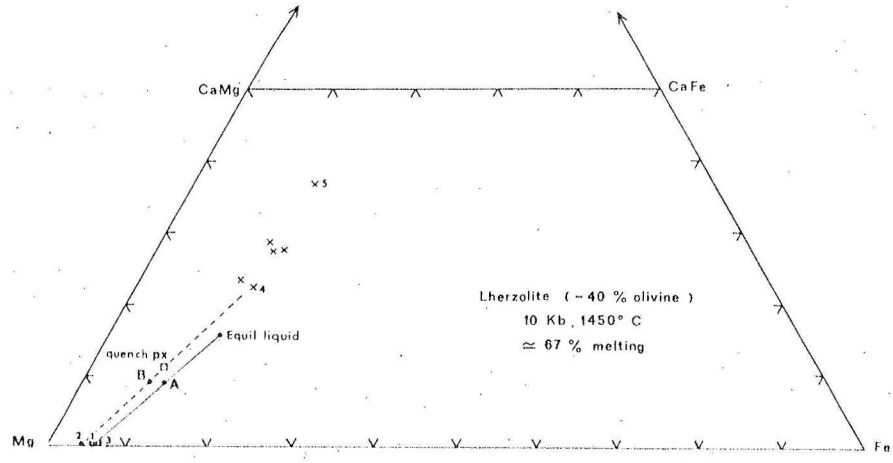

Fig. 5. Ca–Mg–Fe diagram illustrating relations in a run with a large amount of partial melting. Solid tie lines connect the starting mix (A) to the calculated equilibrium liquid. Dashed tie line joins analyzed olivine (2) with the bulk charge after the run (B) and the least-modified glass composition (4). Crosses indicate other glass analyses (determined at least 5–10 microns from any observable quench phase). Glass 5 was obtained adjacent (2–5μ) to a quench pyroxene. 3 = range of quench olivine compositions. Compositions given in Table 5.

ing sections we discuss the causes of these problems in determination of liquid compositions in partial melting experiments on peridotite compositions.

Iron loss in experimental runs

Although Stern and Wyllie (1975) showed in an andesite-melting study that iron is not lost uniformly from the charge, there appears to be a belief that equilibrium, once achieved, is maintained throughout the experiment in spite of iron loss. For example, Mysen and Kushiro (1977) claim that a 20 percent iron loss results in only a minor change in the Fe content of the olivine and disregard any greater effect on the liquid composition.

Other data obtained from runs of varying duration at the same pressure and temperature, 10 kbar and 1300°C, are presented in Table 3 to illustrate the problem. Despite attempts to presaturate the Pt capsules, all experienced iron loss [shown by the 100Mg/(Mg+Fe) ratio of the charge; Table 2]; runs in spec-pure iron resulted in iron gain. The effect of iron loss can be very significant; for example, in the 7.5-hour run the iron loss was sufficient to stabilize calcic pyroxene in the residue, whereas only olivine, orthopyroxene, and chrome spinel were present in the residue of other runs. Figure 2 and the data of Table 3 show that as iron is lost from the system, demonstrated by increasing 100Mg/(Mg+Fe) ratio of the bulk charge, orthopyroxene compositions change little, whereas olivine and glass compositions readjust more rapidly to the loss. The different rates of adjustment of the crystalline phases to iron loss are also shown by the greater compositional difference between core and rim compositions of pyroxene relative to olivine. Stern and Wyllie (1975) found that apparent garnet and clinopyroxene Fe/Mg partitioning was dependent on run duration, because garnet adjusted more slowly to Fe loss than clinopyroxene, causing $(Fe/Mg)_{ga}/(Fe/Mg)_{cpx}$ to increase with run duration. Similar differences in the rate of adjustment of garnet and pyroxene to iron loss have been observed in eclogite melting studies (K. L. Harris, personal communication, 1978). The effect of iron loss from the system is shown in Figure 3, where all phases and the bulk composition are displaced from the equilibrium value to more Fe-poor compositions.

The effect of change of the bulk composition is most marked on liquid compositions: the 10-minute run in spec-pure Fe resulted in iron gain by both the charge and the glass, but had little effect on the compositions of residual crystals.

It is apparent that Fe diffusion rates are different for various phases and that iron is lost preferentially in the order liquid > olivine (orthosilicate) > pyroxene (chain silicate). Significant iron loss can result in the formation of olivine considerably more magnesian than the original equilibrium olivine because of attempted re-equilibration of the olivine with the increasingly iron-deficient liquid.

Equilibrium melting requires that equilibrium exists between melt and residue, and between residual phases. *However, the difference in rates of adjustment of the various phases to iron loss produces non-equilibrium assemblages.* Because of the different diffusion

Table 4. Compositions of phase and calculated melt for pyrolite – 40 percent olivine at 15 kbar, 1350°C

	ol[1]	opx	cpx	sp	glass[3]	melt[4]
SiO_2	41.1	54.7	52.4	-	49.9	49.0
TiO_2	-	0.33	0.80	1.23	3.4	3.2
Al_2O_3	-	3.93	5.03	25.3	14.4	12.9
FeO	7.53	6.25	5.09	21.7	8.7	10.2
MnO	0.41	-	-	-	-	0.1
MgO	50.6	30.8	20.5	16.3	8.3	11.6
CaO	0.35	2.76	14.3	0.27	10.9	9.1
Na_2O	-	-	0.55	-	3.3	3.1
K_2O	-	-	-	-	0.9	0.7
Cr_2O_3	-	1.15	1.42	35.2	-	-
$\frac{100\ Mg}{Mg + Fe}$	92.3	89.8	87.8	57	63	67
Ca		5.5	30.6		37.4	27.6
Mg		84.9	60.9		39.2	48.5
Fe		9.6	8.5		23.3	23.9

1. Equilibrium olivine used in liquid calculation was calculated assuming $K_D^{ol}/opx = 1.1$ i.e. 100 Mg/Mg+Fe = 88.9
2. Total iron as FeO
3. Least modified glass
4. Melt calculated by mass balance; using modal analysis, analyzed crystalline phases (olivine corrected for Fe loss) and original bulk composition

Table 5. Compositions of phases and calculated melt for lherzolite – 40 percent olivine at 10 kbar, 1450°C

	olivine	quench olivine	quench	spinel	glass[2]	melt[3]
SiO_2	41.6	44.5	50.9	-	54.8	51.6
TiO_2	-	0.12	0.32	0.13	0.4	0.2
Al_2O_3	-	1.34	6.46	11.5	8.9	7.8
FeO[1]	4.37	5.36	6.14	11.2	7.5	8.4
MnO	0.32	-	-	-	-	0.2
MgO	53.5	47.2	29.6	18.8	18.5	23.9
CaO	0.27	0.95	5.74	0.27	9.2	7.4
Na_2O	-	-	-	-	-	0.45
K_2O	-	-	-	-	-	0.04
Cr_2O_3	-	0.56	0.70	58.1	-	-
$\frac{100\ Mg}{Mg + Fe}$	95.6	94	89.6	74.9	81.4	83.8
Ca			11.1		22.6	15.7
Mg			79.7		63.0	70.5
Fe			9.3		14.4	13.9

1. Total iron as FeO
2. Least modified glass composition
3. Equilibrium melt calculated from K_D^{ol}/liq 1 0.3 after correction for iron loss (Green, 1973).

rates in liquid and different residual crystals, measured Fe/Mg partition coefficients are dependent on run time. For example, the $K_D$ol/opx = $(Fe/Mg)_{ol}/(Fe/Mg)_{opx}$ has been shown to be insensitive to temperature and pressure, and has been determined experimentally as equal to 1.1±0.1 (*e.g.* Mori and Green, 1978, and others). Equilibrated olivine–orthopyroxene pairs from natural peridotites have K_D values in this range (*e.g.* Nixon and Boyd, 1973; Himmelberg and Loney, 1973; Frey and Green, 1974), as do olivine–orthopyroxene pairs in experimental runs in capsule materials other than platinum-group metals (*e.g.* Kushiro *et al.*, 1972). Our data in Tables 2 and 3 commonly exhibit non-equilibrium Fe/Mg partitioning between olivine and orthopyroxene. This is also evident in some previous partial melting studies where iron loss has occurred; for example, the data of Mysen and Kushiro (1977) show $K_D$ol/opx ranging from 0.72 to 0.85, and these values can be attributed to Fe loss and preferential readjustment of olivine to more magnesian compositions. The extent of iron loss from their experiments can also be gauged by the fact that in some of their runs the starting composition lies outside the field defined by the analyzed phases.

Several methods of alloying Pt capsules with iron have been suggested to reduce iron loss (*e.g.* Nicholls, 1974; Ford, 1978). In order to avoid net exchange of Fe, the activity of Fe in the capsule must exactly match that in the silicate charge, *i.e.* this must be determined for each bulk composition, *T*, *P*, and run duration. Moreover Fe-alloyed Pt becomes brittle, difficult to seal, and may result in capsule fracture during the experiment. Methods such as those proposed by Ford (1978) and Johannes and Bode (1978) may considerably reduce iron loss, but do not remove the necessity for the investigator to thoroughly evaluate the nature and extent of compositional interchange between sample and container.

Quench modification of equilibrium melts

Scanning electron microscope photographs (Fig. 1) reveal the presence of some quench material in all our experiments, even where none was discernible

optically. The extent of quench material varies from narrow (0.5–1 micron) rims of pyroxene or olivine on primary phases to broader (2–5 microns) blades of quench pyroxene both as rims and as discrete dendrites in the glass. The dominant quench phase in these anhydrous runs is clinopyroxene with varying Ca content. Quench clinopyroxene is not surprising, since this phase most closely approximates the liquid composition over most of the melting range. Quench clinopyroxene commonly contains 6 to 12 percent Al_2O_3 and 6 to 16 percent CaO and has a high TiO_2 content (2–3 percent). These features, together with the generally lower 100Mg/(Mg+Fe) ratio and skeletal or dendritic form, serve to distinguish quench pyroxene from stable primary calcic pyroxene. In addition, quench pyroxene analyses generally are not stoichiometric. In most cases the 100Mg/(Mg+Fe) ratios of the quench and primary phases are distinct, but in some experiments a continuum was found. Because abundant quench material drastically reduces the liquid volume and results in increased concentration of highly incompatible elements in the residual melt fraction, the presence of quench rims and crystals will cause errors in any method of estimation of degree of melting or melt composition based on analysis of the glass in experimental runs.

Quench crystallization has been shown to significantly modify equilibrium melt compositions in hydrous melting of peridotite (Green, 1973, 1976), and we have therefore examined the effect of quenching on liquids in anhydrous melting experiments. Data from two experiments, one at low to moderate degrees of melting (15 kbar, 1350°C) and the other at a high degree of melting (10 kbar, 1450°C), are presented in Tables 4 and 5 and plotted on Ca–Mg–Fe (atomic) diagrams (Figs. 4 and 5). Diffusion studies (*e.g.* Hofmann and Magaritz, 1977) have shown a high efficiency of diffusion over short distances (*e.g.* $D = 10^{-6}$ cm^2 at 1400°C), but the quenching rate in solid-media apparatus is such as to produce large compositional differences within the glass where quench phases and outgrowths occur. Moreover, the glass compositions bear little relationship to the composition of the equilibrium liquid calculated by mass balance from the proportions and compositions of the residual phases (Table 4, Fig. 4) or using published partition coefficients (Roeder and Emslie, 1970) after correction for iron loss for simple residues (Table 5, Fig. 5). Glass analyses made adjacent to quench crystals show a marked compositional difference to those obtained in larger "quench-free" pools. In neither case can these be considered as equilibrium melts.

The new data reaffirm earlier studies of the quenching problem (Green, 1973, 1976; Cawthorn *et al.*, 1973) and show that marked changes in the liquid composition may result in partial-melting experiments where quench phases occur, even in anhydrous melting. This problem is especially severe at low degrees of melting, and previous studies have shown that the problem increases at higher pressure and in the presence of volatiles (Green, 1973, 1976; Nicholls, 1974; Mysen and Kushiro, 1977).

Conclusions

We believe that the problems of iron loss and quench crystallization in anhydrous partial melting studies employing piston-cylinder apparatus are severe enough in most cases to preclude direct determination of the equilibrium melt composition. At high degrees of partial melting quench modification is far from trivial, and at low degrees of partial melting modification of the melt may be as severe under anhydrous as under hydrous conditions. In all cases, iron loss problems in anhydrous melting are greater than under hydrous melting conditions because of the higher melting temperatures. Therefore we are forced to conclude that most, perhaps all, previously published partial melt compositions obtained by direct analysis of quenched glasses from piston–cylinder runs are in error. At the very least, all such compositions should be regarded with suspicion.

We have attempted to show that, provided run times are not unduly long (this must be determined empirically by repeated experiments of varying duration), it is possible to calculate the equilibrium liquid composition by mass balance from the compositions of the residual phases which adjust more slowly to iron loss (and using known K_D's for those phases which do adjust rapidly), provided the modal proportions of the phases (including the percentage of melt + quench) can be determined. This is possible by point counting of reflected light and SEM photographs of the polished mount where all phases, including quench phases and overgrowths, can be discriminated. Replicates are generally required to overcome inhomogeneous distribution and crystal settling. However, no liquid determined by partial-melting experiments can be regarded as safely estab-

lished in the absence of reversal studies (*i.e.* crystallization of the liquid composition under the same experimental conditions).

Acknowledgments

We thank W. O. Hibberson and W. C. Doran for technical assistance and advice, and Dr. A. McKee and B. J. Griffin for instruction in the use of the SEM microprobe. Comments on the draft manuscript by K. L. Harris and D. J. Ellis and reviews by W. C. Luth, P. L. Roeder, and R. F. Fudali are gratefully acknowledged.

References

Bottinga, Y. and F. F. Weill (1970) Densities of liquid silicate systems calculated from partial molar volumes of oxide components. *Am. J. Sci., 269,* 169–182.

Cawthorn, R. G., C. E. Ford, G. M. Biggar, M. S. Bravo and D. B. Clarke (1973) Determination of the liquid composition in experimental samples: discrepancies between microprobe analyses and other methods. *Earth Planet. Sci. Lett., 21,* 1–5.

Ford, C. E. (1978) Platinum–iron alloy sample containers for melting experiments in iron-bearing rocks, minerals, and related systems. *Mineral. Mag., 42,* 271–275.

Frey, F. A. and D. H. Green (1974) The mineralogy, geochemistry and origin of lherzolite inclusions in Victorian basanites. *Geochim. Cosmochim. Acta, 38,* 1023–1059.

Green, D. H. (1963) Alumina content of enstatite in a Venezuelan high-temperature peridotite. *Geol. Soc. Am. Bull., 74,* 1397–1402.

——— (1973) Experimental melting studies on model upper mantle compositions at high pressure under both water-saturated and water-undersaturated conditions. *Earth Planet. Sci. Lett., 19,* 37–53.

——— (1976) Experimental testing of 'equilibrium' partial melting of peridotite under water-saturated, high pressure conditions. *Can. Mineral., 14,* 255–268.

——— and A. E. Ringwood (1967) The genesis of basaltic magmas. *Contrib. Mineral. Petrol., 15,* 103–190.

Himmelberg, G. R. and R. A. Loney (1973) Petrology of the Vulcan Peak alpine-type peridotite, southwest Oregon. *Geol. Soc. Am. Bull., 84,* 1585–1600.

Hofmann, A. W. and M. Magaritz (1977) Diffusion of Ca, Sr, Ba and Co in a basalt melt: implications for the geochemistry of the mantle. *J. Geophys. Res., 82,* 5432–5440.

Ito, K. and G. C. Kennedy (1967) Melting and phase relations in a natural peridotite to 40 kilobars. *Am. J. Sci., 265,* 519–538.

Johannes, W. and B. Bode (1978) Loss of iron to the Pt-container in melting experiments with basalts and a method to reduce it. *Contrib. Mineral. Petrol., 67,* 221–225.

Kushiro, I., N. Shimizu, Y. Nakamura and S. Akimoto (1972) Compositions of coexisting liquid and solid phases formed upon melting of natural garnet and spinel lherzolites at high pressures: a preliminary report. *Earth Planet. Sci. Lett., 14,* 19–25.

———, H. S. Yoder and B. O. Mysen (1976) Viscosities of basalt and andesite melts at high pressures. *J. Geophys. Res., 81,* 6351–6356.

Mori, T. and D. H. Green (1978) Laboratory duplication of phase equilibria observed in natural garnet lherzolites. *J. Geol., 86,* 83–97.

Mysen, B. O. and A. L. Boettcher (1975) Melting of a hydrous mantle. II. Geochemistry of crystals and liquids formed by anatexis of mantle peridotite at high pressures and temperatures as a function of controlled activities of water, hydrogen and carbon dioxide. *J. Petrol., 16,* 549–593.

———and I. Kushiro (1977) Compositional variations of coexisting phases with degree of melting of peridotite in the upper mantle. *Am. Mineral., 62,* 843–865.

———, ———, I. A. Nicholls and A. E. Ringwood (1974) A possible mantle origin for andesitic magmas: discussion of a paper by Nicholls and Ringwood. *Earth Planet. Sci. Lett., 21,* 221–229.

Nehru, C. E. and P. J. Wyllie (1975) Compositions of glasses from St Pauls peridotite partially melted at 20 kb. *J. Geol., 83,* 455–471.

Nicholls, I. A. (1974) Liquids in equilibrium with peridotitic mineral assemblages at high water pressures. *Contrib. Mineral. Petrol., 45,* 289–316.

Nixon, P. H. and F. R. Boyd (1973) Petrogenesis of the granular and sheared ultrabasic nodule suite in kimberlites. In P. H. Nixon, Ed., *Lesotho Kimberlites,* p. 48–56. Lesotho National Development Corporation, Maseru.

O'Hara, M. J. and D. J. Humphreys (1977) Problems of iron gain and loss during experimentation on natural rocks: the experimental crystallization of five lunar basalts at low pressure. *Phil. Trans. R. Soc. Lond., A286,* 313–330.

Reed, S. J. B. and N. G. Ware (1973) Quantitative electron microprobe analysis using a lithium-drifted silicon detector. *X-ray Spectrometry, 2,* 69–74.

——— and ——— (1975) Quantitative electron microprobe analysis of silicates using energy dispersive X-ray spectrometry. *J. Petrol., 16,* 499–519.

Ringwood, A. E. (1966) The composition and origin of the earth. In P. M. Hurley, Ed., *Advances in Earth Science,* p. 287–356. MIT Press, Cambridge, Massachusetts.

Roeder, P. L. and R. F. Emslie (1970) Olivine–liquid equilibrium. *Contrib. Mineral. Petrol., 29,* 275–289.

Stern, C. R. and P. J. Wyllie (1975) Effect of iron absorption by noble-metal capsules on phase boundaries in rock melting experiments at 30 kb. *Am. Mineral., 60,* 681–689.

Manuscript received, August 21, 1978;
accepted for publication, May 16, 1979.